Green Energy and Technology

Santosh K. Tiwari
Michal Bystrzejewski
Vijay Kumar *Editors*

Biomass-Based Functional Carbon Nanostructures for Supercapacitors

Springer

Green Energy and Technology

Climate change, environmental impact and the limited natural resources urge scientific research and novel technical solutions. The monograph series Green Energy and Technology serves as a publishing platform for scientific and technological approaches to "green"—i.e. environmentally friendly and sustainable—technologies. While a focus lies on energy and power supply, it also covers "green" solutions in industrial engineering and engineering design. Green Energy and Technology addresses researchers, advanced students, technical consultants as well as decision makers in industries and politics. Hence, the level of presentation spans from instructional to highly technical.

Indexed in Scopus.

Indexed in Ei Compendex.

Santosh K. Tiwari · Michal Bystrzejewski ·
Vijay Kumar
Editors

Biomass-Based Functional Carbon Nanostructures for Supercapacitors

Springer

Editors
Santosh K. Tiwari
Department of Chemistry
NMAM Institute of Technology, Nitte
(Deemed to be University)
Karnataka, India

Michal Bystrzejewski
Faculty of Chemistry
Warsaw University
Warsaw, Poland

Vijay Kumar
Department of Physics
National Institute of Technology Srinagar
Srinagar, Jammu and Kashmir, India

ISSN 1865-3529 ISSN 1865-3537 (electronic)
Green Energy and Technology
ISBN 978-981-99-0995-7 ISBN 978-981-99-0996-4 (eBook)
https://doi.org/10.1007/978-981-99-0996-4

Preface

"We simply must balance our demand for energy with our rapidly shrinking resources. By acting now, we can control our future instead of letting the future control us." A quote by former US President Jimmy Carter. These words are really fitting for our future. At present, energy catastrophe is one of the key issues facing the globe. To solve this problem, the proper use of biomass can play a vital role. The approximate amount of biomass in the world is ~1,800 Pg and 70% of which exists as biomass waste. An estimated 140 Pg of agricultural biomass waste is produced annually around the globe, which is equivalent to 50 billion tons of oil, whereas the globe's annual oil consumption is ~4000 billion tons. Thus, the chosen subject of turning biomass waste into useful energy will make a significant contribution to the current energy crisis.

For most of the renewable energy sources, storing energy for the required time is a big challenge, even with the availability of sources. Among the many energy storage techniques, supercapacitors have been regarded as one of the most advanced and effective technologies. At the electrode-electrolyte interface, supercapacitors have the ability to store electrical charge in an electric double layer. The market for supercapacitors was projected to reach $2 billion globally in 2025, and demand for them is expected to continue growing and double in the following years. Due to the versatility of supercapacitors, advanced research has led to rapid improvements in their availability, cost of fabrication, and efficiency. However, these technologies still require significant improvements, both in terms of technical promise and commercial viability. Meanwhile, secondary batteries are among the most commonly used in electronic devices of the twenty-first century. Secondary batteries (such as lithium-air batteries and lithium-ion batteries) are crucial in our daily lives because of their special characteristics, and they are widely utilized because of their slow self-discharge, high energy density, minimal maintenance requirements, wide range of availability, etc. Due to the limited supply of lithium in the earth's crust, these batteries experience significant problems with aging, inadequate protection, flexibility, transportation, and high cost, which forces materials scientists to look for alternative materials for batteries that can be produced in large quantities at a reasonable price. Sodium batteries have been tested as a lithium substitute recently, but they have a

number of drawbacks that have prevented them from taking over the market. In recent years, biomass-derived nano- and microcarbon materials have received much attention as a green source of activated carbon due to their renewable, abundant, affordable, and environmentally friendly nature. Numerous carbon compounds, including graphene, mesoporous carbon, carbon nanotubes, carbon fiber, and their composites, have been researched as electrode materials for energy storage applications.

Given the significance of carbon nanostructures made from biomass for supercapacitors, a few review papers on this category of materials have been published. But in recent years, significant progress has been made in producing useful carbon nanostructures from biomass and applying these structures in a variety of fields. Furthermore, several crucial issues concerning carbon nanostructures produced from biomass and their uses have not been covered up to this point. To address this issue, we chose to produce a book on Biomass-Based Functional Carbon Nanostructures for Supercapacitors and to generalize and organize the findings of the relevant research. To our knowledge, this is the first time a comprehensive overview of the creation, advancement, and use of cutting-edge carbon nanostructures derived from biomass for supercapacitor applications has been published.

The book is aimed at scientists and researchers who are already working in the field of biomass-based carbon nanostructures or who aspire to do so, i.e., scientists and researchers whose research focuses on carbon nanostructures made from biomass for energy storage applications. This book will serve as a significant and insightful source of valuable information, giving scientists and engineers new insights for comprehending and improving existing carbon nanostructures derived from biomass and for designing new carbon-based nanostructures from biomass with new and unexpected possibilities.

We believe that academicians, postdocs, and university students would all greatly benefit from this book. The book's organizational framework provides a foundation for courses in numerous fields of science and engineering. Graduate students may also find the book to be extremely helpful in their research and comprehension of the characteristics of carbon nanostructures produced from biomass and their use in supercapacitors. We are confident that the material will be helpful to all of them in their endeavors.

Finally, we would like to express our gratitude to all the authors who contributed to the book's production. We appreciate their cooperation in working on this project and their efforts in getting the book ready. The completion of this project would not have been feasible without their involvement. We also thank Springer for allowing us to publish the book and for their support. We would like to express our sincere gratitude to the editorial staff at Springer for their patience and support during the course of this project's development.

Karnataka, India — Santosh K. Tiwari
Warsaw, Poland — Michal Bystrzejewski
Jammu and Kashmir, India — Vijay Kumar

Contents

About the Editors

Dr. Santosh K. Tiwari is an Assistant Professor at NMAMIT (Visiting Scientist, Guangxi Institute Fullerene Technology, GU, Nanning, China), Nitte, India. Dr. Tiwari received a Ph.D. in 2D materials-based polymer nanocomposite from IIT Dhanbad, India. And then worked for more than five years with several high-ranked research labs and universities around the globe, including HSCL, Hanynag University, Seoul Korea, GIFT, GU, Nanning, China, and the University of Warsaw, Poland. He has published more than 55 articles (Total citation 2000+, h-index: 24) & five books with reputed international publishers His research interests are in the areas of new materials, 2D nanomaterials, polymer composites, and mechanical properties.

Prof. Michal Bystrzejewski is a full professor in the Department of Chemistry, Warsaw University, Poland, and has a deep research interest in synthesis and characterizations of carbon nanomaterials, carbon capsules, magnetic nanoparticles, and separation based adsorption. He received his M.Sc and Ph.D. from the University of Warsaw, Poland, and postdoctoral training from Germany as a Marie Curie Fellow. He published more than 150 research articles related to nanomaterials and carbon nanostructures. He finished several research projects granted by the European Union and the government of Poland.

Dr. Vijay Kumar is currently working as an Assistant Professor at the National Institute of Technology Srinagar, J&K, India. He obtained his Ph.D. degree in Physics (Material Science) from the Sant Longowal Institute of Engineering & Technology (SLIET), Longowal, Punjab (Deemed to be University) in 2013. He has received several awards and honors, including the best poster and oral presentation awards, the Young Scientist Award under the fast-track scheme of the Department of Science and Technology (DST), Government of India, and the Teacher with the Best Research Contribution Award. He is also a visiting research fellow in the Department of Physics at the University of the Free State, South Africa. He has been selected as an Early Career Advisory Board member of Vacuum (Elsevier). He has been selected under the SERB International Research Experience (SIRE) Fellowship extended by the Science and Engineering Research Board, DST, Government of India. He has been inducted

as a member of the Indian National Young Academy of Sciences (INYAS) for a five-year term. He has been nominated as a member of the Scientific Advisory Committee for the Initiative for Research and Innovation in Science by DST. He has more than 80 research papers in international peer-reviewed journals, 10 peer-reviewed conference proceedings, 15 book chapters, and has edited 9 books (authored and co-authored). He has more than 4580 citations with an h-index of 36 and an i10-index of 85. He serves as a reviewer for several reputed journals and is also on the editorial board of Vacuum, Results in Surfaces and Interfaces, Frontiers in Energy Research under Section Nano Energy, etc. He has edited the Virtual Special Issue of Vacuum—Journal—Elsevier and Materials Today: Proceedings. He has worked extensively on irradiation-induced modifications in polymeric materials. His current research focuses on synthesizing, processing, and characterizing functional materials, solid-state luminescent materials, soft and ceramic materials, biopolymers, drug delivery devices, wastewater treatment, etc.

Biomass-Based Functional Carbon Nanostructures for Supercapacitors

Vandana Molahalli, Apoorva Shetty, Kiran Bijapur, Gowri Soman, Aman Sharma, Jasmine Joseph, and Gurumurthy Hegde

Abstract For the creation of next-generation biocompatible energy technologies, it is urgently necessary to examine environmentally acceptable, low-cost electrode materials with high adsorption, rapid ion/electron transit, and programmable surface chemistry. Because of their wide availability, environmentally friendly nature, and affordability, carbon electrode materials made from biomass have received a lot of interest lately. The biological structures they naturally possess are regular and accurate, and they can be used as templates to create electrode materials with precise geometries. The current study is primarily concerned with recent developments in research pertaining to biomass-derived carbon electrode materials for supercapacitor applications, including plant, fruit, vegetable, and microorganism-based carbon electrode materials. Also provided is a summary of alternative synthesis methods for the conversion and activation of biomass waste.

1 Introduction

The relevance of the worldwide clean energy storage device has been gaining attention for the last few centuries. It is impossible for humans to even imagine a world without a continuous supply of energy. Although fossil fuels are the main source of energy, their scarcity and high demand have made them an expensive and unreliable energy source. Globally, the combustion of fossil fuel has resulted in the production of enormous amounts of CO_2, a greenhouse gas that significantly contributes to climate change. Other conventionally used devices to meet the growing demand for energy source were fuel cells, batteries, and capacitors. Batteries are used to serve the purpose of energy requirements. They function by converting chemical energy into electrical energy through redox reactions. Over a period of time, the chemical

V. Molahalli · A. Shetty · K. Bijapur · G. Soman · A. Sharma · J. Joseph · G. Hegde (✉)
Department of Chemistry, CHRIST (Deemed to Be University), Bangalore 560029, India
e-mail: murthyhegde@gmail.com; gurumurthy.hegde@christuniversity.in

Centre for Advanced Research and Development (CARD), CHRIST (Deemed to Be University), Bangalore 560029, India

S. K. Tiwari et al. (eds.), *Biomass-Based Functional Carbon Nanostructures for Supercapacitors*, Green Energy and Technology,
https://doi.org/10.1007/978-981-99-0996-4_1

reactants in the battery will get consumed completely. Afterwards, the battery has to be either recharged or disposed (Fig. 1).

Later on, the discovery of Fuel cells could solve this issue to some extent. Batteries and fuel cells operate similarly, with the exception that fuel cells feature an extra layer known as a catalyst layer that speeds up the chemical reactions. Fuel cells can produce energy endlessly as long as fuel is given to them. In contrast to conventional cells and batteries, these cells do not lose voltage or current over time. Fuel cells possess an extra layer known as the catalyst layer which helps to improve the chemical

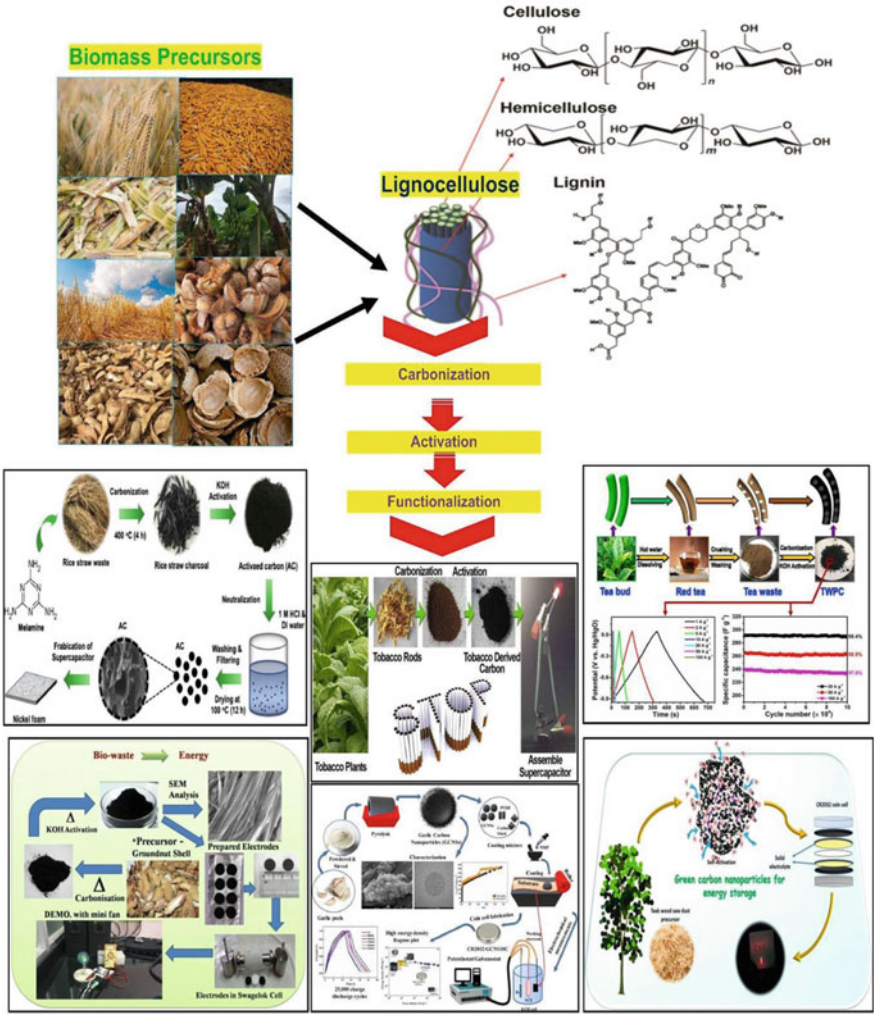

Fig. 1 An illustration of the steps taken to create biomass-based functional carbon nanostructures for use in supercapacitors. Adapted with permission from ref [1–6]

reaction. Despite their benefits, they were unable to completely replace batteries due to their major demerits such as handling gaseous fuel cells, expensive catalysts for the electrode reactions, and the electrolytes employed in fuel cells seem to raise a number of practical issues. The invention of supercapacitors (SCs) proved beneficial in overcoming these circumstances and meeting the need for energy.

Supercapacitors (SCs) also known as ultracapacitors differ from regular capacitors due to their quick charge–discharge rates, longer life cycles, high power, and high energy density. They are specially designed energy storage devices that store energy through mainly two mechanisms: double-layer capacitance or pseudo capacitance. These two mechanisms differ in origin. Double-layer capacitance is of electrostatic origin whereas pseudocapacitance is of electrochemical origin. This indicates why supercapacitors excel in their performance when compared to the normal supercapacitors and batteries, as the working of the SCs is a combination of both. Normally, an electrostatic capacitor operates at a maximum voltage range; the typical maximum charge voltage range of SCs lies between 2.5 and 2.7 V. Supercapacitors have evolved to be a potential replacement for electrochemical capacitors, as there is a huge demand for electric vehicles. SCs are efficient in delivering desirable power density and rate response, but they possess low energy density. The choice of electrode material is very crucial when it comes to SCs, as they affect electrical properties. Due to the fact that double-layer charge storage is a surface process, the electrode material's surface characteristics have a significant impact on the cell's capacitance. One of the challenges faced while using SCs is low voltage per cell, low energy density, and high production cost. This prompted scientists to create novel storage materials and increase electrolytes with high operating potential in order to offer a solution that would improve the performance of SCs [7]. Carbon materials, metal oxides, and conducting polymers are now the most common electrode materials used in the manufacturing of electrodes for SCs applications. Carbon materials have been employed since the beginning of supercapacitor production because of their high surface area. On the other hand, metal oxides offer high specific capacitance and low resistance, making them attractive choices for electrode materials. In numerous studies, a wide range of cutting-edge materials is investigated and evaluated as SC electrode materials. Among the various developments in the area of SCs, biomass precursors have found much attention. Biomass precursors like wood, dried leaves, stems, flowers, seeds, fruits, and agricultural waste are excellent sources of carbon materials as they are non-toxic, sustainable, abundant, and environment friendly. For instance, some papers concentrate on activated carbons made from specific precursors like lignocellulosic precursors, oil palm, wood, plant components, and agricultural waste, while other researchers have written papers about the uses of activated carbons made from biomass in removing heavy metals, storing dyes, making electrode materials for hybrid electrochemical capacitors, and adsorption.

2 Origin of Biomass Usage

See Fig. 2

The waste products generated in the food and agricultural industries are collectively referred to as biomass. Biomass is critical for the manufacture of a number of commercially significant goods in addition to being a good source of energy. As a result, biomass is properly viewed as a renewable source of energy that can be used to create energy or energy-carrying materials [8]. Some of the sources of the biomass which are easily available are listed below.

2.1 Agricultural and Forest Residue

Agricultural waste accounts for the majority of the bio waste produced which includes dry leaves, rice/wheat husks, nut shells, peels of fruits, corn straw, etc. Waste produced

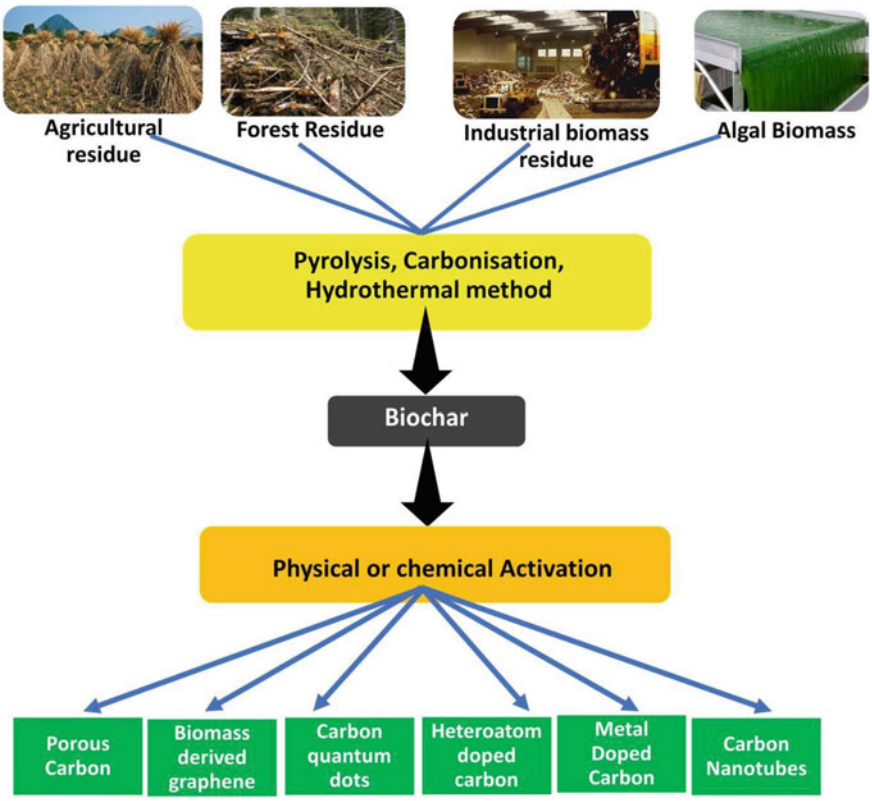

Fig. 2 Origin of biomass usage

by industries reliant on forests, such as stems, treetops, and branches, is referred to as forest residue. These wastes due to a lack of strategies for the disposal are simply burnt which results in the release of large amounts of CO_2 into the atmosphere. However, these materials can be converted into value-added products and can be utilized as feed stocks for the production of carbon-based nanostructures which are of great importance as electrode materials in energy storage applications. By using ferrocene as an effective, low-cost catalyst in a straightforward catalytic oxidation process, Tamilselvi Ramasamy and the team showed that readily available coconut waste could be effectively converted into reduced graphene oxide and examined as an electrode material for supercapacitor application [9]. Bhat et al. studied the porous carbons synthesized from garlic peel via catalyst-free pyrolysis technique for the evaluation of high-performance supercapacitor [4].

2.2 Industrial Biomass Residue

The industrial biomass residue is generally generated by paper mills, sugar mills, oil mills, furniture industries, etc. The paper industry generates "Pulp Sludge" as a ubiquitous solid byproduct of the manufacturing process. Pulp sludge is currently disposed of through incineration or placed into landfills. The sludge releases CO_2 into the atmosphere as it either burns or decomposes. The scale of its availability and negative cost make pulp sludge a very attractive feedstock for high surface area carbons. Huanlei Wang and group demonstrated the synthesis of carbon material derived from paper sludge, yielding controlled levels of micro and mesoporosity, and studied them for supercapacitor application [9]. Vijayakumar and team collected waste cotton from the cotton industry and obtained high surface area activated porous carbon fibers as high-performance supercapacitor electrodes with commercial level mass loading [10].

2.3 Algal Biomass

The term "algae as feedstocks" describes a wide range of extraordinarily fruitful organisms, such as microalgae, macroalgae (seaweed), and cyanobacteria, also known as "blue-green algae". Most of them use sunlight and nutrition to produce biomass, which contains essential elements like lipids, proteins, and carbohydrates that may be transformed and improved into a range of biofuels and goods. Algae can thrive in fresh, salty, or brackish water that comes from groundwater, surface water sources, or ocean, depending on the strain. They can also flourish in water that has been used a second time, including produced water from oil and gas drilling or treated industrial effluent as well as municipal, agricultural, or aquaculture wastewater. In comparison to lignocellulose-derived biochar, the algal biochar is nitrogen-rich, has a higher pH, and a higher H/C and O/C ratio [11]. Consequently, the intrinsic

heteroatom functions make it advantageous to produce carbon nanostructures from the algal feedstock.

Bingjun Zhu and group reported a high-performance carbon-based supercapacitor electrode material synthesized from selected algae microspheres, which were grown under controlled cultivation conditions. The best-performed sample possessed a high specific surface area 1337.9m^2g^{-1} with a hierarchically porous structure and naturally intrinsic nitrogen dopant with a specific capacitance of 353 Fg^{-1} at 1 Ag^{-1} and 92% capacitance retention even after 10,000 charge–discharge cycles at 20 Ag^{-1}.

Thus, the origin of the biomass plays a significant role in the inherited structural and chemical composition of the carbon nanostructures that are synthesized from them, and as a result, the chosen biomass will have the capacity to enhance the properties of the materials such as surface area, functionality, porosity, thermal stability, and electrical conductivity, which are crucial for supercapacitor applications.

3 Nanostructured Bio-based Carbon Materials: Preparation and Characterization

Bio-based materials are products whose primary components were first derived from living things. These substances can be created synthetically or from naturally occurring organic compounds. Although it typically relates to modern materials, this term does encompass natural materials like wood and leather. Many recent innovations create biodegradable items using bio-based components. Plant-based materials are the bio wastes that are most frequently utilized to create carbon nanostructured materials (Fig. 3).

CNPs are a promising electrode material for high-performance supercapacitors because of their high electrical conductivity, ability to display a reduced ion-transport resistance, and ability to demonstrate a shorter diffusion pathway [17].

3.1 Pyrolysis

Pyrolysis is a thermochemical process that degrades materials into smaller components at high temperatures without oxygen. This technology has recently received increased attention for its usage in the conversion of organic wastes into usable and advanced application materials [18]. Biomass is thermally decomposed at temperatures between 300 and 900 °C to produce charcoal, bio-oil, and syngas. The amount of biochar produced depends on the feedstock type and the operating circumstances [20]. On the basis of temperature and heating rate, pyrolysis is further separated into slow and rapid pyrolysis. Pyrolysis is further divided into slow and quick pyrolysis based on temperature and heating rate. Fast pyrolysis is conducted at a higher heating rate (100–200 C/min) with a shorter residence time (10 s), whereas slow pyrolysis

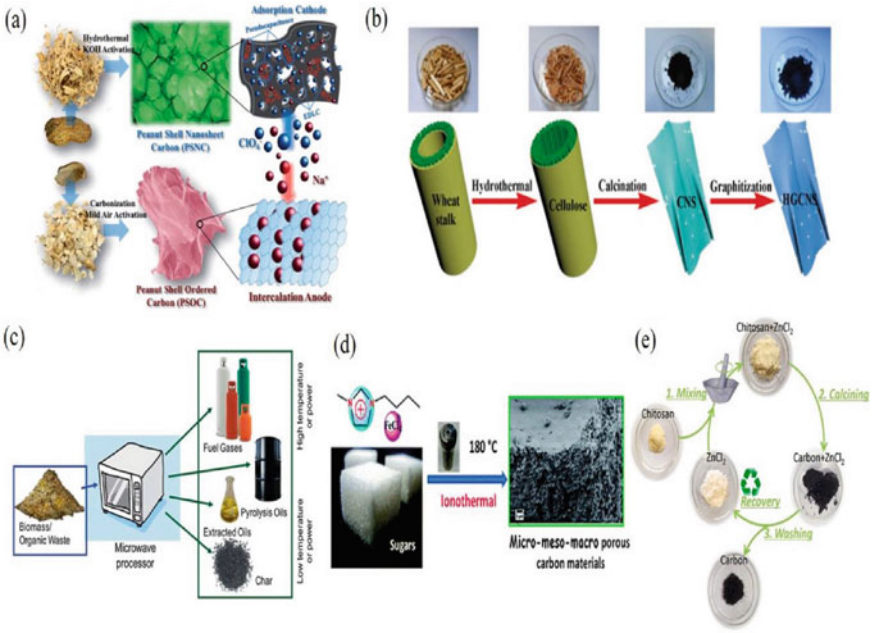

Fig. 3 Illustration of several synthesis techniques used to create biochars made from biomass. **a** Carbon from peanut shells was produced using a combination of hydrothermal carbonization and activation. Adapted with permission from ref [12]. **b** Carbon from wheat stalks was obtained by hydrothermal and calcination-graphitization processes. Adapted with permission from ref [13]. **c** Organic waste is pyrolyzed using a microwave. Adapted with permission from ref [14] **d** Porous carbon is produced by ionothermal means from sugars. Adapted with permission from ref [15] **e** Chitosan carbon was formed from molten salt. Adapted with permission from ref [16]

runs at a lower heating rate (5–7 C/min) and longer residence duration (>1 h) [19]. The microstructure of the resulting carbon can also be modified through pyrolysis (for example, by increasing the amount of graphitic material), making pyrolysis-assisted production is becoming more popular in now a day. These materials can be generated using lithographic processes as micro- and nano-scale pre-patterned structures, films on a substrate, or substrate-attached components, depending on the kind of carbon and the size of the reaction [22].

3.2 Chemical Vapor Deposition

The most often utilized method of thin-film deposition for creating nanomaterials is CVD. The chemical vapor deposition (CVD) approach is currently the standard, extensively used method in the synthesis of nanotubes due to its simplicity and low cost. This process was created in the 1960s and 1970s and has been effectively

applied for more than 20 years to the manufacturing of carbon fibers and carbon nanofibers [20]. In the CVD method of making carbon nanotubes, the catalyst is first applied to the substrate, and then it is nucleated either through thermal annealing or chemical etching (using ammonia as the etching agent). After that, the pre-prepared supporting material is put into a tubular reactor to begin the growth process. A mixture of hydrocarbon gas (ethylene, methane, acetylene, etc.) and a process gas (nitrogen, hydrogen, argon) is made to react in a reaction chamber over the surface of metal catalysts for a given time period (typically 15–60 min), and when the decomposition of the carbon precursor takes place, CNTs grow on the catalyst particle in the reactor and are collected from the reactor after it has been heated to the necessary reaction temperature (600–1200 °C) [21]. Similarly, nanostructured bio-based carbon nanomaterials can be synthesized.

3.3 Arc Discharge

One essential requirement for stabilizing arc discharge is to keep the distance between the graphite electrodes constant at around 1 mm [20]. Two graphitic rods are maintained at a distance of a few millimeters, and an arc is generated between them. This process is economical. Normally, a carbon-containing gas is decomposed at a high temperature in the presence of a metal catalyst to create carbon nanotubes using the thermal chemical vapor deposition process [22]. When creating 1D and 2D nanostructures from carbon anodes, pulsed arc discharges can enhance arc control and customize the ablation process. After the pulsed arc, carbon nanostructures such as carbon nanotubes and graphene nanoplatelets were deposited on the cathode. The production of semiconducting nanomaterials with adjustable electrical and optical characteristics is possible using this deposition technique [23].

3.4 Laser Ablation

Carbon nanostructure materials (CNMs) can be successfully created on a graphite target submerged in deionized water by pulsed laser ablation. To irradiate the target, different laser strengths (between 60 and 220 mJ) and a laser pulse duration of ns (1064 nm) were used. The graphite target submerged in deionized water was ablated using a Q-switched pulsed Nd: YAG laser operating at 1064 nm wavelength with a pulse repetition rate of 1 Hz and pulse duration of 9 ns (mm) [24].

3.5 Hydrothermal Method

Several investigations have been carried out to produce carbon-rich compounds from a variety of biomasses by combining hydrothermal carbonization and pyrolysis with a range of residence durations and reaction temperatures [28]. This technique has a number of benefits, including the ability to produce vast quantities of nanomaterials at a low cost and the ability to produce highly crystalline nanocrystals with precisely regulated dimensions. It can be used in conjunction with microwaves and magnetic fields to create materials with significantly enhanced repeatability and high quality [25]. A stable colloidal suspension of spherical carbon nanoparticles (CNPs) with good size and shape homogeneity was produced using the hydrothermal technique [17]. Carbon nanoparticles were created by hydrothermally oxidizing carbohydrates (glucose, sucrose, and starch) in water with the use of acids and alkalis [26].

Various activation methods are used while synthesizing the different carbon structures from the biomass precursors. The activation methods are inevitable for ensuring the porosity, size, and morphology of the carbon structures from biomass, which includes physical activation, chemical activation, and microwave activation methods. The chemical activation method is the most prominent among the researchers in synthesizing bio-carbon. Usually, common oxidizing and dehydrating agents like sulfuric acid, phosphoric acid, zinc chloride, and potassium hydroxide are used as activating agents. The activating agent is mixed with the precursor material and can be treated between the temperatures of 500 and 800 °C. The cellulose will break down and dehydration will remove the moisture content. As a result of this, the carbon skeleton is formed due to charring, and the aromatization of the structure takes place easily. The resultant structure also will be porous in nature. Table 1 summarized some of the relevant nano-carbon prepared from various biomass giving good specific capacitance.

4 Preparation and Evaluation of Newly Developed Bio-derived Precursor as Electrodes in Energy Storage Applications

Energy is essential to our daily activities, and as the need for batteries and other energy storage devices rises steadily, there are some fascinating aspects that will need to be taken into account. For instance, it is still uncertain if lithium-ion batteries will remain desirable and viable. It is crucial to emphasize that these batteries are not made at a low cost to the environment. A sustainable method of manufacturing high-performance electrochemical devices is required to solve this problem. Additionally, it is preferred that materials and procedures be inexpensive to enable the mass manufacture of electrodes to satisfy current industry demands [38].

Supercapacitors can offer numerous advantageous features over conventional batteries, including high power density, quick charging, and extremely extended

Table 1 Analysis of the different activation methods used in the synthesis of various Bio-nanocarbon materials

Precursor	Activation method	Activation agent	Surface area (m^2g^{-1})	Specific capacitance (Fg^{-1})	Refs.
Celtuse leaves	Pyrolysis in Ar/Alkali treatment	KOH	3404	421	[27]
Potato peel	Pyrolysis followed by metal chloride treatment	$ZnCl_2$	1052	255	[28]
Aloe Vera	Carbonization/Alkali treatment	KOH	1890	410	[29]
Hemp stem	Carbonization/self-activation	$KMnO_4$	1193	255.5	[30]
Prosopis Juliflora wood	Carbonization in N_2 /alkali treatment	KOH	2943	588	[31]
Parthenium hysterophorus	Carbonization/Alkali activation	KOH	4014	270	[32]
Bamboo shaving	CO_2 catalyzed induction	K_2CO_3	1980	273	[33]
Averrhoa bilimbi leaves	One-way KOH impregnation	KOH, CO_2	–	293	[34]
Soyabean residues	HTC/Alkali activation	KOH	1943	497	[35]
Metaplexis Japonica	Carbonization/Alkali activation	KOH	3635	127	[36, 37]
Bamboo chips	Pyrolysis in NH_3	K_2CO_3 and $K_2C_2O_4$	755	208	[37]

cycle life [18]. The performance of supercapacitors is directly impacted by the characteristics of the electrode materials and the electrode/electrolyte interface [39]. A lot of research has been done on carbon-based electrodes for supercapacitor applications due to their exceptional electrical and chemical stability. The hydrothermal reaction is the best option for use in the preparation of CNPs, since it is significantly easier, less expensive, and less damaging than the other techniques mentioned. This technique also consumes less oxygen and operates at a lower temperature. Due to these factors, the hydrothermal reaction is a practical method for creating high-quality CNPs that can be used as supercapacitor electrodes [44].

The two most widely utilized methods for activating biomass are chemical activation and physical activation. One benefit of employing chemical activation over physical activation is the ability to produce materials with greater surface areas and activated carbons with porous structures. Miscanthus × giganteus lignocellulosic biomass was used to create value-added products like activated carbon and carbon nanotubes. An alternate method for creating activated carbon from Miscanthus × giganteus was described. The activated carbon that was created had a high surface area and pore volume of 0.92 cm^3g^{-1} after two phases of activation using phosphoric

acid and potassium hydroxide. Following the first and second activation procedures, the SBET of the raw biomass revealed 17, 1142, and 1368 m^2g^{-1}, respectively [40].

A family of electrochemical energy storage devices known as electrochemical double-layer capacitors (EDLCs), also known as supercapacitors, ultracapacitors, and capacitors, are often used names for these devices. These devices are perfect for the quick storage and release of energy [41]. Carbon materials have long been used as supports for active materials, electro-conductive additives, substrates for current leads, electron transfer catalysts, intercalation hosts, and as agents for the control of surface area, porosity, heat transfer, and capacitance in energy storage devices. Carbons are naturally a good choice for EDLC electrode materials due to these factors [42].

Pandolfo et al. claim that the following physical–chemical characteristics of an electrode material in a supercapacitor can be identified: high electric conductivity, low cost, good thermal stability, high corrosion resistance, high specific surface (>2000 $m^2\ g^{-1}$), high material purity, and homogeneous pore structure [41].

Due to their superior performance, carbon-based electrodes are widely researched for energy storage devices. High electrochemical stability, simple modification, variable and porous morphologies, and particular capacitance combine to give the highly regarded performance. The electrochemical performance of carbon electrodes generated from biomass and bio waste is a key factor in figuring out whether bio-based carbon precursors are viable for use in energy storage applications. The electrochemical performance of a carbon-based electrode is frequently connected with its shape, porosity and pore size, specific surface area, and doping level. Unique nanostructures, a sizable specific surface area, and a high heteroatom doping level distinguish bio-based carbon electrodes [48, 49].

In [43], six different forms of carbon materials from potato waste were created using the hydrothermal carbonization (HTC) method. The biomass was heated to 200, 220, and 240 degrees Celsius for two and five hours, respectively. A stainless-steel autoclave with a capacity of 250 mL was filled with 25 g of dry biomass and 150 g of water before each carbonization procedure. This is equivalent to a 1:6 ratio. The autoclave was then heated in a gas chromatography oven to the appropriate temperature. The reaction time was noted as soon as the autoclaves attained the desired reaction temperature. The autoclave was quenched in a 20 °C cold water bath at the conclusion of the reaction. Vacuum filtration was used to separate the solid and liquid phases. For this, filter paper with a particle retention of 5–13 m (VWR) was employed. The filter cake was dried at 105 °C for the entire night [43] (Fig. 4).

5 Nanostructure Morphology and the Kind of Precursor

Agreen and sustainable platform for the production of diverse functional carbon materials (porous carbon, heteroatom doped biochar, carbon nanotubes, graphene, carbon quantum dots, etc.) for advanced applications is provided by biochar produced from

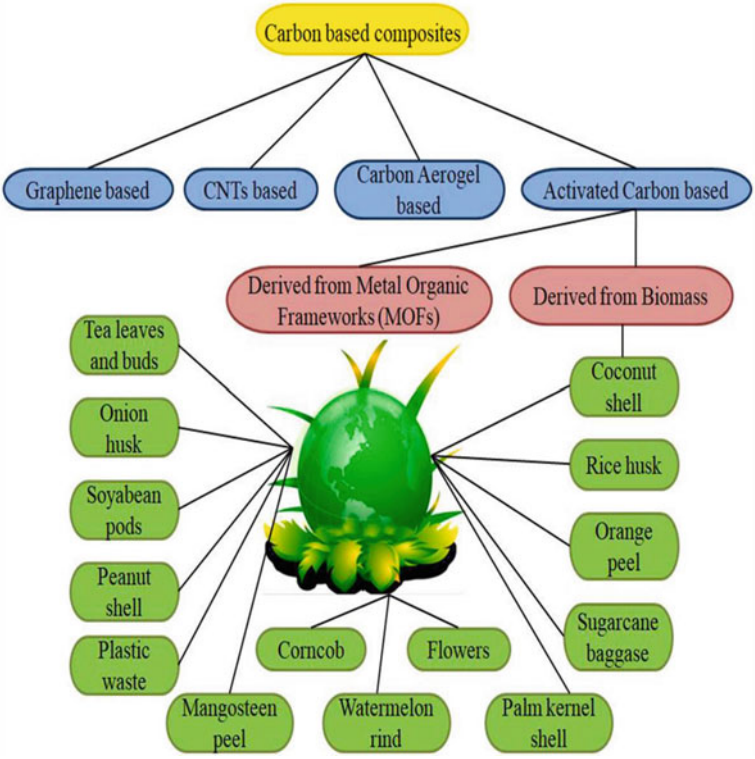

Fig. 4 Various carbon-based composites and biowaste. Adapted with permission from ref [44]

the thermochemical conversion of biomass. Recent studies on carbon compounds generated from biochar have broadened their usage in supercapacitors and fuel cells, respectively, for electrochemical energy generation and storage [44]. Because it is less expensive, changeable and controlled shape, high specific surface area, and superior electrical conductivity, porous carbon is an excellent electrode material for supercapacitors[45, 46]. It has been demonstrated that the capacitive characteristics of porous carbon are significantly influenced by pore structure [47]. These factors cause all of the carbon materials listed above to behave in an EDLC-like manner when ions are adsorbed at the electrode interface. The use of carbon materials derived from biomass in supercapacitors has advanced recently, demonstrating how easy it is to boost the energy density of the manufactured electrodes by applying various electrolytic systems [48]. Due to their low cost and variety of species, many biomass, including fish scale, rice, cornstalk, sorghum, loofah sponge, rice straw, bagasse, and jujube, have been used to make porous carbon. The large pore size distribution of activated carbon contributes significantly to improving the electrochemical performance of supercapacitor devices when they are being charged and discharged ($\geq$50 nm) [49].

Batteries typically have an energy density of between 100 and 250 Wh/kg, while supercapacitors have an energy density of around 20 Wh/kg but a high power density of over 10 kW/kg. Therefore, the primary objective is to increase SC energy density to a level that is comparable to rechargeable battery energy density. This can be accomplished by modifying the nanostructure of the carbon material to achieve a high surface area and narrow pores size distribution in the mesoporous region [50]. In this chapter, we discussed the different nanostructures which are derived from bio waste, for the development of SCs.

5.1 Biomass-Derived Carbon Nanotubes (CNT)

With single-walled CNT having a diameter of 0.8–2 nm and multi-walled CNT having a diameter of 5 to 20 nm, the term "CNT" refers to a collection of carbon components that are assembled into cylindrical tubes [51]. CNTs are used in a wide range of applications, including biosensors, drug delivery systems, and biomedical imaging. Additionally, CNTs enhance ionic conductivity and reduce the electrode's self-discharge, which lowers the supercapacitor's potential and results in energy loss [52].

Through the hydrothermal carbonization of glucose in the presence of carbon nanotubes, Natalia et al. developed a carbon nanotube hybrid material. Following the addition of 2 weight percent of carbon nanotubes, the electrode materials produce $206Fg^{-1}$ and 78% capacitance retention up to 0.8 V and 20 Ag^{-1}, as well as high rate cyclability (97% after 5000 cycles). The huge surface area is responsible for the exceptional performance [53]. Even though CNTs having high surface area and high conductivity, the SCs based on CNTs failed to achieve a good optimum capacitance in the absence of pseudocapacitive material [54]. There is a direct relationship between the amounts of the charge stored to the capacitance of the material. Taberna et al. [55] developed a composite of CNTs with activated carbon prepared by coconut shells for the development of electrodes. The capacitance of the activated carbon was $92Fg^{-1}$, it got decreased when they were composed with the CNT, to 88 to $55Fg^{-1}$, at 15 and 50 wt%. This test was performed under the presence of a non-aqueous electrolyte (NEt4BF4 1.5 M in acetonitrile). From these results, we can conclude that CNTs are not good for composite for the development of electrodes for SCs.

5.2 Biomass-Derived Carbon Nanosphere

High surface area and hierarchical porosity—two properties necessary for efficient energy storage devices—are inherent to CNs generated from biomass. Carbon nanospheres have attracted a great deal of interest in recent years for supercapacitor applications. Bio-cellulose waste and hemicellulose, which are the structural

elements of cells, are appropriate for energy storage technologies. The main component of solid biowaste, consisting of 35–50% cellulose, is called lignocellulosic biomass [56]. It can be used to make porous carbons, which can be used to make free-standing electrode materials, at a low cost [57]. Numerous industries use activated carbon nanospheres, including those that treat drug overdose and poisoning, purify air and water, raise cattle, make wine, store hydrogen and natural gas, filter beverages, remove mercury, and many more.

Gomma et al. [57] synthesized porous CNs with garlic peels for the evolution of high-performance SCs. The developed devices show the following results: the highest possible specific capacitance measured in a 4.0 M KOH electrolyte was 174 F/g at 0.1 A/g. The symmetric supercapacitor had a specific energy of 32.6 Wh/kg and a specific capacitance of 119.2 F/g at 0.1 A/g. With 97.8% coulombic efficiency, the device demonstrated perfect stability over 25,000 charge–discharge cycles. Even at the ending of the 10,000th cycle, a 93% retention of capacitance was recorded. The porous carbon that Erman [58] and his team produced from shallot peel agricultural waste had a specific surface area of 1182.3 m^2g^{-1}. The outstanding electrochemical performance of the supercapacitor cell system was shown by a specific capacitance of 170 Fg^{-1} at a current density of 1.0 Ag^{-1} using a two-electrode design in 1 M H_2SO_4 aqueous electrolyte. The maximum specific energy was found to be 16.67 Wh kg^{-1} and the maximum specific power was found to be 86.40 Wkg^{-1}. Diab [59] and his team synthesized CNs from potato feel and then co-doped them with sulfur and phosphorus for the effective development of electrodes with a high specific area. The constructed SC properties are as follows: After 5000 cycles, the electrode has a high specific capacitance of 323 Fg^{-1} at 1 Ag^{-1}, an acceptable rate capability, and good cycling stability. The developed symmetric supercapacitor device has an increased extended cycle life and a wide operational potential window of 1.6 V, achieving a maximum energy density of 45.5 Wh kg^{-1} at a power density of 800 W kg^{-1} (94.3 retention after 10,000 consecutive cycles). Yubing [60] and team synthesized CNs for the successful development of SC by making use of bio waste, i.e., flaxseed residue from the edible oil industry. The proposed material has high specific surfaces that can reach 3230 m^2g^{-1}, and large micropores account for more than 70.1% of the volume of the micropore. The resulting material has a maximum specific capacitance of 369 and 398 Fg^{-1} in the KOH and H_2SO_4 electrolytes, respectively. And its cyclic performance was great. Even with a high current density of 20 Ag^{-1}, more than 92.7% of the initial capacitance is retained intact, and after 10,000 cycles in a KOH electrolyte, the capacitance retention is greater than 98.1%. At a power density of 468.8 W kg^{-1} and a high energy density of 43.5 Wh kg^{-1} in an ionic liquid electrolyte called $EMIMBF_4$, the supercapacitor device energy density reaches 61.2 Wh kg. As can be seen in Fig. 5a–c, the typical SEM images of the pyrolysis carbon PC–700 display a composite morphology of carbon nanosphere and disordered stacked amorphous carbon.

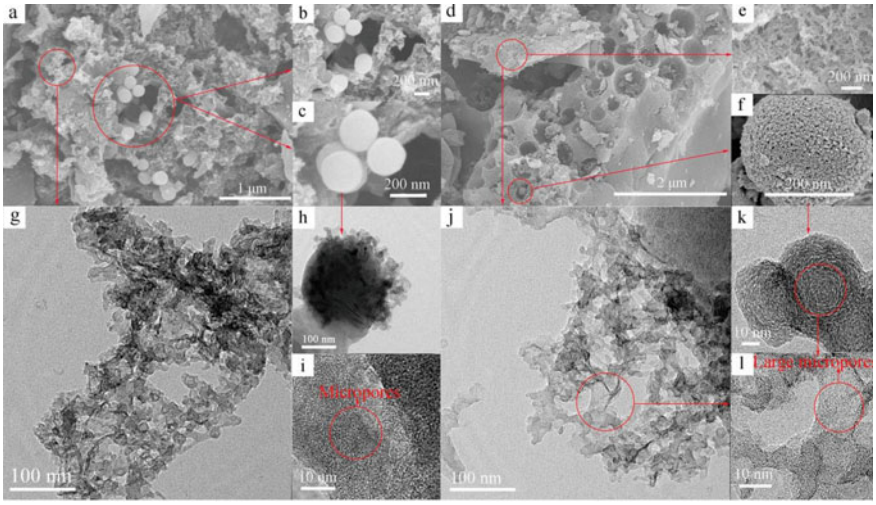

Fig. 5 Typical SEM images of the pyrolysis carbon PC-700 **a~c** and sample $LMiPC_2$ **d~f**, and TEM images of PC-700 **g~i** and $LMiPC_2$ **j~l**. Adapted with permission from ref [60]

5.3 Biomass-Derived Carbon Nanosheets

The porous activated carbon nanosheet was synthesized by Erman et al. [61] from the biomass of Syzygium oleana leaves. The two-electrode system demonstrates an increase in specific capacitance from 114 to 188 Fg^{-1}, leading to high energy and power densities of 26 Wh kg^{-1} and 96 W kg. However, ACS700 is thought to be more stable at various scan speeds, including 1, 2, 5, and 10 mV s^{-1}. Arthi [62] and team developed electrode, novel few-layer graphene-like microporous carbon nanosheets obtained from a ginger root. According to electrochemical tests, the carbon electrode made from ginger root has a very high specific capacitance of 390 Fg^{-1} at 1 Ag^{-1} of current density. Additionally, the carbon electrode made from ginger has a capacitance retention rate of 93.3% for 3500 charge/discharge cycles. This method suggests significant potential for achieving large scale, low cost, easy, and sustainable manufacturing of carbon compounds generated from renewable biomass for effective energy storage applications in the future. By using a tube furnace (CVD) and an Ar inert environment at 800 C, Thirumal et al. [63] reported tamarind shell pyrolysis into extremely microporous three-dimensional (3D) carbon nanosheets. The developed device shows good electrochemical performance, the specific capacitance observed was 245.07 F/g at 1A/g when compared to pure ACNSs, which have an R_{ct} value of 5.03, the electrochemical impedance spectroscopy (EIS) was conducted using K-ACNSs, which have a low Rct value of 0.65. Specifically, the galvanostatic charge–discharge test results for the materials ACNSs and KCNSs were 77 and 245.03 F/g in relation to 1 A/g current density, respectively. Figure 6

showed SEM images to conclude that the surface morphology of pure bio-activated carbon nanosheets (ACNSs).

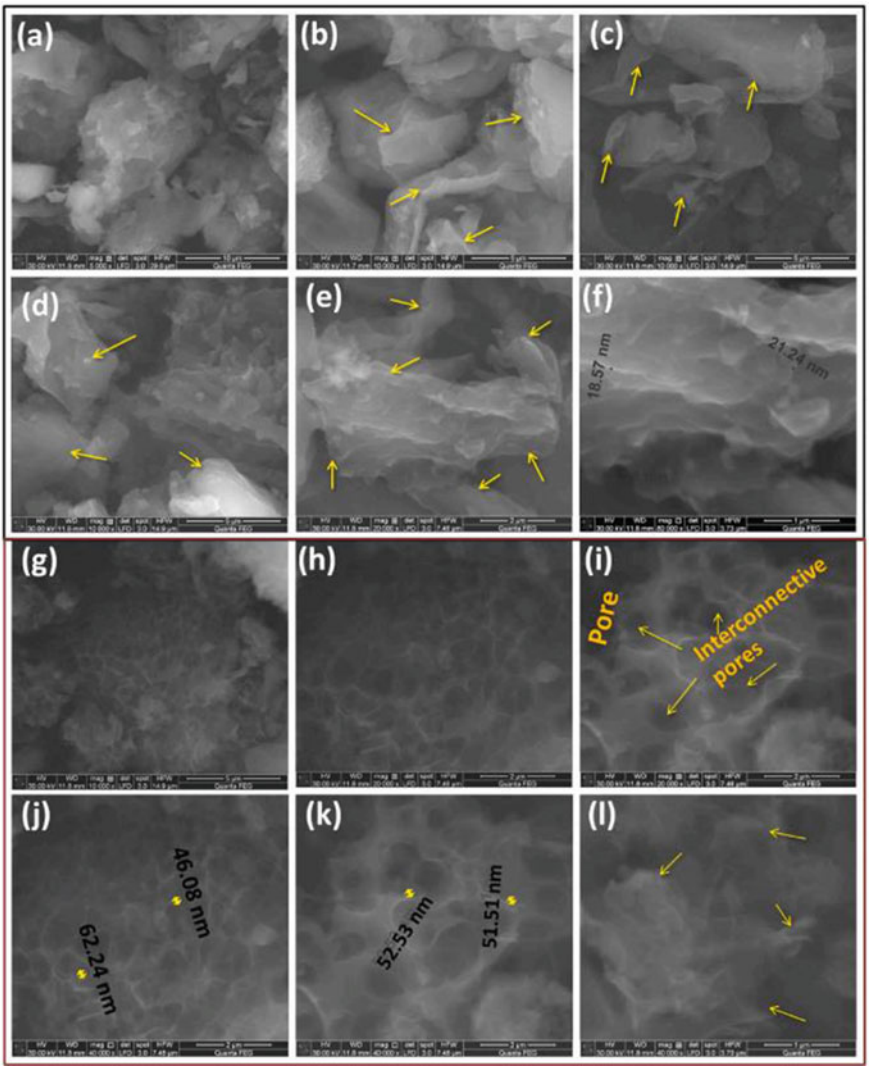

Fig. 6 SEM images of TFSs after pyrolysis—CVD pure ACNSs **a, b, c, d, e, and f** and KOH treated TFSs after pyrolysis KACNSs **g, h, i, j, k, and l** both samples at different magnification. Adapted with permission from ref [63]

5.4 Biomass-Derived Carbon Dots

Since their discovery, carbon dots (CDs) have drawn interest for a variety of uses, including bioimaging, photovoltaics, optical sensing, and drug delivery. This is due to their appealing qualities, which include chemical inertness, tunable photoluminescence, nontoxicity, and biocompatibility [64, 65] Recently published studies describe the development of CD/graphene composites with improved capacitance. For instance, securing CDs to RGO resulted in a composite specific capacitance of 211.9 Fg^{1} at 0.5 Ag^{1}, which was 74.3 percent greater than that of RGO (121.6 Fg) [66]. Similarly to this, Zhao et al. [67] produced a 3D CDs/GO composite with outstanding specific capacitance (308 Fg^{-1} at 0.5 Ag^{-1}) and cycle life. 264 Fg^{-1} of specific capacitance was recently achieved using RGO hydrogel/CDs, which was stable after 5000 cycles [68]. Van and his team recently developed biomass-derived CDs from cauliflower leaf waste and composed with graphene oxide. With varying GO to CDs mass ratios, the electrodes' electrochemical performance was examined. High specific capacitance was shown by the RGO/CD composite with a 2:1 mass ratio (RC-21), with maximal discharge capacitances of 278 and 227 Fg^{-1} at 0.2 $Ag^{-}1$ and 2 mV s^{-1}, respectively. As the current density grew from 0.2 to 100 Ag^{-1} and from 2 to 1000 mV s-1, respectively, it also showed outstanding capacitance retention, rising from 60 to 63% [69]. The use of polymer-carbon dot composite in energy storage devices has gained a special interest in recent years from energy researchers. As high-performance SCs, Ghasem [76] and his associates introduced a mix of polyaniline, polypyrrole, graphene, and CDs produced from biomass. Carrot was used to create CDs. The created composite showed that 396 Fg^{-1} is the highest achievable specific capacitance. Figure 7 displays the results of research using TEM and SEM to examine the morphologies of graphene as a precursor for the creation of polymer nanocomposites and carbon dots (CDs) in their as-prepared state.

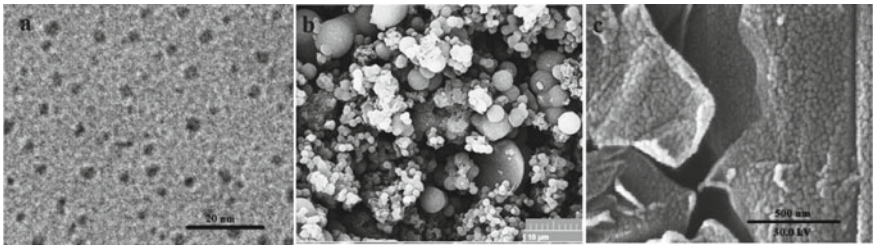

Fig. 7 TEM image of CDs **a**, SEM image of CDs **b** and graphene. Adapted with permission from ref [70]

5.5 *Biomass-Derived Carbon Nanoflowers*

CNF have 2D nanostructures and they significantly increase the high conductivity of electrode material. Cellulose is the main source of porous carbon nanofiber. Erman et al. prepared an electrode by using lemongrass as a biomass precursor which resulted in specific energy of 35.6 $Whkg^{-1}$ and power density of 128.3 Wkg^{-1}, and electrochemical testing shows the low potential of 0–1 C with a scan rate of $1mVS^{-1}$ in the presence of electrolyte H_2SO_4 [71].

6 Novel Nanoelectrode Materials in 0-, 1-, 2-, and 3-Dimensional Materials from Biomass-Derived Carbons Including an Overview of the Design

As electrode materials for SC, a variety of materials including porous materials, metal oxides, and conducting polymers were studied. High surface area and the proper pore size of the electrode material for a particular electrolyte are two factors that define SC performance. Electrochemical storage systems must have a large surface area in order to store energy on their surface. Carbon materials are becoming more popular as perspective electrode materials because they are accessible in a number of shapes and dimensions, including 0D, 1D, 2D, and 3D. Additionally, the electrodes made from biomass-derived activated carbon have excellent qualities like low cost, high surface area, customizable pore distribution, high thermal stability, high electrical conductivity, excellent corrosion resistance, and reasonable compatibility to create composites with a variety of different materials (Fig. 8).

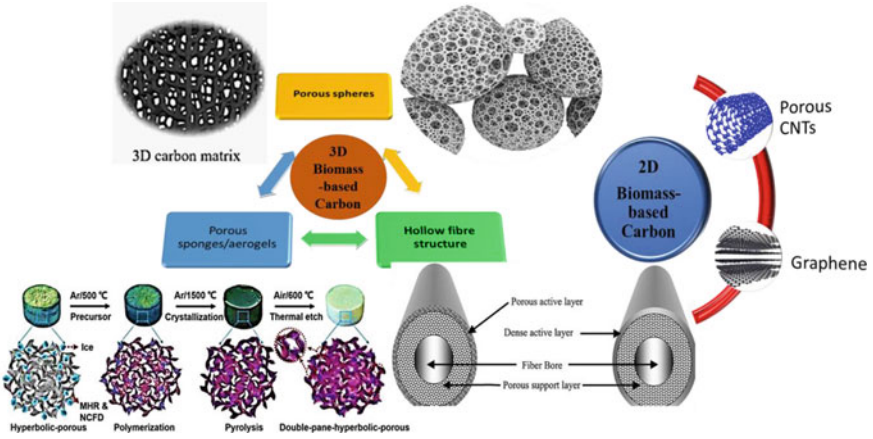

Fig. 8 3D and 2D images of biomass-derived carbon materials used for SCs application

The resultant biomass-derived carbons typically preserve the diversity of their structures and compositions following pyrolysis since biomasses have their own distinct microstructures and compositions. The electrochemical performance of carbons obtained from biomass is significantly influenced by their various morphologies, compositions, and structural types, such as hard, soft, and hybrid carbons, N-doped carbons, and other atom-doped carbons. Around the world, researchers are currently examining the electrochemical performance of 0D, 1D, 2D, and 3D carbon composites derived from biomass precursors. These materials have numerous applications based on the orientation [72].

7 Comparison of Performance of the Various Bio Waste-Based Supercapacitors

Biowaste materials	Surface area (m^2/g)	Electrode	Electrolyte (M)	Specific capacitance (F/g)	Energy density (Wh/Kg)	Power density (kW/Kg)	No. of cycles	Refs.
Rice husk	3333	Ni foam	KOH (6 M)	400	8.06	12.85	10,000	[73]
Chestnut shell	691.8	Ni foam	KOH (6 M)	402.8	26.6	0.44	20,000	[74]
Terminalia Catappa shell	1350	TCFSMC	PHF	200	120	43	90,000	[75]
Jack fruit	511.4	ITO	KOH (0.5 M)	292	40	1.48	10,000	[76]
Watermelon seeds	1920	Carbon electrode	$NaClO_4$	120	79	22.5	150,000	[77]
Coffee grounds	3549	Ni foam	KOH (6 M)	440	101	0.9	10,000	[78]
Olive seed	1700	Graphitic discs	1 M H_2SO_4, 1 M Na_2SO_4	224/193	3–5	20–30	12,500	[79]
Neem leaves	1230	Glassy carbon	H_2SO_4 (1 M)	400	55	10	–	[80]
Albizia flowers	2757	Ni foam	KOH (6 M)	406	26.3	0.429	10,000	[81]
Bamboo shoot	3300	Ni foam	KOH (6 M)	209	12.6	0.299	10,000	[82]
Human hair	1306	Aluminum foil	$LiPF_6$ (1 M)	340	29	2.2	20,000	[83, 84]
Coconut fibers	2898	Stainless steel coin cell	KOH (6 M)	142	53	8.2	10,000	[85]
Silkworm	2258	Carbon Cloth	Na_2SO_4 (1 M)	41.71	23.17	0.5	10,000	[84]
Mushroom	935.8	–	Na_2SO_4 (1 M)	253	35.9	0.36	10,000	[86]
Bean sprout	1114	Ni foam	KOH (6 M)	421	5.44	0.3	10,000	[87]
Sunflower stalk	1505	Ni foam	KOH (6 M)	365	35.7	0.98	15,000	[88]
Aloe vera	1890	Stainless steel mesh	KOH (6 M)	312	13.9	0.025	10,000	[29]

(continued)

(continued)

Biowaste materials	Surface area (m^2/g)	Electrode	Electrolyte (M)	Specific capacitance (F/g)	Energy density (Wh/Kg)	Power density (kW/Kg)	No. of cycles	Refs.
Cherry flower	2500	Carbon cloth	–	334	–	–	38,000	[89]
Wolfberry fruit	1423	Ni foam	KOH (6 M)	365	23.2	0.225	10,000	[90]
Sugarcane bagasse	1993	Graphite sheet	GPE (PVdF-HFP/EMITf/NaTf)	193	31–32	55	10,000	[91]

8 Function of Biomass-Derived Carbon Electrodes in Energy Storage Application

Energy has been the driving force behind national progress, and as a result, humankind's energy requirements have increased, particularly for transportation, agricultural, industrial, and construction operations. Oil-derived fuel is the primary source of energy for vehicles, whereas electricity, which is mostly sourced from fossil fuels, nuclear power, and/or renewable energy sources like solar and hydropower, is the primary source of energy for buildings. Fossil fuels and electric energy are combined to power industrial and agricultural processes. It is critical to employ better monitoring and control systems and produce more energy from renewable sources in order to promote the sustainability of energy production and efficient energy use. This prompts the need for a life cycle analysis of energy processes to help with the choices in the energy sector and the development of more environmentally friendly energy systems as well as creating better, more intelligent electric power grids, where storage energy technologies are crucial (Fig. 9).

Modern electric devices are in high demand as a result of population growth and rapid economic growth. Energy storage systems must be continuously improved to achieve the highest conversion efficiency at the lowest cost possible, as well as faster charging and longer lifetimes. Enhancing the utilization of biomass for more effective electricity production (through direct carbon fuel cells) and bio-based carbon materials for energy storage applications could be a solution to these problems. Recent research claims that carbon compounds made from bio-based sources have qualities that are comparable to or even superior to those of their fossil counterparts.

Due to their exceptional conductivity, adaptable porous structure, and surface area, carbon-based materials have received a lot of interest as supercapacitor electrodes. However, due to their abundance, affordability, and environmental friendliness, carbon nanomaterials, and activated carbon produced from biomass are particularly appealing as electrodes when compared to activated carbons that are prepared conventionally. Mi et al. [98] used a hydrothermal process, The coconut shells are carbonized, followed by pyrolysis and steam activation, to create high porosity and pore volume with adjustable micro/mesopores. The activated carbon samples had an

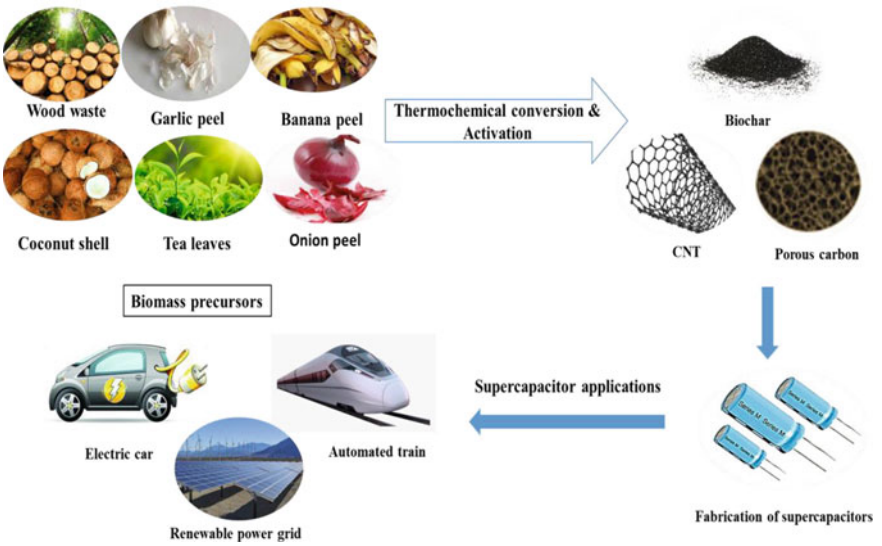

Fig. 9 Application of biomass-based electrodes in energy storage

energy density of 38.5 Wh kg^{-1} and a specific capacitance of 228 Fg^{-1} at 5 mV^{-1} with barely any voltage drop.

Zhang and his coworkers [99] showed how easy it is to chemically activate garlic skin to produce 3D-hierarchical porous carbon. The as-prepared carbon from garlic peels has a huge surface area of 2818 m^2g^{-1}, which results in the formation of hierarchically porous structures, primarily macro-, meso- (2–4 nm), and micro- (0.6–1 nm) porous frameworks. At current densities of 0.5 and 50 Ag^{-1}, material-specific capacitances of 427 and 315 Fg^{-1}, respectively, were recorded. In a similar study, Kishore et al. used coconut kernel pulp to generate activated carbon with a surface area of 1200 m^2g^{-1} and a Csp of 173 Fg^{-1} at 0.25 Ag^{-1} in 1 M H_2SO_4 electrolyte [100].

Willow catkins were used to make nitrogen self-doped porous carbon microtubes. Xie et al. [101] demonstrated the straightforward carbonization and activation processes. A high surface area of 1775.7 m2 g^{-1} and a small pore volume of 0.8516 cm^3 g^{-1} were both characteristics of the carbon microtubes that were produced. At a current density of 1 Ag^{-1}, they also demonstrated a specific capacitance of 292 Fg^{-1}.

Tea leaves, which are a great source of nitrogen and phenolic compounds, have been utilized as a precursor material to create activated carbon utilizing pyrolysis and KOH activators. 911.92 m^2 g^{-1} of surface area and 0.512 cm^3g^{-1} of pore volume were present in the final carbon produced at 1200 °C, respectively. The specific capacity of symmetric supercapacitors constructed from activated carbon derived from tea leaves was 167 Fg^{-1} at a current density of 1 Ag^{-1} [102]. By carbonizing and activating with KOH, Xu et al. [103] produced dual-doped porous carbon materials containing

sulfur and nitrogen using broad bean shells. A specific capacitance of 202 Fg^{-1} was seen in porous carbon at a current density of 0.1 Ag^{-1}.

By activating sugar cane bagasse and urea with $CaCl_2$ in a single step, N-doped carbons with various nitrogen contents, medium-range specific surface areas, and interconnected porosities were successfully created in this literature. The quasirectangular forms of the CV curves in Fig. 10a point to the optimal capacitive behavior of a two-electrode capacitor in a 6.0 M KOH electrolyte. The charge/discharge waveforms of the S_{122} electrode at various charge/discharge current densities are shown in Fig. 10b. The specific capacitance of the S_{122} electrode was reduced from 300 to 132 Fg^{-1} when the current density was raised from 0.25 to 5 Ag^{-1}. The IR drop rose correspondingly from 0.3 to 3.2 mV. The Ragone plots for the supercapacitor sample S122 are shown in Fig. 10c. The S122 capacitor has an energy density of 10.41 and 4.58 Wh kg^{-1}, respectively, with specific power densities of 250.0 and 4892.5 W $kg^{-}1$. The Nyquist plots (Fig. 10d) recorded from 0.1 to 100 000 Hz at open circuit potential in 6 M KOH, which are analyzed by the software of Z View on the basis of the electrical equivalent circuit, as shown in the inset modeled equivalent circuit of EIS, can be used to confirm electrochemical impedance spectroscopy (EIS) analysis. The S_{122} samples, as seen in Fig. 10d, have a low interfacial charge-transfer resistance of 1.45 and a low ionic resistance of 2.74.

This literature describes the use of corncob-derived activated porous carbon for supercapacitors in aqueous and non-aqueous electrolytes. The activated corncob was designated as CC-AA-600 after being activated at 600 °C. The activated corncob carbon has an estimated BET surface area of 800 $m^2\ g^{-1}$ and is meso and microporous in nature. SEM and HR-TEM analyses are used to further validate the carbon's porous nature. Electrochemical tests in aqueous solutions show a very high specific capacitance of 390 Fg^{-1} at 0.5 Ag^{-1} current density. To evaluate the electrochemical performance of activated corncob electrodes, three different ionic liquids are employed; among them, the EMIMBF4 exhibits strong capacitive behavior and a wide potential window, which results in a high energy density of 25 Wh kg^{-1} and a high power density of 174W kg^{-1}. A red LED could be powered for more than 4 min by the supercapacitor made using ionic liquid after a 10-s charge. In a symmetric cell with a potential range of 0 to 1.2 V and a 1 M H_2SO_4 electrolyte, the CD profile of the CC-AA-600 electrodes is depicted in Fig. 11a. The computed capacitance is 120, 104, and 98 Fg^{-1}, respectively, for current densities of 2, 3, and 4 Ag^{-1}. A maximum specific capacitance of 164 Fg^{-1} was found at 1 Ag^{-1}. (Fig. 11b). Charge–discharge cycling at a current density of 4 Ag^{-1} was done for 10,000 cycles to examine the stability of the electrodes in the two-electrode systems (Fig. 11c). After 10,000 charge–discharge cycles, 85% of the initial capacitance was still retained. Electrochemical impedance spectroscopic (EIS) analysis was performed at the frequency range of 100 kHz to 10 MHz with an amplitude of 10 mV in order to understand the various resistances, such as internal resistance, charge-transfer resistance, and solution resistance (Fig. 11d).

The discovered chestnut shell-derived carbons display significant heteroatom content (3.79 at.% N, 13.35 at.% O, and 0.52 at.% S), a high specific area (691.8 $m^2\ g^{-1}$), a great number of interconnected micropores/mesopores, a suitable level

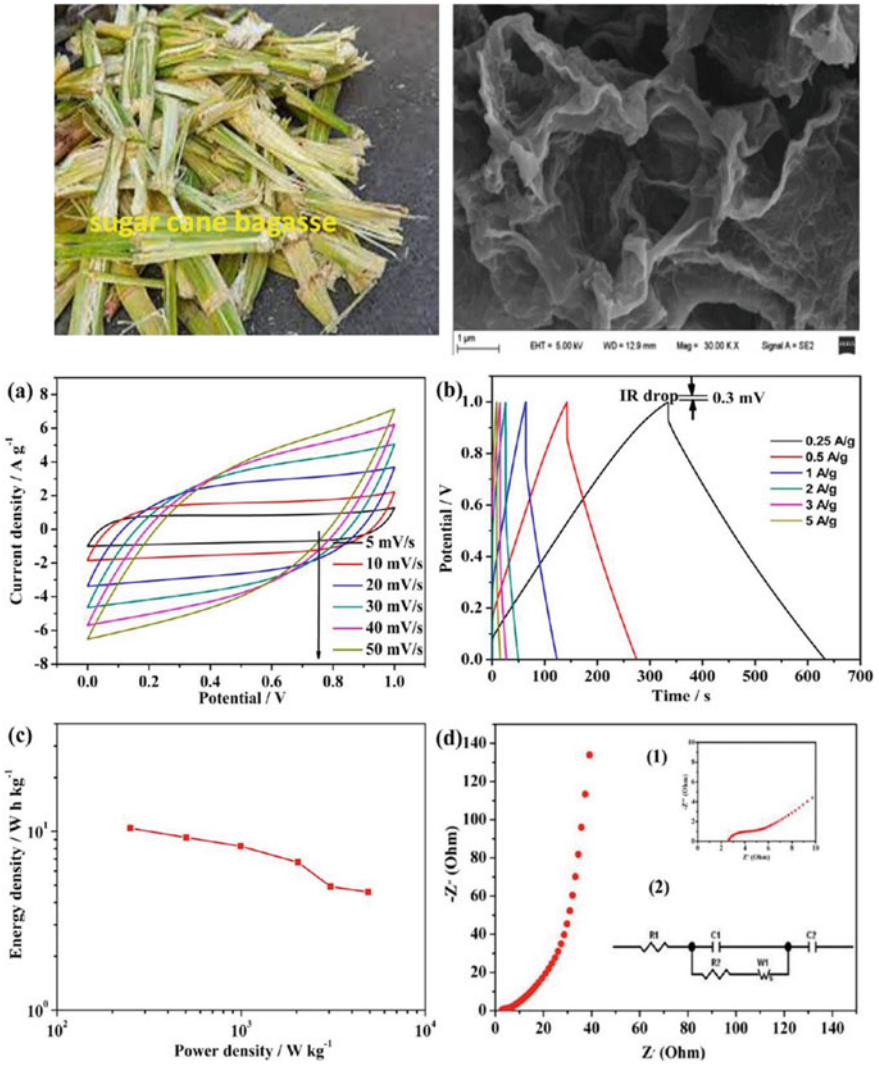

Fig. 10 Two electrodes were used to measure the device's electrochemical capabilities. **a** Three-dimensional nitrogen-rich porous carbon sample S_{122} CV curves at various scan rates. **b** In a 6 M KOH aqueous solution, the S_{122} electrode was done. **c** Ragone plot. **d** Spectra of electrochemical impedance (inset: magnified region). Adapted with permission from ref [92]

of graphitization, and all of these characteristics. In KOH electrolyte, the produced carbon electrode displays remarkable rate capability (45.3% capacitance retention at 100 Ag^{-1}) and a high specific capacitance (402.8 Fg^{-1} at 0.5 Ag^{-1}) as a result of these superior properties. A better energy density of 26.6Wh kg^{-1} is delivered by the manufactured symmetric supercapacitor at a power density of 445.5 W kg^{-1}. Additionally,

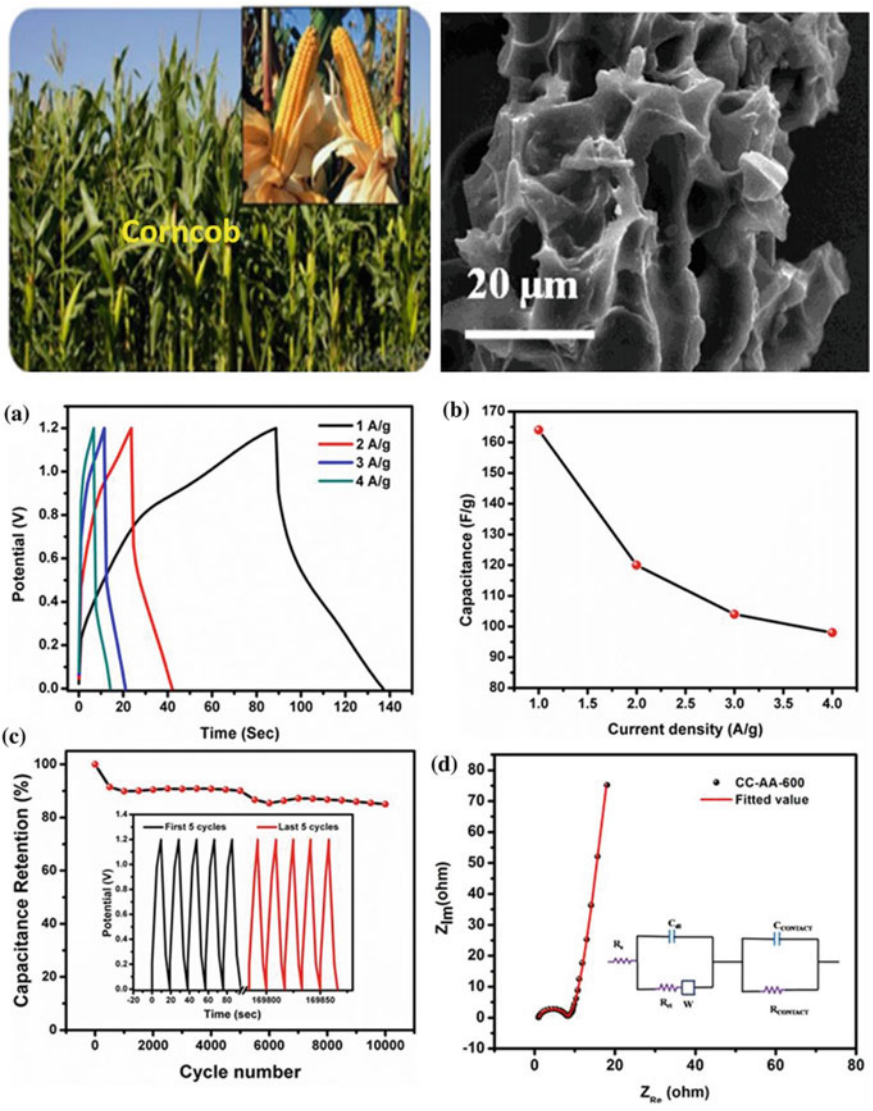

Fig. 11 **a** The CD profile of the CC-AA-600 electrodes in a symmetric two-electrode cell **b** The specific capacitance of the CC-AA-600 electrodes in a symmetric two-electrode cell **c** The cyclability of the CC-AA-600 electrodes in a symmetric two-electrode cell **d** The EIS spectrum of the CC-AA-600 electrodes in a symmetric two-elect (inset). Adapted with permission from ref [93]

with 96.6% cycle stability, the supercapacitor device exhibits good performance. retention of capacitance after 20,000 cycles. These findings show that the carbonaceous materials as prepared have excellent promise for low-cost high-performance supercapacitors.

Broad beans are widely grown all over the world because they are high in vitamins and amino acids. Broad bean shells, a significant portion of which are byproducts from the sintering, are abandoned and damage the environment. Here, we describe the production of dual-doped porous carbon materials for energy storage devices' electrode materials by carbonizing broad bean shells via a chemical activation. The as-prepared porous carbon material exhibits a specific capacitance of up to 202 Fg^{-1} and better cycle performance for electric double-layer capacitors at a current density of 0.5 Ag^{-1}. Even at scan rates as high as 30 mV s^{-1}, the roughly rectangular form of the CV curve can still be seen (Fig. 12a), proving that ACSB is capable of supporting rapid ion transport. The ACSB electrode's galvanostatic charge/discharge curves exhibit almost isosceles triangle forms at various current densities (Fig. 13b), which illustrates the perfect charge and discharge characteristics for EDLCs. The specific capacitance is still up to 129 Fg^{-1} even at a current density of 10 Ag^{-1}. Furthermore, as illustrated in Fig. 13c, ACSB has a greater rate performance. A further indication of the ACSB electrode's strong cycling stability is the specific capacitance retention, which is close to 90% after 3000 cycles (Fig. 13d).

Choosing an appropriate biomass source and processing technique is crucial to producing high-quality carbon compounds that are more effective. The process of turning biomasses into carbon compounds is expensive because of the thermal or chemical treatments that are employed. For a variety of energy-intensive biomass conversion processes, using high-temperature carbonization/pyrolysis technologies is still frequently necessary. As a result, larger advancements would be made for the carbon compounds derived from biomass to be established as useful goods for society if the study focused on the development of an energy-efficient technique.

Improved electrolyte wettability, higher charge storage, and moderate electrode strength can be achieved using techniques like the synthesis of carbonaceous materials with micro- and mesoporous nature. Additionally, the production of nanofibrous carbonaceous materials from lignocellulosic fibers may aid in the advancement of flexible and wearable electronics, an important technical area of interest. The systematic understanding and relationship between the carbon structure and electrochemical performance would be aided by the use of modern in-situ analytical instruments, which would also offer real-time information on the charge and ion storage capacities. Enhanced electrolyte wettability, improved charge storage, and moderate electrode strength can all be attained by employing approaches such as producing carbonaceous materials with micro- and mesoporous nature. Additionally, the creation of nanofibrous carbonaceous materials from lignocellulosic fibers may aid in the advancement of flexible and wearable electronics, an important technical area of interest.

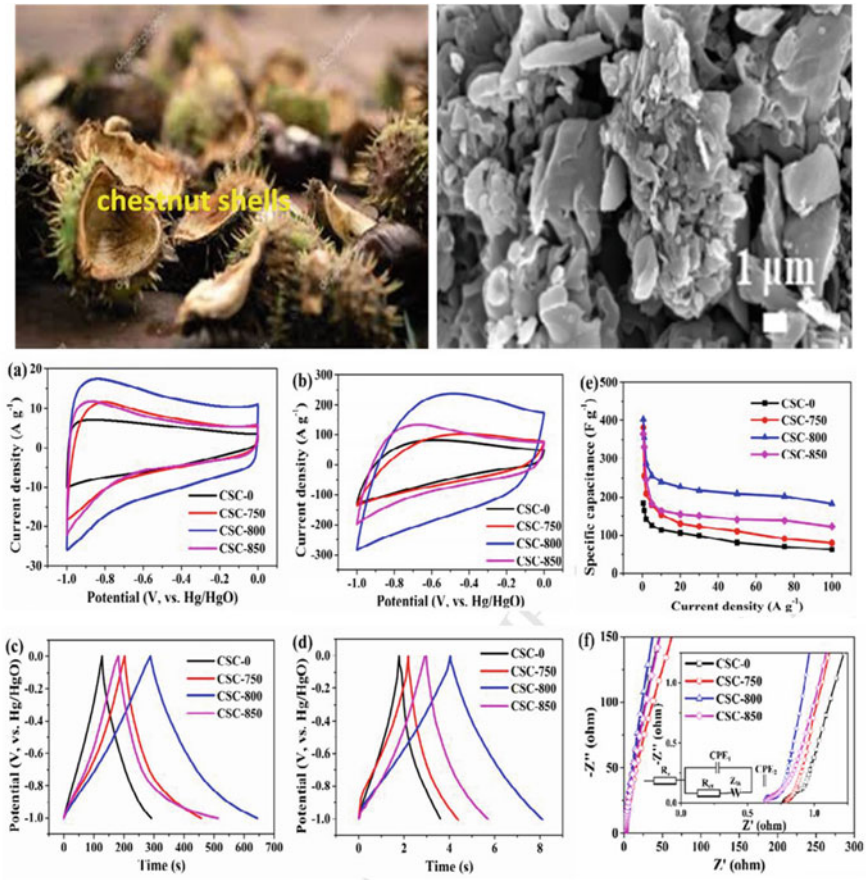

Fig. 12 All CSC samples performed electrochemically in a three-electrode experiment with a 6.0 M KOH aqueous electrolyte. All CSC electrodes cyclic voltammograms at scan rates of **a** 50 mV s^{-1} and **b** 1000 mV s^{-1}. Galvanostatic charge–discharge curves at **c** 1.0 Ag^{-1} and **d** 50.0 Ag^{-1} current densities. **e** All CSC electrodes' specific capacitance at various current densities. **f** Equivalent circuit model and Nyquist graphs. Adapted with permission from ref [74]

9 The Recent Development and Challenges of Biowaste-Based Electrode Materials for Storage Applications

Biomass materials have a wide range of morphological dimensions. Active carbon generated from biomass can be perfectly preserved or molded into novel frameworks such as spherical, tubular, honeycomb, or graphene-like carbon. Biomass materials typically exhibit fascinating structures, such as hierarchical organization, periodic pattern, or specific nano architectures, which equip them with unique capabilities

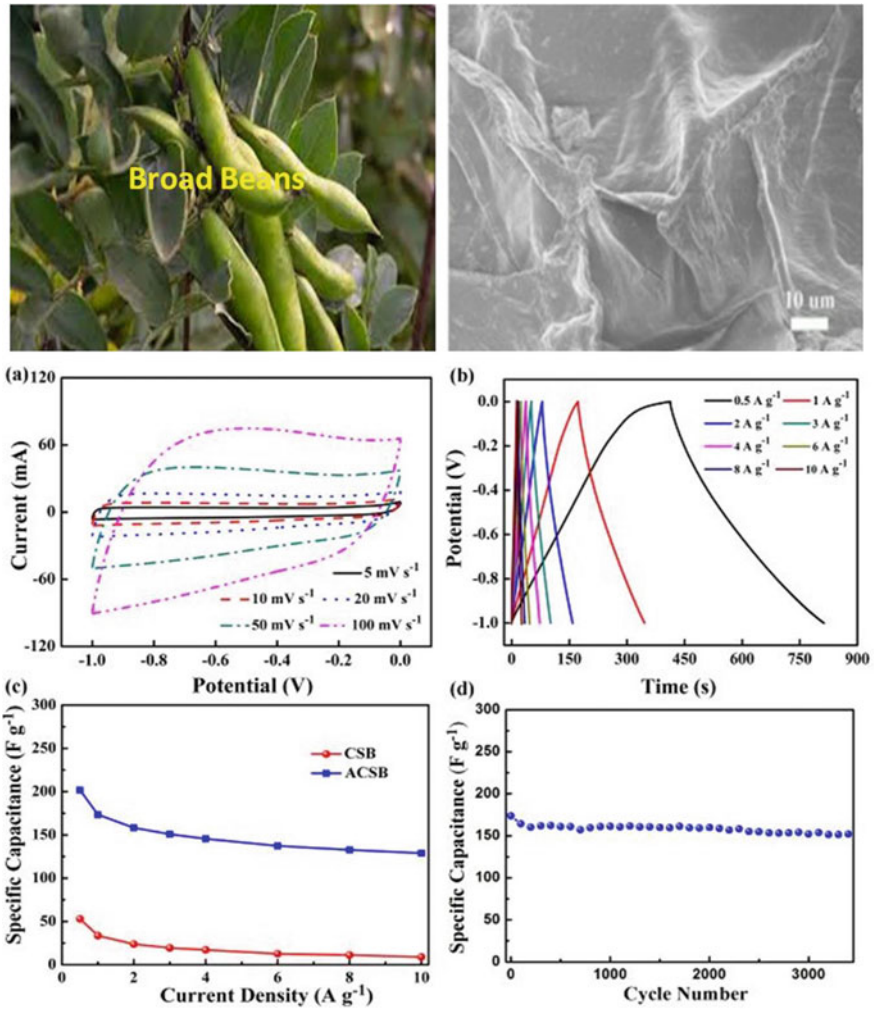

Fig. 13 **a** The galvanostatic charge–discharge curves of the ACSB electrode in 6 M KOH aqueous solution at different scan rates, **b** The 20 specific capacitances determined from the discharge curves under different scan rates, **c**, and **d** cyclic stability of the ACSB-based EDLCs at a current density of 1 Ag^{-1}. Adapted with permission from ref [94]

such as anti-reflection, super-hydrophobicity, structural coloring, and biological self-assembly [95]. The biomass-derived carbon-based supercapacitor electrodes have the distinct benefits of high power density and exceptional cycle performance due to their intrinsic fine structure and the richness of race components in biological tissue [96]. The vast surface area and porous network of the electrode materials used in supercapacitors allow the charge to be stored by electrostatic attraction and facile

ion diffusion in the electrolyte. Presently, the work on the fabrication of supercapacitors derived from biomass is mainly focused on the optimization of different experimental parameters such as the amount of activation agent, synthesis temperature [97], and the type of activation agent [98]. The N, O, S, and P co-doped porous carbon material from the protein-rich soyabean is developed as a negative electrode for asymmetric supercapacitor applications. The material synthesis involves low-temperature hydrothermal carbonization and KOH activation of soya bean precursor material. The prepared material exhibited outstanding specific capacitance in acidic and alkaline aqueous solutions. Particularly, the produced porous carbon demonstrated extremely high specific capacitances of 685.1 F/g at 0.5 A/g in 2 M KOH and 439.5 F/g at 1 A/g in 1 M H_2SO_4 [110, 111]. The report from Zhimin Zou et al. demonstrated highly mesoporous carbon material derived from kapok fiber, which can be used for organic electrolyte-based electrochemical storage with high power density. The material is a nano-carbon flake having a BET surface area of 3010 m^2/g with an ultra-high mesoporous volumetric ratio of 97.6%. The prepared carbon flakes exhibited excellent energy density of about 24 Wh kg^{-1} at high power density 24, 029 W kg^{-1}. This electrode material is used as symmetric supercapacitors in the organic electrolyte, which was one of the highest values recorded so far on biomass-derived porous carbon electrodes [99]. The porous carbon electrode derived from tobacco rods exhibited high capacitance with 286.6 Fg^{-1} at 0.5A/g and at 30 A/g also showed excellent capacitive performance of 212.72 Fg^{-1}. Furthermore, the capacitance retention of about 96% after 10,000 cycles was observed. In addition, the supercapacitor material provided an energy density of 31.3 Wh kg^{-1} at 0.5 Ag^{-1} and a power density of 11.8 kW kg^{-1} at 15 Ag^{-1} [5]. There are some reports in which the carbon nanomaterials derived from biomass through pyrolysis without any chemical activation gave supercapacitor electrode material with excellent performance. Neem leaves, for instance, have a specific capacitance of 400 F/g and an energy density of 55 Wh/Kg. Similarly, Sargassum wightii has a specific capacitance of 354 F/g and an energy density of 44.25 Wh/Kg, and Turbinaria conoides have a specific capacitance of 416 F/g with an energy density of 52 Wh/Kg [80, 100–102].

Biomass-based lignocellulosic materials are used to synthesize flexible supercapacitors. High-performance flexible supercapacitors derived from bamboo are used for temperature-dependent energy applications. The carbonized bamboo fibers showed a specific capacitance of 510 F/g at 0.4 A/g. The energy and power density of the material is 7.9 kW/Kg and 54 Wh/Kg, respectively. The material showed excellent flexibility without any reduction in the charge storage capacity during the bending and twisting of the electrode. The performance of the supercapacitor showed an enhancement of about 65% at high temperatures [103]. Cellulose materials have been found to be an excellent choice for synthesizing the flexible supercapacitor due to their high flexibility, low weight, and less expense. Han et al. developed a flexible supercapacitor from the composite made from the wood powder extracted from nanocellulose crystals. They combined electrospinning technology and in-situ polymerization to synthesize the composite. Due to the extensive intermolecular crosslinking of the material, it exhibited good thermal stability and mechanical strength. After 2000 cycles, nanofibrous electrodes showed a specific capacitance of 164.6 F/g and

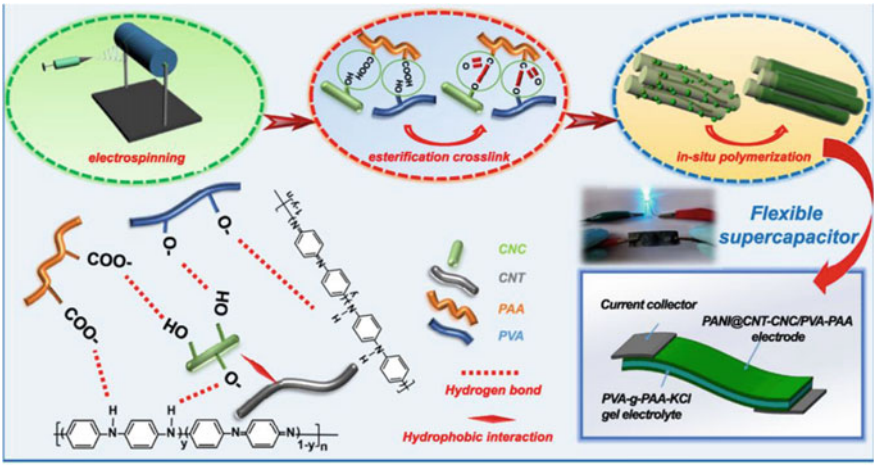

Fig. 14 The figure represents the nano-cellulose membrane fabrication process with a core–shell structure. Adapted with permission from ref [104]

retained about 91% of their initial capacitance. The symmetrical solid-state supercapacitor constructed from nanofibrous electrodes has a good capacitance of 155.5 F/g and remarkable capacitance retention of 92, 90, and 89% after 2000 cycles under flat, bending, and twisting deformations, respectively [104] (Fig. 14).

Photo-supercapacitors that combine solar cells with supercapacitors can transform and store solar energy at the same time. It helps to minimize the usage of fossil fuels by using solar energy as an alternative [105]. The integrated devices with the dual capability of energy conversion and storage are gaining popularity due to stored energy that can be used to deliver continuous energy independent of solar uncertainties [106]**.** Keppetipola et al developed coconut shell-derived carbonized carbon for photo-supercapacitor application. The prepared carbon particle exhibited a surface area of $1998 m^2 g^{-1}$ and $1.09\ cm^3 g^{-1}$. When the ionic liquid (1-methyl-1-propyl-pyrrolidinium bis(fluorosulfonyl)imide) is acting as an electrolyte, the carbon particle exhibited outstanding storage properties over a wide potential range (up to 3.5 V) [107]. The specific energy of the combined system was 92.1 Wh/kg, adding to the power density of 2046.9 W/kg. It was feasible to link a carbon supercapacitor and a carbon-perovskite solar cell directly. At large areal discharge currents of 18 and 30 mA cm^{-2}, the dual-functional device (photo-storage) was able to retain its high overall peak efficiencies of 5.63 and 4.07%. So far, this is the best-documented result for maintaining high efficiencies at high discharge current, demonstrating the promise of a Perovskite solar cell/supercapacitor combination for high power electronic applications [108].

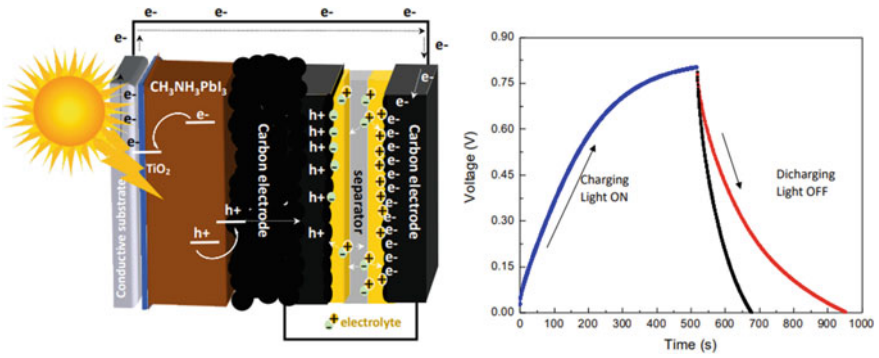

Fig. 15 PSC-based integrated power conversion and storage device operational mechanism. Adapted with permission from ref [106]

Asymmetric supercapacitors (ASCs) made from supercapacitors provide numerous advantages for energy storage applications. For example, the high operational voltage in aqueous-based electrolytes may improve grid storage and zero-power mobility with high energy density with in coming decades. ASCs development with a Faradaic/pseudocapacitive positive electrode and a capacitive negative electrode is a viable technique for improving SC overall performance. These devices often have a high power density and a broad potential window. The very low energy density of ASCs is a significant barrier that requires quick addressing [109]. When ASCs are formed using traditional nanostructured electrode materials, additional issues including high cost, slow manufacturing rate, trouble doping heteroatoms, and creation of toxic byproducts for the environment are also present. By using biomass-derived/green carbon sources with natural hierarchical structures, these issues can be avoided or reduced to some extent. Here in Fig. 15, the power density and energy density obtained from ASCs prepared from different biomass-derived carbon structures are shown (Fig. 16).

CNB/MnO_2@CNB from tofu plant [111], AMC/ZnCO from almond shell [96], EDAC/MnS from eggplant [112], NPC/PC@MnO_2 from loofah sponge, NKGLC/Ni$(OH)_2$-MnO_2-RGO from ginkgo leaves [113], PC/$NiCo_2S_4$@PC from popcorn [114], APC/$NiCo_2O_4$ from walnut shells, HC/MnO_2@HC from hemp stems, PFN/PFNC from pomelo fruit [115], BioHPC/$NiCo_2O_4$-NS from corncob, N-CBC/CBC-N@LDH/p-BC-N/MnO_2@p-BC from bacterial cellulose CCNS/MnO_2@CCNS, PCMT/βNi$(OH)_2$@ACMT from Willow Catkin, FBC/FCBC from Cladophora glomerata [116], Fe_2O_3@BPC/CNT@CoNiLDH from Wheat straw [117], GPCN-SS/MnO_2@GPCN-SS from Salvia splendens [116], and MnSi-C/Ni$(OH)_2$ from Bamboo leaves [118].

Despite the long history of carbon-based electrode development, more work needs to be done before the technology can be commercialized, particularly with regard to rechargeable systems. Numerous excellent studies have been conducted to address the issues they face, but most carbon materials are still lacking sufficient energy

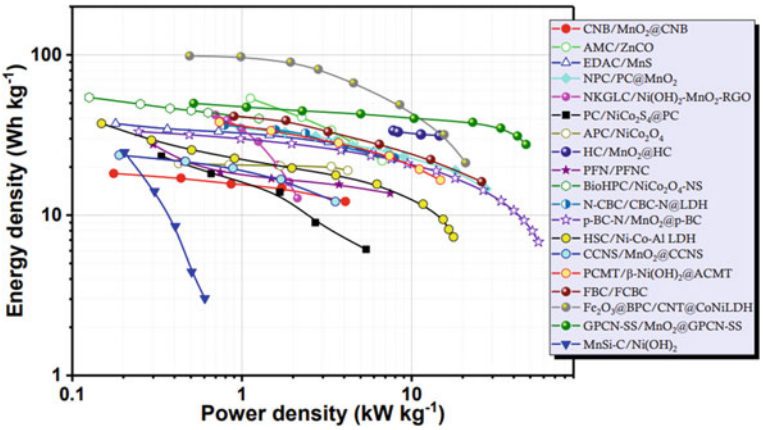

Fig. 16 An analysis of the Ragone plots generated for ASCs developed using BDC materials. Adapted with permission from ref [110]

density to be used commercially. There are still many aspects that need to be further researched and improved. (a) Low yield of carbon: as previously discussed the total carbon content obtained from available biomass varies according to the elemental and chemical composition of the precursor, ranging around 5.5 and 52.1 wt%. It, therefore, generates severe concerns for the carbonaceous materials obtained from the low-carbon content biomass precursor restricting their commercial production remarkably. (b) The relative low value of energy density: despite having relatively high specific capacitances (C_{sp}) of over 400 Fg^{-1}, carbons generated from biomass cannot yet be compared to materials possessing pseudocapacitance, which can have C_{sp} of over 1000 Fg^{-1} [119]. (c) Optimization of morphology and microstructure of carbon: currently, there exists no improved method that can control the effects like graphitization and carbonization of the precursors as the preparation and production of carbons derived from biomass have somewhat always followed an unmanaged process. The result of this ignorance is a randomized dispersion of porosities (micropores, meso, and macro) over the carbonized biomass as well as an irregular arrangement of graphitized structures, which significantly reduces the efficiency of charge and ion transfer.

A path forward is needed for the device system's commercialization despite the effective use of biochar as diverse components for supercapacitors. To actualize the useful applications for biochar, innovative improvements are still required. Supercapacitors are most likely the next generation of useful energy storage devices because of their great gravimetric and volumetric density. One way to improve the life cycle of the device is by making substantial changes in design strategies, which include the synthesis procedure as well as the surface chemistry of the biochar. Furthermore, a few properties/concepts must be taken into account when it comes to commercialization such as (i) high energy density storage devices by increasing the loading of active material (ii) economic factors which include low cost readily available

precursors and synthesis methods. Adopting different energy storage technologies in accordance with technological requirements may be carefully evaluated with such substantial breakthroughs.

Despite the drawbacks that are already existing in the field of energy storage device fabrication from biomass precursors, significant efforts have been made to improve the device's performance. The newly built devices are found to be an excellent replacement for the existing device in the market. Moreover, the device is enhanced by making changes keeping in mind the waste-to-wealth concept.

10 Conclusion and Future Scope

Biochar-based materials for supercapacitors' electrodes showed enhanced capacitance and cycle stability. Electrochemical performance can be enhanced to obtain desired energy and power density by activation (both chemical and physical), which results in a high surface area (Meso, micro, and macro) porous structure. In addition, heteroatoms such as phosphorus, sulfur, and nitrogen can be incorporated into the carbon structure via self-doping or post-biochar synthesis method. These methods improve the storage capacity and lead to higher capacitances. Basically, it is crucial to comprehend the chemical makeup of the wide variety of biomasses that represent forestry, agriculture, urban, sludge, domestic trash, etc., because the elements vary depending on the sort of biomass that is readily available. Understanding the various chemical components found in the various forms of biomass precursors can help determine whether or not they are appropriate for achieving specific objectives.

The use of carbon-based materials to enhance the electrochemical capabilities of energy generation and storage systems has advanced to a critical point. As a result, the researchers are forced to come up with innovative and affordable solutions to the problem of source depletion for the synthesis of these materials. Recent research demonstrates that biomass offers a real ocean to solve this issue with various benefits. Particularly for supercapacitors, dependable changes are required, and carbon-based materials obtained from biomass are essential. After thorough research, it was discovered that biomass can synthesize highly porous carbon compounds with the addition of a permanent, low-cost precursor. The research that has been published demonstrates that the produced biomass-derived materials enhance the electrochemical adhesion of the ions, increasing the specific capacitance of the electrode and improving the cycling ability and stability of the supercapacitor. The selection of biomass, the synthesis process, the preprocessing, and the type of supercapacitor are listed as the key factors in the manufacturing of products produced from biomass. Because the pore size and dispersion greatly differ depending on the precursor's content and the pretreatment procedure, precursor material and pretreatment play a significant role. It is very essential to closely evaluate the inorganics and other contaminants present in the biomass precursor that builds up in the production of biochar-based products. The presence of the contaminants can drastically change the specific capacitance. The charge storage efficiency is hsighly dependent on the

interaction between ionic, organic, and quasisolid-state electrolytes. It is also important to study the combined effect of biochar-based carbon electrode material in different electrolytes. In this review, the details of the control over phase, surface functional groups, and morphology for materials exhibiting both electrostatic and electrochemical charge storage behavior were summarized.

References

1. Muthu Balasubramanian M, Subramani M, Murugan D, Ponnusamy S (2020) Groundnut shell–derived porous carbon-based supercapacitor with high areal mass loading using carbon cloth as current collector. Ionics 26:6297–6308
2. Charoensook K, Huang C-L, Tai H-C, Lanjapalli VVK, Chiang L-M, Hosseini S, Lin Y-T, Li Y-Y (2021) Preparation of porous nitrogen-doped activated carbon derived from rice straw for high-performance supercapacitor application. J Taiwan Inst Chem Eng 120:246–256
3. Khan A, Senthil RA, Pan J, Osman S, Sun Y, Shu X (2020) A new biomass derived rod-like porous carbon from tea-waste as inexpensive and sustainable energy material for advanced supercapacitor application. Electrochim Acta 335:135588
4. Bhat VS, Kanagavalli P, Sriram G, Ramya Prabhu B, John NS, Veerapandian M, Kurkuri M, Hegde G (2020) Low cost, catalyst free, high performance supercapacitors based on porous nano carbon derived from agriculture waste. J Energy Storage 32:101829
5. Zhao Y-Q, Min L, Tao P-Y, Zhang Y-J, Gong X-T, Yang Z, Zhang G-Q, Li H-L (2016) Hierarchically porous and heteroatom doped carbon derived from tobacco rods for supercapacitors. J Power Sources 307:391–400
6. Bhat VS, Krishnan SG, Jayeoye TJ, Rujiralai T, Sirimahachai U, Viswanatha R, Khalid M, Hegde G (2021) Self-activated "green" carbon nanoparticles for symmetric solid-state supercapacitors. J Mater Sci 56:13271–13290
7. Bhat VS, Hegde G, Nasrollahzadeh M (2020) A sustainable technique to solve growing energy demand: porous carbon nanoparticles as electrode materials for high-performance supercapacitors. J Appl Electrochem 50:1243–1255
8. Serrano-Ruiz JC (2020) Biomass: a renewable source of fuels, chemicals and carbon materials. Molecules https://doi.org/10.3390/molecules25215217
9. Wang H, Li Z, Tak JK et al (2013) Supercapacitors based on carbons with tuned porosity derived from paper pulp mill sludge biowaste. Carbon N Y 57:317–328
10. Vijayakumar M, Santhosh R, Adduru J, Rao TN, Karthik M (2018) Activated carbon fibres as high performance supercapacitor electrodes with commercial level mass loading. Carbon N Y 140:465–476
11. Yu KL, Lau BF, Show PL, Ong HC, Ling TC, Chen W-H, Ng EP, Chang J-S (2017) Recent developments on algal biochar production and characterization. Bioresour Technol 246:2–11
12. Ding M, Chen G, Xu W, Jia C, Luo H (2020) Bio-inspired synthesis of nanomaterials and smart structures for electrochemical energy storage and conversion. Nano Mater Sci 2:264–280
13. Zhou X, Chen F, Bai T, Long B, Liao Q, Ren Y, Yang J (2016) Interconnected highly graphitic carbon nanosheets derived from wheat stalk as high performance anode materials for lithium ion batteries. Green Chem 18:2078–2088
14. Luque R, Angel Menéndez J, Arenillas A, Cot J (2012) Microwave-assisted pyrolysis of biomass feedstocks: the way forward? Energy Environ Sci 5:5481–5488
15. Xie Z-L, White RJ, Weber J, Taubert A, Titirici MM (2011) Hierarchical porous carbonaceous materials via ionothermal carbonization of carbohydrates. J Mater Chem 21:7434–7442
16. Deng X, Zhao B, Zhu L, Shao Z (2015) Molten salt synthesis of nitrogen-doped carbon with hierarchical pore structures for use as high-performance electrodes in supercapacitors. Carbon N Y 93:48–58

17. Sedira S, Mendaci B (2020) Hydrothermal synthesis of spherical carbon nanoparticles (CNPs) for supercapacitor electrodes uses. Mater Renew Sustain Energy. https://doi.org/10.1007/s40243-019-0161-0
18. Zahid MU, Pervaiz E, Hussain A, Shahzad MI, Niazi MBK (2018) Synthesis of carbon nanomaterials from different pyrolysis techniques: a review. Mater Res Express 5:052002
19. Dhyani V, Bhaskar T (2018) A comprehensive review on the pyrolysis of lignocellulosic biomass. Renew Energy 129:695–716
20. Koziol K, Boskovic BO, Yahya N (2010) Synthesis of carbon nanostructures by CVD method. Advanced structured materials. Springer, Berlin Heidelberg, Berlin, Heidelberg, pp 23–49
21. Shah KA, Tali BA (2016) Synthesis of carbon nanotubes by catalytic chemical vapour deposition: a review on carbon sources, catalysts and substrates. Mater Sci Semicond Process 41:67–82
22. Sharma R, Sharma AK, Sharma V (2015) Synthesis of carbon nanotubes by arc-discharge and chemical vapor deposition method with analysis of its morphology, dispersion and functionalization characteristics. Cogent Eng 2:1094017
23. Corbella C, Portal S, Zolotukhin DB, Martinez L, Lin L, Kundrapu MN, Keidar M (2019) Pulsed anodic arc discharge for the synthesis of carbon nanomaterials. Plasma Sources Sci Technol 28:045016
24. AlMalki FA, Khashan KS, Jabir MS, Hadi AA, Sulaiman GM, Abdulameer FA, Albukhaty S, Al-Karagoly H, Albaqami J (2022) Eco-friendly synthesis of carbon nanoparticles by laser ablation in water and evaluation of their antibacterial activity. J Nanomater 2022:1–8
25. Li J, Wu Q, Wu J (2016) Synthesis of nanoparticles via solvothermal and hydrothermal methods. Handbook of Nanoparticles. Springer International Publishing, Cham, pp 295–328
26. He X, Li H, Liu Y, Huang H, Kang Z, Lee S-T (2011) Water soluble carbon nanoparticles: hydrothermal synthesis and excellent photoluminescence properties. Colloids Surf B Biointerfaces 87:326–332
27. Wang R, Wang P, Yan X, Lang J, Peng C, Xue Q (2012) Promising porous carbon derived from celtuce leaves with outstanding supercapacitance and CO_2 capture performance. ACS Appl Mater Interfaces 4:5800–5806
28. Ma G, Yang Q, Sun K, Peng H, Ran F, Zhao X, Lei Z (2015) Nitrogen-doped porous carbon derived from biomass waste for high-performance supercapacitor. Bioresour Technol 197:137–142
29. Karnan M, Subramani K, Sudhan N, Ilayaraja N, Sathish M (2016) Aloe vera derived activated high-surface-area carbon for flexible and high-energy supercapacitors. ACS Appl Mater Interfaces 8:35191–35202
30. Qiu D, Kang C, Gao A, Xie Z, Li Y, Li M, Wang F, Yang R (2019) Sustainable low-temperature activation to customize pore structure and heteroatoms of biomass-derived carbon enabling unprecedented durable supercapacitors. ACS Sustain Chem Eng 7:14629–14638
31. Selvaraj AR, Muthusamy A, Inho-Cho K-J, Senthil K, Prabakar K (2021) Ultrahigh surface area biomass derived 3D hierarchical porous carbon nanosheet electrodes for high energy density supercapacitors. Carbon N Y 174:463–474
32. Aruchamy K, Dharmalingam K, Lee CW, Mondal D, Kotrappanavar NS (2022) Creating ultrahigh surface area functional carbon from biomass for high performance supercapacitor and facile removal of emerging pollutants. Chem Eng J 427:31477
33. Qiu G, Miao Z, Guo Y, Xu J, Jia W, Zhang Y, Guo F, Wu J (2022) Bamboo-based hierarchical porous carbon for high-performance supercapacitors: the role of different components. Colloids Surf A Physicochem Eng Asp 650:129575
34. Taer E, Apriwandi A, Nursyafni N, Taslim R (2022) Averrhoa bilimbi leaves-derived oxygen doped 3D-linked hierarchical porous carbon as high-quality electrode material for symmetric supercapacitor. J Energy Storage 52:104911
35. Chung H-Y, Pan G-T, Hong Z-Y, Hsu C-T, Chong S, Yang TC-K, Huang C-M (2020) Biomass-derived porous carbons derived from soybean residues for high performance solid state supercapacitors. Molecules 25:4050

36. Zhang F, Xiao X, Gandla D, Liu Z, Tan DQ, Ein-Eli Y (2021) Bio-derived carbon with tailored hierarchical pore structures and ultra-high specific surface area for superior and advanced supercapacitors. Nanomaterials 12:27
37. Li Y, Li Z, Xing B, Li H, Ma Z, Zhang W, Reubroycharoen P, Wang S (2021) Green conversion of bamboo chips into high-performance phenol adsorbent and supercapacitor electrodes by simultaneous activation and nitrogen doping. J Anal Appl Pyrolysis 155:105072
38. Santhiago M, Garcia PS, Strauss M (2018) Bio-based nanostructured carbons toward sustainable technologies. Curr Opin Green Sustain Chem 12:22–26
39. Izadi-Najafabadi A, Yasuda S, Kobashi K, Yamada T, Futaba DN, Hatori H, Yumura M, Iijima S, Hata K (2010) Extracting the full potential of single-walled carbon nanotubes as durable supercapacitor electrodes operable at 4 V with high power and energy density. Adv Mater 22:E235–E241
40. Osman AI, Farrell C, Al-Muhtaseb AH, Harrison J, Rooney DW (2020) The production and application of carbon nanomaterials from high alkali silicate herbaceous biomass. Sci Rep 10:1–13
41. Pandolfo AG, Hollenkamp AF (2006) Carbon properties and their role in supercapacitors. J Power Sources 157:11–27
42. Fialkov AS (2000) Carbon application in chemical power sources. Russian J Electrochem 36:345–366
43. Hoffmann V, Jung D, Alhnidi MJ, Mackle L, Kruse A (2020) Bio-based carbon materials from potato waste as electrode materials in supercapacitors. Energies 13:2406
44. Joshi SSPC (2021) Biomass derived carbon for supercapacitor applications: review. J Energy Storage. https://doi.org/10.1016/j.est.2021.102646
45. Jayaramulu K, Dubal DP, Nagar B, Ranc V, Tomanec O, Petr M, Datta KKR, Zboril R, Gómez-Romero P, Fischer RA (2018) Ultrathin hierarchical porous carbon nanosheets for high-performance supercapacitors and redox electrolyte energy storage. Adv Mater 30:e1705789
46. Han J-W, Zheng H-F, Cui Y et al (2009) Genome-wide association study in a Chinese Han population identifies nine new susceptibility loci for systemic lupus erythematosus. Nat Genet 41:1234–1237
47. Hou J, Jiang K, Wei R, Tahir M, Wu X, Shen M, Wang X, Cao C (2017) Popcorn-derived porous carbon flakes with an ultrahigh specific surface area for superior performance supercapacitors. ACS Appl Mater Interfaces 9:30626–30634
48. Karamanova B, Shipochka M, Georgiev M, Stankulov T, Stoyanova A, Stoyanova R (2021) Biomass-derived carbonaceous materials to achieve high-energy-density supercapacitors. Front Mater Sci. https://doi.org/10.3389/fmats.2021.654841
49. Saini S, Chand P, Joshi A (2021) Biomass derived carbon for supercapacitor applications: review. J. Energy Storage 102646
50. Haoshen Z, Shenmin Z, Mitsuhiro H, Itaru H (2003) Electrochemical capacitance of self-ordered mesoporous carbon. J Power Sources 122:219–223
51. Chen C, Wang H (2016) Biomedical applications and toxicology of carbon nanomaterials. John Wiley & Sons
52. Fan L-Q, Tu Q-M, Geng CL, Huang JL, Gu Y, Lin JM, Huang YF, Wu JH (2020) High energy density and low self-discharge of a quasi-solid-state supercapacitor with carbon nanotubes incorporated redox-active ionic liquid-based gel polymer electrolyte. Electrochim Acta 331:135425
53. Rey-Raap N, Enterría M, Martins JI, Pereira MFR, Figueiredo JL (2019) Influence of multiwalled carbon nanotubes as additives in biomass-derived carbons for supercapacitor applications. Appl Mater Interferences 11:6066–6077
54. Yang H, Kannappan S, Pandian AS, Jang J-H, Lee YS, Lu W (2017) Graphene supercapacitor with both high power and energy density. Nanotechnology 28:445401
55. Taberna P-L, Chevallier G, Simona P, Plée D, Aubert T (2006) Activated carbon–carbon nanotube composite porous film for supercapacitor applications. Mater Res Bull 41:478–484
56. van Wyk JPH (2001) Biotechnology and the utilization of biowaste as a resource for bioproduct development. Trends Biotechnol 19:172–177

57. Ali GA, Manaf SAA, Divyashree A, Chong KF, Hegde G (2016) Superior supercapacitive performance in porous nanocarbons. J Mater Chem A Mater Energy Sustain 25:734–739
58. Taera E, Apriwandi A, Andani DR, Taslim R (2021) Solid coin-like design activated carbon nanospheres derived from shallot peel precursor for boosting supercapacitor performance. J Market Res 15:1732–1741
59. Khalafallah D, Quan X, Ouyang C, Zhi M, Hong Z (2021) Heteroatoms doped porous carbon derived from waste potato peel for supercapacitors. Renewable Energy 170:60–71
60. Li Y, Zhang D, Zhang Y, He J, Wang Y, Wang K, Xu Y, Li H, Wanga Y (2020) Biomass-derived microporous carbon with large micropore size for high-performance supercapacitors. J Power Sources 448:227396
61. Taer E, Apriwandi A, Taslim R, Agutino A, AfdalYusra D (2020) Conversion Syzygium oleana leaves biomass waste to porous activated carbon nanosheet for boosting supercapacitor performances. J Market Res 9:13332–13340
62. Gopalakrishnan A, Kong CY, Badhulika S (2019) Scalable, large-area synthesis of heteroatom-doped few-layer graphene-like microporous carbon nanosheets from biomass for high-capacitance supercapacitors. New J Chem 43:1186–1194
63. Thirumal V, Dhamodharan K, Yuvakkumar R, Ravi G, Saravanakumar B, Thambidurai M, Dang C, Velauthapillai D (2021) Cleaner production of tamarind fruit shell into biomass derived porous 3D-activated carbon nanosheets by CVD technique for supercapacitor applications. Chemosphere 282:131033
64. Shamsipur M, Barati A, Karami S (2017) Long-wavelength, multicolor, and white-light emitting carbon-based dots: achievements made, challenges remaining, and applications. Carbon N Y 124:429–472
65. Wang S, Cole IS, Zhao D, Li Q (2016) The dual roles of functional groups in the photoluminescence of graphene quantum dots. Nanoscale 8:7449–7458
66. Dang Y-Q, Ren S-Z, Liu G, Cai J, Zhang Y, Qiu J (2016) Electrochemical and capacitive properties of carbon dots/reduced graphene oxide supercapacitors. Nanomaterials (Basel). https://doi.org/10.3390/nano6110212
67. Zhong C, Deng Y, Hu W, Sun D, Han X, Qiao J, Zhang J (2016) Electrolytes for electrochemical supercapacitors. CRC Press
68. Feng H, Xie P, Xue S, Li L, Hou X, Liu Z, Wu D, Wang L, Chu PK (2018) Synthesis of three-dimensional porous reduced graphene oxide hydrogel/carbon dots for high-performance supercapacitor. J Electroanal Chem 808:321–328
69. Hoang VC, Nguyen LH, Gomes VG (2019) High efficiency supercapacitor derived from biomass based carbon dots and reduced graphene oxide composite. J Electroanal Chem 832:87–96
70. Oskueyan G, Mansour Lakouraj M, Mahyari M (2021) Fabrication of polyaniline–carrot derived carbon dots/polypyrrole–graphene nanocomposite for wide potential window supercapacitor. Carbon Lett 31:269–276
71. Taer E, Effendi NY, Taslim R, Apriwandi A (2022) Interconnected micro-mesoporous carbon nanofiber derived from lemongrass for high symmetric supercapacitor performance. J Jpn Res Inst Adv Copper-Base Mater Technol 19:4721–4732
72. Bi Z, Kong Q, Cao Y, Sun G, Su F, Wei X, Li X, Ahmad A, Xie L, Chen C-M (2019) Biomass-derived porous carbon materials with different dimensions for supercapacitor electrodes: a review. J Mater Chem A Mater Energy Sustain 7:16028–16045
73. Jina H, Hua J, Wua S, Wanga X, Zhanga H, Xua H, Liana K (2018) Three-dimensional interconnected porous graphitic carbon derived from rice straw for high performance supercapacitors. J Power Sources 384:270–277
74. Wan L, Li X, Li N, Xie M, Cheng D, Zhang Y, Chen J (2019) Multi-heteroatom-doped hierarchical porous carbon derived from chestnut shell with superior performance in supercapacitors. J Alloys Compd 790:760–771
75. Lal MS, Ariharan A, Viswanathan B, Ramaprabhu S (2020) Redox-active polymer hydrogel electrolyte in biowaste-derived microporous carbon-based high capacitance and energy density ultracapacitors. J Electroanal Chem 870:114236

76. Lee K, Shabnam L, Faisal SN, Gomes VG (2020) Aerogel from fruit biowaste produces ultracapacitors with high energy density and stability. J Energy Storage 27:101152
77. Thangavel R, Kannan AG, Ponraj R, Thangavel V, Kim D-W, Lee Y-S (2018) Nitrogen- and sulfur-enriched porous carbon from waste watermelon seeds for high-energy, high-temperature green ultracapacitors. J Mater Chem A Mater Energy Sustain 6:17751–17762
78. Liu X, Zhang S, Wen X, Chen X, Wen Y, Shi X, Mijowska E (2020) High yield conversion of biowaste coffee grounds into hierarchical porous carbon for superior capacitive energy storage. Sci Rep 10:1–12
79. Elmouwahidi A, Bailon-Garc E, Perez-Cadenas AF, Francisco J. Maldonado-Hódar FJ, Carrasco-Marín F (2017) Activated carbons from KOH and H3PO4-activation of olive residues and its application as supercapacitor electrodes. Electrochim Acta 229:219–228
80. Biswal M, Banerjee A, Deo M, Ogale S (2013) From dead leaves to high energy density supercapacitors. Energy Environ Sci 6:1249
81. Wu F, Gao J, Zhai X, Xie M, Sun Y, Kang H, Tian Q, Qiu H (2019) Hierarchical porous carbon microrods derived from albizia flowers for high performance supercapacitors. Carbon N Y 147:242–251
82. Huang G, Wang Y, Zhang T, Wu X, Cai J (2019) High-performance hierarchical N-doped porous carbons from hydrothermally carbonized bamboo shoot shells for symmetric supercapacitors. J Taiwan Inst Chem Eng 96:672–680
83. Qian W, Sun F, Xu Y, Qiu L, Liu C, Wang S, Yan F (2013) Human hair-derived carbon flakes for electrochemical supercapacitors. Energy Environ Sci 7:379–386
84. Lei S, Chen L, Zhou W, Deng P, Liu Y, Fei L, Lu W, Xiao Y, Cheng B (2018) Tetra-heteroatom self-doped carbon nanosheets derived from silkworm excrement for high-performance supercapacitors. J Power Sources 379:74–83
85. Yin L, Chen Y, Zhao X, Hou B, Cao B (2016) 3-Dimensional hierarchical porous activated carbon derived from coconut fibers with high-rate performance for symmetric supercapacitors. Mater Des 111:44–50
86. Bian Z, Zhao G, Chao L, Liu C, Zhao M, Wang H, Chen C (2020) Nitrogen and oxygen co-doped hierarchical porous carbon derived from pine mushroom biomass for high-performance supercapacitor. Int J Electrochem Sci 15:8296–8310
87. Yang Z, Xiang M, Wu Z, Hui J, Huang Q, Zhang J, Qin H (2020) A three-dimensional carbon electrode derived from bean sprout for supercapacitors. Ionics. https://doi.org/10.1007/s11581-020-03682-7
88. Wang X, Yun S, Fang W, Chen Zhang X, Liang ZL, Liu Z (2018) Layer-stacking activated carbon derived from sunflower stalk as electrode materials for high-performance supercapacitors. ACS Sustain Chem Eng. https://doi.org/10.1021/acssuschemeng.8b01334
89. Bhattarai RM, Chhetri K, Natarajan S, Saud S, Kim SJ, Mok YS (2022) Activated carbon derived from cherry flower biowaste with a self-doped heteroatom and large specific surface area for supercapacitor and sodium-ion battery applications. Chemosphere 303:135290
90. Xu X, Sielicki K, Min J, Li J, Hao C, Wen X, Mijowska E (2022) One-step converting biowaste wolfberry fruits into hierarchical porous carbon and its application for high-performance supercapacitors. Renew Energy 185:187–195
91. Hashmi MA (2022) High energy density solid-state supercapacitors based on porous carbon electrodes derived from pre-treated bio-waste precursor sugarcane bagasse. J Energy Storage 55:105421
92. Liu J, Deng Y, Li X, Wang L (2016) Promising nitrogen-rich porous carbons derived from one-step calcium chloride activation of biomass-based waste for high performance supercapacitors. ACS Sustain Chem Eng 4:177–187
93. Karnan M, Subramani K, Srividhya PK, Sathish M (2017) Electrochemical studies on corncob derived activated porous carbon for supercapacitors application in aqueous and non-aqueous electrolytes. Electrochim Acta 228:586–596
94. Xu G, Han J, Ding B, Nie P, Pan J, Dou H, Li H, Zhang X (2015) Biomass-derived porous carbon materials with sulfur and nitrogen dual-doping for energy storage. Green Chem 17:1668–1674

95. Zhou H, Fan T, Zhang D (2011) Biotemplated materials for sustainable energy and environment: current status and challenges. Chemsuschem 4:1344–1387
96. Chun W, Yang S, Cai J, Zhang Q, Zhu Y, Zhang K (2016) Activated microporous carbon derived from almond shells for high energy density asymmetric supercapacitors. Adv Mater. https://doi.org/10.1021/acsami.6b02942
97. Bhat VS, Jayeoye TJ, Thitima Rujiralai,Uraiwan Sirimahachai,Kwok Feng Chong,Gurumurthy Hegde (july2020) Influence of surface properties on electro-chemical supercapacitors utilizing Callerya atropurpurea pod derived porous nanocarbons: Structure property relationship between porous structures to energy storage devices. Nano Select https://doi.org/10.1002/nano.202000013
98. Tay T, Ucar S, Karagöz S (2009) Preparation and characterization of activated carbon from waste biomass. J Hazard Mater 165:481–485
99. Jiang ZTC (2019) Highly mesoporous carbon flakes derived from a tubular biomass for high power electrochemical energy storage in organic electrolyte. Mater Chem Phys 223:16–23
100. Rajalakshmi PDR (2020a) Facile synthesis of micro/mesoporous functional carbon from Turbinaria conoides seaweed for high performance of supercapacitors. Mater Today Proc 27:44–53
101. Rajalakshmi PDR (2020b) Renewable low cost green functional mesoporous electrodes from Solanum lycopersicum leaves for supercapacitors. J Energy Storage 27:101149
102. Priya MS, Divya P, Rajalakshmi R (2020) A review status on characterization and electrochemical behaviour of biomass derived carbon materials for energy storage supercapacitors. Sustain Chem Pharm 16:100243
103. Zequine C, Ranaweera CK, Wang Z et al (2016) High performance and flexible supercapacitors based on carbonized bamboo fibers for wide temperature applications. Sci Rep 6:1–10
104. Han J, Wang S, Zhu S, Huang C, Yue Y, Mei C, Xu X, Xia C (2019) Electrospun core-shell nanofibrous membranes with nanocellulose-stabilized carbon nanotubes for use as high-performance flexible supercapacitor electrodes with enhanced water resistance, thermal stability, and mechanical toughness. ACS Appl Mater Interfaces 11:44624–44635
105. Zheng R, Li H, Hu Z, Wang L, Lü W, Li F (2022) Photo-supercapacitor based on quantum dot-sensitized solar cells and active carbon supercapacitors. J Mater Sci: Mater Electron 33:22309–22318
106. Keppetipola NM, Olivier C, Toupance T, Cojocaru L (2021) Biomass-derived carbon electrodes for supercapacitors and hybrid solar cells: towards sustainable photo-supercapacitors. Sustain Energy Fuels 5:4784–4806
107. Keppetipola NM, Dissanayake M, Dissanayake P et al (2021) Graphite-type activated carbon from coconut shell: a natural source for eco-friendly non-volatile storage devices. RSC Adv 11:2854–2865
108. Keppetipola NM, Kumara GRA, Tennakone K, Dourges M-A, Olivier C, Toupance T, Cojocaru L (2022) Sustainable photo-supercapacitors using biomass waste as source of carbon for electrodes. Proc Int Conf Hybrid Organic Photovolt (HOPV22)
109. Wang Y, Song Y, Xia Y (2016) Electrochemical capacitors: mechanism, materials, systems, characterization and applications. Chem Soc Rev 45:5925–5950
110. Divya ML, Natarajan S, Lee Y-S, Aravindan V (2019) Biomass-derived carbon: a value-added journey towards constructing high-energy supercapacitors in an asymmetric fashion. Chemsuschem 12:4353–4382
111. Ouyang T, Cheng K, Yang F, Zhou L, Zhu K, Ye K, Wang G, Cao D (2017) From biomass with irregular structures to 1D carbon nanobelts: a stripping and cutting strategy to fabricate high performance supercapacitor materials. J Mater Chem A Mater Energy Sustain 5:14551–14561
112. Chen T, Tang Y, Qiao Y, Liu Z, Guo W, Song J, Mu S, Yu S, Zhao Y, Gao F (2016) All-solid-state high performance asymmetric supercapacitors based on novel MnS nanocrystal and activated carbon materials. Sci Rep 6:1–9
113. Zhu X, Yu S, Xu K, Zhang Y, Zhang L, Lou G, Fu S (2018) Sustainable activated carbons from dead ginkgo leaves for supercapacitor electrode active materials. Chem Eng Sci 181:36–45

114. Yingying MY, Wang HYLJLL (2019) Improving electrochemical activity of activated carbon derived from popcorn by NiCo2S4 nanoparticle coating. Appl Surf Sci 463:1001–1010
115. Gan Q, Jia S, Wang H, Cao F, Li L, Qing C, Sun D, Wang B, Tang Y, Wang J (2016) Asymmetric supercapacitor based on porous n-doped carbon derived from pomelo peel and NiO arrays. ACS Appl Mater Interfaces. https://doi.org/10.1021/acsami.6b06630
116. Liu B, Liu Y, Chen H, Yang M, Li H (2019) MnO2 nanostructures deposited on graphene-like porous carbon nanosheets for high-rate performance and high-energy density asymmetric supercapacitors. ACS Sustain Chem Eng. https://doi.org/10.1021/acssuschemeng.8b04817
117. Fang K, Chen J, Zhou X, Mei C, Tian Q, Xu J, Wong CP (2018) Decorating biomass-derived porous carbon with Fe2O3 ultrathin film for high-performance supercapacitors. Electrochim Acta 261:198–205
118. Wang Q, Zhang Y, Jiang H, Meng C (2019) In-situ grown manganese silicate from biomass-derived heteroatom-doped porous carbon for supercapacitors with high performance. J Colloid Interface Sci 534:142–155
119. Augustyn V, Simon P, Dunn B (2014) Pseudocapacitive oxide materials for high-rate electrochemical energy storage. Energy Environ Sci 7:1597–1614

Methods for Production of Functional Carbon Nanostructures from Biomass

Arpita Roy and Kalipada Manna

Abstract Biomass is high abundant, easily available, and renewable in nature. Thus this chapter explores the suitability of biomass as a source for the synthesis of various carbonaceous nano materials (CNMs). CNMs are nanomaterials which have extraordinarily desired shapes. They also retain various striking features which are extensively used in several of arenas, including the health sectors to energy sectors. This chapter summarizes the synthetic designs, unique features, and functionalization/modification strategies of CNMs including graphene, carbon nanotubes (CNTs), Carbon nano-onions (CNOs), and carbon nanofibers (CNFs) which have been developed using biomass as a precursor material. Primarily biomass contains 60–90% cellulose. Due to highly crystalline in nature the cellulose ha e very lower solubility, hence ionic liquids (ILs) are introduced as the media to dissolute the cellulose-comprising biomass to produce starting material for the synthesis of CNMs.

Keywords Carbonaceous nano materials · Biomass · Modification strategies · Synthetic designs

1 Introduction

Worldwide, there is an upsurge in technical growth, which is to help life on the earth more sustainable. This caused in a bigger claim for various materials being used in the development of various products. Amongst these substances CNMs were reported first by Kroto et al. in 1985 [1]. Subsequently, there have been many inquiries and abundant reports on CNMs. Investigation has been focused by various unique properties exhibited by CNMs, including high surface to volume ratio, great mechanical strength, improved optical absorption, and better carrier (holes and electrons) features [2, 3]. These features improves applicability of the CNMs in various functions like sensing, [4] catalysis, [5] energy storage [6] harvesting and conversion, and so on [7, 8]. Maximum of these uses necessitate a specific type of CNMs to be

A. Roy (✉) · K. Manna
Department of Chemistry and Chemical Biology, IIT(ISM), Dhanbad 826004, India
e-mail: arpitachem28@gmail.com

S. K. Tiwari et al. (eds.), *Biomass-Based Functional Carbon Nanostructures for Supercapacitors*, Green Energy and Technology,
https://doi.org/10.1007/978-981-99-0996-4_2

extremely effective. Hence, a different variety of CNMs with different shapes have been introduced such as fibres, [9] spheres, [10] ribbons, [11] cylindrical tubes, [12] etc.

The synthesis of these kinds of CNMs of different shapes mainly depends on the properties of the carbon precursors used and also depend on the conditions of the reactions. Bai et al. reported that use of benzene and ferrocene produces two dissimilar kinds of CNMs, one is carbon nanotubes both single and multiwalled and the other is carbon nanofibers [13]. They established that ratio of starting material to catalyst controls the production of product. This phenomenon is also suggested by Nyamori and Coville [14]. In their case iron to carbon ratio played an important role in case of the size and shape of the CNMs. Furthermore, Sevilla et al. [15] reported the synthesis of graphitic carbon nano-structures consuming gluconate dehydrates of Fe and Co. Besides they have also conveyed that Fe and Co nanoparticles acted as catalyst to the reaction (required temperature 900 or 1000 °C). Various structures of CNMs were generated using Au and Si containing starting materials [16].

In several reports there are description for the synthesis of CNMs including CNTs, CNFs, and so on using hydrocarbons consisting long chains and aromatic moieties as the carbon source where various metal salt were served as catalysts [17, 18]. Usually, CNMs are produced through the bulk pyrolysis and followed by solvothermal treatment to obtain pure product. In pyrolysis using heat a mixture comprising soluble metal salt (catalyst) and organic materials rich in carbon (carbon source) decomposes to form char under inert environment (may be slightly reducing sometimes). In many cases, H_2O or O_2 are used for the partial combustion [19]. Consequently, in case of pyrolysis, there are two steps; initially, the metal nanoparticles synthesis are synthesized and then secondly, the coating material were grown utilizing the synthesized nanoparticles as templates [20]. Besides, in case of solvothermal process the purification of the synthesized nanomaterials after synthesis using various solvents in an autoclave is required, and when solvent used for treatment is H_2O then it is known to be the hydrothermal process. The economical and large scale production is a prime challenge of these types of synthesis processes as they leads to very small scale synthesis of products [15]. Consequently, there is a requirement for more research works that emphasis on the use of carbon precursors that are naturally abundant and cheap. Henceforth, various substitute substances based on biomass and fossil as renewable starting materials are extremely favorable. Thus widespread research is currently on going for the surface modification and functionalization of various CNMs like CNTs and graphene. Nevertheless, there are various limits regarding the electrical conductivity, mechanical properties, optical absorptivity, and dispersibility. Furthermore in many cases there are also the difficulties in the synthetic processes have been detected.

So, in the present chapter we have discussed about various forms of carbonaceous nanomaterials such as 0D, 1D, 2D, and 3D, [21, 22] developing the CNMs from biomass, classification of biomass, and also various synthetic strategy, functionalization, and surface modification of CNMs like carbon nanotubes (CNTs), carbon nanofibers (CNFs), and graphene.

2 Carbon Nanostructures

Carbonaceous nano materials (CNMs) are a special class of materials where the main structural units like crystallites, molecule, or clusters of the materials are in nano dimensions (1–100 nm).

All the nanostructured carbon allotropes irrespective of their synthetic techniques can be generated in the nanoscale. Carbonaceous nanomaterials have many benefits, and they have been extensively used in various industries as well as in scientific laboratories. Due to the catination properties of the carbon, it can exhibit three types of (sp, sp^2, and sp^3) hybridization.

These special features helps carbon to develop various crystalline and amorphous forms including variable dimensionalities. Typically carbon allotropes can be zero dimensional (fullerene), [23] one dimensional (single and multi-walled carbon nanotubes (CNT) and nanofibers (CNF)), two dimensional (carbon nanohorns [24] and graphene [25]), and three dimensional (micelles, foams, aerogel, and hydrogel [26–29]).

2.1 Various Forms of Carbonaceous Nano Materials (CNMs)

2.1.1 0D CNMs

Greek term "nanos" mean dwarf and from this term the "nano" term has been introduced [30].

0D CNMs involves both uniform as well as heterogeneous particles arrays. Some examples of 0D CNMs are quantum dots, nanolenses, fullerene, onion, hollow spheres, etc. From last decades there is a huge progress in the synthesis and control of dimensionality of 0D CNMs. Different 0D CNMs (graphene clusters, Buckminster fullerene, nanocones or nanohorns, nanotoroids, nested giant fullerenes or graphitic onions; short carbon chains) have been exhibited in Fig. 1. Several approaches have been utilized to develop 0D CNMs [31–34]. 0D CNMs are so far widely utilized in light emitting diodes (LEDs), [34] single-electron transistors, [35] lasers, [36] composite materials for energy storage, [37] solar cells [38], and so on.

2.1.2 1D CNMs

From last few years, research on 1D CNMs have increased importance owing to their unique properties and their potential application. 1D CNMs are in general used for the investigation of various nanoscale phenomena. Therefore they have been widely explored in the development of LEDs, security devices, composite materials, electronic materials, and optoelectronic materials [39]. Nanotubes were introduced by Iijima [40], and they have widespread usage as 1D CNMs. Different 1D CNMs

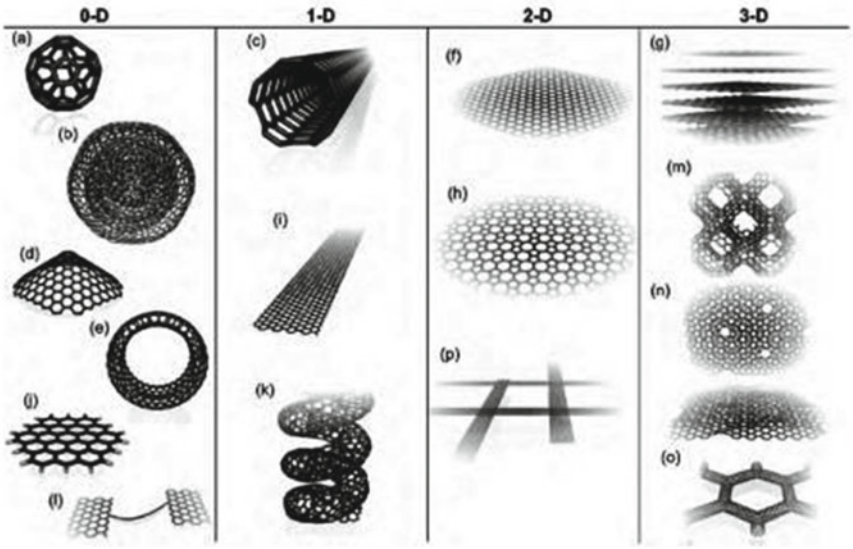

Fig. 1 Different CNMs **a** C60; **b** graphitic onions or nested gigantic fullerenes; **c** CNT; **d** nanocones; **e** nanotoroids; **f** 2D graphene layer; **g** 3D graphite crystal; **h** Haeckelite layer; **i** graphene nanoribbons; **j** graphene nanoclusters; **k** helicoidal CNT; **l** short carbon chains; **m** 3D Schwarzite crystals; **n** nanofoams; **o** 3D CNT networks, and **p** nanoribbon (Reproduced from [54])

(carbon nanotubes, graphene nanoribbons, and helicoidal carbon nanotubes) has been represented in Fig. 1. These 1D CNMs were successfully developed and used by various researchers [41, 42].

2.1.3 2D CNMs

2D CNMs consist of nanosized two dimensions. Newly, the development of 2D CNMs have created potential interest in the field of materials research. The main reason is that they possess several unique properties in low dimension which is dissimilar from the bulk. 2D CNMs are found to be used as the structural units of nanodevices owing to their certain unique geometries and shape-dependent features [43, 44]. Various 2D CNMs structures have been shown in Fig. 1. Moreover, 2D CNMs are predominantly remarkable for their several potential applications like sensing, photocatalysis, and so on [45].

2.1.4 3D CNMs

Owing to the high superficial area, quantum size effect, and several other exclusive properties as compared to the bulk, 3D CNMs have exhibited extensive research

attention and various 3D CNMs have so far been developed [46–49]. The performances of CNMs are intensely dependent on their sizes, dimensionality, structures, shapes, and their architectures. Thus controlling the structure and morphology of 3D CNMs is very essential. Furthermore, nanostructures with 3 dimensions are very essential substance owing to their application ranging from the area of biology to batteries [46–50]. Due to large surface area, high porosity and presence of various functionalities on the surface these 3D CNMs can be used as absorption sites for several molecules in a small molecules and can actively transport them to the desired site [51–53]. Various 3D CNMs structures have been shown in Fig. 1.

3 Biomass: A Renewable Source of Carbon

3.1 Biomass

Biomass is a natural waste material and organic in nature. These are generally obtained as waste from woods, animals, crops, and seaweed and is a renewable source of carbon. Hence the biomass can be used to develop various CNMs which could be further used for several applications. Different sources of biomass are demonstrated in Fig. 2. From the ancient age, the wood is used in household for cooking purposes. Thus biomass is considered as the oldest energy source after the sun. The nature collects the solar energy and conserves it in it. Through photosynthesis, the planes collect energy from sunlight and transform H_2O and CO_2 into O_2 and sugars. The sugar acts as an energy source to the plants and animals. Thus the energy is also stored in the biomass and the energy supply is not restricted. More interestingly so far the plants and animals are there, the waste (biomass) will always be produced and thus biomass is a renewable source of carbon and energy [55].

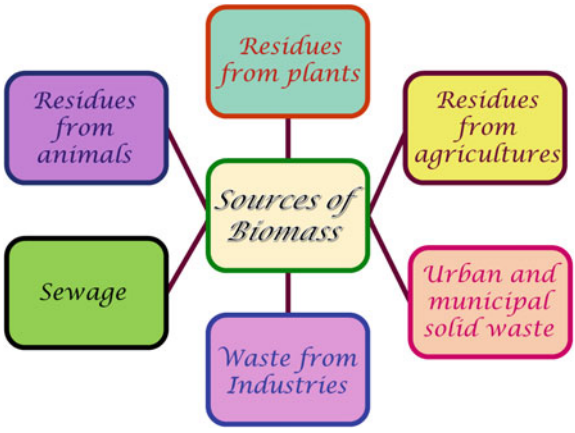

Fig. 2 Different biomass sources

Table 1 Classification of biomass [56]

Biomass	Species and types
Wood and woody biomass	Coniferous or deciduous; Angiospermous or gymnospermous; Stems, sawdust, branches, foliage, lumps, bark, chips, pellets, briquettes, sawmill, and various other different wood species
Herbaceous biomass	Flowers and grasses (cynara, bana, alfalfa grass, bamboo, brassica, cane, miscanthus, switchgrass, timothy, and so on) Various straws (sunflower, various beans, oat, barley, corn, mint, rape, rice, rye, sesame, wheat and so on) Natural residues (fruits and their skins, pulps, pips, shells, husks, hulls, grains, various seeds, coir, stalks, cobs, cereals, bagasse, residual food, fodder, cakes, and so on)
Waterlife biomass	Freshwater or marine algae; various macroalgae including brown, blue, green, red etc. Various microalgae; sea and lake weeds, kelp, water hyacinth, and so on
Animal and human waste biomass	Meat-bone meal; Bones, various manures, and so on

3.2 Classification of Biomass

Owing to the extensive variances of biomass epically in terms of diversity, amount of and compositional features, so far there is no such univocal means for the classification of biomass. Thus they can be classified depending upon the scope and purpose. According to source, purpose, and ultimate products, in general biomass is divided in two groups-

I. Biomass obtained in environment (depending upon the ecosystem or variety of vegetation);
II. Application of biomass as feedstock [56]. Table 1 represents the classification of biomass.

3.3 Chemical Characterization of Biomass

The biomass can consist numerous composition. For instance, biomass derived from plants predominantly consist lignin, cellulose, and hemicellulose. These components also have different percentages in different cases (Fig. 3 and Table 2). Whereas the cattle manure contain high proteins and starch is the main component of the cereals. It is obvious that due to various chemical structures biomass possess different chemical properties [57].

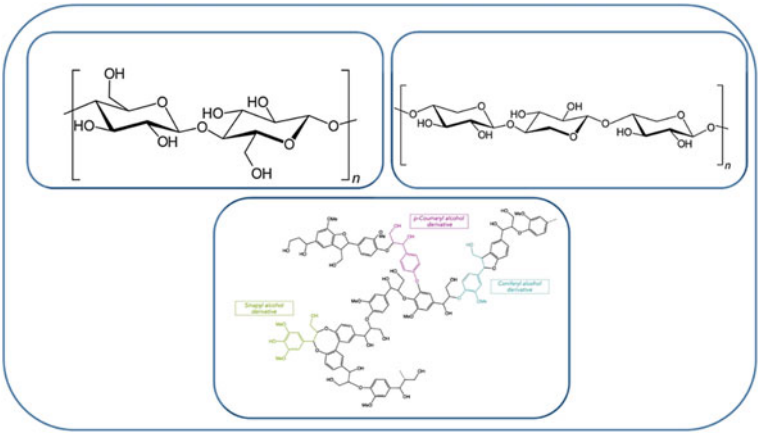

Fig. 3 Structure of **a** cellulose, **b** hemicellulose, **c** lignin. (Reproduced from [55])

Table 2 Chemical configuration and the structure of cellulose, hemicellulose, and lignin in herbal cell walls [58, 59]

Element	Subunits	Type of bonds in Subunits	Composition	Polymer
Cellulose	D-Pyranglucose units	β-1,4-Glycosidic bonds	β-Glucan	Several hundred to tens of thousands
Hemicellulose	D-Xylose, mannose, arabinose, galactose, glucuronic acid	β-1,4-Glycosidic bonds in L-main chains; β-1.2-, β -1.3-, β-1.6-glycosidic bonds in side chains	Polyxylose Galactoglucomannan (Gal-Glu-Man) Glucomannan (Glu-Man)	Less than 200
Lignin	Guaiacylpropane (G), syringylpropane (S), p-hydroxyphenylpropane (H)	Various ether bonds (mainly β-O-4); carbon–carbon bond	G lignin, GS lignin, GSH lignin	4,000

4 Biomass as a Renewable Carbon Source for CNMs Synthesis

So far there are very few reports on the use of biomass for the synthesis of CNMs. This may be owing to the fact that the conversion is somehow critical and requires a well-established protocol as the biomass has various complex structure. Additionally, the biomass in general does not dissolve in various solvents thus reacting them to form

CNMs are limited [60–62]. Nevertheless, there are some process for conversion of biomass to CNMs which has been discussed below. In normal procedure they are macromolecular materials and under heat treatment they produce prospective precursors for CNMs [63]. For example, lignocellulosic is considered as a potential chemical resource as it consist of various biopolymers like cellulose, hemicellulose, and lignin [64]. Cell wall of normal eukaryotic cells of living organisms are made up of cellulose. It is considered as the most abundant organic substance with exceptional properties like relatively high chemical and thermal steadiness, biodegradability, and biocompatibility [65]. Cellulose is linear and possess high molecular weight [66]. Cellulose, when exposed to high temperature, is certainly able to produce carbon remains without melting and develop appropriate CNMs starting materials [63]. Besides, various types of small gaseous molecules like CO, alcohols, CO_2, and ketones are generated from biomass during their pyrolysis (Scheme 1).

Sometimes is has been observed that very low oxygen containing starting material is beneficial for CNMs synthesis [68]. Besides various fossil-based hydrocarbon starting materials comprising acetylene, toluene, methane, and benzene are very useful.

From the reports on the synthesis of CNMs from biomass, it is also known that sometimes there are very low yields in case of pyrolysis. As in these cases before pyrolysis of the final carbonaceous solid, the biomass need a hydrothermal pre-treatment of sodium carboxymethylecellose using an autoclave at 800 ℃ under inert atmosphere, followed by extraction and filtration [69].

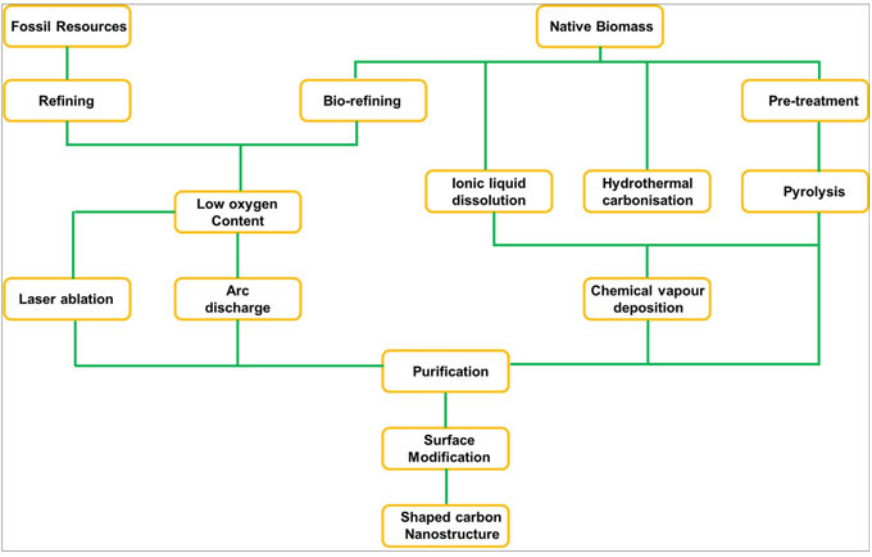

Scheme 1. Flow chart of the production of starting materials for the synthesis of CNMs. (Reproduced from [67])

5 Preparation of CNMs from Biomass

5.1 Carbon Nanotubes (CNTs)

CNTs have continuous hollow cylindrical structures, and they are exceptionally lightweight usually developed by sp^2 carbon atoms which are covalently linked. They possess good mechanical features comprising high toughness, extraordinary mechanical/tensile strength. Thus they are appropriate as reinforcement materials [70]. Furthermore, CNTs possess some other exclusive features like high conductivity (electrical and thermal both), [71, 72] striking optical features, [73] and high flexibility [74]. Moreover, metallic or semiconducting features are typically detected only with single or double-walled CNTs. This metallic type nature of CNTs provide them great conductivity (even higher than that of Cu). Besides, CNTs demonstrated high thermal conductivity as well as large heat capacity [75, 76]. The optical features of the CNTs can be in between transparent to ideal black body absorber. Thus so far CNTs have widely been used as electromagnetic interference defensive materials. Various transparent films and coatings have also been prepared using CNTs [76].

Biomass cellulose and lignocellulosic have been utilized for the preparation of CNTs through bulk pyrolysis [77]. For example, spongy cotton, [78] when treated under 400–600 °C, generated CNTs typically with outer and inner diameters of 80 and 10 nm correspondingly. In this type of synthesis a purification of the developed material using ethanol and water is necessary. On the other hand, CNTs with 24–38 nm diameter have been synthesized though the pyrolysis of cellulose acetate at 750 ºC in the presence of polyisocyanate and $NiCl_2$ (pre-catalyst) [79].

CNTs can also be prepared from biomass lignocellulosic including wood fiber [60] or wood sawdust [80]. When carbonization was accomplished under oxidative environments at temperatures 250–400 °C the synthesized products have diameters between 10 to 20 nm. In this process extraction with acid (HCl) is required for purification [60]. Another report was there where gumwood was pyrolysed under inert atmosphere using microwave [81] at 500 °C for the synthesis of CNTs having diameter ~ 50 nm using SiC. Bamboo charcoal also can be pyrolised at 1000–1500 °C in the presence of ethanol vapour to yield CNTs using chemical vapour deposition techniques (CVD) [82]. Grass when treated at 600 °C produces MWCNTs (diameters ~ 30–50 nm) [12].

These aforesaid examples demonstrate that CNTs can be effectively synthesized using various biomass sources. Nevertheless, controlling the diameters or lengths of the CNTs is still a great challenge.

5.2 Graphene

Physically, graphene occurs as atomic mono layer of graphite and it also possess the basic structural element for CNTs and fullerenes [83]. Graphene possess carbon

atoms with both sp^2 and sp^3 hybridization closely packed into a honeycomb like lattice structure. It also contains delocalized pi electrons [84]. Graphene is a 2D material possessing exceptionally good electrical, thermal as well as mechanical features. Therefore, they have been extensively used in energy devices [85].

Usually, graphene can be developed from only one chemical precursor [86]. Nevertheless, there are some reports on the use of various complex biomass-derived materials to synthesize graphene. For instance, chitosan extracted from crustacean waste is helpful to produce a single layered nitrogen-doped graphene. This synthesis involved pyrolysis of the material at 800 °C [87]. Shams et al. in a work used camphor leaf to generate graphene through pyrolysis at 1200 °C, [88] followed by a purification process to isolate graphene from the amorphous carbon particles. Chen et al. effectively generated graphene using wheat straw, through hydrothermal and graphitization techniques [89]. Remarkably, when grapheme oxide (GO) and milled sheep horn was pyrolysed, a 3D porous nitrogen and sulphur doped graphene was generated [90]. Most importantly, here synthesis process does not involve any catalysts or strong acid treatment to produce graphene. Thus using renewable resources for CNMs synthesis is now a striking area of investigation with exciting prospects.

5.3 Carbon Nanofibers (CNFs)

Carbon nanofibers (CNFs) are one of the well-known CNM, which are fibre like and contains covalently bonded sp^2 hybridized carbon atoms. They have structural resemblance with CNTs when observed using a low-resolution scanning electron microscope (SEM). Conversely, when they are observed under a high-resolution transmission electron microscope (TEM), they look like a solid substance because they do not possess the hollow pipe like structure like the CNTs. CNFs have been used as reinforcement ingredients in composites due to their excellent mechanical features. Moreover, CNFs have also exhibit high electrical conductivity due to which they are also used in energy devices.

The generation of CNFs has been described from the bacterial cellulose. This biomass were usually pre-treated with a solution comprising doping heteroatoms, before pyrolysis [91, 92]. Thus a 3D heteroatom doped (P or N/P or B/P) CNF has been generated. The amount of doping of nitrogen can be controlled by controlling the conc. of NH_3 in the solution [93]. Extraction with acid is the purification step for these kinds of reactions. However, it is very problematic to modify the material features because of the acid treatment. The acid action makes some morphological and surface changes.

5.4 Carbon Nano-onions

Carbon nano-onions are a new introduction to CNMs. They have multi-layered quasi-spherical and polyhedral shaped shells with concentrically layered structures [94]. Here also sp^2 bonded carbon atoms are present. This type of substances demonstrate various striking physical and chemical features, including good optical features and reasonable capacitance; henceforth, they are used in supercapacitors [94, 95]. So far, only there is a single report where carbon nano-onions were produced from biomass wood wool [96]. Once wood wool is pyrolysed under a mixed environment of oxygen and nitrogen at 600 °C carbon nano-onion is produced.

5.5 Carbon Nano-Spheres

Carbon nano-spheres (CNSs) are layered carbonaceous structure which possess broken concentric layers. These concentric layers are held together through van derWaals forces of interactions in agglomerates [97]. CNSs have extensively been used in electrode material in lithium-ion batteries [98] and supercapacitors [99] From biomass cassava/tapioca flour or carrageenan, CNSs were produced through hydrothermal and carbonization approach after some chemical initiation steps [100, 101].

6 Modifications of CNMs

CNMs generally agglomerate due to presence of strong Vander Waals forces interactions; [102] thus it is essential to disperse them after synthesis. Throughout the purification procedure, dispersion is attainable. Sometimes, this procedures lead to the introduction of various functionalities on the surfaces of the CNMs and thus the normal structures are modified. The modification of CNMs can be accomplished using some key methods. They are (a) covalent bonding between various functionalities and the pi-conjugated backbones of CNMs, (b) non-covalent attachments or covering with numerous functionalities, and (c) endohedral filling of the vacant interior cavities [102].

The covalent functionalization of CNMs are mainly two types: (a) on the CNMs structural sides or (b) at the site of defects. This mainly depends on the position of the functionalities [67]. Functionalization in the fullerenes can be achieved using both electron-withdrawing and donating moieties on the aromatic rings [103]. Surface functionalization of fullerenes vary from the general aromatic reaction outlines. Moreover, the reactions for the fullerene surface functionalization be similar to the reactions of confined electron-lacking polyolefins, i.e., dienophilic, electrophilic, and

dipolarophilic. Thus in general the fullerenes are find to undertake cycloaddition reactions, reacting with various nucleophiles. They also take part in addition reactions and form complexes with the transition metal causing the surface modifications [104]. CNMs based on graphene are hard to modify due to the large interlayer cohesive forces of attraction. Consequently, precise chemical reaction designs are essential for functionalization like click chemistry (cycloaddition), fluorination/bromination, biomolecules modification, electrophilic/radical/nucleophilic addition, and grafting of polymers. Generally, mechanical and electrical features of covalently functionalized CNMs alter due to the defects in the structures which is introduced by the breakdown of the carbon–carbon double bonds of the main graphitic backbone during the chemical procedures involved [67].

6.1 Modification Procedures of CNTs: Primary Designs

The chemical functionalization of CNTs is a developing arena of modern materials science. Many uses of CNTs depend on the effective surface modification. Herein, we have tried to summarize all the reported literatures on the covalent surface modification chemistry of CNTs (Fig. 4) and also concisely discussed about the chemical procedures to modify the CNTs.

6.1.1 Carboxylation Reactions of the Terminal Carbons and Defect Sites of CNTs

Initially, the modification of CNTs can be done through acid cutting using HNO_3 or mixed acids [106]. In this case, the terminal carbon atoms and the carbons atoms situated at the defect spots were transformed into–COOH groups. Haddon group reported that utilizing the acid groups for the attachments of long alkyl chains to SWCNTs can be achieved through the formation of amide linkages17 or by carboxylate-ammonium salt interactions. Sun et al. reported that the carboxylic acids can also be modified to esters to solubilise the CNTs having any effective length [107, 108]. These soluble CNTs permit various characterizations which are solution based. There is now sufficient investigational indication that a various functionalities can be deposited or loaded onto the CNTs. This involves reactions with the various –COOH groups present in the CNTs [109]. Thus modified CNTs have extensive application in the biomedical areas (Fig. 4).

6.1.2 Halogenation Reactions

Due to the high electronegativity, fluorine (F) can fluorinate the lateral walls of the CNTs. The fluorination can take place in room temperature, or it may require high temperature (600 °C) [110, 111] (Fig. 4). HR-TEM, [110, 112] scanning tunnelling

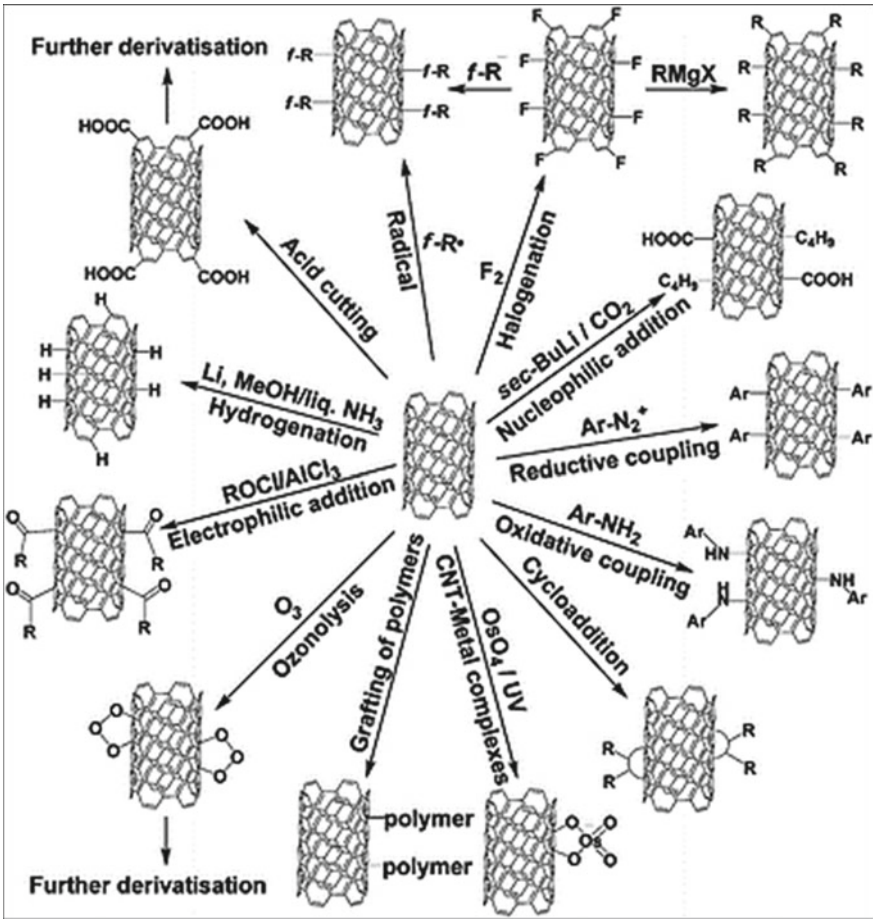

Fig. 4 Various surface functionalization techniques of CNTs. (Reproduced from [105])

microscopy (STM), [113] and X-ray photoemission spectroscopy (XPS) [114] are the general characterization tools to investigate the fluorinated CNTs. The fluorinated carbon atoms present in the sidewall the CNTs exhibit sp^3 hybridization with a tetrahedral structure. Due to this tetrahedral structure the electronic band structure CNTs (metallic or semiconducting) destroys resulting an insulating compound [115]. There is argument on the topic of the most favourable design of F-addition onto the lateral walls of CNTs being either 1,4-addition or 1,2-addition. Though, theoretical DFT calculations proposed that 1,2-addition is more favourable due to 4 kcal/mol energy gain, but as there is not large energy gap so both types of addition reactions might co-occur. From elemental analysis it is observed that so far C_2F can achieve the highest extent of functionalization [112]. Thus Fluorine functionalized CNTs have a moderate solubility in alcohols (1 mg/mL) [116].

The fluorine functionalization is very beneficial because further by replacing F atoms other more useful functional units can be synthesized [117]. Some common methods to substitute F atoms are (a) Grignard reactions through which they can be replaced by the fluorine atom can be alkyl [118] or (b) use of organo-lithium reagents [119]. These alkylated CNTs can be well dispersed in many organic media and can be dealkylated entirely when heated at 500 °C under inert conditions, thus pristine CNTs can be recovered. Various diols [120] and diamines [121] were also found to replace F atoms of fluorinated CNTs. This F substitution of CNTs can be confirmed from IR spectroscopy if there is absence of the C-F bond stretching at 1225 cm^{-1}. These functionalized CNTs, like aminoalkylated CNTs can be modified more. Thus amino groups can be converted to more important functional groups, [122] which can exhibit binding efficacy towards various biomolecules for biomedical applications.

Furthermore, chlorination or bromination of CNTs was achieved by electrochemical reactions but the resultant products comprise noteworthy extents of –COOH or –OH groups.

6.1.3 Cycloadditions Reactions

In Fig. 5 we have discussed the cycloaddition reactions of CNTs. Both carbenes as well as nitrenes smoothly react with CNTs to produce cycloaddition adducts. Dichlorocarbene produced in-situ consuming a $CHCl_3$/NaOH or a phenyl(bromodichloromethyl) mercury substrate was first used by Haddon research group [123]. The attachment of CCl_2 unit on the surface of CNTs was established using XPS, IR spectra, and other chemical analyses. The –COOH groups added on the CNTs can again be modified for other purposes. A latest report of Bingel cyclopropanation was for the modification of extremely short nanotubes (20–80 nm sizes) with malonic acid bis-(3-tert-butoxycarbonylaminopropyl) ester in CBr_4/DBU to yield products of small dimensions. The covalent linkage and fitted packaging of the products arms around CNTs were established by through thermogravimetry (TGA) and solid-state NMR spectra.

Alkoxycarbonylnitrene was synthesized via thermal dissociation of organic azide. The resulting nitrene was attached to the lateral walls of CNTs, leading to alkoxycarbonylaziridino- CNT [124, 125]. Various different functionalities have been added onto CNTs using various azides [126, 127]. The added functionalities can be utilized in chelating metal ions, molecular recognition, cross-linking, and so on. Functionalized CNTs are solvable in dimethyl sulfoxide (DMSO) or 1, 2-dichlorobenzene and can be studied by NMR, UV–vis, XPS, and IR analyses [128, 129].

In an altered method, azomethine ylides (can be produced thermally in-situ by condensation reaction of an aldehyde and an α-amino acid) were effectively attached to the surface of the CNT through 1,3-dipolar cycloaddition generating pyrrolidine rings fused with each other [130, 131]. This approach is unique for formulating an extensive variety of modified CNTs. This design of chemistry has been applied in

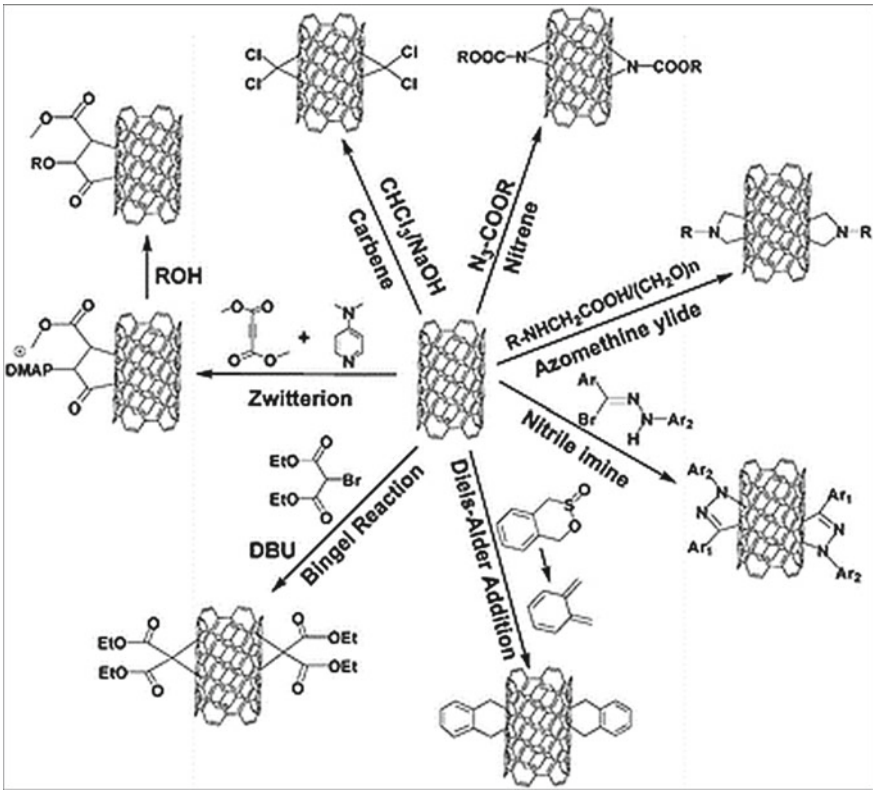

Fig. 5 Functionalization of CNTs using various cycloaddition reactions. (Reproduced from [105])

energy sectors, solar energy harvesting, medicinal chemistry, and sensing of specific chemicals [132, 133].

There is an another report by Alvaro et al. where a different approach was opted for the modification of CNT using microwave assisted 1, 3-dipolar cycloaddition of nitrile imines [134]. Thus functionalized CNTs were thoroughly investigated using various spectroscopic techniques like FT-IR UV–vis-NIR, NMR, and so on. Theoretical studies also support that 1, 3-dipolar cycloadditions are very effective to functionalize the lateral walls of CNTs [135]. Besides various other kinds of cycloadditions have been so far explored to functionalize the CNTs. Using microwave and Diels–Alder cycloaddition reactions the lateral walls of SWNTs can be modified. In this process o-quinodimethane is used [136]. This reaction intermediates are stable by aromaticity and gives the more stable products as suggested from the theoretical calculations [137]. Swager group recently reported a cycloaddition method group using zwitterions [138]. Initially the nucleophile of the reaction (4-dimethylaminopyridine) attack dimethyl acetylenedicarboxylate which acts as an

electrophile. Finally the nucleophilic moiety attached is substituted with other nucleophile including alcohols leading to the generation of the anticipated functional groups.

6.1.4 Free Radical Addition Reactions to CNTs

The lateral walls of the CNTs are highly reactive towards the radical reactions as proved from the molecular modelling studies [139]. There are also experimental evidence of this type of modification reactions. One example is that using radical reaction of diazonium salts (Fig. 5) the lateral walls of CNTs have been functionalized. However, in case of aryl substituted diazonium salts electrochemical reduction process is required. These salts produce an aryl radical in the reaction media and that radical can be added covalently to the CNTs [140]. The electrons are transferred from CNTs to aryl diazonium salts to form the radicals and this helped the modification process. Another report was there where diazonium salts which are soluble in water have been employed to specifically functionalize the metallic CNTs [141, 142]. Thus modified CNTs can be dispersed well in aqueous media as well as in DMF. *In-situ* modification of CNTs using electro chemical methods was exhibited by addition of substituted phenyl groups [143]. So far there are reports on two types of coupling reactions. One is reductive coupling where aryl diazonium salts are required, and the other is namely oxidative coupling where the aromatic amines are used. Radicals are generated on the CNT surface, and they attack the carbon structure and develop the covalent linkages. In the previous situation, the reaction formed a C–C linkage at the surface. However in the latter case, the direct attachment of amines to the CNTs is observed.

Reductive alkylation reaction of SWNTs using Li in liq. NH_3 and then addition of either alkyl or aryl sulphides/ iodides is too anticipated for a radical reaction [144, 145]. The reductive intercalation of Li^+ on the surface of CNTs in the presence of NH_3 or in some other polar aprotic media has been detected using AFM and TEM analyses. The negative charge present on the CNTs was initiated to the exchange of electrons with aryl/alkyliodides having long chains, leading to the generation of a transitory aryl/alkyl radical. An alike reaction pattern was described for the modification of CNTs through single electron reduction of benzophenone using K metal [146]. There is a generation of radical anion in the presence of K metal, and this leads to the transfer of an electron from the K to the benzophenone. Thus *in-situ* generated radical anion is easily attached to the lateral walls of the CNTs to produce diphenylcarbinol-modified SWNTs [146].

Photochemical and thermal approaches are also explored for the effective covalent modification of CNTs using free radicals. Aryl and Alkyl peroxides were dissociated by heating, and the generated free radicals were attached to the graphitic units [147]. For example the reaction of CNTs with glutaric or succinic acid in the presence of acyl peroxides generated carboxyalkyl free radicals which are added successfully onto the lateral walls. These acid-modified CNTs can then be transformed into various kinds of important substrates. Attachments of perfluoroalkyl free radicals on

CNTs were achieved by photoinitiated processes [148]. Under irradiation of light with a proper wavelength an alkyl iodide dissociated homolytically to yield the free radical. Besides, a silylation approach was established by the Wong and the research group for the attachment of silanes to the SWCNTs. Such as hexaphenyldisilane and trimethoxysilane can be added to SWCNTs using the irradiation of UV light. This process is also known as a photo-initiated free radical reaction approach [149].

6.1.5 Modification Through the Grafting of Polymers

The presence of non-covalent interactions between the CNTs and polymers has been widely explored using various groups. Several findings about the non-covalent polymer-CNT composites have significantly progressive field of research [150, 151]. In contrast, the covalent interactions of polymers with CNTs are similarly significant as the long polymeric chains support to solubilization the CNTs into an extensive range of media even when there is a very little amount of modification. Two primary approaches have been so far opted for the formation of covalent linkages of polymeric chains to the superficial graphitic structures of CNTs, which are known as "grafting from" and "grafting to" approaches (Fig. 4).

The "grafting from" approach is centred on the immobilization of the polymer precursors onto the main backbone of CNTs and afterwards the polymerization reactions and elongation of polymer chains in the presence of the monomers. In this approach, the macromolecules produce at the outwards of CNTs [152, 153]. For example, Qin et al. described polystyrenesulfonate grafting on the surface of CNTs through *in-situ* free radical polymerization [154]. An analogous design was used by Viswanathan et al. Using *in-situ* anionic polymerization they have incorporated the polystyrene chains to the raw CNTs [155]. The pristine CNTs were treated with secondary-butyllithium, to introduce carbanion moieties on the surface and origins the exfoliation of the bundles. Afterwards, once monomers are supplied, the CNT-carbanions starts the polymerization leading covalent grafting of the polystyrene.

The "grafting to" approach depend on the synthesis of a macromolecule having reactive functionalities and succeeding formation of covalent linkage between the synthesized polymer chain and the surface of CNTs using coupling reactions. For instance, in monochlorobenzene solvent, poly(methyl methacrylate) (pMMa) react with CNTs using ultrasonication method [156]. In another example, Wu et al. used poly(vinylcarbozole) or poly(butadiene) and treated them using NaOH or Bu-Li to produce the macromolecular anions and afterwards grafted them with CNTs [157]. Otherwise, CNTs can be functionalized with n-Bu-Li and consequently can be attached with halogenated polymers which was suggested by the Blau group [158]. Besides, various other reactions including radical coupling [159] or cycloaddition [160] can be utilized to graft the chains of some macromolecules on the surface of to CNTs.

The polymeric chains can be grafted on CNTs using another polymerization technique known as atomic transfer radical polymerization (ATRP) [108]. ATRP involves

the usage of initiators which are restrained covalently on the backbone of CNTs. In this case the backbone of CNTs acts as a grafting agent. Adronov et al. used an initiator which were very effective towards the polymerization of MMa and t-Bu-acrylate. Nevertheless, these kinds of polymerization reactions were not controlled and produce macromolecules with high molecular weight. Thus, the authors recommended that, if the polymerization time increased, there is an increment in mass. As a result there is an increment in the number of nanotube-immobilized macro-initiators which cause the rapid and uncontrolled elongation of the polymer chains [108].

The synthesis of various nanocomposites including *in-situ* Ziegler–Natta catalyst assisted polymerization of ethylene [161] or formation of nanotube-polyaniline composites [162] on CNTs was also explored. Though, the proper mechanism for the formation and the interactions present in the nanotube-polymer composites is still to be invented.

6.1.6 Modification Using Electrophilic Additions

Among the various process of the modification of CNTs the electrophilic addition is a well-established one. In this regard the electrophilic addition of chloroform to SWCNTs was explored by Prato et al. This addition was carried out in presence of a Lewis acid afterward a hydrolysis leading to the addition of -OH units to the exterior of CNTs [163]. Additional esterification using propionyl chloride developed corresponding esters. This ester functinalized SWCNTs demonstrates a greater water solubility and thus characterization of their structure become easy. Further multipurpose electronic addition to CNTs was accomplished by Balaban et al. Friedel–Crafts reaction condition was applied to produce polyacylate nanotubes [164]. This modification restricts CNTs to become soluble in typical organic media. The overview of this approach permits the effective penetration not only of standard acyl chains but also of perfluorinated acyl remainders (Fig. 4).

6.1.7 Modification Through Nucleophilic Additions

Nucleophilic substitution reactions to modify CNTs have been reported first by Hirsch and co-workers. Thus they have attached carbenes to the CNTs [124]. In many cases the zwitterionic products were obtained instead of the cyclopropane moieties (Fig. 4). The functionalized CNTs have good solubility in DMSO and can be investigated using mass spectroscopy. Basiuk et al. explored nucleophilic addition of octadecylamine to CNTs [105]. A direct amination method was adopted in this case. This amination was taken place in the five member rings of the graphitic structures, whereas the six membered aromatic rings are inert towards the addition. The lateral walls of the CNTs must possess several five membered rings as defects so that they can be functionalized using octadecylamine to a comparatively higher amount. Another example of a nucleophilic addition [165]. They have treated primeval CNTs with secondary-Butyl Li and afterwards with CO_2 [166]. In this case the pristine

CNTs were observed to be functionalized with both carboxylic and alkyl groups. The resultant carboxylic and alkyl functionalized CNTs can be separately dispersed in aqueous media opting a conc. of 0.5 mg/mL.

6.1.8 Ozonolysis: A Simple Approach

SWNTs in presence of CH_3OH undergoes ozonolysis at bother at room temperature [167] and at elevated temperature like 78 °C [165] then a precised modification can also be carried out. The action of various reactants like $NaBH_4$, H_2O_2, and DMS on SWNT-ozonides produce a large amount of various functional groups (–COOH, –COOR, –CHO, > CO, and –OH) on the surface of CNTs (Fig. 4). These reactive functionalities can further be modified to develop CNTs with anticipated functionalization. In this regards Banerjee et al. reported that the reactivity of lateral wall of CNTs towards ozonation depends on the diameter of CNTs [168]. CNTs with comparatively smaller diameter have high energy of strain per carbon atom because of high curvature and larger rehybridization energy. Therefore they demonstrate greater affinity towards the ozonolysis in solution-phase.

6.2 Chemical Modification Strategies of Graphene

The preparation of graphene is carried out in various processes like chemically, thermally, or photochemically by the reduction of graphene oxide. However, dispersion of graphene oxide without stabilizer are not possible, it can easily precipitate out as graphite particles because it has inherent rapid and irreversible aggregation property. Therefore, need to covalent or non-covalent functionalization through surface modification of graphene oxide sheet by reduction process [169]. In this process, organic solvent dispersible functionalized graphene sheets can be produced by the reduction of alkylamine-modified graphene oxide. Also, in this process carboxylic or sulfonate groups inducing GO produce water dispersion of functionalized graphene sheets [169]. However, in this dispersible graphene oxide has been also synthesized directly from natural graphite. Also, it has been synthesized electrochemically by modification of ionic liquid [170, 171]. Several different techniques have also been said for the guidance of strong dispersion of non-functionalized graphene with excessive yields [172].

6.2.1 Modification of Graphene Using Covalent Functionalizations

In this section, we focus completely on the covalent functionalization of the graphene structure. The modification of the graphene framework can only occur at the end of the sheet or the surface of the sheet. After functionalization of surface structure, the hybridization of one or more sp^2 carbon atoms can change into sp^3 hybridization

[173]. The modification or functionalization of grapheme framework can be accomplished by four different methods: nucleophilic substitution, electrophilic addition, and condensation (Fig. 6).

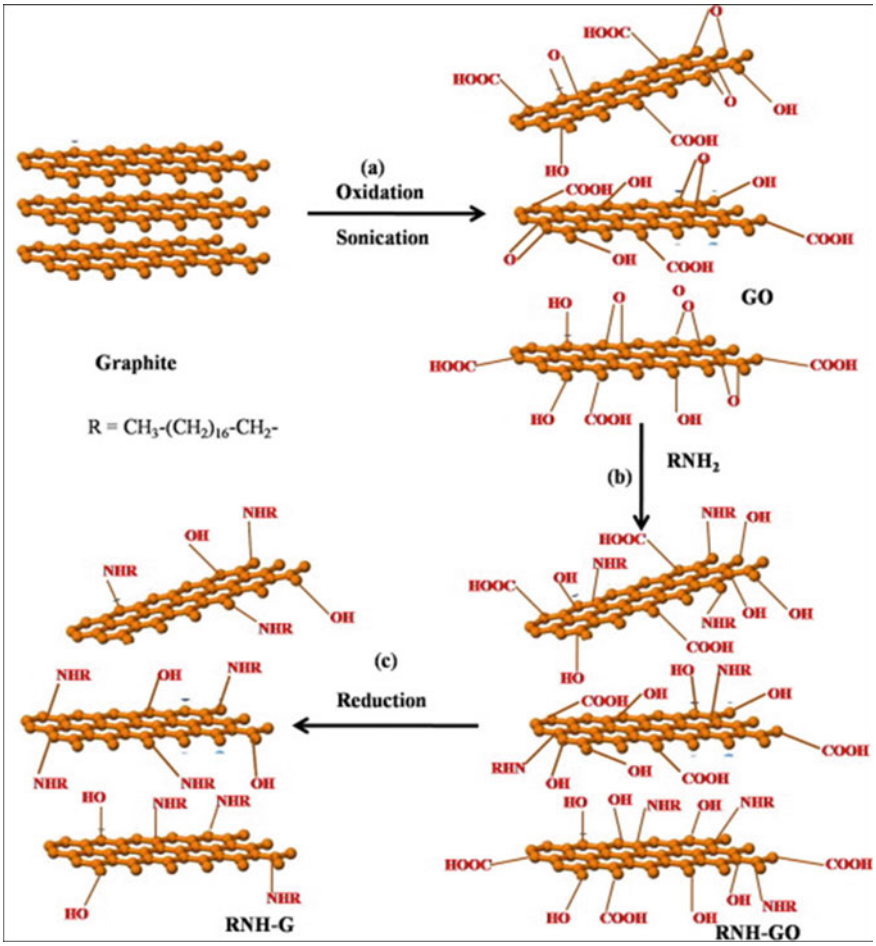

Fig. 6 An easy pathway for the synthesis procedure of graphene sheets from graphite: **a** Oxidation process of normal graphite flake to form graphite oxide (GO), **b** an aqueous dispersed solution of GO is reacted with alkylamine to produce amine-functionalized GO (RNH-GO); **c** RNH-GO is subsequently reduced utilizing hydrazine to synthesize amine-functionalized graphene (RNH-G). (Reproduced from [180])

6.2.2 Nucleophilic Substitution Reactions

For the nucleophilic substitution reaction, here epoxide group of the graphene oxide (GO) is the main reactive site. Basically, lone pair of amine groups can attack the epoxide group of the GO. The main advantage of the nucleophilic substitution reaction occurs at room temperature and in a water medium. Therefore, it is a good method for the preparation of large-scale surface modification of graphene. Accordingly, the preparation of functionalized graphene by use of various aliphatic or aromatic compounds like amino acids, ionic liquids, aromatic amines, small molecular weight polymers, etc., [174–177].

Bourlinos et al. reported surface-modified graphite oxide by the use of primary amine, $C_nH_{2n} + NH_2$ (n = 2, 4, 8, 12, 18) [178]. He has completed the grafting process at room temperature with $C_nH_{2n} + NH_2$ (n = 2, 4, 8, 12,) for small-chain primary amines and (n = 18) for long-chain amines with the heated of the reaction mixture for 24 h. After that XRD analysis exhibits interlayer distance of the amine-modified GO derivatives depending on the chain lengths of amine. Also, he represents the tilted orientation of GO which is due to the hydrophilic nature of the graphite oxide [179]. However, the reaction occurs in an alkaline medium of amino acid the single bond NH_2 end group is simply attached to the epoxide group of GO. From XRD evaluation indicates that the amino acid molecules adopt a flat alignment within the interlayer sector of GO. Another, Kuila et al. and Wang et al. have also reported the synthesis of organophilic graphene by use of dodecyl amine (DA) and octadecyal amine (ODA) [174]. Figure 6 is a schematic representation of the synthesis of alkyl amine-modified graphene.

6.2.3 Electrophilic Substitution Reaction

In order to electrophilic substitution reactions of graphene with the dissociation of H-atom occurs by an electrophile. For example, the surface modification of graphene by the grafting of aryl diazonium salt with the help of an electrophilic substitution reaction. Moreover, graphene surface can be grafted by the diazonium salt of para-nitro aniline [181]. Lomeda et al. and Zhu et al. reported organosoluble graphene, which can be prepared by the surface modification of graphene with aryl diazonium salt by electrophilic substitution [182, 183] Fig. 7 is a schematic representation of the functionalization of graphene by diazonium salt. In presence of hydrazine monohydrate the sodium dodecyl benzene sulfonate (SDBS) surfactant can be wrapped on the surface of GO by the reduction process at 80 °C for 24 h at a pH ~10. The formation of functionalized graphene is dispersible in DMF solvent with high extent. Another Sun et al. reported the edge-selective graphene functionalization with the help of diazonium salt of 4-bromo-aniline. For this modification it is more dispersible than virgin graphene. Microscopy data show that over 70% of the chemically modified graphene flakes are less than 5 layers thick [184]. Also Si and Samulski et al. reported various simplistic synthetic method for sulfonated graphene. These sulfonated graphene was showed electrical conductivity around 1250 S m^{-1}. From this, we can conclude that

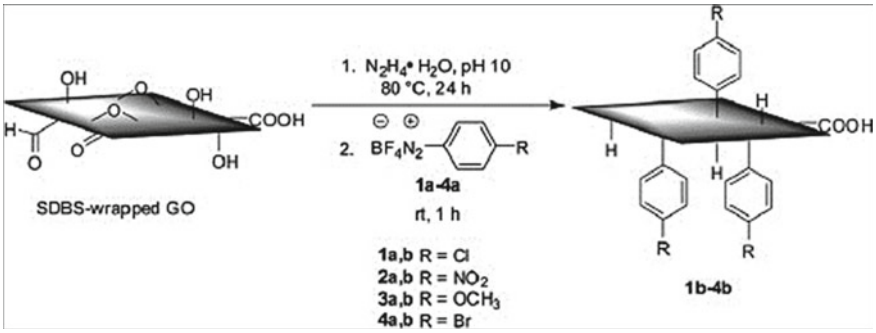

Fig. 7 Reduction modification of transitional SDBS-enfolded CCG with diazonium salts, starting with SDBS-enfolded GO. (Reproduced from [182])

the sulfonated graphene show higher electrical conductivity than other functionalized graphenes [185].

In recent times, Avinash et al. have established Friedel–Crafts acylation of GO by Ferrocene. The preparation of covalently-bonded ferrocene-GO hybrid materials by the reaction of solid phase alumina and trifluoroacetic anhydride at room temperature [186]. Another, Pham et al. reported solvothermal process, this is the new idea for the preparation of functionalization of graphene by using graphene oxide (GO) and *N*-Methyl-2-Pyrrolidone (NMP) as starting materials [187]. During this process NMP can produce free radical, which can assist the functionalization of graphene by aryl diazonium salts. With increase in reaction time it was found that the conjugation of C = C in graphene increases. That's why the dispersible property increases with DMF, NMP, polycarbonate (PC), THF, and ethanol solvent. Also, electrical conductivity value increases which was found to be ~21,600 S m^{-1} at room temperature [188].

6.2.4 Condensation Reactions

In order to condensation reaction, two molecules combine together to form a single molecule with a decrease of entropy. In these case for graphene, condensation reaction takes place with isocyanates, diisocyanates, and amine compounds to form amide and carbamate ester bonds. Stankovich et al. reported various types of isocyanate series compounds for the surface functionalization of graphene oxide [189]. Figure 8 depicts the formation of isocyanate-modified graphene oxide. This reaction takes place when solid isocyanate and graphene oxide dissolve in DMF under an inert atmosphere. After completion of the reaction, the isocyanide-modified GO dispersed in DMF and it is suitable for polymer nanocomposites preparation [190].

Parallelly like isocyanate, diisocyanate is also more important for the functionalization and crosslinking of graphene oxide [191]. The surface modification of graphene oxide by organic diisocyanate through the grafting process can be achieved by activation of the carboxylic acid group of graphene oxide using thionyl chloride.

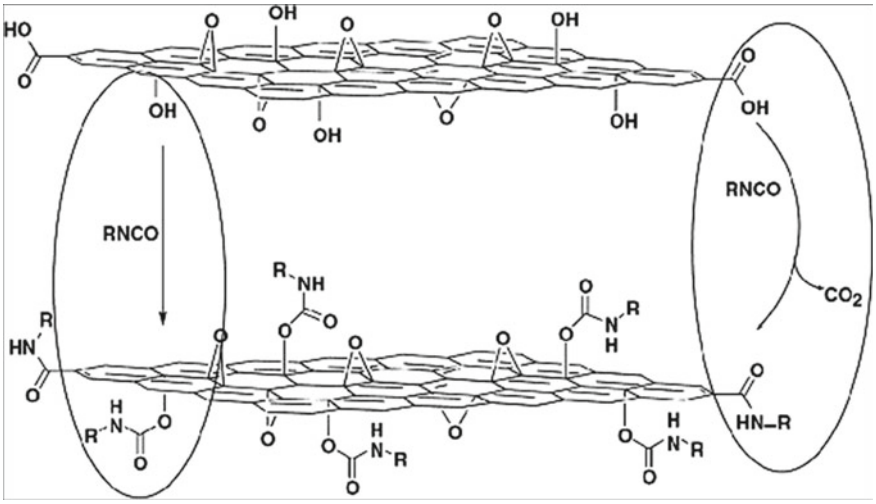

Fig. 8 Anticipated reactions during the action of on isocyanate GO, in which organic isocyanates react with the –OH (left oval) and –COOH (right oval) of GO to form carbamate and amide functional groups, correspondingly. (Reproduced from [189])

Upon functionalization the formation of amide bond between amine ($–NH_2$) functional group of diisocyante and carbonyl chloride (–COCl) functional groups of activated graphene oxide. The formation of product G-CO $NH(CH_2)_{17}CH_3$ is highly dispersible in THF and also soluble in CCl_4 and DCM [192]. Also, Worsley et al. suggested that the functionalized graphene can be produced by the reaction between tetramethylethylenediamine (TMEDA) and graphite fluoride in hexane medium at 0 °C [193]. After that, the reaction was continued for 3 days and then it was quenched with isopropanol and ethanol. The subsequent can be well dispersed in halogenated solvents like dichlorobenzene, DCM, and THF.

6.2.5 Noncovalent Functionalization

In this noncovalent functionalization is mainly induced by various physical interactions such as van der Waals force, hydrophobic interaction as well as electrostatic forces and also physical adsorption. So this functionalization is accomplished by polymer wrapping, adsorption of surfactants or small aromatic molecules, and interaction with porphyrins or biomolecules such as deoxyribonucleic acid (DNA) and peptides. Basically, this technique is most useful for the preparation of surface functionalized carbon-based nano-materials [194, 195]. Previously this technique has been used mostly in the surface functionalized of the sp^2 framework of carbon nanotubes. In the current research appearances that the same skill can be applied on the graphene using various type of organic modifiers [196–201].

Firstly, Stankovich et al. proposed poly(sodium 4-styrene sulfonate) (PSS) for the preparation of graphitic nanoplatelets by noncovalent functionalization way [202]. In presence of poly(sodium 4-styrenesulfonate) the formation of noncovalent-functionalized graphitic nanoplatelets can be highly dispersed in a water medium. Moreover, the stable dispersion formed by the use of surface modifier sulfonated polyaniline (SPANI). Due to its well electrical and electrochemical property it can be shown acceptable electrical conductivity (30 S m^{-1}) and exceptional electrochemical properties [203].

7 Conclusion and Future Out-Scope

Biomass has been recognised as a substitute, easy available, cheap, and renewable source of carbon for the production of various CNMs. It is informed that the generated CNMs and their specific features differ depending upon the types of biomass used. This indicates that the nature of the biomass and its analogous amorphous carbon plays an important role. Therefore, proper choice of an appropriate biomass and modification the properties of the analogous amorphous carbons to generate more suitable amorphous carbon starting materials for the successful generation of CNMs is a main fact. This chapter has summarized about the current advances in synthesis CNMs from biomass. In the starting part we have studied the recent literatures available and categorised the CNMs. In the second part we have discussed about the synthesis procedures of various CNMs from biomass including graphene, CNT, CNF, and so on. Furthermore, we have also tried to accumulate various surface functionalization procedures of CNTs and graphene. In view of the effectiveness of surface-functionalized CNMs, more research should be carried out to develop various easy and favourable approaches for reproducible, well-regulated, and large-scale modification of CNMs for various applications. The polymeric surface functionalizations may alter the stability, non-toxicity, and tissue reformative features of CNMs where the shape, charge, building units, size, structure, and contact angle with various solvents of the CNMs have a great influence. Using the surface modification of CNMs using some important biomaterials through non-covalent or covalent interactions the field of nanomedicine enriched. To extend the possibility of bio-applications of the CNMs, furthermore investigation is needed on the surface functionalizations and its effects in various biological and biomedical applications. The serious issue restricting the investigation of nanomedicine is the uncertainty in the real interactions between CNMs and the biological moieties. A clear knowledge on the actions of the nanomaterial, interactions with the biological entities, and clear mechanism of interactions could simplify the use of them in future.

References

1. Kroto H, Heath J, O'Brien S, Curl R, Smalley R (1985) Buckminsterfullerene. Nature 318:162–163. https://doi.org/10.1038/318162a0. GoogleScholarThereisnocorrespondingrecordforthisreference
2. Cha C, Shin SR, Annabi N, Dokmeci MR, Khademhosseini A (2013) Carbon-based nanomaterials: multifunctional materials for biomedical engineering. ACS Nano 7:2891–2897
3. Hwang J-Y, Kim H-S, Kim JH, Shin US, Lee S-H (2015) Carbon nanotube nanocomposites with highly enhanced strength and conductivity for flexible electric circuits. Langmuir 31:7844–7851
4. Llobet E (2013) Gas sensors using carbon nanomaterials: a review. Sens Actuat B Chem 179:32–45
5. Lee WJ, Maiti UN, Lee JM, Lim J, Han TH, Kim SO (2014) Nitrogen-doped carbon nanotubes and graphene composite structures for energy and catalytic applications. Chem Commun 50:6818–6830
6. Guldi DM, Sgobba V (2011) Carbon nanostructures for solar energy conversion schemes. Chem Commun 47:606–610
7. Yang L, Zhang L, Webster TJ (2011) Carbon nanostructures for orthopedic medical applications. Nanomedicine 6:1231–1244
8. Lahiri I, Das S, Kang C, Choi W (2011) Application of carbon nanostructures—energy to electronics. Jom 63:70–76
9. Liu Y, Kumar S (2012) Recent progress in fabrication, structure, and properties of carbon fibers. Polym Rev 52:234–258
10. Mhlanga S, Coville N, Iyuke S, Afolabi A, Abdulkareem A, Kunjuzwa N (2010) Controlled syntheses of carbon spheres in a swirled floating catalytic chemical vapour deposition vertical reactor. J Exp Nanosci 5:40–51
11. Stamatin I, Morozan A, Dumitru A, Vulpe S (2005) Highly oriented carbon ribbons for advanced multifunctional material engineering. Fullerenes Nanotubes Carbon Nanostruct 13:543–551
12. Mugadza K, Nyamori VO, Mola GT, Simoyi RH, Ndungu PG (2017) Low temperature synthesis of multiwalled carbon nanotubes and incorporation into an organic solar cell. J Exp Nanosci 12:363–383
13. Bai S, Li F, Yang Q, Cheng H-M, Bai J (2003) Influence of ferrocene/benzene mole ratio on the synthesis of carbon nanostructures. Chem Phys Lett 376:83–89
14. Nyamori VO, Coville NJ (2007) Effect of ferrocene/carbon ratio on the size and shape of carbon nanotubes and microspheres. Organometallics 26:4083–4085
15. Sevilla M, Martinez-de Lecea CS, Valdés-Solís T, Morallón E, Fuertes A (2008) Solid-phase synthesis of graphitic carbon nanostructures from iron and cobalt gluconates and their utilization as electrocatalyst supports. Phys Chem Chem Phys 10:1433–1442
16. Mutuma BK, Matsoso B, Ranganathan K, Wamwangi D, Coville NJ (2016) Generation of open-ended, worm-like and graphene-like structures from layered spherical carbon materials. RSC Adv 6:20399–20408
17. Kairi MI, Khavarian M, Bakar SA, Vigolo B, Mohamed AR (2018) Recent trends in graphene materials synthesized by CVD with various carbon precursors. J Mater Sci 53:851–879
18. Yadav MD, Dasgupta K, Patwardhan AW, Joshi JB (2017) High performance fibers from carbon nanotubes: synthesis, characterization, and applications in composites: A Review. Ind Eng Chem Res 56:12407–12437
19. Bridgwater A, Bridge S (1991) A review of biomass pyrolysis and pyrolysis technologies. In: Biomass pyrolysis liquids upgrading and utilization, pp 11–92
20. Zhu M, Diao G (2011) Review on the progress in synthesis and application of magnetic carbon nanocomposites. Nanoscale 3:2748–2767
21. Roy A, Maity CK (2021) Nanostructured 2D materials for biomedical, nano bioengineering, and nanomechanical devices. In: Advanced applications of 2D nanostructures. Springer, pp 211–29

22. Roy A, Maity CK (2022) Defective carbon nanostructures for biomedical application. In: defect engineering of carbon nanostructures. Springer, pp 1–34
23. Grausova L, Vacik J, Vorlicek V, Svorcik V, Slepicka P, Bilkova P et al (2009) Fullerene C60 films of continuous and micropatterned morphology as substrates for adhesion and growth of bone cells. Diam Relat Mater 18:578–586
24. Stankova L, Fraczek-Szczypta A, Blazewicz M, Filova E, Blazewicz S, Lisa V et al (2014) Human osteoblast-like MG 63 cells on polysulfone modified with carbon nanotubes or carbon nanohorns. Carbon 67:578–591
25. Verdanova M, Rezek B, Broz A, Ukraintsev E, Babchenko O, Artemenko A et al (2016) Nanocarbon allotropes—graphene and nanocrystalline diamond—promote cell proliferation. Small 12:2499–2509
26. Roy A, Manna K, Ray PG, Dhara S, Pal S (2022) β-Cyclodextrin-based ultrahigh stretchable, flexible, electro-and pressure-responsive, adhesive, transparent hydrogel as motion sensor. ACS Appl Mater Interfaces 14:17065–17080
27. Subramanian B, Agarwal T, Roy A, Parida S, Kundu B, Maiti TK et al (2020) Synthesis and characterization of PCL-DA: PEG-DA based polymeric blends grafted with SMA hydrogel as bio-degradable intrauterine contraceptive implant. Mater Sci Eng C 116:111159
28. Manna K, Patra P, Roy A, Roy RK, Chaitanya Sunka K, Dhara S, et al (2022) Amino acid inspired alginate-based ph sensitive polymeric micelles via reversible addition–fragmentation chain transfer polymerization. ACS Appl Polym Mater
29. Roy A, Guha Ray P, Manna K, Banerjee C, Dhara S, Pal S (2021) Poly (N-vinyl imidazole) cross-linked β-Cyclodextrin hydrogel for rapid hemostasis in severe renal arterial hemorrhagic model. Biomacromolecules 22:5256–5269
30. Fang M, Zeisberg W-M, Condon C, Ogryzko V, Danchin A, Mechold U (2009) Degradation of nanoRNA is performed by multiple redundant RNases in Bacillus subtilis. Nucleic Acids Res 37:5114–5125
31. Roy A, Samanta S, Singha K, Maity P, Kumari N, Ghosh A et al (2020) Development of a thermoresponsive polymeric composite film using cross-linked β-cyclodextrin embedded with carbon quantum dots as a transdermal drug carrier. ACS Appl Bio Mater 3:3285–3293
32. Kim YT, Han JH, Hong BH, Kwon YU (2010) Electrochemical synthesis of CdSe quantum-dot arrays on a graphene basal plane using mesoporous silica thin-film templates. Adv Mater 22:515–518
33. Wang J, Lin M, Yan Y, Wang Z, Ho PC, Loh KP (2009) CdSe/AsS core−shell quantum dots: preparation and two-photon fluorescence. J Am Chem Soc 131:11300–11301
34. Stouwdam JW, Janssen RA (2008) Red, green, and blue quantum dot LEDs with solution processable ZnO nanocrystal electron injection layers. J Mater Chem 18:1889–1894
35. Mokerov V, Fedorov YV, Velikovski L, Scherbakova MY (2001) New quantum dot transistor. Nanotechnology 12:552
36. Ustinov V, Zhukov A, Kovsh A, Mikhrin S, Maleev N, Volovik B et al (2000) Long-wavelength quantum dot lasers on GaAs substrates. Nanotechnology 11:397
37. Liu Q, Sun J, Gao K, Chen N, Sun X, Ti D et al (2020) Graphene quantum dots for energy storage and conversion: from fabrication to applications. Mater Chem Front 4:421–436
38. Lee W, Kang SH, Kim J-Y, Kolekar GB, Sung Y-E, Han S-H (2009) TiO2 nanotubes with a ZnO thin energy barrier for improved current efficiency of CdSe quantum-dot-sensitized solar cells. Nanotechnology 20:335706
39. Kuchibhatla SV, Karakoti A, Bera D, Seal S (2007) One dimensional nanostructured materials. Prog Mater Sci 52:699–913
40. Iijima S (1991) Helical microtubules of graphitic carbon. Nature 354, 56–58
41. Li G-R, Feng Z-P, Zhong J-H, Wang Z-L, Tong Y-X (2010) Electrochemical synthesis of polyaniline nanobelts with predominant electrochemical performances. Macromolecules 43:2178–2183
42. Xia H, Feng J, Wang H, Lai MO, Lu L (2010) MnO2 nanotube and nanowire arrays by electrochemical deposition for supercapacitors. J Power Sources 195:4410–4413

43. Bae S, Kim H, Lee Y, Xu X, Park J-S, Zheng Y et al (2010) Roll-to-roll production of 30-inch graphene films for transparent electrodes. Nat Nanotechnol 5:574–578
44. Kim KS, Zhao Y, Jang H, Lee SY, Kim JM, Kim KS, et al (2009) Large-scale pattern growth of graphene films for stretchable transparent electrodes. Nature 457:706–710
45. Pradhan D, Leung K (2008) Vertical growth of two-dimensional zinc oxide nanostructures on ITO-coated glass: effects of deposition temperature and deposition time. J Phys Chem C 112:1357–1364
46. Chen H, Cong TN, Yang W, Tan C, Li Y, Ding Y (2009) Progress in electrical energy storage system: a critical review. Prog Nat Sci 19:291–312
47. Kamarudin SK, Achmad F, Daud WRW (2009) Overview on the application of direct methanol fuel cell (DMFC) for portable electronic devices. Int J Hydrogen Energy 34:6902–6916
48. Roy A, Guha Ray P, Bose A, Dhara S, Pal S (2022) pH-responsive copolymeric network gel using methacrylated β-Cyclodextrin for controlled codelivery of hydrophilic and hydrophobic drugs. ACS Appl Bio Mater 5:3530–3543
49. Roy A, Manna K, Pal S (2022) Recent advances in various stimuli-responsive hydrogels: from synthetic designs to emerging healthcare applications. Mater Chem Front
50. Dey S, Roy A, Manna K, Pal S (2022) The UCST phase transition of a dextran based copolymer in aqueous media with tunable thermoresponsive behavior. Polym Chem 13:3865–3869
51. Shen Q, Jiang L, Zhang H, Min Q, Hou W, Zhu J-J (2008) Three-dimensional dendritic Pt nanostructures: sonoelectrochemical synthesis and electrochemical applications. J Phys Chem C 112:16385–16392
52. Lee H, Habas SE, Kweskin S, Butcher D, Somorjai GA, Yang P (2006) Morphological control of catalytically active platinum nanocrystals. Angew Chem Int Ed 45:7824–7828
53. Roy A, Maity PP, Bose A, Dhara S, Pal S (2019) β-Cyclodextrin based pH and thermo-responsive biopolymeric hydrogel as a dual drug carrier. Mater Chem Front 3:385–393
54. Terrones M, Botello-Méndez AR, Campos-Delgado J, López-Urías F, Vega-Cantú YI, Rodríguez-Macías FJ et al (2010) Graphene and graphite nanoribbons: morphology, properties, synthesis, defects and applications. Nano Today 5:351–372
55. Kaltschmitt M (2019) Renewable energy from biomass: introduction. In: Energy from Organic Materials (Biomass). Springer, pp 1–14
56. Vassilev SV, Baxter D, Andersen LK, Vassileva CG, Morgan TJ (2012) An overview of the organic and inorganic phase composition of biomass. Fuel 94:1–33
57. Yokoyama S, Matsumura Y (2008) The Asian biomass handbook: a guide for biomass production and utilization. Japan Instit Energy 1:61–62
58. Xu F, Zhong X, Sun R, Jones G (2005) Lignin distribution and ultrastructure of Salix psammophila. Trans Chin Pul Pap 20:6–9
59. Chen H (2014) Chemical composition and structure of natural lignocellulose. In: Biotechnology of lignocellulose. Springer pp 25–71
60. Goodell B, Xie X, Qian Y, Daniel G, Peterson M, Jellison J (2008) Carbon nanotubes produced from natural cellulosic materials. J Nanosci Nanotechnol 8:2472–2474
61. Bazaka K, Jacob MV, Ostrikov K (2016) Sustainable life cycles of natural-precursor-derived nanocarbons. Chem Rev 116:163–214
62. Qu J, Luo C, Cong Q, Yuan X (2012) Carbon nanotubes and Cu–Zn nanoparticles synthesis using hyperaccumulator plants. Environ Chem Lett 10:153–158
63. Watt W, Perov B (1985) Strong fibres. Elsevier Science Limited
64. Demirbas A, Arin G (2002) An overview of biomass pyrolysis. Energy Sources 24:471–482
65. Gupta V, Carrott P, Singh R, Chaudhary M, Kushwaha S (2016) Cellulose: a review as natural, modified and activated carbon adsorbent. Biores Technol 216:1066–1076
66. Karimi K, Taherzadeh MJ (2016) A critical review of analytical methods in pretreatment of lignocelluloses: composition, imaging, and crystallinity. Biores Technol 200:1008–1018
67. Mugadza K, Stark A, Ndungu PG, Nyamori VO (2020) Synthesis of carbon nanomaterials from biomass utilizing ionic liquids for potential application in solar energy conversion and storage. Materials 13:3945

68. Prasek J, Drbohlavova J, Chomoucka J, Hubalek J, Jasek O, Adam V et al (2011) Methods for carbon nanotubes synthesis. J Mater Chem 21:15872–15884
69. Gan L, Geng A, Xu L, Chen M, Wang L, Liu J et al (2018) The fabrication of bio-renewable and recyclable cellulose based carbon microspheres incorporated by CoFe2O4 and the photocatalytic properties. J Clean Prod 196:594–603
70. Abdalla S, Al-Marzouki F, Al-Ghamdi AA, Abdel-Daiem A (2015) Different technical applications of carbon nanotubes. Nanoscale Res Lett 10:1–10
71. Lekawa-Raus A, Patmore J, Kurzepa L, Bulmer J, Koziol K (2014) Electrical properties of carbon nanotube based fibers and their future use in electrical wiring. Adv Func Mater 24:3661–3682
72. Chu K, Guo H, Jia C, Yin F, Zhang X, Liang X et al (2010) Thermal properties of carbon nanotube–copper composites for thermal management applications. Nanoscale Res Lett 5:868–874
73. Gharbavi K, Badehian H (2015) Optical properties of armchair (7, 7) single walled carbon nanotubes. AIP Adv 5:077155
74. Sun D-M, Timmermans MY, Tian Y, Nasibulin AG, Kauppinen EI, Kishimoto S, et al (2011) Flexible high-performance carbon nanotube integrated circuits. Nat Nanotechnol 6:156–161
75. Marconnet AM, Panzer MA, Goodson KE (2013) Thermal conduction phenomena in carbon nanotubes and related nanostructured materials. Rev Mod Phys 85:1295
76. De Volder MF, Tawfick SH, Baughman RH, Hart AJ (2013) Carbon nanotubes: present and future commercial applications. Science 339:535–539
77. Vivekanandhan S, Schreiber M, Muthuramkumar S, Misra M, Mohanty AK (2017) Carbon nanotubes from renewable feedstocks: A move toward sustainable nanofabrication. J Appl Polym Sci 134
78. Qu J, Luo C, Cong Q (2011) Synthesis of multi-walled carbon nanotubes/ZnO nanocomposites using absorbent cotton. Nano-Micro Lett 3:115–120
79. Osman AI, Farrell C, Al-Muhtaseb A, Harrison J, Rooney DW (2010) The production and application of carbon nanomaterials from high alkali silicate herbaceous biomass. Sci Rep 10:1–13
80. Bernd MGS, Bragança SR, Heck N, da Silva Filho LC (2017) Synthesis of carbon nanostructures by the pyrolysis of wood sawdust in a tubular reactor. J Market Res 6:171–177
81. Shi K, Yan J, Lester E, Wu T (2014) Catalyst-free synthesis of multiwalled carbon nanotubes via microwave-induced processing of biomass. Ind Eng Chem Res 53:15012–15019
82. Zhu J, Jia J, Kwong FL, Ng DHL, Tjong SC (2012) Synthesis of multiwalled carbon nanotubes from bamboo charcoal and the roles of minerals on their growth. Biomass Bioenergy 36:12–19
83. Skoda M, Dudek I, Jarosz A, Szukiewicz D (2014) Graphene: one material, many possibilities—application difficulties in biological systems. J Nanomater 2014
84. Geim AK (2009) Graphene: status and prospects. Science 324:1530–1534
85. Abergel D, Apalkov V, Berashevich J, Ziegler K, Chakraborty T (2010) Properties of graphene: a theoretical perspective. Adv Phys 59:261–482
86. Mombeshora ET, Ndungu PG, Nyamori VO (2017) Effect of graphite/sodium nitrate ratio and reaction time on the physicochemical properties of graphene oxide. New Carbon Mater 32:174–187
87. Primo A, Atienzar P, Sanchez E, Delgado JM, García H (2012) From biomass wastes to large-area, high-quality, N-doped graphene: catalyst-free carbonization of chitosan coatings on arbitrary substrates. Chem Commun 48:9254–9256
88. Shams SS, Zhang LS, Hu R, Zhang R, Zhu J (2015) Synthesis of graphene from biomass: a green chemistry approach. Mater Lett 161:476–479
89. Chen F, Yang J, Bai T, Long B, Zhou X (2016) Facile synthesis of few-layer graphene from biomass waste and its application in lithium ion batteries. J Electroanal Chem 768:18–26
90. Amiinu IS, Zhang J, Kou Z, Liu X, Asare OK, Zhou H et al (2016) Self-organized 3D porous graphene dual-doped with biomass-sponsored nitrogen and sulfur for oxygen reduction and evolution. ACS Appl Mater Interfaces 8:29408–29418

91. Chen LF, Huang ZH, Liang HW, Gao HL, Yu SH (2014) Three-dimensional heteroatom-doped carbon nanofiber networks derived from bacterial cellulose for supercapacitors. Adv Func Mater 24:5104–5111
92. Liu W-J, Tian K, Jiang H (2015) One-pot synthesis of Ni–NiFe 2 O 4/carbon nanofiber composites from biomass for selective hydrogenation of aromatic nitro compounds. Green Chem 17:821–826
93. Chen L-F, Huang Z-H, Liang H-W, Yao W-T, Yu Z-Y, Yu S-H (2013) Flexible all-solid-state high-power supercapacitor fabricated with nitrogen-doped carbon nanofiber electrode material derived from bacterial cellulose. Energy Environ Sci 6:3331–3338
94. Bartelmess J, Giordani S (2014) Carbon nano-onions (multi-layer fullerenes): chemistry and applications. Beilstein J Nanotechnol 5:1980–1998
95. Plonska-Brzezinska ME, Echegoyen L (2013) Carbon nano-onions for supercapacitor electrodes: recent developments and applications. J Mater Chem A 1:13703–13714
96. Ghosh M, Sonkar SK, Saxena M, Sarkar S (2011) Carbon nano-onions for imaging the life cycle of Drosophila melanogaster. Small 7:3170–3177
97. Tripathi PK, Durbach S, Coville NJ (2019) CVD Synthesis of solid, hollow, and nitrogen-doped hollow carbon spheres from polypropylene waste materials. Appl Sci 9:2451
98. Roberts AD, Li X, Zhang H (2014) Porous carbon spheres and monoliths: morphology control, pore size tuning and their applications as Li-ion battery anode materials. Chem Soc Rev 43:4341–4356
99. Ma X, Liu M, Gan L, Zhao Y, Chen L (2013) Synthesis of micro-and mesoporous carbon spheres for supercapacitor electrode. J Solid State Electrochem 17:2293–2301
100. Fan Y, Yang X, Zhu B, Liu P-F, Lu H-T (2014) Micro-mesoporous carbon spheres derived from carrageenan as electrode material for supercapacitors. J Power Sources 268:584–590
101. Pari G, Darmawan S, Prihandoko B (2014) Porous carbon spheres from hydrothermal carbonization and KOH activation on cassava and tapioca flour raw material. Procedia Environ Sci 20:342–351
102. Conroy D, Moisala A, Cardoso S, Windle A, Davidson J (2010) Carbon nanotube reactor: Ferrocene decomposition, iron particle growth, nanotube aggregation and scale-up. Chem Eng Sci 65:2965–2977
103. He C-L, Liu R, Li D-D, Zhu S-E, Wang G-W (2013) Synthesis and functionalization of [60] fullerene-fused imidazolines. Org Lett 15:1532–1535
104. Yurovskaya M, Trushkov I (2002) Cycloaddition to buckminsterfullerene C60: advancements and future prospects. Russ Chem Bull 51:367–443
105. Wu H-C, Chang X, Liu L, Zhao F, Zhao Y (2010) Chemistry of carbon nanotubes in biomedical applications. J Mater Chem 20:1036–1052
106. Liu J, Rinzler AG, Dai H, Hafner JH, Bradley RK, Boul PJ et al (1998) Fullerene pipes. Science 280:1253–1256
107. Riggs JE, Guo Z, Carroll DL, Sun Y-P (2000) Strong luminescence of solubilized carbon nanotubes. J Am Chem Soc 122:5879–5880
108. Yao Z, Braidy N, Botton GA, Adronov A (2003) Polymerization from the surface of single-walled carbon nanotubes−preparation and characterization of nanocomposites. J Am Chem Soc 125:16015–16024
109. Sun Y-P, Fu K, Lin Y, Huang W (2002) Functionalized carbon nanotubes: properties and applications. Acc Chem Res 35:1096–1104
110. Touhara H, Okino F (2000) Property control of carbon materials by fluorination. Carbon 38:241–267
111. Khabashesku VN, Billups WE, Margrave JL (2002) Fluorination of single-wall carbon nanotubes and subsequent derivatization reactions. Acc Chem Res 35:1087–1095
112. Mickelson E, Huffman C, Rinzler A, Smalley R, Hauge R, Margrave J (1998) Fluorination of single-wall carbon nanotubes. Chem Phys Lett 296:188–194
113. Kelly K, Chiang I, Mickelson E, Hauge R, Margrave J, Wang X et al (1999) Insight into the mechanism of sidewall functionalization of single-walled nanotubes: an STM study. Chem Phys Lett 313:445–450

114. An KH, Heo JG, Jeon KG, Bae DJ, Jo C, Yang CW et al (2002) X-ray photoemission spectroscopy study of fluorinated single-walled carbon nanotubes. Appl Phys Lett 80:4235–4237
115. Wilson SR, Cayetano V, Yurchenko M (2002) Advanced materials: fluorous fullerenes and nanotubes. Tetrahedron 58:4041–4047
116. Mickelson E, Chiang I, Zimmerman J, Boul P, Lozano J, Liu J et al (1999) Solvation of fluorinated single-wall carbon nanotubes in alcohol solvents. J Phys Chem B 103:4318–4322
117. Khabashesku VW, Billups WE, Margrave JL (2002) Fluorination of single-wall carbon nanotubes and subsequent derivatization reactions. Acc Chem Res 35:1087
118. Boul P, Liu J, Mickelson E, Human CB, Ericson LM, Chiang IW, Smith KA, Colbert DT, Hauge RH, Margrave JL, Smalley RE (1999) Fluorination of single-wall carbon nanotubes and subsequent derivatization reactions. Chem Phys Lett 35:310–367
119. Saini RK, Chiang IW, Peng H, Smalley R, Billups W, Hauge RH et al (2003) Covalent sidewall functionalization of single wall carbon nanotubes. J Am Chem Soc 125:3617–3621
120. Liu Y, Gu Z, Margrave JL, Khabashesku VN,Lobo FM, Rui JL, Margrave VN (2004) Functionalization of nanoscale diamond powder: fluoro-, alkyl-, amino-, and amino acid-nanodiamond derivatives. Chem Mater 16:2055
121. Stevens JL, Huang AY, Peng H, Chiang IW, Khabashesku VN, Margrave JL (2003) Sidewall amino-functionalization of single-walled carbon nanotubes through fluorination and subsequent reactions with terminal diamines. Nano Lett 3:331–336
122. Dresselhaus MS, Avouris P (2001) Introduction to carbon materials research. In: Carbon nanotubes. Springer pp 1–9
123. Chen Y, Haddon R, Fang S, Rao AM, Eklund P, Lee W et al (1998) Chemical attachment of organic functional groups to single-walled carbon nanotube material. J Mater Res 13:2423–2431
124. Holzinger M, Vostrowsky O, Hirsch A, Hennrich F, Kappes M, Weiss R et al (2001) Sidewall functionalization of carbon nanotubes. Angew Chem Int Ed 40:4002–4005
125. Holzinger M, Abraham J, Whelan P, Graupner R, Ley L, Hennrich F et al (2003) Functionalization of single-walled carbon nanotubes with (R-) oxycarbonyl nitrenes. J Am Chem Soc 125:8566–8580
126. Holzinger M, Steinmetz J, Samaille D, Glerup M, Paillet M, Bernier P et al (2004) [2+ 1] cycloaddition for cross-linking SWCNTs. Carbon 42:941–947
127. Hirsch A, Vostrowsky O (2005) Functionalization of carbon nanotubes. Funct Mol Nanostruct 193–237
128. Moghaddam MJ, Taylor S, Gao M, Huang S, Dai L, McCall MJ (2004) Highly efficient binding of DNA on the sidewalls and tips of carbon nanotubes using photochemistry. Nano Lett 4:89–93
129. Lee KM, Li L, Dai L (2005) Asymmetric end-functionalization of multi-walled carbon nanotubes. J Am Chem Soc 127:4122–4123
130. Georgakilas V, Kordatos K, Prato M, Guldi DM, Holzinger M, Hirsch A (2002) Organic functionalization of carbon nanotubes. J Am Chem Soc 124:760–761
131. Tagmatarchis N, Prato M (2004) Functionalization of carbon nanotubes via 1, 3-dipolar cycloadditions. J Mater Chem 14:437–439
132. Pantarotto D, Briand J-P, Prato M, Bianco A (2004) Translocation of bioactive peptides across cell membranes by carbon nanotubes. Chem Commun 16–17
133. Bianco A, Hoebeke J, Godefroy S, Chaloin O, Pantarotto D, Briand J-P et al (2005) Cationic carbon nanotubes bind to CpG oligodeoxynucleotides and enhance their immunostimulatory properties. J Am Chem Soc 127:58–59
134. Alvaro M, Atienzar P, de la Cruz P, Delgado JL, Garcia H, Langa F (2004) Sidewall functionalization of single-walled carbon nanotubes with nitrile imines. Electron transfer from the substituent to the carbon nanotube. J Phys Chem B 108:12691–71269
135. Lu X, Tian F, Xu X, Wang N, Zhang Q (2003) A theoretical exploration of the 1, 3-dipolar cycloadditions onto the sidewalls of (n, n) armchair single-wall carbon nanotubes. J Am Chem Soc 125:10459–10464

136. Delgado JL, de la Cruz P, Langa F, Urbina A, Casado J, Navarrete JTL (2004) Microwave-assisted sidewall functionalization of single-wall carbon nanotubes by Diels–Alder cycloaddition. Chem Commun 1734–1735
137. Lu X, Tian F, Wang N, Zhang Q (2002) Organic functionalization of the sidewalls of carbon nanotubes by Diels−Alder reactions: a theoretical prediction. Org Lett 4:4313–4315
138. Zhang W, Swager TM (2007) Functionalization of single-walled carbon nanotubes and fullerenes via a dimethyl acetylenedicarboxylate− 4-dimethylaminopyridine zwitterion approach. J Am Chem Soc 129:7714–7715
139. Mylvaganam K, Zhang L (2004) Nanotube functionalization and polymer grafting: an ab initio study. J Phys Chem B 108:15009–15012
140. Dyke CA, Stewart MP, Maya F, Tour JM (2004) Diazonium-based functionalization of carbon nanotubes: XPS and GC-MS analysis and mechanistic implications. Synlett 2004:155–160
141. Dyke CA, Tour JM (2003) Unbundled and highly functionalized carbon nanotubes from aqueous reactions. Nano Lett 3:1215–1218
142. Strano MS, Dyke CA, Usrey ML, Barone PW, Allen MJ, Shan H et al (2003) Electronic structure control of single-walled carbon nanotube functionalization. Science 301:1519–1522
143. Badhulika S, Tlili C, Mulchandani A (2014) Poly (3-aminophenylboronic acid)-functionalized carbon nanotubes-based chemiresistive sensors for detection of sugars. Analyst 139:3077–3082
144. Liang F, Sadana AK, Peera A, Chattopadhyay J, Gu Z, Hauge RH et al (2004) A convenient route to functionalized carbon nanotubes. Nano Lett 4:1257–1260
145. Pénicaud A, Poulin P, Derré A, Anglaret E, Petit P (2005) Spontaneous dissolution of a single-wall carbon nanotube salt. J Am Chem Soc 127:8–9
146. Chua T, Mariatti M, Azizan A, Rashid A (2009) Surface functionalization of multi-walled carbon nanotubes via electron reduction of benzophenone by potassium metal. J Alloy Compd 480:534–536
147. Peng H, Reverdy P, Khabashesku VN, Margrave JL (2003) Sidewall functionalization of single-walled carbon nanotubes with organic peroxides. Chem Commun 362–363
148. Umek P, Seo JW, Hernadi K, Mrzel A, Pechy P, Mihailovic DD et al (2003) Addition of carbon radicals generated from organic peroxides to single wall carbon nanotubes. Chem Mater 15:4751–4755
149. Hemraj-Benny T, Wong SS (2006) Silylation of single-walled carbon nanotubes. Chem Mater 18:4827–4839
150. Andrews R, Jacques D, Qian D, Rantell T (2002) Multiwall carbon nanotubes: synthesis and application. Acc Chem Res 35:1008–1017
151. Zhang J, Lee J-K, Wu Y, Murray RW (2003) Photoluminescence and electronic interaction of anthracene derivatives adsorbed on sidewalls of single-walled carbon nanotubes. Nano Lett 3:403–407
152. Shaffer M, Koziol K (2002) Polystyrene grafted multi-walled carbon nanotubes. Chem Commun 2074–2075
153. Sung JH, Kim HS, Jin H-J, Choi HJ, Chin I-J (2004) Nanofibrous membranes prepared by multiwalled carbon nanotube/poly (methyl methacrylate) composites. Macromolecules 37:9899–9902
154. Qin S, Qin D, Ford WT, Herrera JE, Resasco DE, Bachilo SM et al (2004) Solubilization and purification of single-wall carbon nanotubes in water by in situ radical polymerization of sodium 4-styrenesulfonate. Macromolecules 37:3965–3967
155. Viswanathan G, Chakrapani N, Yang H, Wei B, Chung H, Cho K et al (2003) Single-step in situ synthesis of polymer-grafted single-wall nanotube composites. J Am Chem Soc 125:9258–9259
156. Koshio A, Yudasaka M, Zhang M, Iijima S (2001) A simple way to chemically react single-wall carbon nanotubes with organic materials using ultrasonication. Nano Lett 1:361–363
157. Wu W, Zhang S, Li Y, Li J, Liu L, Qin Y et al (2003) PVK-modified single-walled carbon nanotubes with effective photoinduced electron transfer. Macromolecules 36:6286–6288

158. Blake R, Gun'ko YK, Coleman J, Cadek M, Fonseca A, Nagy JB et al (2004) A generic organometallic approach toward ultra-strong carbon nanotube polymer composites. J Am Chem Soc 126:10226–10227
159. Liu Y, Yao Z, Adronov A (2005) Functionalization of single-walled carbon nanotubes with well-defined polymers by radical coupling. Macromolecules 38:1172–1179
160. Qin S, Qin D, Ford WT, Resasco DE, Herrera JE (2004) Functionalization of single-walled carbon nanotubes with polystyrene via grafting to and grafting from methods. Macromolecules 37:752–757
161. Tong X, Liu C, Cheng HM, Zhao H, Yang F, Zhang X (2004) Surface modification of single-walled carbon nanotubes with polyethylene via in situ Ziegler-Natta polymerization. J Appl Polym Sci 92:3697–3700
162. Sainz R, Benito AM, Martínez MT, Galindo JF, Sotres J, Baró AM et al (2005) Soluble self-aligned carbon nanotube/polyaniline composites. Adv Mater 17:278–281
163. Tagmatarchis N, Georgakilas V, Prato M, Shinohara H (2002) Sidewall functionalization of single-walled carbon nanotubes through electrophilic addition. Chem Commun 2010–2011
164. Balaban TS, Balaban MC, Malik S, Hennrich F, Fischer R, Rösner H et al (2006) Polyacylation of single-walled nanotubes under Friedel-crafts conditions: an efficient method for functionalizing, purifying, decorating, and linking carbon allotropes. Adv Mater 18:2763–2767
165. Banerjee S, Wong SS (2002) Rational sidewall functionalization and purification of single-walled carbon nanotubes by solution-phase ozonolysis. J Phys Chem B 106:12144–12151
166. Chen S, Shen W, Wu G, Chen D, Jiang M (2005) A new approach to the functionalization of single-walled carbon nanotubes with both alkyl and carboxyl groups. Chem Phys Lett 402:312–317
167. Mawhinney DB, Naumenko V, Kuznetsova A, Yates JT, Liu J, Smalley R (2000) Infrared spectral evidence for the etching of carbon nanotubes: ozone oxidation at 298 K. J Am Chem Soc 122:2383–2384
168. Banerjee S, Wong SS (2004) Demonstration of diameter-selective reactivity in the sidewall ozonation of SWNTs by resonance Raman spectroscopy. Nano Lett 4:1445–1450
169. Fang M, Wang K, Lu H, Yang Y, Nutt S (2010) Single-layer graphene nanosheets with controlled grafting of polymer chains. J Mater Chem 20:1982–1992
170. Liu N, Luo F, Wu H, Liu Y, Zhang C, Chen J (2008) One-step ionic-liquid-assisted electrochemical synthesis of ionic-liquid-functionalized graphene sheets directly from graphite. Adv Func Mater 18:1518–1525
171. Matsuo Y, Sakai Y, Fukutsuka T, Sugie Y (2007) Preparation of pillared carbons by pyrolysis of silylated graphite oxide. Chem Lett 36:1050–1051
172. Hamilton CE, Lomeda JR, Sun Z, Tour JM, Barron AR (2009) High-yield organic dispersions of unfunctionalized graphene. Nano Lett 9:3460–3462
173. Park MJ, Lee JK, Lee BS, Lee Y-W, Choi IS, Lee S-G (2006) Covalent modification of multi-walled carbon nanotubes with imidazolium-based ionic liquids: effect of anions on solubility. Chem Mater 18:1546–1551
174. Kuila T, Bose S, Hong CE, Uddin ME, Khanra P, Kim NH et al (2011) Preparation of functionalized graphene/linear low density polyethylene composites by a solution mixing method. Carbon 49:1033–1037
175. Laaksonen P, Kainlauri M, Laaksonen T, Shchepetov A, Jiang H, Ahopelto J et al (2010) Interfacial engineering by proteins: exfoliation and functionalization of graphene by hydrophobins. Angew Chem Int Ed 49:4946–4949
176. Kang SM, Park S, Kim D, Park SY, Ruoff RS, Lee H (2011) Simultaneous reduction and surface functionalization of graphene oxide by mussel-inspired chemistry. Adv Func Mater 21:108–112
177. Cui Y, Kim SN, Jones SE, Wissler LL, Naik RR, McAlpine MC (2010) Chemical functionalization of graphene enabled by phage displayed peptides. Nano Lett 10:4559–4565
178. Bourlinos AB, Gournis D, Petridis D, Szabó T, Szeri A, Dékány I (2003) Graphite oxide: chemical reduction to graphite and surface modification with primary aliphatic amines and amino acids. Langmuir 19:6050–6055

179. Matsuo Y, Miyabe T, Fukutsuka T, Sugie Y (2007) Preparation and characterization of alkylamine-intercalated graphite oxides. Carbon 45:1005–1012
180. Kuila T, Bose S, Mishra AK, Khanra P, Kim NH, Lee JH (2012) Chemical functionalization of graphene and its applications. Prog Mater Sci 57:1061–1105
181. Bekyarova E, Itkis ME, Ramesh P, Berger C, Sprinkle M, de Heer WA et al (2009) Chemical modification of epitaxial graphene: spontaneous grafting of aryl groups. J Am Chem Soc 131:1336–1337
182. Lomeda JR, Doyle CD, Kosynkin DV, Hwang W-F, Tour JM (2008) Diazonium functionalization of surfactant-wrapped chemically converted graphene sheets. J Am Chem Soc 130:16201–16206
183. Zhu Y, Higginbotham AL, Tour JM (2009) Covalent functionalization of surfactant-wrapped graphene nanoribbons. Chem Mater 21:5284–5291
184. Sun Z, Kohama S-I, Zhang Z, Lomeda JR, Tour JM (2010) Soluble graphene through edge-selective functionalization. Nano Res 3:117–125
185. Si Y, Samulski ET (2008) Synthesis of water soluble graphene. Nano Lett 8:1679–1682
186. Avinash M, Subrahmanyam K, Sundarayya Y, Govindaraju T (2010) Covalent modification and exfoliation of graphene oxide using ferrocene. Nanoscale 2:1762–1766
187. Pham VH, Cuong TV, Hur SH, Oh E, Kim EJ, Shin EW et al (2011) Chemical functionalization of graphene sheets by solvothermal reduction of a graphene oxide suspension in N-methyl-2-pyrrolidone. J Mater Chem 21:3371–3377
188. Jin Z, Lomeda JR, Price BK, Lu W, Zhu Y, Tour JM (2009) Mechanically assisted exfoliation and functionalization of thermally converted graphene sheets. Chem Mater 21:3045–3047
189. Stankovich S, Piner RD, Nguyen ST, Ruoff RS (2006) Synthesis and exfoliation of isocyanate-treated graphene oxide nanoplatelets. Carbon 44:3342–3347
190. Stankovich S, Dikin DA, Dommett GH, Kohlhaas KM, Zimney EJ, Stach EA, et al (2006) Graphene-based composite materials. Nature 442:282–286
191. Zhang D-D, Zu S-Z, Han B-H (2009) Inorganic–organic hybrid porous materials based on graphite oxide sheets. Carbon 47:2993–3000
192. Niyogi S, Bekyarova E, Itkis ME, McWilliams JL, Hamon MA, Haddon RC (2006) Solution properties of graphite and graphene. J Am Chem Soc 128:7720–7721
193. Worsley KA, Ramesh P, Mandal SK, Niyogi S, Itkis ME, Haddon RC (2007) Soluble graphene derived from graphite fluoride. Chem Phys Lett 445:51–56
194. Nakayama-Ratchford N, Bangsaruntip S, Sun X, Welsher K, Dai H (2007) Noncovalent functionalization of carbon nanotubes by fluorescein−polyethylene glycol: supramolecular conjugates with pH-dependent absorbance and fluorescence. J Am Chem Soc 129:2448–2449
195. Zhao Y-L, Stoddart JF (2009) Noncovalent functionalization of single-walled carbon nanotubes. Acc Chem Res 42:1161–1171
196. Chen C, Zhai W, Lu D, Zhang H, Zheng W (2011) A facile method to prepare stable noncovalent functionalized graphene solution by using thionine. Mater Res Bull 46:583–587
197. Liu H, Gao J, Xue M, Zhu N, Zhang M, Cao T (2009) Processing of graphene for electrochemical application: noncovalently functionalize graphene sheets with water-soluble electroactive methylene green. Langmuir 25:12006–12010
198. Kamada S, Nomoto H, Fukuda K, Fukawa T, Shirai H, Kimura M (2011) Noncovalent wrapping of chemically modified graphene with π-conjugated disk-like molecules. Colloid Polym Sci 289:925–932
199. Yang Q, Pan X, Huang F, Li K (2010) Fabrication of high-concentration and stable aqueous suspensions of graphene nanosheets by noncovalent functionalization with lignin and cellulose derivatives. J Phys Chem C 114:3811–3816
200. Ren L, Liu T, Guo J, Guo S, Wang X, Wang W (2010) A smart pH responsive graphene/polyacrylamide complex via noncovalent interaction. Nanotechnology 21:335701

201. Kodali VK, Scrimgeour J, Kim S, Hankinson JH, Carroll KM, De Heer WA et al (2011) Nonperturbative chemical modification of graphene for protein micropatterning. Langmuir 27:863–865
202. Stankovich S, Piner RD, Chen X, Wu N, Nguyen ST, Ruoff RS (2006) Stable aqueous dispersions of graphitic nanoplatelets via the reduction of exfoliated graphite oxide in the presence of poly (sodium 4-styrenesulfonate). J Mater Chem 16:155–158
203. Bai H, Xu Y, Zhao L, Li C, Shi G (2009) Non-covalent functionalization of graphene sheets by sulfonated polyaniline. Chem Commun 1667–1669

Key Limitations of Biomass-Derived Carbon Nanostructures for Energy Application

Vinicius G. C. Madriaga, Vinicius Rossa, Luanne E. M. Ferreira, Sancler da Costa Vasconcelos, and Thiago M. Lima

Abstract As sustainability practices and Green Chemistry's principles gathered attention, the use of renewable sources became an urgent topic to be addressed by the scientific community. In that way, biomass has become pivotal in a more sustainable future, especially for energy applications. Compared to the conventional carbon nanostructures obtained from non-renewable sources, biomass has a great potential for their replacement and to furnish similar materials for carbon-based supercapacitors. However, to accomplish that biomass has to overcome a large variety of drawbacks as suitable methods for increased porosity (hierarchical pore sizes and high surface areas), reduced tortuosity, reduction of the number of some oxygenated functional groups (avoiding secondary reactions that induce charge loss), and increased wettability. The structure of carbon-based materials can directly influence their electrical properties and thus affect their resistivity/conductivity, which is related to the activation or preparation procedure employed to produce them from biomass. Despite the efforts made on lignocellulosic-based supercapacitors, structural uniformity continues to be a fundamental challenge for the field. Even the slightest change in any treatment parameter causes critical differences in the final physicochemical supercapacitor. In addition, it should also be mentioned that biomass source implies the transformation of the electrochemical activities, needing to establish a comparison between them. Also, biomass cultivation and the circular economy might represent a vital bottleneck to be overcome. Despite these issues mentioned above, it is worth noting that biomass efforts for replacing non-renewable sources of carbon-based supercapacitors are essential to devote great attention to overcoming them to achieve a more sustainable future for energy purposes.

Keywords Biomass · Carbon nanostructures · Energy application · Green chemistry · Supercapacitor

V. G. C. Madriaga · V. Rossa · L. E. M. Ferreira · S. da Costa Vasconcelos · T. M. Lima (✉)
Instituto de Química, Universidade Federal Fluminense, Outeiro São João Batista, s/n, Campus do Valonguinho, Centro, Niterói, Rio de Janeiro 24020-141, Brazil
e-mail: tmlima@id.uff.br

S. K. Tiwari et al. (eds.), *Biomass-Based Functional Carbon Nanostructures for Supercapacitors*, Green Energy and Technology,
https://doi.org/10.1007/978-981-99-0996-4_3

1 Introduction

From the second industrial revolution until today, the world has become highly dependent on oil, both for energy production (fossil fuels) and petrochemicals (reagents, solvents, and polymers) [1]. However, the high consumption of oil and its derivatives is very worrying since it is one of the main responsible factors for climate change. In this context, the interest in biomass, as a renewable raw material, to partially replace oil and its derivatives has been growing over the years [2–8]. Biomass is an alternative and promising renewable raw material source for manufacturing biofuels and essential building blocks. Lignocellulosic biomass is generally composed of 35–50% cellulose (C6 sugars); 20–35% hemicellulose (C5 and C6 sugars); 10–25% lignin (phenyl, guaiacyl, and syringyl groups); and a small amount of ashes (metal oxides), extractives (essential oils and waxes), and water/moisture [6, 9–12].

The lignocellulosic biomass bioavailable on Earth is in the form of agricultural, industrial, and forestry residues. In 2017, the total amount of bioavailable biomass on the planet reached 550 gigatons of carbon in dry weight, of which about 80% came from plants [13–18]. Its excellent bioavailability has aroused great interest in science and technology, intending to use it as a raw material to produce bio-oils, biofuels, lignin, biochars, and syngas (CO and H_2) [2, 19–22].

As sustainability practices and Green Chemistry's principles gathered attention [23, 24], the use of renewable sources became an urgent topic addressed by the scientific community. This urge relied on energy field-related materials, especially for constructing power storage devices such as supercapacitors [25, 26]. In this way, employing renewable sources for making carbon-based electrodes to perform as supercapacitors is an encouraging pathway to achieving more sustainable materials and the future. Carbon-based supercapacitors are propitious materials since carbon is a very abundant element in nature, presenting several allotropes with different hybridizations (diamond, graphite, nanotubes, and fullerene), dimensionality (0 to 3D structures), textural properties, and more organizations. The electrical conductivity of carbon-based electrodes will depend on several parameters such as microtexture, hybridization, heteroatom content, thermal treatment, and many others [27–29].

2 Overview of Carbon-Based Supercapacitor Requirements

Supercapacitors are energy-storage devices whose mechanisms can be classified into electrochemical double-layer capacitors (EDLC) and pseudocapacitors. Capacitance is based on the electrostatic adsorption of electrolyte ions on the surface area of porous electrically conductive electrodes in the first case. Second, energy is stored through reversible redox reactions at the electrode/electrolyte interface. These devices operate by two main mechanisms (namely, charge separation in the electrical double layer),

and many tasks are located in high surface area electrodes. The utilization of carbon-based materials (CBMs) for that purpose is particularly interesting since they can be easily modulated to achieve the desired physical–chemical properties. These properties are closely related to how the charges from an electrolyte solution will cross these carbonaceous materials and how ions will move through the electrode's surfaces [26]. It is worth mentioning that beyond textural properties, carbon-based electrodes also should present (i) high conductivity, (ii) corrosion resistance, (iii) thermal stability, (iv) controlled pore structure, (v) compatibility in composites, and (vi) low cost [26].

CBMs are widely applied due to their physicochemical properties, good electrical conductivity, adjustable porosity, ease of processability, and variety of shapes [30]. Biomass-derived carbon materials are used as electrodes in supercapacitors, and their performance might be improved compared to non-biomass materials. The most common synthesis method for this type of material is direct pyrolysis or carbonization of the biomass, but it offers limited control over the physicochemical properties of CBMs [30–32].

The structure of carbon materials can directly influence their electrical properties, impacting mainly their resistivity/conductivity, which is related to the activation or preparation procedure employed to produce them. In that sense, the material's conductivity depends on the temperature used for converting carbon-rich precursors. This conversion might form a large amount of conjugated carbon in sp^2 hybridization, which plays a vital role in the electrochemical properties (as more efficient charge carriers). Therefore, highly disordered materials do not possess good conductivity and thus require a high graphitization degree, which is highly dependent on the thermal treatment temperature [26]. In addition to this intrinsic resistivity, the electrical resistance of carbon particles should be considered. The particle contact resistance plays an essential role in the aggregated carbon powders. This resistance depends on carbon particle morphology and overall pressure applied to the final material in the supercapacitor, which is higher in smaller carbon particles [26].

Another essential requirement for an excellent carbon-based supercapacitor is the presence of surface oxygen groups. High oxygen content in these materials increases the barrier for electron transfer among the microcrystalline elements. However, the company of these groups is still under debate in the specialized literature, and there needs to be a consensus on their ultimately detrimental character to the functioning of a supercapacitor [26]. The treatment of carbon precursors in an oxygen-rich atmosphere is an issue to be addressed since it yields a material with a high amount of this heteroatom and a supercapacitor with high electrical resistivity. These surface groups are pivotal in the whole behavior of the carbon material [26]. They might influence the wettability, ion adsorption, self-discharge, point of zero charge, and electrical contact resistance.

Moreover, these materials also present other heteroatoms such as hydrogen, nitrogen, sulfur, and halogens derived from the starting materials used to produce them and incorporated due to the thermal treatments. Still, regarding oxygenated carbons, the surface oxides can be classified as acid, basic, or neutral, as displayed in Fig. 1 [26]. Typically, the acidic functionalities are not desired since they lead to high

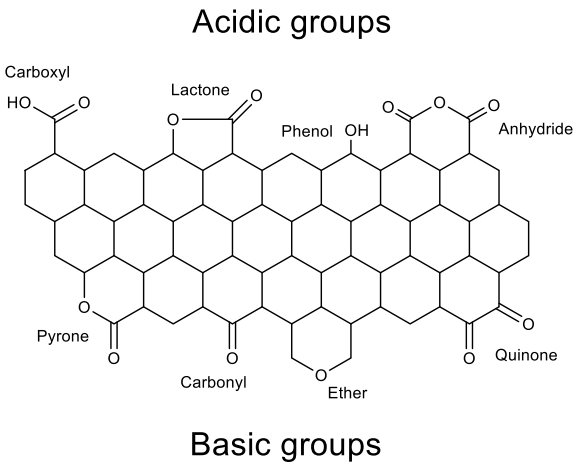

Fig. 1 Surface oxygen functional groups are commonly present in CBMs

rates of self-discharges. On the other hand, basic and neutral oxygenated functionalities are required because of the improved wettability, leading to increased specific capacitance [26]. Carbons with a low functionality on their surface can lead to a broader potential window, and higher energy density since functional groups might react with the electrolytes, solvent molecules, and additives. Moreover, oxygenated groups also might react with themselves, promoting their oxidation or reduction, leading to current leakage and low stability [28]. From this perspective, controlling the presence of functional groups is considered a factor of higher relevance when compared to other essential features, such as textural properties, since these groups will determine the supercapacitor performance [28].

In this context, the following reactions (1)–(3) are typically found in oxygenated surface groups in carbon-based electrodes [27]:

$$-\mathrm{C}-\mathrm{OH} \rightleftharpoons -\mathrm{C}=\mathrm{O} + \mathrm{H}^{+} + \mathrm{e}^{-} \tag{1}$$

$$-\mathrm{COOH} \rightleftharpoons -\mathrm{COO} + \mathrm{H}^{+} + \mathrm{e}^{-} \tag{2}$$

$$-\mathrm{C}=\mathrm{O} + \mathrm{e}^{-} \rightleftharpoons -\mathrm{C}-\mathrm{O}^{-} \tag{3}$$

As mentioned before, the surface characteristics of the electrode material are of pivotal importance to the supercapacitor performance [33, 34]. In that matter, heteroatom doping with elements such as N, O, B, S, and P has been drawing attention since they can enhance the material's capacitance because of the pseudocapacitance effect related to Faradaic redox reactions [13, 33–35]. The presence of heteroatoms that acts as electron donors or electron acceptors provides chemical polarity to surrounding carbons, improving ion adsorption increasing the number of

active sites, and decreasing hydrophobicity, thus impacting the penetration of guest species on the inner pores of the structure [13, 34].

Usually, doping can be performed using heteroatom-rich biomass as feedstock, post-treatment of the material, or during the carbonization step. The oxygen doping can be performed during chemical activation with alkaline treatment with NaOH and KOH, while phosphorous doping occurs in the acid treatment with H_3PO_4 [13, 33, 34]. Nitrogen atoms can be inserted into the structure through simple pyrolysis with precursors containing N or by adding a nitrogen source, such as NH_3 or HCN. Three nitrogen-containing functionalities can be formed in a carbon matrix: pyridinic nitrogen, pyrrolic nitrogen, and quaternary nitrogen. The first two present a pseudocapacitance role, while the last improves the charge transfer through the carbon electrode [13, 33].

Considering the porosity of a carbon-based supercapacitor, when the electrode pores are smaller than electrolyte ions, it is known that the electrode cannot provide charge storage. Therefore, a material's pore size must be appropriate for a selected electrolyte [29]. The size and distribution of pores on carbonaceous electrode materials are critical for electrolyte adsorption at the electrode–electrolyte interface. The most desired property in a carbon-based material applied as an electrode is high porosity and specific surface area. It is suggested that larger specific surface areas lead to higher capacities; however, this correlation reaches a limit determined by the porosity of the carbon-based electrodes [29]. The pore size exerts a critical role in the carbon-based supercapacitors, and the carbonaceous precursor can directly affect the size of these porous materials. In the electrochemical charge/discharge process, the macropore, mesopore, and micropore structures play different roles. Although some micropores are inaccessible to adsorb ions, it still affects the charge status by controlling ion diffusion and molecular sieve effects and then changing the capacitance. Macropores serve as ion-buffering reservoirs for meso- and micropores; mesopores provide abundant transport channels for ions' diffusion [34]. Micropores, particularly 0.7 nm in aqueous electrolytes and 0.8 nm in organic electrolytes, are the most efficient diameters for ion accumulation, resulting in higher capacitances. On the other hand, micropores centered at 1.3 nm are the most required for providing the highest number of active sites for ion adsorption [34].

Typically, the high specific surface area of carbons is assigned to the majority of micropores in their structure. Micropores can be both beneficial and deleterious to the final electrochemical behavior of carbons. This type of porosity can directly affect the capacitance by variations in the discharge current due to the possible restrictions in the electrolyte's diffusion, particularly organic electrolytes [26]. Micropores often fall in the double-layer dimensions, and the electrolyte ions' limitation to form this double layer will not significantly contribute to the overall capacitance. In addition, since narrow micropores limit the ions' diffusion, they also will retard their movement in charging/discharging and thus poorly cooperate for the charge-storage capacity [26]. Of course, which electrolyte is used and its hydrodynamic size should be considered for these considerations. On the other hand, micropores can selectively impose specific adsorption processes, thus acting as a molecular sieve and possessing a greater adsorbent–adsorbate affinity [26].

Larger pores, such as mesopores, allow improved accessibility because they provide a more comprehensive transport of electrolytes, especially those of bulkier molecules. In contrast, macropores do not contribute remarkably and are more critical in allowing the access of electrolytes to narrower pores [26]. Mesopores provide low-resistance channels for fast ion transport to the inner space of electrodes, resulting in higher rate capacity and power density. At the same time, macropores may reduce the ion diffusion distance by acting as ion-buffering reservoirs. Multiscale pores (hierarchical structure or pores) inside carbons are favorable for achieving superior electrochemical performance. Hierarchical carbons with micro-/mesopores can accommodate large ions, whereas meso-/macropores have many channels for ion transport and mass diffusion, resulting in high capacitances and rate performances [34]. In summary, pore size is vital for improving supercapacitors' efficiency. Carbon-based materials from natural sources, such as biomass, often present all porosity types but commonly display a higher degree of microporosity [26].

However, porosity is still a matter of debate in the scientific community [27, 28, 34, 36]. For example, it is possible to find studies regarding micropores as vital for high energy storage for the same reasons mentioned as drawbacks before, such as controlled diffusion effects. Still, the presence of hierarchical pores is often required, especially the carbons with interconnected hierarchical porosity, which promote the electrochemical pathways.

The wettability of the carbon surface, which is governed by the type of surface functionality, is another factor that influences the capacitance values (using organic or aqueous electrolytes), as shown in Fig. 2. The capacitance of porous carbon materials should be measured after the electrodes have been entirely soaked [29]. Suppose the electrolyte has a low wettability on the electrode surface. In that case, it becomes difficult for the electrolyte solution to penetrate the pores, thus resulting in a low utilization rate of its surface area. Since the energy density of supercapacitors is related to the surface area, a low utilization rate results in a low energy density [37].

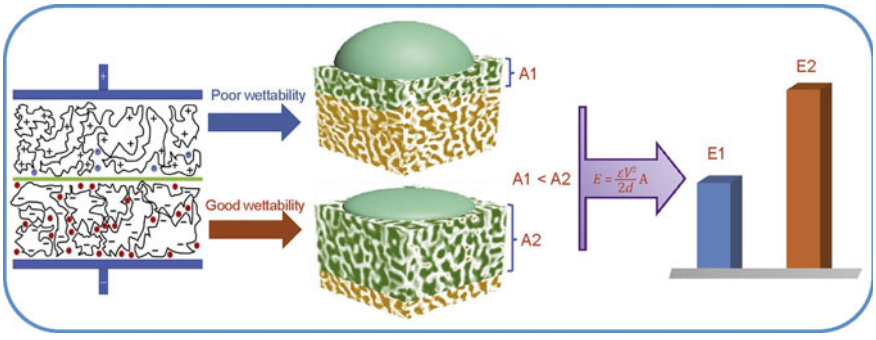

Fig. 2 Role of wettability in the carbon-based electrode area [37] (Copyright © 2019 Institute of Process Engineering, Chinese Academy of Sciences. Publishing services by Elsevier B.V. on behalf of KeAi Communications Co., Ltd.)

Another essential requirement of a carbon-based supercapacitor is the tortuosity factor. The tortuosity is a variable linked to the solid carbon structure that describes the difference between theoretical and measured (or practical) diffusion in a single dimensionless parameter, including all deviations from straight diffusion routes. Thus, this parameter reflects the random porosity in the carbon-based supercapacitor, which will negatively affect the electrolyte diffusion and energy density [38, 39]. Ordered porous carbons are desired to decrease the tortuosity through a rapid diffusion of the electrolytes into their structure to avoid this issue.

3 A Brief Review of the Strategies to Improve Carbon-Based Material Properties for Supercapacitors

Although CBMs have been highlighted in the energy field due to their desired properties, their characteristics, when derived from biomass, might need to be more satisfactory compared to metal oxides and other materials. In this sense, it became necessary to develop strategies to enhance some electrochemical and electrical properties of these CBMs, especially for building supercapacitors with higher power density [34]. As mentioned in the previous section, some critical characteristics are the focus of these procedures, like specific area, electrical conductivity, safety, low cost, and the pore structure [34]. Fortunately, CBMs have been studied for several applications, making possible a rapid development of procedures to tune their properties. These strategies may include doping, chemical, physical activation, functionalization with various functional groups, distinct structural shapes, and large pore distribution. Here, we will briefly explore some of these strategies, their fundamental limitations, and their impact on these materials' properties [34, 40]. Table 1 compares carbons prepared from different sources and their main properties [13].

CBMs derived from biomass are rich in functional groups and produced more sustainably than fossil fuel-based activated carbons and carbon black. In addition, they provide several advantages: (1) it is a by-product of the biomass industry; (2) it is

Table 1 CBMs preparation from different sources and their features and preparation methods

	Biochar	Activated carbons	Carbon black
Source	Biomass	Asphalt, coal, biomass, etc.	Oil, asphalt and coal tar, etc.
Carbon amount (%)	40–90	80–95	>95
Features	Enriched surface functional groups, amorphous, and porous	Porous and amorphous	Carbon particles, microcrystal, or amorphous
Preparation	Pyrolysis (400–600 °C) followed by activation (physical or chemical)	Carbonization (700–1000 °C) followed by activation (physical or chemical)	Combustion in the presence of air

cost-effective and environmentally friendly since it uses thermal conversions to make bio-oil; (3) it is plentiful; (4) it is chemically and physically stable; (5) it has a variety of surface functional groups (e.g., different types of polymers) that contain oxygen or nitrogen, which can be tweaked by changing the feedstock or the thermochemical conditions; (5) because it is permeable or hierarchically structured by nature, it can enhance electrolyte accessibility to electrodes and reduce ion transport time [26, 41].

Thermochemical decomposition processes must be performed to convert feedstock biomass into carbon energy-storage materials. Two thermal methods are widely used to obtain such products: hydrothermal carbonization (HTC) and pyrolysis [13]. Although pyrolysis conditions might be optimized for biochar production, the material formed presents low conductivity, low specific surface area, and inferior pore characteristics [13, 35, 42]. HTC is a thermochemical transformation technique carried out in sub-critical liquid water media and high autogenous pressure [13, 34, 35, 43, 44].

Both methods present vantages and disadvantages, but the materials obtained in both cases still need improvement to be used in energy-storage systems. Hence, carbonization methods are usually combined with activation methods to improve characteristics such as specific surface area and porous structure and to form functional groups. The activation methods are divided into two categories: physical/thermal activation and chemical activation [13].

Physical activation consists of the controlled gasification of the biochar at high temperatures in the presence of oxidizing gases [13, 26, 45, 46]. The desired characteristics for the final product can be tuned by changing the activation conditions. It is possible to control not only the materials' porosity but also the pore size and the nature of internal surfaces through alterations in the activation temperature and flow. The pores and specific surface area are increased due to the elimination of volatile products [13, 26, 44, 45]. By increasing activation time, micropores and mesopores are generated, but a high duration will lead to the collapse of the porous structures [13, 34].

Among the advantages of using physical activation, the elevation in the content of oxygen-containing functional groups can be mentioned, leading to increased polarity and hydrophilicity of the material's surface. On the other hand, this process requires high temperatures, is highly energy-consuming, and presents poor porosity control compared to chemical activation [33, 46].

Chemical activation occurs at slightly lower temperatures, which vary from 400 to 900 °C, and acids, strong bases, or salts are added to the precursors acting as dehydrating and oxidizing agents. Several activating reagents, such as KOH, NaOH, H_3PO_4, $ZnCl_2$, $MgCl_2$, and K_2CO_3, can be used in this process [13, 26, 33, 34, 44, 45]. Chemical treatments present several advantages, such as high control in the development of pores and their sizes, high surface area and porosity, high carbon yield, and lower temperature and duration of the procedure. In contrast, activating reagents are corrosive, and washing is required to remove reactants and inorganic residues, leading to waste generation [13, 26, 35, 46].

When it comes to supercapacitors, one of the most exciting insights is how specific surface area is related to capacitance, as aforementioned. Several methods to activate

CBMs aim to enhance the particular area values by modifying the porous structure using heat or chemicals (KOH, $ZnCl_2$, and many others). Different temperatures might be selected depending on the carbon source (500–1200 °C). However, the principle is the same for all procedures: high temperatures can promote the oxidation of structural carbons, forming gases such as CO_2, CO, and other oxides [47, 48]. Removing these carbons as gaseous molecules allows the formation of new pores and cavities, causing an increase in specific area values. On the other hand, the removal of these molecules can be performed through chemical reactions with structural carbons on the surface. One of the most popular methods consists in to submit the CBM to high temperatures, in the presence of KOH or other bases, to remove carbons, as shown by the reactions (4)–(7) in the following [49]:

$$6KOH + 2C \rightarrow 2\ K + 3H_2\uparrow + 2K_2CO_3 \tag{4}$$

$$6KOH + CO_2 \rightarrow H_2O\uparrow + 2K_2CO_3 \tag{5}$$

$$2K_2CO_3 + 2C \rightarrow K_2O + 2CO\uparrow \tag{6}$$

$$K_2O + CO \rightarrow 2K + CO\uparrow \tag{7}$$

The parameter selection is also a crucial attention point in these procedures. The pore structure and the specific area might be different by modifying the reaction time, temperature, atmosphere, and other parameters. Also, various carbon sources may interfere with these results, especially for biomass sources that contain different concentrations of other species and dopants. Activated CBMs generally present specific area values around 1000–3500 m^2/g, which leads to a capacitance of 150–350 F/g in aqueous media [50, 51]. It is also expected that the pore structure might contribute to these values. Some studies have established the relationship between pore size distribution with capacitance values and power density, revealing that monodisperse distributions and narrow pores can tune some of the electrical properties of these materials. As already mentioned, the pore size might determine the carbon-based supercapacitor functionality, in which larger pores can be used as buffers. In comparison, the smaller pores might help the diffusion of the ions and charge storage [52, 53].

For supercapacitors, the presence of functional groups is also a promising pathway to optimize the CBMs properties. It is essential to address that functionalization does not insert atoms in the lattice as a dopant; instead, heteroatom-containing groups are attached to the material's surface. Functionalization is an encouraging way to overcome the hydrophobicity of CBMs, which may reduce their power density in some electrolytes. Furthermore, these groups give extra pseudocapacitance and resistance, especially in non-aqueous electrolytes [46].

The shape of the CBMs is also a point of discussion in energy utilization as supercapacitors. Some studies discuss that it may influence the capacitance value by

limiting the electrolyte access to the material's surface. In this way, it is suggested that plane and aligned carbon nanotube structures present better performances as supercapacitors, allowing the improvement of charge storage. On the other hand, there are proper ways to facilitate electrolyte access to the surface, introducing vacancies in the structure to overcome that issue [33, 54, 55].

In all these cases, the advance in CBM chemistry helps to design materials with improved properties. This is particularly important for sources like biomass due to their non-homogeneous structure and composition. As different kinds of biomass might present other properties and performances, improving these CBM's final properties is a promising pathway to be used as supercapacitors. In that way, Table 2 shows several carbon-based supercapacitors prepared from different types of biomasses and submitted to specific activation treatments [13, 56].

Table 2 Comparison of textural and electrochemical properties of CBMs prepared from different biomass sources

Biomass source	Activation	Surface area (m^2/g)	Specific capacitance (F/g)
Coconut shell	Steam	1532	228 at 5 mVs^{-1}
Onion husk	K_2CO_3	2571	188 at 1 Ag^{-1}
Peanut shell	$ZnCl_2$	1549	340 at 1 Ag^{-1}
Palm kernel shell	KOH	–	210 at 0.5 Ag^{-1}
Watermelon rind	KOH	2277	333.4 at 1 Ag^{-1}
Tea leaves	KOH	2841	330 at 1 Ag^{-1}
Tea waste buds	KOH	1610	332 at 1 Ag^{-1}
Sugarcane bagasse	KOH/KNO_3	1940	298 at 1 Ag^{-1}
Withered rose flower	KOH	1980	350 at 1 Ag^{-1}
Albizia flowers	NaOH	2757.6	406 at 0.5 Ag^{-1}
Jujube fruit	KOH	1135	460 at 1 Ag^{-1}
American popular fruit waste	KOH	942	423 at 1 Ag^{-1}
Corncob	KOH	800	390 at 0.5 Ag^{-1}
plastic waste	KOH	2326	169 at 0.2 Ag^{-1}
Rice husk	KOH	3145	367 at 5 mVs^{-1}
Soyabean pods	NaOH	2612	352.6 at 0.5 Ag-1
Orange peel	KOH	2160	460 at 1 Ag^{-1}
Mangosteen peels	NaOH	2623	357 at 1 Ag^{-1}

4 Main Challenges of Biomass Utilization to Produce Supercapacitors

As explored previously in this chapter, biomass can generate a variety of materials for special applications, including energy storage. Since biomass is a renewable and cheap source, scientists have been developing methods to convert it into desired materials. Each biomass presents different compositions, producing various compounds with distinct properties. However, some challenges will be overcome, which will be further explored in this section [57].

Firstly, for preparing carbon-based supercapacitors, the pyrolysis of the raw precursors is a classical methodology in this field. This thermal treatment submits the raw biomass to high temperatures under a controlled atmosphere to produce biochar. Also, biomass fractions can be depolymerized, primarily to obtain lignin-based materials, as this fraction has a higher carbon content and high hydrophobicity [58, 59]. Several biomass sources are suitable for this, including tea leaves, tree products, bagasse, sawdust, shells, wood, and wastes. However, depending on the origin of the biomass source, it might be more challenging to control the CBMs' properties. The selection of a suitable source relies on the desired properties of CBM for the chosen application. The produced materials might differ in properties like aromaticity, inorganic compound content, presence of heteroatoms, and others [58, 59].

Plant biomass draws attention to the search for more sustainable alternatives and renewable sources. It is produced in large quantities as a by-product in industry, agriculture and forestry, bioethanol fermentation, pulp and paper manufacturing, and crop planting. Billions of tons of biomass residues are produced in these sectors each year. Therefore, when consumed in manufacturing CBMs, these biomasses cease to be waste and act as a precursor, becoming a possible solution to an urgent environmental problem [60]. Pyrolysis is one of the most common methods for synthesizing conventional CBMs like biochars. Despite being a standard method, there are some challenges, including scalability cost and low-yield manufacturing [61, 62].

Still, it is challenging to predict essential properties for biochar or lignin-based materials, such as specific area, porous structure, and composition. Beyond the biomass selection, the methodology might produce different materials in biochars, e.g., the influence of the pyrolysis atmosphere and temperature in biochars' porous structure. Also, the pyrolysis time and temperature can interfere with the material's aromaticity and stability level, and even the concentration of heteroatoms (especially oxygen) in the structure might be affected [63–65].

In addition, it is vital to address that another challenging issue in biomass utilization is finding a balance between eco-friendly low-cost sources and the efficiency of CBM to required employment, respecting the eco-friendly proposal. Usually, physical activation offers a sustainable pathway, but there needs to be more property control. On the other hand, chemical methods increase the system cost and reduce the sustainable character. Moreover, the energy investment must be considered in all

cases because these processes often need high temperatures for a long-time synthesis [49, 54]. These materials generally do not have large porosity or surface area, and further action is required in most cases. Also, introducing some groups in the structure through distinct functionalization methods is a common strategy for these materials. These post-synthesis methods improve some of the electrical properties of these materials; however, they often use harmful chemicals to achieve this purpose. Moreover, these additional activation methodologies often increase the cost of these supercapacitors. Another drawback, in this case, is the non-homogeneous structure of these materials, which can impair the reproducibility of these anodes and hinder their use as supercapacitors [34, 56, 66].

Another exciting aspect of biomass pyrolysis is the gas released during the process. Biomass pyrolysis, in general, can generate three fractions: biochar, the desired material for energy application; bio-oil; and pyrolysis gases. Usually, to be considered a green process, these gases need to be converted into other chemicals to avoid their release into the atmosphere; however, on an industrial scale, this might be harder. The pyrolysis gas is mainly composed of CO_2, but also some hazardous compounds like SO_2, NO_x, HCl, and many other gases are released during this process. Again, it is crucial to consider this topic as an issue in producing these materials since releasing these gases represents an environmental problem [58, 59].

The different porosity developed according to the composition of the raw biomass starting material and related to the activation process employed is another challenging barrier, as illustrated in Table 3 [13]. For example, the pyrolysis process of lignocellulosic biomass yields carbon materials with different specific surface areas, micropore and mesopore volumes, and pore diameters due to their distinct composition. It is well known that lignocellulosic-derived starting materials present a wide range of wt.% of cellulose, hemicellulose, and lignin constitution. Each fraction is typically decomposed at different temperatures. Since these fractions are deeply interconnected, their percentage is closely related to the plant species and growth stage [13].

In this context, preparing biochar to use as carbon electrodes in supercapacitors will depend on the lignocellulosic biomass source, yielding materials difficult to reproduce regarding their physical–chemical properties, especially textural properties. Typical treatment processes, such as pyrolysis, furnish biochars with a hierarchical structure, i.e., containing both micro- and mesopores, however, in distinct amounts and not interconnected. These different types of pores should present a high degree of interconnection to allow good electrolyte diffusion and avoid loss of capacity [34]. The linked porous network of biomass-derived nanostructured carbon materials can provide multimodal electron transport channels and reduce transport lengths between electrodes and electrolytes, which are essential for supercapacitors with higher energy density. In this way, even though graphitic carbon materials are created from biomass-derived CBMs, it isn't easy to regulate the pore geometry, pore size, and pore connectivity using chemical activators to achieve high specific surface area and hierarchical porous structure [35]. To surpass this issue, some strategies are used to obtention biomass-derived CBMs, but they still mainly employ soft/hard templates, which might represent a high cost and residue formation [34]. However, it is worth mentioning that some biomasses might naturally furnish interconnected

Table 3 Lignocellulosic compositions of commonly used materials for carbon production [13]

Lignocellulosic materials	Cellulose (%)	Hemicellulose (%)	Lignin (%)
Hardwood stems	40–55	24–40	18–25
Softwood stems	45–50	25–35	25–35
Nut shells	25–30	25–30	30–40
Corn cobs	45	35	15
Grasses	25–40	35–50	10–30
Miscanthus	34–36.5	42–44.8	28–30
Sugarcane bagasse	25–27.7	48–50.3	31–32.2
Paper	85–99	0	0–15
Wheat straw	30	50	15
Cotton seed hairs	80–95	5–20	0
Newspaper	40–55	25–40	18–30
Waste paper from chemical pulps	60–70	10–20	5–10
Solid cattle manure	1.6–4.7	1.4–3.3	2.7–5.7
Coastal bermudagrass	25	35.7	6.4
Switchgrass	45	31.4	12
Swine waste	6	28	n.a

mesopores, such as those comprised of fibrous structures [34]. Moreover, since these pores are mostly randomly organized and poorly ordered due to the decomposition reactions of cellulose, hemicellulose, and lignin, they often present a significant degree of tortuosity and thus decrease the supercapacitor efficiency [38, 39].

Lignocellulosic biomass typically possesses a high amount of oxygen in its fractions, i.e., cellulose, hemicellulose, and lignin. In that perspective, porous carbons present more oxygenated compounds in their structures. Although it is suggested that these compounds are closely related to a good wettability of the carbon materials, they are widely accepted to be deleterious for a supercapacitor operation, as aforementioned in Eqs. (1)–(3). Considering that, the adjustment of the oxygen content in the final carbon materials needs to be addressed for a broad application of lignocellulosic biomass as a renewable source. Thermal treatments can achieve this in a unique atmosphere, such as nitrogen, argon, or hydrogen, representing a cost increase for a broad application of this renewable source.

Despite the efforts made on lignocellulose electrodes, structural uniformity continues to be a fundamental challenge for the field. Even the slightest change in any parameter causes lignocellulosic biomass characteristics to change. Different surface morphologies can be seen depending on the pre-treatment technique and biomass source. Because the surface and structural morphology of the biomass-derived active material differs depending on the method utilized, different electrode preparation procedures alter capacitive performance. It is also possible that functional groups and their bonding may vary. Each lignocellulosic biomass source has different

surface chemistry and morphology, which causes differences in capacitive performances. Therefore, these sources yield a carbon material with variable capacitance, energy density, and power density due to the peculiar structure of cellulose, hemicellulose, and lignin. The electrodes derived from these several lignocellulosic origins will have relatively low energy densities, despite their high specific capacitance and power density values, as shown in Fig. 3 [63].

Furthermore, Fig. 4 presents the capacitance of biochars prepared from different biomass sources and their pore size and specific surface area (SBET) [44].

The adjustment of microstructure and pore homogeneity is imperative to employ biomass as the carbon material source, which consequently requires a deep knowledge of the different physical or chemical activation methods, i.e., to establish a standard procedure for the treatments of the raw material to achieve more reproducible carbon [63]. As mentioned in this chapter, there needs to be more progress in creating biomass-derived materials with finely adjusted structural and property characteristics for commercial electrochemical energy devices with large-scale manufacturing capabilities that are both inexpensive and ecologically beneficial [35]. Several efforts must be directed to fabricate hierarchical porous carbons with well-established synthesis parameters through further thermal treatments or chemical agents' activation [33]. Because biomass has unpredictable morphologies, it is challenging to precisely regulate pore parameters like shape and structure, limiting rate performance, and power

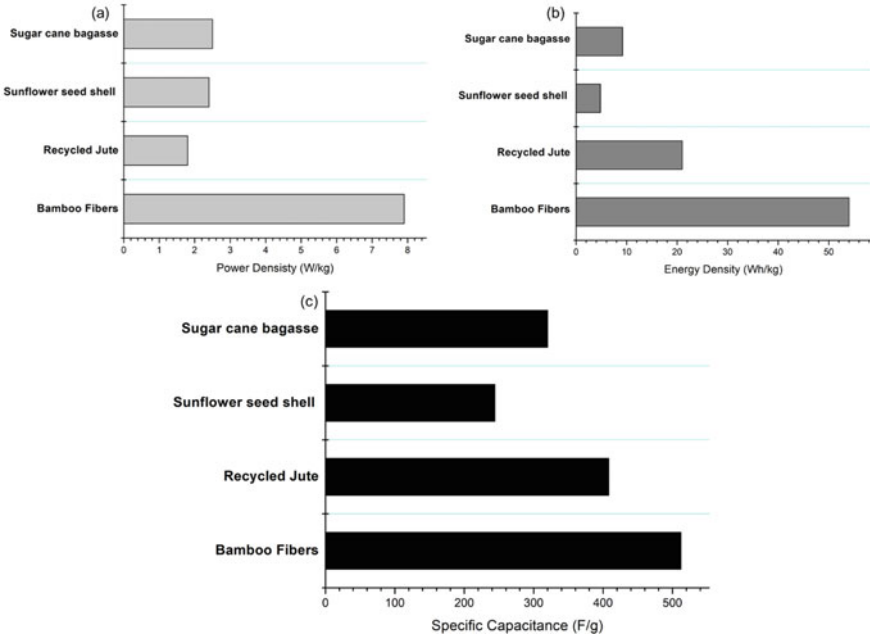

Fig. 3 Specific capacitance, energy density, and power density of different biomass sources

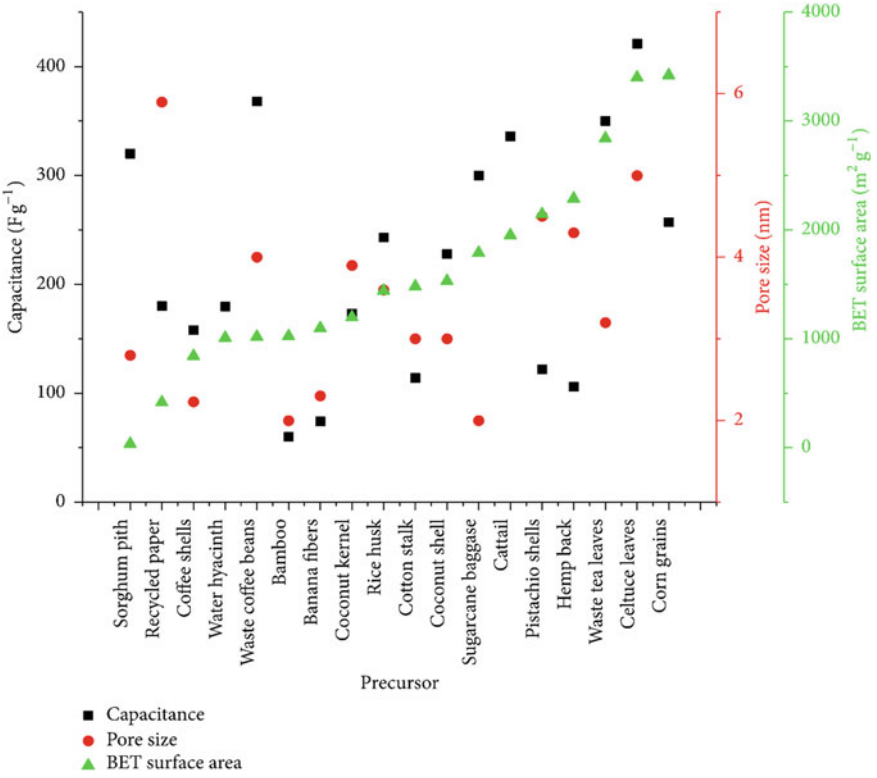

Fig. 4 Capacitance, pore size, and surface area as a function of biomass source [44]

density. Furthermore, the electrochemical performance of biomass-derived energy-storage devices is unknown mainly due to pore size, surface area, and surface chemistry impacts. Investigating the ion diffusion mechanism in hierarchical pore structure remains a significant issue [63]. Also, it should be mentioned that even for the same type of lignocellulosic biomass, the seasonality of the crops is another barrier to be overcome due to the different compositions of cellulose, hemicellulose, and lignin.

The graphitization degree is also a crucial parameter to be adjusted since biomass-based carbon materials have various electrochemical properties, such as internal resistance, rate capability, power delivery, and energy efficiency. Improving the graphitization of active carbon increases the electrode's surface in an aqueous electrolyte, speeds up ion diffusion and charge transfer, and enhances supercapacitor performance [33]. Since a high electrical conductivity is closely related to a high graphitization degree, biochars produced from biomass pyrolysis typically present a low degree and thus represent a barrier to be surpassed to achieve more efficient materials [33, 59, 67]. Moreover, there is a compromise between the graphitization degree and the specific surface area since these carbons often present low areas and porosity, as presented in Fig. 5 [68]. Electrochemical characteristics such as internal

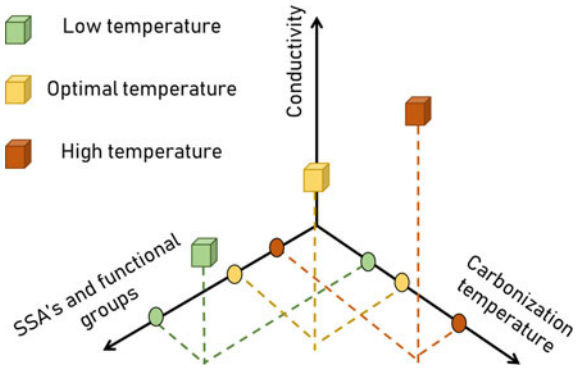

Fig. 5 Specific surface area, functional groups, and conductivity as a function of the carbonization temperature [68]

resistance and energy efficiency are related to the materials' graphitization degree. A high level of graphitization provides a high electrical conductivity and surface hydrophilicity, enhancing ion diffusion and charge transport. On the other hand, it is also related to a small surface area and undeveloped pore structure. Consequently, there must be a trade-off between the graphitization degree and the porous structure to obtain a better electrochemical performance [33].

The mechanisms proposed for the catalytic graphitization process are (i) dissolution–precipitation, where amorphous carbon is dissolved into metallic particles, then precipitated as graphitic carbon and (ii) formation–decomposition of carbide intermediates, where metal carbides are formed, as an intermediate, and them they decomposed at a specific temperature, leaving graphitic carbon [69, 70]. As discussed, catalytic graphitization and thermochemical activation produce layered graphitic and porous nanostructured carbon materials. Therefore, it became interesting to investigate the combination of the two methods. Through the studies developed, it was observed that some parameters influence the material obtained. These are the type of precursor, pre-treatment, and operating parameters applied [71–74]. In addition, another difficulty is the obtention from biomass of some carbon structures that are highly efficient and already used as supercapacitors. We can mention structures such as nanotubes, nanofibers, and nanosheets [71–74].

Another critical factor to be mentioned is the presence of heteroatoms in the lignocellulosic biomass, such as O, H, S, and N. Several thermal or chemical treatments might remove these heteroatoms, but oxygen is a persistent heteroatom in the final carbon material. However, oxygenated groups can be beneficial for good wettability and widening the working voltage window, thus increasing the energy density. In contrast to oxygen, nitrogenated groups (pyridinic, pyrrolic, and quaternary ammonium) are less reactive, and their presence in the carbon structure increases the conductivity and the pseudocapacitance. In addition, mineral traces, such as Ca, K, Mg, Na, and Si, can significantly affect the electrochemical properties of the final carbon-based electrodes [33].

Despite this, the production of carbon from biomass faces some difficulties. For instance, the various growth circumstances, harvest periods, and essential micronutrients for many plants may be found in different parts of the world because of their abundance. Because of this, it is challenging to replicate all these effects for obtaining the same carbons with similar electrochemical properties. The decomposition of biomass and pest damage are significant issues for a feasible action plan. Meanwhile, market prices also have to be considered considering the economic benefit, a lack of storage, a substantial financial commitment to farming, and avoiding using large-scale use with high economic value [68].

The use of biomass as a raw material for supercapacitor production has been drawing more and more attention, and several studies on the subject have already been carried out. Some of the characteristics that explain this interest are related to the fact that biomass is a low-cost renewable feedstock that is also widely available in nature. Furthermore, it has the advantage of presenting an intrinsically porous structure; different functional groups; and heteroatoms such as nitrogen, phosphorous, and sulfur, which generate various active sites in the material [13, 34, 35, 46, 63].

Using lignocellulosic biomass to produce biochar makes the process economical and ecological, with excellent waste management and recovery method [13, 75–78]. However, they also release CO, CO_2, SO_x, NO_x, and CH_4, which are harmful to the planet and contribute to the greenhouse effect. This fact can be remedied by inserting a Fischer–Tropsch process in the plant to produce hydrocarbons and alcohols [46, 79, 80].

Scale-up from a laboratory process to a pilot plant is challenging, as the results obtained in laboratories generally present many variations concerning the results obtained in the scale-up. In addition, scale-up requires a large amount of raw material, adequate conditions of transport and storage, efficient process management, product purification and recovery, quality control, waste treatment, and concerns with the legislation in force in each country. The increase in scale also involves economic studies; process flowcharts; process modeling and simulation; evaluation and monitoring; improvements and development of new processes; and analysis of costs, risks, and environmental impacts [19].

Lignocellulosic biomass processing plants exist in Asia, Europe, and the Americas. In this context, the expenditure on biomass pre-treatment reaches 40% [22, 81], and pre-processing, transport, and storage are responsible for 50% of the total cost of processing. The other 50% is concentrated on expenses with energy, chemical reactants, and operation/maintenance of the reactor, necessary for the pre-treatment [22, 82].

This fact prompted the industry to review its lignocellulosic biomass technologies due to the complexity of the process and pre-treatment difficulties. At first, the studies were carried out to reduce operating costs from an economic point of view. However, currently, they are more focused on reducing environmental impacts and ensuring sustainability throughout the process [19, 22, 82].

The main factors to boost lignocellulosic biomass commercialization are bioavailability; conversion costs into products with added value; public policies and investments implementation; process automation; and process expansion, development,

and technological maturity [19, 22]. Currently, governments of several countries in Asia, Europe, and the Americas are financing these projects. Still, the industrial sector also needs to be engaged in production, commercialization, sustainability, and reduction of environmental impacts [19, 22, 83].

In the USA, agricultural residues and other crops result in the highest bioavailability of biomass (577 million dry tons per year). In contrast, in Canada, this bioavailability is concentrated in bulk crops and forest residues (561 million dry tons per year). This difference is due to the greater agricultural area of the USA than Canada. The icy climate significantly limits agriculture in Canada, making it difficult to grow and harvest crops. In addition, forest fires, insect infestations, and poor forest management also contribute to reduced biomass production [19, 22].

In Brazil, the tropical climate favors agriculture and lignocellulosic biomass bioavailability. Examples of Brazilian lignocellulosic biomasses are residual sugarcane bagasse (186 million tons per year) from first-generation ethanol production and forest residues from eucalyptus cultivation for the paper and cellulose industry. Brazil has already established itself as one of the primary producers of biofuels in the world [19, 22].

In Europe, the bioavailability of biomass is concentrated in waste from water treatment plants, municipal solid waste, and agricultural and forestry waste. It has been predicted that biofuels from lignocellulosic biomass could result in around 70–85% reduction in greenhouse gas emissions by 2050, including a 10% target for domestic biofuel production through the implantation of non-food and lignocellulosic biomasses. However, as these biomasses require very complex technologies, they increase the costs of collection, transport, storage, handling, bioprocessing, and final product purification [22].

Many African countries face devaluation in their agricultural exports, and many losses to their competitors occur. The impact of bioenergy on African food security has resulted in land competition issues and a neglect of the expected potential to promote rural development. However, the continent has great potential for lignocellulosic biomass bioavailability. Like straw, grasses and wood do not require complex farming techniques. In addition, grasses grow and regenerate in degraded soils and dry lands [22].

The bioavailable lignocellulosic biomasses on the Asiatic continent are residues of rice, cotton, wheat, corn, and pineapple; banana stem; sugarcane bagasse; and coconut husk. Other potential lignocellulosic biomasses include forest residues, wood, straw from paper and cellulose industries, logging activities, and other agricultural residues. China is the world's largest producer of rice and wheat, ranking second in corn production after the USA. They have generated annually and cause environmental problems of degradation and recycling in bulk. Such situations open the prospects for deriving liquid fuels and chemicals from these lignocellulosic materials [19, 22].

Most of Oceania's lignocellulosic biomass comes from residues from forest management practices and decomposed residues. Lignocellulosic biomass is the most cost-effective opportunity to complement the continent's dependence on fossil

fuels for primary energy for electricity, transport, and heating. The supply of lignocellulosic biomass generally increases with the development of new forestry and agricultural technologies integrated into arable land, without any need for wastewater and competing with food and fiber production [22].

Thermochemical methods have yet to be evaluated for large-scale production, which may contribute to the lack of control over global warming and climate change. Making it necessary to create a route that aims to increase productivity and reduce environmental impacts [19, 22, 83]. According to the literature, only some models study all the variables of the lignocellulosic biomass conversion process. Some authors address the bioavailability and biomass type; others are more concerned with location, storage, and biomass transport, and other authors address conversion statistics, process development, and operating cost. Therefore, it is necessary to create a single model where all variables are considered whole and not separated [19, 22].

5 Conclusions

It is undeniable that biomass possesses a high potential for the replacement of carbon-based electrodes for supercapacitors obtained from non-renewable sources. Biomass is an abundant carbon source and might yield auspicious materials to achieve this goal. However, as demonstrated in this chapter, several issues must be faced to be suitable as materials for supercapacitor construction, such as high specific surface area, the presence of a hierarchical system of pores sizes, good wettability, and the absence of some oxygenated groups (mainly the acid ones) that might contribute to a fast discharging and a higher graphitization degree. In addition, since carbons produced from biomass-derived sources often present low specific surface area, an efficient and well-consolidated method for activation must be used, which is reproducible and easy to perform. The biomass source also plays an essential role as materials derived from distinct lignocellulosic might furnish different carbons with very dependent electrochemical properties. One of the most critical issues to overcome is the consolidation of a circular economy for a high amount of biomass production without affecting the regional production center. After all, a carbon with reproducible properties will be employed at a large scale.

References

1. Ahove MA, Bankole SI (2018) Petroleum industry activities and climate change: global to national perspective. In: Ndimele PE (ed) The political ecology of oil and gas activities in the Nigerian aquatic ecosystem. Elsevier, pp 277–292
2. Cha JS, Park SH, Jung S-C, Ryu C, Jeon J-K, Shin M-C et al (2016) J Ind Eng Chem 40:1–15. https://doi.org/10.1016/j.jiec.2016.06.002
3. Zou R, Qian M, Wang C, Mateo W, Wang Y, Dai L et al (2022) Chem Eng J 441:135972. https://doi.org/10.1016/j.cej.2022.135972

4. Qin F, Zhang C, Zeng G, Huang D, Tan X, Duan A (2022) Renew Sust Energ Rev 157:112056. https://doi.org/10.1016/j.rser.2021.112056
5. Azzi ES, Karltun E, Sundberg C (2019) Environ Sci Technol 53:8466–8476. https://doi.org/10.1021/acs.est.9b01615
6. Romaní A, Larramendi A, Yáñez R, Cancela Á, Sánchez Á, Teixeira JA et al (2019) Ind Crop Prod 132:327–335. https://doi.org/10.1016/j.indcrop.2019.02.040
7. Azzi ES, Karltun E, Sundberg C (2021) J Clean Prod 280:124873. https://doi.org/10.1016/j.jclepro.2020.124873
8. Cornelissen G, Pandit NR, Taylor P, Pandit BH, Sparrevik M, Schmidt HP (2016) Plos One 1–16. https://doi.org/10.1371/journal.pone.0154617
9. Santos FA, de Queiróz JH, Colodette JL, Fernandes SA, Guimarães VM, Rezende ST (2012) Quim Nova 35(5):1004–1010. https://doi.org/10.1590/S0100-40422012000500025
10. Almeida Ribeiro RS, Monteiro Ferreira LE, Rossa V, Lima CGS, Paixão MW, Varma RS et al (2020) Chemsuschem 13(16):3992–4004. https://doi.org/10.1002/cssc.202001017
11. Canilha L, Chandel AK, Suzane dos Santos Milessi T, Antunes FAF, Luiz da Costa Freitas W, das Graças Almeida Felipe M et al (2012) J Biomed Biotechnol 2012:1–15
12. Xin D, Saha N, Reza MT, Hudson J, Chiu PC (2021) ACS Sustain Chem Eng 9(19):6821–6831. https://doi.org/10.1021/acssuschemeng.1c01251
13. Zhu Z, Xu Z (2020) Renew Sust Energ Rev 134:110308. https://doi.org/10.1016/j.rser.2020.110308
14. Saini R, Osorio-Gonzalez CS, Hegde K, Brar SK, Magdouli S, Vezina P et al (2020) Curr Sustain/Renew Energy Rep 7:122–136. https://doi.org/10.1007/s40518-020-00157-1
15. Roy P, Dias G (2017) Renew Sust Energ Rev 77:59–69. https://doi.org/10.1016/j.rser.2017.03.136
16. Rutherford DW, Wershaw RL, Rostad CE, Kelly CN (2012) Biomass Bioenerg 46:693–701. https://doi.org/10.1016/j.biombioe.2012.06.026
17. Cha JS, Park SH, Jung S-C, Ryu C, Jeon J-K, Shin M-C et al (2016) Production and utilization of biochar: a review. J Indus Eng Chem. Korean Soc Indus Eng Chem 40:1–15 (REPETIDO)
18. Nanda S, Azargohar R, Dalai AK, Kozinski JA (2015) Renew Sust Energ Rev 50:925–941. https://doi.org/10.1016/j.rser.2015.05.058
19. Saini R, Osorio-Gonzalez CS, Hegde K, Brar SK, Magdouli S, Vezina P et al (2020) Lignocellulosic biomass-based biorefinery: an insight into commercialization and economic standout. Curr Sustain/Renew Energy Rep 7:122–136
20. Roy P, Dias G (2017) Prospects for pyrolysis technologies in the bioenergy sector: a review. Renew Sustain Energy Rev. Elsevier Ltd., 77:59–69
21. Rutherford DW, Wershaw RL, Rostad CE, Kelly CN (2012) Effect of formation conditions on biochars: compositional and structural properties of cellulose, lignin, and pine biochars. Biomass Bioenergy. Elsevier Ltd., 46:693–701
22. Nanda S, Azargohar R, Dalai AK, Kozinski JA (2015) An assessment on the sustainability of lignocellulosic biomass for biorefining. Renew Sustain Energy Rev 50:925–941
23. Anastas PT, Eghbali N (2010) Chem Soc Rev 39:301–312. https://doi.org/10.1039/B918763B
24. Anastas PT, Warner JC (1998) Green chemistry: theory and practice. Oxford University Press
25. Zhen Q, Bashir S, Liu JL (eds) Nanostructured materials for next-generation energy storage and conversion. Springer Berlin Heidelberg, Berlin. https://doi.org/10.1007/978-3-662-58675-4
26. Pandolfo AG, Hollenkamp AF (2006) J Power Sour 157:11–27. https://doi.org/10.1016/j.jpowsour.2006.02.065
27. Frackowiak E, Béguin F (2001) Carbon 39(6):937–950. https://doi.org/10.1016/S0008-6223(00)00183-4
28. Liu C-F, Liu Y-C, Yi T-Y, Hu C-C (2019) Carbon 145:529–548. https://doi.org/10.1016/j.carbon.2018.12.009
29. Siraj N, Macchi S, Berry B, Viswanathan T (2020) Electrochem 1(4):410–438. https://doi.org/10.3390/electrochem1040028
30. Deng J, Li M, Wang Y (2016) Green Chem 18:4824–4854. https://doi.org/10.1039/C6GC01172A

31. Fan Y, Yang X, Zhu B, Liu PF, Lu HT (2014) J Power Sour 268:584–590. https://doi.org/10.1016/j.jpowsour.2014.06.100
32. Li Y, Wang G, Wei T, Fan Z, Yan P (2016) Nano Energy 19:165–175. https://doi.org/10.1016/j.nanoen.2015.10.038
33. Wang J, Zhang X, Li Z, Ma Y, Ma L (2020) J Power Sour 451:227794. https://doi.org/10.1016/j.jpowsour.2020.227794
34. Yang H, Ye S, Zhou J, Liang T (2019) Front Chem 7:274. https://doi.org/10.3389/fchem.2019.00274
35. Tang X, Liu D, Wang Y-J, Cui L, Ignaszak A, Yu Y et al (2021) Prog Mater Sci 118:100770. https://doi.org/10.1016/j.pmatsci.2020.100770
36. Wang D-W, Li F, Liu M, Lu GQ, Cheng H-M (2007) Angew Chem Int Edit 47(2):373–376. https://doi.org/10.1002/anie.200702721
37. Liu T, Wang K, Chen Y, Zhao S, Han Y (2019) Green Energy Environ 4:171–179. https://doi.org/10.1016/j.gee.2019.01.010
38. Chen C, Zhang Y, Li Y, Dai J, Song J, Yao Y et al (2017) Energy Environ Sci 10:538–545. https://doi.org/10.1039/C6EE03716J
39. Flores-López SL, Ramírez-Montoya LA, Casal MD, Montes-Morán MA, Menéndez JA, Arenillas A (2021) Carbon 171:921–930. https://doi.org/10.1016/j.carbon.2020.09.079
40. Chen T, Dai L (2013) Mater Today 16:272–280. https://doi.org/10.1016/j.mattod.2013.07.002
41. Saini S, Chand P, Joshi A (2021) J Energy Storage 39:102646. https://doi.org/10.1016/j.est.2021.102646
42. Brewer CE, Hu Y-Y, Schmidt-Rohr K, Loynachan TE, Laird DA, Brown RC (2012) J Environ Qual 41:1115–1122. https://doi.org/10.2134/jeq2011.0118
43. Reza MT, Andert J, Wirth B, Busch D, Pielert J, Lynam JG et al (2014) Appl Bioenergy 1:11–29. https://doi.org/10.2478/apbi-2014-0001
44. Enock TK, King'ondu CK, Pogrebnoi A, Jande YAC (2017) Int J Electrochem 2017:1–14. https://doi.org/10.1155/2017/6453420
45. Abioye AM, Ani FN (2015) Renew Sust Energ Rev 52:1282–1293. https://doi.org/10.1016/j.rser.2015.07.129
46. Saini S, Chand P, Joshi A (2021) Biomass derived carbon for supercapacitor applications: review. J Energy Storage. Elsevier Ltd., 39:102646
47. Jin H, Wang X, Gu Z, Polin J (2013) J Power Sour 236:285–292. https://doi.org/10.1016/j.jpowsour.2013.02.088
48. Dehkhoda AM, Gyenge E, Ellis N (2016) Biomass Bioenergy 87:107–121. https://doi.org/10.1016/j.biombioe.2016.02.023
49. Dehkhoda AM, Gyenge E, Ellis N (2016) A novel method to tailor the porous structure of KOH-activated biochar and its application in capacitive deionization and energy storage. Biomass Bioenergy 87:107–121
50. Yao F, Pham DT, Lee YH (2015) Chemsuschem 8:2284–2311. https://doi.org/10.1002/cssc.201403490
51. Demirbas A, Arin G (2002) Energy Sour 24:471–482. https://doi.org/10.1080/00908310252889979
52. Tang W, Zhang Y, Zhong Y, Shen T, Wang X, Xia X et al (2017) Natural biomass-derived carbons for electrochemical energy storage. Mater Res Bull 88:234–241
53. Yao F, Pham DT, Lee YH (2015) Carbon-based materials for lithium-ion batteries, electrochemical capacitors, and their hybrid devices. Chemsuschem 8:2284–2311
54. Frackowiak E (2007) Carbon materials for supercapacitor application. Phys Chem Chem Phys 9:1774–1785
55. Chen T, Dai L (2013) Carbon nanomaterials for high-performance supercapacitors. Mater Today. Elsevier Ltd., 16:272–280
56. Fahmy TYA, Fahmy Y, Mobarak F, El-Sakhawy M, Abou-Zeid RE (2020) Biomass pyrolysis: past, present, and future. Environ Dev Sustain 22:17–32
57. Demirbas MF, Balat M, Balat H (2009) Potential contribution of biomass to the sustainable energy development. Energy Convers Manage 50:1746–1760

58. EBC (2012) Guidelines for a sustainable production of biochar. Eur Biochar Found 1–22
59. Conte P, Bertani R, Sgarbossa P, Bambina P, Schmidt H-P, Raga R et al (2021) Recent developments in understanding biochar's physical–chemistry. Agronomy 11:615. https://www.mdpi.com/2073-4395/11/4/615
60. Wang Z, Shen D, Wu C, Gu S (2018) State-of-the-art on the production and application of carbon nanomaterials from biomass. Green Chem. Royal Soc Chem 20:5031–5057
61. Zhu M, Diao G (2011) Review on the progress in synthesis and application of magnetic carbon nanocomposites. Nanoscale 2748–2767
62. Sevilla M, Salinas Martínez-De Lecea C, Valdés-Solís T, Morallón E, Fuertes AB (2008) Solid-phase synthesis of graphitic carbon nanostructures from iron and cobalt gluconates and their utilization as electrocatalyst supports. Phys Chem Chem Phys 10:1433–1442
63. Mehta S, Jha S, Liang H (2020) Lignocellulose materials for supercapacitor and battery electrodes: a review. Renew Sustain Energy Rev 134:110345. https://linkinghub.elsevier.com/retrieve/pii/S136403212030633X
64. Watkins D, Nuruddin M, Hosur M, Tcherbi-Narteh A, Jeelani S. Extraction and characterization of lignin from different biomass resources. J Mater Res Technol. Korea Inst Orient Med 4:26–32
65. Demirbaş A, Arin G (2002) An overview of biomass pyrolysis. Energy Sour 24:471–482
66. Abioye AM, Ani FN (2015) Recent development in the production of activated carbon electrodes from agricultural waste biomass for supercapacitors: a review. Renew Sustain Energy Rev. Elsevier Ltd., 52:1282–1293
67. Schuepfer DB, Badaczewski F, Guerra-Castro JM, Hofmann DM, Heiliger C, Smarsly B et al (2020) Assessing the structural properties of graphitic and non-graphitic carbons by Raman spectroscopy. Carbon N Y. 161:359–372. https://linkinghub.elsevier.com/retrieve/pii/S0008622319313417
68. Lyu L, Seong K, Ko D, Choi J, Lee C, Hwang T et al (2019) Recent development of biomass-derived carbons and composites as electrode materials for supercapacitors. Mater Chem Front 3:2543–2570. http://xlink.rsc.org/?DOI=C9QM00348G
69. Oya A, Marsh H (1982) Review Phenomena of catalytic graphitization. J Mater Sci 17:309–322
70. Derbyshire FJ, Presland AEB, Trimm DL (1975) Graphite formation by the dissolution-precipitation of carbon in cobalt, nickel and iron. Carbon N Y
71. Barin GB, de Fátima Gimenez I, da Costa LP, Filho AGS, Barreto LS (2014) Influence of hydrothermal carbonization on formation of curved graphite structures obtained from a lignocellulosic precursor. Carbon N Y. Elsevier Ltd., 609–612
72. Niu Q, Gao K, Tang Q, Wang L, Han L, Fang H et al (2017) Large-size graphene-like porous carbon nanosheets with controllable N-doped surface derived from sugarcane bagasse pith/chitosan for high performance supercapacitors. Carbon N Y. Elsevier Ltd., 123:290–298
73. Zhou D, Wang H, Mao N, Chen Y, Zhou Y, Yin T et al (2017) High energy supercapacitors based on interconnected porous carbon nanosheets with ionic liquid electrolyte. Microporous Mesoporous Mater. Elsevier B.V., 241:202–209
74. Sun Z, Zheng M, Hu H, Dong H, Liang Y, Xiao Y et al (2018) From biomass wastes to vertically aligned graphene nanosheet arrays: a catalyst-free synthetic strategy towards high-quality graphene for electrochemical energy storage. Chem Eng J. Elsevier B.V., 336:550–561
75. Tang W, Zhang Y, Zhong Y, Shen T, Wang X, Xia X et al (2017) Natural biomass-derived carbons for electrochemical energy storage. Mater Res Bull. Elsevier Ltd., 88:234–241
76. Ghosh S, Santhosh R, Jeniffer S, Raghavan V, Jacob G, Nanaji K et al (2019) Natural biomass derived hard carbon and activated carbons as electrochemical supercapacitor electrodes. Sci Rep. Springer US, 9:1–15
77. Jiang J, Zhang L, Wang X, Holm N, Rajagopalan K, Chen F et al (2013) Highly ordered macroporous woody biochar with ultra-high carbon content as supercapacitor electrodes. Electrochimica Acta. Elsevier Ltd., 113:481–489
78. Lonappan L, Liu Y, Rouissi T, Brar SK, Surampalli RY (2020) Development of biochar-based green functional materials using organic acids for environmental applications. J Clean Prod. Elsevier B.V., 244

79. Rangabhashiyam S, Balasubramanian P (2019) The potential of lignocellulosic biomass precursors for biochar production: performance, mechanism and wastewater application—a review. Indus Crops Prod. Elsevier, 128:405–423
80. Sun Y, Yu IKM, Tsang DCW, Fan J, Clark JH, Luo G et al (2020) Tailored design of graphitic biochar for high-efficiency and chemical-free microwave-assisted removal of refractory organic contaminants. Chem Eng J. Elsevier, 398:125505
81. Sindhu R, Binod P, Pandey A (2016) Biological pre-treatment of lignocellulosic biomass—an overview. Biores Technol 199:76–82
82. Searcy E, Flynn P, Ghafoori E, Kumar A (2007) The relative cost of biomass energy transport. Appl Biochem Biotechnol 136–140:639–652
83. Azzi ES, Karltun E, Sundberg C (2021) Small-scale biochar production on Swedish farms: A model for estimating potential, variability, and environmental performance. J Clean Prod. Elsevier Ltd., 280:124873

Carbon Nanostructures with the Ultra-High Surface Area and Porosity Derived from Biomass

Ha H. Phan and Anh N. Phan

Abstract This chapter discusses the role of surface morphology/architecture, different pore types, and pore size distribution on the performance of supercapacitors. A honeycomb-like structure of pores in surface morphology/architecture together with pores distributing evenly appeared to be the most beneficial morphology for the supercapacitors. Each of pore types (macropore, micropore and mesopore) contributes differently to the electrostatic double-layer capacitor, with macropore being the gateway for bulk electrolyte to enter the pore network, mesopore enhancing the diffusion of electrolyte into micropore, and micropore being the active sites for the electric double layer to interact with carbon electrode. The use of carbon black and binder when preparing electrodes can block micropores and mesopores, so this could be the reason why pore size distributions did not show a significant correlation to the supercapacitors. The chemical activation (KOH, $ZnCl_2$, etc.) or physical activation (CO_2) can be used to alter the pore structures with surface area up to 3326 $m^2\ g^{-1}$ and total pore volume 2.372 $cm^3\ g^{-1}$. More comprehensive analysis, focusing on morphology and macropore structure of not only biomass-derived carbon activated through chemical and physical methods but also the mixture of carbon with additives and binders in future studies, is necessary to enhance the adoption of biomass carbons in supercapacitors.

Keywords Carbon nanostructures · Ultra-high surface area · Porosity · Biomass · Supercapacitors

H. H. Phan (✉) · A. N. Phan (✉)
School of Engineering, Newcastle University, Newcastle Upon Tyne NE1 7RU, UK
e-mail: ha.phan@newcastle.ac.uk

A. N. Phan
e-mail: anh.phan@newcastle.ac.uk

S. K. Tiwari et al. (eds.), *Biomass-Based Functional Carbon Nanostructures for Supercapacitors*, Green Energy and Technology,
https://doi.org/10.1007/978-981-99-0996-4_4

1 Introduction to the Nanostructure of Carbon Electrodes in Supercapacitors

Electrostatic double-layer capacitor (EDLC) depends on the ability of generating electrical double layers on the surface between a conductive electrode and the liquid electrolyte. Therefore, materials with high surface area are commonly used as the electrode material in EDLC. Biomass is a redundant and renewable source of carbon (up to 50 wt%), so biomass-derived carbon is potentially applied in EDLC. However, there are many factors influencing the surface area of biomass-derived carbon such as biomass precursors, heat treatment temperatures and activating methods. The structures of biomass-derived carbon (the morphology and the volumes of micropores, mesopores and macropores) control the diffusion of electrolyte ions and the accessibility of ions to the surface.

The surface area and porosity of biomass-derived carbon are normally measured by gas adsorption–desorption techniques via N_2 adsorption–desorption isotherm at −196 °C and Brunauer–Emmett–Teller (BET) equation to analyze the surface area (BET SA) and total pore volume, and CO_2 adsorption–desorption at 0 °C and Dubinin Radushkevich (DR) equation to determine the ultra-micropore volume <0.7 nm (DR V_{CO2}) [11, 30]. The former provides a general view on specific surface area of the material, total pore volume (V_{total}), BET micropore volume (V_{micro}) and mesopore volume (V_{meso}). However, using BET equation to calculate the BET SA could be misleading if the adsorption isotherm falls into type I according to IUPAC classification [26]. One essential requirement to apply BET equation is the infinite accumulation of adsorbate layers on the surface of the adsorbent. In the case of type I adsorption isotherm (which is frequently observed for carbon materials), the number of adsorbate layers is likely to be inhibited due to narrow micropores, and this results in the pore filling phenomenon instead of forming adsorbate layers. The low temperature at −196 °C also inhibits the diffusion of the adsorbate e.g., N_2, leading to activated diffusion effect. Therefore, BET SA values do not reflect the correct surface area of the carbon samples, and V_{micro} may only account to bigger micropores in the range of 0–2 nm. The latter (CO_2 adsorption) is a suitable method to complement the V_{micro} measured from N_2 adsorption isotherms at −196 °C. However, these two methods do not cover the macropore volume. Until now, the main method to examine the macropore volume is the mercury porosimetry [27]. The mercury intrusion method can provide information of any pore higher than 6 nm and cover most pores in the scale of micrometer. Performing all these analyses on one sample is imperative to understand the performance of the supercapacitor, but it could be difficult due to limits in experimental instruments. The complexity of micropore, mesopore and macropore also hinders the understanding of the surface area and porosity even if all analysis could be performed. To visualize the pore architecture in one carbon sample, imaging techniques such as transmission electron microscope (TEM) and scanning electron microscope (SEM) are conducted [6, 40]. These techniques help understand how pores are organized in the carbon and how they are connected to each other because

this information could not be obtained through the gas adsorption–desorption techniques. This chapter will try to unveil the relations between surface area, pore types and surface morphology and the performance of supercapacitors.

Biomass-derived carbon is commonly obtained via thermochemical process such as pyrolysis at a temperature range of 250–900 °C in an inert environment e.g. N_2. However, solely pyrolysis has little enhancement in BET SA and V_{total} e.g. BET SA of biomass-derived carbon was only 2–8 $m^2\ g^{-1}$ at a temperature range of 350–700 °C [7, 8]. Increasing temperature only has a small increase in BET SA [8]. Therefore, activation methods are required to improve BET SA and V_{total} of biomass-derived carbon. This chapter will also discuss on some methods to improve the surface area, pore volume and morphology of biomass-derived carbon.

2 Roles of Morphology, Surface Areas, Pore Size and Pore Distribution on Specific Capacitance and Energy Density

2.1 Surface Morphology and Pore Size Distribution

Table 1 summarizes the specific capacitance of biomass-derived carbons with their porosity properties. The majority of biomass-derived carbons demonstrated high specific capacitances >200 F g^{-1} at a current density of 0.5–1 A g^{-1}, and the capacitance range of 374–409.7 F g^{-1} was among the highest capacitances reported. The morphologies of carbons demonstrating high specific capacitance in the range of 374–409.7 F g^{-1} at 0.5 A g^{-1} are illustrated in Fig. 1, presenting honeycomb-like structure carbons with pores up to 2–3 μm. The pore networks are channeled through the whole samples in the micrometer scale, and the pores were distributed evenly with thin pore walls. Furthermore, these carbons showed the sheet-like carbon layer structures without any carbon lumps and various small pores in the nanometer scale. This architecture supported the electrolyte diffusion throughout the carbon samples, allowed EDLCs to form on the surface of carbon and helped explain the high supercapacitances in all five carbons despite the differences in biomass precursors and preparation processes. Although BET SA and V_{total} of these carbons varied significantly in a range of 973.5–3326 $m^2\ g^{-1}$ and 0.54–2.372 $cm^3\ g^{-1}$, the change in specific capacitances is negligible. These reveal that pore shapes and pore architectures are crucial for supercapacitors as shown in Fig. 1, and the measured BET SA and V_{total} were not the main factors governing the performance of the supercapacitors.

Figure 2 summarizes the SEM and TEM images of some carbons with specific capacitances in the range of 162–194 F g^{-1} using 6 M KOH electrolyte at 0.5 A g^{-1}, exhibiting specific capacitances lower than those illustrated in Fig. 1. Pores with thick pore walls were randomly distributed in these carbon particles, and there were big carbon flakes rather than pore network structures. Also, they appeared to have multilayer structures in a particle at the nanometer scale, so this structure decreased the number of carbon active sites and the EDLC on the carbon surface subsequently,

Table 1 Surface area, pore volumes and specific capacitances values of different carbon materials

Carbon	BET SA ($m^2\ g^{-1}$)	V_{total} ($cm^3\ g^{-1}$)	V_{micro} ($cm^3\ g^{-1}$)	V_{meso} ($cm^3\ g^{-1}$)	Electrolyte	Specific capacitance ($F\ g^{-1}$)	Current density ($A\ g^{-1}$)	Scan rate ($mV\ s^{-1}$)	Refs.
AC	2059				Na_2SO_4 1 M	358.4	0.5		[18]
AC	2059				Na_2SO_4 1 M	270.4	20		
AC	2059				Na_2SO_4 1 M	200.2	100		
CO_2-AC	603.5		0.416		H_2SO_4 1 M	56.8	1		[3]
NaOH-AC	1011		0.486		H_2SO_4 1 M	125.9	1		[3]
LMiPC2	3230	1.67	1.41	0.26	KOH 6 M	369	0.5		[19]
LMiPC2	3230	1.67	1.41	0.26	KOH 6 M	344	1		
LMiPC2	3230	1.67	1.41	0.26	KOH 6 M	267	2		
LMiPC2	3230	1.67	1.41	0.26	H_2SO_4	398	0.5		[19]
ABC-700	1728.7	0.697	0.671	0.026	KOH 1 M				[29]
ABC-800	2279.5	0.988	0.907	0.081	KOH 1 M				
ABC-900	2330.9	1.914	0.975	0.939	KOH 1 M	175.6	0.5		
DDLGC/GO8	893.9	0.515			KOH 6 M	366	1		[37]
DDLGC/GO8	893.9	0.515			KOH 6 M	176	20		
DAC-800	1140	0.584	0.171	0.413	H_2SO_4 2 M	298	0.5		[5]
DAC-800	1140	0.584	0.171	0.413	H_2SO_4 2 M	131	20		
MAC	1726	0.890	0.442	0.448	H_2SO_4 2 M	367	0.5		[5]
MAC	1726	0.890	0.442	0.448	H_2SO_4 2 M	244	20		
ANPC-1	679	0.490	0.276	0.214	KOH 6 M	150.5	0.5		[20]

(continued)

Table 1 (continued)

Carbon	BET SA ($m^2\ g^{-1}$)	V_{total} ($cm^3\ g^{-1}$)	V_{micro} ($cm^3\ g^{-1}$)	V_{meso} ($cm^3\ g^{-1}$)	Electrolyte	Specific capacitance ($F\ g^{-1}$)	Current density ($A\ g^{-1}$)	Scan rate ($mV\ s^{-1}$)	Refs.
ANPC-2	1083	0.628	0.431	0.197	KOH 6 M	187.5	0.5		[20]
ANPC-3	1749	0.924	0.698	0.226	KOH 6 M	243.2	0.5		
ANPC-3	1749	0.924	0.698	0.226	KOH 6 M	197.7	10		
NKGLC	906	0.400	0.29	0.11	KOH 1 M	345	0.2		[41]
NKGLC	906	0.400	0.29	0.11	KOH 1 M	290	0.5		
NKGLC	906	0.400	0.29	0.11	KOH 1 M	268	1		
KGLC						300	0.2		[41]
HFC-2	1577	0.86			KOH 6 M	177	1		[39]
HFC-3	1700	0.95			KOH 6 M	238	0.5		[39]
HFC-3	1700	0.95			KOH 6 M	216	1		
HFC-3	1700	0.95			KOH 6 M	176	8		
HFC-4	1726	1.07			KOH 6 M	184	1		[39]
SE-600	261	0.169			H_2SO_4 0.5 M	149		5	[14]
SE-600	261	0.169			H_2SO_4 0.5 M	43	2		
SE-700	476	0.453			H_2SO_4 0.5 M	334	1		
SE-700	476	0.453			H_2SO_4 0.5 M	273	2		
SE-700	476	0.453			H_2SO_4 0.5 M	150	10		
SE-700	476	0.453			H_2SO_4 0.5 M	509		5	
SE-700	476	0.453			KOH 1 M	149		5	

(continued)

Table 1 (continued)

Carbon	BET SA ($m^2\ g^{-1}$)	V_{total} ($cm^3\ g^{-1}$)	V_{micro} ($cm^3\ g^{-1}$)	V_{meso} ($cm^3\ g^{-1}$)	Electrolyte	Specific capacitance ($F\ g^{-1}$)	Current density ($A\ g^{-1}$)	Scan rate ($mV\ s^{-1}$)	Refs.
SE-700	476	0.453			Na_2SO_4 0.5 M	124		5	
SE-800	450	0.330			H_2SO_4 0.5 M	300		5	
SE-800	450	0.330			H_2SO_4 0.5 M	180	2		
AC_F-3	1175	0.598	0.212	0.212	KOH 6 M	195.2	1		[44]
AC_F-4	1232	0.647	0.276	0.276	KOH 6 M	256.2	1		
AC_F-4.5	1904	1.019	0.553	0.466	KOH 6 M	286.8	1		
AC_F-4.5	1904	1.019	0.553	0.466	KOH 6 M	180	10		
AC_F-5	1254	0.565	0.232	0.232	KOH 6 M	269.4	1		
GC	21.3	0.03			H_2SO_4 1 M	39		10	[46]
KGC	853.4	0.38	0.26	0.12	H_2SO_4 1 M	281		10	
ZnGC	824.6	0.43	0.23	0.20	H_2SO_4 1 M	102		10	
BGC	346.4	0.34	0.09	0.25	H_2SO_4 1 M	45		10	
KGC	853.4	0.38	0.26	0.12	H_2SO_4 1 M	374	0.5		[46]
KGC	853.4	0.38	0.26	0.12	H_2SO_4 1 M	335	1		
CBAC	786	0.212			KOH 6 M	449	1		[35]
CBAC	786	0.212			KOH 6 M	176	20		
WFT-700	2739	1.452	0.974	0.478	KOH 6 M	286	2		[22]
WFT-700	2739	1.452	0.974	0.478	KOH 6 M	236	10		
WFT-800	3977	2.215	1.062	1.153	KOH 6 M	379.7	0.5		

(continued)

Table 1 (continued)

Carbon	BET SA ($m^2\ g^{-1}$)	V_{total} ($cm^3\ g^{-1}$)	V_{micro} ($cm^3\ g^{-1}$)	V_{meso} ($cm^3\ g^{-1}$)	Electrolyte	Specific capacitance ($F\ g^{-1}$)	Current density ($A\ g^{-1}$)	Scan rate ($mV\ s^{-1}$)	Refs.
WFT-800	3977	2.215	1.062	1.153	KOH 6 M	321.4	2		
WFT-800	3977	2.215	1.062	1.153	KOH 6 M	268	10		
WFT-900	3326	2.372	0.208	2.164	KOH 6 M	409.7	0.5		
WFT-900	3326	2.372	0.208	2.164	KOH 6 M	354.4	2		
WFT-900	3326	2.372	0.208	2.164	KOH 6 M	297	10		
EWC-1	2838	1.333	0.830	0.503	KOH 6 M	284	0.5		[47]
EWC-2	2918	1.281	1.091	0.190	KOH 6 M	335	0.5		
EWC-2	2918	1.281	1.091	0.190	KOH 6 M	240	20		
EWC-3	2839	1.322	0.661	0.663	KOH 6 M	306	0.5		
MG-6	1705	0.920	0.215	0.705	KOH 6 M	75	0.5		[38]
MG-12	2062	1.148	0.205	0.943	KOH 6 M	112	0.5		
MG-18	1816	0.897	0.262	0.635	KOH 6 M	162	0.5		
MG-24	1953	0.981	0.216	0.765	KOH 6 M	84	0.5		
MG-48	1444	0.788	0.085	0.703	KOH 6 M	58	0.5		
SSC-600	421.2	0.185	0.154	0.031	KOH 1 M	93.6	0.5		[15]
SSC-700	2012.6	0.849	0.713	0.136	KOH 1 M	380.5	0.5		
SSC-700	2012.6	0.849	0.713	0.136	KOH 1 M	251.6	10		
SSC-800	2266.2	1.022	0.811	0.211	KOH 1 M	204.5	0.5		
AC-600	624.1	0.34			KOH 6 M	202.9	0.5		[32]

(continued)

Table 1 (continued)

Carbon	BET SA ($m^2\ g^{-1}$)	V_{total} ($cm^3\ g^{-1}$)	V_{micro} ($cm^3\ g^{-1}$)	V_{meso} ($cm^3\ g^{-1}$)	Electrolyte	Specific capacitance ($F\ g^{-1}$)	Current density ($A\ g^{-1}$)	Scan rate ($mV\ s^{-1}$)	Refs.
AC-700	771.6	0.61			KOH 6 M	237.4	0.5		
AC-800	973.5	0.75			KOH 6 M	408.8	0.5		
PCBL-3	992.4	0.618	0.471	0.147	H_2SO_4 1 M				
PCBL-5	936.1	0.573	0.502	0.071	H_2SO_4 1 M	293	1		[34]
PCBL-7	900.8	0.548	0.425	0.125	H_2SO_4 1 M	215	1		
PCBL-3	992.4	0.618	0.471	0.147	NaOH 1 M	111	1		
PCBL-5	936.1	0.573	0.502	0.071	NaOH 1 M	197	1		
PCBL-7	900.8	0.548	0.425	0.125	NaOH 1 M	168	1		
PCBL-3	992.4	0.618	0.471	0.147	Na_2SO_4 1 M	111	1		
PCBL-5	936.1	0.573	0.502	0.071	Na_2SO_4 1 M	197	1		
PCBL-7	900.8	0.548	0.425	0.125	Na_2SO_4 1 M	168	1		
2 M-800°C	1288	0.75	0.48	0.27	KOH 6 M	376	0.5		[43]
2 M-800°C	1288	0.75	0.48	0.27	KOH 6 M	354	1		
2 M-800°C	1288	0.75	0.48	0.27	KOH 6 M	255	50		
WBC-1	1846	0.95	0.88	0.07	KOH 6 M	243	1		[17]
WBC-2	2352	1.17	1.11	0.06	KOH 6 M	268	1		
WBC-2	2352	1.17	1.11	0.06	KOH 6 M	222	10		
WBC-3	1905	0.93	0.89	0.04	KOH 6 M	186	1		
AC-$ZnCl_2$	1571				KOH 6 M	2.45			[16]

(continued)

Table 1 (continued)

Carbon	BET SA ($m^2\ g^{-1}$)	V_{total} ($cm^3\ g^{-1}$)	V_{micro} ($cm^3\ g^{-1}$)	V_{meso} ($cm^3\ g^{-1}$)	Electrolyte	Specific capacitance ($F\ g^{-1}$)	Current density ($A\ g^{-1}$)	Scan rate ($mV\ s^{-1}$)	Refs.
AC-2	1422.7	0.767	0.328	0.439	KOH 6 M	156			[2]
CSPCN8	675	0.268			KOH 1 M	144.6	0.5		[4]
CSPCN8	675	0.268			KOH 4 M	202.9	0.5		
CSPCN8	675	0.268			KOH 5 M	261.8	0.5		
HPC-0.25	1273.9	0.66	0.340	0.320	KOH 6 M				[24]
HPC-0.5	2027.7	1.06	0.580	0.480	KOH 6 M				
HPC-1	2787.5	1.60	0.036	1.564	KOH 6 M	253	0.5		
HPC-1	2787.5	1.60	0.036	1.564	KOH 6 M	199	10		
NC	28	0.127		0.127	KOH 6 M	41.1	0.5		[45]
NC	28	0.127		0.127	KOH 6 M	30.5	1		
NC	28	0.127		0.127	KOH 6 M	7	15		
NHPC	1067	0.486	0.244	0.243	KOH 6 M	233.3	0.5		
NHPC	1067	0.486	0.244	0.243	KOH 6 M	228.7	1		
NHPC	1067	0.486	0.244	0.243	KOH 6 M	198	10		
NHPC	1067	0.486	0.244	0.243	KOH 6 M	174	20		
BHPC-AP	1624.8	0.931	0.788	0.143	KOH 6 M	253.7	1		[9]
BHPC-AP	1624.8	0.931	0.788	0.143	KOH 6 M	225.6	50		
SC-700	236.4	0.147	0.084	0.063	KOH 6 M	125	0.5		[13]
SC-Mg-700	624.3	0.912	0.171	0.741	KOH 6 M	172	0.5		

(continued)

Table 1 (continued)

Carbon	BET SA ($m^2\ g^{-1}$)	V_{total} ($cm^3\ g^{-1}$)	V_{micro} ($cm^3\ g^{-1}$)	V_{meso} ($cm^3\ g^{-1}$)	Electrolyte	Specific capacitance ($F\ g^{-1}$)	Current density ($A\ g^{-1}$)	Scan rate ($mV\ s^{-1}$)	Refs.
SC-Zn-700	950.3	1.286	0.086	1.200	KOH 6 M	263	0.5		
SC-Zn-700	950.3	1.286	0.086	1.200	KOH 6 M	140	10		
HHC	2189.2	1.1			KOH 6 M	294	0.5		[36]
HHC	2189.2	1.1			KOH 6 M	290	1		
PGC	1103	0.54			KOH 6 M	374	0.5		[23]
KOH-0.1	717	0.34	0.18	0.16	KOH 6 M				[1]
KOH-0.5	1351	0.55	0.34	0.21	KOH 6 M	162	1		
KOH-1	1063	0.47	0.30	0.17	KOH 6 M	161	1		
KOH-2	1579	0.59	0.39	0.20	KOH 6 M				[28]

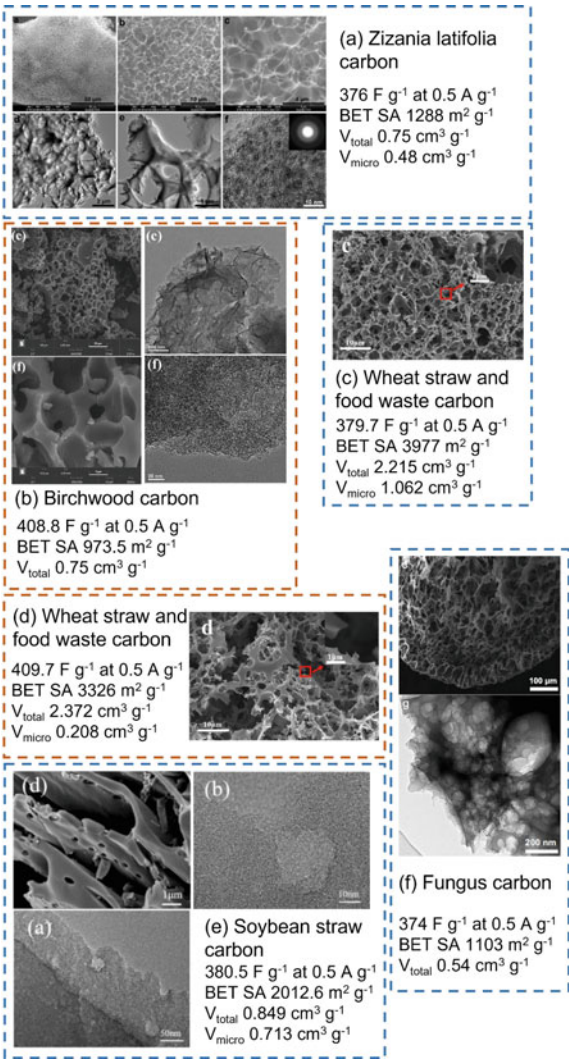

Fig. 1 Carbon materials with similar morphology demonstrated high specific capacitances of 335–409.7 F g^{-1}: **a** Zizania latifolia carbon (2 M-800°C) (adapted from [43]). **b** Birchwood carbon (AC-800) (adapted from [32]). **c** Wheat straw and food waste carbonized at 800 °C (WFT-800) and **d** at 900 °C (WFT-900) (adapted from [22]). **e** Soybean straw carbon (SSC-700) (adapted from [15]). **f** Fungus carbon (PGC) (adapted from [23]). The specific capacitances were obtained from galvanostatic charge–discharge curve using three electrode systems in KOH 6 M as electrolyte (SSC-700 used KOH 1 M). *Note* BET SA: BET surface area, V_{total}: total pore volume, V_{micro}: micropore volume. These were obtained from N_2 adsorption isotherm at −196 °C

leading to lower specific capacitances. This structure is significantly different from the honeycomb-like structure observed in Fig. 1. BET SA and V_{total} of these carbons varied in the ranges of 950.3–2787.3 m^2 g^{-1} and 0.486–1.60 cm^3 g^{-1}, overlapping with the surface areas and pore volumes reported in Fig. 1. Therefore, it can be concluded that these carbons did not provide excellent electrolyte diffusion and accessibility although they have similar BET SA and V_{total}. This further ascertains that the BET SA and V_{total} are not the only factors controlling the performance of biomass-derived carbons, and it is required to use imaging technique such as SEM and TEM to have a better understanding on the pore structure of carbons.

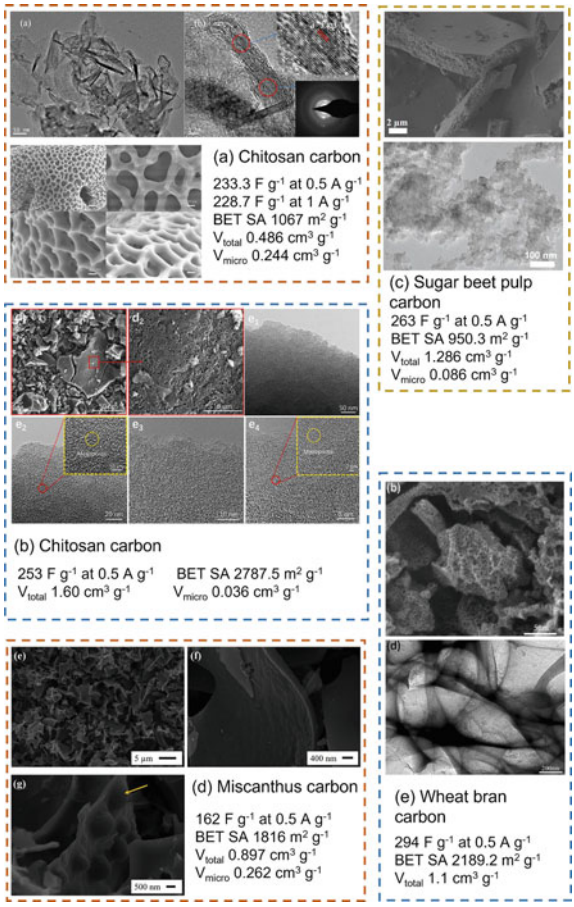

Fig. 2 Carbon materials with different morphologies demonstrated specific capacitances of 162–294 F g^{-1}: **a** Chitosan carbon (NHPC) [45], **b** Chitosan carbon (HPC-1) [24], **c** Sugar beet pulp carbon (SC-Zn-700) [13], **d** Miscanthus carbon (MG-18) [38], **e** Wheat bran carbon (HHC) [36]. The specific capacitances were obtained from galvanostatic charge-discharged curve using three electrode systems using KOH 6 M as the electrolyte

Figure 3 presents the pore size distributions of all biomass-derived carbons that have a majority of micropores in the range of 0.5–2 nm with small portions of mesopores in the range of 2–20 nm. No pore sizes <0.5 nm was observed due to activated diffusion effect at extremely low temperatures (−196 °C), which inhibited N_2 from diffusing into ultra-micropores of carbons. In addition, no pore size distribution >50 nm (macropores) was shown, indicating the limits of gas adsorption–desorption techniques, so no relation between pore observed in SEM images and pore volumes could be concluded. In the cases of carbon AC-800 °C (Fig. 3b), the pore sizes <20 nm were not demonstrated clearly, which hindered the understanding of relations between micropores and mesopores and the performance of supercapacitors.

Pore size distributions of carbons in high specific capacitance range (335–409.7 F g^{-1}) are illustrated in Fig. 3a–e. Majority of pores in carbon 2 M–800 °C (Fig. 3a) were micropores <2 nm with little mesopores [43]. The pores of WFT-800 were

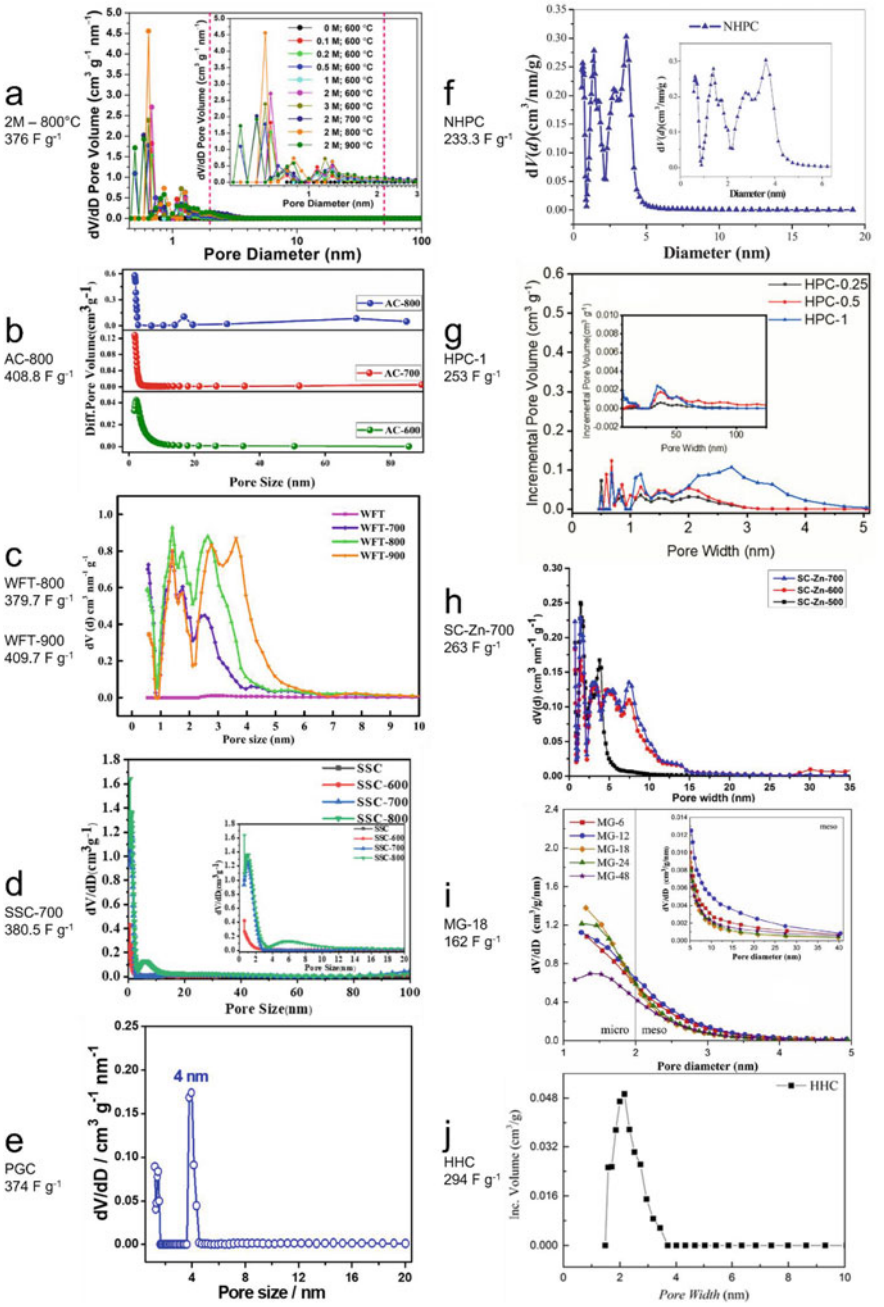

Fig. 3 Pore size distribution of different biomass carbons **a** 2 M-800 °C [43], **b** AC-800 [32], **c** WFT-800 and WFT-900 [22], **d** SSC-700 [15], **e** PGC [23], **f** NHPC [45], **g** HPC-1 [24], **h** SC-Zn-700 [13], **i** MG-18 [38] and **j** HHC [36]. The specific capacitance values were measured at 0.5 A g^{-1} in KOH 6 M electrolyte

distributed relatively even in the range of 0.5–4 nm (Fig. 3c) [22]. Most micropores of SSC-700 were smaller than 2 nm with little mesopores (Fig. 3d) [15] whereas PGC had some micropores at ~1 nm and only mesopores at 4 nm (Fig. 3e) [23]. The pore size distribution of AC-800 did not provide a clear insight due to the lack of resolution (Fig. 3b) [32]. When comparing carbon samples in the same studies, WFT-900 had more pores in the range 3–5 nm and a slightly higher capacitance (409.7 F g^{-1}) compared to WFT-800 (379.7 F g^{-1}) [22]. However, SSC-800 had lower capacitance (204.5 F g^{-1}) compared to SSC-700 (380.5 F g^{-1}) even though there was an addition of mesopores in the range of 4–8 nm to SSC-800 [15]. By comparing the surface morphology (Fig. 1) and pore size distributions (Fig. 3a–e), it showed that the differences of pore size distributions of carbons (Fig. 3a–e) from N_2 adsorption–desorption isotherm could not describe the changes in carbon morphologies and pore architectures observed in SEM and TEM images (Fig. 1). The comparison of the pore distributions of carbons with lower specific capacitances (162–294 F g^{-1}) (Fig. 3f–g) and their corresponding surface morphologies (Fig. 2) also gave a similar conclusion. SEM and TEM images provided specific information about surface morphology and complemented the understanding of pore size distributions.

This also revealed that there is a little relation between pore distributions and the performances of supercapacitors. NHPC carbon (Fig. 3f) had more micropores and mesopores distributing in the range of 0.5–5 nm compared to PGC (Fig. 3e) [45] although the capacitance of NHPC (233.3 F g^{-1}) was lower than PGC (374 F g^{-1}). Majority of pores in MG-18 (Fig. 3i) were micropores [38], similar to 2 M–800 °C (Fig. 3a) [43], but MG-18 demonstrated a much lower capacitance at only 162 F g^{-1}. HPC-1 (Fig. 3g) had the same pore distribution but less pores at each diameter compared to NHPC (Fig. 3f), but HPC-1 still showed a slightly higher capacitance compared to NHPC. Therefore, there is no significant correlation between pore size distributions and capacitance values. The presence of hierarchical pore structures in all biomass-derived carbons with plenty micropores and mesopores does not guarantee the optimal performance of supercapacitors.

2.2 Role of Each Pore Type in Supercapacitors

Honeycomb-like structures might play an important role in supercapacitors, but it is evident in different studies that increasing surface area and pore size still have effect on the supercapacitors. For example, the study on chitosan carbon showed that a lack of BET SA (28 m^2 g^{-1}) and V_{total} (0.127 cm^3 g^{-1}) resulted in a low capacitance of 41.1 F g^{-1} at 0.5 A g^{-1} in KOH 6 M, compared to 233.3 F g^{-1} of NHPC carbon with BET SA 1067 m^2 g^{-1} and V_{total} 0.486 cm^3 g^{-1} [45]. In some studies, the correlation between BET SA and V_{total} were well observed, such as chitosan carbons obtained through freeze-drying and activation with KOH showed that the increase in BET SA from 1273.9 m^2 g^{-1} to 2787.5 m^2 g^{-1} and V_{total} from 0.66 cm^3 g^{-1} to 1.60 cm^3 g^{-1} improved the specific capacitance to 253 F g^{-1} at 0.5 A g^{-1} in KOH 6 M [24]. The correlation of specific capacitances of hibiscus flower derived carbon electrode and

BET SA and V_{total} was also reported [39]: increasing BET SA increased from 1577 $m^2\ g^{-1}$ to 1700 $m^2\ g^{-1}$ and V_{total} from 0.86 $cm^3\ g^{-1}$ to 0.95 $cm^3\ g^{-1}$ enhanced the specific capacitance from 177 F g^{-1} to 216 F g^{-1}. This also followed the trend of soybean powder carbons [20]. However, further increase in BET SA (1726 $m^2\ g^{-1}$) and V_{total} (1.07 $cm^3\ g^{-1}$) of hibiscus flower derived carbon decreased the specific capacitance from 216 F g^{-1} to 184 F g^{-1} [39]. More amorphous carbon could be generated due to the activating reactions between KOH and carbon materials, and subsequently this decreased the size of ordered carbon crystals that were responsible for the transport of electrons.

The differences in these studies and the results discussed in Sect. 2.1 reveal that there is a discrepancy in interpretating the influence of surface area and pore size on supercapacitors. Besides the honeycomb-like structures assembling from sheet-like carbon layers (observed in TEM and SEM images), biomass-derived carbons require certain pores and surface areas to form the EDLC, and the relations between these characteristics of carbon with supercapacitors need to be explored.

Micropores are important for the formation of EDLC because they (0.7–2 nm) serve as a storage for electrolyte ions in the electrodes where electron exchanges occur. Therefore, depending upon the properties of electrolytes, the requirements of the size of micropores and pore distributions may vary, and increasing micropores should generally enhance the capacitances. Micropores >0.7 nm benefit the specific capacitances due to the ability to create the EDLC in this pore range [10]. However, micropores in the range of <0.7 nm—at the expense of micropores of 0.7–2 nm—decreased the capacitance of the electrodes [1] since they decrease the available electrode surfaces, inhibit the accessibility of electrolyte ions onto the surface of electrodes, and prevent the formation of EDLC. Mesopores (2–50 nm) are the pathways connecting micropores and macropores for the diffusion of electrolyte ions. The mesopore volume (V_{meso}) in the range of 20–50% of V_{total} benefits the specific capacitances because it enhances the diffusion of electrolyte ions into micropores, and some electron exchanges could occur in this pore range [12]. However, increasing the mesopore volume ratio beyond this range decreased the specific capacitances due to the decrease in carbon active sites [38]. For example, miscanthus grass was directly soaked with KOH at a mass ratio biomass/KOH 1:4 at different soaking times and is activated at 800 °C in N_2 [38]. The V_{micro} varied only in the range of 0.205–0.262 $cm^3\ g^{-1}$, indicating the soaking time of 6–24 h did not influence micropore structures. However, the minimum V_{meso} 0.635 $cm^3\ g^{-1}$ was achieved at 18 h of soaking time, yielding the specific capacitance of 162 F g^{-1} at 0.5 A g^{-1}, but the capacitance decreased to only 112 F g^{-1} at the maximum mesopore volume of 0.943 $cm^3\ g^{-1}$. High V_{meso} decreased the number of active sites, and the EDLC could not form on the surface of the material, leading to the reduction in capacitance.

Unlike micropores and mesopores, macroporosity could only be obtained from mercury porosimetry, so there is a limited number of studies reporting macroporosity. The micropores, mesopores and macropores of cellulose derived carbons were analyzed in the study of Abouelamaiem et al. [1]. The α-cellulose was dispersed in H_2O and stirred for 2 min in a blender to create a homogeneous mixture. This mixture was pressed to remove the water, and the obtained cellulose was mixed with

KOH at the mass ratio KOH/cellulose 0.005:1 (KOH-0.005), 0.1:1 (KOH-0.1), 0.5:1 (KOH-0.5) and 2:1 (KOH-2). These mixtures of KOH and cellulose were carbonized at 850 °C for 2 h under N_2.

The mercury porosimetry revealed that the macropore volume (V_{macro}) of KOH-0.5 carbon (1.01 $cm^3\ g^{-1}$) was significantly higher than KOH-0.005 (0.008 $cm^3\ g^{-1}$), indicating that increasing the mass of KOH remarkably enhanced V_{macro}. When mixing these two carbons KOH-0.005 and KOH-0.5 with carbon black and polyvinylidene fluoride (as a binder), KOH-0.5 retained most of its micropores and mesopores (2–10 nm) while all micropores and mesopores of KOH-0.005 were blocked. The results demonstrated the importance of macropores in preserving the micropore and mesopore structures for EDLC with the areas under cyclic voltammetry curve of these samples increased with the increase of V_{macro} from 0.008 to 1.01 $cm^3\ g^{-1}$. Mixing carbon black and polyvinylidene fluoride blocked all micropores and mesopores in the carbon and turned the carbon into an open surface electrode, but this phenomenon was not observed with other cellulose carbons with higher V_{macro} (1.01–5.17 $cm^3\ g^{-1}$). Increasing mass ratio KOH/cellulose to 1:1 improved the V_{macro} of KOH-1–3.45 $cm^3\ g^{-1}$ but it did not result in any remarkable difference in supercapacitance between KOH-0.5 and KOH-1 (162 and 161 F g^{-1} respectively). V_{macro} higher than 1.01 $cm^3\ g^{-1}$ is suitable for the carbons used in the supercapacitor electrode [1], and the pore blocking effect observed in this study may also explain why there is a significant change in the pore structures among carbons in Table 1 although their specific capacitances were similar.

Table 2 summarizes the energy density of some biomass-derived carbons. The energy density is related to the amount of energy that a supercapacitor can store and release in one charge—discharge cycle, and the energy densities in Table 2 were obtained from the two electrode systems simulating a real supercapacitor. Energy densities varied remarkably with changing carbon samples and the electrolyte ions. When using KOH 6 M as the electrolyte, NHPC presented the highest energy density of 25.7 Wh kg^{-1} with power density of 500 W kg^{-1} [45], and HPC-1 showed the lowest energy density of 6.53 at a power density of 250.1 W kg^{-1} [24]. Higher BET SA and V_{total} of HPC-1 (2787.5 $m^2\ g^{-1}$ and 1.60 $cm^3\ g^{-1}$) compared to 1067 $m^2\ g^{-1}$ and 0.486 $cm^3\ g^{-1}$ of NHPC did not correlate with the energy density of the supercapacitor. This showed that the energy densities did not correlate with surface areas and pore volumes, similar to specific capacitance in Table 1. Furthermore, most studies only reported energy densities of one single carbon among a range of prepared carbons, resulting in a lack of data in literature. A wide range of electrolytes and concentrations available in the literature also made the data scattered. Different ion activities of electrolytes directly influence the energy density, so future studies of supercapacitors should pay more attention to how surface areas and morphologies control the energy density of the supercapacitor.

Table 2 Energy density and power density of some biomass-derived carbon materials

Carbon	BET SA ($m^2\ g^{-1}$)	V_{micro} ($cm^3\ g^{-1}$)	V_{meso} ($cm^3\ g^{-1}$)	V_{total} ($cm^3\ g^{-1}$)	Electrolyte	Energy density (Wh kg^{-1})	Power density (W kg^{-1})	Refs.
ANPC-3	1749	0.924	0.698	0.226	KOH 6 M	12.5	450	[20]
WFT-900	3326	2.372	0.208	2.164	KOH 6 M	11.3	240	[22]
WFT-900	3326	2.372	0.208	2.164	KOH 6 M	7.6	4716.1	
EWC-2	2918	1.281	1.091	0.190	KOH 6 M	13.6	300	[47]
EWC-2	2918	1.281	1.091	0.190	KOH 6 M	8.4	6048	
MG-12	2062	1.148	0.205	0.943	KOH 6 M	8	377	[38]
AC-800	973.5	0.75			KOH 6 M	6.9	112.7	[32]
AC-800	973.5	0.75			KOH 6 M	20.6	350.3	[32]
N-ACU1	640.6	0.73			KOH 6 M	11.05	795.77	[31]
N-ACU2	477.5	0.43			KOH 6 M	13.48	970.24	
N-ACU3	445.2	0.30			KOH 6 M	19.89	1431.20	
HPC-1	2787.5	1.60	0.036	1.564	KOH 6 M	6.53	250.1	[24]
HPC-1	2787.5	1.60	0.036	1.564	KOH 6 M	5.83	4997.1	
NHPC	1067	0.486	0.244	0.243	KOH 6 M	25.7	500	[45]
NHPC	1067	0.486	0.244	0.243	KOH 6 M	22.6	800	
NHPC	1067	0.486	0.244	0.243	KOH 6 M	7.2	20,000	
BHPC-AP	1624.8	0.931	0.788	0.143	KOH 6 M	12.11	250	[9]
CSPCN8	675	0.268			KOH 5 M	12.6	105.7	[4]
NKGLC	906	0.400	0.29	0.11	KOH 1 M	42.2	700	[41]
SSC-700	2012.6	0.849	0.713	0.136	KOH 1 M	8.95	25	[15]
SSC-700	2012.6	0.849	0.713	0.136	KOH 1 M	5	2500	

(continued)

Table 2 (continued)

Carbon	BET SA ($m^2\ g^{-1}$)	V_{micro} ($cm^3\ g^{-1}$)	V_{meso} ($cm^3\ g^{-1}$)	V_{total} ($cm^3\ g^{-1}$)	Electrolyte	Energy density (Wh kg^{-1})	Power density (W kg^{-1})	Refs.
PCBL-3	992.4	0.618	0.471	0.147	NaOH 1 M	8.29	139.19	
PCBL-5	936.1	0.573	0.502	0.071	NaOH 1 M	21.85	162.78	
PCBL-7	900.8	0.548	0.425	0.125	NaOH 1 M	15.37	146.72	
PCBL-3	992.4	0.618	0.471	0.147	Na_2SO_4 1 M	11.78	163.47	
PCBL-5	936.1	0.573	0.502	0.071	Na_2SO_4 1 M	16.12	178.44	
PCBL-7	900.8	0.548	0.425	0.125	Na_2SO_4 1 M	8.01	124.34	
2 M-800°C	1288	0.75	0.48	0.27	Na_2SO_4 1 M	20.07	500	[43]
	2059				Na_2SO_4 1 M	49.7	247.8	[18]
	2059				Na_2SO_4 1 M	27.8	16,400	[18]
MAC	1726	0.890	0.442	0.448	H_2SO_4 2 M	9.55	478	[5]
PCBL-5	936.1	0.573	0.502	0.071	H_2SO_4 1 M	26.5	173.45	[34]
SE-700	476	0.453			H_2SO_4 0.5 M	63.33		[14]
LMiPC2	3230	1.67	1.41	0.26	$EMIMBF_4$	61.2	468.8	[19]
LMiPC2	3230	1.67	1.41	0.26	$EMIMBF_4$	43.5	13,300	

3 Biomass-Derived Carbons

KOH is commonly used to prepare high surface area and porous carbon materials [7, 19, 29]. Either original biomass or the biochar from pyrolysis can be activated with KOH at high temperatures (700–900 °C). In the case of biochar, the temperatures of the pyrolysis process significantly influenced the porosity of the material, which affected the permeability of KOH. High pre-treatment pyrolysis temperatures e.g. >750 °C, created a rigid structure of biochar, and KOH activation has little effect on BET SA [7]. At lower temperatures of pyrolysis (≤700 °C), the biochar activated in KOH (AC) demonstrated the improvement in specific capacitance due to an increase in micropores (1–2 nm) in flaxseed derived carbon (LMiPC2) (the biochar pyrolyzed at 700 °C was activated with KOH at mass ratio biochar/KOH 1:4) [19] and pine sawdust-derived carbon (the biochar pyrolyzed at 700 °C was activated with KOH at the mass ratio biochar/KOH 1:4) [29]. The micropore of LMiPC2 carbon was in the range of 1–2 nm, up to 70.1% of total V_{micro}, equal to 0.988 $cm^3\ g^{-1}$, leading to a high specific capacitance of LMiPC2 of 369 F g^{-1} at 0.5 F g^{-1} in KOH 6 M [19]. Micropores of pine sawdust AC were dominant with the portion up to 92–96% of V_{total} at 700–800 °C, while increasing the activation temperatures to 900 °C enhanced the V_{meso} to 0.939 $cm^3\ g^{-1}$ (49% of V_{total}). The differences in pore structure from AC showed that heat treatment temperatures played an important role in determining the ratio of micropores and mesopores. High treatment temperatures (900 °C) enhanced the etching reactions between KOH and carbon, resulting in more carbon consumption and widened pores. This high mesopore volume supports the diffusion of KOH electrolyte, resulting in the capacitance of 176 F g^{-1} at 0.5 A g^{-1} [29]. However, one drawback in the experimental approach of this study was the lack of the graphitic carbon structure in the electrode. High pre-treatment temperature at 700 °C changed the sawdust into turbostratic carbon, and further treatment with KOH at 900 °C could not promote the formation of any graphitic carbon structure to support the electron conductivity.

Increasing activation temperatures is effective to increase BET SA when using KOH. The BET SA of Amygdalus pedunculata shell derived carbon increased to 2054 $m^2\ g^{-1}$ after being treated with KOH at 900 °C for 1 h at the mass ratio biomass/KOH 1:2.5 [18]. This is significantly higher than BET SA of KOH activated birch wood carbon obtained at 800 °C (Fig. 1b) (973.5 $m^2\ g^{-1}$) [32] but lower than the BET SA of wheat straw and food waste carbon activated with KOH at 900 °C (WFT-900) (Fig. 1d) (3326 $m^2\ g^{-1}$, V_{micro} 0.208 $cm^3\ g^{-1}$ and V_{meso} 2.164 $cm^3\ g^{-1}$) [22]. Birch wood was pyrolyzed in N_2 at 300 °C for 4 h, and the biochar was activated with KOH at 800 °C at the mass ratio 1:2 for 4 h in N_2 (AC-800) [32]. This increased the BET SA of AC-800 to 973.5 $m^2\ g^{-1}$ and V_{total} to 0.75 $cm^3\ g^{-1}$ [32]. Analysis of the morphology of birch wood carbon also revealed that the BET SA and V_{total} increased with increasing temperatures: at 600 °C the BET SA and V_{total} were 624 $m^2\ g^{-1}$ and 0.34 $cm^3\ g^{-1}$, respectively. This agrees with the activating mechanism of KOH that heat treatment temperature of 600 °C was not sufficient for the reaction between KOH and carbon. When increasing temperatures to 700–900 °C, the KOH

started to react with carbon in the biochar/biomass to form the pore network, and the etching effect of KOH increased with increasing temperatures.

Wheat straw and food waste were used to cultivate the trichoderma viride (a type of fungus) and used as the precursor for carbon materials [22]. The mixture of wheat straw, food waste and trichoderma viride after being cultivated were hydrothermally treated at 200 °C for 12 h before being activated with KOH at the mass ratio 1:4 at 700 °C (WFT-700), 800 °C (WFT-800), and 900 °C (WFT-900) for 2 h in N_2 [22]. The WFT-900 carbon presented the BET SA of 3326 $m^2\ g^{-1}$ with V_{total} of 2.372 $cm^3\ g^{-1}$, and these supported the high specific capacitance of 409.7 F g^{-1} at 0.5 A g^{-1}, and even 297 F g^{-1} at 10 A g^{-1}. This is higher than the specific capacitance observed in other studies. The reason for the high BET SA and pore volumes among these carbons could be due to the cultivation process prior to heat treatment. During the cultivation procedure, trichoderma viride used the materials in wheat straw and food waste, degraded cellulose and lignin inside the biomass, made the structure of the biomass more fragile and allowed more KOH to be adsorbed into the original cellulose and lignin. The increase in interactions between cellulose and lignin of wheat straw and food waste and KOH resulted in a better catalytic activity during heat treatment, generated more micropores and mesopores and enhanced the surface area of the obtained carbons.

Another method to increase the immersion of KOH into the biomass is through freeze-drying. The egg white was freeze dried at −51 °C before being pyrolyzed at 400 °C in N_2 [47]. The obtained biochar was mixed with KOH at the mass ratio biochar/KOH 1:1 (EWC-1), 1:2 (EWC-2), and 1:3 (EWC-3) and then carbonized at 800° for 2 h in N_2. BET SA of these three carbons varied in the range of 2838–2918 $m^2\ g^{-1}$, but EWC-2 presented the highest specific capacitance of 335 F g^{-1} at 0.5 A g^{-1} due to the balance between the micropore (0.661 $cm^3\ g^{-1}$) and mesopore (0.663 $cm^3\ g^{-1}$). This indicates the importance of a well-balanced structure between the micropore and mesopore in supercapacitor electrodes.

The soybean powder was used to synthesize AC for the supercapacitor [20]. The synthesis route was more complex than other studies due to the attempt of doping nitrogen functional groups into the carbon. 3 g soybean powder was mixed with 0.25 mL aqueous ammonia, 10 mL of ethanol, 25 mL of DI water and 0.75 g of tetraethoxysilane, and this mixture was carbonized at 800 °C in N_2 for 2 h. The solid product was washed with hot NaOH 2 M to remove the silica template, and the obtained biochar was further activated with KOH at the mass ratio biochar/KOH from 1:1 to 1:3 at 700 °C for 2 h in N_2 to obtain carbons ANPC-1, ANPC-2 and ANPC-3 [20]. Increasing the KOH content fostered the reaction between KOH and carbon skeleton and increased BET SA from 679 $m^2\ g^{-1}$ to 1749 $m^2\ g^{-1}$ and V_{total} from 0.490 $cm^3\ g^{-1}$ to 0.924 $cm^3\ g^{-1}$ [20]. This increase in BET SA and V_{total} led to the increase in capacitance from 150.5 F g^{-1} (ANPC-1) to 243.2 F g^{-1} (ANPC-3) at 0.5 A g^{-1} in KOH 6 M, and the highest capacitance of ANPC-3 was ascribed to the superior BET SA and V_{total}. However, due to the high temperatures in the first carbonization step, carbonaceous structure of these carbons remained at turbostratic, and limited the electric conductivity of the electrodes. Furthermore, the specific capacitance of ANPC-3 was in the same range with those in Fig. 2 and lower than those in Fig. 1,

indicating that the increase in nitrogen contents did not lead to a superior performance and several pores were blocked during the preparation of electrodes.

When adjusting the ratio between the biochar and activating agent such as KOH, there is no universal ratio which could be applied to all types of biomass. The kapok flower was pyrolyzed at 500 °C in N_2 for 2 h before being activated with KOH at 700 °C at different mass ratios [44]. The mass ratio of kapok flower biochar/KOH 1:4.5 (AC_F-4.5) was optimal to achieve the BET SA of 1904 $m^2\ g^{-1}$ and V_{total} of 1.019 $cm^3\ g^{-1}$ in the mass ratio range from 1:3 to 1:5 [44]. When increasing the mass ratio from 1:3 to 1:4.5, it fostered the reaction with carbons in the biochar, formed new pores and widened micropores into mesopores with the maximum micropore and mesopore volumes of 0.533 and 0.466 $cm^3\ g^{-1}$ in AC_F-4.5 respectively. Increasing the mass ratio to 1:5 led to the significant consumption of carbon and remarkably decreased the V_{micro} to 0.333 $cm^3\ g^{-1}$ and V_{meso} to 0.232 $cm^3\ g^{-1}$. The high V_{micro} and V_{meso} improved the specific capacitance to 286.8 F g^{-1} at 1 A g^{-1} in KOH 6 M, and the capacitance is still retained at 180 F g^{-1} at 10 A g^{-1}, indicating 62.7% retention with increasing current density.

In the attempt to simplify the activation procedure, the one step activation of sechium edule leaves was conducted [14]. The sechium edule leaves were mixed with NH_4Cl and KOH at the mass ratio 1:1:2 respectively using a mortar, and the mixture were carbonized at 600 °C (SE-600), 700 °C (SE-700) and 800 °C (SE-800) for 2 h in N_2. The maximum BET SA was 476 $m^2\ g^{-1}$ (SE-700), much lower compared to other carbons, due to the low activating temperature (700 °C compared to 800–900 °C) inhibiting the reactions between carbon in biomass and KOH. Despite the low BET SA, SE-700 demonstrated the specific capacitance of 273 F g^{-1} in H_2SO_4 0.5 M at 2 A g^{-1} compared to 43 F g^{-1} of SE-600 and 180 F g^{-1} of SE-800 [14]. This indicates there were improvement in the macropore structure to enhance the electrolyte diffusion, but it was not measured in the study.

Besides the conventional heat treatment approach, microwave-assisted conversion of biomass is also a promising method to increase the pore structure to enhance the supercapacitor. The squeezed camellia oleifera residue was first pyrolyzed at 400 °C for 2 h in N_2, and the obtained biochar was mixed with KOH at the mass ratio 1:3 before being activated in the microwave at 2450 MHz for 2 min [5]. This resulted in the carbon MAC with V_{total} of 0.890 $cm^3\ g^{-1}$, V_{meso} 0.448 $cm^3\ g^{-1}$ (50% of V_{total}) and BET SA of 1726 $m^2\ g^{-1}$. The increased the capacitance of MAC carbon to 367 F g^{-1} at 0.5 A g^{-1} in H_2SO_4 2 M, and still retained at 244 F g^{-1} at 20 A g^{-1}. This performance was superior to the camellia oleifera residue carbon obtained through KOH conventional heat activation DAC-800 (pre-carbonized at 400 °C and activated with KOH at the mass ratio 1:3 at 800 °C) with the capacitance of 298 F g^{-1} at 0.5 A g^{-1} [5]. The DAC-800 had the BET SA of 1140 $m^2\ g^{-1}$ and V_{total} of 0.584 $cm^3\ g^{-1}$, smaller than those of MAC. Furthermore, the Raman spectrum of DAC-800 also showed more broadening D and G peaks compared to MAC, indicating that the carbon structure of MAC was more ordered than DAC-800, and this benefited the electric conductivity of the carbon.

KOH appeared to be more effective than $ZnCl_2$ and H_3BO_3 in improving the morphology and surface area of carbon. The dead gingko leaves were carbonized at

900 °C in N_2 for 2 h, and the obtained biochar was activated with KOH, $ZnCl_2$ and H_3BO_3 at the mass ratio biochar/activating agent 1:4 at 900 °C for 2 h in N_2 [46]. BET SA and V_{total} of KOH activated gingko leaves carbon (KGC) were 853.4 $m^2\ g^{-1}$ and 0.38 $cm^3\ g^{-1}$, which were superior to H_3BO_3 activated carbon (BGC) with BET SA 346.4 $m^2\ g^{-1}$ and V_{total} 0.34 $cm^3\ g^{-1}$. The $ZnCl_2$ gingko leaves carbon (ZnGC) had BET SA of 824.6 $m^2\ g^{-1}$ and V_{total} of 0.43 $cm^3\ g^{-1}$, similar to the morphology of KGC, but ZnGC demonstrated a lower capacitance of 102 F g^{-1} compared to 281 F g^{-1} of BGC when scanning at 10 mV s^{-1} in H_2SO_4 1 M. This indicates the influence of the activating agent on the performance of carbon. The activation with KOH resulted in a hierarchical nanoarchitecture from macropores, mesopores and micropores while the activation with $ZnCl_2$ significantly lacked macropores. The addition of macropores in KOH activation supported the movement of the electrolytes and increased the specific capacitance compared to $ZnCl_2$ activation.

Some studies explored other activating agents such as $ZnCl_2$ for the activating process. Chitosan carbon was prepared by hydrothermally treating the mixture of 1 g of chitosan +1 mL 1 M CH_3COOH + 3 g of $ZnCl_2$ in 40 mL of H_2O at 160 °C for 8 h, and the hydrochar was carbonized at 800 °C in N_2 for 1 h (10 °C min^{-1}) to obtained carbon NHPC [45]. $ZnCl_2$ acted as a dehydration agent to absorb the moisture inside the biomass and increased the BET SA of NHPC to 1067 $m^2\ g^{-1}$ and V_{total} of 0.486 $cm^3\ g^{-1}$, which helped increase the specific capacitance to 233.3 F g^{-1} at 0.5 A g^{-1} in KOH 6 M. This was superior to the chitosan carbon synthesized without $ZnCl_2$ (NC) with the capacitance of only 41.1 F g^{-1} at 0.5 A g^{-1}. This indicates the importance of the porosity of carbon which aided the transport of electrolyte ions and formation of EDLC.

The specific capacitance of sugar beet pulp carbon was 216 F g^{-1} at 0.5 A g^{-1} in KOH 6 M [13]. Sugar beet pulp was mixed with water and citric acid monohydrate at mass ratio 1:10:0.03, hydrothermally treated at 200 °C for 2.5 h, and the hydrochar was mixed with $Mg(CH_3COO)_2.4H_2O$ at the mass ratio 1:1 or $ZnCl_2$ at the mass ratio 1:3 before being carbonized at 700 °C to attain SC-Mg-700 and SC-Zn-700 respectively. At 700 °C, $Mg(CH_3COO)_2.4H_2O$ decomposed into CH_3COOH and $Mg(OH)CH_3COO$ and MgO subsequently [21, 25]. This process encouraged the formation of V_{meso} of 0.741 $cm^3\ g^{-1}$ compared to 0.171 $cm^3\ g^{-1}$ of V_{micro} in SC-Mg-700, resulting in the high BET SA of 624.3 $m^2\ g^{-1}$. On the other hand, $ZnCl_2$ influenced the surface area and pore volume through the dehydration, and increased BET SA to 950.3 $m^2\ g^{-1}$ and V_{meso} to 1.200 $cm^3\ g^{-1}$, while V_{micro} was only 0.086 $cm^3\ g^{-1}$. The higher specific capacitance of SC-Zn-700 of 263 F g^{-1} at 0.5 A g^{-1} compared to 172 F g^{-1} of SC-Zn-700 can be ascribed to the formation of V_{meso} which facilitated the diffusion of electrolyte ions.

Not all the activated carbons had the high specific capacitances in supercapacitors. The empty fruit bunch was first de-ashed by immersing in HF for 1 h, and the obtained precursor was hydrothermally treated at the mass ratio biomass/$ZnCl_2$/H_2O 1:2:3 at 275 °C for 1 h [16]. This hydrochar was activated in CO_2 at 800 °C for 2 h (10 °C min^{-1}) to obtained AC-$ZnCl_2$. $ZnCl_2$ enhanced the BET SA of AC-$ZnCl_2$ to 1571 $m^2\ g^{-1}$. However, the specific capacitance of this AC-$ZnCl_2$ was only 2.45 F g^{-1} in KOH 6 M, so that prepared carbon was not suitable for the supercapacitor.

SEM images of AC-$ZnCl_2$ showed large particles of carbon, so the low capacitance could be ascribed to the lack of pore network. This inhibited the transport of the electrolyte and decreased the electric double layer capacitor on the carbon surface, and $ZnCl_2$ is more selective than KOH in activating the effect on biomass carbons.

Changes in the pre-treatment environment from inert e.g. N_2 to CO_2 affects the properties of the carbon. At elevated temperatures (>700 °C), carbon reacts with CO_2 via Boudouard reaction to form CO [42]. The reaction between carbon and CO_2 results in the consumption of carbon, creates more pores in the structure, connects existing pores, and decreases the thickness of the pore walls. Furthermore, it leads to the shrinkages of production particles. However, this activation method was not favored in the literature survey although a previous study [35] demonstrated that the electrochemical behavior of the carbon obtained from CO_2 activation was similar to other carbons activated using KOH and K_2CO_3. Soap nut seed was first carbonized in N_2 at 700 °C for 3 h, and then activated with CO_2 at the same temperatures for 2 h [35]. BET SA of soap nut seed carbon (CBAC) was 786 $m^2\ g^{-1}$ and V_{total} was 0.212 $cm^3\ g^{-1}$, lower than other biomass carbon activated by KOH. Interestingly, this CBAC carbon demonstrated the specific capacitance of 449 F g^{-1} at 1 A g^{-1} in 6 M KOH, higher than 286.8 F g^{-1} (kapok flower carbon AC_F-4.5) [44]. The cyclic voltammetry of CBAC showed a small peak at −0.6 V, indicating that it may involve pseudo-capacitance from redox reactions. This suggested that the heat treatment temperature at only 700 °C retained some oxygen functional groups in CBAC and these groups join in the redox reactions to enhance pseudo-capacitance.

In some rare cases, such as activated carbon from caesalpinia sappan pods, the direct pyrolysis under N_2 atmosphere at 800 °C for 1 h was conducted (CSPCN8) [4]. BET SA increased to 675 $m^2\ g^{-1}$ with V_{total} of 0.268 $cm^3\ g^{-1}$, and the specific capacitance was 261.8 F g^{-1} at 0.5 A g^{-1} in KOH 5 M. The relatively high surface area of CSPCN8 could be due to the release of volatile out of biomass during pyrolysis, but it is not common for the biomass-derived carbon to achieve high BET SA because of the shrinkage of carbon skeleton during heat treatment, and it is not recommended to use direct pyrolysis to prepare carbon materials for supercapacitors.

4 Current Challenges and Conclusions

This chapter discusses the surface morphology, surface area, pore types, and pore size distributions of biomass-derived carbons, how these properties influence the performance of supercapacitors, and the activation methods. It reveals that:

- Evenly distributed honeycomb-like pore network assembling from thin pore walls and a few-layer carbon structures prove to be the most suitable carbon architectures for supercapacitors. The honeycomb-like structure ensures that the electrolytes can equally transport to the entire surface of biomass-derived carbons.
- Macropores are important for supercapacitors because they act as a gateway for the bulk electrolyte to enter the surface of carbon, and macropores also protect the

micropores (<2 nm) and mesopores (2–10 nm) from being blocked by additives and binders used during the electrode preparation. However, the lack of reports on macropores in literature inhibits the optimization and scaling-up of biomass-derived carbon for supercapacitors. Furthermore, the lack of data on macropores also explains why the remarkable differences in BET SA, V_{total}, V_{micro} and V_{meso} were observed in Table 1. despite relatively similar specific capacitances of those biomass-derived carbons.

- Mesopores are the pathways connecting micropores and macropores, so maintaining a percentage of mesopores benefits the diffusion of electrolytes in carbon's structure.
- Micropores in the range of 0.7–2 nm act as the active sites for the EDLC, so the increase of micropores should increase the capacitance of carbons. Narrower micropores (<0.7 nm) are inaccessible for electrolyte ions and do not benefit the supercapacitors.
- There is no correlation between the pore size distributions and surface morphologies, and no correlation between pore size distributions and the performance of supercapacitors was observed in the reported studies. Due to the blocking effect of binders and additives when preparing electrodes, EDLC does not form on most micropores and mesopores in carbons. For many studies, the shortage of data on surface area, porosity, and pore distribution of not only biomass-derived carbon but also the mixture of biomass-derived carbon, binder and additive creates difficulties in comparing and analyzing data. A more comprehensive analysis of surface morphology and porosity of the mixture of biomass-derived carbon, binder and additive in future studies will solve the discrepancy of the data and create a better relation between surface morphology, porosity, and electrochemical performance.
- To increase the surface area and pore volumes, chemical activation (KOH, K_2CO_3, $ZnCl_2$) and physical activation (CO_2 gasification) are frequently applied. Most studies focus on the influence of mass ratio of the activating agent and biomass/biochar, temperatures on the surface area and pore volumes, but it is evident that they also control the surface morphology and macropore structures. With a better understanding about how these activating methods affect the surface morphologies and macropore structures, it will help the scaling up and adoption of biomass-derived carbon in supercapacitors.
- Many studies used only a small amount of biomass precursors, and the vast array of biomass used in literature posed difficulties in scaling up the biomass-derived carbon production. This is crucial for the mass production of biomass-derived carbon. More studies on the transition of laboratory scale testing into pilot scale testing are therefore encouraged.
- Even though this is still at an early stage, more study on the techno-economic challenges of biomass-derived carbon in supercapacitors will support a sustainable adoption of this material in the future.

Acknowledgements The authors gratefully acknowledged the financial support from the Royal Academy of Engineering (Grant No: FF\1920\1\45), United Kingdom.

References

1. Abouelamaiem DI, He G, Parkin I, Neville TP, Jorge AB, Ji S, Wang R, Titirici M-M, Shearing PR, Brett DJL (2018) Synergistic relationship between the three-dimensional nanostructure and electrochemical performance in biocarbon supercapacitor electrode materials. Sustain Energy Fuels 2:772–785. https://doi.org/10.1039/C7SE00519A
2. Ahmed S, Ahmed A, Rafat M (2019) Investigation on activated carbon derived from biomass Butnea monosperma and its application as a high performance supercapacitor electrode. J Energy Storage 26:100988. https://doi.org/10.1016/j.est.2019.100988
3. Alhebshi NA, Salah N, Hussain H, Salah YN, Yin J (2021) Structural and electrochemical properties of physically and chemically activated carbon nanoparticles for supercapacitors. Nanomaterials 12:122. https://doi.org/10.3390/nano12010122
4. Bhat VS, Toghan A, Hegde G, Varma RS (2022) Capacitive dominated charge storage in supermicropores of self-activated carbon electrodes for symmetric supercapacitors. J Energy Storage 52:104776. https://doi.org/10.1016/j.est.2022.104776
5. Bo X, Xiang K, Zhang Y, Shen Y, Chen S, Wang Y, Xie M, Guo X (2019) Microwave-assisted conversion of biomass wastes to pseudocapacitive mesoporous carbon for high-performance supercapacitor. J Energy Chem 39:1–7. https://doi.org/10.1016/j.jechem.2019.01.006
6. Bonnamy S, Oberlin A (2016) Chapter 4—transmission electron microscopy. Mater Sci Eng Carbon 45–70. https://doi.org/10.1016/B978-0-12-805256-3.00004-0
7. Chen H, Liu D, Shen Z, Bao B, Zhao S, Wu L (2015) Functional biomass carbons with hierarchical porous structure for supercapacitor electrode materials. Electrochim Acta 180:241–251. https://doi.org/10.1016/j.electacta.2015.08.133
8. Chen W, Wei R, Yang L, Yang Y, Li G, Ni J (2019) Characteristics of wood-derived biochars produced at different temperatures before and after deashing: their different potential advantages in environmental applications. Sci Total Environ 651:2762–2771. https://doi.org/10.1016/j.scitotenv.2018.10.141
9. Cui J, Zhang Z-X, Quan H, Hu Y, Wang S, Chen D (2022) Effect of various ammonium salts as activating additive on the capacitance performance of hierarchical porous carbon derived from camellia husk. J Energy Storage 51:104347. https://doi.org/10.1016/j.est.2022.104347
10. Fernández JA, Tennison S, Kozynchenko O, Rubiera F, Stoeckli F, Centeno TA (2009) Effect of mesoporosity on specific capacitance of carbons. Carbon N Y 47:1598–1604. https://doi.org/10.1016/j.carbon.2009.02.012
11. Garrido J, Linares-Solano A, Martin-Martinez JM, Molina-Sabio M, Rodriguez-Reinoso F, Torregrosa R (1987) Use of nitrogen versus carbon dioxide in the characterization of activated carbons. Langmuir 3:76–81. https://doi.org/10.1021/la00073a013
12. Gryglewicz G, Machnikowski J, Lorenc-Grabowska E, Lota G, Frackowiak E (2005) Effect of pore size distribution of coal-based activated carbons on double layer capacitance. Electrochim Acta 50:1197–1206. https://doi.org/10.1016/j.electacta.2004.07.045
13. Gür E, Semerci TG, Semerci F (2022) Sugar beet pulp derived oxygen-rich porous carbons for supercapacitor applications. J Energy Storage 51:104363. https://doi.org/10.1016/j.est.2022.104363
14. Jalalah M, Rudra S, Aljafari B, Irfan M, Almasabi SS, Alsuwian T, Patil AA, Nayak AK, Harraz FA (2022) Novel porous heteroatom-doped biomass activated carbon nanoflakes for efficient solid-state symmetric supercapacitor devices. J Taiwan Inst Chem Eng 132:104148. https://doi.org/10.1016/j.jtice.2021.11.015
15. Jiao S, Zhang L, Li C, Zhang H, Zhang J, Li P, Tao Y, Zhao X, Chen H, Jiang J (2022) Efficient construction of a carbon-based symmetric supercapacitor from soybean straw by coupling multi-stage carbonization and mild activation. Ind Crops Prod 183:114906. https://doi.org/10.1016/j.indcrop.2022.114906
16. Larasati TD, Prakoso T, Rizkiana J, Devianto H, Widiatmoko P, Nurdin I (2019) Nano carbon produced by advanced mild hydrothermal process of oil palm biomass for supercapacitor material. IOP Conf Ser Mater Sci Eng 543:012031. https://doi.org/10.1088/1757-899X/543/1/012031

17. Li J, Wu Q (2015) Water bamboo-derived porous carbons as electrode materials for supercapacitors. New J Chem 39:3859–3864. https://doi.org/10.1039/C4NJ01853B
18. Li W, Ding Y, Zhang W, Shu Y, Zhang L, Yang F, Shen Y (2016) Lignocellulosic biomass for ethanol production and preparation of activated carbon applied for supercapacitor. J Taiwan Inst Chem Eng 64:166–172. https://doi.org/10.1016/j.jtice.2016.04.010
19. Li Y, Zhang D, Zhang Y, He J, Wang Y, Wang K, Xu Y, Li H, Wang Y (2020) Biomass-derived microporous carbon with large micropore size for high-performance supercapacitors. J Power Sources 448:227396. https://doi.org/10.1016/j.jpowsour.2019.227396
20. Lin G, Ma R, Zhou Y, Liu Q, Dong X, Wang J (2018) KOH activation of biomass-derived nitrogen-doped carbons for supercapacitor and electrocatalytic oxygen reduction. Electrochim Acta 261:49–57. https://doi.org/10.1016/j.electacta.2017.12.107
21. Liu W-J, Jiang H, Tian K, Ding Y-W, Yu H-Q (2013) Mesoporous carbon stabilized MgO nanoparticles synthesized by pyrolysis of MgCl2 preloaded waste biomass for highly efficient CO_2 capture. Environ Sci Technol 47:9397–9403. https://doi.org/10.1021/es401286p
22. Liu Z, Hu J, Shen F, Tian D, Huang M, He J, Zou J, Zhao L, Zeng Y (2021) Trichoderma bridges waste biomass and ultra-high specific surface area carbon to achieve a high-performance supercapacitor. J Power Sources 497:229880. https://doi.org/10.1016/j.jpowsour.2021.229880
23. Long C, Chen X, Jiang L, Zhi L, Fan Z (2015) Porous layer-stacking carbon derived from in-built template in biomass for high volumetric performance supercapacitors. Nano Energy 12:141–151. https://doi.org/10.1016/j.nanoen.2014.12.014
24. Meng D, Hu Y, Jing Y, Zhang X, Mahmud S, Su S, Zhu J (2022) One-step carbonization strategy of freeze-dried chitosan to prepare nitrogen-oxygen co-doped porous carbon supercapacitors with ultra-large specific surface area. Fuel 320:124002. https://doi.org/10.1016/j.fuel.2022.124002
25. Morishita T, Soneda Y, Tsumura T, Inagaki M (2006) Preparation of porous carbons from thermoplastic precursors and their performance for electric double layer capacitors. Carbon N Y 44:2360–2367. https://doi.org/10.1016/j.carbon.2006.04.030
26. Nishi Y, Inagaki M (2016) Chapter 11—gas adsorption/desorption isotherm for pore structure characterization. In: Inagaki M, Kang F (eds) Materials science and engineering of carbon. Butterworth-Heinemann, pp 227–247
27. Pawelec KM, White AA, Best SM (2019) Properties and characterization of bone repair materials. In: Bone repair biomaterials. Elsevier, pp 65–102
28. Pulikkottil M, Antony H, Muralidharan MN, Gopalan EV, Ansari S (2022) Cashew nut shell derived porous activated carbon electrodes for "water-in-salt" electrolyte based symmetric supercapacitor. ChemistrySelect 7. https://doi.org/10.1002/slct.202200984
29. Quan C, Su R, Gao N (2020) Preparation of activated biomass carbon from pine sawdust for supercapacitor and CO_2 capture. Int J Energy Res 44:4335–4351. https://doi.org/10.1002/er.5206
30. Rexer TF, Mathia EJ, Aplin AC, Thomas KM (2014) High-pressure methane adsorption and characterization of pores in posidonia shales and isolated kerogens. Energy Fuels 28:2886–2901. https://doi.org/10.1021/ef402466m
31. Rustamaji H, Prakoso T, Devianto H, Widiatmoko P, Saputera WH (2022) Urea nitrogenated mesoporous activated carbon derived from oil palm empty fruit bunch for high-performance supercapacitor. J Energy Storage 52:104724. https://doi.org/10.1016/j.est.2022.104724
32. Selvaraj AR, Chinnadurai D, Cho I, Bak J-S, Prabakar K (2022) Bio-waste wood-derived porous activated carbon with tuned microporosity for high performance supercapacitors. J Energy Storage 52:104928. https://doi.org/10.1016/J.EST.2022.104928
33. Sharma RK, Wooten JB, Baliga VL, Lin X, Geoffrey Chan W, Hajaligol MR (2004) Characterization of chars from pyrolysis of lignin. Fuel 83:1469–1482. https://doi.org/10.1016/j.fuel.2003.11.015
34. Taer E, Apriwandi A, Nursyafni N, Taslim R (2022) Averrhoa bilimbi leaves-derived oxygen doped 3D-linked hierarchical porous carbon as high-quality electrode material for symmetric supercapacitor. J Energy Storage 52:104911. https://doi.org/10.1016/J.EST.2022.104911

35. Vinayagam M, Suresh Babu R, Sivasamy A, de Barros ALF (2021) Biomass-derived porous activated carbon nanofibers from Sapindus trifoliatus nut shells for high-performance symmetric supercapacitor applications. Carbon Lett 31:1133–1143. https://doi.org/10.1007/s42823-021-00235-4
36. Wang D, Min Y, Yu Y (2015) Facile synthesis of wheat bran-derived honeycomb-like hierarchical carbon for advanced symmetric supercapacitor applications. J Solid State Electrochem 19:577–584. https://doi.org/10.1007/s10008-014-2639-0
37. Xu M, Wang A, Xiang Y, Niu J (2021) Biomass-based porous carbon/graphene self-assembled composite aerogels for high-rate performance supercapacitor. J Clean Prod 315:128110. https://doi.org/10.1016/j.jclepro.2021.128110
38. Yakaboylu GA, Jiang C, Yumak T, Zondlo JW, Wang J, Sabolsky EM (2021) Engineered hierarchical porous carbons for supercapacitor applications through chemical pretreatment and activation of biomass precursors. Renew Energy 163:276–287. https://doi.org/10.1016/j.renene.2020.08.092
39. Yan D, Liu L, Wang X, Xu K, Zhong J (2022) Biomass-derived activated carbon nanoarchitectonics with hibiscus flowers for high-performance supercapacitor electrode applications. Chem Eng Technol 45:649–657. https://doi.org/10.1002/ceat.202100585
40. Yoshida A, Kaburagi Y, Hishiyama Y (2016) Chapter 5—Scanning electron microscopy. Mater Sci Eng Carbon 71–93. https://doi.org/10.1016/B978-0-12-805256-3.00005-2
41. Yu S, Zhu X, Lou G, Wu Y, Xu K, Zhang Y, Zhang L, Zhu E, Chen H, Shen Z, Bao B, Fu S (2018) Sustainable hierarchical porous biomass carbons enriched with pyridinic and pyrrolic nitrogen for asymmetric supercapacitor. Mater Des 149:184–193. https://doi.org/10.1016/j.matdes.2018.04.023
42. Zhang J, Shao J, Huang D, Feng Y, Zhang X, Zhang S, Chen H (2020) Influence of different precursors on the characteristic of nitrogen-enriched biochar and SO_2 adsorption properties. Chem Eng J 385:123932. https://doi.org/10.1016/j.cej.2019.123932
43. Zhao K, Zhao L, Zhou W, Rao L, Wen S, Xiao Y, Cheng B, Lei S (2022) Pore regulation of well-developed honeycomb-like carbon materials from Zizania latifolia for supercapacitors. J Energy Storage 52:104910. https://doi.org/10.1016/j.est.2022.104910
44. Zheng L-H, Chen M-H, Liang S-X, Lü Q-F (2021) Oxygen-rich hierarchical porous carbon derived from biomass waste-kapok flower for supercapacitor electrode. Diam Relat Mater 113:108267. https://doi.org/10.1016/j.diamond.2021.108267
45. Zhou J, Wang H, Yang W, Wu S, Han W (2018) Sustainable nitrogen-rich hierarchical porous carbon nest for supercapacitor application. Carbohydr Polym 198:364–374. https://doi.org/10.1016/j.carbpol.2018.06.095
46. Zhu X, Yu S, Xu K, Zhang Y, Zhang L, Lou G, Wu Y, Zhu E, Chen H, Shen Z, Bao B, Fu S (2018) Sustainable activated carbons from dead ginkgo leaves for supercapacitor electrode active materials. Chem Eng Sci 181:36–45. https://doi.org/10.1016/j.ces.2018.02.004
47. Zhu Y, Fang T, Hua J, Qiu S, Chu H, Zou Y, Xiang C, Huang P, Zhang K, Lin X, Yan E, Zhang H, Xu F, Sun L, Zeng J (2019) Biomass-derived porous carbon prepared from egg white for high-performance supercapacitor electrode materials. ChemistrySelect 4:7358–7365. https://doi.org/10.1002/slct.201901632

Biomass-Derived N and S Doped Carbon Nano-shapers for Supercapacitor Applications: Effect of Doping on Energy Density

Debajani Tripathy, Bibhuti B. Sahu, Ankita Subhrasmita Gadtya, and Srikanta Moharana

Abstract Porous nanostructured nitrogen and S-doped carbon derived from biomass have been extensively studied as electrode materials for supercapacitor applications. Supercapacitors are high-surface-area electrode-based electrochemical energy storage technologies that may be dominant in applications requiring high power supply or absorption. In high-performance supercapacitors, several electrodes, including biomass-derived carbonaceous electrodes, have subsequently shown significant potential due to their ubiquitous availability, renewable behavior, and cheap power storage. However, it is possible to design and optimize biomass with or without the presence of nitrogen in order to produce porous nanostructured nitrogen doped carbon by a variety of processes, including pyrolysis, hydrothermal carbonization, and several other routes. The N doped carbon increases ion absorption sites, electronic conductivity, carbon–sulfur bonding, and electrochemical catalysis. This chapter discusses the synthesis routes of natural biomass-derived porous nanostructured N and S doped carbon, as well as heteroatomic doping of biomass-derived carbon and its end-use applicability in the field of supercapacitors.

Keywords Biomass derived carbon · N & S doped · Heteroatom doping · Fuel cell · Supercapacitor

1 Introduction

The cumulative reliance on fossil fuels has made meeting the demands for both energy and environmental sustainability a pressing problem on a worldwide scale. Fuel cells, wind, lunar, and tidal energy are just some of the renewable energy options

D. Tripathy · A. S. Gadtya · S. Moharana (✉)
School of Applied Sciences, Department of Chemistry, Centurion University of Technology and Management, R.Sitapur, Paralakhemundi 761211, Odisha, India
e-mail: srikanta.moharana@cutm.ac.in

B. B. Sahu
Basic Science and Humanities Department, Nalanda Institute of Technology (NIT), Bhubaneswar, Biju Pattanaik University of Technology (BPUT), Bhubaneswar, Odisha, India

S. K. Tiwari et al. (eds.), *Biomass-Based Functional Carbon Nanostructures for Supercapacitors*, Green Energy and Technology,
https://doi.org/10.1007/978-981-99-0996-4_5

that have emerged as a result of rising demand and related environmental concerns [1, 2]. But for safe and continuous power acquisition, the sporadic energy supply from these devices needs an effective storage mechanism [2]. Supercapacitors and lithium-ion batteries (LIB) have been mentioned as viable storage technologies in terms of energy [3, 4]. Despite having an elevated energy density (gravimetric), LIB has a low power density, limited availability, and a sluggish stored energy transfer rate [3]. Moreover, the supercapacitors have attracted a lot of interest due to the fact that they have a superior density of power, a rapid charge or discharge rate, and the capacity to tolerate harsh environmental scenarios [4, 5]. The supercapacitors bridge the gap between lithium-ion batteries (LIBs) and regular capacitors, which have excellent power densities but limited energy storage capabilities (energy density increases with diminished power) [6]. The supercapacitors may theoretically supply energy to a broad avenue of transportable electronic gadgets, hybrid electric cars, and emergency power systems [7, 8].

The greatest drawback of a supercapacitor is its diminished energy density value, which restricts the variety of uses for it [5]. So, researchers have tried to come up with different electrode supplies and electrolytes with superior-recital output in order to increase the density of energy. According to their charge storage method, supercapacitors are often divided into two main classes: electrochemical double-layer capacitors (EDLCs) and pseudo capacitors. EDLCs (stimulated carbon, graphene, and others) concentrate on electrostatic charge storage at the electrode/electrolyte interface, while pseudo capacitors (conductive polymers, nano-metal oxides, sulfurides, and others) use the method of charge storage through redox processes [5, 9]. The pseudo capacitors have a higher specific capacitance than that of EDLCs, but they have low cycle stability, and their electrode structure changes when redox reactions occur [10]. EDLCs, on the other hand, have a higher rate capability and extremely long cycle lives with no electrode deterioration. Researchers have therefore concentrated on creating a cutting-edge porous carbon electrode material for supercapacitors. It is necessary to consider the graphitization level, specific surface area, and surface properties of the EDLC electrode material in the research, development, and design processes in order to produce great performance from the EDLC electrode material. As a consequence of this, scientists have studied a diverse selection of electrodes (carbon-based), ranging from zero-dimensional nanostructures to 3-dimensional nanostructured materials like fullerenes [11], carbon nanotubes [12], graphene [13], triggered carbon [14], and porous carbon made from metal organic frameworks (MOFs) [15, 16]. The manufacturing of these carbon electrode materials is complex, time-consuming, and energy-intensive; hence, their usage is restricted, despite the fact that they possess excellent electrochemical and structural qualities. The petroleum coke and graphite-derived activated carbons are non-renewable and were produced in polluted environments [17, 18]. In contrast to previous carbon nanostructures, the development of carbon materials derived from biomass has garnered a lot of interest. As renewable carbon precursors, biomass resources are plentiful, non-toxic, and sustainable [19]. They are also thought to be environmentally beneficial. Animals, plants, and microbes that are used for waste disposal provide a wide variety of biomass precursors, including scales of fish [20], shells of coconut [21], wood [22], algae [23], etc.

Using a straightforward conversion procedure, the carbon obtained from the biomass precursors can take on certain shapes and develop leaky behavior [24]. Activation and carbonization processes were used to create porous carbon electrode materials. In the carbonization process, biomass is pyrolyzed at temperatures between 400 and 900 °C to produce carbon nanostructures in an inert gas environment. Activation techniques such as chemical or physical activation convert pyrolyzed biomass into useful porous carbon compounds. The two stages of the physical activation approach are carbonization at low temperature and activation at elevated temperature, employing vapor or CO_2 as activating agents. For instance, using a physical activation approach, porous activated carbon was created from coconut shells [25]. After carbonization, the coconut shell biochar is treated with hydrochloric and hydrofluoric acids before being rinsed with deionized water (DI). The acid-activated biochar was then put through physical activation while being heated to 900 °C by CO_2 gas. Because the stimulated carbon does not have a large surface area with proper porous structure development, this activation procedure requires more energy than chemical activation. Alternatively, the chemical activation process consists of three distinct steps, including low-temperature pyrolysis, chemical agent activation, and carbonization at high temperatures between 500 and 900 °C. The activation process uses a number of chemical activating agents, including KOH, NaOH, KCl, NaCl, H_3PO_4, and $ZnCl_2$, to produce an extensive variety of pore sizes with big conduits for quick ion transmission and effective stowage [26]. KOH is the chemical substance used to activate most frequently because it produces carbon with a large, specific area of surface, in contrast with physical initiation. For instance, Wang et al. [27] produced stimulated carbon from lettuce leaves that had been activated with a KOH solution that was tuned. The vegetables were first pyrolyzed at 600 °C, triggered with KOH, and then carbonized at high temperatures before being washed with hydrochloric acid and DI water to remove potassium ions. The permeable carbon with doped nitrogen produced from bovine gelatin directly through carbonization and NaOH activation without the use of any additional doping chemicals is one example of this [28]. The use of doped processes, which produce a larger specific capacitance of 385 F/g and great rate capability, was made possible by the presence of different proteins. In contrast to artificial doping, the self-doping procedure is therefore extra affordable, straightforward, and environmentally friendly. Review articles on the doped heteroatoms in the network of carbon for energy storage applications focus on different doping techniques and how they affect the performance of electrochemical reactions. For numerous applications in energy systems, including supercapacitors, batteries, fuel cells, and hydrogen storage, an indication of the nobbling of carbon with N, P, and B was published [29]. Although self-doped carbon compounds have shown promise as a viable option for energy storage, there have been very few studies summarizing the landscape of the most efficient and environmentally friendly approaches. Here, we provide a concise introduction to the use of supercapacitors containing carbon produced from biomass that has been doped by itself with different atoms (mostly nitrogen, sulfur, and phosphorus). Before a single heteroatom doped carbon material can be discussed as a supercapacitor electrode, the behavior of different atom bonding and the consequences of doping must be described. After providing some

background information on dual and multiple diverse-atom doping with biomass carbon for applicability in the domain of supercapacitors, we move on to discuss the most important future doping insights.

2 Fabrication of the N and S Self-doped Hierarchical Porous Carbon

The permeability and electrochemical efficiency of carbon materials have been thought to be greatly improved by heteroatom doping techniques [30, 31]. Although N-doping improves the conductivity and electrochemical activities of the carbon matrix as well as its permeability, nitrogen-doped carbon is widely used to discuss energy-related issues [32–34]. Research on S-doping is still limited when compared to N-doping. The Fermi level in the carbon material has been shown to change significantly toward the conductive band as a result of S-doping [35]. This process will create a surface that is more polarized, improving the permeability of the carbon surface while accelerating the transport of electrolyte ions inside the porous carbon matrix [36]. Consequently, S-doped carbon has a huge capacity for energy storage. The latest evidence by certain organizations has focused on N and S co-doped star carbons, such as graphene and carbon nanotubes, in the hopes that the combined effects of nitrogen and sulfur doping will also enhance the star's carbon electrochemical performance [37–41]. For instance, in a step-by-step doping process, Gopalsamy et al. [42] synthesized co-doping with N and S graphene by employing cyanamide and benzyl disulfide as the N and S sources, respectively. The results indicated that the dual-doped graphene performed better electrochemically compared to the single-doped and undoped graphene. Wang et al. [43] developed a one-step procedure that results in the co-doping of carbon with N and S made up of pomelo peel with superior specific capacitance (317 F/g^{-1}) and a remarkable capability rate (69.7%). However, the same technology was used in the processing of another two, specifically bamboo fiber and sugarcane bagasse, both of which exhibited remarkable electrochemical activity. This is primarily because the morphology and conformation of the pomelo peel and subsequent carbon are quite similar to those of the pomelo peel.

According to the X-ray diffraction (XRD) analysis (shown in Fig. 1), synergistic activation was discovered in pomelo peel resulting carbon samples processed in a step-by-step process by carbonization at different temperatures. Finally, the results reveal the significant application of symmetric supercapacitors for energy storage by showing high energy density (30,624.6 Wh kg^{-1}). Similarly, Lei and her coworkers investigated the three dimensional structure of dually doped carbon fibres, that is, nitrogen and sulphur doped carbon fibers, by utilizing an absorption-swelling method. As per the report, it was found to have a best specific capacitance of 202 F/g^{-1} for dual doped NSCF as compared to a pristine, un-doped one, which is 2 times less than the doped one. It demonstrates the manufacture of a supercapacitor electrode that has excellent power performance as a result of optimal electrical conductivity, quick ion

transport, and the greatest wettability [44]. Wan et al. [45] have presented a hierarchical absorbent carbon candidate made from rape pollen and directly activated with amalgamated salts of $ZnCl_2$ and $FeCl_3$, which is co-doped with nitrogen and sulfur. Due to the interaction between the consistent hierarchical aperture structure and the congenital spherical shape, the resulting hierarchically porous carbon displays a high specific capacitance of 361.6 F g^{-1} at a current density of 1 A g^{-1} and exceptional rate capability. But the plentiful surface unfastened channels, and number of doped N, S atoms had the right level of graphitization (217.0 F g^{-1} at 100 A g^{-1}). Additionally, it exhibits improved cycle steadiness with 94.5% capacitance preservation after 20,000 cycles at 5 A g^{-1}.

These amazing discoveries could offer a novel strategy for converting biomass into superior-performing carbon compounds for applicability in supercapacitor applications. Dai and his team fabricated a unique, low-cost supercapacitor with high power density and energy. Herein, they apply the methods of activation, electrospinning, and carbonization to N and S co-doped graphene with polyacrylonitrile, which is based on the biomass of lignin in carbon nanofibers. In order to successfully collect HCN, NH_3, and SO_2 produced from lignin and PAN during carbonization, GN is utilized as a nitrogen and sulfur immobilization mediator. As a result, the concentration of heteroatoms of N and S in ACNFs is enhanced. The produced ACNF has a maximum specific surface area of 2439 m^2 g^{-1} and a GN content of 0.30 wt%. It exhibits the highest heteroatom doping and a characteristic 3-dimensional porous network structure with high crystallinity. The assembled supercapacitor performs

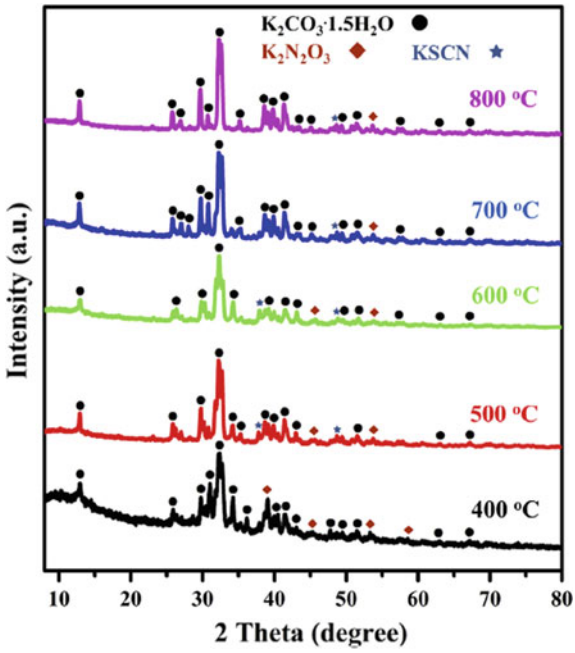

Fig. 1 X-ray diffraction (XRD) spectra of co-doped N, S pomelo peel at different temperature. Reproduce with permission from the Ref. [43]. Copyright 2020, Elsevier

better electrochemically because of its extremely up surging specific capacitance of 267.32 F g^{-1}, diminished corresponding series resistance of 5.67, and excellent cyclable stability of 96.7%, giving a maximum of 5000 cycles of charge/discharge in both techniques with 6 mol L^{-1} KOH as electrolyte. The built-in symmetrical supercapacitor most clearly demonstrates that doping ACNFs with GNs enhances their energy–density value from 4.12 to 9.28 Wh kg^{-1} without slightly reducing power density [46].

3 Effect of Heteroatoms Doping into Carbon

Doping carbon with a wide range of heteroatom mixtures makes it possible to study in depth how these mixtures affect the electrochemical performance and properties of the doped carbon.

3.1 Nitrogen Doping (N-doping)

In the case of doping strategies, which are mainly used in carbon materials, the most common heteroatom is nitrogen. The following factors are particularly effective for N-doping carbon [47]:

i. Since N is an adjacent element to C in the periodic table, doping may cause many electrons to be tuned.
ii. Most of the electrons that N gives to the delocalized carbon chain are what make the electronic conductivity of the carbon network go up.
iii. The occurrence of N atoms, which have a radius close to that of C atoms, makes it less probable that the lattice would crack.
iv. The C–N bond is formed in a manner analogous to n-type semiconductors, and it has several potential uses in the electrical industry.

In a broad sense, it has been shown that adding N atoms to sp^2 carbon chains may lead to the production of four distinct nitrogen bonding forms. These nitrogen bonding forms are referred to as pyridine-N, pyrrolic/pyridone-N, graphitic/quaternary-N, and pyridine-N (oxidized). While pyrrolic-N is chemically similar to pyridine, which forms rings with sp^2-hybridized carbon atoms in the five-carbon family via a single hydroxylic group, pyridine-N forms rings with di-sp^2 carbon atoms in the six-carbon family via the contribution of electron lone pairs [48]. Graphitic-quaternary-N has a significant N-doping effect because the majority of its unpaired electrons are covalently bonded to neighboring carbon atoms through three-bonds, filling the sp^2 carbon atoms'—state with one electron from N and pushing the other into the conduction band [49]. In addition, nitrogen and a plethora of oxygenated functional groups in the carbon obtained from biomass all play a role in the faradaic reactions [50]. Therefore, N's presence in carbon modifies its

symmetry and other features that are advantageous for electrochemical performance by facilitating redox processes. Analytically and conceptually, Wang et al. [51] investigated how N doping affects redox reactions during electrochemical processes. Their research was published in the journal Electrochemistry Communications. According to the conclusions drawn from the theoretical research, redox pairs are formed when oxidized pyridine-N with a high affinity for electrons and oxidized pyridine-N with a lower positive charge interact. This well-described method, which first increases the amount of space available for storing hydrogen atoms and subsequently endorses the binding of protons, is exemplified by the interaction among pyridine-N and pyrrolic-N.

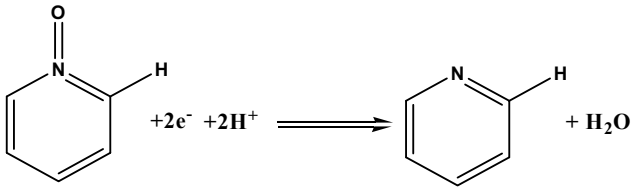

N-doping of carbon occurs since nitrogen-rich biomass has regular nitrogen dispersion worldwide. In addition, in order to produce superior performance, the combination of several types of N-species (pyridine-N, pyrrolic/pyridone-N, graphitic-quaternary-N, and oxidized pyridine-N) would definitely be beneficial. Li and colleagues created a material using cherry stones as a source to create porous carbon with a carbon support that was functionalized using heteroatom nitrogen atom doping. The whole process of development was carried out using a chemical activation approach, and the high mechanical strength and shape of carbon obtained from cherry stone (CS) that was produced as a consequence made it a major contender for use in industrial applications. These cherry stones turn black at calcination temperatures of 800 °C while retaining their spherical shape and high mechanical strength (as shown in Fig. 2). Furthermore, scanning electron microscopy (SEM) surface morphology (Fig. 3a, b) reveals an intriguing fact about CS: it is composed of stacked flakes, each with numerous cavities on its surface. The majority of the cavities are large, and some of them aren't even through. Figure 3c, d depict TEM characterization of this unusual texture, where the holes remain perplexing due to their varying orientations (highlighted in red dashed box). Because there are always channels present in cellulose materials, we conclude that the macro-pores likely originated in the cherry stone's primary structure. According to HRTEM (see Fig. 3e), CS is predominantly made up of amorphous carbon with minimal graphitization. Moreover, with the application of N-doping, the material exhibited a sizable surface area of around 1155 m^2/g in addition to a characteristic hierarchical pore structure that was associated with macro and micro pores [52].

Guo et al. [53] developed a carboxymethyl chitosan nanocomposite material that combined crystalline Mn_3O_4 particles of nanoscale porous carbon spheres with

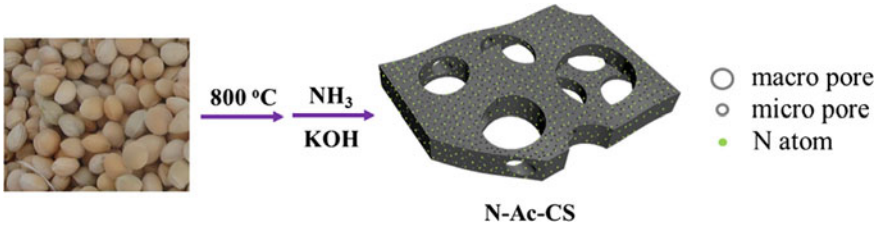

Fig. 2 Schematic depicting the manufacture of N-doped hierarchical porous carbon from cherry stones. Reproduce with permission from the Ref. [52]. Copyright 2018, Elsevier

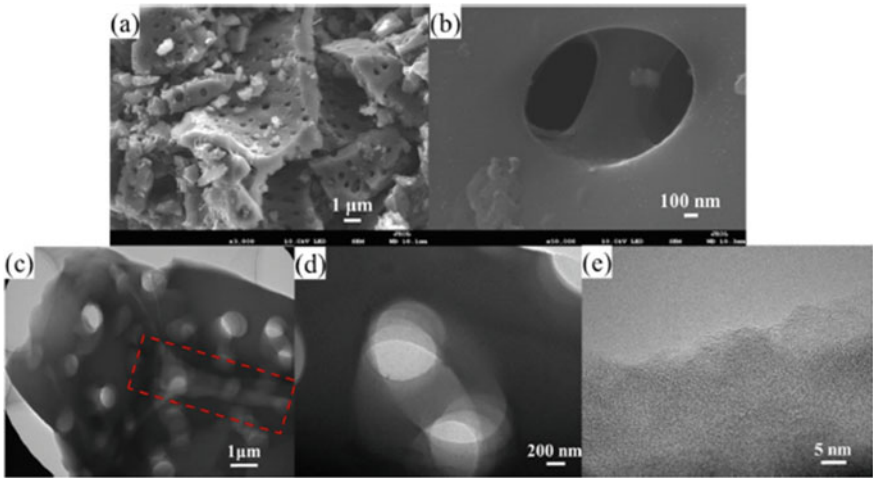

Fig. 3 Characterization of CS material by SEM (**a**, **b**) and TEM (**c–e**). Reproduce with permission from the Ref. [52]. Copyright 2018, Elsevier

doped nitrogen. However, lithium ion batteries that employ Mn_3O_4–NPCS nanocomposite as an anode material show an elevated specific capacity of 1629 mAh g^{-1} at 100 mA g^{-1} after 100 cycles, compared to the values for neat Mn_3O_4 and NPCS, respectively. The exceptional electrochemical activity of the Mn_3O_4–NPCS nanoscale-particle may be attributed to both the N-doped and the one-of-a-kind hybrid structure of the nanocomposites. The majority of the carbon-based nanosheets with N-doping pores were created by Zuo et al. [54] by a hydrothermal procedure and carbonization using pemole peel and melamine as the starting materials. The inherent sponge-like structure of the pomelo peel was exploited as a carbon source, and melamine was used to control the development of nanosheets by acting as a nitrogen precursor. The outcome showed that the carbonization temperature, pomelo peel to melamine ratio, amount of nitrogen doping, and surface area were all related. Following the loading of Pd onto a porous carbon-based nanosheet doped with nitrogen, the catalytic hydrogenation of nitrobenzene was assessed. Because of

the designed pore structure, increased nitrogen, and very low Pd particle, the consequences disclosed that Pd@PCN had nearly 100% adaptation and virtuous cycle activity towards the hydrogenation of nitro-benzene; it was better than some other nanoparticles and supports and demonstrates significant application potential [54].

3.2 Sulfur Doping (S-doping)

Sulfur interacts with carbon to create thiols, sulfides, and disulfides, functional groups that are structurally analogous to oxygen's alcohols, ethers, and peroxides (sulfur is part of the oxygen group and hence is positioned in the period IInd of the periodic table). The incorporation of second-row atoms with a larger radius than carbon disrupts a flat geometry because these imperfections serve as active species in redox reactions [55]. According to a survey, different sulphur bonding species, including thiol, thiophene (aromatic sulphur), thioether/sulfides (aliphatic sulphur), sulfoxide, sulfone, and sulfonic acid, are produced when sulphur atoms are added to the sp^2 carbon framework. Zhao et al. [56] described the function of S doped inside the network-carbon, so that had an impact on improving the capacitance efficiency in S-doped mesoporous carbon structures. The results are owing to (i) a larger density of electrons being present on the interface of carbon as a result of its harmonious instigation with the electron-efficient sulphur and (ii) a sequence of redox reactions (i.e., faradaic reactions) involving sulfone and sulfoxide types [57]. An increased electric dipole moment during the electrochemical process causes the overall polarization of the medium to increase within an applied electrical field. According to the following equation, the total polarization (P) is multiplied by the electrolyte's dielectric constant (r), increasing the normalized capacitance. Therefore, a greater r increases capacitance, and surface polarization facilitates the charge transfer mechanism.

$$C/A = \varepsilon_r \varepsilon_0 / d \text{ and } P = (\varepsilon_r - 1)/(\varepsilon_r + 2)$$

where A is the electrode's electro active surface area, ε_r and ε_0 are the dielectric constants of the electrolyte and free space, and d is the average ionic distance from the electrode surface.

So, S-doping of the carbon framework causes the band gap to open and localized states to form, which change the electro negativity by causing polarization impact. Additionally, S-doping can effectively change the distribution of spin/charge densities that modify the carbon matrix by generating a significant number of electroactive sites. Chen et al. [58] synthesized an ecologically friendly approach that was used to create S-doped microporous carbon nanospheres with a TiO_2 nano-covering (CNS-S@TiO_2) (as shown in Fig. 4a), which were then investigated as a potential anode material for SIBs/LIBs. Greater as predicted values of both graphite and TiO_2 for Li^+ and Na^+ stowage, the composites used as anodic demonstrated superior revocable capabilities of 768 and 480 mAh g^{-1}, that might be attributed to surface

storing because of availability in sulphur atoms. It has been found that S-doping may significantly boost the binding energy of sodium ions on graphite and enhance the efficacy of C_4Na surface production. Additionally, TiO_2 nano-coverings are having a significant impact on the constancy of Li^+-ion and Na^+-ion storage in these materials, leading to an extremely extended life cycle. However, CNS@TiO_2 hybrids with almost monodisperse widths of around 200 nm are shown in Fig. 4b1. Further, it is suggested that the (enlarged TEM image, Fig. 4b2) i.e., CNS interface was coated by TiO_2 nanoscale-particles. Figure 4b3 shows presence of TiO_2 nano-units (yellow ellipse) through sizes extending from 4 to 8 nm in CNSs. Figure 4c1 shows the CNS-S@TiO_2 nanohybrid was found after S-doping. In high-resolution TEM images (Fig. 4c2) show that CNS-S@TiO_2 is greatly sander than CNS@TiO_2, with the exception of several giant TiO_2 nanoparticles. However, three nanocoatings, indicated by yellow lines in Fig. 4c3, are displayed on CNS-S@TiO_2. The widths of the lattice fringes (0.33 nm for rutile and 0.35 nm for anatase) and the presence of polymorphs of TiO_2, as shown by selected area electron diffraction (SAED), show that nanospheres were heavily coated with TiO_2 nano-coatings. Figure 4d1, d2 demonstrate that the TiO_2 shell treated over carbon of nano-spherical shapes of diameters vacillating from 100 to 200 nm have retained after a portion of the carbon core was removed by calcinating CNS-S@TiO_2 in air, indicating the excellent stability of TiO_2 nano-coatings. The SAED (inset) shows that the TiO_2 is polycrystalline and conforms to the (101), (004), (200), and (105) planes of anatase TiO_2, which are shown in Fig. 4d3.

He et al. [59] investigated chemical activation using potassium hydroxide, a lignin-based pitch recovered from dark liquor has been employed as a preliminary to create triggered carbon (AC) exhibiting lofty specific pore volume and interfacial area (KOH). It was also investigated how the characteristics of activated carbon were affected by the activation temperature. At an stimulation temperature of 850 °C, the improved activated carbon (PAC-5-850-60) was made. The PAC-5-850-60 attained its maximum specific surface area and total pore volume at this temperature. Gassy benzene has been employed by way of adsorbing agent in the adsorption investigation, and only a dynamic adsorption experiment has been run to examine the adsorption activity and process of PACs. The partition coefficient and adsorption capability for gassy benzene on PAC-5-850-60 under 5000 ppm (or 500 Pa partial pressure) seem to have been 802.06 mg g^{-1} and 0.20 mol kg^{-1} Pa^{-1} at 10% breakthrough level and 819.77 mg g^{-1} and 0.02 mol kg^{-1} Pa^{-1} at the 100% breakthrough level, respectively. The recycling adsorption performance of PAC-5-850-60 was excellent, and it may work effectively as an absorbent to get rid of gaseous benzene. Similarly, Raj et al. [60] propose a significant contender for supercapacitor applications after a fruitful conversion of Borassus flabellifer flower into stimulated carbon (AC), by the greatest uptake of sulphur (S) levels in the doped-S AC method. As per report, at the current density of 1 A/g, S-doped activated carbon exhibits an excellent specific capacitance of 275 F/g at a current density of 1 A/g^{-1}. The specific surface area (PM6) for AC is 474.99 m^2/g, with the maximum 10 wt% S achieved after activation at 600 °C for an hour via 30 wt% KOH [60].

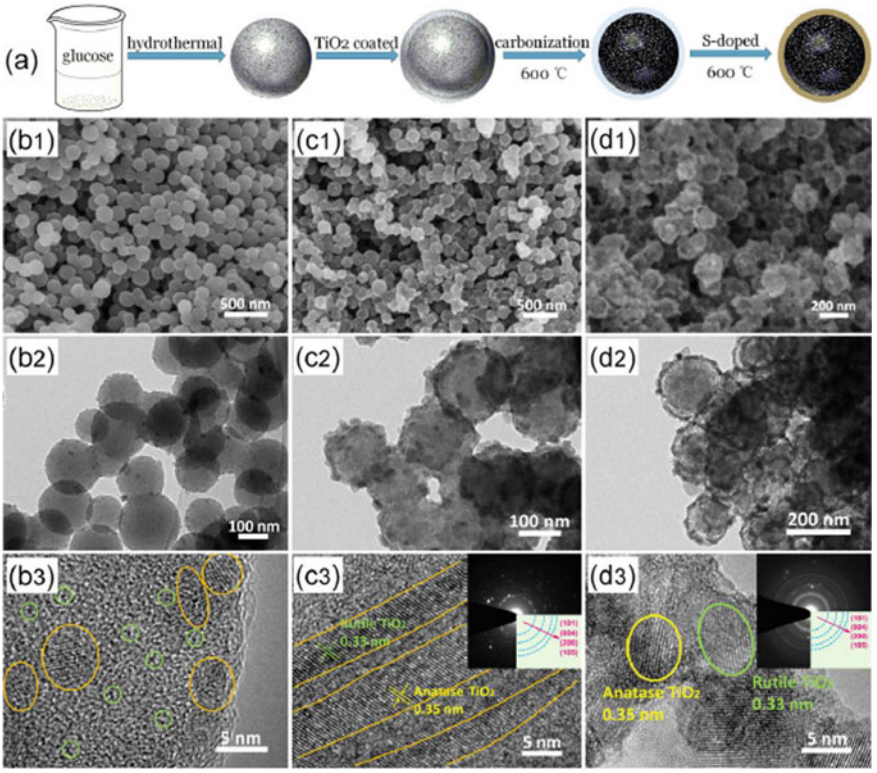

Fig. 4 Morphology and structural characteristics: (**a**) CNS-S@TiO_2 material. TiO_2 nanoparticles and micro-pores are shown in a ellipse of yellow colour and a tiny green ring in the SEM and TEM images of CNS@TiO_2 (**b1–b3**). TiO_2 exhibits nanocoatings shown by yellow lines in the S-doped CNS-S@TiO_2 as exposed in (**c1–c3**) SEM and TEM images. Neat TiO_2 remained after part of the carbon was removed from CNS-S@TiO_2 in medium of air at a temperature 450 °C, as shown by the matching SEM and TEM (**d1–d3**). Reproduce with permission from the Ref. [58]. Copyright 2018, Elsevier

4 Biomass-Derived and Self-doped Heteroatoms-Built Carbon Materials

In the past ten years, a lot of biomass precursors have been used for energy storage purposes. Due to their very porous nature and heteroatom doping, electrodes' electrochemical performance has increased. Heteroatoms appear spontaneously in a variety of protein configurations in certain biomass precursors. However, these were utilized as a low-cost, environmentally acceptable method of uniformly doping carbon, which serves as a strategy leading to applications involving storing of energy. On the basis of mentioned benefits, individual-doped biomass carbon as an anode/cathode for supercapacitors can be used for and has the following features: Zou et al. [61] investigated a material with a sustainable and low-cost carbon-based electrode, which is

used as the most abundant resource other than fossil fuel for energy device applications. These materials are used in this study to create suitably doped heteroatom carbon materials in order to determine the outstanding electrochemical behaviors and porosity via alkaline activation and carbonization. However, the activation method increases the pore distribution, specific surface area as well as helps in the construction of active sites for heteroatom doping. Similarly, Ma and colleagues proposed a self-doped heteroatom concept based on porous carbon materials with low-cost and renewable precursors. Herein, they used the concept of carbonization and activation strategies to achieve hierarchical multi-heteroatom co-doped porous carbon materials. Initially, the biomass porous carbon was derived from tea leaves, which function as an ideal precursor to provide the secondary hetero-atomically functionalized carbon nanosheets. Hence, these nanosheets are adjustable by changing the different conditions of pyrolysis, which successfully increases the petrochemical activity of porous carbon. Thus, it results in outstanding capacitance retention of nearly 94.8% over 14,000 cycles at 3 A/g^{-1} and reveals the best strategy for storing energy at high performance for use in the industrial sector. The self-doping method is still improving their ability to use supercapacitors by resulting biomass derived from various carbon-containing materials [62]. Bhattarai et al. [63] proposed the concept of self-doped nitrogen atoms with activated carbon, which is derived from wastes of cherry flowers, to function as variable energy storage materials for green and sustainable energy solutions. However, they examined the energy storage applications of activated carbon derived materials like an electric double layer capacitance and sodium-ion battery electrode material.

4.1 Solitary Heteroatom Doped Biomass Carbon

Numerous biomass resources high in nitrogen are readily available out of usual resources and used in the process of conversion for applicability in the field, energy storage. The N-efficient biomass may be divided to three categories: microorganisms, plants, and animals. The use of this N-doped carbon produced from biomass in supercapacitor applications is described in more depth below. Plant-based biomass consists of the seeds, fruits, leaves, and stems/bark of plants, which are rich in minerals, proteins, and other compounds, including collagen and chitin. The by-products of animal life, such as skin, bones, and other body parts, include a large no. of hetero-atom functions in the form of keratin protein, amino acids, and chitin. Animal waste is a cheap, plentiful, renewable, and eco-friendly source of doped carbon nanostructures.

4.2 Biomass with Carbon with Dual-heteroatom Doping

A carbon network's dual doping may provide a harmonious coupling consequence among hetero-atoms, enhancing the network's chemical or corporal characteristics. N-doped primary element, while co-dopants such as S, P, and O are often utilized. Co-doping with nitrogen and sulfur occurs naturally in close-packed carbon hexagonal rings, and their combined effect may increase the total doping level. The N–H–S– and N–H–S– =hydrogen bonding groups allow pyridinic and graphitic nitrogen to communicate [64]. While S and P widen the gap between layers and provide electrochemically dynamic regions for pseudo capacitance, graphitic N-doping allows electricity to flow more freely through the material. Density functional theory (DFT) was used by Zhou et al. to determine that nitrogen and sulphur co-doped carbon had a larger binding energy (Eb) associated with the LiSH molecule than nitrogen and sulphur alone (E_b = 1.43 and 1.02 eV, respectively) [65]. In contrast to graphene without doping, E_b at the thionic S site increases while E_b at the thio-phenic S site decreases. In contrast, intense contact raises the E_b of LiSH at the pyridinic N and pyrrolic N sites. The LiSH molecule exhibits a higher binding energy in the case of N- and S-co-doped graphene, with thionic S and pyridinic or pyrrolic N closed. Because N and S atoms are more electronegative than C atoms, they act as electron withdrawing agents, polarizing nearby C atoms and the group C–O and forming hydrophilic interfaces. DFT simulations show that dual-doped graphene is superior to mono-doped graphene as a result of its synergistic impact.

4.3 Multi-heteroatom Doped Biomass Carbon

Carbon atoms receive greater asymmetrical spin and charge density when they are doped with several heteroatoms. These few biomass precursors contain multiple heteroatoms on their own, as opposed to single or co-doped heteroatoms; pyrolysis of these precursors yields multi-heteroatom doped carbon at the nanoscale. To stabilize oxygen functions by enhancing reaction stability, doping with N, S, and P in that order will correspondingly introduce an n-type dopant interface of polarization for pseudo-sites, increase pseudo-capacitive characteristics coupled with electronic conductivity, and increase pseudo-capacitive characteristics. For instance, using a one-step technique, Zhao et al. [66] have synthesized N (11.2 at%), S (0.64 at%), and P (0.82 at%) co-doped hierarchically porous structured carbon (N–P–S–HPC) from peanut meal. To further comprehend the capacitive behavior of N–P–S–HPC and commercially stimulated carbon, the Trasatti analysis has been utilized to quantify the involvement of EDLC as well as pseudo capacitance (AC). This result is more in accordance with the Dunn technique of study, which found that heteroatom-doped carbon showed 23% pseudo-capacitive behavior compared to AC's 8%. However, urea is the primary nitrogen source in human urine, and it can be easily converted to heteroatom-doped porous carbon via pyrolysis and acid action [67]. Moreover, the

chemical compositions of heteroatoms like N, S, and P vary from higher to lower percentages. The most common waste material in sericulture, agronomic waste from silkworm feces, has recently been used in the fabrication of multi-heteroatom doped carbon with appreciable porosity. This waste is comprised of rudimentary forms of proteins, lipids, amino acids, carotenoids, and other substances. Hydrothermal treatment [68] or activation/pyrolysis of silkworm poop yielded heteroatom-doped porous carbon for use as electrodes in high-performance supercapacitors [69]. Chitin, a polymer often found in insect exoskeletons and cell walls, contains amines, as was previously documented. Heteroatom-incorporated porous carbon (PCS) was made by carbonizing and activating cicada slough (cicada shell) [70]. The XPS analysis reveals the presence of heteroatom doping at 2.72 at% for nitrogen, 0.13 at% for sulphur, and 0.27 at% for phosphorus, with all N-species, C–P–C bonds, oxy-phosphorus, and all S-species, like thiophene, sulfonate/sulfate, etc. Yang et al. [71] have claimed that employing a laver to produce porous carbon that was doped with various heteroatoms (P, S, Ca, Mg, K, and Fe) improved the capacity of supercapacitor devices to power LEDs.

5 Biomass Derived N-doped Carbons as Fuel Cell Catalyst Support

Carbon black is made from Vulcan XC-72, and because of its large surface area and high electrical conductivity, it has found widespread use as a catalyst in the advancement of technology for fuel cells. The feeble connection amongst XC-72 blacks of carbon and Pt nano-scale units led to the accumulation of Pt nano-sized particles, which decreased the active sites on the particles [72–74]. As a consequence, the durability of the material was deficient. Moreover, the surface active sites that anchor metal nanoparticles might be introduced by doping carbon with nitrogen, resulting in more homogeneous and better bonding between both the nanoparticles and carbon-based materials. In contrast to non-doped carbon nanotubes, Pt nanoparticles anchored by nitrogen-doped surface carbon nanotubes have been shown in recent studies to have increased durability and ORR activity [73, 74]. The use of nitrogen-doped carbon-based biomass acts as a catalyst for electrochemical activity. A higher electrochemically dynamic area of surface and enhanced properties of electro-catalyst performance for oxidation in alcohol and reduction of oxygen were found in a NCs-supported catalyst in comparison to that of a standard carbon black-supported noble metal nanoparticle [74–76]. Besides, nitrogen, which may alter the Pt chemical state and shape the nanoparticles into their characteristic dendrites, was found to be present in the soybean-derived NC, resulting in the formation of Pt dendrites (Fig. 5a) with a dimension of nearly 20 nm. In addition, as can be shown in Fig. 5b, the Pt dendrites demonstrated increased electro-oxidation of methanol in comparison to that of the normal Pt–C catalysts. Superior-interfacial-area nitrogen doping of carbon aerogel generated from chitosan is an appropriate electrochemical

substrate because it can create highly distributed and uniform Pt nanoparticles with large electrochemically active sites for methanol oxidation. However, because of their mutually influential bond, the electronic configuration of PT was altered when nitrogen was introduced into a carbon support. The results of the XPS experiment also established that the Eb of Pt 4f undergoes a positive transition toward a high-state energy state (Fig. 5c, d), which suggests that it is capable of demonstrating a lowering trend when shown by adsorbates on the surfaces of metals. This helps remove CO-based transitional chemicals and enhances methanol oxidation kinetics, lowering the onset potential and increasing intrinsic activity [72–76].

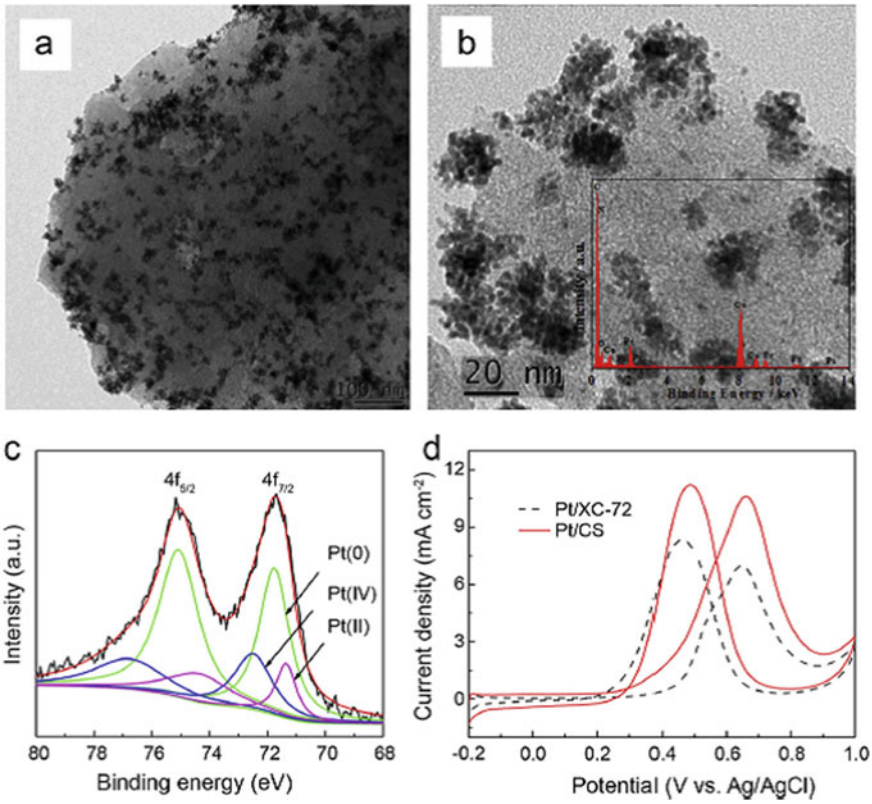

Fig. 5 **a** Pt dendrimers on nitrogen-doped carbon: a morphological picture, **b** Pt–C catalyst, **c** XPS spectra of P–C catalyst and **d** Pt-XC-72 carbon black. Reproduce with permission from the Ref. [75]. Copyright 2014, Elsevier

6 Supercapacitor Activity of N-based Doped-Heteroatom Biomass Carbon Electrodes

Electrochemical capacitors (ECs), sometimes acknowledged as "supercapacitors," are a promising photovoltaic technology for mobile electronics, cold-starting aids, electric automobiles, etc., because of their higher rate capability and longer cycle life compared to battery systems. Rescindable ion adsorption on the superficial high-surface area electrodes charges the electrical dual layers in ECs, which then serve as energy storage devices. The primary elements of an EC, the electrodes, typically comprise absorbent activated carbon. This substance is particularly suited for this application due to the fact that it has great chemical stability, superior electrical conductivity, accessibility, is kind to the environment, and has a cheap cost. Furthermore, the permeability of significantly higher exterior-area carbon can be custom-made and altered to match the properties of the electrolyte used in ECs6. Additionally, the inclusion of certain heteroatoms into the carbon framework can have pseudo-capacitive effects that increase the capacitance of the carbon materials employed as electrodes. For instance, nitrogen groups can increase specific capacitance by combining the charging of the double layer with extra-faradic redox processes. Ferrero et al. [77] have developed a supercapacitor based on Li_2SO_4 that uses electrode material that is inexpensive and kind to the environment. In this work, defatted soybean (i.e., soybean meal), an extensively accessible and lucrative protein-rich biomass, was used as an ingredient in an ecologically sound hydrothermal carbonization procedure, yielding nitrogen-doped carbon through a large specific surface extent, optimized micropore assembly, and surface chemistry.

In Fig. 6, we can see that the rate capabilities of these activated carbons are quite high, and samples produced at low activation temperatures had a capacitance fade of 50% when subjected to a current density of roughly 20 A g^{-1}. Furthermore, at an increased current density of 40 A g^{-1}, the AS-700 and AS-800 samples show a greater value of capacitance of 140 F g^{-1} (87 F cm^{-3}) and 170 F g^{-1} (99 F cm^{-3}), respectively, and outstanding capacitance retention of 45 and 56% for 400 times the rise in discharge rate from 0.2 to 80 A g^{-1}. Zhou et al. [78] have investigated the most environmentally friendly biomass that has carbon pores, which will be vastly utilized in the near future as a domain of energy conversion technology. However, they reveal the use of soybean dreg in a simple KOH activation and high-temperature carbonization process using both aqueous (6.0 M KOH) and ionic liquid (EMIMBF4) electrolytes to make a high efficiency electrode material for supercapacitors. It is favorable for both large-scale ion storage and high-speed ion transport that the material that carbonizes at 800 °C has a significant number of micropores (0.71 cm^3 g^{-1}) and a highly ion-accessible surface (1837.26 m^2 g^{-1}).

Han and his colleague planned the development of high-quality, low-cost electrochemical energy storage systems using activated carbon derived from plant waste. Because of its low cost and simple production procedure as an electrode material for supercapacitors, activated carbon has a promising future, especially compared to graphene, carbon nanotubes, and other pricey carbon materials. By activating KOH

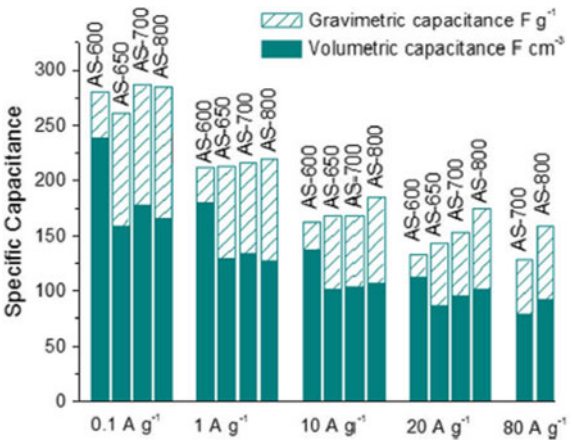

Fig. 6 Specific capacitance of N doped porous carbon in 1 M H_2SO_4 at a voltage window of 1.1 V varies as a function of current density [77]

with bamboo shoot shells, porous carbon (KAC-700) with heteroatoms (O, N) is created. At a current density of 1 A g^{-1} in 1 M H_2SO_4 electrolyte, the symmetric supercapacitor based on KAC-700 possesses gravimetric and volumetric capacitances of 223.21 F g^{-1} and 167.63 F cm^3, respectively. With a power density of 546.60 W kg^{-1} and a high energy density of 13.15 Wh kg^{-1}, this supercapacitor also has a high capacitance retention rate of 93.62% after 4000 cycles at 5 A g^{-1} [79]. Similarly, a research group identified celery derived N-doped microporous carbon material, which is synthesized using a one-step self-activation process. Herein, the manufactured samples demonstrate a hierarchical porous structure with open micropores, with a specific surface area of up to 1186 m^2 g^{-1} and an average micropore width of 0.94 nm. These samples inherit the evolved water transport system found in celery living tissue. The addition of nitrogen heteroatoms increases the manufactured samples' wettability, conductivity, and surface activity, as well as the accessibility of the electrolyte in the micropores, which results in better capacitive performance. The manufactured samples have a capacitance of up to 245 F g^{-1} [80]. Jia and his co-workers have reported the Metasequoia fruit (dawn redwood cone) may be used to obtain naturally nitrogen-doped porous carbon in two simple steps: pre-carbonization and chemical activation. In 6.0 M basic electrolyte, current collectors covered with porous carbon are tested as electrodes for electrochemical capacitor applications. According to the findings, porous carbon that was produced at a temperature of 700 °C for activation maintains the highest specific surface area (1,831 m^2 g^{-1}) and the biggest pore volume (0.92 cm^3 g^{-1}). The carbon-based electrode exhibits a steady cycling characteristic in a three-electrode test, in addition to having an exceptional capacitive performance up to 326 and 236 F g^{-1} at current densities of 0.5 and 10 A g^{-1}, respectively. Due to the accessibility of materials, our research implies that the cone may be used as a viable and nearly cost-free precursor in the fabrication of porous carbon samples for supercapacitors [81].

7 Supercapacitor Performance of S-based Heteroatom Doped Biomass Carbon Electrodes

Chadha et al. [82] proposed the concept of lithium–sulfur batteries using carbon-based electrode material as well as describing the recent development of a flexible Li–S battery device. Due to their high energy density, theoretical capacity, and low price, lithium–sulfur batteries are one of the fastest-growing categories of rechargeable batteries. However, a number of obstacles, such as degradation brought on by polysulfide dissolution, low conductivity, and other limiting factors, delay their widespread application. Li–S batteries have been developed for decades with the goal of enhancing battery performance by changing the electrode material to address these issues. Meanwhile, the need for process modifications to enhance battery performance is more critical than ever due to the depletion of fossil fuels and rising energy demand. Due to their low cost, accessibility, high cycle stability, and remarkable electrical, thermal, and mechanical qualities, carbon-based materials, including conducting polymers, carbon nanotubes, graphene, and activated carbon, have drawn a lot of attention. A comparison of Li–S batteries and their rival rechargeable batteries based on comparable characteristics is also covered, as is a comparison with various non-carbon-based electrodes used in the lithium–sulfur battery. A basic conclusion and recommendations for the future are provided. Similarly, Gu et al. [83] analyze the new technique to obtain lithium–sulfur batteries with a significant potential by replacing lithium-ion batteries. This study examines the different uses of carbonaceous materials in Li–S batteries and offers ideas for their future development with the goal of creating a sulfur-based cathode with a high energy density, extended cycle life, and little impact on the environment. Because the impacts of climate change are just now becoming apparent, society must develop measures to lessen the influence of humans on the environment. It is apparent that more ecologically friendly power sources are needed because energy production is one of the main causes of greenhouse gas emissions. Research is constantly being done to improve renewable energy sources such as solar and wind power. However, due to the intermittent nature of their power generation, efforts must be made to develop methods of storing this sustainable energy for times when production circumstances are not at their optimal level. One potential addition to these renewable energy sources is battery storage, but as present Li-ion technology has reached its theoretical capacity, new battery technology needs to be researched. Sustainable carbonaceous materials have been sought after for applications such as carbon–sulfur (C–S) composite cathodes, carbon interlayers, and carbon-modified separators in an effort to reduce environmental impact.

8 Supercapacitor Performance of Dual N and S Based Heteroatom Doped Biomass Carbon Electrodes

Multi-heteroatom doping makes the spin and charge density of carbon atoms more asymmetrical than either single-heteroatom doping or co-doping of heteroatoms. There are only a handful of biomass precursors that naturally contain multiple heteroatoms, but when pyrolyzed, they yield multi-heteroatom doped carbon nanostructures with sequential N, S, and P doping, resulting in n-type nanoparticles with a polarized surface for pseudo-sites that improve quasi-properties and electron mobility and stabilize oxygen functions for greater reaction stability. One example is the production of nitrogen (11.2 at%), sulphur (0.64 at%), and phosphorus (0.82 at%) co-doped hierarchical porous carbon (N–P–S–HPC) from peanut meal by Zhao et al. [84], utilizing a one-step technique. In order to appreciate the capacitive behavior of N–P–S–HPC and commercial activated carbon, the Trasatti analysis was used to evaluate the contribution of EDLC and pseudo capacitance. This was done using the EDLC and pseudo capacitance values (AC). It reveals that the heteroatom-doped carbon exhibited 23% pseudo capacitive behavior as compared to AC's 8%, which is more in keeping with the results of the Dunn method of analysis as given above. AC's behavior was measured at 8%. In addition, the human organic waste, often known as "urine," which contains urea as the principal source of nitrogen in addition to other organic and inorganic elements, was readily turned into heteroatom doped porous carbon material by the processes of pyrolysis and acid treatment [85]. The chemical makeup of heteroatoms containing nitrogen, sulphur, and phosphorus, respectively, is 5.7, 0.8, and 0.2 at%. Recently, multi-heteroatom doped porous carbon nanosheets were manufactured utilizing agricultural waste from silkworm feces. Silkworm excrement is the primary byproduct of the silkworm farming industry and is comprised of crude proteins, lipids, amino acids, and other substances. Excreta from silkworms were subjected to hydrothermal treatment [68] or activation/pyrolysis [69] in order to produce heteroatom-doped porous carbons for use as electrodes in high-performance supercapacitors [70]. Activation/pyrolysis [86] according to the findings of a recent study, the polysaccharide chitin, which is normally found in the exoskeletons and cell walls of insects, has a significant quantity of amines. Cicada slough, also known as cicada shell, was one of the materials that were used during the carbonization and activation procedure [87] in order to produce heteroatom-incorporated porous carbon (PCCS). According to the results of the XPS analysis, the elements nitrogen (2.72 at%), sulphur (0.13 at%), and phosphorus (0.27 at%) are all heteroatom-doped. Among all of the species of nitrogen are all of the species of sulphur, including thiophene, sulfonate, and sulfate, and phosphorus is oxidized. The ability of a solid-state supercapacitor device to power LEDs was shown by Yang et al. [43] after they used a laver to create multi-heteroatom doped porous carbon (P, S, Ca, Mg, and K) and then used the porous carbon to power LEDs. Si et al. successfully used the hydrothermal carbonization approach as well as KOH activation to prepare N-doped or dual N- and S-doped microporous carbons using glucose and human hair as carbon precursors. Its goal is to alter the amount of human hair used in

N- or S-doping. The generated carbons exhibited a considerable pseudo-capacitance as a result of the synergistic effects of the various N, O, and S-doped species. It is possible for the capacitance of AHC-4 in KOH electrolyte to reach 264 F g^{-1}. With a good cycle life of 1000 cycles and a very high capacitance value of 154 F $g^{-}1$, the AHC-1 has proven to be an excellent choice. Utilizing renewable biomass allows for the production of adjustable dual heteroatom-doped carbon composites with high surface area and capacitive performance [88]. In a similar vein, Wang and one of his co-workers have successfully synthesized N, S co-doped pomelo peel-derived carbon using a one-step technology. Because of its large SBET, high heteroatom doping rate, and acceptable graphitization degree, the carbon that was obtained demonstrates a high specific capacitance (317 F g^{-1}) and an exceptional rate capability (69.7% of capacitance retention at 15 A g^{-1}), These outcomes are superior to those obtained with PPC and NSPPC2, for which the respective capacitance retentions are 59.3% and 66.9% (as shown in Fig. 7). The one-step approach is used to deal with the other two biomasses (bamboo fiber and sugarcane bagasse). Because of their comparable microstructure and chemical make-up to the generated carbon from pomelo peel, the other two biomasses still display outstanding electrochemical performance. This indicates that the one-step approach may be used on a wide variety of other types of materials. All of the carbon materials used in the series of symmetric supercapacitors have been found to have high energy densities (30.6–24.6 Wh kg^{-1}), which indicates that there may be potential uses for such carbon materials in the field of energy storage [43].

Heteroatom-doped, biomass-derived carbon has gotten a lot of attention lately because its precursors are cheap and there is a lot of it. This is especially true in oxygen

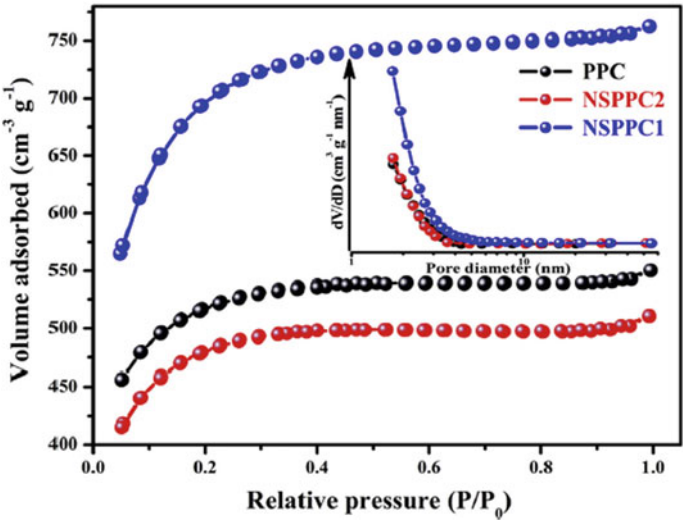

Fig. 7 Three different EIS curves for PPC, NSPPC2, and NSPPC1. Reproduce with permission from the Ref. [43]. Copyright 2020, Elsevier

reduction processes and supercapacitors. He and his co-workers manufactured a porous carbon material, like a ladder, from mulberry leaves. This material has a high nitrogen content (8.17 at%), a high sulfur content (1.97 at%), a large surface area (1689 m^2 g^{-1}) and a porous structure with a mass of micropores and mesopores. The nitrogen–sulfur dual-doped ladder-like carbon has a huge specific capacitance of 243.4 F g^{-1} at 0.1 A g^{-1} and exceptional durability (94% retention after 5000 cycles at 3 A g^{-1}). This is the electrode material for the supercapacitor. Additionally, as compared to the Pt/C catalyst, the ladder-like porous carbon doped with nitrogen and sulfur demonstrates superior electrochemical performance in terms of long-term stability (90.2% retention after 20,000 s) and resistance to methanol crossover for the oxygen reduction process. This research may successfully offer a new device for exploiting natural resources to make heteroatom-doped carbon for energy conversion and storage [88].

9 Conclusion and Outlooks

An overview of the recent developments in high-performance electrochemical energy storage and conversion applications using porous nanostructured nitrogen and sulfur-doped carbon produced from biomass is presented in this current chapter. A better understanding of the factors that limit the efficiency of electrochemical catalysts and energy storage devices and strategies for overcoming these challenges are discussed. There are two techniques that may be used to convert biomass into PNCs: pyrolysis and hydrothermal carbonization. When dealing with biomass that is deficient in nitrogen, the reaction system may need the addition of ammonia in order to acquire nitrogen. In addition, the presence of nitrogen functional groups within the carbon crystal structure impacts the kinetics of catalytic reactions as well as the sites of absorption for ion storage. For instance, pyridinic N and quaternary N are both active in oxidation reduction reactions, and the production of these compounds at low temperatures would result in an increase in the amount of iron present in the compounds. Moreover, the nanostructured materials produced from biomass have the potential to be widely employed in high performance electrode materials for supercapacitor (SC) applications. These materials developed from biomass are a cost-effective, environmentally responsible, and sustainable product.

This chapter examines the relationship between the dimensionality, chemical composition, and microstructure of biomass-derived carbon materials and the electrochemical performance of SC electrodes. The precursors are great for making large quantities of carbon materials made from biomass that have specific functions for SC applications. In this way, optimal carbon materials derived from biomass can be engineered by selecting appropriate precursor techniques, carbonization or activation methods, and structures to facilitate the synthesis of carbon electrodes with a specific surface area and pore size. Thus, biomass-derived carbon materials may be rationally designed to meet high-performance SC criteria for SSA, pore size distribution, and

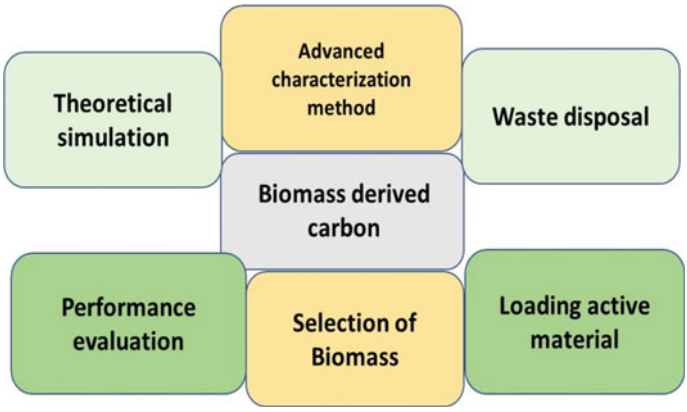

Fig. 8 Prospects for porous carbon materials generated from biomass

composition. Using biomass-derived carbon sources to make high-performance SCs has made progress, but challenges remain (as shown in Fig. 8).

Selection of precursors: It is crucial to understand the similarities and distinctions of biomass precursors, especially microorganisms, biological minerals, plant organs, and bio-macromolecule precursors. By selecting the right biomass precursors, low-cost, high-quality carbon products may be produced.

Activation and Carbonization: The structural transition of organic precursors into inorganic carbon compounds during carbonization needs more study. During carbon activation, the link between chemical additions and carbon structural characteristics must be determined. To increase biomass precursor conversion efficiency, carbon yields, heteroatom contents, and tap densities should be considered, as should cost-effective ways for scaling up production.

Composite electrodes: To maximize gravimetric and volumetric energy densities, SC electrode components must have a high theoretical capacity, acceptable interfacial carbon compatibility, and/or good structural stability. New solutions like highly concentrated electrolytes or aqueous solutions may help resolve interfacial difficulties.

Theoretical simulation: Theoretical models of capacitor operations, molecular interactions, and chemical reactions may guide capacitance augmentation. These models can predict ion diffusion and dynamics.

Performance and evaluation: Traditional gravimetric capacitance data leave out mass loading, electrolytes, and SC volume, which makes them useless. For high-performance SCs, an effective method for evaluating biomass-based, high-mass-loading carbon electrodes is required.

Effect on the environment: Creating clean and efficient SCs is a practical and effective way out of the energy crisis. Improvements in the disposal of waste SCs and other device enhancements might have a significant impact on waste management,

carbon emission reduction, and energy security, all of which would contribute to global carbon management targets and clean air programs.

Acknowledgements The authors thankfully acknowledge the support provided by Centurion University of Technology and Management, Odisha, India for carrying out the current research.

Conflicts of Interest The authors declared that no conflict of interest.

References

1. Chen X, Li C, Grätzel M, Kostecki R, Mao SS (2012) Chem Soc Rev 41(23):7909–7937
2. Hatfield-Dodds S, Schandl H, Newth D, Obersteiner M, Cai Y, Baynes T, Havlik P (2017) J Clean Prod 144:403–414
3. Yu Z, Tetard L, Zhai L, Thomas J (2015) Energy Environ Sci 8(3):702–730
4. Jiang J, Zhang Y, Nie P, Xu G, Shi M, Wang J, Zhang X (2018) Adv Sustain Syst 2(1):1700110
5. Gopalakrishnan A, Sahatiya P, Badhulika S (2018) Chem Electro Chem 5(3):531–539
6. Bai Y, Shen B, Zhang S, Zhu Z, Sun S, Gao J, Wei F (2019) Adv Mater 31(9):1800680
7. Simon P, Gogotsi Y (2008) Nat Mater 7(11):845–854
8. Jiang H, Lee PS, Li C (2013) Energy Environ Sci 6(1):41–53
9. Gopalakrishnan A, Yang D, Ince JC, Truong YB, Yu A, Badhulika S (2019) J Energy Storage 25:100893
10. Kang Z, Li Y, Yu Y, Liao Q, Zhang Z, Guo H, Zhang Y (2018) J Mater Sci 53(14):10292–10301
11. Wang H, Yan X, Piao G (2017) Electrochim Acta 231:264–271
12. Zhao F, Vicenzo A, Hashempour M, Bestetti M (2014) Electrochim Acta 150:35–45
13. Sun K, Zhang S, Li P, Xia Y, Zhang X, Du D, Ouyang J (2015) J Mater Sci: Mater Electron 26(7):4438–4462
14. Gopalakrishnan A, Badhulika S (2018) J Ind Eng Chem 68:257–266
15. Osman S, Senthil RA, Pan J, Li W (2018) J Power Sources 391:162–169
16. Osman S, Senthil RA, Pan J, Sun Y (2019) J Power Sources 414:401–411
17. Kim KS, Zhao Y, Jang H, Lee SY, Kim JM, Kim KS, Hong BH (2009) Nature 457(7230):706–710
18. Yang H, Ye S, Zhou J, Liang T (2019) Front Chem 7:274
19. Gopalakrishnan A, Sahatiya P, Badhulika S (2017) Mater Lett 198:46–49
20. Liu M, Niu J, Zhang Z, Dou M, Wang F (2018) Nano Energy 51:366–372
21. Xia J, Zhang N, Chong S, Chen Y, Sun C (2018) Green Chem 20(3):694–700
22. Zhang X, Liu Y, Zhu B, Zhao H, Mi R, Wang Z, He P (2022) Appl Phys Lett 121(6):063901
23. Pourhosseini SEM, Norouzi O, Salimi P, Naderi HR (2018) ACS Sustain Chem Eng 6(4):4746–4758
24. Ranaweera CK, Kahol PK, Ghimire M, Mishra SR, Gupta RKC (2017) Nanoscience 3(3):25
25. Yoshizawa N, Maruyama K, Yamada Y, Zielinska-Blajet M (2000) Fuel 79(12):1461–1466
26. Wei L, Yushin G (2012) Nano Energy 1(4):552–565
27. Wang R, Wang P, Yan X, Lang J, Peng C, Xue Q (2012) ACS Appl Mater Interfaces 4(11):5800–5806
28. Xu B, Hou S, Cao G, Wu F, Yang Y (2012) J Mater Chem 22(36):19088–19093
29. Paraknowitsch JP, Thomas A (2013) Energy Environ Sci 6(10):2839–2855
30. Paraknowitsch JP, Thomas A (2013) Energy Environ Sci 6:2839–2855
31. Zdol_sek N, Rocha RP, Krstic J, Trtic-Petrovic T, Sljukic B, Figueiredo JL (2019) Electrochim Acta 298:541–551
32. Deng YF, Xie Y, Zou KX, Ji XL (2016) J Mater Chem A 4:1144–1173
33. Liu XC, Li SM, Mi R, Mei J, Liu LM, Cao L (2015) J Appl Energy 153:32–40

34. Lai QX, Zhao YX, Liang YY, He JP, Chen JH (2016) Adv Funct Mater 26:8334–8344
35. Lee MS, Choi HJ, Baek JB, Chang DW (2017) Appl Energy 195:1071–1078
36. Zhang DY, Han M, Wang B, Li YB, Lei LY, Wang KJ, Wang Y (2017) J Power Sources 358:112–120
37. Li JH, Zhang GP, Fu CP, Deng LB, Sun R, Wong CP (2017) J Power Sources 345:146–155
38. Zhou SC, Zhou QX, Su HX, Wang Y, Dong Z, Dai XP (2019) J Colloid Interface Sci 533:311–318
39. Zhang WJ, Chen ZT, Guo XL, Jin K, Wang YX, Li L, Zhang Y (2018) Electrochim Acta 278:51–60
40. Cai DD, Wang CS, Shi CY, Tan N (2018) J Alloy Comp 731:235–242
41. Cheng LL, Hu YY, Qiao DD, Zhu Y, Wang H, Jiao Z (2018) Electrochim Acta 259:587–597
42. Gopalsamy K, Balamurugan J, Thanh TD, Kim NH, Lee JH (2017) Chem Eng J 312:180–190
43. Wang B, Ji L, Yu Y, Wang N, Wang J, Zhao J (2019) Electrochim Acta 309:34–43
44. Lei W, Zhang H, Liu D, Lin L (2019) Appl Surf Sci 495:143572
45. Wan L, Wei W, Xie M, Zhang Y, Li X, Xiao R, Du C (2019) Electrochim Acta 311:72–82
46. Dai Z, Ren PG, Jin YL, Zhang H, Ren F, Zhang Q (2019) J Power Sources 437:226937
47. Jeon IY, Noh HJ, Baek JB (2020) Chem Asian J 15(15):2282–2293
48. Lherbier A, Blase X, Niquet YM, Triozon F, Roche S (2008) Phys Rev Lett 101(3):036808
49. Zhao M, Xia Y, Lewis JP, Zhang RJ (2003) Appl Phys 94(4):2398–2402
50. Lee YH, Chang KH, Hu CC (2013) J Power Sources 227:300–308
51. Wang DW, Li F, Yin LC, Lu X, Chen ZG, Gentle IR, Cheng HM (2012) Chem Eur J 18(17):5345–5351
52. Li X, Tie K, Li Z, Guo Y, Liu Z, Liu X, Zhao XS (2018) Appl Surf Sci 447:57–62
53. Guo L, Ding Y, Qin C, Song W, Sun S, Fang K, Wang F (2018) J Alloys Compd 7351:209–217
54. Zuo P, Duan J, Fan H, Qu S, Shen W (2018) Appl Surf Sci 435:1020–1028
55. Gopalakrishnan A, Badhulika S (2020) Renew Energy 161:173–183
56. Zhao X, Zhang Q, Chen CM, Zhang B, Reiche S, Wang A, Su DS (2012) Nano Energy 1(4):624–630
57. Gu W, Sevilla M, Magasinski A, Fuertes AB, Yushin G (2013) Yushin G. Energy Environ Sci 6(8):2465–2476
58. Chen C, Yang Y, Ding S, Wei Z, Tang X, Li P, Zhang M (2018) Energy Storage Mater 13:215–222
59. He S, Shi G, Xiao H, Sun G, Shi Y, Chen G, Yang X (2021) Chem Eng J 410:128286
60. Raj FRMS, Jaya NV, Boopathi G, Kalpana D, Pandurangan A (2020) Mater Chem Phys 240:122151
61. Zou J, Xu J, Wu H, Li Z, Zhao F, Zeng X, Huang J (2022) J Energy Storage 55:105448
62. Ma Q, Xi H, Cui F, Zhang J, Chen P, Cui T (2022) J Energy Storage 45:103509
63. Bhattarai RM, Chhetri K, Natarajan S, Saud S, Kim SJ, Mok YS (2022) Chemosphere 135290
64. Wang T, Wang LX, Wu DL, Xia W, Jia DZ (2015) Sci Rep 5(1):1–9
65. Zhou G, Paek E, Hwang GS, Manthiram A (2015) Nat Commun 6(1):1–11
66. Zhao G, Li Y, Zhu G, Shi J, Lu T, Pan L (2019) ACS Sustain Chem Eng 7(14):12052–12060
67. Razmjooei F, Singh K, Kang TH, Chaudhari N, Yuan J, Yu JS (2017) Sci Rep 7(1):1–14
68. Deng P, Lei S, Wang W, Zhou W, Ou X, Chen L, Cheng B (2018) J Mater Sci 53(20):14536–14547
69. Lei S, Chen L, Zhou W, Deng P, Liu Y, Fei L, Cheng B (2018) J Power Sources 379:74–83
70. Jia H, Sun J, Xie X, Yin K, Sun L (2019) Carbon 143:309–317
71. Liu W, Wang X, O'Connor M, Wang G, Han F (2020) Neural Plast
72. Pinheiro VS, Souza FM, Gentil TC, Nascimento AN, Parreira LS, Sairre MI, Santos MC (2022) J Alloys Compd 899:163361
73. Yan L, Yu J, Houston J, Flores N, Luo H (2017) Green Energy Environ 2(2):84–99
74. Huang K, Sasaki K, Adzic RR, Xing Y (2012) J Mater Chem 22(33):16824–16832
75. Zhou T, Wang H, Ji S, Linkov V, Wang R (2014) J Power Sources 248:427–433
76. Zhao X, Zhu J, Liang L, Li C, Liu C, Liao J, Xing W (2014) Appl Catal B 154:177–182
77. Ferrero GA, Fuertes AB, Sevilla M (2015) Sci Rep 5(1):1–13

78. Zhou Y, Ren J, Xia L, Zheng Q, Liao J, Long E, Lin D (2018) Electrochim Acta 284:336–345
79. Han J, Li Q, Wang J, Ye J, Fu G, Zhai L, Zhu Y (2018) J Mater Sci: Mater Electron 29(24):20991–21001
80. He J, Zhang D, Han M, Liu X, Wang Y, Li Y, Zhang X, Wang K, Feng H, Wang YJ (2019) Energy Storage 21:94–104
81. Jia H, Wang S, Sun J, Yin K, Xie X, Sun L (2019) J Alloys Compd 794:163–170
82. Chadha U, Bhardwaj P, Padmanaban S, Suneel RM, Milton K, Subair N, Kumar A (2022) J Electrochem Soc 169(2):020530
83. Gu X, Hencz L, Zhang S (2016) Batteries 2(4):33
84. Qu R, Zhang W, Liu N, Zhang Q, Liu Y, Li X, Feng L (2018) ACS Sustain Chem Eng 6(6):8019–8028
85. Razmjooei F, Singh K, Kang TH, Chaudhari N, Yuan J, Yu JS (2017) Sci Rep 7(1):1–14
86. Yang L, Lu X, Wang S, Wang J, Guan X, Guan X, Wang G (2020) Nanoscale 12(3):1921–1938
87. Si W, Zhou J, Zhang S, Li S, Xing W, Zhuo S (2013) Electrochim Acta 107:397–405
88. He D, Zhao W, Li P, Sun S, Tan Q, Han K, Qu X (2019) J Alloys Compd 773:11–20

Carbon Nanotubes and Similar Nanostructures Derived from Biomass for Supercapacitors Application

İnal Kaan Duygun and Ayse Celik Bedeloglu

Abstract Carbon nanotubes are advanced carbon materials with unique physicochemical and mechanical properties that make them important candidates for supercapacitor applications. However, their synthesis mostly requires carbon precursors derived from fossil fuel-related compounds. Recently, the use of biomass as a carbon source for energy storage materials has attracted great attention. Biomass precursors are considered an alternative carbon source to fossil fuel-related compounds in energy storage devices. In this section, the importance of biomass-based carbon nanotubes, their composites, and similar nanostructures for supercapacitor applications is evaluated. The potential use and common applications of biomass-based carbon nanotubes for high-performance SC applications are assessed. The synthesis methods for carbon nanotubes from biomass precursors are presented. A future perspective of biomass-derived carbon nanotubes and the fabrication of high-performance supercapacitors are also discussed.

Keywords Carbon nanotubes · Biomass · Supercapacitors · Carbon nanostructures

1 Introduction

Fossil fuels are the main energy sources today for heating, electricity generation, transportation, and other fields of modern life. Fossil fuels, including coal, natural gas, and petroleum are formed naturally over millions of years by the decomposition of plant, animal, and plankton remains that are subjected to tremendous heat and pressure below the Earth's crust [9, 57]. The limited resources of the nature make necessary the replacement of fossil fuels with alternating and efficient energy resources. In addition, the possible energy crisis and related environmental issues may cause the important problems for the world economy and the future of the environment [53]. Moreover, global warming and the depletion of natural energy sources encourage scientists to find alternative energy sources. In order to bring efficient

İ. K. Duygun · A. C. Bedeloglu (✉)
Department of Polymer Materials Engineering, Bursa Technical University, Bursa, Turkey
e-mail: ayse.bedeloglu@btu.edu.tr

S. K. Tiwari et al. (eds.), *Biomass-Based Functional Carbon Nanostructures for Supercapacitors*, Green Energy and Technology,
https://doi.org/10.1007/978-981-99-0996-4_6

solutions to these problems, biomass-derived energy sources have attracted a great interest as an alternative to fossil fuels [30].

Sustainability and renewability of an energy source have a critical importance in terms of using the limited sources of the nature efficiently. On the other hand, the storage of the produced energy for later demand, energy shortage, and different applications is another important issue due to the depleted fossil energy sources. Supercapacitors (SCs) are the most promising energy storage devices with excellent specific capacitance values compared to the conventional capacitors [52, 62]. SCs have a high power density and lower energy density unlike lithium-ion batteries and therefore, they take place in many improved electronic devices that require high power densities and good cyclability [62, 88]. SCs are mostly used in portable electronic devices, hybrid electric vehicles, various power systems, UPS, active filters, and similar electronic systems [8, 41, 52]. There are three different classes of SCs: electric double-layer capacitors (EDLC), pseudocapacitors, and hybrid capacitors [52]. EDLC's electrodes mainly consist of carbon-based electroactive materials because of their high specific surface area, electrical conductivity, good chemical, and thermal stability [8, 52]. In this type of SCs, electrical energy is stored by non-faradaic reactions (ion adsorption and desorption) at the interface of porous carbon-based electrodes and electrolytes [8]. On the other hand, pseudocapacitor electrodes are basically derived from conducting polymers or metal oxide materials and faradaic reactions take place for energy storage [12, 14, 20]. The properties of EDLCs and pseudocapacitors are combined in hybrid capacitors and higher specific capacitance and energy densities are obtained owing to the resultant faradaic and non-faradaic reactions during charge storage [8].

Carbon-based materials and their composites have a great importance especially for SCs applications. Carbon nanotubes, graphene, graphene nanoribbons, activated carbon, hierarchical porous carbon, carbon nanofibers, and carbon aerogels are widely used for the fabrication of high-performance SC electrodes [13, 37, 40]. In the last few years, the use of biomass materials as precursors to produce carbon nanotube (CNT) and similar nanostructures has attracted a great deal of interest and is regarded as an alternative way to obtain energy materials for energy storage devices, instead of fossil fuel-related sources [57].

Biomass is basically a biomaterial that comes from woods, plants, agricultural products, or household wastes [9, 30, 57]. In this regard, biomass is promising, versatile, and less expensive carbon source especially for the production of advanced carbon nanomaterials and high-performance energy storage devices. In this chapter, it is aimed to evaluate the current status of biomass-based carbon nanotubes and similar nanostructures for SCs. The potential use and common applications of biomass-based CNT materials for high-performance SC applications are assessed. The production methods of these unique materials are presented. A future perspective of biomass materials for CNT production and the fabrication of high-performance SCs is also discussed.

2 Carbon Nanotubes

Carbon nanotubes (CNTs) are advanced one-dimensional (1D) carbon nanomaterials with cylindrical shape on a nanometer scale. They were first discovered by Japanese scientist Sumio Iijima using arc-discharge method in 1991 [70, 93]. CNTs are one of the most investigated carbon allotropes since their first discovery in many different research areas. In CNT structure, the sp^2 hybridized carbon atoms make bonds in a hexagonal structure and form a tubular shape with a high length/diameter ratio (the length up to micrometers and diameter in nanometer scale) [6, 70]. CNT structure can also be described as a tubular structure consisting of single or multiple graphene layers. In addition, CNTs have also been classified as a subfamily of fullerenes which were discovered by Harry Kroto and his colleagues in 1985 [6, 56]. CNTs are generally divided into single-walled nanotubes (SWCNTs) and multi-walled carbon nanotubes (MWCNTs) depending on the number of outer graphite layers [56]. The general structures of SWCNT and MWCNT were given in Fig. 1. The diameter of SWCNTs is approximately 1.4 nm, while those of MWCNT are between 2 and 25 nm [6, 56, 93]. These nanostructures can also be synthesized as aligned arrays by using different synthesis methods. Especially, chemical vapor deposition (CVD) and microwave plasma CVD methods are often used for aligned CNT production [26, 61]. These unique architectures of CNTs are also used in many different applications, such as field emitters and flat panel displays [56]. In the synthesis of CNTs and similar nanostructures, it is a well-known fact that the control of the process parameters that determine nanotube size, shell numbers, and the nanotube structure is highly important, since these factors are decisive to obtain desired properties of CNTs [6, 56, 70]. The specific characteristics of CNTs and similar nanostructures make them one of the most investigated electroactive materials in various nanotechnology applications especially for SCs. Besides the use in EDLC electrodes, they can also be used in pseudocapacitors by combining them with other functional nanomaterials and fabricating electrode materials with high mechanical and electrochemical performance. CNTs possess high electrical (up to 10^6 to 10^7 S/m for pure CNT) and thermal conductivity (2800–6000 W/m K for a single nanotube at room temperature), aspect ratio, specific surface area (1300 m^2/g), and excellent mechanical properties, such as flexibility and high tensile strength [25, 43, 61]. These properties make them important candidates for the fabrication of improved energy storage devices. The production of macroscopic CNT structures is especially advantageous for flexible SCs. They could be fabricated as 1D fibers, 2D films, and 3D sponges and used for SC electrodes [93].

It is a well-known fact that chirality of SWCNT determines its electronic structure and other related electronic properties (The bandgap energy) [24, 56]. Chirality can be defined as a vector connecting the centers of two hexagons in a nanotube structure [24, 44]. Chirality can be expressed by two integers as n and m. For $m = 0$, a zigzag structure forms, while $n = m$, an armchair CNT structure forms. The other possibilities result in the formation of a chiral structure. The three different SWCNT types in different formations were given in Fig. 2.

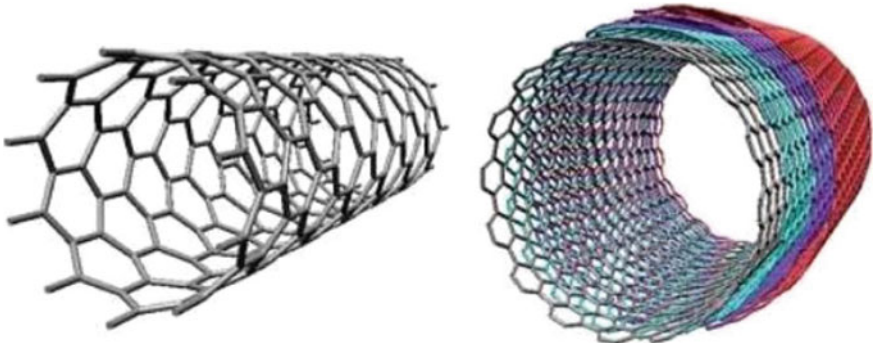

Fig. 1 The structure of SWCNT and MWCNT. Reproduced from Ref. [24] with permission from Elsevier

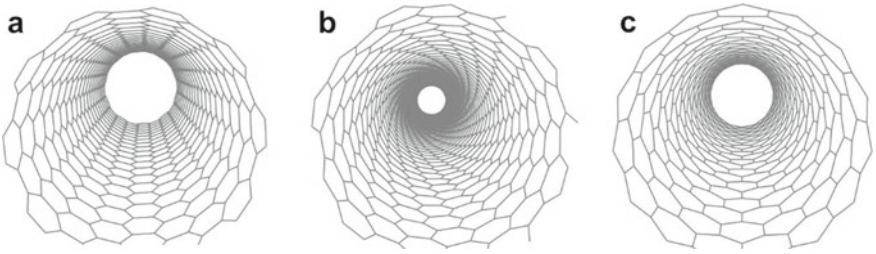

Fig. 2 Schematic illustration of three typical SWNT structures, **a** Armchair (10, 10), **b** Chiral (13, 6), and **c** Zigzag (14, 0). Reproduced from Ref. [44] with permission from Elsevier

3 CNT Production Techniques

There are different CNT production methods. Electric-arc discharge, chemical vapor deposition (CVD), and laser ablation are the most performed techniques for CNT production [56, 70]. The comparison of the most used CNT synthesis methods depending on the process properties was given in Table 1. Beside the aforementioned methods, other techniques have been developed such as pyrolysis, electrolysis, and flame synthesis methods for CNT production [70]. Electric-arc discharge technique is the first reported method by IIjima in 1991 for the production of CNT [6]. In this method, carbon atoms are evaporated by an electric arc in plasma by applying a required current to the carbon source. However, the produced CNT in this method contains more impurities and the control of morphological properties of tubes is difficult compared to other methods [6, 56, 70].

In the laser ablation method, the graphite targets are evaporated by laser irradiation in an inert atmosphere. It was shown that the yield and quality of CNT produced from this method depend highly on the process temperature (approximately 1200 °C) and the low temperatures could result in a low-quality structure and imperfections in CNT structure [56].

Table 1 The comparison of different CNT synthesis methods. Reproduced from Ref. [56] with permission from Elsevier

Process	Arc-discharge	Laser ablation	CVD method
Yield of process [54]	Moderate (70%)	High (80–85%)	High (95–99%)
Temperature	1700 °C	1200 °C	700–900 °C
Diameter	4–30 nm	10–20 nm	20–25 nm [65]
Purity	High	High	High
Production rate	Low	Low	Low
Cost	High	High	Low
Process control	Difficult	Difficult	Easy
Energy requirement	High	High	Moderate
Advantages [10]	Simple, inexpensive, high-quality NT	High purity, synthesis in room temperature production	Simple, high purity, large-scale production
Disadvantages	High temperature, less purified, tangled NT	Limited method to the lab scale	Defects in MWNTs

CVD technique is a more advantageous way for CNT production in comparison with the former methods [6, 61, 70]. Contrary to the other methods, CVD is carried out at lower process temperatures and allows to define the type of CNT, and the control of vertical alignment [26, 61]. Furthermore, large-scale production is possible in this way. In this technique, a hydrocarbon gas mixture (ethylene, methane, acetylene) is deposited onto a substrate coated by a metal as a catalyst in a temperature range of 700–900 °C [26, 56, 61]. The nature of the substrate and the type of the catalyst also determines CNT structure and quality [56].

Biomass Resources

Biomass is a widely used term to define organic materials coming from plants or animals. The energy of these living or once-living organisms can be converted into a more usable form of energy in different ways to use it for various purposes. As an abundant and renewable energy resource, biomass-based materials are widely used in various areas, such as hydrogen storage, energy storage, sustainable water purification, and CO_2 capture and storage [51, 69].

The selected carbonization method is of great importance for obtaining desired properties in the final product, such as morphology, porosity, functional groups, and components [69]. Thermochemical conversion is a well-known carbonization method that was used to obtain desired products from biomass resource. The biomass feedstock, reactor type, and selected reactor conditions are important parameters determining the product quality [51]. The chemical composition of biomass may differ depending on the source.

Cellulose is one of the most abundant biopolymers in the world and it provides an important resource for biomass [51, 63]. In many different application areas, plants or other agricultural residues are used as biomass precursors. In plant-based

resources, the biomass structure mainly consists of cellulose, hemicellulose, and lignin which were distributed in the plant cell and structure [51, 63]. Organic extractives and other inorganic minerals are also present in biomass chemical structure [51]. The carbonization of biomass through thermochemical methods is an important step for the following uses. In this process, oxygen and hydrogen are removed from the biomass structure, and carbon remains as a single substance [51, 63, 69]. The transformation of biomass to the carbon can be carried out using different pyrolysis temperatures depending on the chemical components of biomass materials [77]. In general, the decomposition of biomass takes place in the temperature range of 200–400 °C [51, 63, 77]. It was reported by different studies that the degradation of cellulosic and hemicellulosic structures in plant biomass takes place at the temperature ranges of 250–350 and 290–400 °C, respectively [63, 77]. On the other hand, lignin structures degrade at higher temperatures (140–900 °C) [77].

Apart from other carbonization methods, hydrothermal carbonization is also used to convert biomass precursors into the carbon-rich substances. In this method, it is easily controlled the structure, morphology, and components of the final product [63, 69]. Titirici and Antonietti [68] described the carbonization process of biomass in three steps. They stated that in the first step hydrolysis of biomass happens. In the following step, polyfurans form because of the polymerization. In the last step, the intermolecular dehydration phenomena result in the carbonization of the structure. Furthermore, the carbonization of biomass results in the formation of various functional groups, such as carboxyl, carbonyl, phenol, quinone, lactone, and other functional groups which give the unique properties of biomass precursors [51, 63]. The main classification of different biomass varieties and species were given in Table 2.

4 Biomass Resources for CNT Synthesis

Carbon-based improved materials constitute an important material group for various engineering and scientific research areas. On the other hand, the main components for the synthesis are petroleum or coal-based materials. Therefore, new resources and their use in CNT materials or other improved carbon nanomaterial synthesis became an important issue in terms of the use eco-friendly, renewable, low cost, and easily accessible materials. It is clearly seen that the conventional production methods require high process temperatures, mostly complex reactor designs, and non-renewable carbon sources which result in toxic process wastes. Moreover, it is also possible to obtain low process yield and CNT materials with structural defects. On the other hand, CNT production requires stable carbon sources which is mostly a problem in CNT synthesis [6, 56]. At this point, biomass sources have become promising candidates as widely distributed, eco-friendly, and low-cost carbon sources for CNT synthesis [77]. It was proven that biomass sources contain a high amount of carbon which could be used effectively for CNT synthesis. In addition, it has been shown by many different studies that suitable precursors for CNT synthesis

Table 2 The classification of different biomass groups according to their biological origin. Reproduced from Ref. [69] with permission from Elsevier

Biomass groups	Biomass sub-groups, varieties, and species
1. Wood and woody biomass	Coniferous or deciduous; angiospermous or gymnospermous; soft or hard; stems, branches, foliage, bark, chips, lumps, pellets, briquettes, sawdust, sawmill, and others from various wood species
2. Herbaceous and agricultural biomass	Annual or perennial and field-based or processed-based such as:
	2.1. Grasses and flowers (alfalfa, arundo, bamboo, bana, brassica, cane, cynara, miscanthus, switchgrass, timothy, others)
	2.2. Straws (barley, bean, flax, corn, mint, oat, rape, rice, rye, sesame, sunflower, wheat, others)
	2.3. Other residues (fruits, shells, husks, hulls, pits, pips, grains, seeds, coir, stalks, cobs, kernels, bagasse, food, fodder, pulps, cakes, others)
3. Aquatic biomass	Marine or freshwater algae; macroalgae (blue, green, blue-green, brown, red) or microalgae; seaweed, kelp, lake weed, water hyacinth, others
4. Animal and human biomass wastes	Bones, meat-bone meal, chicken litter, various manures, others
5. Contaminated biomass and industrial biomass wastes (semi-biomass)	Municipal solid waste, demolition wood, refuse-derived fuel, sewage sludge, hospital waste, paper-pulp sludge, waste papers, paperboard waste, chipboard, fibreboard, plywood, wood pallets and boxes, railway sleepers, tannery waste, others
6. Biomass mixtures	Blends from the above varieties

could be obtained by the pyrolysis of lignocellulosic biomass at a certain pressure and process temperature [51, 68, 77]. There are many different biomass sources for CNT synthesis, such as plants (catkin, grass, corn, cotton, bamboo, gumwood), bio-extracts (chitosan, cotton fiber, wood fiber), bio-products (wheat flours, palm oil, sesame oil), and bio wastes (wood sawdust, crop stalks, grain wastes, sugarcane bagasse, nut shells, roots, leaves, egg yolks). Various pyrolysis techniques are widely used for the thermochemical conversion of the biomass to the CNT [57, 68, 77].

There are different studies using various biomass materials as precursors for CNT synthesis. Ghosh et al. [22] have used eucalyptus oil as biomass precursor to synthesize SWCNT by catalytic decomposition. In this study, spray pyrolysis method was performed using silica/zeolite support with Fe/Co catalyst at a temperature of 850 °C. During a CNT synthesis, the catalyst material may cause contamination on the CNT structure which influences adversely the properties of nanotubes. Therefore, there were a lot of studies investigating different precursors which may act as catalyst material during CNT synthesis. In some studies, it was reported that the selected biomass

precursor can also contribute to the use of a lower amount of catalyst. In such a study, Kumar and Ando [32] have synthesized aligned carbon nanotubes from camphor as a precursor. Camphor is a waxy and flammable terpenoid ($C_{10}H_{16}O$) that is found in the Cinnamomum camphora tree, a large tree found in Asian countries [34]. The authors stated that the presence of hexagonal and pentagonal carbon rings in camphor molecular structures, nanotubes, and fullerene structures can be easily synthesized. In this work, vertically aligned MWCNTs were grown on quartz substrate by the pyrolysis of biomass material with ferrocene catalyst in an argon atmosphere at 900 °C. They also claimed that camphor as a biomass required a remarkably low amount of ferrocene as catalyst material and this resulted in a less metal contamination on the synthesized aligned MWCNTs. Afre et al. [2] investigated turpentine oil as biomass precursor for CNT production by spray pyrolysis technique. In this work, CNT structure was synthesized at different temperatures using the bimetallic catalyst Co and Fe on the silica gel particles. Turpentine oil is an eco-friendly carbon source which is produced from the oleoresin of the longleaf pine (Pinus palustris) family found in Southeastern United States [59]. They stated that the highest yield was obtained at the synthesis temperature of 700 °C and nanotubes diameter are affected by the process temperature significantly. In another study, Suriani et al. [66] have synthesized vertically aligned CNTs on a silicon substrate by CVD technique using natural palm oil as biomass precursor. The palm oil is obtained from palm tree fruits and contains hydrocarbons ($C_{67}H_{127}O_8$) which provides precursors for CNT synthesis. In their experiments, they reported that SWCNT or MWCNT synthesis is possible by controlling process parameters such as the amount of the catalyst, gas flow rate, and synthesis temperature. In the synthesis of nanotubes, the nanostructure of the selected biomass is also critical to be able to obtain high-quality CNTs. Such a novel approach to CNT synthesis was carried out by Kang et al. [28]. In their work, grass as a biomass source was used to synthesize MWCNTs in the presence of oxygen at 600 °C. The authors noted that grass contains vascular bundles that can be effectively converted into carbon nanotube structure. In addition, the presence of cellulose, hemicellulose, and lignin in the grass makes it a useful biomass precursor for CNT production. They claimed that the presence of oxygen facilitates the pyrolytic reactions of tubular structures and the formation of the complex C–O–H system results in the formation of CNT structure. Apart from the studies in which several catalysts were used, there are other studies investigating the efficiency of biomass precursors without using any catalyst. In such a work, Goodell et al. [23], used six different biomass materials with distinct forms and morphologies (wood fiber, organosolved lignin, ashless filter paper, avicel, α-cellulose, and bamboo). For CNT synthesis, biomass precursors were exposed to heating/cooling cycle (heating to 40 °C and cooling to room temperature). They claimed that plant and wood cells are suitable carbon sources for CNT in a low-temperature heating cycling process. Furthermore, it is noteworthy that these structures possess nanochannels and chemical components in the cell walls which facilitate the formation of CNTs.

5 CNT Production Techniques

Pyrolysis, CVD, microwave irradiation, and mechanical milling techniques are the main production methods for CNT synthesis from biomass resources [92]. The different approaches for CNT production from biomass sources were given in Fig. 3.

5.1 Pyrolysis Method

One of the most used methods for CNT production is the catalytic pyrolysis of biomass materials. This process is generally carried out as one-step or two-step pyrolysis which is more advantageous in terms of process control and CNT quality [77, 90, 92]. In this process, only the mixture of biomass materials and catalysis are used for CNT growth. Biomass decomposition takes place and activated carbon is formed. The metal salts produced by decomposition act as catalysis during the process [92]. After this step, activated carbon begins to dissolve and ordered tubular shape formation occurs. Another pyrolysis method includes microwave irradiation. In this method, biomass mixture is subjected to a certain temperature by the microwave-induced electromagnetic field. Thereby, amorphous carbon nanospheres form as CNT structure [42].

It has been shown that catalyst type has also a significant importance in the CNT synthesis process. Aboul-enein et al. [1] investigated the catalytic pyrolysis of sugarcane bagasse by zeolite catalyst for the synthesis of MWCNT. On the other hand, Thompson et al. [67] studied the graphitic CNT synthesis from one-step catalytic pyrolysis of softwood sawdust which is lignocellulose biomass. In this work, iron

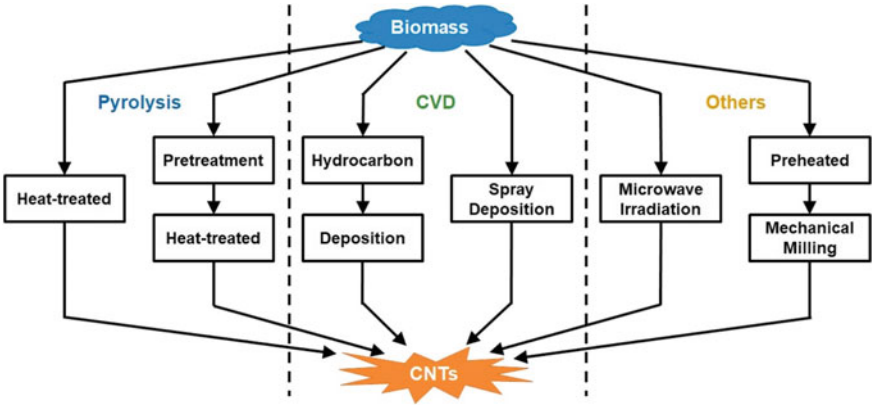

Fig. 3 CNT synthesis methods from biomass precursors. Reproduced from Ref. [92] with permission from Elsevier

carbide (Fe_3C) nanoparticles were used as catalyst and the tubular graphitic structure formed at 800 °C under a nitrogen atmosphere. They claimed that this technique enables the production of large-scale and sustainable synthesis of biomass-based advanced carbon nanostructures. Rey-Raap et al. [58] investigated the effect of biomass-based MWCNT addition to the SC electrodes. They developed activated glucose-derived carbon/CNT hybrids and assessed the effect of biomass-derived CNT on the SC performance. They claimed that the presence of CNT with 4 and 8 wt% results in a better electronic transportation and capacitance retention compared to the electrodes without CNT addition (Table 3).

5.2 CVD Method

Another important method for CNT synthesis from biomass is CVD [61]. The several hydrocarbons are the main precursors for CNT and many other advanced carbon nanostructures. The mostly used carbon feedstock for the CVD process is fossil fuel-related gases such as benzene, xylene, and toluene [45, 54]. Hydrocarbon vapor with an inert gas is heated in a reactor chamber generally in the temperature range of 600–1200 °C, and thereby, it is decomposed to hydrogen and carbon. Hydrogen gas is removed by evaporation and carbon dissolves into the metal catalyst [6, 54, 61]. Gas, liquid, and solid precursor hydrocarbon sources can be used in the CVD method. In addition, CVD allows to obtain different architectures of CNT, such as entangled, aligned, and straight nanotubes as well as 2D films with different thicknesses. The CVD technique is also advantageous for obtaining high-quality CNT structure since process parameters are easily controlled in this method. Iron (Fe), Nickel (Ni), and cobalt (Co) are the most efficient catalysts for CNT production by the CVD method due to their high carbon diffusion rate and carbon solubility [54]. Hydrocarbon gas derived from fossil fuels could be replaced with biogas which is obtained from biomass wastes. In this regard, the importance of agricultural wastes or organic wastes is obvious. In this method, biomass mixture is firstly decomposed to gaseous phase and then, transferred into the reactor chamber with substrate and catalysis to form CNT [54, 61]. The most used biomass materials and catalysts for CNT synthesis by CVD method were given in Table 4.

5.3 Microwave Irradiation

Over the years, the use of microwave irradiation for organic synthesis applications has increased remarkably [15]. Microwave irradiation is another method especially for large-scale CNT production, using microwave radiation to reach pyrolysis temperature [47]. Contrary to the conventional heating methods, in microwave-assisted pyrolysis the target material is heated from the center of the material to the surface because of the forming temperature gradient [39]. Furthermore, compared to the

Table 3 The most used biomass precursors for CNT synthesis by pyrolysis method. Reproduced from Ref. [92] with permission from Elsevier

Method	Biomass category	Catalyst	Condition	CNT diameter (nm)	CNT length	Yield	Year	Ref
Cyclic pyrolysis	Grass	N/A	600 °C 20 min × 50	30–50	1 μm	15%	2005	[28]
Cyclic pyrolysis	Wood fiber	N/A	400 °C 10 min × 35	10–20	N/A	N/A	2008	[23]
Pyrolysis	D-Glucosamine hydrochloride	$Ni(NO_3)_2$	1000 °C 1 h	50–70	2–10 μm	N/A	2015	[74]
Pyrolysis	–	$FeCl_3/C_4H_6CoO_4{\cdot}4H_2O$	850 °C 1 h, 900 °C 1 h	35–45	N/A	N/A	2015	[71]
Pyrolysis	Catkin	$FeCl_3$	800 °C 2 h	~80	N/A	N/A	2015	[35]
Pyrolysis	Wood sawdust	$C_{10}H_{10}Fe$ or Fe/Mo/MgO	750 °C 3 h	25	N/A	N/A	2017	[7]
Pyrolysis	Stillage residue	$NiCl_2$	750 °C 2 h, 500 °C 2 h, 700–900 °C 2 h	10–15	0.1–0.3 μm	N/A	2017	[83]
Pyrolysis	Chlorella	$C_4H_6CoO_4$	900 °C 1 h	~40	0.1–2 μm	N/A	2017	[72]
Pyrolysis	Egg yolks	$C_6N_6FeK_3$	900–1100 °C 2 h	~50–80	N/A	N/A	2018	[84]
Pyrolysis	Chitosan	$Co(Ac)_2/CH_4N_2O$	800 °C 2 h	~20	N/A	N/A	2018	[86]
Pyrolysis	Wheat flour	Yeast	750 °C 2 h	100–200	3–20 μm	N/A	2018	[21]
Pyrolysis	Potato peels	FeC_2O_4	600 °C 3 h, 900 °C 1 h	~10–25	N/A	N/A	2019	[48]
Pyrolysis	Grain wastes	FeC_2O_4	600 °C 3 h, 900 °C 1 h	15–35	N/A	N/A	2019	[49]
Pyrolysis	Industrial paper sludge	Fe	900 °C 2 h	50	N/A	N/A	2020	[91]

(continued)

Table 3 (continued)

Method	Biomass category	Catalyst	Condition	CNT diameter (nm)	CNT length	Yield	Year	Ref
Pyrolysis	Cotton fiber	$Co(NO_3)_2$	480 °C 2 h, 900 °C 2 h	50	0.5 μm	N/A	2020	[81]
Microwave induced pyrolysis	Gumwood	Minerals in gumwood	500 °C 30 min	50	0.6–1.6 μm	5.78%	2014	[64]
Microwave induced pyrolysis	Rice husks	Ni	640 °C 10–38 min	50–200	10–100 μm	N/A	2015	[78]

Table 4 The most used biomass precursors for CNT synthesis by CVD method […] Reproduced from Ref. [92] with permission from Elsevier

Method	Biomass category	Catalyst	Condition	CNT diameter (nm)	CNT length	Yield	Year	Ref
CVD	Camphor	$C_{10}H_{10}Fe$	850 °C, 15 min	N/A	N/A	N/A	2007	[31]
CVD	Palm oil	$C_{10}H_{10}Fe$	450/750 °C, 30 min	0.6–1.2	110 μm	N/A	2009	[66]
CVD	Sugarcane bagasse	Stainless steel	600–1000/1000 °C, N/A	20–50	50 μm	N/A	2012	[4]
CVD	Reed	Reed seeds	1200 °C, 2 h	10–15	N/A	N/A	2013	[46]
CVD	Camphor	$C_{10}H_{10}Fe$	250 °C, 1 h, 800 °C, 2 h	22	N/A	41–44%	2017	[19]
Spray pyrolysis-assisted CVD	Castor oil	$C_{10}H_{10}Fe$	850 °C, 15 min	20–60	5–10 μm	N/A	2011	[5]
Spray pyrolysis-assisted CVD	Jatropha	$C_{10}H_{10}Fe$	800–900 °C, 20 min	20–50	20 μm	N/A	2012	[33]

conventional heating and pyrolysis processes, this method is advantageous in terms of heating rate, low cost, and fast decomposition reaction [29, 39, 54]. In addition, it was reported that the use of a suitable catalyst, gaseous carbon source, or an inert atmosphere for CNT production like in CVD method, is not necessary in microwave radiation method [29, 39].

The frequency range of microwaves in electromagnetic spectrum is between 300 MHz and 300 GHz which is a wavelength range from 1 m down to 1 mm [15]. In this method, microwaves which are between infrared waves and radio waves in the electromagnetic spectrum are used to convert electromagnetic radiations to thermal heating for reaching a desired temperature [15, 39, 47]. On the other hand, heating, by using the microwaves, is highly dependent on the molecular structure of the target material bib39|. Microwave absorber materials absorb microwave irradiation and thereby, heating takes place [15, 29]. On the other hand, it is a well-known fact that the reflection or transparency of microwaves by target material does not result in heating and in this case, the required pyrolysis temperatures cannot be reached. Therefore, it is important to provide a microwave and molecular interaction during the pyrolysis process, since the heating process occurs due to the molecular interactions of microwaves [15, 29, 39, 47]. The vibrational energy of molecules that absorb microwave radiation results in a temperature generation in the target material. It is a well-known fact that only polar molecules can absorb microwaves and turn them to heat energy. In addition, the pyrolysis by means of microwave radiation, the process yield, and final product quality are affected by the shape, biomass particle size, selected biomass type and properties, and microwave output power level [15, 39].

In microwave-assisted pyrolysis process, it was also shown that CNT synthesis from different biomass sources is possible without using any catalyst. There are many studies investigating CNT synthesis using microwave-assisted pyrolysis with or without a catalyst material. The synthesis of CNT without catalyst has been conducted by many different researchers. It was claimed that the presence of different inorganic materials in biomass materials results in the formation of catalyst. The selected biomass precursors may also contribute to the decrease of the used catalyst amount. Shi et al. [64] studied a catalyst-free MWCNT synthesis using the microwave pyrolysis method. They used gumwood as a biomass source and the process was carried out at 500 °C as a relatively lower target temperature without using any catalyst or substrate during the reaction. They stated the minerals in gumwood could act as catalysts, and the graphitized carbon in the superheated active sites forms MWCNT structure. Omoriyekomwan et al. [18] have synthesized superlong CNT using cellulosic biomass (from palm kernel shell) under microwave pyrolysis without any catalyst or external carbon source. They reported that 0.7–2 mm of CNT structures were produced under the temperatures of 1200–1400 °C. They also stated that palm kernel shell (PKS) is not a good microwave absorber and therefore, activated carbon as a microwave receptor was mixed with PKS biomass. Another approach for CNT synthesis is the use of biochar as a carbon source which is a porous material derived from the thermal treatment of agricultural wastes or other biomass sources. The high surface area of biochar makes it also an important precursor for the synthesis of

various advanced carbon nanomaterials. In such a study, Hidalgo et al. [27] have investigated a biochar precursor which was obtained from agro-industrial wastes using pyrolysis at 400 and 600 °C. In this work, ferrocene was used as a catalyst. They claimed that the best quality of CNT was obtained from biochar derived from hazelnut hull and wheat straw. On the other hand, the pyrolysis at 600 °C resulted in a higher CNT concentration. In another study carried out by Zhang et al. [85], microwave-assisted CVD technique was used to synthesize CNT from biochar source (pine nutshell) at 600 °C. For the synthesis, Ni was also used as catalyst material. They claimed that biochar substrate exhibited a good microwave absorption ability for the required local synthesis temperature to form. In addition, in their experiments, they observed that a higher surface area of biochar substrate forms compared to other substrate types, which facilitated Ni catalyst dispersion on the substrate surface. Thereby, it has been shown that these positive effects of biochar led to the easy decomposition of methane for CNT growth.

6 Supercapacitor Applications

SCs are one of the most investigated energy storage devices with their higher specific capacitance values, good cycling stability, and energy density than those of conventional capacitors. SCs possess high power density values, faster charge–discharge rates, longer cycle life, and more eco-friendly fabrication methods compared to the Li-ion batteries [8, 12]. On the other hand, their relatively lower energy density values limit their use in various applications that require higher energy density values. An SC usually consists of current collectors, electrodes, separators, and electrolytes. SCs are in general divided into two main groups depending on their charge storage mechanisms: electrical double-layer capacitors (EDLC) and pseudocapacitors [8, 41]. In an EDLC, the charge process is carried out by the non-faradaic reactions. The porous electrode surface of EDLCs provides a large specific surface area which is important for ion diffusions and storage. On the other hand, in a pseudocapacitor, faradaic reactions take place for energy storage. The electron transfer results in the changes in the chemical states of electroactive materials, and thereby, energy storage process occurs due to the redox reactions. Pseudo-capacitors show higher energy densities than those of EDLCs and thus, they attracted a great interest in energy storage studies [8, 12, 20, 41]. Furthermore, hybrid SCs could combine the properties of EDLCs and pseudocapacitors in one device and show excellent capacitance and good energy density values [8].

Over the years, particularly carbon-based nanostructures became the most investigated electroactive materials for the fabrication of high-performance SC devices. Carbon nanomaterials have excellent electrical conductivity and electrochemical performance due to their unique geometric and shape characteristics. Moreover, they can be prepared in different designs such as films, textile products, and coatings in different substrates to improve the electronic device performance. Besides carbon-based nanomaterials, conducting polymers, transition metal oxides, their composites

with carbon materials and similar structures have been also often used in SC applications. Recently, the fabrication of flexible and free-standing electrodes for SCs has become an important research area, particularly for portable and wearable electronic devices [11, 38]. As flexible structures, CNT films were frequently fabricated as flexible SC electrodes for various SC applications such as portable, and wearable electronics [38]. Especially wearable energy storage devices have a great potential for future applications [11, 38]. Since the mechanical properties (Young's modulus, large elastic strain limit, and tensile properties) of CNTs provide a good flexibility to the electrodes or current collectors, the number of applications of flexible electrode fabrication increased rapidly.

Although carbon-based materials are highly functional and effective for energy storage applications, some properties may restrict their applications fields. One of the most used carbon-based materials for SC electrodes is activated carbon (AC). AC materials have a high specific surface area and electrical conductivity. However, the distribution of the pore size in AC is not always suitable for an efficient ion diffusion, and this may lower the device performance. On the other hand, graphene-based electroactive materials are frequently affected by the agglomeration of graphene nanoparticles and resulting performance decrease of energy storage devices. In this regard, the advantages of CNTs have attracted a great interest in high-performance SC fabrication. CNT-based nanomaterials and their composites are one of the most promising electroactive materials for SC electrodes owing to their electronic, physical, and chemical properties. Their high electronic conductivity (5000 S cm^{-1}), high aspect ratio and good specific surface area (SWNT > 1600 m^2 g^{-1}, MWNT > 430 m^2 g^{-1}) make them highly efficient materials for SC electrodes [6, 70, 93]. The free-standing CNT structures can be used as both current collectors and electrodes in an SC device. SWCNT and MWCNT structures are widely used as electroactive materials in SC electrodes. Furthermore, their composites are also good candidates as electrode active materials. It was suggested that pure CNT film electrodes have higher power densities and good charge/discharge cycles, however, lower specific capacitance and energy density values than those of other carbon-based nanostructures [6, 56, 70, 93]. Therefore, their properties should be improved for pseudocapacitor electrodes and high-performance SCs. Therefore, it can be stated that the electrode design and suitable composite structures are very important parameters for improved energy densities and specific capacitance values. The advantages and unique properties of CNTs and their composites with various active materials for SC applications were revealed by many different studies. Pan et al. [50] stated that the percolation of active nanotubes is more efficient compared to the other conventional carbon materials. The mesoporous CNT structure results from the entanglement of CNTs, and this facilitates the diffusion of electrolyte ions to the active composite surfaces. These unique properties lead to a decrease in the equivalent series resistance (R_s) and an increase in the power density of the device. On the other hand, they also claimed that the high number of charge and discharge cycles could cause the volumetric changes in the SC electrodes which negatively affect the electrodes performances. However, CNT and their composites result in a more adaptive electrode structure

during charge/discharge processes, and this improves the cycling stability of the SCs [6, 25, 70, 93].

The composite structures of different CNT materials are widely used as electrodes in SC applications. The synergistic effect of the carbon-based electroactive materials mostly contributes to an improvement in the electrode performance in many ways. Zhang et al. [87] have investigated the SC and CO_2 capture properties of MWCNT/carbon foam nanocomposites. In this work, the poor mechanical properties of porous carbon foam structure were improved by combining biomass-derived carbon foam with MWCNT. The authors claimed that the presence of MWCNT in the nanocomposite structure remarkably increased the compressive strength of the nanocomposite material. The nanocomposite SC electrodes exhibited a high specific capacitance of 157.07 F g^{-1} at a current density of 1 A g^{-1}. It was also reported that the nanocomposite electrode showed a capacitance retention over 2000 charge/discharge cycles. Besides carbon nanocomposites, CNT materials were also used with other electroactive materials for SC electrodes. The composites of pseudocapacitive materials (transition metal oxides) and carbon-based materials have been often investigated in terms of their SC electrode performance. In such a composite structure, the properties of EDLCs and pseudocapacitors are combined to enhance energy density and specific capacitance values of SCs. Carbon-based electroactive components provide a porous surface structure and high specific surface area as a result. In addition, pseudocapacitive materials provide a high specific capacitance owing to the faradaic reactions during charge/discharge processes. Ranjithkumar et al. [55] developed an SC electrode using CNT and ZnO. They stated that SC with ZnO/CNT nanocomposite electrode and 1 M Na_2SO_4 electrolyte exhibited 189 F g^{-1} at 1 mV s^{-1} scan rate. In addition, it was also reported that 96%of capacitance retention was achieved over 1000 cycles. The comparison of the cyclic voltammograms of ZnO, CNT, and ZnO/CNT electrodes in different scan mVs^{-1} were given in Fig. 4.

In another work, Sannasi et al. [60] investigated the use of NiO nanoflakes anchored on CNT electrodes which were fabricated by an H_2O_2-assisted microwave irradiation method. According to GCD studies of the NiO/CNTs electrodes a maximum specific capacitance of 258 F g^{-1} at 1 A g^{-1} current density in 2 M KOH aqueous electrolyte was obtained for 1:1 ratio of NiO/CNT composite. They reported that this value is 2 times higher than that of NiO electrode (120 F g^{-1}) which is an indication of the synergistic effect between CNT and NiO in nanocomposite structure. Wang et al. [73] investigated the electrochemical performance of MnO_2/CNT nanocomposite. They reported that the nanocomposite structure was synthesized by a facile direct redox reaction between potassium permanganate and CNTs without using any other oxidant or reductant. They found that the resistance value increases with the increasing MnO_2 content in nanocomposite. They stated that the nanocomposite electrode with 44.4% MnO_2 showed the best electrochemical performance. The electrode exhibited 162.2 F g^{-1} at the current density of 0.2 A g^{-1} and shows excellent capacitance retention (90%) after 2000 cycles at the current density of 5 A g^{-1}. Cyclic voltammograms and Nyquist plots of MnO_2/CNT were given in Fig. 5.

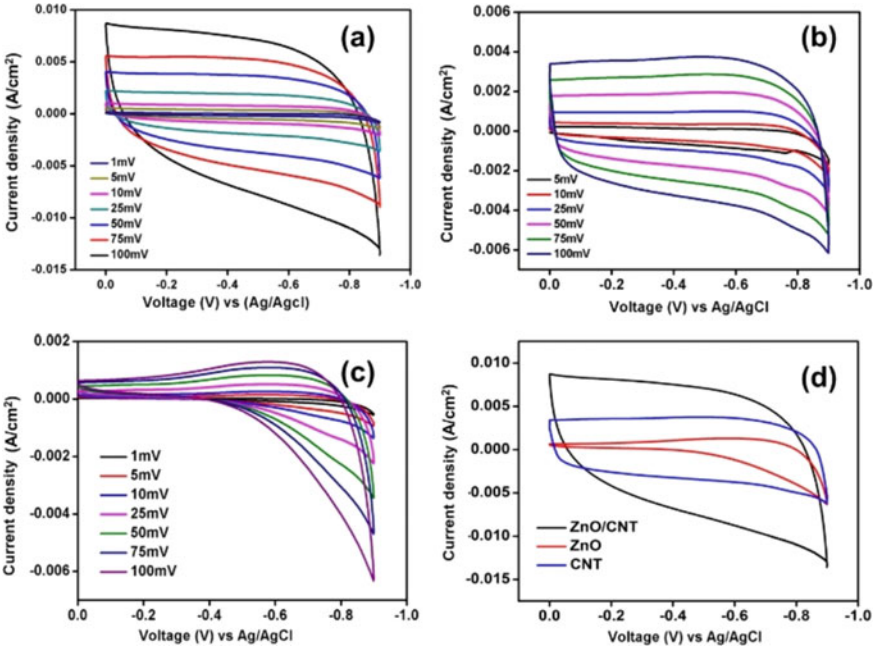

Fig. 4 Cyclic voltammograms of **a** ZnO/CNT, **b** CNT, **c** ZnO and **d** ZnO/CNT, ZnO, and CNT in 100 mV s^{-1}. Reproduced from Ref. [55] with permission from Elsevier

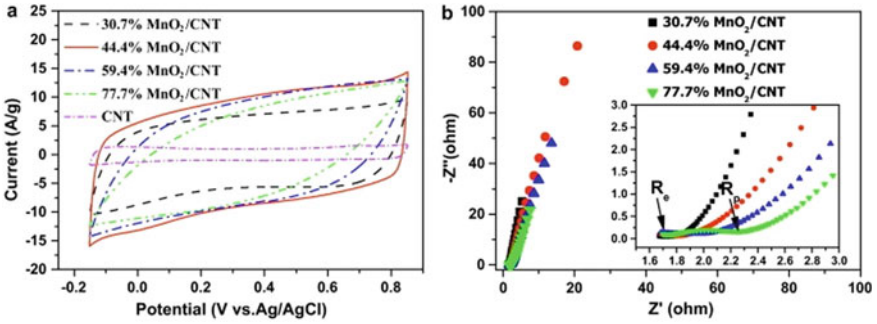

Fig. 5 Cyclic voltammograms and Nyquist plots of MnO_2/CNT nanocomposite electrodes with a different MnO_2 content. Reproduced from Ref. [73] with permission from Elsevier

6.1 Biomass-Derived CNTs for SC Applications

CNTs are of great importance for energy storage applications due to their excellent mechanical and electrical properties. It was shown that many different studies have been carried out investigating the effect of CNTs or their composites on the

electrochemical performance of different SCs electrodes. Their unique characteristics have also made them popular materials in carbon-based nanostructures. Even though there are a lot of studies regarding CNT-based electrodes which was synthesized from conventional precursor materials, it is obvious that the use of biomass as precursors for CNT synthesis is not widely investigated in SC electrodes. This indicates that the effects of biomass precursors on the properties of CNT materials are waiting to be investigated in detail. It is evident that biomass resource has an important effect on the final carbon-based product, such as morphology, porosity, functional groups, and other similar aspects.

The use of CNT and similar nanostructures from biomass in hybrid capacitors electrodes was investigated in several studies. Zhou et al. [89] have developed a hybrid supercapacitor electrode from bamboo biomass using CVD technique. Vacuum sintering at 850 °C was used to produce bamboo-based activated carbon. Co was also used as catalyst material. They have shown that by catalytic decomposition of carbon monoxide, CNT/Co/BAC electrode was obtained. It was claimed that SC electrode showed a high specific capacitance (512 F g^{-1} at 0.1 A g^{-1}) and 98.4% of capacitance was retained after 3000 cycles at a current density of 5 A g^{-1}.

Apart from nanotube structure, carbon microtube structures were also used as high-performance SC electrodes. Xie et al. [80] have developed hierarchical porous carbon microtubes derived from willow tree catkins which is a highly planted tree in China. In this study, the electrode material has been synthesized by means of carbonization of biomass and the following activation process with KOH. The dried willow catkins were carbonized under an inert gas atmosphere at 600 °C for 4 h. The obtained hierarchical structure was then mixed with aqueous KOH solution in a certain weight ratio. The activation processes were carried out at three different temperatures (600, 700, and 800 °C). They have found that the symmetric SC electrodes containing 80% HPNCT-800, acetylene black, and PVDF in 1 M $LiPF_6$ electrolyte showed a good electrochemical performance. The obtained SC exhibited a specific capacitance of 292 F g^{-1} at a 1 A g^{-1} current density and a high electrical conductivity of 35.84 S m^{-1}. In addition, the symmetric SC showed 4000 cycles for 2.8 V working voltage.

One of the most important production wastes is palm oil mill effluent (POME), especially in the countries in which the palm oil production holds a prominent industrial application. POME is a wastewater resulted from the sterilization, hydrocyclone waste, and separator sludge from crude palm oil production [3, 17]. The separator sludge and sterilizer effluent are the main POME sources which cause the highly polluting characteristics of the wastewater [17]. Therefore, the efficient use and removal of these pollution sources are highly important for both the production of biomass-based advanced carbon materials and environmental issues. It was reported by many studies that POME has a great potential to be used as biomass material [3, 17]. Furthermore, POME contains rich organic compounds in its structure, and it has also a great potential as a carbon source for the large-scale production of CNTs. Widiatmoko et al. [79] have used POME as a carbon source for CNT synthesis. They developed supercapacitor electrodes from POME-derived CNTs. In this work, POME was firstly polymerized with a 37% formaldehyde solution using ammonium

hydroxide as catalyst at 95 °C for 4 h. The obtained resin after this process was mixed with ferrocene and then the pyrolysis process was applied to obtain CNT structure at two different temperatures (200 and 900 °C), under natural atmosphere and nitrogen atmosphere. They also reported that the fabricated SC from POME-derived electrodes exhibited a specific capacitance of 13.98 F g^{-1}. However, they stated that EIS which resulted from the weak electrode and electrolyte interaction lowers the SC performance significantly.

The electrodes of SC are the main components that determine the final electrochemical performance of the devices. Electrode morphology is highly important in terms of specific surface area and electrolyte ion diffusion to the electrode surface and electron transport. Therefore, different electroactive materials are composed, and different architectures were used to increase electrode performance. Wang et al. [76] have developed an SC electrode from a new composite material with a hollow tube-on-tube architecture of carbon tube. The new hollow tube-on-tube carbon tube/$NiCo_2S_4$ (CT/NCS tube) composite material was synthesized by the means of thermal synthesis and sulfidation process of $NiCo_2S_4$ precursors on carbon tubes. In this work, Juncus roemerianus which is a flowering plant was used as biomass material for the production of 3D bio-carbon tubes as substrates. They claimed that the hollow carbon tube/NCS tube composite structure resulted in a better ion/electron storage and more diffusion channels to the electrode surface. The prepared SC electrode capacitances were reported as 747, 724.7, 669, and 507.9 F g^{-1} at different current densities at 1, 2, 10, and 20 A g^{-1}, respectively. The cycling stability of SC was also measured at 5000 cycles.

Yang et al. [82] have developed composite fabric electrodes including MWCNT and reduced graphene oxide (RGO) and metallic textiles for high-performance, waterproof, and wearable SCS. In this study, they vacuum filtered MWCNT and RGO directly on the Ni-coated cotton fabric. They reported that the all solid-state fabric SC showed 6.2 F cm^{-2} at an areal current density of 20 mA cm^{-2} and 3.2 F cm^{-2} after 10,000 charge/discharge cycle. They hypothesized that the synergistic effect between 1D MWCNTs and 2D RGO sheets contributed to a porous hybrid 3D framework, and this positive effect may also indicate the use of 1D and 2D materials together as efficient electrode materials for many other applications.

The fabrication of binderless electrodes is also advantageous in terms of electrical conductivity and surface porosity and related electrochemical performance of SC cells. Since most of the binder materials have lower conductivity values, their presence also causes an important performance loss. The use of CNT in such an electrode structure as a conductive and binder material was investigated by previous studies. Dolah et al. [16] have developed a method to fabricate binderless SC electrodes from biomass-derived activated carbon and CNTs. In this work, they used self-adhesive carbon grains from oil palm empty fruit bunch fibers. After carbonization and activation with KOH, they obtained carbon/CNT structure and porous SC electrodes. They reported that the increase of CNT content in electrode structure led to a remarkable decrease in the ESR value of the electrodes and an improvement in the specific power of the devices. However, an increase of CNT content may result

in the formation of a less porous electrode surface which also reduces the specific capacitance of the electrodes.

Wang et al. [75] have developed composites SC electrodes using biomass-derived carbon microtubes decorated with Ni–Co sulfites nanoparticles. They used willow catkins as a biomass source for CMT synthesis. They reported that CMT structure was synthesized from the pre-carbonization of willow catkins at 1000 °C. The SC which was fabricated from the CMTs-1000/Ni–Co-sulfides exhibited 1210 F g^{-1} at a current density of 0.5 A g^{-1}. They also stated that the capacitance retention of composite electrode was found to be 95% over 3000 charge/discharge cycles. In another work, Li et al. [36] used willow catkins as biomass which served as a bio-template for carbon microtube structure. They reported that carbon microtubes were synthesized by carbonization of willow catkins under an argon atmosphere at 500 °C for 4 h. The prepared β-$Ni(OH)_2$@acid-treated carbon microtube composite electrodes exhibited 1568 F g^{-1} specific capacitance at a current density of 1 A g^{-1}, and a good cycle stability of 84.3% over 3000 charge/discharge cycles at 5 A g^{-1}.

7 Conclusion

This chapter summarizes biomass-derived CNT and related structures in terms of biomass sources, synthesis methods, and main applications in the supercapacitors. CNTs have advanced electronic and mechanical properties owing to their physical and chemical structure. Global warming and other important environmental issues increased the importance of renewable and eco-friendly energy resources. As a result of the rapid increasing world population, the energy crisis or long energy shortages are very likely to occur in the near future. This situation indicates the importance of biomass resources for energy materials. As carbon sources, biomass materials provide a wide variety of possibilities for CNT synthesis by means of different methods. They are advantageous candidates for CNT synthesis due to their wide distribution, eco-friendly nature, and low cost. On the other hand, it was shown that the studies on the use of biomass-derived CNTs in SCs are relatively new and it is obvious that more studies are necessary to reveal the effect of different biomass sources on CNT structure and related properties. According to the previous studies, CNTs from biomass precursors and their composites can be effectively used in supercapacitors as high-performance electrode materials. It was shown that especially composite materials of biomass-derived CNTs have an important potential and remain as an outstanding research field waiting to be investigated in detail.

Acknowledgements This chapter is based upon work from COST Action "High-performance Carbon-based composites with Smart properties for Advanced Sensing Applications" (EsSENce Cost Action CA19118, https://www.context-cost.eu) supported by COST (European Cooperation in Science and Technology, https://www.cost.eu).

References

1. Aboul-enein AA et al (2021) Catalytic pyrolysis of sugarcane bagasse by zeolite catalyst for the production of multi-walled carbon nanotubes. Ranliao Huaxue Xuebao/J Fuel Chem Technol 49(10):1421–1434. https://doi.org/10.1016/S1872-5813(21)60127-5
2. Afre RA et al (2006) Carbon nanotubes by spray pyrolysis of turpentine oil at different temperatures and their studies. Microporous Mesoporous Mater 96(1–3):184–190. https://doi.org/10.1016/j.micromeso.2006.06.036
3. Ahmad AL, Ismail S, Bhatia S (2003) Water recycling from palm oil mill effluent (POME) using membrane technology. Desalination 157(1–3):87–95. https://doi.org/10.1016/S0011-9164(03)00387-4
4. Alves JO et al (2012) Characterization of nanomaterials produced from sugarcane bagasse. J Market Res 1(1):31–34. https://doi.org/10.1016/S2238-7854(12)70007-8
5. Awasthi K, Kumar R, Raghubanshi H (2011) Synthesis of nano-carbon (nanotubes, nanofibres, graphene). Materials 34(4):607–614
6. Baddour CE, Briens C (2005) Carbon nanotube synthesis: a review. Int J Chem React Eng 3. https://doi.org/10.2202/1542-6580.1279
7. Bernd MGS et al (2017) Synthesis of carbon nanostructures by the pyrolysis of wood sawdust in a tubular reactor. J Market Res 6(2):171–177. https://doi.org/10.1016/j.jmrt.2016.11.003
8. Berrueta A et al (2019) Supercapacitors: electrical characteristics, modeling, applications, and future trends. IEEE Access 7:50869–50896. https://doi.org/10.1109/ACCESS.2019.2908558
9. Bracmort K, Gorte RW (2010) Biomass: comparison of definitions in legislation. In: Biomass: energy data, multi-year plan and legislative definitions, pp 1–18
10. Brhane Y, Gabriel T (2016) Production, purification and functionalization of carbon nanotubes for medical applications. Int Res J Pharm 7(7):19–27. https://doi.org/10.7897/2230-8407.07780
11. Chen H et al (2015) Fabrication and functionalization of carbon nanotube films for high-performance flexible supercapacitors. Carbon 92:271–296. https://doi.org/10.1016/j.carbon.2015.04.010
12. Chen R et al (2020) The development of pseudocapacitor electrodes and devices with high active mass loading. Adv Energy Mater 10(20):1–33. https://doi.org/10.1002/aenm.201903848
13. Chen T, Dai L (2013) Carbon nanomaterials for high-performance supercapacitors. Mater Today 16(7–8):272–280. https://doi.org/10.1016/j.mattod.2013.07.002
14. Choudhary RB, Ansari S, Majumder M (2021) Recent advances on redox active composites of metal-organic framework and conducting polymers as pseudocapacitor electrode material. Renew Sustain Energy Rev 145:110854. https://doi.org/10.1016/j.rser.2021.110854
15. Díaz-Ortiz Á, Prieto P, de la Hoz A (2019) A critical overview on the effect of microwave irradiation in organic synthesis. Chem Rec 19(1):85–97. https://doi.org/10.1002/tcr.201800059
16. Dolah BNM et al (2014) A method to produce binderless supercapacitor electrode monoliths from biomass carbon and carbon nanotubes. Mater Res Bull 60:10–19. https://doi.org/10.1016/j.materresbull.2014.08.013
17. Esa N et al (2010) Review of current Palm Oil Mill Effluent (POME) treatment methods: vermicomposting as a sustainable practice. World Appl Sci J 10(10):1190–1201
18. Esohe Omoriyekomwan J et al (2022) Synthesis of super-long carbon nanotubes from cellulosic biomass under microwave radiation. Nanomaterials 12(5):737. https://doi.org/10.3390/nano12050737
19. Fathy NA (2017) Carbon nanotubes synthesis using carbonization of pretreated rice straw through chemical vapor deposition of camphor. RSC Adv 7(45):28535–28541. https://doi.org/10.1039/c7ra04882c
20. Fleischmann S et al (2020) Pseudocapacitance: from fundamental understanding to high power energy storage materials. Chem Rev 120(14):6738–6782. https://doi.org/10.1021/acs.chemrev.0c00170

21. Gao Z et al (2018) Carbon nanotubes derived from yeast-fermented wheat flour and their energy storage application. ACS Sustain Chem Eng 6(9):11386–11396. https://doi.org/10.1021/acssuschemeng.8b01292
22. Ghosh S et al (2019) Natural biomass derived hard carbon and activated carbons as electrochemical supercapacitor electrodes. Sci Rep 9(1):1–15. https://doi.org/10.1038/s41598-019-52006-x
23. Goodell B et al (2008) Carbon nanotubes produced from natural cellulosic materials. J Nanosci Nanotechnol 8(5):2472–2474. https://doi.org/10.1166/jnn.2008.235
24. Gupta S, Murthy CN, Prabha CR (2018) Recent advances in carbon nanotube based electrochemical biosensors. Int J Biol Macromol 108:687–703. https://doi.org/10.1016/j.ijbiomac.2017.12.038
25. Han Z, Fina A (2011) Thermal conductivity of carbon nanotubes and their polymer nanocomposites: a review. Prog Polym Sci (Oxford) 36(7):914–944. https://doi.org/10.1016/j.progpolymsci.2010.11.004
26. He D et al (2017) Design of electrically conductive structural composites by modulating aligned CVD-grown carbon nanotube length on glass fibers. ACS Appl Mater Interfaces 9(3):2948–2958. https://doi.org/10.1021/acsami.6b13397
27. Hildago-Oporto P et al (2019) Synthesis of carbon nanotubes using biochar as precursor material under microwave irradiation. J Environ Manag 244(May):83–91. https://doi.org/10.1016/j.jenvman.2019.03.082
28. Kang Z et al (2005) Obtaining carbon nanotubes from grass. Nanotechnology 16(8):1192–1195. https://doi.org/10.1088/0957-4484/16/8/036
29. Kappe CO (2002) High-speed combinatorial synthesis utilizing microwave irradiation. Curr Opin Chem Biol 6(3):314–320. https://doi.org/10.1016/S1367-5931(02)00306-X
30. Koruba D, Piotrowski JZ, Latosińska J (2017) Biomass—alternative renewable energy source to the fossil fuels. E3S Web Conf 14(March 2016):1–10. https://doi.org/10.1051/e3sconf/20171402015
31. Kumar M et al (2007) The use of camphor-grown carbon nanotube array as an efficient field emitter. Carbon 45(9):1899–1904. https://doi.org/10.1016/j.carbon.2007.04.023
32. Kumar M, Ando Y (2003) A simple method of producing aligned carbon nanotubes from an unconventional precursor—camphor. Chem Phys Lett 374(5–6):521–526. https://doi.org/10.1016/S0009-2614(03)00742-5
33. Kumar R et al (2013) Synthesis of carbon and carbon-nitrogen nanotubes using green precursor: Jatropha-derived biodiesel. J Exp Nanosci 8(4):606–620. https://doi.org/10.1080/17458080.2011.577102
34. Li J et al (2021) Thermochemical characteristics and non-isothermal kinetics of camphor biomass waste. J Environ Chem Eng 9(4):105311. https://doi.org/10.1016/j.jece.2021.105311
35. Li M et al (2015) Iron and nitrogen co-doped carbon nanotube@hollow carbon fibers derived from plant biomass as efficient catalysts for the oxygen reduction reaction. J Mater Chem A 3(18):9658–9667. https://doi.org/10.1039/c5ta00958h
36. Li Q et al (2018) β-$Ni(OH)_2$ nanosheet arrays grown on biomass-derived hollow carbon microtubes for high-performance asymmetric supercapacitors. ChemElectroChem 5(9):1279–1287. https://doi.org/10.1002/celc.201800024
37. Li X, Wei B (2013) Supercapacitors based on nanostructured carbon. Nano Energy 2(2):159–173. https://doi.org/10.1016/j.nanoen.2012.09.008
38. Liu L, Niu Z, Chen J (2018) Flexible supercapacitors based on carbon nanotubes. Chin Chem Lett 29(4):571–581. https://doi.org/10.1016/j.cclet.2018.01.013
39. Liu Y et al (2019) Facile growth of carbon nanotubes using microwave ovens: the emerging application of highly efficient domestic plasma reactors. Nanoscale Adv 1(12):4546–4559. https://doi.org/10.1039/c9na00538b
40. Luo XY, Chen Y, Mo Y (2021) A review of charge storage in porous carbon-based supercapacitors. Xinxing Tan Cailiao/New Carbon Mater 36(1):49–68. https://doi.org/10.1016/S1872-5805(21)60004-5
41. Máca J, Sedla M (2018) Supercapacitors: properties and applications. 17(March)

42. Mamaeva A et al (2016) Microwave-assisted catalytic pyrolysis of lignocellulosic biomass for production of phenolic-rich bio-oil. Biores Technol 211:382–389. https://doi.org/10.1016/j.biortech.2016.03.120
43. Meguid SA, Weng GJ (2017) Micromechanics and nanomechanics of composite solids. Micromechanics Nanomechanics Compos Solids. https://doi.org/10.1007/978-3-319-52794-9
44. Meng L et al (2012) Single walled carbon nanotubes as drug delivery vehicles: targeting doxorubicin to tumors. Biomaterials 33(6):1689–1698. https://doi.org/10.1016/j.biomaterials.2011.11.004
45. Mubarak NM et al (2014) An overview on methods for the production of carbon nanotubes. J Ind Eng Chem 20(4):1186–1197. https://doi.org/10.1016/j.jiec.2013.09.001
46. Nersisyan HH et al (2013) Fabrication of tunable carbon micro- and nanotubes using reed as bio-template. Mater Lett 107:79–82. https://doi.org/10.1016/j.matlet.2013.05.102
47. Omoriyekomwan JE et al (2021) A review on the recent advances in the production of carbon nanotubes and carbon nanofibers via microwave-assisted pyrolysis of biomass. Fuel Process Technol 214(November):106686. https://doi.org/10.1016/j.fuproc.2020.106686
48. Osman AI, et al (2019) Production and characterisation of activated carbon and carbon nanotubes from potato peel waste and their application in heavy metal removal. Environ Sci Pollut Res 26(36):37228–37241. https://doi.org/10.1007/s11356-019-06594-w
49. Osman AI et al (2020) Upcycling brewer's spent grain waste into activated carbon and carbon nanotubes for energy and other applications via two-stage activation. J Chem Technol Biotechnol 95(1):183–195. https://doi.org/10.1002/jctb.6220
50. Pan H, Li J, Feng YP (2010) Carbon nanotubes for supercapacitor. Nanoscale Res Lett 5(3):654–668. https://doi.org/10.1007/s11671-009-9508-2
51. Pasangulapati V et al (2012) Effects of cellulose, hemicellulose and lignin on thermochemical conversion characteristics of the selected biomass. Biores Technol 114:663–669. https://doi.org/10.1016/j.biortech.2012.03.036
52. Poonam et al (2019) Review of supercapacitors: materials and devices. J Energy Storage 21(January):801–825. https://doi.org/10.1016/j.est.2019.01.010
53. Popp J et al (2021) Bioeconomy: biomass and biomass-based energy supply and demand. New Biotechnol 60:76–84. https://doi.org/10.1016/j.nbt.2020.10.004
54. Rafique MMA, Iqbal J (2011) Production of carbon nanotubes by different routes—a review. J Encapsulation Adsorpt Sci 01(02):29–34. https://doi.org/10.4236/jeas.2011.12004
55. Ranjithkumar R et al (2019) Enhanced electrochemical studies of ZnO/CNT nanocomposite for supercapacitor devices. Phys B 568(April):51–59. https://doi.org/10.1016/j.physb.2019.05.025
56. Rathinavel S, Priyadharshini K, Panda D (2021) A review on carbon nanotube: an overview of synthesis, properties, functionalization, characterization, and the application. Mater Sci Eng B: Solid-State Mater Adv Technol 268(March):115095. https://doi.org/10.1016/j.mseb.2021.115095
57. Rawat S, Mishra RK, Bhaskar T (2022) Biomass derived functional carbon materials for supercapacitor applications. Chemosphere 286(P3):131961. https://doi.org/10.1016/j.chemosphere.2021.131961
58. Rey-Raap N, et al (2019) Influence of multiwalled carbon nanotubes as additives in biomass-derived carbons for supercapacitor applications. ACS Appl Mater Interfaces [Preprint]. https://doi.org/10.1021/acsami.8b19246
59. Salvador VT, et al (2020) Biomass transformation: hydration and isomerization reactions of turpentine oil using ion exchange resins as catalyst. Sustain Chem Pharm 15(October 2019). https://doi.org/10.1016/j.scp.2020.100214
60. Sannasi V et al (2020) H_2O_2-assisted microwave synthesis of NiO/CNT nanocomposite material for supercapacitor applications. Ionics 26(8):4067–4079. https://doi.org/10.1007/s11581-020-03563-z
61. Shanov V et al (2013) CVD growth, characterization and applications of carbon nanostructured materials. Surf Coat Technol 230:77–86. https://doi.org/10.1016/j.surfcoat.2013.06.017
62. Sharma P, Kumar V (2020) Current technology of supercapacitors: a review. J Electron Mater 49(6):3520–3532. https://doi.org/10.1007/s11664-020-07992-4

63. Shen D et al (2011) The pyrolytic behavior of cellulose in lignocellulosic biomass: a review. RSC Adv 1(9):1641–1660. https://doi.org/10.1039/c1ra00534k
64. Shi K et al (2014) Catalyst-free synthesis of multiwalled carbon nanotubes via microwave-induced processing of biomass. Ind Eng Chem Res 53(39):15012–15019. https://doi.org/10.1021/ie503076n
65. Shukrullah S et al (2016) Effect of ethylene flow rate and CVD process time on diameter distribution of MWCNTs. Mater Manuf Processes 31(12):1537–1542. https://doi.org/10.1080/10426914.2015.1090588
66. Suriani AB et al (2009) Synthesis of vertically aligned carbon nanotubes using natural palm oil as carbon precursor. Mater Lett 63(30):2704–2706. https://doi.org/10.1016/j.matlet.2009.09.048
67. Thompson E et al (2015) Iron-catalyzed graphitization of biomass. Green Chem 17(1):551–556. https://doi.org/10.1039/c4gc01673d
68. Titirici MM, Antonietti M (2010) Chemistry and materials options of sustainable carbon materials made by hydrothermal carbonization. Chem Soc Rev 39(1):103–116. https://doi.org/10.1039/b819318p
69. Vassilev SV et al (2010) An overview of the chemical composition of biomass. Fuel 89(5):913–933. https://doi.org/10.1016/j.fuel.2009.10.022
70. Vetrivel R, Navinselvakumar C, Samuel Ratna Kumar PS (2018) Carbon nanotubes and its applications—a review. Int J Mech Prod Eng Res Dev 8(Special Issue 7):288–293
71. Wang G et al (2015a) A N-, Fe- and Co-tridoped carbon nanotube/nanoporous carbon nanocomposite with synergistically enhanced activity for oxygen reduction in acidic media. J Mater Chem A 3(34):17866–17873. https://doi.org/10.1039/c5ta03523f
72. Wang G et al (2017a) From chlorella to nestlike framework constructed with doped carbon nanotubes: a biomass-derived, high-performance, bifunctional oxygen reduction/evolution catalyst. ACS Appl Mater Interfaces 9(37):32168–32178. https://doi.org/10.1021/acsami.7b10668
73. Wang H et al (2011) Facile synthesis of MnO_2/CNT nanocomposite and its electrochemical performance for supercapacitors. Mater Sci Eng B: Solid-State Mater Adv Tech 176(14):1073–1078. https://doi.org/10.1016/j.mseb.2011.05.043
74. Wang J et al (2015b) Ni-promoted synthesis of graphitic carbon nanotubes from in situ produced graphitic carbon for dehydrogenation of ethylbenzene. Chem Commun 51(64):12859–12862. https://doi.org/10.1039/c5cc02593a
75. Wang K et al (2019) Multi-scale biomass-based carbon microtubes decorated with Ni–Co sulphides nanoparticles for supercapacitors with high rate performance. Electrochim Acta 302:78–91. https://doi.org/10.1016/j.electacta.2019.02.015
76. Wang N et al (2017b) A hollow tube-on-tube architecture of carbon-tube-supported nickel cobalt sulfide nanotubes for advanced supercapacitors. ChemNanoMat 3(4):269–276. https://doi.org/10.1002/cnma.201700016
77. Wang Y et al (2021) Biomass-Derived Carbon Materials: Controllable Preparation and Versatile Applications. Small 17(40):1–32. https://doi.org/10.1002/smll.202008079
78. Wang Z et al (2015c) Nanocarbons from rice husk by microwave plasma irradiation: from graphene and carbon nanotubes to graphenated carbon nanotube hybrids. Carbon 94:479–484. https://doi.org/10.1016/j.carbon.2015.07.037
79. Widiatmoko P, et al (2020) Upscaled synthesis of carbon nanotube from palm oil mill effluent using pyrolysis for supercapacitor application. IOP Conf Ser: Mater Sci Eng 823(1). https://doi.org/10.1088/1757-899X/823/1/012040
80. Xie L et al (2016) Hierarchical porous carbon microtubes derived from willow catkins for supercapacitor applications. J Mater Chem A 4(5):1637–1646. https://doi.org/10.1039/c5ta09043a
81. Yang M et al (2020) Dramatically enhanced electromagnetic wave absorption of hierarchical CNT/Co/C fiber derived from cotton and metal-organic-framework. Carbon 161:517–527. https://doi.org/10.1016/j.carbon.2020.01.073

82. Yang Y, et al (2017) Waterproof, ultrahigh areal-capacitance, wearable supercapacitor fabrics. Adv Mater 29(19). https://doi.org/10.1002/adma.201606679
83. Yao Y et al (2017) Synthesis of "sea urchin"-like carbon nanotubes/porous carbon superstructures derived from waste biomass for treatment of various contaminants. Appl Catal B 219:563–571. https://doi.org/10.1016/j.apcatb.2017.07.064
84. Zhang J et al (2019) In situ encapsulation of iron complex nanoparticles into biomass-derived heteroatom-enriched carbon nanotubes for high-performance supercapacitors. Adv Energy Mater 9(4):1–8. https://doi.org/10.1002/aenm.201803221
85. Zhang X et al (2017) An overview of a novel concept in biomass pyrolysis: microwave irradiation. Sustain Energy Fuels 1(8):1664–1699. https://doi.org/10.1039/C7SE00254H
86. Zhang Y et al (2018) Biomass chitosan derived cobalt/nitrogen doped carbon nanotubes for the electrocatalytic oxygen reduction reaction. J Mater Chem A 6(14):5740–5745. https://doi.org/10.1039/c7ta11258k
87. Zhang Y et al (2021) Multi-walled carbon nanotubes/carbon foam nanocomposites derived from biomass for CO_2 capture and supercapacitor applications. Fuel 305(May):121622. https://doi.org/10.1016/j.fuel.2021.121622
88. Zhao J, Burke AF (2021) Review on supercapacitors: technologies and performance evaluation. J Energy Chem 59:276–291. https://doi.org/10.1016/j.jechem.2020.11.013
89. Zhou F et al (2014) A 3d hierarchical hybrid nanostructure of carbon nanotubes and activated carbon for high-performance supercapacitors. J Mater Chem A 2(10):3505–3512. https://doi.org/10.1039/c3ta14723a
90. Zhou J, et al (2021) Biomass-derived carbon materials for high-performance supercapacitors: current status and perspective, electrochemical energy reviews. Springer, Singapore. https://doi.org/10.1007/s41918-020-00090-3
91. Zhou S et al (2020) Autochthonous N-doped carbon nanotube/activated carbon composites derived from industrial paper sludge for chromate (VI) reduction in microbial fuel cells. Sci Total Environ 712:136513. https://doi.org/10.1016/j.scitotenv.2020.136513
92. Zhou Y et al (2022) Recent advances in biomass-derived graphene and carbon nanotubes. Mater Today Sustain 18:100138. https://doi.org/10.1016/j.mtsust.2022.100138
93. Zhu S, Ni J, Li Y (2020) Carbon nanotube-based electrodes for flexible supercapacitors. Nano Res 13(7):1825–1841. https://doi.org/10.1007/s12274-020-2729-5

Amorphous Carbon with a Graphitic Pattern Derived from Biomass for Supercapacitor Applications

Ha H. Phan and Anh N. Phan

Abstract The graphitic pattern of biomass-derived carbon is deemed to link with the electric conductivity of the carbon, but conventional heat treatment, even up to 3000 °C, is not suitable to convert biomass into highly ordered graphitic carbon. A number of studies on biomass derived carbons that underwent heat treatment exhibited that graphite carbon microcrystals formed during the heat treatment consisted of only a few graphene layers (3–4 layers), with the crystal heights being smaller than those of natural and synthetic graphite (20–300 nm). The interlayer distance between these layers is normally >10% higher than that of graphite (0.335–0.336 nm) due to the presence of impurities and heteroatoms, and these crystals are also distributed randomly in carbon without proper connections, so they cannot conduct electrons and result in poor electric conductivity and supercapacitor performances. However, combining chemical pre-treatment with transitional metal compounds (e.g., $Fe(NO_3)_3$, $Ni(NO_3)_2$) or alkaline and alkaline earth metal compounds (e.g., CaO, KOH) with heat treatments to generate graphitic carbons has been investigated. This chapter critically examines the graphitic structure and surface area/porosity of biomass derived carbons obtained from these chemical activation methods, the influence of operating conditions, and their applications in supercapacitors. Finally, current challenges and further perspectives on graphitic carbon from biomass used in supercapacitors are suggested.

Keywords Amorphous carbon · Graphitic pattern · Biomass · Supercapacitor applications

H. H. Phan (✉) · A. N. Phan (✉)
School of Engineering, Newcastle University, Newcastle upon Tyne NE1 7RU, UK
e-mail: ha.phan@newcastle.ac.uk

A. N. Phan
e-mail: anh.phan@newcastle.ac.uk

S. K. Tiwari et al. (eds.), *Biomass-Based Functional Carbon Nanostructures for Supercapacitors*, Green Energy and Technology,
https://doi.org/10.1007/978-981-99-0996-4_7

1 Introduction

The depletion of fossil fuels and the emergence of hybrid electric vehicles ask for the explorance of efficient energy storage systems to utilise the energy generated from renewable energies. An effective energy storage system should have high energy density, high power density and low cost with easy accessibility [1]. Among current energy storage systems, supercapacitors demonstrate high power density and cycling stability with fast charge–discharge characteristic. However, the main drawback—low energy density (less than 10 Wh kg^{-1}) of supercapacitors [2]—limits its applications in portable devices and electric vehicles [3]. The electrode in supercapacitors directly involves in the interactions of electrolyte ions and electron transfer, so improving properties of the electrode can help boost the performance of supercapacitors [4, 5].

Carbon electrodes materials are conventionally obtained from coke and pitch, with the ability to conduct electricity in carbon electrodes of supercapacitors depends on the carbonaceous/crystalline structure [6]. The mass use of graphite from coke and fossil fuels in supercapacitors is hindered because the high cost for graphite manufacture is costly and this carbon source is non-renewable. Biomass is the renewable source of carbon (up to 50% carbon), which can be converted into graphitic carbon materials to reduce the cost and increase the application of supercapacitors. Carbon obtained from biomass structure can also be tailored to improve electric conductivity, energy density, and power density [5].

The importance of carbonaceous structure, surface area, porosity, and functional groups of biomass derived carbons in supercapacitors have been scrutinised in other studies with pore networks providing pathways for electrolyte ions to diffuse across the electrode surface [7, 8], and functional groups improving the pseudocapacitance through reversible surface reactions [9, 10] while graphitic carbon structure contributing to the electrical double layer capacitance (EDLC) of capacitors [11–14]. The graphitic structure of camphor leaves carbon with >200 layers of ordered carbon and only 4.37 at% of oxygen content significantly exhibited the superior capacitance of 397 F g^{-1} at 1 A g^{-1} [12]. Multiple layers of ordered carbon in cornstalk derived carbon obtained at 1100 °C increased the specific capacitance to 213 F g^{-1} at 1 A g^{-1} and reduced the charge transfer to 0.5663 Ω compared to 0.9106 Ω of turbostratic cornstalk carbon [11]. In graphite, C–C bonds using sp^2 hybrid orbitals create flat planes of carbon hexagon rings where the free π electrons from non-hybrid orbitals on the same plane interact with π electrons from different layers to create stacking [6]. The high electron conductivity of graphite is the result of free π electrons resonating between layers of carbon hexagon rings.

Many studies focused on enhancing surface area and morphology of biomass derived carbon due to the direct influence on electrolyte diffusion onto the electrode interface [15, 16]. However, modifying surface area and morphology of biomass-derived carbon only increases the performance of supercapacitors to a certain limit (162–253 F g^{-1} at 0.5 A g^{-1} for biomass carbons with surface area of 1816–2787 m^2 g^{-1} [17, 18]). Because carbonaceous structure directly links to the electron

conductivity of electrodes, some biomass derived carbons with a dominant amorphous content (through XRD and Raman spectroscopy) could not support this critical feature [19, 20]. As a result, without improving the carbonaceous structure of biomass carbons, it will prevent the widespread application of biomass-derived carbon in supercapacitors [5].

2 Synthetic Process of Carbon Derived from Biomass

Figure 1 illustrates several methods to prepare carbons from biomass. Biomass can be converted through pyrolysis to obtain carbon or chemically activated at high temperatures. The characteristics of these carbon will be discussed in this section.

2.1 Pyrolysis Approach

Pyrolysis is a thermochemical conversion operated in an inert environment such as nitrogen and argon over a range of temperatures (>300 °C) at low heating rates (<20 °C min^{-1}) to obtain carbon materials. Depending upon the heat treatment temperature, heating rate, and holding time, the properties of the carbon vary in which heat treatment temperature is a dominant factor in controlling graphitic structure of carbon materials [22, 23]. Johnson et al. reported that increasing the temperature between 300–2800 °C resulted in a high ordered structure, and crystal diameter of carbon evidenced by a reduction in the D-band width in Raman spectroscopy and an increase in L_a in XRD [22]. The changes of D-band and L_a can be observed clearly at a wide range of temperature. In a temperature range of 900 to 2400 °C, the intensity ratio between D and G peaks (I_D/I_G) of carbon derived from coal increased from 1.1 to 1.7 and the D band widths also reduced, indicating the rearrangement into a higher degree of ordered carbon structure [23]. However, narrowing the temperature range

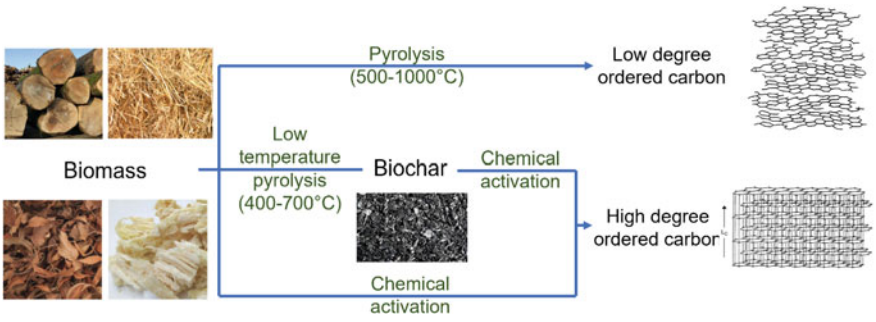

Fig. 1 Process illustration for the preparation of biomass derived carbon (some elements adapted from [6] and [21])

to 1300–2000 °C had no effect on the structure of metallurgic cokes, e.g. the I_D/I_G ratio remaining almost constant at 1.3–1.4. Heating rate, pressure and holding time had little influence on the properties of carbon product derived from charcoals in a range temperature of 400–1000 °C [24]. A similar finding was found for polymer-based carbon activated in CO_2 as shown by a small fluctuation of D band widths in the range 264–289 cm^{-1} at position 1363 ± 2 cm^{-1} and G band at 1593 ± 4 cm^{-1} [25]. With various cross linkages between C, H and O in these carbons, it yields extremely high activation energies (normally not applicable in heat treatment) to break all these bonds and remove all heteroatoms out of carbon, so the carbon cannot go through a nematic discotic liquid crystal phase to form graphitic carbon.

The solid product obtained from pyrolysis of biomass is normally known as biochar containing heteroatoms e.g. oxygen, hydrogen. Therefore, it is difficult to observe the influence of temperatures on the carbonaceous structure of biochar. The carbonaceous structure of biochar showed some small transformation at high temperatures e.g. the carbon crystal diameter (L_a) of spruce wood biochar increased from 2.5 nm in a temperature range of 500–1000 °C to 7.5 nm at 2400 °C, and D band widths decreased from 200 cm^{-1} at 500 °C to ~ 55 cm^{-1} at 2200–2400 °C but no clear change for G band [26]. D band widths of cedar wood-derived biochar decreased from 200 ± 12 cm^{-1} to 150 ± 10 cm^{-1} within a temperature range of 500–1000 °C [27]. The interlayer distance (d_{002}) of Acacia and Eucalyptus-wood biochar obtained at 600–1200 °C slightly declined from 0.39 to 0.37 nm, and L_a increased from 2.2 to 4.0 nm due to the cross linkages of oxygen in the carbon structure [28]. Increasing the holding time from 1 to 5 h for a temperature range of 800–1000 °C did not observe any change to d_{002} and L_a [28]. For cellulose-derived biochar, increasing temperatures from 600 to 2600 °C slightly increased the carbon crystal diameter (L_a) and carbon crystal height (L_c) from 3 to 5 nm, and decreased d_{002} from 0.350 to 0.341 nm and D band widths [29]. These examples of biochar from spruce wood [26], cedar wood [27], and Acacia and Eucalyptus-wood [28] showed that in a conventional pyrolysis treatment (a temperature range of 600–2400 °C in an inert atmosphere), L_a, d_{002}, D peaks and G peaks demonstrated negligible changes. The alteration of carbonaceous structure of biochar mainly occurs in the temperature range of 500–1000 °C. To produce graphitic carbon from biomass, all cross linkages in its structure must be removed.

Graphitic carbons should exhibit a sharp and narrow peak at 26–26.5° in XRD for (002) carbon structure with a prominent peak at 44.5–45° for (100) structure with 20–90 layers in carbon crystals, and a 2D band at ~2750 cm^{-1} could normally be observed in Raman spectroscopy [6, 11, 30]. Although biomass derived carbons were reported to be of graphite structure and used for testing the supercapacitors, the carbonaceous structure of these biochar samples only demonstrated two broad XRD peaks at 20–30° and 44° in XRD patterns, and D and G peaks overlapping each other in Raman spectroscopy. Such evidence normally reveals that there are micro carbon crystals distributed randomly in the amorphous carbon and the carbon is highly disordered. Therefore, a robust method needs to be developed to obtain the graphitic carbon.

2.2 Hybrid Chemical Pre-treatment and Pyrolysis

2.2.1 Transitional Metal-Based Chemical Treatment

Thermochemical processes such as pyrolysis cannot directly produce carbon from biomass with a graphitic structure. Some other procedures, such as hydrocarbon precursors at high temperatures (chemical vapour deposition) and graphite precursor for exfoliation are also not suitable [31]. Coupling chemical pre-treatment and carbonisation can potentially convert biomass to graphitic carbon since it will remove the cross linkages of oxygen, hydrogen, and carbon in the biomass, and promote the formation of ordered carbon layers.

Iron-containing compounds were used to produce biomass-derived graphitic carbon [11, 30]. Porous graphitic carbon nanosheets were successfully synthesised from pyrolysis of cornstalk in the presence of $K_4[Fe(CN)_6]$ at 700 °C in N_2 environment. Increasing the temperature in a range of 1000–1200 °C significantly developed the graphitic structures [11]. The Raman spectra of cornstalk derived carbons obtained in the range 1000–1200 °C revealed the clear G peak at 1575–1581 cm^{-1} without overlapping with D peak at 1361 cm^{-1}, together with a distinctive 2D band emerging with increasing temperatures at 2715–2729 cm^{-1}. Increasing the concentration of $K_4[Fe(CN)_6]$ also increased the contact between biomass and the iron-containing compounds, which supported the formation of graphitic carbon e.g. the crystal height (L_c) of this cornstalk graphitic carbon nanosheets obtained at 1100 °C that increased from 11.37 nm (at a mass ratio cornstalk/$K_4[Fe(CN)_6]$ 1:1.46) to 23.75 nm (at mass ratio cornstalk/$K_4[Fe(CN)_6]$ 1:8.77) [11]. The crystal diameter (L_a) also increased from 14.41 nm to 26.21 nm. The crystal height in the range of 11.37–23.75 nm was equivalent of 34–71 carbon layers in the graphitic structure with the interlayer distance (d_{002}) at 0.3354–0.3373 nm (similar to that of graphite 0.3354 nm [32]). Therefore, oxygen was successfully removed from the biomass during the activation process. The capacitance was 213 F g^{-1} in KOH 6 M for graphitic carbon derived from the combination of pre-treatment at a mass ratio cornstalk/$K_4[Fe(CN)_6]$ 1:2.92 and pyrolysis at 1100 °C compared to 49 F g^{-1} for cornstalk biochar obtained from pyrolysis at 1100 °C only. This is due to the lack of electric conductivity in biochar.

Further evidence for graphitic carbon when using iron-containing compounds was observed when activating coconut shell with $ZnCl_2$ and $FeCl_3$ (Fig. 2b) [30] and activating sawdust with $Fe(NO_3)_3$ (Fig. 2c) [33]. The well-formed G peaks were observed in Raman spectrum from coconut shell carbon obtained at 800–1000 °C, which was similar to the cornstalk derived carbon [11]. XRD of coconut shell derived carbon activated with $FeCl_3$ at 700 °C did not demonstrate the band of carbon at 26.5° but the generation of Fe_3C phase (Fig. 3a). The band of carbon at 26.5 °C started to emerge at 800 °C and increased significantly at 900 °C, implying the development of crystallinity of carbon sheets. Therefore, it can be proposed that during the pyrolysis, $FeCl_3$ impregnated into the coconut shell reacted with gases (CO and H_2) from the decomposition to form metal Fe, which then reacted to form carbide phase Fe_3C (Eq. 1) at <800 °C and decomposed at temperature >800 °C into α-Fe (Eq. 2).

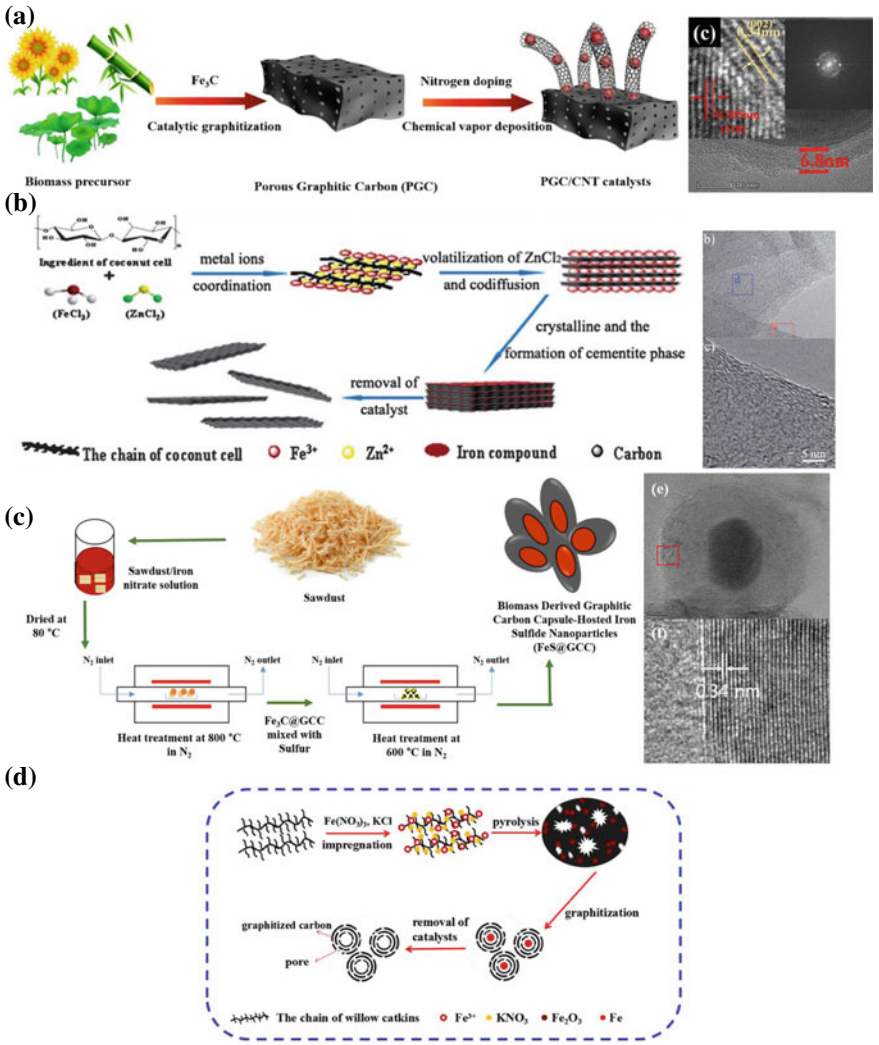

Fig. 2 Schematic illustration of biomass derived carbon using iron-containing compounds and TEM images of the obtained product from **a** bamboo [34], **b** coconut shell [30], **c** sawdust (Adapted with permission from [33]. Copyright 2022 American Chemical Society), and **d** willow catkins [35]

$$\mathrm{Fe} + \mathrm{C_{biomass}} \rightarrow \mathrm{Fe_3C} \tag{1}$$

$$\mathrm{Fe_3C} \rightarrow \alpha - \mathrm{Fe} + \mathrm{C_{graphite}} \tag{2}$$

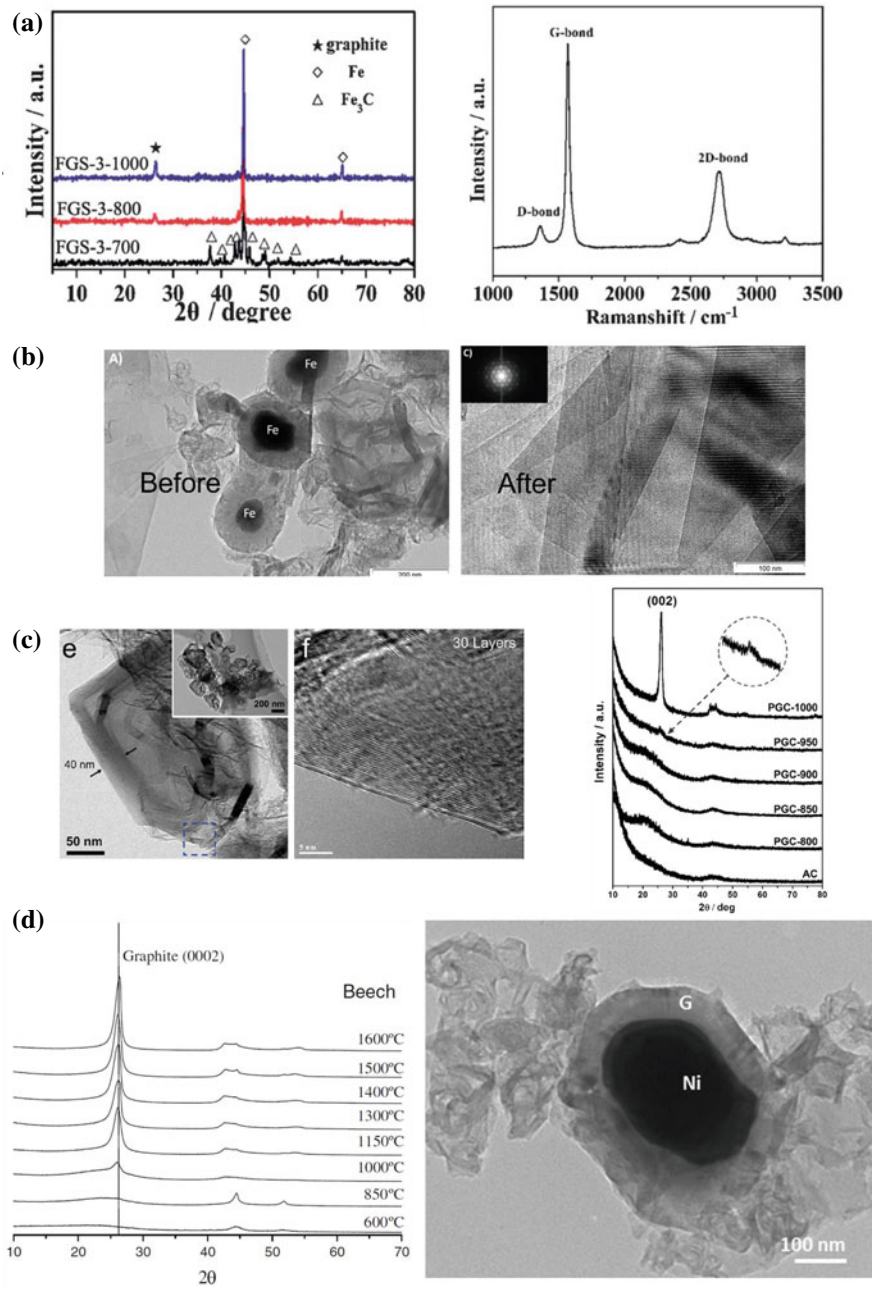

Fig. 3 **a** XRD of coconut shell carbon activated with $FeCl_3$ and $ZnCl_2$ and Raman spectrum of graphitic carbon [30], **b** TEM images of beech wood carbon activated with $FeCl_3$ before and after iron removal [36], **c** TEM images and XRD patterns of Zizania Latifolia leaves activated with $Ni(NO_3)_2$ [37], **d** XRD of beech wood activated with $Ni(NO_3)_2$ at 600–1600 °C and TEM image of the obtained carbon [38]

This promotes the formation of layers of hexagon carbon rings around the Fe metal with new carbon layers stacking on top of each other to form graphite structure [11]. At a mass ratio coconut shell/$ZnCl_2$/$FeCl_3$ 1:3:8 and 900 °C, the coconut shell derived carbon enhanced the surface area to 1874 $m^2\ g^{-1}$ and pore volume of 1.21 $cm^3\ g^{-1}$, which was ideal for the diffusion of electrolyte ion in supercapacitors. The combination of electron conductivity and surface area improved the specific capacitance to 268 F g^{-1} at 1 A g^{-1} in KOH 6 M.

Iron-based compounds can be also used for biochar activation at low temperatures (i.e. 400 °C) to obtain a similar effect [39]. Bamboo biochar derived from pyrolysis at 400 °C was mixed with K_2FeO_4 at a mass ratio biochar/K_2FeO_4 1:1.87 and then heat treated at 800 °C in Ar (2 h, 5 °C min^{-1}) to form graphitic carbon, which evidenced by a clear separation of D and G peaks in Raman spectrum and (002) and (100) peaks at 26.5 and 44.4° in XRD [39]. At 400–600 °C, K_2FeO_4 decomposed to $Fe(OH)_3$ and KOH (Eq. 3). $Fe(OH)_3$ was then reduced into iron oxides and subsequently metal Fe through a series of reactions (Eqs. 4–6) to promote the formation of graphitic carbon whereas KOH reacted with carbon to increase the surface area [40]. The partially decomposed lignin and cellulose in bamboo biochar prepared at 400 °C released H_2 and CO upon further heating which participated in the reduction reaction of $Fe(OH)_3$.

$$4K_2FeO_4 + 10H_2O \rightarrow 8KOH + 4Fe(OH)_3 + 3O_2 \tag{3}$$

$$Fe(OH)_3 \rightarrow FeO(OH) \rightarrow Fe_2O_3 \tag{4}$$

$$3Fe_2O_3 + (H_2,\ C,\ CO) \rightarrow 2Fe_3O_4 + (H_2O,\ CO,\ CO_2) \tag{5}$$

$$Fe_3O_4 + 4(H_2,\ C,\ CO) \rightarrow 3Fe + 4(H_2O,\ CO,\ CO_2) \tag{6}$$

Metal α-Fe then followed the same path to create graphite carbon when heated at temperatures > 800 °C as observed with coconut shell derived carbon (Eqs. 1–2) (Fig. 3b) [30]. The presence of Fe_3C could be ascertained by the XRD pattern recorded on the carbon product after being activated with iron salts with the diffraction peaks at 45.087°, 42.978°, 43.834°, 45.962° for the (121), (201), (103) and (211) structures, while the presence of metal α-Fe was confirmed through the XRD peaks at 44.57° and 65.02° (Fig. 3a) [30, 33, 34, 41]. Since graphitic carbon were formed when using biochar obtained at 400 °C, and it could be reasonably assumed that the carbon in biochar at this temperature was flexible enough for the rearrangement into graphitic carbon at higher temperatures. However, at this point, there are no other studies available for further comparison. Further studies to understand how temperatures in pre-pyrolysis can influence the graphitising process is important.

Even though metal Fe plays an important role in creating graphitic carbon structure, the types of iron salts influenced the graphitic structure formation. $Fe(NO_3)_3$ and $FeCl_3$ decompose to create Fe_2O_3 which later involves in the evolution of Fe_3C. However, $Fe_2(SO_4)_3$ decomposes at temperatures > 530 °C, which is higher than the

decomposition temperature of cellulose and hemicellulose (400–500 °C). Therefore, it limits the reduction reaction of Fe_2O_3 (from $Fe_2(SO_4)_3$) to metal Fe, and subsequently inhibits the formation of graphitic carbon [35]. The (002) band at 26.56° and 26.58° in XRD patterns specifically for the graphitic structure was observed when using $Fe(NO_3)_3$ and $FeCl_3$ but only a broad peak at 24.01° for $Fe_2(SO_4)_3$, indicating the predominance of amorphous carbon. Therefore, $Fe(NO_3)_3$ and $FeCl_3$ are more suitable than $Fe_2(SO_4)_3$ in producing graphitic carbon. Furthermore, since the graphitisation process only occurs around metal Fe ion, the dispersion of iron salts into biomass precursors is crucial. Hunter et al. showed that decreasing the size of a series of biomass precursors (bamboo, almond shell, coconut shell, softwood sawdust, etc.) to 150 μm increased the (002) band intensity in XRD patterns, signalling the increase in stack height of graphite crystals [42]. Decreasing the size of biomass precursors should enhance the penetration of Fe ions into biomass precursors and allow more carbons to be graphitised during heat treatment, and more studies should be conducted to ascertain this.

Heat treatment also controlled the development of graphitic carbon when using iron-containing compounds as observed in cornstalk derived carbon [11] and coconut shell derived carbon [30]. Increasing temperatures significantly increased the intensity of 2D peak in Raman spectroscopy, indicating the development of highly ordered carbon structure [11, 29]. The ratio of intensity of 2D peak compared to G peak (I_{2D}/I_G) was 0.187 at 800 °C, increasing to 0.443 at 900 °C and to 0.547 at 1000 °C [43]. The intensity of D peak also decreased with I_D/I_G decreasing from 1.004 at 800 °C to 0.699 at 1000 °C [43]. The L_c of wood derived carbons increased significantly from 9.3 nm at 850 °C to 30.2 nm at 1200 °C and increased gradually to 46.8 nm at 2000 °C, and D band intensity in Raman spectra also reduced with increasing temperatures indicating the decrease in defects of carbon [41].

The effect of concentration of iron salts on the evolution of graphitic structure in biomass derived carbons was only observed at high amount of iron salts e.g. biomass/iron salts from 1:1 to 1:8 [30, 43]. This is because the graphitising reaction occurs around the iron molecules (Fig. 3b), and low iron concentrations result in low contact and hinder the graphitisation of biomass. Table 1 summarises the characteristics of biomass derived carbon activated with iron salts. Despite the difference in experimental procedures, the peak (002) at $2\theta = 26$–$26.5°$ was observed in all carbons. The interlayer distance of graphite (0.335 nm) indicates the formation of graphitic structure in carbons. Furthermore, the sharp peaks (002) and (100) in XRD and sharp Raman D and G bands also supported the formation of graphitic carbon. This showed that iron-containing compounds are suitable for promoting the formation of graphitic carbon (Table 2).

Surface morphology is an important property of biomass derived carbon materials. Table 3 shows that some graphitic carbon activated with iron compounds had low surface area with mainly mesopores e.g. 348 $m^2\ g^{-1}$ for bamboo [42], 314.73–341.92 $m^2\ g^{-1}$ for chestnut shell [45], 353.42 $m^2\ g^{-1}$ for cotton stalk [45]. The N_2 adsorption–desorption isotherms of these biomass derived graphitic carbons fell into the mixed type I/IV with high N_2 uptakes at low p/p_0 and a large hysteresis at high p/p_0, indicating the development of mesopore structure in these graphitic

Table 1 Carbonaceous structure of biomass derived carbon using X-ray diffraction and Raman spectroscopy

Carbon	Experimental procedures	X-ray diffraction					Raman spectroscopy				Refs.
		2θ (002)°	d_{002} (nm)	L_a (nm)	L_c (nm)	# layers	D band (cm^{-1})	G band (cm^{-1})	2D band (cm^{-1})	I_D/I_G	
Cornstalk	Cornstalk immersed in $K_4[Fe(CN)_6]$ 0.1 M solution for 4 h. Carbonised at 1000 °C in N_2	26.43	0.337	19.27	16.82	50.90	1361	1579	2715	0.71	[11]
	Cornstalk immersed in $K_4[Fe(CN)_6]$ 0.1 M solution for 4 h. Carbonised at 1100 °C in N_2	26.43	0.336	20.25	19.22	58.12	1361	1575	2725	0.62	
	Cornstalk immersed in $K_4[Fe(CN)_6]$ 0.1 M solution for 4 h. Carbonised at 1200 °C in N_2	26.55	0.336	24.58	20.19	61.16	1361	1575	2829	0.29	

(continued)

Table 1 (continued)

Carbon	Experimental procedures	X-ray diffraction					Raman spectroscopy				Refs.
		2θ (002)°	d_{002} (nm)	L_a (nm)	L_c (nm)	# layers	D band (cm^{-1})	G band (cm^{-1})	2D band (cm^{-1})	I_D/I_G	
	Cornstalk immersed in $K_4[Fe(CN)_6]$ 0.3 M solution for 4 h. Carbonised at 1100 °C in N_2	26.57	0.335	26.21	23.752	71.82	1361	1575	2719	0.22	
	Cornstalk immersed in $K_4[Fe(CN)_6]$ 0.05 M solution for 4 h. Carbonised at 1100 °C in N_2	26.42	0.337	14.42	11.37	34.72	1361	1581	2721	0.83	

(continued)

Table 1 (continued)

Carbon	Experimental procedures	X-ray diffraction					Raman spectroscopy				Refs.
		2θ (002)°	d_{002} (nm)	L_a (nm)	L_c (nm)	# layers	D band (cm^{-1})	G band (cm^{-1})	2D band (cm^{-1})	I_D/I_G	
Willow catkins	1.5 g willow catkins mixed with 30 mL 0.1 M $Fe(NO_3)_3$ and 0.4 M KCl. The mixture was carbonised at 900 °C for 2 h in N_2 (PGCN)	26.50	0.3361	ND			ND			0.95	[35]
	1.5 g willow catkins mixed with 30 mL 0.1 M $Fe(NO_3)_3$. The mixture was carbonised at 900 °C for 2 h in N_2	26.56	0.3353	ND			ND			0.94	

(continued)

Table 1 (continued)

Carbon	Experimental procedures	X-ray diffraction					Raman spectroscopy				Refs.
		2θ (002)°	d_{002} (nm)	L_a (nm)	L_c (nm)	# layers	D band (cm^{-1})	G band (cm^{-1})	2D band (cm^{-1})	I_D/I_G	
	1.5 g willow catkins mixed with 30 mL 0.05 M $Fe_2(SO_4)_3$ and 0.4 M KCl. The mixture was carbonised at 900 °C for 2 h in N_2	24.01	ND	ND			ND			0.97	
	1.5 g willow catkins mixed with 30 mL 0.1 M $FeCl_3$ and 0.4 M KCl. The mixture was carbonised at 900 °C for 2 h in N_2	26.58	0.3351	ND			ND			0.77	

(continued)

Table 1 (continued)

Carbon	Experimental procedures	X-ray diffraction					Raman spectroscopy				Refs.
		2θ (002)°	d_{002} (nm)	L_a (nm)	L_c (nm)	# layers	D band (cm^{-1})	G band (cm^{-1})	2D band (cm^{-1})	I_D/I_G	
Bamboo powder	1 g bamboo powder was impregnated in 1 mmol $Fe(NO_3)_3$ and pyrolysed at 850 °C	26.1	ND	ND			ND			ND	[34]
Wood	Commercial wood impregnated with $FeCl_3$ 1.0 M. Pyrolysis in N_2 up to 500 °C (1 °C min^{-1}), and to 850 °C (10 °C min^{-1})	26	0.3395	8.3	9.3	28	~1350	~1580	ND	2.33	[41]

(continued)

Table 1 (continued)

Carbon	Experimental procedures	X-ray diffraction					Raman spectroscopy				Refs.
		2θ (002)°	d_{002} (nm)	L_a (nm)	L_c (nm)	# layers	D band (cm^{-1})	G band (cm^{-1})	2D band (cm^{-1})	I_D/I_G	
	Commercial wood impregnated with $FeCl_3$ 1.0 M. Pyrolysis in N_2 up to 500 °C (1 °C min^{-1}), and to 1000 °C (10 °C min^{-1})	26	0.3391	9.1	9.8	29	~1350	~1580	ND	2.11	

(continued)

Table 1 (continued)

Carbon	Experimental procedures	X-ray diffraction					Raman spectroscopy				Refs.
		2θ (002)°	d_{002} (nm)	L_a (nm)	L_c (nm)	# layers	D band (cm^{-1})	G band (cm^{-1})	2D band (cm^{-1})	I_D/I_G	
	Commercial wood impregnated with $FeCl_3$ 1.0 M. Pyrolysis in N_2 up to 500 °C (1 °C min^{-1}), and to 1200 °C (10 °C min^{-1})	26	0.3357	13.1	30.2	90	~1350	~1580	ND	1.47	

(continued)

Table 1 (continued)

Carbon	Experimental procedures	X-ray diffraction					Raman spectroscopy				Refs.
		2θ (002)°	d_{002} (nm)	L_a (nm)	L_c (nm)	# layers	D band (cm^{-1})	G band (cm^{-1})	2D band (cm^{-1})	I_D/I_G	
	Commercial wood impregnated with $FeCl_3$ 1.0 M. Pyrolysis in N_2 up to 500 °C (1 °C min^{-1}), and to 1400 °C (10 °C min^{-1})	26	0.3356	13.4	45.0	135	~1350	~1580	ND	1.44	
	Commercial wood impregnated with $FeCl_3$ 1.0 M. Pyrolysis in N_2 up to 500 °C (1 °C min^{-1}), and to 1600 °C (10 °C min^{-1})	26	0.3355	19.8	41.7	125	~1350	~1580	ND	0.97	

(continued)

Table 1 (continued)

Carbon	Experimental procedures	X-ray diffraction					Raman spectroscopy				Refs.
		2θ (002)°	d_{002} (nm)	L_a (nm)	L_c (nm)	# layers	D band (cm^{-1})	G band (cm^{-1})	2D band (cm^{-1})	I_D/I_G	
	Commercial wood impregnated with $FeCl_3$ 1.0 M. Pyrolysis in N_2 up to 500 °C (1 °C min^{-1}), and to 2000 °C (10 °C min^{-1})	26	0.3355	40.9	46.8	140	~1350	~1580	ND	0.47	

Note d_{002}: Interlayer distance (nm), L_a: Carbon crystal width (nm), L_c: Carbon crystal height (nm), ND: Not determined/not reported

Table 2 Surface morphology of biomass derived graphitic carbon using iron-containing compounds

Carbon	Preparation method	Surface morphology				Refs.
		S_{BET} ($m^2\ g^{-1}$)	V_{total} ($cm^3\ g^{-1}$)	V_{micro} ($cm^3\ g^{-1}$)	V_{meso} ($cm^3\ g^{-1}$)	
Milled corn stover carbon	Hydrothermal carbonised in $Ni(NO_3)_2$ 5 wt% solution at mass ratio biomass/water 1:10 for 2 h, 275 °C. The hydrochar obtained was activated with $ZnCl_2$ at mass ratio hydrochar/$ZnCl_2$ 1:1 at 450 °C for 2 h	1060	0.4	ND	ND	[44]
Coconut shell carbon	3 g of coconut shell was mixed with 9 g $ZnCl_2$ in 50 mL of $FeCl_3$ 3 M. The mixture was dried and carbonised at 700 °C for 1 h in N_2 (5 °C min^{-1})	1281	0.35	ND	ND	[30]
	3 g of coconut shell was mixed with 9 g $ZnCl_2$ in 50 mL of $FeCl_3$ 3 M. The mixture was dried and carbonised at 800 °C for 1 h in N_2 (5 °C min^{-1})	1519	0.89	ND	ND	
	3 g of coconut shell was mixed with 9 g $ZnCl_2$ in 50 mL of $FeCl_3$ 3 M. The mixture was dried and carbonised at 900 °C for 1 h in N_2 (5 °C min^{-1})	1874	1.21	ND	ND	
	3 g of coconut shell was mixed with 9 g $ZnCl_2$ in 50 mL of $FeCl_3$ 3 M. The mixture was dried and carbonised at 1000 °C for 1 h in N_2 (5 °C min^{-1})	1538	0.93	ND	ND	

(continued)

Table 2 (continued)

Carbon	Preparation method	Surface morphology				Refs.
		S_{BET} ($m^2\ g^{-1}$)	V_{total} ($cm^3\ g^{-1}$)	V_{micro} ($cm^3\ g^{-1}$)	V_{meso} ($cm^3\ g^{-1}$)	
	3 g of coconut shell was mixed with 9 g $ZnCl_2$ in 50 mL of $FeCl_3$ 1 M. The mixture was dried and carbonised at 900 °C for 1 h in N_2 (5 °C min^{-1})	896	0.26	ND	ND	
	3 g of coconut shell was mixed with 9 g $ZnCl_2$ in 50 mL of $FeCl_3$ 5 M. The mixture was dried and carbonised at 900 °C for 1 h in N_2 (5 °C min^{-1})	1668	0.97	ND	ND	
Dried zizania latifolia leaves carbon	Pyrolysed at 500 °C in vacuum. The biochar was activated with NaOH at 750 °C. The AC was impregnated with $Ni(NO_3)_2$ 1 M overnight, and the mixture after dried was carbonised at 800 °C in N_2	1558	0.82	0.55	0.27	[37]

(continued)

Table 2 (continued)

Carbon	Preparation method	Surface morphology				Refs.
		S_{BET} ($m^2\ g^{-1}$)	V_{total} ($cm^3\ g^{-1}$)	V_{micro} ($cm^3\ g^{-1}$)	V_{meso} ($cm^3\ g^{-1}$)	
	Pyrolysed at 500 °C in vacuum. The biochar was activated with NaOH at 750 °C. The AC was impregnated with $Ni(NO_3)_2$ 1 M overnight, and the mixture after dried was carbonised at 850 °C in N_2	1619	0.87	0.56	0.31	
	Pyrolysed at 500 °C in vacuum. The biochar was activated with NaOH at 750 °C. The AC was impregnated with $Ni(NO_3)_2$ 1 M overnight, and the mixture after dried was carbonised at 900 °C in N_2	1622	0.87	0.57	0.3	

(continued)

Table 2 (continued)

Carbon	Preparation method	Surface morphology				Refs.
		S_{BET} ($m^2\ g^{-1}$)	V_{total} ($cm^3\ g^{-1}$)	V_{micro} ($cm^3\ g^{-1}$)	V_{meso} ($cm^3\ g^{-1}$)	
	Pyrolysed at 500 °C in vacuum. The biochar was activated with NaOH at 750 °C. The AC was impregnated with $Ni(NO_3)_2$ 1 M overnight, and the mixture after dried was carbonised at 950 °C in N_2	1461	0.83	0.49	0.34	
	Pyrolysed at 500 °C in vacuum. The biochar was activated with NaOH at 750 °C. The AC was impregnated with $Ni(NO_3)_2$ 1 M overnight, and the mixture after dried was carbonised at 1000 °C in N_2	907	0.64	0.28	0.36	

(continued)

Table 2 (continued)

Carbon	Preparation method	Surface morphology				Refs.
		S_{BET} ($m^2\ g^{-1}$)	V_{total} ($cm^3\ g^{-1}$)	V_{micro} ($cm^3\ g^{-1}$)	V_{meso} ($cm^3\ g^{-1}$)	
Bamboo	Bamboo was milled, sieved through 150 μm sieve, and then mixed with $Fe(NO_3)_3$. The mixture was dried at 70 °C and carbonised at 800 °C in N_2 for 1 h (5 °C min^{-1})	348	0.39	0.10	0.29	[42]
Chestnut shell	Chestnut shell was crushed to particle size < 2 mm, and mixed with $Fe(NO_3)_3$ at ratio 1 g chestnut shell: 0.25 mmol $Fe(NO_3)_3$. Pyrolysed at 800 °C in N_2	326.5	0.33	0.13	0.20	[45]
	Chestnut shell was crushed to particle size < 2 mm, and mixed with $Fe(NO_3)_3$ at ratio 1 g chestnut shell: 0.5 mmol $Fe(NO_3)_3$. Pyrolysed at 800 °C in N_2	314.7	0.33	0.12	0.21	

(continued)

Table 2 (continued)

Carbon	Preparation method	Surface morphology				Refs.
		S_{BET} ($m^2\ g^{-1}$)	V_{total} ($cm^3\ g^{-1}$)	V_{micro} ($cm^3\ g^{-1}$)	V_{meso} ($cm^3\ g^{-1}$)	
	Chestnut shell was crushed to particle size < 2 mm, and mixed with $Fe(NO_3)_3$ at ratio 1 g chestnut shell: 0.75 mmol $Fe(NO_3)_3$. Pyrolysed at 800 °C in N_2	341.9	0.38	0.13	0.25	
	Chestnut shell was crushed to particle size < 2 mm, and mixed with $Fe(NO_3)_3$ at ratio 1 g chestnut shell: 1.0 mmol $Fe(NO_3)_3$. Pyrolysed at 800 °C in N_2	329.1	0.46	0.15	0.31	
Poplar	Poplar was crushed to particle size < 2 mm, and mixed with $Fe(NO_3)_3$ at ratio 1 g poplar: 1.0 mmol $Fe(NO_3)_3$. Pyrolysed at 800 °C in N_2	381.2	0.67	0.05	0.64	[45]

(continued)

Table 2 (continued)

Carbon	Preparation method	Surface morphology				Refs.
		S_{BET} ($m^2\ g^{-1}$)	V_{total} ($cm^3\ g^{-1}$)	V_{micro} ($cm^3\ g^{-1}$)	V_{meso} ($cm^3\ g^{-1}$)	
Cotton stalk	Cotton stalk was crushed to particle size < 2 mm, and mixed with $Fe(NO_3)_3$ at ratio 1 g cotton stalk: 1.0 mmol $Fe(NO_3)_3$. Pyrolysed at 800 °C in N_2	353.4	0.70	0.07	0.63	[45]
Willow catkins	1.5 g willow catkins mixed with 30 mL 0.1 M $Fe(NO_3)_3$ and 0.4 M KCl. The mixture was carbonised at 900 °C for 2 h in N_2	1488.6	1.24	0.33	0.91	[35]
	1.5 g willow catkins mixed with 30 mL 0.1 M $Fe(NO_3)_3$. The mixture was carbonised at 900 °C for 2 h in N_2	449.3	0.58	0.06	0.52	
	1.5 g willow catkins mixed with 30 mL 0.05 M $Fe_2(SO_4)_3$ and 0.4 M KCl. The mixture was carbonised at 900 °C for 2 h in N_2	893.7	0.72	0.20	0.52	

(continued)

Table 2 (continued)

Carbon	Preparation method	Surface morphology				Refs.
		S_{BET} ($m^2\ g^{-1}$)	V_{total} ($cm^3\ g^{-1}$)	V_{micro} ($cm^3\ g^{-1}$)	V_{meso} ($cm^3\ g^{-1}$)	
	1.5 g willow catkins mixed with 30 mL 0.1 M $FeCl_3$ and 0.4 M KCl. The mixture was carbonised at 900 °C for 2 h in N_2	32.4	0.22	0	0.22	
Bamboo carbon	1 g bamboo powder was impregnated in 1 mmol $Fe(NO_3)_3$ and pyrolysed at 850 °C	205.0	0.45	0.01	0.44	[34]
Bamboo powder and melamine carbon	1 g bamboo powder was impregnated in 1 mmol $Fe(NO_3)_3$ and pyrolysed at 850 °C. 1 g of the obtained carbon was mixed with 10 g melamine in 150 mL C_2H_5OH and dried at 50 °C. The mixture was pyrolysed at 850 °C for 2 h in Ar (10 °C min^{-1})	272.7	0.45	0.03	0.43	

(continued)

Table 2 (continued)

Carbon	Preparation method	Surface morphology				Refs.
		S_{BET} ($m^2\ g^{-1}$)	V_{total} ($cm^3\ g^{-1}$)	V_{micro} ($cm^3\ g^{-1}$)	V_{meso} ($cm^3\ g^{-1}$)	
Softwood sawdust carbon	5.0 g softwood sawdust impregnated in 20 mL solution of 0.005 mol of $Fe(NO_3)_3$. Pyrolysis in N_2 at 800 °C for 1 h (5 °C min^{-1})	220	ND			[46]
	5.0 g softwood sawdust impregnated in 20 mL solution of 0.0038 mol of $Fe(NO_3)_3$. Pyrolysis in N_2 at 800 °C for 1 h (5 °C min^{-1})	280	ND			
	5.0 g softwood sawdust impregnated in 20 mL solution of 0.0025 mol of $Fe(NO_3)_3$. Pyrolysis in N_2 at 800 °C for 1 h (5 °C min^{-1})	270	ND			
	5.0 g softwood sawdust impregnated in 20 mL solution of 0.0013 mol of $Fe(NO_3)_3$. Pyrolysis in N_2 at 800 °C for 1 h (5 °C min^{-1})	340	ND			

(continued)

Table 2 (continued)

Carbon	Preparation method	Surface morphology				Refs.
		S_{BET} ($m^2\ g^{-1}$)	V_{total} ($cm^3\ g^{-1}$)	V_{micro} ($cm^3\ g^{-1}$)	V_{meso} ($cm^3\ g^{-1}$)	
Sugarcane bagasse carbon	5 g of sugarcane bagasse impregnated in 20 mL solution containing 0.005 mol $Fe(NO_3)_3$. Pyrolysed at 800 °C in a vacuum muffle furnace for 1 h (5 °C min^{-1})	311	0.45	ND		[43]

ND: Not detected

Table 3 Surface morphology of biomass derived graphitic carbon using alkaline/alkaline earth compounds

Carbon	Preparation method	Surface morphology				Refs
		S_{BET} ($m^2\ g^{-1}$)	V_{total} ($cm^3\ g^{-1}$)	V_{micro} ($cm^3\ g^{-1}$)	V_{meso} ($cm^3\ g^{-1}$)	
Tissue paper carbon	Tissue paper was mixed with KOH as mass ratio tissue paper: KOH = 1: 1 in aqueous solution and dried at 100 °C. Heat treated at 900 °C for 1 h in Ar	1397	ND	ND	ND	[47]
	Tissue paper was mixed with KOH as mass ratio tissue paper: KOH = 1: 2 in aqueous solution and dried at 100 °C. Heat treated at 900 °C for 1 h in Ar	1684	ND	ND	ND	
Pomelo peel	5 g pomelo peel was pyrolysed at 700 °C in N_2 for 1 h. Biochar was mixed with KOH in a mass ratio biochar/KOH 1:4. Carbonised at 700 °C in N_2 for 3 h (8 °C min^{-1})	1064	0.58	ND		[48]
	5 g pomelo peel was pyrolysed at 700 °C in N_2 for 1 h. Biochar was mixed with KOH in a mass ratio biochar/ΛKOH 1:4. Carbonised at 800 °C in N_2 for 3 h (8 °C min^{-1})	1525	0.80	ND		

(continued)

Table 3 (continued)

Carbon	Preparation method	Surface morphology				Refs
		S_{BET} ($m^2\ g^{-1}$)	V_{total} ($cm^3\ g^{-1}$)	V_{micro} ($cm^3\ g^{-1}$)	V_{meso} ($cm^3\ g^{-1}$)	
	5 g pomelo peel was pyrolysed at 700 °C in N_2 for 1 h. Biochar was mixed with KOH in a mass ratio biochar/KOH 1:4. Carbonised at 900 °C in N_2 for 3 h (8 °C min^{-1})	2167	0.98	0.78	0.20	
Camphor leaf carbon	In situ self-catalysing $CaCO_3$. Activated with KOH at 700 °C in N_2 for 1 h (2 °C min^{-1})	2532.9	1.35	0.65	0.7	[12]
	In situ self-catalysing $CaCO_3$. Activated with KOH at 800 °C in N_2 for 1 h	2751	1.26	0.81	0.45	
	In situ self-catalysing $CaCO_3$. Activated with KOH at 900 °C in N_2 for 1 h	2794	1.44	0.7	0.74	
	In situ self-catalysing $CaCO_3$. Activated with KOH at 1000 °C in N_2 for 1 h	1973.2	1.83	0.28	1.55	
Lotus leaf carbon	In situ self-catalysing $CaCO_3$. Pyrolysed at 950 °C in N_2 for 4 h (2 °C min^{-1})	247.41	0.19	0.06	0.13	[13]
	In situ self-catalysing $CaCO_3$. Pyrolysed at 1000 °C in N_2 for 4 h (2 °C min^{-1})	659.01	0.36	0.2	0.16	
	In situ self-catalysing $CaCO_3$. Pyrolysed at 1100 °C in N_2 for 4 h (2 °C min^{-1})	548.71	0.36	0.13	0.23	

ND: Not determined/not reported

carbons. According to the mechanism of graphitic carbon formation using transition metal compounds, the graphitic carbon formed around the metal particles, and these metal particles were removed when washing with HCl solution to reveal the mesoporous structures [34]. The increase in iron compound loadings resulted in an increase in mesoporous structure e.g. from 0.1993 to 0.3094 $cm^3\ g^{-1}$ with a mass ratio of chestnut shell/$Fe(NO_3)_3$ increasing from 1:0.06 to 1:0.24 while the micropore volumes remained almost constant (0.1191–0.1467 $cm^3\ g^{-1}$) for chestnut shell graphitic carbon [45]. The choice of iron salts also influenced the morphology of carbons. Replacing $Fe(NO_3)_3$ by $Fe_2(SO_4)_3$ and $FeCl_3$ decreased the surface area and the mesopore volume of willow catkins graphitic carbon e.g. from 1488.6 $m^2\ g^{-1}$ to 893.69 $m^2\ g^{-1}$ and 32.37 $m^2\ g^{-1}$ [35], and from 0.91 $cm^3\ g^{-1}$ to 0.52 and 0.22 $cm^3\ g^{-1}$ respectively [35].

The graphitisation procedure does not support the formation of micropore. This explains a low micropore content and surface area in the graphitic carbon when using transitional metal compounds. BET N_2 surface area of wood graphitic carbon activated with $FeCl_3$ was 200.0 $m^2\ g^{-1}$ after being heat treated at 850 °C and decreased gradually to 155.4 $mm^2\ g^{-1}$ at 1000 °C and 34.5 $m^2\ g^{-1}$ at 2000 °C [41]. Sugarcane bagasse derived carbon also had the BET surface area of 311 $m^2\ g^{-1}$ and total pore volume of 0.45 $cm^3\ g^{-1}$ after being activated with $Fe(NO_3)_3$ at 800 °C [43]. However, using other activating agents such as $ZnCl_2$ in coconut shell [30] or NaOH in zizania latifolia leaves [37], a high surface area of 896–1622 $m^2\ g^{-1}$ was achieved. Therefore, a more comprehensive method to simultaneously achieve both high surface area/porosity and graphitic structure should be considered and implemented, which allows a full potential application of biomass carbon in supercapacitors.

Nickel nitrate $Ni(NO_3)_2$ is also effectively used as an activating agent for forming graphitic carbon. α-D-glucose and starch mixed with $Ni(NO_3)_2$ at ratios of 0.4–0.8 mmol Ni^{2+} to 1 g of D-glucose/starch were carbonised at 900–1000 °C under N_2 atmosphere for 3 h (3 °C min^{-1}) to obtain the glucose derived graphitic carbon (Fig. 3d) [49]. The interlayer distance d_{002} in a range 0.34–0.342 nm with L_c of 9.1–9.8 nm from XRD analysis indicates that there are approximately 27–29 layers of carbon stacking together. Beech wood graphitic carbon was achieved from the carbonisation of impregnated beech wood ($15 \times 15 \times 75\ mm^3$) in $Ni(NO_3)_2$ solution 4 M for 2 h at 600–1600 °C under N_2 (5 °C min^{-1}, 30 min) [38]. The (002) peak at 26.6° appeared at a temperature of 1000 °C and intensified up to 1600 °C, which is evident for the composition of the graphite structure in solid carbon product [38]. This is because nickel acts as the substrate for carbon to deposit to form hexagonal carbon rings. However, this process only occurs at temperatures >950 °C for the formation of graphitic structure [37], slightly higher than the temperature required for α-D-glucose and starch (900 °C) [49] due to a more complex structure of cellulose and lignin in beech wood.

Both iron and nickel demonstrated catalytic activities towards generating graphitic carbon structure in biomass derived carbon, but there is evidence that iron is more effective than nickel in creating a higher ordered carbon structure [49, 50]. The first evidence is the interlayer distance between the layers of carbon. The d_{002} of starch graphitic carbon decreased from 0.342 to 0.339 nm when increasing Fe concentration

from 0.4 to 0.8 mmol g^{-1} [49], and decreased even further to 0.336 in pine wood carbons [50]. Furthermore, the d_{002} remained constant at 0.341–0.342 nm in both pine wood carbons and starch carbons when using nickel as the catalyst regardless of concentrations. This indicates that the turbostratic structure presents among the graphite stack when using nickel as the catalyst. The second factor is the growth of crystal height L_c. L_c increased from 5.8 to 7 nm with increasing concentration from 0.4 to 0.8 mmol g^{-1} [49] and increased to 12.3 nm with increasing concentration to 5 mmol g^{-1} [50] while L_c only varied at 9.1–10 nm for both the pine wood and starch graphitic carbon. Furthermore, increasing the heat treatment in the presence of iron catalyst fostered the growth of crystal height from 12.3 to 16.3 nm as observed in pine wood graphitic carbon. Therefore, iron metal salts demonstrated supreme catalytic activity compared to nickel in forming graphitic carbon from biomass.

The main reason for the difference between catalytic activity of Fe and Ni compounds is due to the formation enthalpy of carbides. During the heat treatment, iron reacted with carbon atoms to form iron carbides Fe_3C. The formation enthalpy of carbides is in the order of Fe–C < Ni-C [51], so the Fe_3C could be formed at lower temperatures compared to Ni-C. When the heat treatment continues, the carbide is exuded into metal Fe and C, which is a crucial step in the formation of layers of carbon hexagonal rings, and iron carbide requires lower temperatures to decompose compared to nickel carbides. Therefore, iron is more effective than nickel to form the graphitic carbon.

The evolvement of biomass into graphitic carbon was also explored in other studies such as mangosteen peel graphitic carbon using $CoCl_2$ [52]. However, these studies are limited in number and the application of these carbons in supercapacitors needs to be further explored.

2.2.2 Alkaline and Alkaline Earth Metal Compounds

Alkali and alkaline earth metal compounds perform as catalysts for the formation of graphitic carbon from biomass precursors during carbonisation. In heat treatment, alkali and alkaline earth metal compounds turn into metal oxides, and carbon molecules in biomass deposit on the alkali and alkaline earth metal oxides in heat treatment to form ordered graphitic carbon structure.

Biomass contains alkaline and alkaline earth metals in ash such as Ca, K, and Na [53], and the ash contents generally decrease from the leave sub-groups to the root sub-groups, namely leaves > branches > barks > pruning > cones > stems > roots. Temperature is an important factor controlling the graphitic structure formation in biomass derived carbon as these compounds catalyse the formation of graphitic carbon at high temperatures, depending upon the type of compounds e.g. > 900 °C for $CaCO_3$ (Fig. 4a) [12, 13]. At low temperatures e.g. 700–850 °C, the garlic skin containing $CaCO_3$ cannot transform into the graphitic structure [54] as shown by a broad (002) peak at 24° in the XRD pattern of the garlic skin carbon and the overlapping D and G bands.

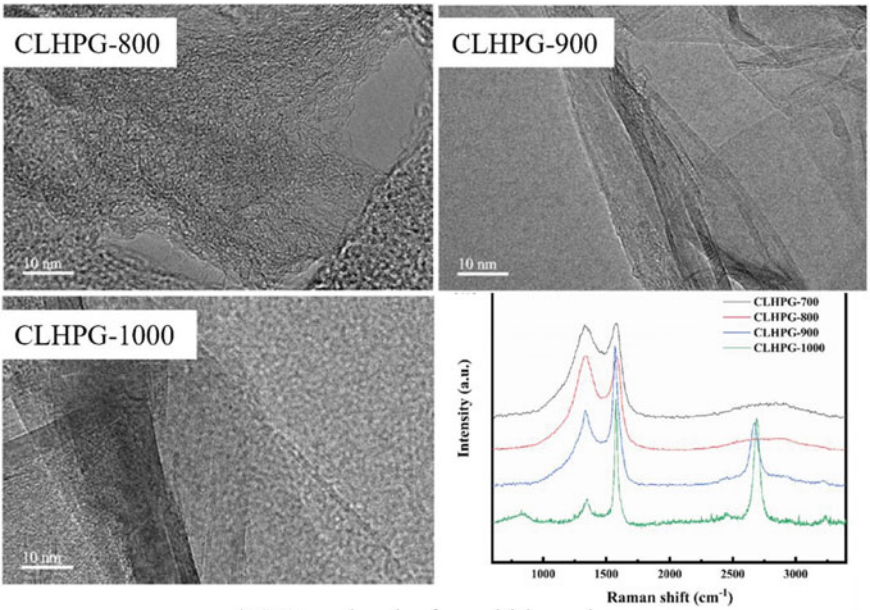

(A) Camphor leaf graphitic carbon

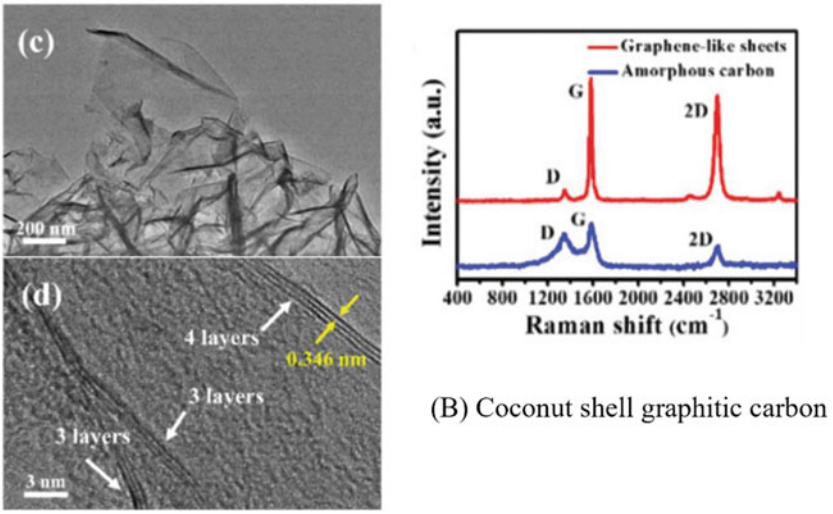

(B) Coconut shell graphitic carbon

Fig. 4 Graphitic carbon from biomass: **a** Camphor leaf graphitic carbon, self-activated with CaO at 700 °C (CLHPG-700) to 1000 °C (CLHPG-1000 °C) [12], **b** Coconut shell graphitic carbon at 900 °C with K_2CO_3 [55], **c** Pomelo carbon activated with KOH at 700 °C (PAC-700), 800 °C (PAC-800) and 900 °C (PAC-900) [56], and **d** Tissue paper carbon activated with KOH at mass ratio biomass/KOH 1:1 (GCS-1) and 1:2 (GCS-2) at 900 °C [47]

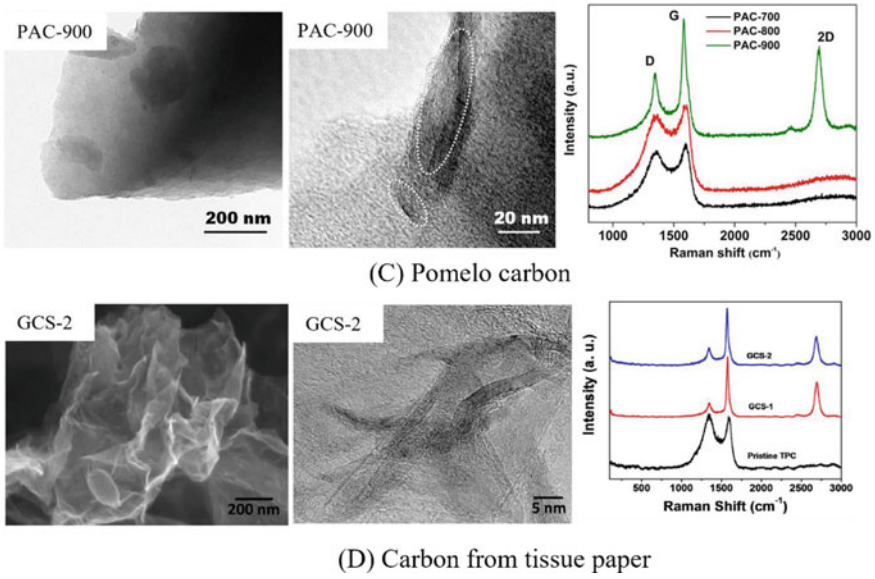

Fig. 4 (continued)

However, the temperature to activate the compounds in ash content for K_2CO_3 is around 600 °C [55]. At this temperatures, some K_2CO_3 reacted with the carbons in the coconut shell (Eq. 7):

$$K_2CO_3 + C \rightarrow 2K + 3CO \tag{7}$$

to create metallic K and to remove C sp^3 portion [57]. At higher temperatures i.e. $\geq$ 900 °C, the remaining K_2CO_3 became liquid and allowed the free movement of small carbon crystals in which the metal K (produced from the above reaction) substituted the hydrogen atoms on the edge of small carbon crystals to create carbons with free electron pairs. These carbon atoms replace hydrogen atoms in other carbon crystals through nucleophilic substitution mechanism to form new C–C bonds and expand the carbon crystals [55]. This is the crucial step for the formation of graphitic carbon in biomass (Fig. 4b). However, pre-treatment step at 400 °C is important to remove the tar from coconut shell because high molecular weight compounds inhibited the catalytic effect of K_2CO_3. The coconut shell carbon obtained at 900 °C showed a specific capacitance of 91.15 F g^{-1} at 0.2 A g^{-1} in organic electrolyte (1 M $TEMABF_4$/PC). K_2CO_3 has been used as an activating agent to enhance the surface area and morphology of carbon materials, but the impact of tar on the formation of graphene sheet in the presence of K_2CO_3 is not well known. Therefore, more studies should be carried out to understand this phenomenon. Since Na_2CO_3 has the same melting point as K_2CO_3, it can be used to obtain graphene carbon sheets [55].

The using of NaOH in graphitising crayfish shell and heavy fraction of bio-oil derived from thr pyrolysis process was conducted [58]. The graphitic structure was only observed at temperatures ≥ 900 °C, evident from the emergence of (002) band at 25.8° in XRD pattern and the G band at 1582 cm^{-1} and 2D band at 2689 cm^{-1} in Raman spectra. This implicates that NaOH needs to go through the liquid phase for the graphitic structure formation to occur.

Higher temperatures ≥ 900 °C are required when using alkaline and alkaline earth metal compounds (Fig. 4) compared to graphitic carbon activated with transitional metal salts (800 °C). For KOH, it can either promote the formation graphitic structure from raw materials e.g. tissue paper (Fig. 4d) [47] or coconut shell biochar (obtained at a pyrolysis temperature of 500 °C) [59], pomelo peel biochar (obtained at 700 °C) (Fig. 4c) [56]. Agricultural waste biomass does not have high planarity and stacking, which does not benefit the growth of the graphitic structure upon heat treatment. Alkaline and alkaline earth metals go through the melting phase which incentivises the creation of planarity and stacking structure through the free movement of carbon, and subsequently the development of graphitic carbon. On the other hand, iron salts transform into metallic iron at lower temperatures (500–600 °C) and form carbides Fe_3C which decompose into graphitic carbon at temperatures 800–900 °C. In both cases, the porosity of the precursors affects the diffusion of metal compounds and distributes these compounds evenly in biomass precursors, fostering the graphitising procedure.

Using alkaline activating agents such as KOH and K_2CO_3 is more effective than transitional-metal compounds in improving the surface area and morphology due to a combined reaction between alkaline activating agents and carbon. In detail, the activation reactions of KOH and K_2CO_3 involved many steps to create micropores and increase the surface area. The activation mechanism of KOH and K_2CO_3 is involved the reaction with carbon in biomass to form alkaline and alkaline earth metals to release H_2 and CO. The evolution of these gases created the micropores in the carbon. Furthermore, the consumption of carbon during these reactions also creates the pores in the carbon and enlarges the micropore structure. The gas released from biomass could also react with carbon through secondary reactions to form micropores. This explains why the surface area of carbons obtained from alkaline and alkaline earth activation are normally higher than graphitic carbon obtained from transition metal compounds. Table 3 shows that carbons activated with alkaline activating agents can easily increase the surface area to 1064–2794 $m^2\ g^{-1}$, which is substantially higher than those activated by transitional metal compounds (Table 2).

3 Performance of Biomass Derived Graphitic Carbon as Electrode Material in Supercapacitors

Section 2 illustrates the properties of carbons obtained through different routes. A challenge is the lack of studies focusing on graphitic carbon in supercapacitors. A significant number of research showed amorphous carbons derived from biomass with broad (002) and (100) bands in XRD and overlapping D and G bands in Raman

spectroscopy, and this created a discrepancy in literature and should be avoided. Because using transitional metal compounds and alkali/alkaline earth compounds directly influence carbonaceous structure and the surface area/morphology, this section will try to elucidate the relationship between these properties and the performance of supercapacitors.

3.1 Carbons Activated with Transitional Metal Compounds

The graphitic structure in biomass derived carbon is deemed to enhance the performance of supercapacitors by improving the electric conductivity of the electrodes. For example, coconut shell carbon (directly activated with both $FeCl_3$ and $ZnCl_2$ at 900 °C (PGNS-3–900)) demonstrated a specific capacitance of 268 F g^{-1} at 1 A g^{-1}, much higher than that obtained from the coconut shell activated only with $ZnCl_2$ at 900 °C (AC-900) (210 F g^{-1}). The higher specific capacitance in this case was due to the significant ordered graphitic structure in PGNS-3–900 even though it had a lower surface area 1874 m^2 g^{-1} than AC-900 (2007 m^2 g^{-1}). This also improved the energy density of PGNS-3–900 carbon in KOH 6 M (9.58 Wh kg^{-1} at a power density of 500 W kg^{-1} or 54.7 Wh kg^{-1} at 10,000 W kg^{-1} in tetraethylammonium tetrafluoroborate in propylene carbonate 1 M), which is compatible with commercial supercapacitors [30]. However, the graphitic structure alone does not guarantee the high performance of supercapacitors. It was found [11] that the combination of graphitic structure with the porosity of the carbons are substantial for the performance of supercapacitors:

- The specific capacitance decreased due to the reduction of total pore volume to 0.41 cm^3 g^{-1} at 1200 °C (PGCS-1–1200) compared to 0.48 cm^3 g^{-1} at 1100 °C (PGCS-1–1100) although the graphitic structure of cornstalk carbon was enhanced. The cornstalk carbon at 1100 °C PGCS-1–1100, on the other hand, demonstrated a higher specific capacitance of 213 F g^{-1} at 1 A g^{-1} in the solution of KOH 6 M [11]. The high conductivity of the carbon electrode is due to the high conductivity of graphitic carbon coupling with the porosity structure of 0.48 cm^3 g^{-1} and surface area of 540 m^2 g^{-1}. The capacitance of the symmetric two electrode cell was 63.5 F g^{-1} in KOH 6 M and 47.3 F g^{-1} in tetraethylammonium tetrafluoroborate in propylene carbonate. Also, the energy density was 9.4 Wh kg^{-1} at the specific power of 10,500 W kg^{-1}.
- The specific capacitance of beech wood graphitic carbon also decreased from 133 F g^{-1} for carbon treated at 1000 °C to 24 F g^{-1} for carbon treated at 1600 °C (KOH 1 M, current density 20 mA g^{-1}) although the activation with $FeCl_3$ at 1000, 1300, 1600 °C is developed of graphitic carbon structure with increasing temperatures [36]. This could be assigned to the decline of pore volume of carbon from 0.24 cm^3 g^{-1} to 0.15 cm^3 g^{-1} at higher temperatures. Higher temperatures supported the rearrangement of carbon into graphitic layers as the expense of the removal of pore structures, which limited the access of electrolyte ions to graphitic carbon and reduced the capacitance. This phenomenon was also observed in the

coconut shell graphitic carbon where the carbon obtained at 1000 °C had the BET SA 1538 $m^2\ g^{-1}$ compared to 1874 $m^2\ g^{-1}$ of carbon treated at 900 °C, which resulted in a lower specific capacitance of 237 F g^{-1} compared to 268 F g^{-1} at 1 A g^{-1} [30].

- Chitosan carbon was activated with $FeCl_3$ in the mixture of acid boron to create a chitosan carbon incorporated with both boron and nitrogen [60]. The chitosan carbon treated with $FeCl_3$ showed a specific capacitance of 207 F g^{-1} at current density of 1 A g^{-1} and decreased to 167 F g^{-1} at 20 A g^{-1} in KOH 6 M electrolyte, showing 80.7% capacitance retention with increasing current density. However, when incorporating the boron into the carbon structure and increasing the surface area and porosity using $ZnCl_2$, the specific capacitance increased to 313 F g^{-1} at 1 A g^{-1} and decreased to 257 F g^{-1} at 20 A g^{-1} (82.1% capacitance retention with increasing current density). This indicates that while graphitic structure in carbon is important to increase the performance of the supercapacitor, improving carbon morphology and functional groups also benefits supercapacitors. Graphitic structure is crucial for the conductivity of carbon electrode, but not the dominant factor influencing supercapacitor performance.

The results from cornstalk graphitic carbon [11], beech wood graphitic carbon [36] and chitosan carbon [60] showed that the graphitic structure is crucial because it determines the electric conductivity of electrode in supercapacitors, and increasing temperatures when using metal catalysts could lead to more ordered carbon structure. However, these results also demonstrated that the development of graphitic structure using transitional-metal compounds also hindered the development of carbon morphology and resulted in lower performances. Some studies tried to overcome the obstacle by using metal catalysts that simultaneously activated the surface morphology and develop graphitic structure. For example, the filter paper was carbonised with $K_3[Fe(C_2O_4)_3]$ at 750 °C to enhance both graphitic structure and porosity [61]. The three-electrode system showed a significant specific capacitance of 313.0 F g^{-1} at 1 A g^{-1} in KOH 6 M and maintained a high capacitance of 240.5 F g^{-1} at 30 A g^{-1} of the obtained carbon CS@CF-KFe (76.8% retention). The graphitic carbon had the surface area of 1515.6 $m^2\ g^{-1}$ with pore volume of 0.56 $cm^3\ g^{-1}$, and the high ordered carbonaceous crystals were distributed evenly in the carbon structure besides the amorphous carbon, which supported the electrical conductivity. The $K_3[Fe(C_2O_4)_3]$ simplified the preparation process because it acted as an activating agent to improve the surface morphology and a graphitising agent to develop the graphitic structure simultaneously. The dual effects of $K_3[Fe(C_2O_4)_3]$ are similar to the use of potassium ferrate K_2FeO_4 [39]. The surface area of bamboo carbon after being treated with K_2FeO_4 increased to 1732 $m^2\ g^{-1}$ and 0.97 $cm^3\ g^{-1}$ pore volume with the specific capacitance 171.4 F g^{-1} at 1.0 A g^{-1} decreasing to 115.0 F g^{-1} at 20 A g^{-1} (67% retention rate). This high specific capacitance stemmed from the cooperation of both the graphitic structure and morphology in this bamboo carbon.

3.2 Carbons Activated with Alkaline/Alkaline Earth Compounds

The alkaline and alkaline earth metals normally promoted the formation of large surface areas and morphology in graphitic carbon to improve the specific capacitance of supercapacitors. Furthermore, the graphitic structure that developed in the biomass derived carbon also supported the electron conductivity and enhanced the performance of supercapacitors:

- Camphor leaf carbon prepared at 900 °C demonstrated the specific capacitance up to 397 F g^{-1} at 1 A g^{-1} and even 293 F g^{-1} at 20 A g^{-1} in KOH 6 M, showing 74% capacitance retention [12]. The superior performance of this graphitic carbon was assigned to the high conductivity of the graphitic structure. The first factor that influenced the performance of camphor leaf graphitic carbon was the surface morphology. The carbon was prepared at 700–1000 °C, the surface areas remained constant at 2532–2794 m^2 g^{-1} at 700–900 °C but declined to 1973 m^2 g^{-1} at 1000 °C. Furthermore, amorphous carbon was dominant at 700–800 °C, and only at 900 °C it started to emerge under the catalytic activity of CaO. Therefore, the temperature at 900 °C was optimal for both surface morphology and carbonaceous structure, so it supported the highest specific capacitance of 397 F g^{-1}. The sample also presented the energy density of 54.2 Wh kg^{-1} at 522 W kg^{-1}, and was maintained at 32.9 Wh kg^{-1} at 9461 W kg^{-1} [12].
- Pomelo peel graphitic carbon MPC-900 that was activated with KOH was used as a framework to incorporate SnO_2 particles on [48], and the electrodes in a symmetric supercapacitor was fabricated using carbon MPC-900-SnO_2 material with tetraethylammonium tetrafluoroborate in propylene carbonate as the electrolyte. The supercapacitor showed a high energy density of 50.9 Wh kg^{-1} at a power density of 4,400 W kg^{-1}, and the energy density was still retained at 25.3 Wh kg^{-1} when increasing the power density to 25,300 W kg^{-1}. The high performance of this carbon-SnO_2 material should be attributed to the graphitic structure of carbon after being treated with KOH at 900 °C to create a partial graphitic structure (indicating through a narrow D band with $I_D/I_G = 0.42$ and a strong 2D band at 2695 cm^{-1}). The high surface area of pomelo peel carbon also contributed to the performance of the supercapacitor with BET N_2 SA of 2167 cm^3 g^{-1} and mesopore volume of 0.20 cm^3 g^{-1}.

Compared to role of the graphitic structure and surface morphology of biomass derived carbon, some studies showed that the surface morphology was more crucial than the carbonaceous structure in determining the supercapacitor performance, which is similar to carbons obtained from transitional metal compound activation. The graphitic carbon CSB-800 derived from crayfish shell and bio-oil at 800 °C showed the highest capacitance of 351 F g^{-1} was compared to 225 F g^{-1} of CSB-900 (obtained at 900 °C) at 1 A g^{-1} [58]. The carbon CSB-900 which was treated at 900 °C in NaOH had higher ordered carbon structure in expense of the surface morphology. The BET SA of CSB-900 reduced to 2053 m^2 g^{-1} and 1.57 cm^3 g^{-1}

total pore volume compared to 3095 $m^2\ g^{-1}$ and 1.66 $cm^3\ g^{-1}$ of CSB-800, and this resulted in a substantial lower capacitance [58]. Some studies such as the garlic skin carbon obtained at 800 °C with a large range of amorphous carbon but demonstrated the specific capacitance up to 315 F g^{-1} even at 50 A g^{-1} due to the surface area of 2818 $m^2\ g^{-1}$ and 1.33 $cm^3\ g^{-1}$ although it was amorphous carbon (a broadened peak around 24.4° in XRD pattern) [54].

This showed that a balance between the carbonaceous structure and the surface morphology are important for the performance of the supercapacitor. The use of metal compounds to create the graphitic structure in biomass derived carbon results in low surface area and pore volume, and this highly influenced the performance of the supercapacitor. The sawdust carbon PGC-4–850 that was activated with $K_2C_2O_4$ and $FeCl_3$ to enhance porosity and develop the graphitic structure demonstrated the capacitance of 219.6 F g^{-1} at at 0.5 A g^{-1}, which is significantly higher than sawdust graphitic carbon GC-850 treated with $FeCl_3$ of 21.6 F g^{-1} at 0.5 A g^{-1} (KOH 6 M) [62]. Cyclic voltammetry of PGC-4–850 also had a larger curved area compared to PC-850 (activated only with $K_2C_2O_4$), indicating that the graphitic structure in carbon is crucial for the electric conductivity and improved the capacitance [62].

In conclusion, the results from these studies confirmed the important role of graphitic carbon in the supercapacitor performance. This also highlighted that a synergy of the graphitic carbon with surface area and in some cases, functional groups would be beneficial for the performance of supercapacitors. Therefore, more robust methods are required to develop the morphology of the obtained carbon besides having a highly ordered graphitic structure.

4 Conclusions

In this chapter, the characteristics of biomass derived graphitic carbon were discussed. Graphitic carbons were prepared from biomass using transitional metal compounds and alkaline and alkaline earth metal compounds. Biomass derived carbon activated with transitional metal compounds had a highly ordered carbon structure but in the expense of the surface area and morphology, which resulted in low specific capacitances. Using alkaline and alkaline earth metal compounds to develop graphitic structure in biomass carbon required higher temperatures than transitional metal compounds but resulted in a higher surface area and morphology for the diffusion of electrolytes in carbon. In this chapter, it was also shown that the graphitic structure benefits the performance of supercapacitors through the enhancement of electric conductivity, and the graphitic structure should act in conjunction with other properties such as surface morphology to deliver the desirable performance of supercapacitors. More studies specifically on graphitic carbon and performance of supercapacitors should be conducted to enhance the understanding on applying graphitic carbon in supercapacitors.

Acknowledgements The authors gratefully acknowledge the financial support from the Royal Academy of Engineering (Grant No: FF\1920\1\45) United Kingdom.

References

1. Davies DM, Verde MG, Mnyshenko O et al (2019) Combined economic and technological evaluation of battery energy storage for grid applications. Nat Energy 4:42–50. https://doi.org/10.1038/s41560-018-0290-1
2. Jiang J, Zhang Y, Nie P et al (2018) Progress of nanostructured electrode materials for supercapacitors. Adv Sustain Syst 2:1700110. https://doi.org/10.1002/adsu.201700110
3. González A, Goikolea E, Barrena JA, Mysyk R (2016) Review on supercapacitors: technologies and materials. Renew Sustain Energy Rev 58:1189–1206. https://doi.org/10.1016/j.rser.2015.12.249
4. Kumar NA, Baek J-B (2015) Doped graphene supercapacitors. Nanotechnology 26:492001. https://doi.org/10.1088/0957-4484/26/49/492001
5. Chen Q, Tan X, Liu Y et al (2020) Biomass-derived porous graphitic carbon materials for energy and environmental applications. J Mater Chem A 8:5773–5811. https://doi.org/10.1039/C9TA11618D
6. Wissler M (2006) Graphite and carbon powders for electrochemical applications. J Power Sources 156:142–150. https://doi.org/10.1016/j.jpowsour.2006.02.064
7. Salanne M, Rotenberg B, Naoi K et al (2016) Efficient storage mechanisms for building better supercapacitors. Nat Energy 1:16070. https://doi.org/10.1038/nenergy.2016.70
8. Kim H-C, Huh S (2020) Porous carbon-based supercapacitors directly derived from metal-organic frameworks. Materials (Basel) 13:4215. https://doi.org/10.3390/ma13184215
9. Gopalakrishnan A, Badhulika S (2020) Effect of self-doped heteroatoms on the performance of biomass-derived carbon for supercapacitor applications. J Power Sources 480:228830. https://doi.org/10.1016/j.jpowsour.2020.228830
10. Hu L, Zhai T, Li H, Wang Y (2019) Redox-mediator-enhanced electrochemical capacitors: recent advances and future perspectives. Chemsuschem 12:1118–1132. https://doi.org/10.1002/cssc.201802450
11. Wang L, Mu G, Tian C et al (2013) Porous graphitic carbon nanosheets derived from cornstalk biomass for advanced supercapacitors. Chemsuschem 6:880–889. https://doi.org/10.1002/cssc.201200990
12. Liu H, Chen W, Zhang R et al (2021) Bioinspired in situ self-catalyzing strategy towards graphene nanosheets with hierarchical structure derived from biomass for advanced supercapacitors. Appl Surf Sci 566:150692. https://doi.org/10.1016/j.apsusc.2021.150692
13. Liu H, Chen W, Zhang R et al (2021) Biomass-derived CaO in situ catalyzing approach towards hierarchical porous graphene nanosheets for high-rate performance supercapacitors. J Alloys Compd 884:161127. https://doi.org/10.1016/j.jallcom.2021.161127
14. Tian W, Gao Q, VahidMohammadi A et al (2021) Liquid-phase exfoliation of layered biochars into multifunctional heteroatom (Fe, N, S) co-doped graphene-like carbon nanosheets. Chem Eng J 420:127601. https://doi.org/10.1016/j.cej.2020.127601
15. Yan D, Liu L, Wang X et al (2022) Biomass-derived activated carbon nanoarchitectonics with hibiscus flowers for high-performance supercapacitor electrode applications. Chem Eng Technol 45:649–657. https://doi.org/10.1002/ceat.202100585
16. Jalalah M, Rudra S, Aljafari B et al (2022) Novel porous heteroatom-doped biomass activated carbon nanoflakes for efficient solid-state symmetric supercapacitor devices. J Taiwan Inst Chem Eng 132:104148. https://doi.org/10.1016/j.jtice.2021.11.015
17. Meng D, Hu Y, Jing Y et al (2022) One-step carbonization strategy of freeze-dried chitosan to prepare nitrogen-oxygen co-doped porous carbon supercapacitors with ultra-large specific surface area. Fuel 320:124002. https://doi.org/10.1016/j.fuel.2022.124002

18. Yakaboylu GA, Jiang C, Yumak T et al (2021) Engineered hierarchical porous carbons for supercapacitor applications through chemical pretreatment and activation of biomass precursors. Renew Energy 163:276–287. https://doi.org/10.1016/j.renene.2020.08.092
19. Wan L, Li N, Li X et al (2019) One-step synthesis of N, S-codoped porous graphitic carbon derived from lotus leaves for high-performance supercapacitors. Ionics (Kiel) 25:4891–4903. https://doi.org/10.1007/s11581-019-03105-2
20. Wang C, Sui G, Guo D et al (2021) Enhanced supercapacitive and hydrogen evolution reaction performance using hierarchically porous carbon derived from Viburnum Sargenti fruits. Ionics (Kiel) 27:1723–1731. https://doi.org/10.1007/s11581-021-03929-x
21. Dasgupta K, Sathiyamoorthy D (2003) Disordered carbon–its preparation, structure, and characterisation. Mater Sci Technol 19:995–1002. https://doi.org/10.1179/026708303225004693
22. Johnson CA, Patrick JW, Mark Thomas K (1986) Characterization of coal chars by Raman spectroscopy, X-ray diffraction and reflectance measurements. Fuel 65:1284–1290. https://doi.org/10.1016/0016-2361(86)90243-7
23. Dong S, Alvarez P, Paterson N et al (2009) Study on the effect of heat treatment and gasification on the carbon structure of coal chars and metallurgical cokes using fourier transform raman spectroscopy. Energy Fuels 23:1651–1661. https://doi.org/10.1021/ef800961g
24. Johnson CA, Thomas KM (1987) The thermal history of char samples taken from a gasifier. Fuel 66:17–21. https://doi.org/10.1016/0016-2361(87)90205-5
25. Baek J, Shin H-S, Chung DC, Kim B-J (2017) Studies on the correlation between nanostructure and pore development of polymeric precursor-based activated hard carbons: II. Transmission electron microscopy and Raman spectroscopy studies. J Ind Eng Chem 54:324–331. https://doi.org/10.1016/j.jiec.2017.06.007
26. Zickler GA, Smarsly B, Gierlinger N, et al (2006) A reconsideration of the relationship between the crystallite size La of carbons determined by X-ray diffraction and Raman spectroscopy. Carbon N Y 44:3239–3246. https://doi.org/10.1016/j.carbon.2006.06.029
27. Ishimaru K, Hata T, Bronsveld P et al (2007) Spectroscopic analysis of carbonization behavior of wood, cellulose and lignin. J Mater Sci 42:122–129. https://doi.org/10.1007/s10853-006-1042-3
28. Kumar M, Gupta RC, Sharma T (1993) X-ray diffraction studies of Acacia and Eucalyptus wood chars. J Mater Sci 28:805–810. https://doi.org/10.1007/bf01151261
29. Lee Y-J (2004) The second order Raman spectroscopy in carbon crystallinity. J Nucl Mater 325:174–179. https://doi.org/10.1016/j.jnucmat.2003.12.005
30. Sun L, Tian C, Li M et al (2013) From coconut shell to porous graphene-like nanosheets for high-power supercapacitors. J Mater Chem A 1:6462–6470
31. Verma D, Goh KL (2019) Chapter 11 - Functionalized Graphene-Based Nanocomposites for Energy Applications. In: Functionalized Graphene Nanocomposites and their Derivatives. Elsevier, pp 219–243
32. Inagaki Michio KF (2014) 2. Fundamental Science of Carbon Materials. Mater. Sci. Eng. Carbon Fundam. (2nd Ed.
33. Haridas AK, Jeon J, Heo J et al (2019) In-Situ Construction of Iron Sulfide Nanoparticle Loaded Graphitic Carbon Capsules from Waste Biomass for Sustainable Lithium-Ion Storage. ACS Sustain Chem Eng 7:6870–6879. https://doi.org/10.1021/acssuschemeng.8b06346
34. Xia S, Guo W, Cai N et al (2021) Synthesis and application in oxygen reduction reaction of N-doping porous graphitic carbon from biomass waste. Fuel Process Technol 224:107028. https://doi.org/10.1016/j.fuproc.2021.107028
35. Zhang X, Zhang K, Li H et al (2018) Synthesis of porous graphitic carbon from biomass by one-step method and its role in the electrode for supercapacitor. J Appl Electrochem 48:415–426. https://doi.org/10.1007/s10800-018-1170-x
36. Gutiérrez-Pardo A, Ramírez-Rico J, Cabezas-Rodríguez R, Martínez-Fernández J (2015) Effect of catalytic graphitization on the electrochemical behavior of wood derived carbons for use in supercapacitors. J Power Sources 278:18–26. https://doi.org/10.1016/j.jpowsour.2014.12.030

37. Liu Y, Liu Q, Gu J et al (2013) Highly porous graphitic materials prepared by catalytic graphitization. Carbon N Y 64:132–140. https://doi.org/10.1016/j.carbon.2013.07.044
38. Gutiérrez-Pardo A, Ramírez-Rico J, de Arellano-López AR, Martínez-Fernández J (2014) Characterization of porous graphitic monoliths from pyrolyzed wood. J Mater Sci 49:7688–7696. https://doi.org/10.1007/s10853-014-8477-8
39. Gong Y, Li D, Luo C et al (2017) Highly porous graphitic biomass carbon as advanced electrode materials for supercapacitors. Green Chem 19:4132–4140. https://doi.org/10.1039/C7GC01681F
40. Khalid B, Meng Q, Akram R, Cao B (2016) Effects of KOH activation on surface area, porosity and desalination performance of coconut carbon electrodes. Desalin Water Treat 57:2195–2202. https://doi.org/10.1080/19443994.2014.979448
41. Gomez-Martin A, Martinez-Fernandez J, Ruttert M et al (2018) Iron-Catalyzed Graphitic Carbon Materials from Biomass Resources as Anodes for Lithium-Ion Batteries. Chemsuschem 11:2776–2787. https://doi.org/10.1002/cssc.201800831
42. Hunter RD, Davies J, Hérou SJA et al (2021) Milling as a route to porous graphitic carbons from biomass. Philos Trans R Soc A Math Phys Eng Sci 379. https://doi.org/10.1098/rsta.2020.0336
43. Gai L, Li J, Wang Q et al (2021) Evolution of biomass to porous graphite carbon by catalytic graphitization. J Environ Chem Eng 9:106678. https://doi.org/10.1016/j.jece.2021.106678
44. Shell KM, Amar VS, Bobb JA et al (2022) Graphitized Biocarbon Derived from Hydrothermally Liquefied Low-Ash Corn Stover. Ind Eng Chem Res 61:392–402. https://doi.org/10.1021/acs.iecr.1c03820
45. Xia S, Cai N, Wu J et al (2020) Synthesis and formation mechanism of biomass-based mesoporous graphitic carbon. Fuel Process Technol 209:106543. https://doi.org/10.1016/j.fuproc.2020.106543
46. Thompson E, Danks AE, Bourgeois L, Schnepp Z (2015) Iron-catalyzed graphitization of biomass. Green Chem 17:551–556. https://doi.org/10.1039/C4GC01673D
47. Hari Mohan E, Nanaji K, Anandan S et al (2019) One-step induced porous graphitic carbon sheets as supercapacitor electrode material with improved rate capability. Mater Lett 236:205–209. https://doi.org/10.1016/j.matlet.2018.10.044
48. Sun F, Wang L, Peng Y, et al (2018) Converting biomass waste into microporous carbon with simultaneously high surface area and carbon purity as advanced electrochemical energy storage materials. Appl Surf Sci 436:486–494. https://doi.org/10.1016/j.apsusc.2017.12.067
49. Sevilla M, Sanchís C, Valdés-Solís T et al (2008) Direct synthesis of graphitic carbon nanostructures from saccharides and their use as electrocatalytic supports. Carbon N Y 46:931–939. https://doi.org/10.1016/j.carbon.2008.02.019
50. Sevilla M, Sanchís C, Valdés-Solís T et al (2007) Synthesis of Graphitic Carbon Nanostructures from Sawdust and Their Application as Electrocatalyst Supports. J Phys Chem C 111:9749–9756. https://doi.org/10.1021/jp072246x
51. Wang ZH, Choi CJ, Kim BK et al (2003) Characterization and magnetic properties of carbon-coated cobalt nanocapsules synthesized by the chemical vapor-condensation process. Carbon N Y 41:1751–1758. https://doi.org/10.1016/S0008-6223(03)00127-1
52. Zha Z, Zhang Z, Xiang P et al (2021) Porous graphitic carbon from mangosteen peel as efficient electrocatalyst in microbial fuel cells. Sci Total Environ 764:142918. https://doi.org/10.1016/j.scitotenv.2020.142918
53. Vassilev SV, Vassileva CG, Song Y-C et al (2017) Ash contents and ash-forming elements of biomass and their significance for solid biofuel combustion. Fuel 208:377–409. https://doi.org/10.1016/j.fuel.2017.07.036
54. Zhang Q, Han K, Li S et al (2018) Synthesis of garlic skin-derived 3D hierarchical porous carbon for high-performance supercapacitors. Nanoscale 10:2427–2437. https://doi.org/10.1039/C7NR07158B
55. Xia J, Zhang N, Chong S et al (2018) Three-dimensional porous graphene-like sheets synthesized from biocarbon via low-temperature graphitization for a supercapacitor. Green Chem 20:694–700. https://doi.org/10.1039/C7GC03426A

56. Sun F, Gao J, Zhu Y et al (2017) A high performance lithium ion capacitor achieved by the integration of a Sn-C anode and a biomass-derived microporous activated carbon cathode. Sci Rep 7:40990. https://doi.org/10.1038/srep40990
57. Hayashi J, Horikawa T, Takeda I, et al (2002) Preparing activated carbon from various nutshells by chemical activation with K2CO3. Carbon N Y 40:2381–2386. https://doi.org/10.1016/S0008-6223(02)00118-5
58. Luo Z, Lin N, Sun M et al (2021) Synthesis of 3D-interconnected hierarchical porous carbon from heavy fraction of bio-oil using crayfish shell as the biological template for high-performance supercapacitors. Carbon N Y 173:910–917. https://doi.org/10.1016/j.carbon.2020.11.083
59. Govind Raj K, Joy PA (2017) Role of localized graphitization on the electrical and magnetic properties of activated carbon. J Am Ceram Soc 100:5151–5161. https://doi.org/10.1111/jace.15035
60. Sun L, Fu Y, Tian C et al (2014) Isolated Boron and Nitrogen Sites on Porous Graphitic Carbon Synthesized from Nitrogen-Containing Chitosan for Supercapacitors. Chemsuschem 7:1637–1646. https://doi.org/10.1002/cssc.201400048
61. Zhang X, Li H, Qin B et al (2019) Direct synthesis of porous graphitic carbon sheets grafted on carbon fibers for high-performance supercapacitors. J Mater Chem A 7:3298–3306. https://doi.org/10.1039/C8TA11844B
62. Zhang X, Li H, Zhang K et al (2018) Strategy for Preparing Porous Graphitic Carbon for Supercapacitor: Balance on Porous Structure and Graphitization Degree. J Electrochem Soc 165:A2084–A2092. https://doi.org/10.1149/2.0491910jes

Graphene and Graphene-Like Materials Derived from Biomass for Supercapacitor Applications

Ankita Subhrasmita Gadtya, Debajani Tripathy, and Srikanta Moharana

Abstract Graphene, a sp^2-hybridized 2D atomic crystal, is one of the most important materials of the twenty-first century. Graphene and graphene-based materials have garnered a lot of interest from researchers because of their potential as superior electrode materials for energy storage systems on account of their high electrical and thermal conductivity, low resistance to corrosion, and high surface area. In the last ten years, there has been a huge increase in research into graphene-like carbon compounds made from biomass that can be used in new ways to store energy. Graphene-like structures can be made from biomass at a low cost and with almost no carbon emissions. This is a promising step towards a more sustainable energy future. Furthermore, due to their sustainability and good performance for high-power and short-term energy needs, they are perfect candidates for carbon-based supercapacitor devices, which are seen as the key to the future electrification of green transportation. Graphene is thus used in a variety of applications, such as polymer composites, energy storage, fuel cells, and biomedical applications. Bio-waste products are considered to be a superior source of carbon generation. However, bio-waste materials are numerous, and adequate disposal methods are required. This chapter has focused on the production of graphene using various bio-sources such as rice husks, paper cups, hemp, chitosan, banana peels, and peanuts, along with its applications as a suitable electrode material in the field of supercapacitors.

Keywords Graphene · Graphene oxide · Biomass · Supercapacitors · Energy storage

A. S. Gadtya · D. Tripathy · S. Moharana (✉)
School of Applied Sciences, Centurion University of Technology and Management, Odisha, India
e-mail: srikanta.moharana@cutm.ac.in

S. K. Tiwari et al. (eds.), *Biomass-Based Functional Carbon Nanostructures for Supercapacitors*, Green Energy and Technology,
https://doi.org/10.1007/978-981-99-0996-4_8

1 Introduction

Graphene is one of the most researched materials because it is a single-atom-thick sheet of sp2-hybridized carbon atoms arranged in a honeycomb lattice [1, 2]. Its exceptional features, including high specific surface area and good electrical and thermal conductivity, have piqued the interest of researchers since its discovery in the 1990s [3] and 2004 [4]. Graphene has several potential uses, including field emission [5, 6], gas sensors and biosensors [7, 8], field effect transistors [9, 10], transparent electrodes [11, 12], energy storage and conversion [13, 14], and many others. It is a two-dimensional atomic crystal with extraordinary properties such as electron mobility of approximately 2.5×10^5 cm^2 V^{-1} S^{-1} at room temperature, a Young's modulus of 1 Tpa, a surface area of approximately 2675 m2/g, and an inherent strength of approximately 130 GPa [15, 16]. Most notably, chemically modified graphene has proven to be a low-cost, mechanically and electrically stable material. Also, the templates protect the active sites of the catalysts by stopping the nanosized metals from randomly moving off the surface. This makes the final product made with graphene composites more stable, even in harsh conditions [17, 18]. Graphene materials have many possible uses because of their unique two-dimensional (2D) structure and unique properties. Because of its heterogeneous electronic structure, graphene has potential properties including flexibility, optical transparency, high mobility, and fluorescence over a broad range of wavelengths, which are desirable features for optoelectronic devices [19, 20]. Moreover, graphene-like carbons have been explored in the field of catalysis. Consequently, expanding the range of graphene's potential applications is still a possibility [21]. The graphene like carbon is to be used in a wide range of situations; it is important to figure out how to make the graphene-like material, especially the feedstock or precursors from which the graphene-like material can be made [22, 23]. Graphite, which is made up of graphene sheets, has been used in the first few attempts to obtain single-layer and few-layer graphene by micromechanical cleavage with very low production efficiency [24, 25]. Methane, ethylene, and acetylene are only a few of the gaseous precursors that have been employed to create graphene-like materials in future studies. Moreover, traditional carbonaceous feedstocks have environmental and health consequences [26–28].

Biomass is an alternate precursor for the fabrication of graphene and graphene-like carbon, also known as G-carbons [29–31]. For activated carbon, biomass is plentiful and very inexpensive. Corn husks [32], sunflower seeds [33], cotton stalks [34], rice hulls [35], grape seeds, and even feathers [32–37] have all been processed for this purpose by scientists. Also, knowing the characteristics of the biomass helps choose the best synthetic parameters, such as reaction temperature, biomass scale, carrier gas, chemical agents, and gas flow rate. In this chapter, we discuss graphene synthesis techniques and its potential use as an electrode material in supercapacitors, as well as its production from a variety of bio-sources such as rice husks, paper cups, hemp, chitosan, banana peels, and peanuts.

2 Synthesis Techniques of Graphene

There are numerous methods for synthesizing graphene, including chemical reduction, chemical vapor deposition (CVD), chemical exfoliation, mechanical cleaving exfoliation, chemical synthesis, microwave synthesis, nanotube unzipping, etc.

2.1 Chemical Reduction

The chemical reduction process is a traditional method for the production of graphene from graphene oxide (GO). Different reducing agents used are $NaBH_4$, phenyl hydrazine, hydroxyl amine, glucose, hydroquinone, ascorbic acid, etc. Hummer's method was used to prepare GO first in this process. A homogeneous aqueous solution was obtained by first diffusing 5 mg of GO into 50 ml of deionized water, and then subjecting the mixture to ultrasonication treatment. The mixture solution was separated into two beakers, and 10 mL of GO solution was transferred to one of them. In that beaker, 100 μL of 1 mM metal salts and 10mg $NaBH_4$ were added and stirred for 1 h. The product was collected after centrifugation. Then the product was washed with a 3% HCl solution and deionized water for 3–5 times. When the washing was done, the metal solution was concentrated and used as a catalyst to reduce the GO. Finally, graphene, or reduced GO, was obtained [38].

2.2 Electrochemical Reduction

For large scale production of graphene, the electrochemical reduction method is used. The GO solution can be sonicated by suspending it in water to get the nanoplatelets of GO. Then, from there, the oxygen can be removed by a suitable agent like hydrazine. The solution is then deposited on the surface to form single-or double-layered GO. By reducing the GO, the resultant after being reduced thermally or chemically via the solvo-thermal method yields graphene films. The chemically modified graphene prepared by colloidal suspensions is ornamented with small organic molecules. Graphene functionalizes with the help of poly (m-phenylenevinylene-co-2,5-dioctoxy-p-phenylene-vinylene) (PmPV), poly (tert-butyl acrylate) [39].

2.3 Chemical Vapor Deposition (CVD)

In the CVD process, a substrate will be dispersed at high temperature onto the thermally disintegrated precursors. CVD-produced graphene is a polycrystalline film

whose size may differ from micrometer- to millimeter-sized domains. The depositions will occur on different precursors (which may be solid, liquid, crystalline, or gaseous), thin films, etc. In the deposition process of graphene, various transition metal substrates are used, like Ni, Pd, Cu, Ru, etc. But most of the time, Cu and Ni have been best suited for CVD growth. The low-cost precursor camphor was used to synthesize graphene on the nickel foils. Camphor was first heated to 180 °Cand then evaporated. After that, it was pyrolyzed in another CVD furnace chamber at 700 to 850 °C by using argon gas, which acts as the carrier. When the temperature was decreased to room temperature, a few layers of graphene sheets were formed on the nickel foil. Similarly, in the thermal CVD technique, 1−2 nm thick graphene sheets were produced that were grown on Ni substrates. Here, the precursor used was a gas mixture of H_2 and CH_4 in a 92:8 ratio. A total gas pressure of 80 Torr was activated by the DC discharge. Then the graphitic films, which were only a few nanometers thick, were found to be separated by ridges. The ridge formed as a result of the difference in thermal expansion coefficients of Ni and graphite. Then, due to the nucleation process, graphene was formed on the surface of Ni [40].

2.4 Chemical Exfoliation

Exfoliation is basically the peeling-off process. Graphene can be prepared from a highly pure graphite sheet when the Van der Waals force, which is weak and can be broken, is released. The exfoliation method is used to weaken the bonds between the graphite sheets by using chemical and mechanical energy. In this method, a highly oriented pyrolytic graphite (HOPG) sheet of 1 mm thickness has been taken, and a dry etching process has been started in the plasma of oxygen to make 5 m-deep mesas. The mixture was then placed in a photoresist and heated until the mesas adhered to it. Then, with the help of Scotch tape, the graphite sheet was peeled off. Inside the photoresist, a few thin flakes were still stuck, which were released in acetone and taken to a silicon substrate. After some time, it was discovered that the substrate contained single and some layers of graphene sheets. This process of preparing graphene is very reliable. Apart from this, the exfoliation in the liquid phase has a slightly different approach. The exfoliation of GO nanosheets was done through the ultrasonication method in the aqueous solution. The produced films were reduced when placed inside the hydrazine and hydrated at 100 °C for 24 h. It can be known as “partially reduced” exfoliated nanographite oxide sheets, as the product formed wasn’t completely reduced. Pure graphite in N-methyl pyrrolidone was also used for dispersion and exfoliation. The yield was 1–12 wt% of monolayer graphene [41].

2.5 Thermal Decomposition

One unique method of preparation of graphene is the thermal decomposition of silicon on the surface of a single crystal of 6H-SiC. When the hydrogen etched surface of 6H-SiC was heated at a temperature of 1250 to 1450 °C for 5–10 minutes, graphene sheets of 1–3 layers were formed on the surface. In another method of thermal decomposition, films of graphene were prepared on a nickel thin film coated SiC substrate at a temperature of 750 °C. This method aids in the production of a large amount of graphene, so it was advantageous to the researchers [42].

2.6 Synthesis of Graphene on Gold

This method used gold foil that was 25 m thick. Before using the gold foil, it was first annealed for 20 min in a hydrogen flame. After annealing, the gold foil was placed inside a quartz chamber, in which argon gas was passed for 5 min. The gold foil was heated to a temperature of 975 °C under the flow of argon and hydrogen. At that time, methane gas was passed inside the chamber for 10 min. After that, the heating was stopped, and the chamber was cooled down. When the flow of methane was stopped, it was seen that layers of graphene had developed on the gold foil. Then polydimethylsiloxane (PDMS) was applied. With the help of the transfer printing method, graphene was transferred from the gold foil to the dielectric substrate. The gold layer was then etched by gold etchant, and after the completion of etching (as shown in Fig. 1), the graphene layer formed on the surface of PDMS was applied to 100 nm SiO_2 coated silicon wafers. From there, when they peeled the PDMS surface, graphene was released on the surface of the dielectric [43].

3 Graphene Based Materials as Applications of Super Capacitor Electrode Materials

Recently, there has been a lot of interest in increasing the demand for energy, and electronic devices are in high demand. There are more portable electronic devices, hybrid electric vehicles (HEVs), and other vehicles on the market presently. The high amount of energy that a supercapacitor can store also makes it an ultracapacitor or an electrochemical capacitor [44]. These supercapacitors have different characteristics, including higher power density, long cycle life performance, low maintenance, fast dynamics of charge propagation, and high charge and discharge rates [45]. Supercapacitors are used in memory backup systems, industrial power and energy management, consumer electronics, etc. The performance of a supercapacitor is based on low self-discharging, safe operation, low cost, excellent cycle ability, which is more than 100 times that of batteries, and greater power density, which is higher than batteries. A

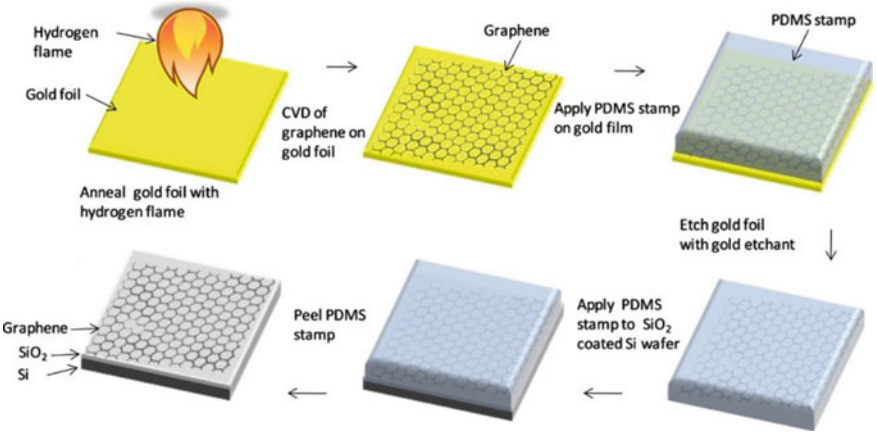

Fig. 1 Schematic representation of the steps of the deposition and transfer processes of graphene growth on gold film. Reproduce with permission from the reference [43]. Copyright 2011, Applied Physics Letter

supercapacitor is classified into two types; electric double layer capacitors (EDLCs) and pseudocapacitors. For better power delivery and energy storage capacity, the pore size and surface area of the electrode should be carefully considered in the EDLCs [46–49]. The graphene has a honeycomb network with various dimensionalities and carbon allotropes. These graphene-based materials have a conducting network to support the redox reactions of transition metal oxides, oxides, and conducting polymers. The nano-hybrid electrode with graphene and nanoparticles shows excellent electrochemical performance due to the synergistic effect of the graphene layers. Graphene's high surface area, higher electrical conductivity, greater flexibility, and other properties make it an excellent electrode material for supercapacitors. The prepared graphene films are being used as a stretchable electrode. Apart from the flexibility and stretch ability; the graphene films also promote the easy fabrication of supercapacitor devices [50, 51]. Due to the lack of yield in high-quality graphene, the higher specific conductance value of graphene isn't of any use. But the graphene can be prepared by the chemical vapor deposition (CVD) method, and these nanosheets have a capacitance value of 0.076 Fcm^{-2} in the H_2SO_4 solution. So, the capacitance of the graphene-based supercapacitor was found to be 1.49×10^4 F. Ruoff et al. have reported a method of preparing graphene-polymer composites through an exfoliation method [52]. The percolation threshold of the polystyrene-graphene composite was found to be 0.1 vol%. The specific conductance value was determined to be 191 f/g when KOH electrolyte was used as an electrode in ultracapacitors. Yang et al. have synthesized hydrothermally reduced graphene-MnO_2 composites. In this experiment, the researchers have found the specific capacitance value of the HRG-MnO_2 composite reaches 211.5 F/g at the potential scan rate of 2 mVs^{-1}. The composite shows 75% capacitance retention after 1000 cycles of charge/discharge in 1 M Na_2SO_4 electrolyte, which indicates a good potential for the supercapacitor

and power system [53]. Similarly, for the electrochemical pseudocapacitor materials, $Ni(OH)_2$ nanoplates were grown on graphene. This electrode shows a high specific capacitance value of 1335 F/g^{-1} at a 2.8 A/g charge discharge rate. It also shows an improved value for power density and energy density. All of these improved properties point to promising applications in supercapacitors for higher power sources [54]. Jian and his co-workers developed a flexible graphene paper by adding carbon black nanoparticles between the graphene sheets for better electrochemical performance. The incorporation of carbon black in the graphene sheet gave it an open structure for charge storage and ion diffusion channels. The specific capacitance of the pillared graphene paper was found to be 138 F/g^{-1} and 83.2 F/g^{-1} in the aqueous electrolyte and organic electrolyte, respectively, at a scan rate of 10 mVs^{-1}. The capacitance loss was 3.85% after 2000 cycles at a current of $10Ag^{-1}$. The ability to maintain high conductivity and a large surface area provides high-performance energy-storage devices with better energy and power densities [55]. Murugan and his co-workers [56] have synthesized graphene nanosheets and polyaniline nanocomposites for energy storage devices. The composite with 50 wt% graphene showed EDLC and pseudocapacitance with a specific capacitance of 408 F/g^{-1}. This composite can be used in energy storage and conversion applications along with microelectronics. Duan et al. prepared functionalized graphene hydrogels (FGHs)-based high performance supercapacitors. The FGHs are used as the electrodes in supercapacitors with an excellent specific capacitance value of 441 F/g in 1 M H_2SO_4 aqueous solution, whose value is higher than that of the unfunctionalized graphene hydrogels, i.e., 211 F/g [57]. The FGHs show an excellent 80% capacitance rate at 20 A/g along with 86% retention over 10,000 cycles. All these data can prove that these electrodes can show greater properties if they are used in the supercapacitor [58]. A.N. Grace and colleagues used the solvothermal method to create a series of vanadium pentoxide-doped graphene and investigated its applications in supercapacitors. In this work, they have found out that the V_2O_5 doped graphene showed a maximum specific capacitance of 1032.6 F/g^{-1} at a 1 mVs^{-1} scan rate. It also provides greater cyclic stability with an energy density of 185.86 Wh/Kg and a power density of 37.20 W/Kg^{-1} (Fig. 2). The graphene moieties show a fast and smooth electronic transfer between the V_2O_5 materials, which leads to their prominent use in the supercapacitor as the electrode. In another experiment, the potential use of graphene-based material in the field of energy storage applications, especially in supercapacitors and the green energy field has been described [59]. The graphene substrate's synergistic effect has been improved due to its high surface area and conductivity.

4 Different Bioprecusors

Rice Husk

The rice husk is the outer layer of rice kernels. The graphene can now be prepared from rice husks and can also be used as an activator for the preparation of activated

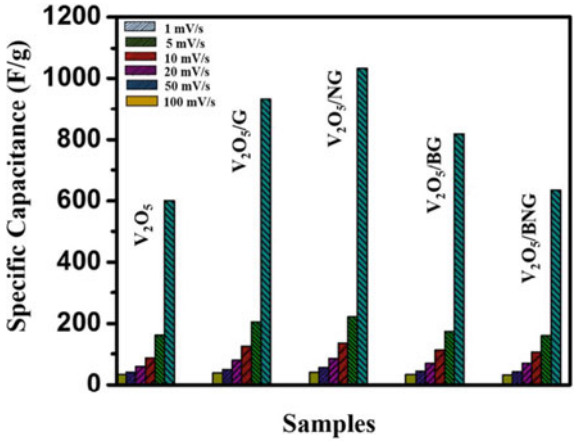

Fig. 2 Graphical illustration of specific capacitance at different scan rates for a variety of compositions of the samples. Reproduce with permission from the reference [58]. Copyright 2018, Elsevier

carbon. Rice husk has a major silicon concentration, so it is also used to prepare silica and its derivatives and is also used for nanocarbon preparation. The preparation of graphene from rice husk was described by Hiroyuki et al. by taking rice husk and adding KOH to it [60]. The mixture was taken for calcination at 1123K. When the activation of KOH starts, a 3D network of large volumetric capacitance can be achieved. The KOH helps in removing the silica impurities. The prepared graphene has greater porosity and an active edge, along with hydrogen stability. Singh et al. reported on another method of producing graphene from rice husk. They activated the rice husk with KOH before annealing it at 9000 °C. The resultant graphene has a few layers of graphene with agglomerations of silica particles. In another method, rice husk was taken to form rice husk carbon (RHC) and rice husk graphene quantum dots (RH-GQDs). First, 5.0 gms of rice husk were taken, washed with deionized (DI) water, and grinded in order to make RHC. The powder was then taken inside a tube furnace at 700 ºC for 2 h, and nitrogen gas was passed through it. The carbon and silica-containing rice husk ash (RHA) was then collected. That RHA was reacted with an excess of NaOH for 2 hours at 900 ºC. When the reaction was completed, it was again washed with DI water, and RHC was obtained, which was dried at 80 ºC for 12 h. In another experiment to make GQD from rice husk, 50 mg of RHC was mixed with a 10 ml solution of H2SO4 and 3 ml of DI water. The mixture was then taken for ultrasonication for 5 hours. In that solution, 20 mL of HNO_3 was added and again taken for ultrasonication for 10 hours. After that, the solution was properly washed and again diffused in 30 ml of DI water with 1.0 M NaOH aqueous solution, which was then transferred to an autoclave for 10 h at 200 °C. Then it was cooled down to room temperature and filtered where RH-GQD was finally obtained [61–63].

Hemp

The cannabis plant is the source of hemp bast fiber. This plant is full of fiber, which is used to make different products like ropes, clothes, oils, etc. Researchers recently

created a graphene-like material from it. Hemp bast fiber was taken for activation and then carbonization for the hydrothermal product of carbon nanosheets. Firstly, 3.0 gms of hemp straw were taken and dispersed in 50 ml of H_2SO_4, which was then placed inside a stainless-steel autoclave for 24 h at 180 ºC. Then it was cooled down to room temperature, resulting in a carbonaceous solid known as biochar. The biochar was then filtered, thoroughly washed with distilled water, and taken for drying. After completion of the drying of the biochar, it was chemically activated by adding KOH. The mixture of biochar and KOH was taken into an agate mortar and grinded properly. Then the mixture was heated at around 750 ºC for 1 h by passing argon gas. When the heating was done, the mixture was washed again with 10% HCl and distilled water, and finally, the carbon sheets were prepared by drying it in the oven for 12 h at 100 ºC [64].

Paper Cups

The paper cups are made of lignin and hemicelluloses from wood. The graphene can be prepared from disposable paper cups by using iron as a catalyst. Firstly, the paper cups were passed through active treatment by using KOH; where K^+ ions get adsorbed into paper pulp. The Fe^{2+} ions in the catalyst iron are exchanged for K^+ ions. Then, a layer of Fe_3C is formed through the graphitization process. The C-atom disperses as the temperature drops, forming a multi-layered structure of graphene or iron. The preparation of graphene from disposable paper cups is economically beneficial. Researchers have gained interest in the production of graphene sheets from paper cups as it helps in the manufacturing of high yield energy-consuming products. The produced graphene is obtained by removing the Fe template and is used in Li-ion batteries [65].

Chitosan

Chitosan is a nitrogen containing polysaccharide biopolymer that is derived from the outer skeleton of crustacean animals like shellfish, crab, lobster, etc. Chitosan is able to produce graphene, which is used as an electrocatalyst. In its structure, nitrogen atoms are present inside the sheet of graphene, which increases the electronic bonds and makes it a semiconductor. Chitosan is produced by the deacetylation of chitin. By heating the chitosan to 1300 °C, a series of hard carbons (HC) were produced. Then it was taken for thermal treatment by passing argon gas at a 5 °C per min heating rate. The annealing temperature was chosen as a good compromise between the concentration of defects, porosity, and d-spacing. The hard carbon chitosan (HC-chs) was synthesized by multiple surface and bulk techniques. However, the chitosan was heated at 800 °C by flowing argon gas through it. The resultant graphene was obtained in the form of a thin film. Activated carbon can also be prepared by chitosan through the carbonization process (as shown in Fig. 3) at high temperatures and then activation by different chemical reagents like H_3PO_4. This activated carbon is being used in the supercapacitor for energy storage purposes [66].

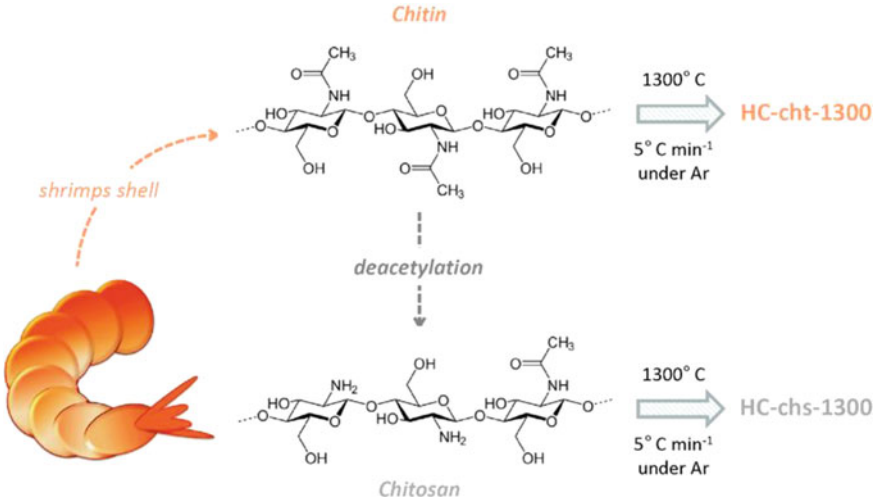

Fig. 3 Schematic diagram of the preparation of hard carbons from chitin and chitosan. Reproduce with permission from the Reference [66]. Copyright 2019, American Chemical Society

Coal

Coal is one of the most affordable energy resources, but it is non-renewable in nature. Coal structures are made up of very small, nanometer-sized crystalline carbon with defects that are linked by aliphatic amorphous carbon. Graphene quantum dots (GQDs) are being synthesized from mostly bituminous coal, anthracite, and coke, which are used in energy storage devices. Ye and his co-workers [67] have reported about the synthesis technique of GQDs (Fig. 4) from these three types of coal. GQDs were derived from bituminous coal in their experiment by first sonicating the bituminous coal and dispersing it in a solution of H_2SO_4 and HNO_3. When sonication was completed, it was heated at 1200 ℃ for 24 h. Finally, we will get the b-GQD, where we can find hexagonal lattices and many crystalline domains having dots that are linked by the amorphous carbon. GQDs can also be synthesized from anthracite and coke using the same method as bituminous coal.

In another experiment, synthesized humic acid (HA) powders from lignite coal were prepared, which have properties like GO sheets. Firstly, the lignite coal was placed in an aqueous solution of leonardite. Then the solution mixture was acidified to produce HA powder [68]. The particles produced are useful in the application of obtaining specific GO particles. Vijapur et al. have taken sub-bituminous coal to prepare graphene by the pyrolysis method [69]. At first, the sub-bituminous coal was heated without oxygen, which helped the coal get decomposed into hydrocarbon gases that act as thermal precursors. Then the derived carbon compound was adsorbed with the help of copper, and it produced a hybrid carbon film. That carbon film was then graphitized to produce graphene films in the presence of hydrogen. The produced

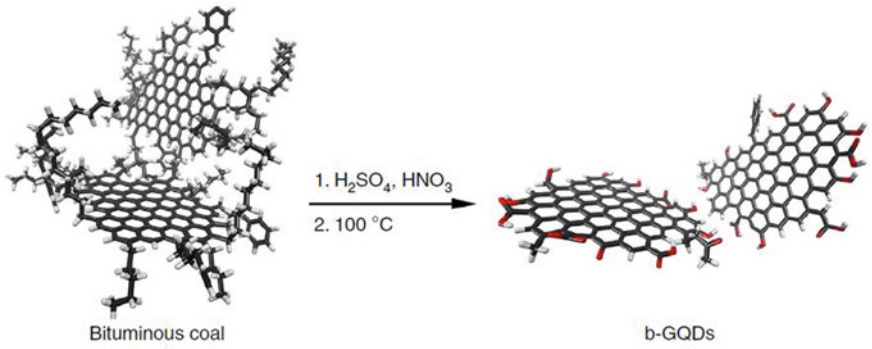

Fig. 4 Schematic illustration of the synthesis of b-GQDs. Oxygenated sites are shown in red. Reproduce with permission from the Reference [67]. Copyright 2013, Nature Publishing Group

graphene films can be useful in the application of solar cells, light emitting diodes, etc.

Bougainvillea

The bougainvillea flower is a member of the Nyctaginaceae family that originated in South America but is now found in almost every country. It is filled with natural antioxidants having phenolic groups like caffeic acid, chlorogenic acid, tannins, carbohydrates, etc. For the preparation of graphene from bougainvillea, dead flowers (Fig. 5) were taken and washed properly. The washed flowers were dried in the oven at 80 °C. The flowers were crushed into a fine powder after drying. 10 g of the crushed powder was pyrolyzed in a pure quartz crucible at 600 and 800 ºC for 5 h by passing argon. From that, perforated graphene was obtained [70].

Mahendran et al. collected fresh bougainvillea and separated 20 g of petals, which were washed with demineralized water to remove the impurities. After complete washing, the petals were boiled in 200 ml of demineralized water for 30 min at 95 °C. The boiled petals were then filtered and stored at −4 ºC in a refrigerator. The GO powder was also synthesized by Hummer's method. 100 mg of GO powder was taken,

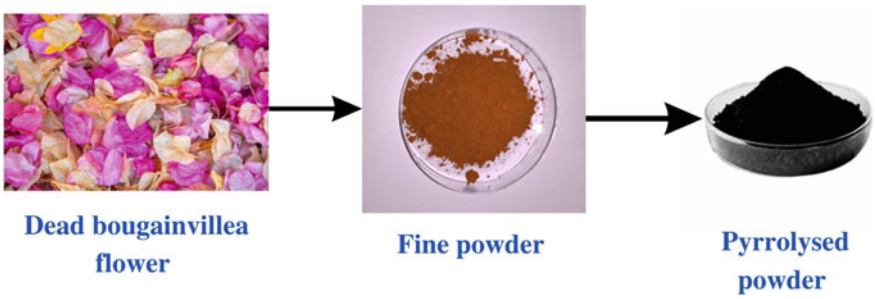

Fig. 5 Schematic representation for preparation of perforated graphene from dead flowers

30 ml of demineralized water was added to it, and it was taken for ultrasonication for 30 min. In that mixture, 20 ml of the bougainvillea flower extract was added and refluxed for 5 h at 95 °C. The mixture was then centrifuged and washed with demineralized water. Finally, the mixture was dried in an oven for 12h at 60 °C to get a black colored powder. The formation of reduced GO was indicated by a transition from dark brown to black in the mixture [71].

Corn Stalk

The corn stalk consists of leaves and stems, where the stems consist of cortex and pith. A corn stalk with a large pith in the stem is one of its features. These corn stalks have high nutritional value. Different kinds of products are being manufactured from the corn stalk, like paper, biodegradable fiber material, oligosaccharides, etc. Apart from this, it is also used in the energy sector for the production of biodiesel, gas fuels, and graphene sheets, which are used as electrodes in supercapacitors. Li et al. reported the efficient catalytic conversion of corn stalk and xylose into furfural in valerolactone over sulfonated graphene [72]. In order to investigate the variation in the furfural production from corn stalks in the aqueous phase, several tests were carried out at 50, 100, 150, 200, and 250 min at 190 °C (Fig. 6). At the same time, a low 5-HMF yield was obtained. When the time was stretched out, the most furfural was made after 150 min, when it was 16.5%. After that, it slowly went down [72].

Carbon microspheres (CSs) of reasonably uniform size were initially used as spacers in carbon microsphere/reduced graphene oxide composite hydrogels (CS-rGOs) to prevent the restacking of graphene sheets. These CS were produced without carbonization or activation from waste biomass corn stalks. As electrode materials for supercapacitors, the produced composite hydrogels performed very well owing to their high oxygen content and high hydrophilicity. Specific capacitance was found to be excellent for CS-rGO-3 sample-based symmetric supercapacitors (281.5 F g^{-1}

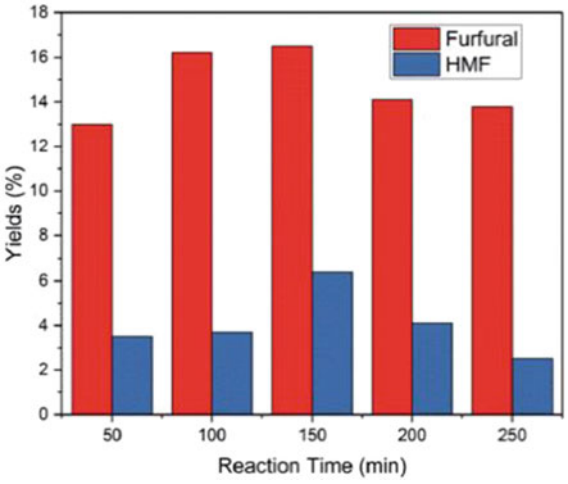

Fig. 6 Corn stalk conversions in 10 mL of clean water with 75 mg of corn stalk and 35 mg of catalyst at 190 °C. Reproduced with permission from the Reference [72]. Copyright 2019, Royal Society of Chemistry

at 0.3 A g^{-1}), rate performance was high (81.87%), and capacitance retention was outstanding (102.2% after 10,000 cycles at 10 A g^{-1}). This work offers a new way to turn waste biomass into something with more value and to make high-performance electrode materials for supercapacitors [73, 74].

Soybean Oil

Soybean oil is derived from soybeans, which is a great source of saturated and polyunsaturated fatty acids. It is composed of mainly 5 fatty acids, i.e., linoleic acid, oleic acid, palmitic acid, stearic acid, and linolenic acid. Kim et al. have reported a paper on photo-cross linked polymer networks based on graphene functionalized soybean oil and their properties. Here, they have prepared four different types of soybean oil/graphene-based photo-cross linked polymer networks. They have found a 48% increase in tensile strength in their experiment. The filler was homogeneously mixed with the polymer matrix when functionalization was done, and the optical property was also increased [75].

Wheat Straw

Wheat straw is the stalk left over after wheat grains are harvested, which is abundant and very cost effective. It can also be an edible grain used to produce different foods. Sadeghi et al. have reduced wheat straw to graphene, and the modification was done with the help of cross-linking. When wheat straw was converted into graphene, the surface area was expanded from 4 to 415 m^2g^{-1}. The modified graphene sheets have a solution temperature of 30–60 ℃, a pH value of 3–11, and many more. The Eriochrone Black T (EBT) removal and dye removal remained high, allowing it to be used as an adsorbent against EBT in aqueous media [76]. Another study used a hydrothermal and graphitization procedure to create high-quality graphene nanosheets from wheat straw. The prepared few-layer graphene was used as an electrode for the lithium-ion batteries that showed greater electrochemical properties like high cycling stability; charge/discharge rate, and reversible capacity. This process was adopted by researchers due to its cost effectiveness, eco-friendly nature, catalyst-free nature, and sustainability as an energy source. Graphene made from wheat straw had improved physical and chemical properties, making it useful for applications such as sodium ion batteries, ultra-capacitors, lithium-ion oxygen batteries, etc [77].

Coconut Shells

Coconut shell consists of cellulose fiber and is low cost, commercially available, environmentally safe, a sustainable biological resource, and abundantly available. As a result, coconut shell (Fig. 7) is becoming a popular carbon resource for the production of activated carbon [64]. Fu and his coworkers have synthesized porous graphene-like nanosheets (PGNS) materials with increased surface area using the simultaneous activation graphitization (SAG) method and coconut shell as the carbon resource [78]. Here $ZnCl_2$ and $FeCl_3$ act as activating agents and graphitic catalysts, respectively. Here, 3 gm of coconut shell was taken and mixed with 9 gm of $ZnCl_2$ in 50 ml of 3M $FeCl_3$ solution. The mixture was then evaporated at 80 °C for 2 h and dried at 1000 °C in an oven, where the carbon precursor was obtained. Then the

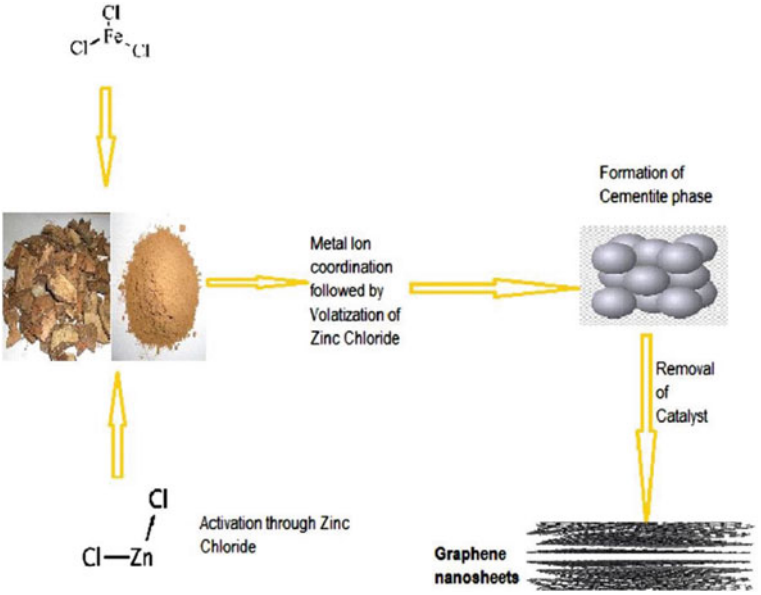

Fig. 7 Schematic diagram of preparation of graphene nanosheets from coconut shell. Reproduced with permission from the Reference [65]. Copyright 2020, John Wiley and Sons

activation and graphitization processes were done in a furnace by passing nitrogen gas at 5C min^{-1} up to 900 °C for 1 h. The sample was then treated with 2 M HCl to remove iron impurities and dried at 60 °C for 12 h, and the resultant product was found to be distorted graphene sheets. The prepared PGNSs showed excellent specific capacitances of 268 F/g^{-1} and 196 F/g^{-1} in an aqueous electrolyte and an organic electrolyte, respectively. It also showed a better cycling rate, higher energy and power density, and better capacity retention [65].

The coconut shell was placed in a glass vessel for the cracking process. As the glass is an inert material, it slowly donates electrons to the coconut shell. The entropy effect slowly cracked the coconut shell. Then the shell was taken for pyrolysis at 600 °C. But due to the higher temperature, the transfer of electrons into the carbon of the coconut shell becomes slower. Finally, small and broad carbon atoms were formed along with the graphene nanosheets [79].

Nori

Nori is a type of red algae marine seaweed that is edible in nature and has a thin film structure that consists of nitrogen, phosphorous, etc. It is used as a better precursor for preparing a doped carbon catalyst. Fan and his colleagues created nori carbon (NC) through the carbonization of biomass, as well as activated nori carbon (ANC) in a study. The NC was prepared through the carbonization process, first by taking the nori and washing it properly with the help of distilled water (DI). When it was dried, nori powder was obtained directly. The ANC was prepared by collecting the nori and

activating it. Then it was filtered and dried in an oven at 80 ºC and carbonized at 800 ºC for 2 h by passing argon gas. The NC was added to a KOH solution in an agate mortar for 30 min and then annealed for 2 h at 800 ºC. The prepared solution was washed properly with DI water to remove excess KOH. The prepared NC and ANC have characteristics of fast growth and short maturity cycle when used in Lithium-ion batteries. The ANC has sufficient nitrogen and oxygen groups and provides multiple polar sites and results in high rate performance of 626 mAh/g at 5 °C. This nori-based carbon derivative gives a significant enhancement in the electrochemical performance of the batteries [80]. Liao and his co-workers have prepared high performance doped carbon catalysts with the help of nori as the precursor and melamine as the promoter. The prepared catalyst has a high surface area and thin-film structure. The catalyst showed high oxygen reduction reaction (ORR) performance in 0.1 M KOH along with greater stability rate and methanol tolerance [81]. Similarly, Liao, they have prepared carbon doped catalyst from nori as the precursor called NORI and used that in the lithium oxygen battery. The prepared NORI has a graphene like nano sheet structure with large surface area and good ORR performance. The NORI electrode showed superior cycling stability with 100 cycles at 1000 mAh/g^{-1} and efficiency [82].

Banana Peel

Banana peel is the outer cover of the banana, which is filled with polyphenols, carotenoids, and different other antioxidants that help fight cancer. X. Li et al. have taken banana peels and converted them into porous activated carbon scaffolds for energy storage applications. Banana peels were first cut or punched into different sizes and frozen inside a refrigerator. The frozen pieces were lyophilized in a dryer for 3 hours before being placed in an argon-gas-filled furnace for 1 h at 900 ºC. After canonization, banana peel pieces shrank in size, and finally, the activated banana peel (ABP) pieces were washed with DI water and dried for 2 h at 75 ºC. The prepared ABP was doped with $NiCo_2O_4$ nanowires to get a high performance electrode material for supercapacitor applications [83]. Lotfabad and his co-workers have created a unique low surface-area carbon that was derived from banana peels, which they called banana peel pseudographite (BPPG). This BPPG worked as a promising electrode for lithium-ion batteries (LIBs), achieving three times more capacity than graphite. By using these electrodes [84], the total charge storage capacity, cycling stability, and Coulombic efficiency have been enhanced in the LIB and NIB (sodium ion batteries). Moreover, the banana peel was used as a precursor for the synthesis of activated carbon and also for the synthesis of a few-layer of graphene. The prepared porous activated carbon has a larger surface area and charge storage capacity, due to which the capacitance of the supercapacitor increases. The electrodes, which are transition metal oxides, allowed the supercapacitor to achieve a high scan rate of 10 mV/s. The supercapacitor showed high energy storing capacity, which can be used for the development of flexible electronics [85].

Peanut Shells

The peanut is a plant of the Fabaceae family, i.e., legumes. The peanut shell is the non-eating outer cover of the legume, and its residues have been found to be between 25 and 30% of the total weight of the legume. The peanut shells were collected and washed properly with DI water for the removal of impurities, then passed through pyrolysis in an oven for 10 h at 60 °C. Then, the shells were grinded into powder form. The powder was placed in a crucible by passing nitrogen gas through it. The produced powder was found to be charcoal filled with carbon having a high surface area, porosity, and oxygen containing groups. It also has greater adsorptive properties [86]. A hybrid sodium ion capacitor (NIC) from peanut shell (Fig. 8) was derived by Miltin et al. The NIC with the peanut shell precursor develops the performance rate of the capacitor along with its cycling retention capability. The cycling rate is also stable at 1000 cycles. This hybrid device achieved a capacity retention of 72 and 88% after 10,000 cycles at 6.4 and 51.2 Ag^{-1}. It shows cycling stability at a current density of 6.4 Ag^{-1} [87].

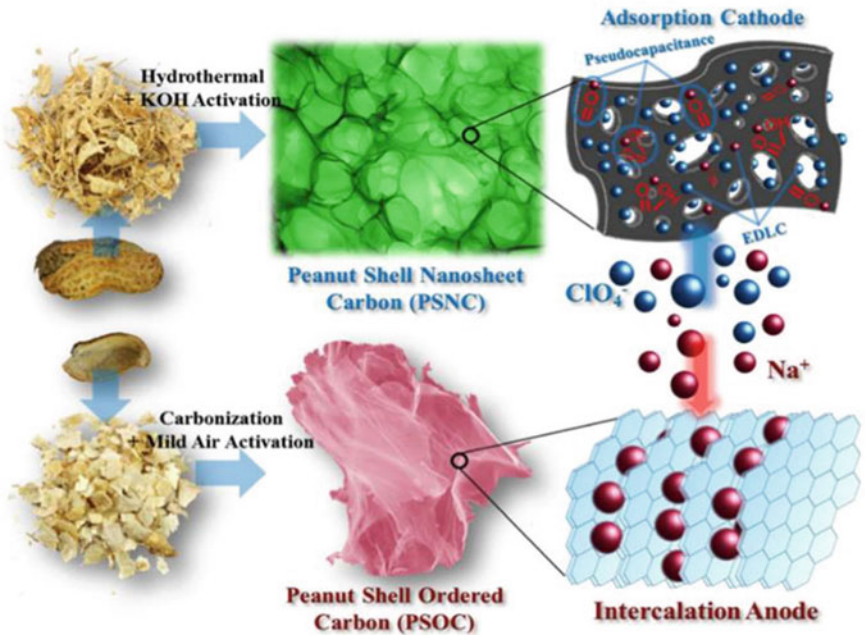

Fig. 8 Making peanut nanosheets from the shell of a peanut. Reproduced with permission from the Reference [87]. Copyright 2015, Royal Society of Chemistry

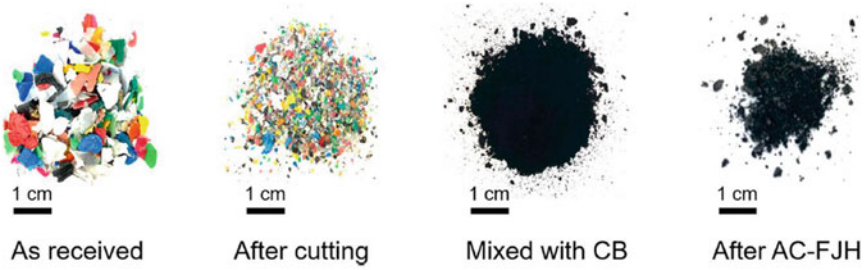

Fig. 9 Images of post-consumer plastic after it was acquired from a recycler, after being cut using a commercial cutter, after being mixed with 5 wt% CB, and after being further converted to FG using AC-FJH are shown (left to right). Reproduced with permission from the Reference [88]. Copyright 2020, American Chemical Society

5 Other Precursors

5.1 Plastic Waste (PW)

Plastic is one of the most commonly generated wastes on the planet, and it is both abundant and extremely harmful to our environment. Plastic is found in many forms, like plastic bags, bottles, toys, sheets, etc., and is left behind after one or two uses. It is non-biodegradable by nature, which makes it more hazardous and a serious threat not only to humans but also to the animal kingdom. Scientists are currently investigating ways to recycle this plastic into usable products. Using flash joule heating (FJH), Tour and his co-workers [88] were able to transform the PW into flash graphene (as shown in Fig. 9). Along with the production of flash graphene, this process also leads to the formation of light hydrocarbons, carbon oligomers, hydrogen, etc. The flash graphene was found to have an interlayer spacing of 3.45 Å which helps in the dispersion of liquids and composites [89].

Waste plastic management is one of the greatest challenges for scientists and researchers. In an attempt to make PW more sustainable and environmentally friendly, Sahoo et al. have synthesized graphene nanosheets from plastic waste [90]. They used DI water to properly wash the PW as part of their experiment. Thereafter, they cut the PW into small pieces and mixed those pieces with nanoclay. The mixture was then transferred to pyrolysis at 4000 °C by passing nitrogen gas, which was followed by fast heating at 750 °C. After this, a black collared charcoal was formed which was again taken for ball milling process to get fine powder of charcoal. In this way, the same procedure was continued for several times and finally few layers of graphene nano sheet were obtained. This graphene is used for many applications like solar cells, fuel cells, for preparing polymer nano composites etc. Similar to this, the same researcher Sahoo et al. used PW's graphene nanosheets in dye-sensitive solar cells and supercapacitors (DSSCs). They have derived graphene nanosheets from PW by pyrolysis at 450 °C and 945 °C in a nitrogen atmosphere. The fabrication with the use of graphene sheets in DSSC showed a high fill factor

of 86.4% and open circuit voltage (V_{oc}) of 0.77V (Fig. 10). Similar results were obtained when the graphene nanosheet was utilized as an electrode in a supercapacitor. It displayed a high specific capacitance of 398 F/g^{-1} with a scan rate of 0.005 V/s. However, it demonstrated a high-power density of 1009.74 Wh/kg and a density of 38 Wh/kg [91].

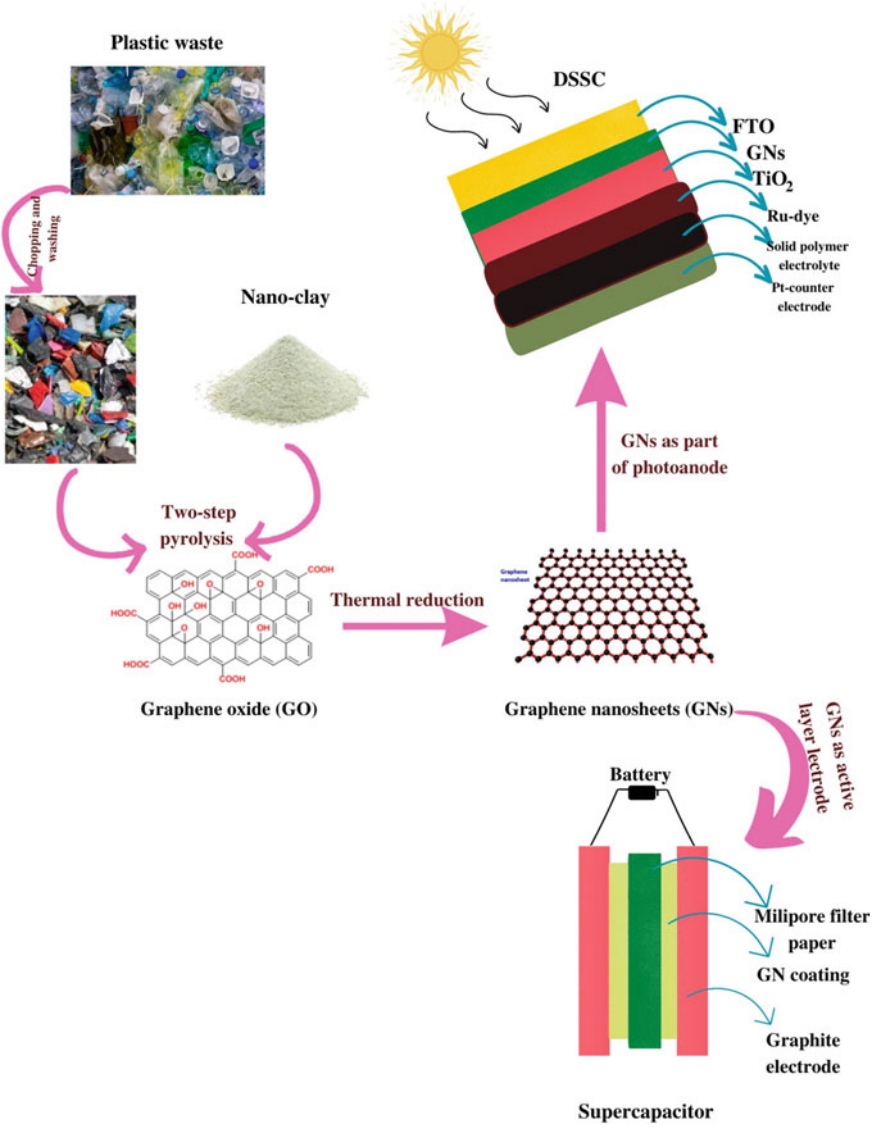

Fig. 10 Schematic illustration for the fabrication of GNs from plastic waste and its application in DSSCs and supercapacitors

6 Conclusions

One of the most significant materials of the twenty-first century is graphene; a sp^2 hybridized 2D atomic crystal. Researchers have lately been interested in graphene owing to its better electrochemical energy-storing capabilities. Over the past 10 years, there has been a significant rise in research on graphene-like carbon compounds derived from biomass that may be used to store energy in novel ways. Biomass may be used to create graphene-like structures at a cheap cost and with nearly no carbon emissions. This is a step in the right direction towards a more sustainable energy future. Furthermore, because of their long-term viability and great performance for high-power and short-term energy demands, they are ideal candidates for carbon-based supercapacitor devices, which are considered the key to future green transportation electrification. As a result, graphene is employed in a wide range of applications, including polymer composites, energy storage, fuel cells, and medicinal applications. Bio-waste products are thought to be an excellent source of carbon production. However, there are various bio-waste products, and proper disposal procedures are necessary. This chapter has concentrated on the manufacture of graphene from diverse bio-sources such as rice husks, paper cups, hemp, chitosan, banana peels, and peanuts, as well as its use as an appropriate electrode material in the area of supercapacitors.

Acknowledgements The author S. Moharana acknowledges Centurion University of Technology and Management, Odisha for the support and facility.

Conflict of Interest The authors declare that we have no conflict of interest.

References

1. Zhang H, He X, Zhao M, Zhang M, Zhao L, Feng X, Luo Y (2012) J Phy Chem C 116:16634–16638
2. Chen Y, Zhang B, Liu G, Zhuang X, Kang ET (2012) Chem Soc Rev 41:4688–4707
3. Lu X, Yu M, Huang H, Ruoff RS (1999) Nanotechnol 10:269
4. Geim AK, Novoselov KS (2010) Nanosci Technol. 11-19
5. Qian M, Feng T, Ding H, Lin L, Li H, Chen Y, Sun Z (2009) Nanotechnol 20:425702
6. Malesevic A, Kemps R, Vanhulsel A, Chowdhury MP, Volodin A, Van Haesendonck C (2008) J Appl Phys 104:084301
7. Pumera M, Ambrosi A, Bonanni A, Chng ELK, Poh HL (2010) Trends Anal Chem 29:954–965
8. Peña-Bahamonde J, Nguyen HN, Fanourakis SK, Rodrigues DF (2018) J Nanobiotechnol 16:1–17
9. Ohno Y, Maehashi K, Matsumoto K (2010) Biosens Bioelectron 26:1727–1730
10. Reddy D, Register LF, Carpenter GD, Banerjee SK (2011) J Phys D 44:313001
11. Xu Y, Liu J (2016) Small 12:1400–1419
12. Liu Z, You P, Xie C, Tang G, Yan F (2016) Nano Energy 28:151–157
13. Quan B, Yu SH, Chung DY, Jin A, Park JH, Sung YE, Piao Y (2014) Sci Rep 4:1–6
14. Mao J, Iocozzia J, Huang J, Meng K, Lai Y, Lin Z (2018) Energy Environ Sci 11:772–799
15. Kretinin AV, Cao Y, Tu JS, Yu GL, Jalil R, Novoselov KS, Haigh SJ, Gholinia A, Mishchenko A, Lozada M, Georgiou T, Gorbachev RV (2014) Nano Lett 14:3270–3276

16. Butler SZ, Hollen SM, Cao L, Cui Y, Gupta JA, Gutiérrez HR, Heinz TF, Hong SS, Huang J, Ismach AF, Goldberger JE (2013) ACS Nano 7:2898–2926
17. Cheng C, Li D (2013) Adv Mater 25:13–30
18. Zhu J, Yang D, Yin Z, Yan Q, Zhang H (2014) Small 10:3480–3498
19. Akinwande D, Petrone N, Hone J (2014) Nat Commun 5:1–12
20. Shrivastava M, Ramgopal Rao V (2021) Nano Lett. 21:6359–6381
21. Bollella P, Fusco G, Tortolini C, Sanzò G, Favero G, Gorton L, Antiochia R (2017) Biosen Bioelectron 89:152–166
22. Reddygunta KKR, Callander A, Šiller L, Faulds K, Berlouis L, Ivaturi A (2022) Int J Energy Res 46:16512–16537
23. Kairi MI, Khavarian M, Bakar SA, Vigolo B, Mohamed AR (2018) J Mater Sci 53:851–879
24. Huang H, Xia Y, Tao X, Du J, Fang J, Gan Y, Zhang W (2012) J Mater Chem 22:10452–10456
25. Phiri J, Gane P, Maloney TC (2017) J Mater Sci 52:8321–8337
26. Yuan GD, Zhang WJ, Yang Y, Tang YB, Li YQ, Wang JX, Meng XM, He ZB, Wu CML, Lee CS, Lee ST (2004) Chem Phys Lett 467:361–364
27. Sun J, Lindvall N, Cole MT, Teo KB, Yurgens A (2011) Appl Phys Lett 98:252107
28. Wei D, Lu Y, Han C, Niu T, Chen W, Wee ATS (2013) Angew Chem 125:14371–14376
29. Gupta K, Gupta D, Khatri OP (2019) Appl Surface Sci 476:647–657
30. Bi Z, Kong Q, Cao Y, Sun G, Su F, Wei X, Li X, Ahmad A, Xie L, Chen CM (2019) J Mater Chem A 7:16028–16045
31. Das VK, Shifrina ZB, Bronstein LM (2017) J Mater Chem A 5:25131–25143
32. Reddy N, Yang Y (2005) Green Chem 7:190–195
33. Stănescu MM, Bolcu A (2022) Polym 14:392
34. Kataria G, Sharma A, Joshi JB, Hameed S, Amiri A (2022) Mater Today: Proc 57:528–1532
35. Steven S, Restiawaty E, Bindar Y (2022) J Eng Technol Sci 54:220304
36. Perra M, Cuena-Lombraña A, Bacchetta G, Manca ML, Manconi M, Maroun RG, Muntoni A, Tuberoso CIG, Gil KA, De Gioannis G (2022) Sustainability 14:10690
37. Manasa P, Sambasivam S, Ran F (2022) J Energy Storage 54:105290
38. Zhuo Q, Gao J, Peng M, Bai L, Deng J, Xia Y, Ma Y, Zhong J, Sun X (2013) Carbon 52:559–564
39. Zhao YL, Stoddart JF (2009) Acc Chem Res 42:1161–1171
40. Li X, Colombo L, Ruoff RS (2016) Adv Mater 28:6247–6252
41. Stankovich S, Dikin DA, Piner RD, Kohlhaas KA, Kleinhammes A, Jia Y, Wu Y, Nguyen S, Ruoff RS (2007) Carbon 45:1558–1565
42. Wu YQ, Ye PD, Capano MA, Xuan Y, Sui Y, Qi M, Cooper J, Shen T, Pandey D, Prakash G, Reifenberger R (2008) Appl Phys Lett 92:092102
43. Oznuluer T, Pince E, Polat EO, Balci O, Salihoglu O, Kocabas C (2011) Appl Phys Lett 98:183101
44. Zhang LL, Zhou R, Zhao XS (2010) J Mater Chem 20:5983–5992
45. Miller JR, Simon P (2008) Sci 321:651–652
46. Winter M, Brodd RJ (2004) Chem Rev 104:4245–4270
47. Libich J, Máca J, Vondrák J, Čech O, Sedlaříková M (2018) J Energy Storage 17:224–227
48. Sharma P, Kumar V (2020) J Electron Mater 49:3520–3532
49. Vangari M, Pryor T, Jiang L (2013) J Energy Eng 2:72–79
50. Ke Q, Wang J (2016) J Materiomics 2:37–54
51. Kim KS, Zhao Y, Jang H, Lee SY, Kim JM, Kim KS, Ahn JH, Kim P, Choi JY, Hong BH (2009) Nature 457:706–710
52. Zhu Y, Murali S, Stoller MD, Velamakanni A, Piner RD, Ruoff RS (2010) Carbon 48:2118–2122
53. Li Z, Wang J, Liu S, Liu X, Yang S (2011) J Power Sources 196:8160–8165
54. Wang H, Casalongue HS, Liang Y, Dai H (2010) J Am Chem Soc 132:7472–7477
55. Wang G, Sun X, Lu F, Sun H, Yu M, Jiang W, Liu C, Lian J (2012) Small 8:452–459
56. Murugan AV, Muraliganth T, Manthiram A (2009) Chem Mater 21:5004–5006
57. Xu Y, Lin Z, Huang X, Wang Y, Huang Y, Duan X (2013) Adv Mater 25:5779–5784

58. Santhosh R, Raman SS, Krishna SM, sai Ravuri S, Sandhya V, Ghosh S, Sahu, NK, Punniyakoti S, Karthik M, Kollu P, Jeong SK, Grace AN (2018) Electrochim Acta 276:284−292
59. Huang L, Liang J, Chen Y (2012) Small 8:1805–1834
60. Rhee I, Kim YA, Shin GO, Kim JH, Muramatsu H (2015) Constr Build Mater 96:189–197
61. Singh P, Bahadur J, Pal K (2017) Graphene 6:61–71
62. Le Van K, Thi TTL (2014) Prog Nat Sci 24:191–198
63. Wang Z, Yu J, Zhang X, Li N, Liu B, Li Y, Wang Y, Wang W, Li Y, Zhang L, Dissanayake S, Suis S, Sun L (2016) ACS Appl Mater Interfaces 8:1434–1439
64. Sodtipinta J, Ieosakulrat C, Poonyayant N, Kidkhunthod P, Chanlek N, Amornsakchai T, Pakawatpanurut P (2017) Ind Crops Prod 104:13–20
65. Poorna AR, Saravanathamizhan R, Balasubramanian N (2021) Electrochem Sci Adv 1
66. Conder J, Vaulot C, Marino C, Villevieille C, Ghimbeu CM (2019) ACS Appl Energy Mater 2:4841–4852
67. Ye R, Xiang C, Lin J, Peng Z, Huang K, Yan Z, Cook NP, Samuel E, Hang CC, Ruan G, Ceriotti G, Raja A, Martin A, Tour JM (2013) Nature commun 4:1–7
68. Powell C, Beal GW (2015) Curr Opin Colloid Interface Sci 20:362–366
69. Vijapur SH, Wang D, Ingram DC, Botte GG (2017) Mater Today Commun 11:147–155
70. Panmand R, Patil P, Sethi Y, Kadam SR, Kulkarni MV, Gosavi SW, Kale BB (2017) Nanoscale 9:4801–4809
71. Mahendran GB, Ramalingam SJ, Rayappan JBB, Kesavan S, Periathambi T, Nesakumar N (2020) J Mater Sci Materi Electron 31:14345–14356
72. Ma J, Li W, Guan S, Liu Q, Li Q, Zhu C, Yang T, Ma L (2019) RSC Adv 9:10569–10577
73. Chen H (2015) Lignocellulose Biorefinery Eng. 219-245
74. Wang J, Zhao B, Huang X, Wang Y, Du X, Wei L, Zhang Y, Ma W (2022) Energy Fuels 36:2268–2276
75. Wang H, Gupta A, Kim BS (2019) Korean J Chem Eng 36:591–599
76. Sadeghi S, Zakeri HR, Saghi MH, Ghadiri SK, Talebi SS, Shams M, Dotto GL (2021) Environ Sci Pollut Res 28:3556–3565
77. Chen F, Yang J, Bai T, Long B, Zhou X (2016) J Electroanal Chem 768:18–26
78. Sun L, Tian C, Li M, Meng X, Wang L, Wang R, Yin J, Fu H (2013) J Mater Chem 1:6462–6470
79. Supeno M, Siburian R (2020) J King Saud Univ Sci 32:189–190
80. Wu X, Fan L, Wang M, Cheng J, Wu H, Guan B, Zhang N, Sun K (2017) ACS Appl Mater Interfaces 9:18889–18896
81. Liu F, Peng H, You C, Fu Z, Huang P, Song H, Liao S (2014) ElectrochimActa 138:353–359
82. Zeng X, Leng L, Liu F, Wang G, Dong Y, Du L, Liu L, Liao S (2016) Electrochim Acta 200:231–238
83. Zhang Y, Gao Z, Song N, Li X (2016) Electrochim Acta 222:1257–1266
84. Lotfabad EM, Ding J, Cui K, Kohandehghan A, Kalisvaart WP, Hazelton M, Mitlin D (2014) ACS nano 8:7115–7129
85. Singh A, Ghosh K, Kumar S, Agrawal A, Jassal M, Goswami P, Chaturvedi H (2019) Few-layer graphene based printed flexible asymmetric supercapacitor
86. Bai S, Wang T, Tian Z, Cao K, Li J (2020) Sci Rep 10:1–9
87. Ding J, Wang H, Li Z, Cui K, Karpuzov D, Tan X, Kohandehghan A, Mitlin D (2015) Energy Environ Sci 8:941–955
88. Algozeeb WA, Savas PE, Luong DX, Chen W, Kittrell C, Bhat M, Shahsavari R, Tour JM (2020) ACS nano 14:15595–15604
89. Vieira O, Ribeiro RS, de Tuesta JLD, Gomes HT, Silva AM (2022) J Chem Eng 428:131399
90. Pandey S, Karakoti M, Dhali S, Karki N, SanthiBhushan B, Tewari C, Rana S, Srivastava A, Melkani AB, Sahoo NG (2019) Waste management 88:48–55
91. Pandey S, Karakoti M, Surana K, Dhapola PS, SanthiBhushan B, Ganguly S, Singh PK, Abbas A, Srivastava A, Sahoo NG (2021) Sci Rep 11:1–17

Metal Doped Nanostructures Derived from Biomass for Supercapacitor Applications: Effect of Doping on Cyclability

Amrita De Adhikari

Abstract In the battle between industrialization and conserving the environment, ecologically viable biomass niches are in high demand. Storing and delivering energy with durability and steadiness has been crucial. Conventionally, carbonaceous materials have been used for years in supercapacitor fabrication. A sustainable supply of energy with minimum cost and huge benefits has made biomass-derived nanostructures suitable for supercapacitor applications. The design of customizable nanostructures (e.g., nanorods, nanoflowers, nanosheets, nanotubes, etc.) has been found to be dependent on dopants, the morphology of precursors, surface area parameters, and many more factors. An enormous number of biowaste and biomass materials have been employed to attain various nanostructures that are beneficial for electrochemical energy storage. Auxiliary, doping metals, and heteroatoms are found to be advantageous as they can lead to the generation of redox active sites, increased cyclability, and reduced resistance to charge transfer. The overall electronic framework has played a significant role in the stability and robustness of the nanostructure in supercapacitors. This chapter discusses the various superstructures derived from biomass, as well as their intrinsic electrochemical performance on metal doping. Metal doped nanostructured carbonaceous materials derived from replenishable, inexpensive, and environmentally friendly biomass have become the "cherry on top" in supercapacitor research communities.

Keywords Biomass · Biowaste · Metal doping · Supercapacitors · Nanostructures · Cyclability

A. De Adhikari (✉)
Department of Chemical Engineering, Indian Institute of Technology Kanpur, Kanpur 208016, India
e-mail: amritainsp.02@gmail.com

S. K. Tiwari et al. (eds.), *Biomass-Based Functional Carbon Nanostructures for Supercapacitors*, Green Energy and Technology,
https://doi.org/10.1007/978-981-99-0996-4_9

1 Introduction

Carbon exists in various forms and allotropes, including mesoporous carbon, fullerenes, graphene, carbon nanotubes, and their composites. [1–3] Each form possesses certain advantages and disadvantages; therefore, the development of their nanostructures can be very challenging and also interesting. Low-cost carbon materials have always been a top priority for industries, as long as economy and profits are considered. Such carbon-based materials have a wide range of applications, but here in this chapter, we shall deal with their supercapacitor (SC) applications. SCs are well-known and extensively researched energy storage systems with a high power density and a long cycle life that aid in renewable energy generation [4]. The deciding parameters for making an SC work efficiently are significantly dependent on the electrode materials. The electrode material that can host facile electrostatic interactions, electron transfers, and good adsorption sites is suitable for SCs applications [5, 6]. Therefore, carbon-based electrode materials have gained attention for their practical and convenient application. Biomass can be an excellent precursor for carbon electrodes. Abundant agricultural residues are produced that can be processed and used for the synthesis of electrode materials. A variety of biomass-based carbonaceous materials have been obtained from different biomass sources, as shown in Table 1. Hydrothermal carbonization (HTC), chemical activation, and pyrolysis are some of the thermochemical treatments carried out in order to obtain porous, high-surface-area products, which are crucial for SCs'application [7].

Also, various studies have shown that carbon materials can indorse in the core-shell nanostructure formation by capturing metal or metal oxide if they are present during the carbonization process. [9, 10] Carbonaceous materials used solely for SCs applications have drawbacks such as low electrical conductivity, poor permittivity, poor polarization ability, and so on [11]. Incorporation of metal/metal oxide species or redox active species (MnO_2, RuO_2, V_2O_5, SnO_2, ZnO, conducting polymers, etc.) influences the energy storage performance at the interface of electrodes and electrolytes [12–19]. Such redox active species are known as the pseudocapacitors in SCs, which can store charge through the transfer of electrons via reversible redox reactions. The carbonaceous materials, on the other hand, store charge via an electrochemical double-layer mechanism (EDLC). Therefore, metal doping or heteroatom doping can improve the electrochemical properties of the SCs device via the synergistic effect between the pseudocapacitors and EDLC materials [20]. This chapter will deal with the physicochemical and electrochemical performance of biomass-based metal-doped electrode materials, which aid in cyclic stability valuation and sustainable routes to the bioeconomy.

Table 1 Some biomass sources and their method of activation for deriving carbon frameworks [8]

Biomass source	Activation
Banana peel	$Zn(NO_3)_2$
Rice husk	$ZnCl_2$
Sugarcane bagasse	$ZnCl_2$
Bamboo	KOH
Seaweed	Thermal
Willow catkins	KOH
Soybeans	KOH
Pomelo peel	KOH
Sunflower seed	KOH
Waxberry	$Fe_2(SO_4)_3$
Perilla frutescens leaf	Thermal
Paulownia sawdust	NaOH
Lessonia nigrescens	Thermal
Celtuce leaves	KOH
Kelp	Thermal
Corn and protein	KOH
Lignosulfonate	Thermal
Auricularia	Thermal
Cassava peel waste	KOH+CO_2
Argan seed shells	KOH

2 Overview

Reduced consumption of fossil fuels and the goal of establishing a low carbon cycle are global necessities for long-term growth. The development of renewable and clean sources of energy is one of the most efficient solutions to reaching this target. This chapter highlights the biomass-derived electrode materials that primarily aim to improve the electrochemical performance and cyclic stability of the electroactive materials. Designing various biomass-derived carbonaceous skeletons from 1D to 3D can become a diverse method to obtain interconnected porous structures. Incorporation of metals or metal oxides contributes to the pseudocapacitance of the electrode material by maximizing the electroactive sites, packing density, and overall capacitance. By adjusting the pore structure, density, doping, electrolyte, and surface area of the biomass-derived carbon, the low volumetric performance can be overcome. Looking into the existing challenges, the scientific community performs in-situ techniques to monitor the functionalization of the biomass-derived carbon that can pave the way from fundamental to operational chemistry. This script can provide a good guideline for designing the next-generation electrode materials for energy storage applications.

3 Cyclic Stability-A Crucial Parameter for SCs Performance

The retention of capacitance of electroactive materials under certain test conditions or after a certain number of charge-discharge cycles is referred to as cyclic stability. Cyclic stability is highly influenced by the type of electrode materials and their process of energy storage. The EDLCs' electrode materials, like carbon materials, are found to belong to type I cyclic stability, where there is no change of phase during charge-discharge cycles and no chemical charge transfer reactions take place in the electrode material. Here, the charge is stored via a reversible adsorption-desorption process at the electrode-electrolyte interface. Thus, there is very little decay of capacitance during many cycles of charge-discharge, and the retention rate is nearly 100%. Such cyclic stability is classified as type I. The second class of cyclic stability is type II, which is generally observed in the case of pseudocapacitive materials (metal/metal oxides, hydroxides, nitrides, carbides, etc.) or battery-type materials, where the charge storage mechanism is via surface-controlled faradic redox reactions. At the initial stages of charge-discharge cycles, there is self-activation of the electrode material, so there is an increase in specific capacitance over the initial value and the retention is always above 100%. After the self-activation step, the rate of retention drops to the initial capacitance or less than 100%; this type is classified as type II. Type III cyclic stability is mostly observed in conducting polymers. In the polymer matrix, rapid, reversible P and N type doping and counter-doping reactions occur. The conducting polymers easily collapse during the charge-discharge process, showing capacitance retention below 100%. The key prompting aspects of cyclic stability include the potential window, electrode materials, scan rate, current density, mass loading, composition of electrolyte, etc.

4 Factors Influencing the Cyclic Stability

4.1 Structural Features of Nanostructured Electrode Materials Derived from Biomass

Tailoring the porosity, geometry, and composition of the biomass-derived nanostructures can lead to enhanced electrochemical performance. There are various methods of synthesizing carbon nanostructures derived from biomass, as noted in Table 1. High specific surface area, heteroatom doping, and high porous structures are some of the interesting traits in regard to increased conductivity and specific capacitance .

4.1.1 High Specific Surface Area

The EDLC mechanism takes place effectively when the carbonaceous electrode materials provide a high specific surface area, leading to better ion adsorption at the electrode/electrolyte interface—a prerequisite for optimizing the specific capacitance [21, 22]. The pore structures and their distribution throughout the architecture greatly influence the electron and ion movements, affecting the electrochemical behavior of the electrode materials. Several crucial parameters of SCs, like power density, energy density, etc., can be improved by optimizing the pore size distribution that is beneficial for the ion transport phenomenon [23]. In aqueous and organic electrolytes, microporous structures (2 nm) with pore sizes of 0.7 and 0.8 nm, respectively, were found to be operative sizes for ion accumulation, confirming high specific capacitance [24]. One of the most versatile procedures to obtain microporous carbons is KOH-assisted pyrolysis, where the reaction between carbon and potassium compounds leads to the production of gases due to the gasification of carbon. Such gasification can create multiple pores within the carbon structure, which are created by washing away the intercalated K^+ ions. [25] CO_2 activation is an alternative approach for the production of microporous carbon at high temperatures, which generates active ion storage and pathways for mass diffusion [26, 27]. Mesoporous (2–50 nm) structures also provide fast transport of ions, leading to higher power densities and rate capacities. Steam activation and ZnCl2 salt activation are some of the methods used to produce mesoporous structures with a mean pore size of 3.2 nm [28]. Elongated time of activation and flow rate of water increase the number of mesopores. ZnCl2 salt acts as a hard template and activating agent to produce mesopores [29]. Macroporous (> 50 nm) structures are large reservoirs of ion-buffering, minimizing the distance of ion diffusion. Micro-and mesoporous structures offer a high specific surface area for accommodation of ions, whereas mesoporous and macroporous structures result in channels for mass diffusion and ion transport [30, 31]. Therefore, it has been observed that pores offer channels for ion transport, ion-buffering spaces, and ion adsorption. However, there is no linear relationship between high surface area and enhanced capacitance. The very small pore size of the micropores restricts the full accessibility of the electrolytic ions, reducing the power and energy density. Again, the ultrahigh pore size of the macro and meso pores causes low packing density, reducing the volumetric capacitance and the electrical conductivity [32]. Thus, the overall architecture with optimal pore sizes, packing density, and sufficient transport channels contributes to the enhanced electrochemical performance [32, 33].

4.1.2 Heteroatom Doping

The doping of heteroatoms within the carbon structure improves the electrical conductivity and wettability. Also, the redox reactions taking place because of the presence of the functional groups at the surface lead to a pseudocapacitance contribution [34, 35]. Biomass-derived nanostructures can be doped with heteroatoms by using precursors enriched with heteroatoms and chemical dopants that can modify

the electronic properties and the surface chemistry [36]. For instance, N doping can provide electroactive sites, improve wettability, and increase electrical conductivity, thereby enhancing the electrochemical activity [37]. The pyridinic and pyrrolic-N atoms have negative charges and provide pseudocapacitance, whereas the pyridinic-N oxide and quarternary-N atoms have a positively charged atom that facilitates electron transfer. Some of the N containing raw biomass includes silk, fish skin, soybean, tree bark, shrimp shell, bamboo shoot, egg white, gelatin, etc [38–45]. The addition of O as a heteroatom has also been found to improve electrochemical performance. O functionalities behaving as electron acceptors improve the wettability of the electrode, increase ion accessibility, and provide pseudocapacitance through redox reactions. O doping can be realized by using O-rich precursors or a suitable activation method like KOH, air, or acid [46–48]. S-doping on the surface of a carbonaceous material acts as an active site for redox reactions and improves wettability [49–51]. S contains one lone pair of electrons on the p-orbital, which overlaps with the p-orbital of the sp2 hybridized graphite; such interaction results in delocalization of electrons within the carbon backbone [52]. S-containing thiourea and thioglycolic acid are good sources of sulfur. Also, the S-doped carbons have low charge transfer resistance owing to the better polarity on the surface of the carbon. Electrochemical properties also depend on the doping degrees and dopant arrangements. However, the mechanism by which the doping effect affects the electrochemical properties still remains unclear.

4.1.3 Hierarchical Nanostructures

Nanostructures derived from biomass show different dimensions of architectures from 1 to 3D, i.e., nanofibers, nanosheets, etc. Such well-defined structures offer high porosity, a specific surface area, and conductivity—all necessary for rapid ion transport leading to high electrochemical performance. 1D nanobelts, nanofibers, nanothreads, etc. have conductive channels for the transport of electrons with exceptional mechanical strength [53–56]. A 1D skeleton enables the migration of ions from bulk electrolytes to interior pores, which is favorable for high rate performance. One of the widely used techniques to produce 1D nanofiber is electrospinning. Controlling the heating rate at the time of carbonization allows the morphologies of the products to be tuned. Cotton and polar catkins are examples of biomass that can be directly converted to 1D fibers due to their tubular structure [57, 58]. Such tubular morphology acts as conductive channels for the rapid transport of ions. Further, the hollow scaffolds of the carbon architecture also act as ion transport and buffering sites, making them beneficial for the high rate capability. Also, the higher length/diameter ratio of the porous nanostructures shortens the diffusion path and offers high surface ion charge storage. 2D nanosheet structures deliver large surface contact areas, good conductivity, and low resistance. [59] But the nanosheets have the possibility of stacking between their adjacent layers, reducing the ion transport and rate capabilities [44, 60]. 3D porous architectures derived from biomass possess less internal resistance, shorter ion diffusion paths, and increased charge transfer kinetics as they

have a large number of pores, a highly interconnected morphology, and good mechanical stability. The 3D honeycomb design hosts the ions and reduces the ion diffusion resistance, resulting in favorable electrochemical performances.

There are also certain inherent biomass nanostructures that possess porous morphology, aiding tunable electrochemical properties. For example, some wood-based carbonaceous materials have vertically allied multi-channels for the transport of ions, which reduce tortuosity, contributing to high rate capability [61]. The interspace between the pores facilitates ion transport and enhances the specific capacitance. There are some inherent free-standing electrodes, like the flat flower petal, whose wrinkled morphology, high conductivity, and 5–10 m thickness make them suitable as self-standing electrodes for flexible SCs. There are also certain biomass-derived electrodes that can be employed as binder-free flexible electrodes, like flax fabric-derived carbon, obtained via facile carbonization [62] (Table 2).

Table 2 Different methods of synthesis of biomass-derived carbon structures and their special features [63]

Method of synthesis			Temperature range	Special features
Pyrolysis	Gas assisted	Air	<500 °C	Incorporation of oxygen functional groups with inherent morphology.
		Steam, CO_2	600–1200°C	Large surface area porous structures
	Self-activated	Physical or chemical activation	600–1700°C	Eco-friendly strategy as no external activating agent is required
	Chemical assisted	NaOH, KOH, H_3PO_4, $CaCl_2$, $ZnCl_2$, $FeCl_3$	400–1000°C	Most commonly used method of activation employing hard templates and activating agents.
Template methods	Soft template	Polymers		Well organized structure obtained with hierarchical morphology with adjustable porosity.
	Hard template	Metal oxides, silica, molten salts		
Hydrothermal carbonization	Graphene oxide assisted		<250°C, followed by carbonization at high temperature	Well-designed architecture porous morphology.

4.1.4 1D Biomass-Derived Carbon Materials

1D fibrous structure possesses various advantages as follows:

(a) It has very good mechanical properties with high strength of 2−3 GPa and Young's modulus of 138 GPa [64–66].
(b) On chemically modifying the surface of the 1D fibers, the surface active sites are created that can improve the electrochemical properties [67–69].
(c) Fibrous geometries have high aspect ratio and can form interconnected binder-free networks for flexible SCs [70, 71].
(d) The linear 1D channel is capable of providing pathways for facile transfer of electrons and ions [72].
(e) The tubular structure can act as a buffer reservoir for the electrolytes offering more active sites for electrochemical reactions [73].

The various 1D biomass-derived precursors include willow catkins, kapok, cotton, flax, bacterial cellulose, ramie, etc [74–79]. Zhang et. al. synthesized MnO_2/carbon microtube bundle composite for SCs electrodes [80]. The carbon microtube was produced from sawdust and MnO_2 nanostructures were obtained by anodic electrodeposition. The deposition of MnO_2 increases the active sites and also the conductivity of the electrode material. The composite offered a specific capacitance of 617.6 F/g at 1 A/g and cyclic stability was tested over 1000 cycles. The electrochemical studies showed that it exhibited very low resistance, high charge storage ability, and good transfer capability. In this study, the researchers exploited the natural tubular features of the existing woods and enhanced their electrochemical performance. Zhang et al. used willow catkins as a precursor to synthesize porous graphitic carbon nanotubes (PGCMT), which acted as a substrate for electrodeposition of MnO_2 [81]. The PGCMT/MnO_2 composite showed excellent specific capacitance of 550.8 F/g at 2 A/g with 89.6% cyclic stability after 5000 cycles. Xu et al. fabricated micro-tubular carbonized kapok fiber/NiO nanocomposites for SCs application [82]. The hollow tubular kapok fibers are used as templates to grow $Ni(OH)_2$ via hydrothermal process, then converted to NiO via carbonization. The composite so prepared has very good supercapacitive properties with specific capacitance of 575.5 F/g at 0.5 A/g with a capacitance retention of 91.7%. Asymmetric SCs device assembled out of this composite has an energy density of 7.5 Wh/Kg and power density of 65.5 W/Kg.

The above discussions highlight some of the fantastic features and electrochemical properties of 1D biomass-derived metal composites along with low cost fabrication and fast charge-discharge rates.

4.1.5 2D Biomass-Derived Carbon Materials

2D nanostructured biomass has great prospective and the following features are essential for electrochemical energy storage:

(a) The 2D structure has strong in-plane covalent bonds and also high conductivity that can speed up the electrons flow [83, 84].
(b) The 2D layered structure has an ultrathin dimension with large lateral size reducing the ion transport path [85, 86].
(c) Open and flat surface exposes the surface active sites, enhancing the surface area for better exchange of ions at the electrode-electrolyte interface [87].
(d) 2D structures have active edges and in-plane defect sites that can facilitate the storage of charges and high specific capacitance [88].

Different precursors of the 2D biomass-derived carbonaceous materials includes silk, Perilla frutescent, bougainvillea flowers, eggplants, puffed rice, etc [38, 89–92]. These precursors intrinsically possess multiple layered structures and rearranges to form 2D sheets on pyrolysis.

4.1.6 3D Biomass-Derived Carbon Materials

3D nanostructures having salient properties that are beneficial for SCs application are:

(a) Increasing the dimensionality, increases the active surface area, therefore improving the supercapacitive performance of the materials.
(b) The 3D microstructures are interconnected with wide range of pores that can provide facile transfer of ions and good electrical conductivity.
(c) They can be tailored into novel structures beneficial for high electrochemical performance.

The assimilated properties, therefore, offer high power delivery and high energy storage with short ion path. For instance, Song et al. studied 3D carbon hierarchical porous structures, synthesized from corn husks via direct pyrolysis of KOH. The internetwork macroporous morphology was obtained because of the inherent cellular architecture of cellulose. Narrow pore size distribution, rich doping of oxygen, and synergistic effect enhances the supercapacitive performance. The specific capacitance obtained was 356 F/g with a rate capability of 84.3% and cyclic stability of 95% over 2500 cycles [93]. Yang et al. synthesized 3D honeycomb porous carbon from pomelo peels via carbonization further by KOH activation [94]. The interconnected honeycomb architecture has high surface area of 2725 m^2/g, efficient for electrolyte diffusion. This was then doped with N which further enhanced the electrochemical performance. The material exhibited a specific capacitance of 342 F/g and volumetric capacitance of 171F/cm^3 at 0.2 A/g. It showed a rate capability of 62% and cyclic stability of 98% over 1000 cycles. Zhao et al. synthesized HPCs from ant powder, in which the exoskeleton of ant contains chitin, facilitating 3D frameworks [95]. Furthermore, the exoskeleton is a rich source of fatty acid and protein, therefore the carbon framework contains many heteroatoms doped skeleton. The ant powder also has many metal salts, making it a natural porous template structure. The obtained biomass possesses high surface area of 2650 m^2/g with suitable pore

sizes. Such morphology enhanced the electrochemical performance of the material with a specific capacity of 352 F/g at 0.1 A/g, high retention rate of 80%, and cyclic stability after 10000 cycles.

4.2 Metal Doping of Biomass-Derived Nanostructures

Metal/metal oxides or hydroxides are often incorporated within the carbon structures in order to contribute to the pseudocapacitive behavior. The typical redox reactions of these materials results in adsorption of ions at the electrode-electrolyte interface and enhances the energy density of the SCs. The sole use of these metal derivatives is restricted because of their low specific surface area, structural instability, and low intrinsic conductivity. But doping of metals within the biomass-derived nanostructures, offers suitable space for the electroactive sites where the redox reactions can take place. The porous structures of the carbon skeleton can promote charge transfer, leading to high energy density and rate performance. Also, the robust biomass architectures are resistant to mechanical stress caused by the faradic reactions and thereby increase the cyclic stability of the hybrids. Therefore, metal-doped biomass-derived structures enhances capacitance, energy density, rate performance, and cyclic stability. The following section will elaborate on some of the metal/metal oxides or hydroxides that have been incorporated within the biomass to enhance the electrochemical performance.

4.2.1 Nickel/Nickel Oxide or Hydroxide Biomass-Derived Nanostructures

Nickel and its derivatives have been regarded as electroactive materials for the SCs application. They have diverse morphologies, easy synthesis, and rapid redox reaction kinetics [96]. They have good synergism with the carbon frameworks as a result provide better electrochemical properties. Li et al. reported the deposition of β-$Ni(OH)_2$ nanosheets within the carbon microtubes derived from catkins via hydrothermal carbonization technique [96]. The willow catkins are biomass precursors having 1D hollow tube structures with a diameter ranging from $6-10\mu m$. They are known to have good capillarity, facilitating transport of nutrients and moisture. It is used as a bio-template to produce hollow carbon microtubes to support active nanomaterials. The porous hollow microtube acted as conductive channel for charge and ion transport and the morphology is regulated and controlled by adjusting the amount of $Ni(NO_3)_2.6H_2O$. The high pseudocapacitance of β-$Ni(OH)_2$ results in high energy density of 37.8 Wh/Kg. The β-$Ni(OH)_2$- catkins derived microtube offered a specific capacitance of 1568 F/g at 1 A/g with a retention of 51% capacitance at 20 A/g and excellent cyclic stability of 84.3% after 3000 cycles. Cao and co-workers derived biochar from waste biomass and then subjected it to Ni sorption. The Ni adsorbed biochar was then employed for supercapacitor application via microwave

treatment [97]. The capacitance was found to be higher in case of microwave assisted Ni-biochar compared to without microwave activation. This enhancement can be attributed to the formation of NiO and NiOOH species from Ni(II). It also exhibited high stability after 1000 cycles with less than 2% loss. This work showed a conjugation of conservation of environment and also storage of energy.

Zhang et al. reported Ni in-situ doping to obtain cellulose based N/Ni co-doped porous carbon [98]. The microcellulose assembly under hydrothermal treatment led to the generation of honeycomb architecture facilitating the uniform distribution of N and Ni within the interconnected networks. The pore size of the porous carbon ranged between 1.7−4 nm, which is beneficial for better ion mobility and adsorption site. The resulting Ni-doped electrode material delivered a specific capacitance of 415 F/g at 0.5 A/g with capacitance retention of 72.22% at 20A/g. The cyclic stability was tested upto 10000 cycles showing a retention rate of 87.87%. They also observed that one-pot hydrothermal treatment strategy to incorporate Ni and N was beneficial for increasing the energy density and cycle life of the electrode material. Zhu and co-workers developed biomass-derived sustainable C/N–$Ni(OH)_2$/Ni_xS_y electrode material having a sandwich structure [99]. The biomass precursor used was egg white, owing to its natural abundance, good sources of N and C, as a source of S to form Ni_xS_y. The doping improves the electrical conductivity and increases the active sites for redox reactions. Ni_xS_y are dispersed and anchored on $Ni(OH)_2$ nanoflakes giving a flake/particle sandwich structure. The electrode material exhibited a specific capacitance of 1731.2 F/g at 0.5 A/g and a hybrid SCs constructed out of this shows an excellent cyclic stability of 107.6% upto 10000 cycles. Fu et al. reported $Ni(OH)_2$/sorghum stalk biomass composite obtained via microwave treatmentx [100]. Herein, biomass was first derived from sorghum stalk and $Ni(OH)_2$ was deposited on it via microwave method of deposition. The electrode material exhibited a specific capacitance of 889.2 F/g at 2A/g and capacitance retention of 95.9% over 30000 cycles. The microwave deposition assisted the uniform growth of $Ni(OH)_2$ on the sorghum stalk, resulting in enhanced electrochemical performance (Fig. 1).

4.2.2 Cobalt/Cobalt Oxide or Hydroxide Biomass-Derived Nanostructures

Cobalt or its oxides and hydroxides have been widely exploited for energy storage applications. On incorporation of cobalt and its derivatives within the porous biomass-derived skeleton, the electroactive spots are increased also increasing the cyclic stability of the system [101]. Madhu et al. reported the synthesis of activated carbon derived from Pongam seed shells and made a composite out of it with cobalt oxide [102]. The nanocomposite PSAC/Co_3O_4 showed a small transfer resistance owing to the synergism between Co_3O_4 and PSAC. Shi et al. studied the sandwich Co_3O_4@carbon fiber@Co_3O_4 for SCs application [75]. The porous hollow structure offers high specific capacitance of 892 F/g at 0.5 A/g with a long cyclic stability of

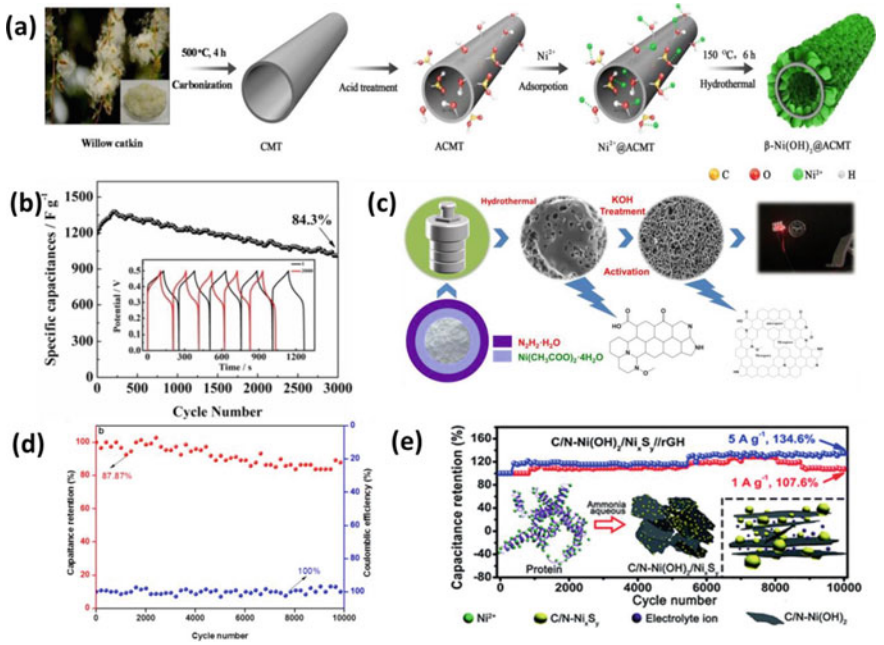

Fig. 1 Some reported nickel/nickel oxide or hydroxide biomass-derived nanostructures. **a**, **b** Scheme showing the synthesis of β-Ni(OH)$_2$@AMCT composite and the cyclic stability of the composite [96]. **c**, **d** Synthesis scheme of cellulose based N/Ni co-doped porous carbon and cyclic stability [98]. **e** C/N–Ni(OH)$_2$/Ni$_x$S$_y$ electrode material and its cyclic stability upto 10000 cycles [99]. (All figures are reprinted with permission)

88% over 6000 cycles. The hollow structure provides inner wall space to accommodate the Co_3O_4 particles and therefore enhances the redox reaction sites and serves as promising electrode material. Ouyang et al. synthesized NiCo-LDHs/BPC porous composite for supercapacitor application [103]. They observed that composite electrode material offered a high specific capacitance of 2047 F/g at a current density of 1 A/g, suggesting good interaction between BPC and LDH. Asymmetric SCs were also assembled where the composite was employed as the cathode, where the SCs delivered a capacitance of 139 F/g at 1 A/g with a cyclic stability of 75.8% after 6000 cycles. The composites were synthesized via single step solvothermal process, where NiCo-LDHs were deposited over the biomass-derived porous carbon, and arrays of nanosheets were assembled to give a spherical structure. Such hierarchical structures possess many electroactive sites facilitating ion transport and diffusion. Another such study of NiCo-LDHs nanosheets for SCs application was reported by Wang et al., where, in-situ growth of NiCo-LDHs was carried out on porous carbon derived from Dicranopteris dichotoma [104]. The synthesis of such a structure avoids the complicated growth process, induces nucleation and controllable growth, and promotes charge transfer ability and rate capability. The special structural features of LDHs nanosheets, like its dimension (6.20 nm), high surface area,

high wettability, and low charge transfer resistance also merits the electrochemical performance of the SCs. A hybrid SCs constructed out of it offers a high energy and power density of 52.47 Wh/Kg and 375 W/Kg respectively, with high capacitance retention of 75.9% after 4000 cycles. Qu et al. reported NiCo-LDH nanosheets regulated by carbon dots derived from fungus bran to form 3D flower-like morphology [105]. The role of carbon dots are ascribed to the formation of 3D spheres from 2D spheres, having more electroactive sites. The optimized obtained electrode material exhibited fair electrochemical performance with a specific capacitance of 2100 F/g at 1 A/g. Asymmetric SCs device was assembled which also delivered a high energy density of 52.5 Wh/Kg at a power density of 750 W/Kg, it can maintain 80% of its initial capacitance upto 5000 cycles. Zhang et al. reported for the first time, SCs devices assembled with metal silicates. They reported the preparation of bamboo leaves derived porous carbon along with Ni-Co silicate as cathode material for SCs [106]. The Co-Ni silicate attains a sheet petal-like structure, offering a specific capacitance of 368 F/g at 0.5 A/g and cyclic stability of 89% upto 10000 cycles. The authors claimed that their work can offer a potential pathway for the synthesis of metal silicates to recycle silicon enriched biomass and synthesize some useful materials (Fig. 2).

4.2.3 Manganese/Manganese Oxide Biomass-Derived Nanostructure

Manganese dioxide has been found to be a very good pseudocapacitive material owing to its high theoretical capacitance of 1370 F/g. The pseudocapacitance arises from the faradic reaction between Mn^{4+} and Mn^{3+} at the interface. A lot of porous carbon skeleton has been employed to grow MnO_2 and its derivatives in order to overcome the low intrinsic conductivity of manganese [107–110]. Wang et al. derived porous carbon from enteromorpha prolifera (ACEP), which acted as a template to grow MnO_2 nanostructure by wet chemical process [110]. The anchoring of the δ-MnO_2 nanosheets were optimized by modulating the reaction time. The ACEP@δ-MnO_2 electrode showed a high specific capacitance of 345.1 F/g at 0.5 A/g with cyclic stability of 92.8% after 5000 cycles and when assembled as a positive electrode in asymmetric SCs, offered a high energy and power density of 31.0 Wh/Kg and 500 W/Kg respectively. Yang et al. reported vertically grown MnO_2 on the surface of the hemp derived porous carbon (HC) [111]. The MnO_2/HC composite was synthesized via one step hydrothermal process, which produced 3D architecture with interconnected network. The porous HC acts as an ideal host to anchor the MnO_2 offering high pseudocapacitance with better ion and electron transport. The composite delivered a specific capacitance of 340 F/g at 1 A/g with rate capability of 88%. Asymmetric SCs were constructed with MnO_2/HC as the positive electrode, which showed an energy density of 33.3 Wh/Kg and power density of 14.8kW/Kg. Gogoi et al. obtained coconut derived porous carbon with $MnCo_2O_4$ nanorods and MnO_2 nanoscales supported on it [112]. The MCO-MnO_2-PC so obtained delivered a specific capacitance of 1330 F/g at 3 A/g and was employed as a positive electrode in flexible asymmetric SCs. The asymmetric device showed a power density of 1600

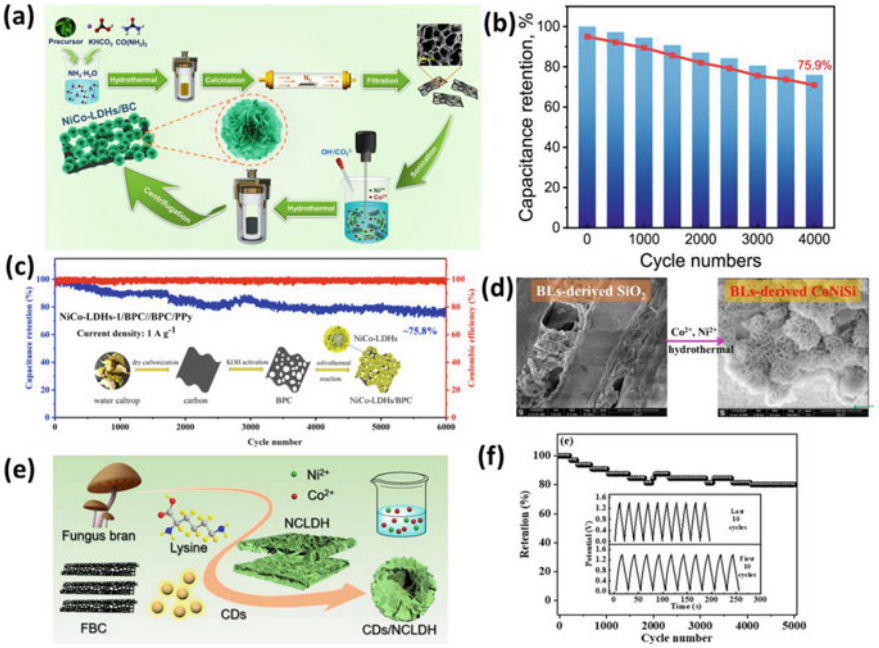

Fig. 2 Some reported cobalt/cobalt oxide or hydroxide biomass-derived nanostructures. **a** Scheme showing in-situ growth of NiCo-LDHs on porous carbon derived from Dicranopteris dichotoma and **b** the cyclic stability of the electrode material [104]. **c** Synthesis and cyclic stability of NiCo-LDHs/BPC porous composite for supercapacitor application [103]. **d** Bamboo leaves derived porous carbon along with Ni-Co silicate as cathode material for SCs [106]. **e** NiCo-LDH nanosheets regulated by carbon dots derived from fungus bran to form 3D flower-like morphology and **f** cyclic stability of the supercapacitor constructed with it [105]. (All figures are reprinted with permission)

W/Kg and energy density of 81.3 Wh/Kg, long shelf life, high rate capability, and cyclic stability of 92% upto 5000 cycles. The PC acts as a solid support for accommodating the MnO_2 and $MnCo_2O_$, providing a shorter ion travel path for the ions with enhanced electrochemical performance. Wang et al. derived porous carbon (EC) by carbonizing the eggplant skin and made a composite with MnO_2 (MnO_2/EC) via hydrothermal method [113]. The composite showed a morphology where the urchin shaped MnO_2 was decorated on the folds of EC surface. The presence of MnO_2 offered pseudocapacitance to the system, enhancing the overall capacitive performance with a specific capacitance of 652.5 F/g at 0.5 A/g and cyclic stability of 79.2% after 10000 cycles. Ganesh et al. studied the low temperature solution process for growing MnO_2 nanorods anchored on carbon framework derived from sweet potato [114]. MnO_2@C composite showed a specific capacitance of 718 F/g at 2 mA/g and a cyclic stability of 89% after 5000 cycles. Mofrad et al. showed the synthesis of carbonaceous aerogel (CA) from watermelon and the Fc-modified MnO_2 obtained by solvothermal route was physically mixed with CA in acetone to obtain MnO_2-Fc/CA [115]. The authors claimed that they synthesized battery-type

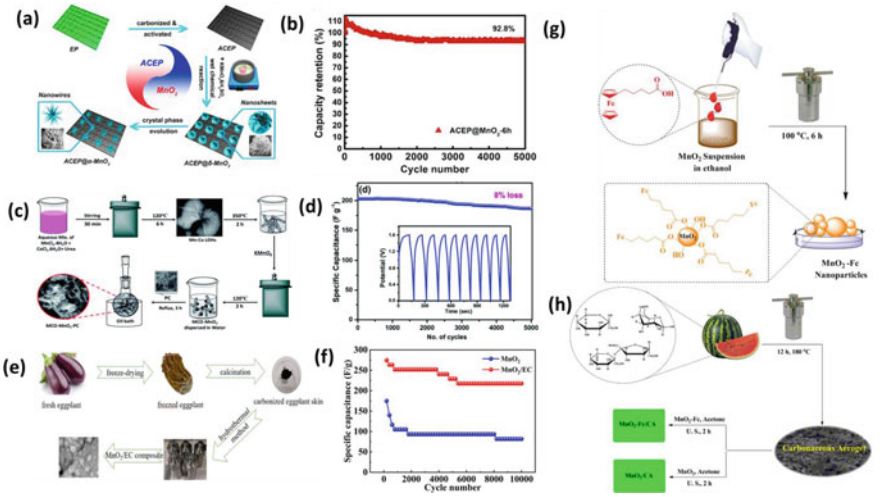

Fig. 3 Some reported Manganese/ manganese oxide biomass-derived nanostructures. **a** MnO_2 nanostructures grown on porous carbon derived from enteromorpha prolifera (ACEP) and **b** Cyclic stability of the electrode material [110]. **c** Synthesis of $MnCo_2O_4$ nanorods and MnO_2 nanoscales decorated on porous carbon derived from coconut composite (MCO-MnO_2-PC) and **d** Its cyclic stability [112]. **e** MnO_2/EC composite synthesized via hydrothermal method using eggplant and **f** Cyclic stability of the material [113]. **g** Synthesis of Fc-modified MnO_2 nanoparticles obtained by solvothermal route. **h** Fc-modified MnO_2 nanoparticles were physically mixed with carbonaceous aerogel (CA) (obtained from watermelon) in acetone to obtain MnO_2-Fc/CA [115]. (All figures are reprinted with permission)

electrode material, where Fc functions as electroactive material on the surface of MnO_2. The nanocomposite delivered a specific capacitance of 963 F/g at 1 A/g with an excellent cyclic stability of 96% after 3000 cycles. A symmetric cell assembled with this electrode material offered a power density of 4556 W/Kg and energy density of 38.1 Wh/Kg (Fig. 3).

4.2.4 Copper/Copper Oxide or Its Other Derivatives Based Biomass-Derived Nanostructure

Copper oxide possesses high chemical stability, ease of availability and environment compatibility, and high theoretical capacitance [116, 117]. Research by various groups has shown that the electrical conductivity of the carbonaceous materials can be enhanced by incorporation of Cu and its derivatives [118–120]. Hu et al. synthesized porous carbon from walnut shell and modified it with Cu/Cu_2O [121] The synthesized material was used as SCs electrode material that delivered a specific capacitance of 360 F/g at 0.5 A/g which offered a cyclic stability of 81.8% after 6000 cycles. Verma and co-workers synthesized PA/AC/CuF as an electrode material for SCs application [122]. In this work, the activated carbon (AC) was derived from coconut shell

via pyrolysis. The fabricated electrode material showed a specific capacitance of 248.3 F/g, energy density of 49.66 Wh/Kg, and power density of 5996.6 W/Kg. The cyclic stability was observed to be 92.8% after 2500 cycles. Copper ferrite (CuF) are somewhat less explored material for SCs application, therefore this work is an example to research such material in future. CuF has diverse oxidation states owing to the presence of Cu^{2+} and Fe^{3+} ions, thus providing bulk redox reactions at the surface and high charge storage ability. Sun et al. reported a new electrode material, 3D bimetallic organic framework/ biomass carbon composite [123]. The carbon was derived from grapefruit peel by carbonization method and then modified with MOF in different ratios. The composite so obtained was employed for SCs application and also for Li ion batteries. The electrochemical performance was obtained best when the doping of carbon was 20% of the active substance.

4.2.5 Iron/Iron Oxide or Its Other derivatives Based Biomass-Derived Nanostructure

Iron oxides or other derivatives of iron are found to be good electrode materials for SCs owing to their natural abundance, low cost, and environment friendly. Iron can undergo reversible redox reactions between Fe^{3+} and Fe^{2+}. Incorporation of iron oxides within the carbonaceous framework improves the conductivity, increases the ionic diffusion, and enhances the cyclic stability of the material [124]. For example, Wu et. al. developed sponge like carbon gels (CGs) from watermelon [125]. To the synthesized gels Fe_3O_4 nanoparticles were incorporated within the carbonaceous network. Fe_3O_4/CGs composite was then transformed into magnetite aerogels via calcination. This aerogel has good conductivity and porous morphology and therefore depicted excellent capacitive behavior with a specific capacitance of 333.1 F/g at 1 A/g and excellent cyclic stability of 96% after 1000 cycles. Zhang et al. studied a simple process to encapsulate nanoparticles of iron into N, P co-doped biomass-derived carbon nanotubes [126]. The precursor used for biomass was egg yolk, which is a rich source of heteroatom. The synthesized electrode material has a very high surface area to accommodate the ions, offering a high pseudocapacitance. A symmetric SCs assembled with this electrode material exhibited a specific capacitance of 392 F/g at 0.5 A/g with a long cyclic stability over 50000 cycles. Butnoi et al. prepared a composite out of lignin based fibers with iron oxide nanoparticles (L-CNFs@Fe_xO_y nanofibers) by electrospinning [127]. Lignin based fibers can be easily obtained at low cost and also the electrospun technique helps to develop interspaced carbon fibers, advantageous for electrolyte accessibility. The nanostructured composite delivered a high energy density of 43 Wh/Kg, specific capacitance of 216 F/g at 0.1 A/g, and power density of 242 W/kg. 97.6% capacitance retention after 1000 cycles also makes it a potential candidate for the SCs. Venkateswarlu et al. synthesized 2D crumbled porous carbon from waste garlic husk and then composite with Fe_3O_4 nanoassemblies were obtained [128]. Fe_3O_4 nanocrystals undergo nucleation in presence of 2D carbon framework and develop a cluster depicting a pomegranate. The crumbled architecture prevents the agglomeration and restacking of the Fe_3O_4

nanoassemblies, enabling excellent ion diffusion within the porous channels. The Fe_3O_4 NAs@2D-CCS composite depicted a power density of 3000−8000 W/Kg, specific capacitance of 820 F/g at 0.5 A/g, and energy density of 115.5−65.9 Wh/Kg with cyclic stability of 90.1% after 2000 cycles.

4.2.6 Transition Metal Dichalocogenides (TMDCs) Based Biomass-Derived Nanostructure

TMDCs are a class of 2D layered inorganic species having a layer of transition metal between two chalcogen layers. They have been recently exploited as pseudocapacitive material owing to its sheet-like structure, good conductivity, and large surface area [129]. Islam et al. studied the electrochemical properties of MoS_2 nanosheets vertically oriented on plasma pyrolyzed cellulose filter paper [130]. Free standing MoS_2-pCMF electrodes have high surface area because of the vertical arrangement and also increase the electrolyte accessibility. It operates in a wide potential window with a cutoff frequency of 103 Hz at −45° and cyclic stability of upto 50000 cycles. Guo et al. synthesized HMD/rGO/MoS_2 composite using a loofah sponge as the carbon source [131]. Hollow microtubular carbon structure obtained from loofah sponge acts as a template to accommodate MoS_2 nanoparticles (Fig. 4).

4.2.7 MXene Based Biomass-Derived Nanostructure

Transition metal carbides or nitrides are known as the MXenes, which have gained tremendous attention in current times for electrochemical energy storage. This have high packing density, electronic conductivity, and charge storage capacity, making it suitable for SCs application [132]. However, they have a tendency to aggregate and tack between the layers, reducing their effective surface area. Therefore various modifications have been done in order to get electrode materials with enhanced electrochemical performance [133]. Pu et al. synthesized N-doped MXene from chitosan derived from waste seafood for SCs application. [134] Chitosan contains amine and acetamide groups and therefore is a favorable precursor for obtaining N-doped products. N-doped MXene possesses lone pair electrons from N and also the interlayer stacking is avoided owing to doping. The electrode material showed a specific capacitance of 286.28 F/g with 98% efficiency and cyclic stability over 10000 cycles. Sun et al. prepared skin/skeleton MXene/CF porous heterostructure for SCs application [135]. The carbon fibers were derived by direct pyrolysis of the cotton fiber wiper. The MXene nanosheet covers the surface of the CF and bridges the gap between CF and MXene. The interlayer stacking of the MXene gets reduced giving a porous pathway for rapid ion exchange. The MXene/CF electrode material possesses high volumetric capacitance of 7.14 F/cm^3, good rate capability, and cyclic stability of 99.8% after 5000 cycles. Wei et al. decorated $Ti_3C_2T_x$ MXene on porous carbon derived from chitosan. [136]. The sandwiched CPCM/MXene heterostructure has electrostatic interaction with less restacking of the MXene layers that can promote ion

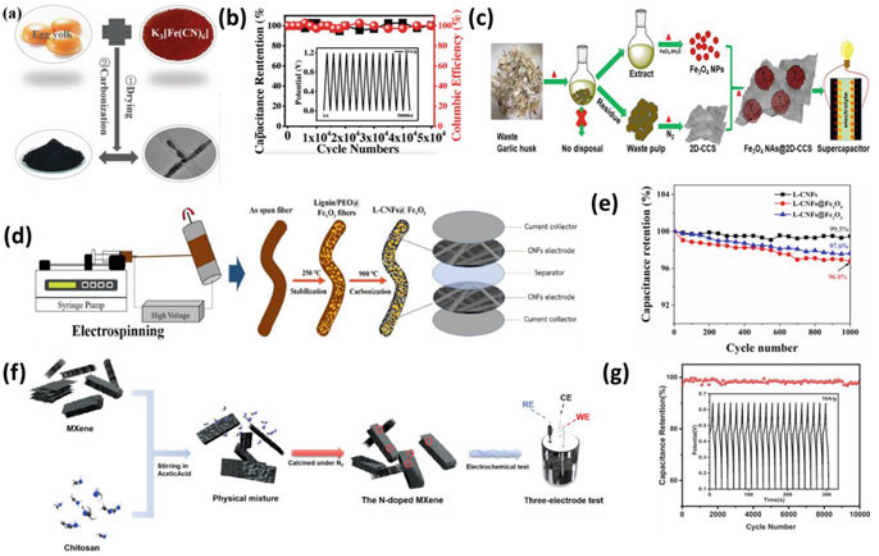

Fig. 4 Some reported iron/iron oxide and MXene based biomass-derived nanostructures. **a** Egg yolk derived biomass iron composite for SCs application and **b** its cyclic stability [126]. **c** Composite made out of 2D crumbled porous carbon from waste garlic husk and Fe_3O_4 nanoassemblies (Fe_3O_4 NAs@2D-CCS) [128]. **d** Lignin based fibers with iron oxide nanoparticles (L-CNFs@Fe_xO_y nanofibers) by electrospinning and **e** its cyclic stability [127]. **f** N-doped MXene from chitosan derived from waste seafood for SCs application and **g** its cyclic stability [134]. (All figures are reprinted with permission)

migration. The good synergism between the components leads to enhanced specific capacitance of 362 F/g at 0.5 A/g, power density 500 W/Kg, energy density 27.8 Wh/Kg, and a cyclic stability of 93.87% after 10000 cycles. Such electrochemical performance provides a new electrode material for SCs application.

4.3 Various Test Parameters

The test parameters like current density, scan rate, and potential window greatly influences the cyclic stability of the electroactive materials. For example, at low current density and scan rate, the specific capacitance is higher while at higher current density and scan rates, capacitance decreases. The reason for such a phenomenon can be explained as, at low scan rates and current density, the ions get enough time to undergo redox reactions and the rate of reactions are equal to the rate of charge transfer. But as the reaction proceeds further, the electroactive material will have a tendency to dissolve or disperse in the electrolyte, thereby decreasing the cyclic stability. However, at some instances, the scan rate and current density are purposefully increased in order to test the cyclic stability. In such cases, only a limited

number of electroactive materials will take part in the electrochemical reactions, and the dissolved materials during the course of the reaction will be replaced by other electroactive materials that are not taking part in the reaction, thereby exhibiting less specific capacitance. Therefore, the testing parameters influence the cyclic stability and must be consistent with cyclic voltammetry and charge-discharge analysis.

5 Challenges and Outlook

This chapter focuses on the recent electrode materials made of biomass-derived carbon and their composites with metal/metal oxide, nitrides, sulfides, etc. Adopting cheap and sustainable raw biomaterial precursors to obtain valued carbonaceous electrodes can reduce the use of non-renewable energy resources. The incorporation of various pseudocapacitive materials within the carbon framework generates rapid redox reactions, high charge transfer, and flexible, stable structures, offering high capacitance and long cyclic stability. However, the biomass-derived carbonaceous materials also face many challenges. For instance, a wide variety of growing environments, harvesting times, and resources of nutrients in the biomass precursor vary at different locations; decay of biomass is very common by insects or animals, etc. All these disadvantages make it difficult to reproduce the electrochemical studies of the materials. Therefore, it is difficult to reproduce the electrochemical properties of carbonaceous materials. Still, taking the economy into consideration, the large-scale use of valuable biomass (e.g., soybean, watermelon, and cocoon silk) for the preparation of porous skeletons outweighs the disadvantages of the biomass-based electrode materials.

The studies have shown that structure modification and biomass activation cannot be separated as both occur simultaneously during the synthesis process. The inherent structural features of the biomass-based materials allow the researchers to perform controlled treatments on them in order to obtain wide, highly porous architectures. The activation step is also found to be an important step for increasing the surface area of the biomass. The prospect of employing a general synthesis process in order to obtain preferred pore structure from a variety of biomass is still a challenge to the scientists. For instance, the molten-salt procedure can be a significant way to control the synthesis of porous structures with variable morphologies [137–140]. Like carbon nanobelts, they were prepared via cutting and stripping techniques in ZnCl2 molten salt, where ZnCl2 acts as a hard template for the generation of pore structure and also acts as a scissor to cut and strip the original materials to obtain the nanobelts [28]. Such carbon materials offer a very high surface area of 1208.0 m2/g and suggest a scalable and controlled approach to achieving biomass-derived carbon heterostructures. Various activation methods, like heteroatom doping, transition metal incorporation, and direct carbonization, have already been explored and employed to build SCs with high volumetric capacitance, but some shortcomings are yet to be met, like low electrical conductivity and bulk density, and weak interaction between carbon and transition metal. Heteroatom doping and pristine

biomass-derived carbon materials possess limited packing density. One such study involved embedding Fe_2O_3/FeS into N,S co-doped carbon material derived from waxberry [93]. The pore morphology was adjusted by controlling the temperature of the hydrothermal reaction and the amount of iron sulfate added. The materials showed very good capacitive performance with a high volumetric capacitance of 1320.4 F/cm^3 at 0.1 A/g, an energy density of 100.9 Wh/Kg, and a power density of 221.9 Wh/L. The material also showed a long cycle life of over 50,000 cycles. Such performance can be attributed to the short diffusion path, porous structure, and multiple heteroatoms due to doping of the carbonaceous skeleton. As a result, the contribution of the pseudocapacitance from the rapid faradic reactions taking place is demonstrated in this work.

A lot of electrolytes have also been investigated in order to obtain a wide potential window for better electrochemical performance. Varieties of electrolytes used are aqueous, non-aqueous, organic, ionic, etc. The operating potential window of an aqueous electrolyte is less than 1 V; non-aqueous electrolytes have a potential window higher than 1.23 V. Ionic liquids and organic electrolytes have a wide potential window of 2.5–4.0 V, making it suitable to obtain SCs with high volumetric energy density, as energy density is proportional to the square of the potential window. However, the electrochemical results obtained with non-aqueous SCs are less than those obtained with aqueous electrolytes, owing to their high viscosity and low ionic conductivity, therefore sacrificing electrochemical performance. The main problem with the non-aqueous SCs is their disparity between the pore structures that are biomass-derived. Still, there have been a lot of challenges with finding the best combination of electrolyte and electrode that can offer better electrochemical properties. It is essential to obtain an in-situ technique of monitoring that can correctly regulate the structural features and charge distribution at the interfaces by properly choosing the best electrolyte for the electrode material.

6 Concluding Remarks

Commercializing SCs is greatly dependent on their cyclic stability and is one of the basic requirements for industrialization. SCs are now trying to make their place in the electronic industries with key technologies and compete for the future market. There are abundant carbon materials that are commercially available, but by using biomass-derived carbon materials, economic benefits can be gained without sacrificing the cycle life. Taking everything into account, the following points must be kept in mind in order to develop high-performance electrode materials for SCs with high cyclic stability:

(a) The cyclic stability of the SCs device is highly dependent on the electrode materials and their stability. The mechanism of energy storage is dependent on the electrode materials and is a deciding factor for the electrochemical performance.

The cyclic stability dependence on the storage mechanism follows the following order: EDLC > intercalation type SCs > pseudocapacitance.

(b) Optimizing different precursors in order to obtain desired structure, surface properties, and composition by properly assessing the type of electrode material for energy storage, improved cyclic stability can be achieved. For instance, by constructing microstructure morphology and coating or encapsulating ions, nanoparticles, and atoms within the system.

(c) Proper selection of cheap and abundant biomass that possesses a high percentage of carbon, a long shelf life, and is easily scalable

(d) Flexible, microstructured, and wearable SCs have become highly fascinating in recent years. Standard and controlled methods of synthesis are used to produce desired textures and morphologies.

(e) In-depth study of pore size distribution, ion storage and transport, and surface area can guide the preparation of carbonaceous structures with enhanced electrochemical performance.

(f) SCs with high specific capacitance and power density have already been achieved, but enhancing energy density is a matter of research, so using proper electrolytes with wide potential windows must be exploited. Electrolyte philicity is an important matter of study for high cycle life and electrochemical performance. Always, an attempt must be made to maintain equilibrium between the electrode and the electrolyte. If the electrode materials have less electrolyte philicity, the electroactive materials will not get wetted properly, and as a result, adsorption, desorption, or intercalation of the ions during the electrochemical reactions will be hindered. Again, if the electroactive materials are overly wetted by the electrode, structure deformation occurs, impeding electrochemical processes.

(g) Stimulating the natural properties of the biomass, which include self-healability, self-power, environmental stability, and sensitive, sophisticated SCs, can be designed.

(h) Cyclic stability is highly influenced by the test conditions. The scan rate and current density must be almost similar in order to obtain maximum capacitance. The potential must also be consistent with the electrochemical analysis. Therefore, as a whole, the cyclic stability test must be carried out with appropriate parameters.

References

1. Tang X, Wen G, Song Y (2018) Appl Surf Sci 436:398
2. Peurifoy SR, Castro E, Liu F, Zhu XY, Ng F, Jockusch S, Steigerwald ML, Echegoyen L, Nuckolls C, Sisto TJ (2018) J Am Chem Soc 140:9341
3. Wang Y, Wang Z, Chen Y, Zhang H, Yousaf M, Wu H, Zou M, Cao A, Han RP (2018) Adv Mater 30:1802074
4. Sharma K, Arora A, Tripathi SK (2019) J Energy Storage 21:801

5. Eftekhari AJ (2018) Mater Chem A 6:2866
6. Sevilla M, Fuertes AB (2009) Chem Eur J 15:4195
7. Hu B, Wang K, Wu L, Yu SH, Antonietti M, Titirici MM (2010) Adv Mater 22:813
8. Jin H, Li J, Yuan Y, Wang J, Lu J, Wang S (2018) Adv Energy Mater 8:1801007
9. Cui X, Antonietti M, Yu SH (2006) Small 2:756
10. Barroso-Bogeat A, Alexandre-Franco M, Fernández-González C, Macías-García A, Gómez-Serrano V (2014) Phys Chem Chem Phys 16:25161
11. Ren Y, Xu Q, Zhang J, Yang H, Wang B, Yang D, Hu J, Liu Z (2014) ACS Appl Mater Interfaces 6:9689
12. 11. Zhang Q, Gu D, Li H, Xu Z, Sun H, Li J, Wang L, Shen L (2021) Electrochim Acta 367:137455
13. Bi W, Deng S, Tang H, Liu Y, Shen J, Gao G, Wu G, Atif M, AlSalhi M S, Cao G. Sci. China Mater. 8, 2022
14. Liu Y, Jiao Y, Zhang Z, Qu F, Umar A, Wu X (2014) ACS Appl Mater Interfaces 6:2174
15. Samuel E, Joshi B, Kim YI, Aldalbahi A, Rahaman M, Yoon SS (2020) ACS Sustain Chem Eng 8:3697
16. Stott A, Tas MO, Matsubara EY, Masteghin MG, Rosolen JM, Sporea RA, Silva SRP (2020) Energy Environ 3:389
17. Huang Y, Li H, Wang Z, Zhu M, Pei Z, Xue Q, Huang Y, Zhi C (2016) Nano Energy 22:422
18. Marriam I, Wang Y, Tebyetekerwa M (2020) Energy Storage Mater 33:336
19. Yu L, Chen GZ (2016) J Power Sources 326:604
20. Yan S, Abhilash KP, Tang L, Yang M, Ma Y, Xia Q, Guo Q, Xia H (2019) Small 15:1804371
21. Wang M, Xia X, Zhong Y, Wu J, Xu R, Yao Z, Wang D, Tang W, Wang X, Tu J (2019) Chem Eur J 25:3710
22. Yamada H, Nakamura H, Nakahara F, Moriguchi I, Kudo T (2007) J Phys Chem C 111:227
23. Yan J, Wang Q, Wei T, Fan Z (2014) Adv Energy Mater 4:1300816
24. Wang J, Kaskel S (2012) J Mater Chem 22:23710
25. Jin Y, Tian K, Wei L, Zhang X, Guo X (2016) J Mater Chem A 4:15968
26. Chmiola J, Yushin G, Gogotsi Y, Portet C, Simon P, Taberna PL (2006) Science 313:1760
27. Mi J, Wang XR, Fan RJ, Qu WH, Li WC (2012) Energ Fuel 26:5321
28. Ouyang T, Cheng K, Yang F, Zhou L, Zhu K, Ye K, Wang G, Cao D (2017) J Mater Chem A 5:14551
29. Liu S, Xu J, Zhu J, Chang Y, Wang H, Liu Z, Xu Y, Zhang C, Liu T (2017) J Mater Chem A 5:19997
30. Wang C, Wu D, Wang H, Gao Z, Xu F, Jiang K (2017) J Power Sources 363:375
31. Simon P, Gogotsi Y (2013) Capacitive energy storage in nanostructured carbon–electrolyte systems. Acc Chem Res 46(5):1094–1103
32. Chao D, Ouyang B, Liang P, Huong TTT, Jia G, Huang H, Xia X, Rawat RS, Fan H (2018) J Adv Mater 30:1804833
33. Montes-Morán MA, Suárez D, Menéndez JA, Fuente E (2004) Carbon 42:1219
34. Lai F, Miao YE, Zuo L, Lu H, Huang Y, Liu T (2016) Small 12:3235
35. Kale VS, Hwang M, Chang H, Kang J, Chae SI, Jeon Y, Yang J, Kim J, Ko YJ, Piao Y, Hyeon T (2018) Adv Funct Mater 28:1803786
36. Berenguer R, García-Mateos FJ, Ruiz-Rosas R, Cazorla-Amorós D, Morallón E, Rodríguez-Mirasol J, Cordero T (2016) Green Chem 18:1506
37. Shen W, Fan W (2013) J Mater Chem A 1:999
38. Hou J, Cao C, Idrees F, Ma X (2015) ACS Nano 9:2556
39. Niu J, Liu M, Xu F, Zhang Z, Dou M, Wang F (2018) Carbon 140:664
40. Teng Y, Liu E, Ding R, Liu K, Liu R, Wang L, Yang Z, Jiang H (2016) Electrochim Acta 194:394
41. Wei T, Zhang Q, Wei X, Gao Y, Li H (2016) Sci Rep 6:1
42. Qu J, Geng C, Lv S, Shao G, Ma S, Wu M (2015) Electrochim Acta 176:982
43. Chen X, Zhang J, Zhang B, Dong S, Guo X, Mu X, Fei B (2017) Sci Rep 7:1

44. Shi Y, Zhang L, Schon TB, Li H, Fan C, Li X, Wang H, Wu X, Xie H, Sun H, Seferos DS (2017) ACS Appl Mater Interfaces 9:42699
45. Li Z, Xu Z, Wang H, Ding J, Zahiri B, Holt CM, Tan X, Mitlin D (2014) Energy Environ Sci 7:1708
46. Zhang LL, Li HH, Shi YH, Fan CY, Wu XL, Wang HF, Sun HZ, Zhang JP (2016) ACS Appl Mater Interfaces 8:4233
47. Yu X, Wang Y, Li L, Li H, Shang Y (2017) Sci rep 7:1
48. Pang J, Zhang WF, Zhang JL, Zhang HM, Cao GP, Han MF, Yang YS (2018) ChemElectroChem 5:1306
49. Liang J, Jiao Y, Jaroniec M, Qiao SZ (2012) Angew Chem Int Ed 51:11496
50. Zhang X, Yan P, Zhang R, Liu K, Liu Y, Liu T, Wang X (2016) J Mater Chem A 4:19053
51. Seredych M, Idrobo JC, Bandosz TJ (2013) J Mater Chem A 1:7059
52. Park SK, Lee H, Choi MS, Suh DH, Nakhanivej P, Park HS (2018) Energy Storage Mater. 12:331
53. Wahid M, Parte G, Fernandes R, Kothari D, Ogale S (2015) RSC Adv 5:51382
54. Tran HD, Li D, Kaner RB (2009) Adv Mater 21:1487
55. Xue J, Zhao Y, Cheng H, Hu C, Hu Y, Meng Y, Shao H, Zhang Z, Qu L (2013) Phys Chem Chem Phys 15:8042
56. Li Y, Wang G, Wei T, Fan Z, Yan P (2016) Nano Energy 19:165
57. Peng L, Fang Z, Zhu Y, Yan C, Yu G (2018) Adv Energy Mater 8:1702179
58. Lee JH, Park N, Kim BG, Jung DS, Im K, Hur J, Choi JW (2013) ACS Nano 7:9366
59. Bae CJ, Erdonmez CK, Halloran JW, Chiang YM (2013) Adv Mater 25:1254
60. Chen C, Zhang Y, Li Y, Dai J, Song J, Yao Y, Gong Y, Kierzewski I, Xie J, Hu L (2017) Energy Environ Sci 10:538
61. Xiao PW, Meng Q, Zhao L, Li JJ, Wei Z, Han BH (2017) Mater Des 129:164
62. Lyu L, Seong KD, Ko D, Choi J, Lee C, Hwang T, Cho Y, Jin X, Zhang W, Pang H, Piao Y (2019) Mater Chem Front 3:2543
63. Wei Q, Xiong F, Tan S, Huang L, Lan EH, Dunn B, Mai L (2017) Adv Mater 29:1602300
64. Jin Z, Yan X, Yu Y, Zhao G (2014) J Mater Chem A 2:11706
65. Sakurada I, Nukushina Y, Ito T (1962) J Polym Sci 57:651
66. Kang YJ, Chun SJ, Lee SS, Kim BY, Kim JH, Chung H, Lee SY, Kim W (2012) ACS Nano 6:6400
67. Wang Z, Carlsson DO, Tammela P, Hua K, Zhang P, Nyholm L, Strømme M (2015) ACS Nano 9:7563
68. Torvinen K, Lehtimäki S, Keränen JT, Sievänen J, Vartiainen J, Hellén E, Lupo D, Tuukkanen S (2015) Electron Mater Lett 11:1040
69. Li S, Huang D, Yang J, Zhang B, Zhang X, Yang G, Wang M, Shen Y (2014) Nano Energy 9:309
70. Mai L, Tian X, Xu X, Chang L, Xu L (2014) Chem Rev 114:11828
71. Chen W, Yu H, Lee SY, Wei T, Li J, Fan Z (2018) Chem Soc Rev 47:2837
72. 72. Cao Y, Xie L, Sun G, Su F, Kong QQ, Li F, Ma W, Shi J, Jiang D, Lu C, Chen CM (2018) Sustain Energy Fuels 2:455
73. Shi Z, Xing L, Liu Y, Gao Y, Liu J (2018) Carbon 129:819
74. Wang X, Kong D, Zhang Y, Wang B, Li X, Qiu T, Song Q, Ning J, Song Y, Zhi L (2016) Nanoscale 8:9146
75. 75. He S, Chen W (2015) Sustain Energy Fuels 294:150
76. Hina K, Zou H, Qian W, Zuo D, Yi C (2018) Cellulose 25:607
77. Zhang X, Meng X, Gong S, Li P, Jin LE, Cao Q (2016) Mater Lett 179:73
78. Zhang X, Zhang K, Li H, Cao Q, Li P (2017) J Power Sources 344:176
79. Xu W, Mu B, Wang A (2016) Electrochim Acta 194:84
80. Tan C, Cao X, Wu XJ, He Q, Yang J, Zhang X, Chen J, Zhao W, Han S, Nam GH, Sindoro M (2017) Chem Rev 117:6225
81. Liu M, Niu J, Zhang Z, Dou M, Wang F (2018) Nano Energy 51:366
82. Hou Y, Lohe MR, Zhang J, Liu S, Zhuang X, Feng X (2016) Energy Environ Sci 9:478

83. Fan Z, Liu Y, Yan J, Ning G, Wang Q, Wei T, Zhi L (2012) Wei Adv Energy Mater 2:419
84. Mendoza-Sánchez B, Gogotsi Y (2016) Adv Mater 28:6104
85. Yi F, Ren H, Shan J, Sun X, Wei D, Liu Z (2018) Chem Soc Rev 47:3152
86. Liu B, Liu Y, Chen H, Yang M, Li H (2017) J Power Sources 341:309
87. Panmand RP, Patil P, Sethi Y, Kadam SR, Kulkarni MV, Gosavi SW, Munirathnam NR, Kale BB (2018) Nanoscale 10:22065
88. Li Z, Lv W, Zhang C, Li B, Kang F, Yang QH (2015) Carbon 92:11
89. Hou J, Jiang K, Tahir M, Wu X, Idrees F, Shen M, Cao C (2017) J Power Sources 371:148
90. Song S, Ma F, Wu G, Ma D, Geng W, Wan J (2015) J Mater Chem 3:18154
91. Liang Q, Ye L, Huang ZH, Xu Q, Bai Y, Kang F, Yang QH (2014) Nanoscale 6:13831
92. Zhao G, Chen C, Yu D, Sun L, Yang C, Zhang H, Sun Y, Besenbacher F, Yu M (2018) Nano Energy 47:547
93. Li Q, Lu C, Xiao D, Zhang H, Chen C, Xie L, Liu Y, Yuan S, Kong Q, Zheng K, Yin J (2018) ChemElectroChem 5:1279
94. Wang Y, Zhang Y, Pei L, Ying D, Xu X, Zhao L, Jia J, Cao X (2017) Sci Rep 7:41523
95. Zhang ZW, Lu CY, Liu GH, Cao YJ, Wang Z, Yang TT, Kang YH, Wei XY, Bai HC (2022) J Mater Res Technol 19:3034
96. Zhang Y, Yu L, Hu R, Zhang J, Wang Y, Niu R, Qian X, Zhu J (2018) J Mater Chem A 6:17417
97. Fu M, Zhu Z, Zhang Z, Zhuang Q, Chen W, Liu Q (2020) J Alloys Compd 846:156376
98. Cui J, Xi Y, Chen S, Li D, She X, Sun J, Han W, Yang D, Guo S (2016) Adv Funct Mater 26:8487
99. Madhu R, Veeramani V, Chen SM, Manikandan A, Lo AY, Chueh YL (2015) ACS Appl Mater Interfaces 7:15812
100. Ouyang Y, Xing T, Chen Y, Zheng L, Peng J, Wu C, Chang B, Luo Z, Wang X (2020) J Energy Storage 30:101454
101. Wang Y, Liu Y, Chen Z, Zhang M, Liu B, Xu Z, Yan K (2022) GreenChE 3:55
102. Qu K, Chen M, Wang W, Yang S, Jing S, Guo S, Tian J, Qi H, Huang Z (2022) J Colloid Interface Sci 616:584
103. Zhang Y, Wang C, Chen X, Dong X, Meng C, Huang C (2021) ACS Appl Energy Mater 4:9328
104. Zhao X, Zhang L, Murali S, Stoller MD, Zhang Q, Zhu Y, Ruoff RS (2012) ACS Nano 6:5404
105. Li Q, Xu Y, Zheng S, Guo X, Xue H, Pang H (2018) Small 14:1800426
106. Tang Y, Zheng S, Xu Y, Xiao X, Xue H, Pang H (2018) Energy Storage Mater 12:284
107. Wang X, Chen S, Li D, Sun S, Peng Z, Komarneni S, Yang D (2018) ACS Sustain Chem Eng 6:633
108. Yang M, Kim DS, Hong SB, Sim JW, Kim J, Kim SS, Choi BG (2017) Langmuir 33:5140
109. 109. Gogoi D, Karmur RS, Das MR, Ghosh NN (2022) Sustain Energy Fuels 6:3599
110. Wang X, Chu J, Yan H J, Zhang H K (2020) Heliyon 10631
111. Ganesh A, Sivakumar T, Sankar G. (2022) J Mater Sci: Mater Electron 1
112. Teimuri-Mofrad R, Payami E, Piriniya A, Hadi R (2022) Appl Organomet Chem 36:6620
113. Wen T, Wu XL, Zhang S, Wang X, Xu AW (2015) Chem Asian J 10:595
114. Zhang Q, Huang L, Kang S, Yin C, Ma Z, Cui L, Wang Y (2017) RSC Adv 7:43642
115. Wang J, Rao M, Ye C, Qiu Y, Su W, Zheng SR, Fan J, Cai SL, Zhang WG (2020) RSC adv 10:4621
116. Sirisomboonchai S, Kongparakul S, Nueangnoraj K, Zhang H, Wei L, Reubroycharoen P, Guan G, Samart C (2018) Appl Surf Sci 436:639
117. Li ZX, Yang BL, Zou KY, Kong L, Yue ML, Duan HH (2019) Carbon 144:540
118. Hu JR, Zhou JW, Jia YX, Li S (2022) New Carbon Mater 37:412
119. Pandey VK, Verma S, Verma B (2022) Chem Phys Lett 802:139780
120. Sun PP, Li YM, Zhang YH, Shi H, Shi FN (2022) J Alloys Compd 896:163081
121. Nithya VD, Arul NS (2016) J Mater Chem A 4:10767
122. Wu XL, Wen T, Guo HL, Yang S, Wang X, Xu AW (2013) ACS Nano 7:3589
123. Zhang J, Zhao H, Li J, Jin H, Yu X, Lei Y, Wang S (2019) Adv Energy Mater 9:1803221
124. Butnoi P, Pangon A, Berger R, Butt HJ, Intasanta V (2021) J Mater Res Technol 12:2153

125. Venkateswarlu S, Mahajan H, Panda A, Lee J, Govindaraju S, Yun K, Yoon M (2021) Chem Eng J 420:127584
126. Choi W, Choudhary N, Han GH, Park J, Akinwande D, Lee YH (2017) Mater Today Commun 20:116
127. Islam N, Wang S, Warzywoda J, Fan Z (2018) J Power Sources 400:277
128. Guo Y, Zhang Y, Wang Y, Zhang D, Lu Y, Luo R, Wang Y, Liu X, Kim JK, Luo Y (2019) Electrochim Acta 296:989
129. Xiong D, Li X, Bai Z, Lu S (2018) Small 14:1703419
130. Zhang Y, Ruan K, Shi X, Qiu H, Pan Y, Yan Y, Gu J (2021) Carbon 175:271
131. Pu L, Zhang J, Jiresse NKL, Gao Y, Zhou H, Naik N, Gao P, Guo Z (2022) Adv Compos Mater 5:356
132. Sun L, Fu Q, Pan C (2021) J Hazard Mater 410:124565
133. Wei L, Deng W, Li S, Wu Z, Cai J, Luo J (2022) J Bioresour Bioprod 7:63
134. Deng X, Zhao B, Zhu L, Shao Z (2015) Carbon 93:48
135. Ouyang T, Cheng K, Gao Y, Kong S, Ye K, Wang G, Cao D (2016) J Mater Chem A 4:9832
136. Liu X, Antonietti M (2014) Carbon 69:460
137. Kamali AR, Fray D (2015) J Chem Commun 51:5594
138. Liu X, Giordano C, Antonietti M (2014) Small 10:193
139. Wang J, Nie P, Ding B, Dong S, Hao X, Dou H, Zhang X (2017) J Mater Chem A 5:2411
140. Ouyang T, Cheng K, Yang F, Zhou L, Zhu K, Ye K, Wang G, Cao DJ (2017) Mater Chem A 5:14551

Porous Hollow Biomass-Based Carbon Nanostructures for High-Performance Supercapacitors

Shivam Rawat, Meenu Jindal, Akinori Muto, Srinivas Hotha, and Thallada Bhaskar

Abstract Biomass is considered a sustainable and renewable raw material for preparing exquisite carbon materials that can be utilized in multiple applications based on the properties required. One such application is in energy storage systems known as supercapacitors. In this chapter, the strategies that involve the usage of biomass to prepare porous carbon materials are discussed in detail. The influence of various activation strategies on the tuning or optimization of the pore structure of the bio-derived carbons has been explained. Furthermore, the charge storage properties of various bio-derived porous carbons have been presented to provide insight into the electrochemical behavior of microporous, mesoporous, and hierarchical porous carbons.

Keywords Porous · Hollow · Biomass · Carbon nanostructures · Supercapacitors

1 Introduction

The dwindling energy resources of non-renewable origin and the environmental pollution associated with their exhaustive use have resulted in the urgent need to harvest renewable energy. Solar, wind, and other renewable sources offer a green

S. Rawat · M. Jindal · T. Bhaskar (✉)
Material Resource Efficiency Division (MRED), CSIR-Indian Institute of Petroleum (IIP), Dehradun, Uttarakhand 248005, India
e-mail: tbhaskar@iip.res.in

Academy of Scientific and Innovative Research (AcSIR), Ghaziabad, Uttar Pradesh 201002, India

A. Muto
Department of Chemical Engineering, Graduate School of Engineering, Osaka Metropolitan University, 1−1 Gakuen-cho, Naka-ku, Sakai-shi, Osaka 599-8531, Japan

S. Hotha
Department of Chemistry, Indian Institute of Science Education and Research, Pune, Maharashtra 411008, India

S. K. Tiwari et al. (eds.), *Biomass-Based Functional Carbon Nanostructures for Supercapacitors*, Green Energy and Technology,
https://doi.org/10.1007/978-981-99-0996-4_10

route towards sustainable energy production. These resources, however, suffer limitations associated with their variable nature and intermittent losses resulting in power fluctuations [1]. To tackle this problem, using supercapacitors in energy storage systems has emerged as an efficient solution [2]. Similarly, supercapacitors have found numerous applications in electric vehicles and portable electronic devices [3, 4]. Supercapacitors store energy through the electrostatic adsorption of electrolyte ions on the surfaces of electrodes once the potential is applied. Also, the presence of redox-active sites provides further assistance through pseudocapacitive behavior via Faradaic reactions. Its specific energy density typically falls between that of conventional capacitors and batteries [5]. Supercapacitors' charge/discharge process is rapid compared to batteries, resulting in a high power density. Moreover, it also has a longer cycle life than typical lithium-ion batteries [6]. All these properties make the use of supercapacitors undoubtedly crucial in this technological era.

From the preparation point of view, numerous materials have been explored for the fabrication of supercapacitors, such as transition metal oxides [7], graphene-based materials [8], or other forms of carbon nanostructures, i.e., activated carbons, carbon nanotubes, and nanosheets [9]. However, the preparation of such material is required to be environmentally benign, sustainable, easily scalable for mass production, and cost-effective. Therefore, the feedstock must be renewable and abundantly available, and most importantly, it should be easily transformed into the desired material with facile preparation methodologies. All these qualities are met by the biomass used to prepare exquisite carbon materials.

Biomass is an organic, carbon-rich feedstock with high bioavailability throughout the globe. Lignocellulose, agriculture industry residues, forestry industry residues, algae, livestock manure, etc., are a few examples of biomass. Thermochemical conversion and subsequent activation or modification can convert these into various carbon nanostructures. When biomass undergoes heat treatment in an inert atmosphere, escaping volatiles and gases generate porosity within the structure of the solid material. Activation is performed using chemical or physical techniques to further modify the porous structure of the prepared biocarbon. Both activations can be carried out either in-situ or after the initial carbonization step, where the obtained biochar is activated. These activations involve using chemical agents such as KOH or $ZnCl_2$ or switching to different carbonization atmospheres like CO_2, NH_3, or steam [10, 11]. These activation techniques impart porosity and modify the carbon materials' surface chemistry. Due to the ease of tuning the physicochemical properties with varying feedstock, operation, and activation parameters, renewable carbon precursors are gaining significant attention.

Recently, different biomass-derived carbon materials have been reported for successful application as active electrode materials for supercapacitors [12]. Among these materials, porous carbon nanostructures have shown tremendous potential. As porosity and surface area are essential factors in determining the energy storage tendency of supercapacitors, a proper understanding of electrolyte-accessible surfaces and porous networks in carbon-based electrode material is required. This chapter discusses different types of porous nanostructures obtained from biomass-derived precursors. Apart from the preparation methodologies, the charge storage

performance of the biomass-derived carbons varies with the pore properties, which are also reviewed.

2 Biomass-Based Feedstocks for Porous Carbon Materials

Biomass can be considered a valuable feedstock for preparing carbon-based materials due to its economic viability, ecological sustainability, and environmental amicability. Biomass is distributed in various forms across the biosphere, ranging from terrestrial waste to marine organisms. It is a green and renewable raw material for numerous value-added applications [13]. One of the most abundant biomass resources is lignocellulosic biomass. It is produced as a by-product from agricultural and forest industry residues, with an estimated annual production of 181.5 billion tonnes [14]. It comprises cellulose, hemicellulose, and lignin, with compositional characteristics depending upon the feedstock [15]. Due to its large-scale bioavailability, it can be considered a sustainable feedstock for producing carbon-based materials.

Another widely available feedstock that has gained significant attention over the past few years is algal biomass. It consists of marine organisms varying from unicellular (microalgae) to multicellular (macroalgae) [16]. With a fast growth rate, even in some species showing an almost four-fold increase within 24 h, algal biomass can fulfill the feedstock's large-scale requirement for value-added applications [17]. Contrary to lignocellulose, algal biomass is rich in nitrogen, which can produce N-doped porous carbons [18, 19]. Heteroatom-doped carbons can improve the electrochemical behavior of carbons through pseudocapacitance and increase wettability, which is much needed in electrode materials [20]. Other forms of biowaste can also be utilized to produce porous carbon materials. One example is lignin, produced as a secondary product from the paper industry. It has a high carbon content and a complex aromatic, rich 3D structure, which can be converted into versatile forms of carbon through high-temperature carbonization and subsequent activation [21]. Food industry residues produced in the form of peels, seeds, bran, oil cake, empty fruit bunches, spent grain, etc., are also considered potential carbon sources [22]. Food industry residues have successfully demonstrated their potential in the preparation of porous carbons suitable for charge storage applications [23, 24]. Livestock manure [25], sewage sludge [26], and municipal waste [27] can also be considered sustainable feedstocks for the preparation of carbon-based supercapacitor electrodes. These feedstocks are high in ash and high in nitrogen and phosphorus. Ash content negatively influences the electrode material, resulting in leakage current and affecting the electrochemical stability [28]. Therefore, ash removal strategies such as fly silicon treatment are required for ash removal and to improve the electrochemical behavior [29]. Similarly, the potential window of sewage sludge-derived porous carbon supercapacitor electrodes can be increased through ash removal by HF washing [30].

3 Preparation of Porous Carbon Nanostructures from Biomass

Various research groups have synthesized porous carbon material from inexpensive renewable biomass such as rice, *Typha Orientalis*, silk proteins, bamboo, bagasse, peanut shells, rice husk, and coffee waste residues [31–38]. Several methods are available for preparing carbon material from biomass and other waste. These include mainly pyrolysis/catalytic pyrolysis [39, 40], hydrothermal carbonization [41, 42], and template-assisted synthesis [43, 44], leading to the formation of carbon materials with different properties like surface area, porosity, and surface functionalities. The physical and chemical activation processes are often employed for tuning pore structures in biomass-derived carbons. In physical activation, the precursor is treated thermally at a high temperature (700 –1000 °C) in a reactive gaseous environment [45]. Such as, activation in CO_2 environment increases the porosity by the Boudouard reaction [46]. The chemical activation requires a lower temperature range in the presence of some chemical agents (NaOH, $ZnCl_2$, KOH, Na_2CO_3, H_3PO_4, K_2CO_3, etc.). These act as dehydrating agents and remove the carbons' non-graphitic parts, resulting in a graphitic structure [47]. Based on porosity, carbon materials can be classified as ultra-microporous, microporous, mesoporous, and hierarchical porous carbon. The detailed preparation strategies for these types of carbons are described below.

3.1 Preparation of Microporous Carbon

The International Union of Pure and Applied Chemistry (IUPAC) classified microporous materials as having pore sizes below 2 nm. There are several strategies to convert biomass residues into microporous carbon materials, of which KOH activation is the most common [48]. Recently, Oginni et al. investigated the direct and indirect KOH activation of Miscanthus and switchgrass biomass to prepare microporous carbon. They reported that direct KOH activation of biomass resulted in a higher specific surface area compared to a two-step process where the biochar was activated using KOH. However, no remarkable change was observed in the pore size distribution of both activated carbons [49]. The KOH and feedstock ratio is essential in determining the biomass-derived carbons' surface area or pore properties. Varying the bamboo biochar: KOH ratio from 1:1 to 1:3 showed increasing specific surface area and micropore volume with increasing KOH amounts. The specific surface area of 980 $m^2\ g^{-1}$ and pore volume of 0.56 $cm^3\ g^{-1}$ were achieved at 800 °C activation in the N_2 environment [50]. However, a reverse trend was observed in the KOH activation of the tobacco stem. The micropores tended to merge, resulting in meso- and macropores with increasing KOH amount [51].

Molten salt activation strategies are also used to impart microporosity in biomass-derived porous carbons. This strategy involves the incorporation of metal chloride

salts such as $CuCl_2$, $ZnCl_2$, LiCl, or KCl into biomass and further carbonization at high temperatures [52]. Cao et al. reportedly synthesized microporous carbon material with a specific surface area above 1,000 $m^2\ g^{-1}$ from peanut shells and watermelon rind through $ZnCl_2$ activation and subsequent acid washing [53]. One-pot synthesis of N-doped microporous carbon was also reported through the NH_3-assisted activation process [54]. While in the case of steam activation of biochar, microporous carbon material with O-rich functionalities was obtained [55].

3.2 Preparation of Mesoporous Carbon

Mesoporous materials have been gaining attention for a few years due to their wide pore structure. Moreover, mesoporous structures with 2D or 3D linked pores have been proven to be highly efficient supercapacitor materials [56]. Hard templating and soft templating are the two most commonly used techniques for the synthesis of mesoporous materials. In the hard templating method, ordered mesoporous silica (such as SBA−15 or MCM-41) is mixed with a carbon source, followed by high-temperature carbonization. Then the template is removed by acid or alkali treatment to generate ordered mesoporous carbon materials. In the soft template process, a carbon-surfactant composite is formed through carbon source and surfactant polymerization. The carbonization of this composite leads to the formation of mesoporous carbons. By carefully selecting the template, the pore size and pore wall structure can be controlled in mesoporous carbons [57]. Milk was converted to ordered mesoporous carbon using SBA−15 as a hard template. The milk concentration and aging temperature also affected the obtained carbon's surface area and pore properties [58]. Pluronic F127 is the typical surfactant used in the soft templating process. Well-ordered mesoporous carbon materials have reportedly been prepared from kraft lignin using F127 as a surfactant [59]. Fructose as a carbon source was used by Kubo et al. for the soft template method with F127. In this method, hydrothermal carbonization was performed at 130 °C with F127, followed by the addition of trimethyl benzene as a swelling agent to get ordered pores with a diameter of 4 nm [60].

Mesoporous carbon with a specific surface area of 2240 $m^2\ g^{-1}$ was prepared using coconut shells as carbon precursors. In this study, coconut shells were hydrothermally carbonized in H_2O_2 solution, followed by chemical activation with $ZnCl_2$ [61]. Li et al. worked on starch to synthesize mesoporous carbon material through a sol–gel process using silica as a template. After subsequent drying of starch silica gel, carbonization was performed at 1000 °C and silica was removed by treating the material with dilute hydrofluoric acid. The synthesized carbon possessed a specific surface area and pore volume of 950 $m^2\ g^{-1}$ and 3.14 $cm^3\ g^{-1}$, respectively [62]. Metal oxides like MgO and ZnO can also be used as endo-templates to obtain mesoporous biocarbon [63]. Mesoporous carbon rods with a specific surface area of 2560 $m^2\ g^{-1}$ were synthesized using ethyl cellulose as a carbon source and MgO as a template [64]. Instead of directly using MgO as a template, magnesium acetate was used as a precursor for activation to generate mesoporous carbon from cotton waste. The

specific surface area and pore volume of 1139 $m^2\ g^{-1}$ and 0.85 $cm^3\ g^{-1}$, respectively, were obtained [65]. Porous carbon with a nanosheet-like structure was obtained from lignosulphonate self-assembly in zinc oxalate and precipitation in ethanol, followed by carbonization at 650 °C. After removing the ZnO endo template formed during the heat treatment, a mesopore-rich carbon quasi-nanosheet was obtained with a specific surface area of 1069 $m^2\ g^{-1}$ [66].

3.3 Preparation of Hierarchical Porous Carbon

Hierarchical porous carbons (HPC) entail micropores, mesopores, and macropores, enhancing the contact area of electrolytes with the electrode material. All these pores perform their specific function, so the overall activity of the prepared HPCs gets highly enhanced. Synthetic strategies for biomass-derived HPCs often combine the micro and meso-synthesis, such as hard/soft template methods, hydrothermal carbonization, or pyrolysis [67]. A mixture of NaCl and KCl salts has also been reported to prepare HPC with micro-mesoporous carbon from egg white. NaCl resulted in the development of mesopores, while KCl resulted in micropore generation [68]. Dual salt activation using Na_2CO_3-K_2CO_3 was performed on peanut shell-derived biochar to produce HPC with micro-mesoporosity [69].

Similarly, two activating agents were used to obtain HPC from cornstalks using $CaCO_3$ and potassium oxalate. $CaCO_3$ acted as a hard template, and potassium oxalate acted as a pore-forming agent, providing an HPC structure [70]. Wang and co-workers elegantly synthesized HPC from wood powder and utilized orange peel as a green activating agent. Wood powder and orange peel were converted into a porous material, thereby doubling the carbon yield. The vertical plot at the low-pressure region in the N_2 adsorption/desorption isotherm revealed the microporous structure, and the hysteresis loop in the high-pressure region confirmed the presence of mesopores, thereby confirming a hierarchical pore structure [71]. Long and co-workers synthesized HPC layer stacked carbon from fungus (*Auricularia*) through the KOH-assisted hydrothermal carbonization process. The carbon material synthesized possessed a specific surface area of 1103 $m^2\ g^{-1}$ and a pore volume of 0.54 $cm^3\ g^{-1}$ [72]. Other strategies involving one-pot synthetic methodologies have also been reported. Activation using $KMnO_4$ resulted in HPC with a surface area of around 1200 $m^2\ g^{-1}$ and 1.17 $cm^3\ g^{-1}$ [73]. While Deng et al. prepared 3D porous HPCs from various biomass residues using a strategy like the bread leavening effect using $KHCO_3$ [74]. Instead of using toxic and corrosive activating agents like KOH, Gopalakrishnan et al. used the KCl-NaCl salt mixture to impart hierarchical porosity in ginger-derived carbon [75]. Using potassium citrate and oxalates for activation can also be considered as they are less environmentally hazardous or corrosive than KOH. Poplar catkin biomass was directly converted to HPC using potassium citrate as an activating agent. The high specific surface area and pore volume of 2186 $m^2\ g^{-1}$ and 1.35 $cm^3\ g^{-1}$, respectively, were obtained [76]. Also, the type and amount of citrate salt can affect the porosity of the carbon material. Activation of cotton waste with

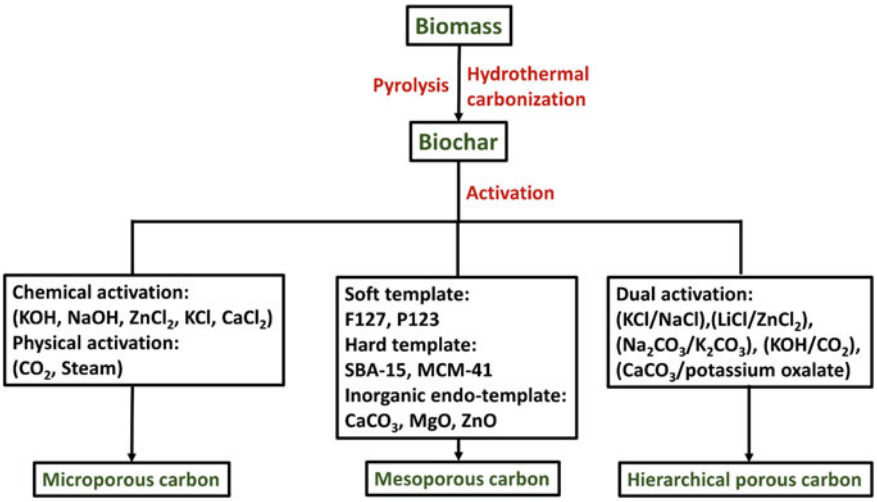

Fig. 1 Overview of activation strategies for the preparation of porous biomass-derived carbon

potassium citrate resulted in the formation of HPC structure with a specific surface area of 1723 $m^2\ g^{-1}$. On the contrary, sodium citrate resulted in microporous carbon. Thus, tailored porosity can be achieved using different citrate salts [77]. Another interesting strategy reported by Wang et al. to produce HPC is through the activation of feedstock in the presence of KOH and Mg. In this strategy, carboxymethylcellulose sodium mixed with KOH/Mg mixture was carbonized to obtain HPC nanosheets with specific surface area and pore volume of 2812 $m^2\ g^{-1}$ and 2.54 $cm^3\ g^{-1}$, respectively [78]. Self-template activation strategies investigated by Song et al. provided a simple route to obtain 3D HPC from corncob biomass. In this method, biomass pretreatment with KOH was performed before carbonization. The HPC consisted of micro, meso, and macropores with surface areas ranging between 800 and 900 $m^2\ g^{-1}$ [79]. An overview of the activation strategies involved in various porous carbon structures is highlighted in Fig. 1.

4 Influence of Porosity on Bio-derived Porous Carbon Supercapacitors

The principal energy storage mechanism in supercapacitors is a surface phenomenon in which the electrolyte ions are adsorbed on the surface of the electrode corresponding to an oppositely charged terminal, typically referred to as "electric double layer capacitance (EDLC)". Therefore, a high surface area and adequate porosity are highly desirable. Also, the pore volume, pore size distribution, and pore interconnectivity play a critical role in the overall electrochemical behavior of the carbon-based

electrode material [80]. Another vital aspect of charge storage in a supercapacitor is reversible Faradaic reactions, known as pseudo capacitance. It is typically governed by the surface chemistry of the electrode material, where the heteroatom functionalities dictate the charge storage mechanism through reversible redox reactions [81].

4.1 Microporous Carbon

Micropores in porous carbons are more critical for storing electrolyte ions than mesopores and macropores because micropores contribute more to the specific surface area and consequently result in high specific capacitance. A good attraction of ions with the pore walls of microporous carbons and a lack of space charge results in the formation of an efficient electric double layer [82]. Carbon material prepared from watermelon seeds using KOH and sodium alginate mixture resulted in 90% porosity in the microporous region. It exhibited a specific capacitance of 385 F g^{-1} at 0.5 A g^{-1} current density [83]. Broad micropores in carbon ranging between 1 and 2 nm were obtained from flaxseed residue after KOH activation. The specific capacitance of 369 and 398 F g^{-1} was obtained at 0.5 A g^{-1} with KOH and H_2SO_4 electrolytes, respectively. Even as the current density was increased to 20 A g^{-1}, more than 90% of the initial capacitance was retained [84]. Microporous carbon prepared from Konjac gel using KOH activation was able to store 274 F g^{-1} at 1 A g^{-1}. Increasing the current density to 10 A g^{-1} resulted in a specific capacitance of 217.5 F g^{-1} [85]. Generally, it is observed that microporous carbons do not favor capacitance retention at higher current density. However, apart from compatible electrolyte ion size, capacitance retention also depends on the ionic conductivity of the electrolyte [86]. KOH activation of walnut shells resulted in a unique microporous sheet-like structure with pore walls as thin as 1–2 carbon layers and specific surface area, pore volume 3577 m^2 g^{-1}, 2.19 cm^3 g^{-1}, respectively. The specific capacitance of 330 F g^{-1} at 0.1 A g^{-1} was achieved, and even when the current density was increased from 0.5 to 100 A g^{-1}, 81% of capacitance was retained. The unique pore size distribution and sheet-like structure resulted in excellent ion transport at high current density. The power and energy density of the fabricated device using ionic liquid as an electrolyte was 100 kW kg^{-1} and 120 Wh kg^{-1}, respectively [87]. Carbon microspheres prepared from hydrothermal treatment of xylose were activated using KOH and H_3PO_4 to generate micropores. The microstructure was retained after the activation, and the porous microsphere delivered a specific capacitance of 277 F g^{-1} [88]. Micropore-dominant carbon nanosheets were prepared using the KOH activation method on fish skin. At 0.1 A g^{-1}, good gravimetric and volumetric capacitance of 374 F g^{-1} and 381 F cm^{-3} were obtained. Even when the current density was increased to 50 A g^{-1}, 183 F g^{-1} and 186 F cm^{-3} of capacitance were retained. The 2D nanosheet structure was responsible for such behaviour, providing accessible surface area for better ionic diffusion and conductivity [89]. Similarly, microporous graphene-like nanosheets were obtained through the carbonization of ginger roots resulting in a

capacitance of 390 F g^{-1} at 1 A g^{-1} [90]. N-doped microporous carbon nanosheets were synthesized from melamine using potassium citrate. The material exhibited a specific capacitance of 350 F g^{-1} at 1 A g^{-1} [91]. Microwave-induced graphitization and activation strategy to obtain microporous graphene nanosheets were reported by Li et al. Black sesame were carbonized and activated using KOH under microwave radiation to obtain a high specific surface area (2414 m^2 g^{-1}) and a high graphitization due to which the specific capacitance 369 F g^{-1} at 1 A g^{-1} was achieved [92].

4.2 Ultra-Microporous Carbon

Ultra-microporous carbon is a sub-class of microporous carbon having a pore size below 0.7 nm. Due to the extremely small pore size distribution in these carbons, the choice of electrolyte should be such that it gets effectively adsorbed inside the pores. When the charge storage was investigated in carbon material with a pore size of 0.55 nm, it was observed that higher capacitance was obtained with KOH electrolyte compared to Et_4NBF_4 (Tetraethylammonium tetrafluoroborate), strongly suggesting the size compatibility requirement in ultra-microporous carbons [93]. In the sub-microporous region, desolvated ions are adsorbed inside the pores, resulting in a high specific capacitance [94]. Nonetheless, a reasonable amount of large pores is also necessary to have a superior charge storage performance [95]. However, low capacitance retention is observed with increasing current density for ultra-microporous carbons with extremely narrow pores between 0.35 to 0.43 nm in 2 M H_2SO_4 electrolyte [96]. Ultra-microporous carbon with high O and N content was prepared using naturally available sodium alginate polysaccharide and examined for energy storage. A combined effect of EDLC and pseudocapacitance was responsible for a high specific capacitance of 342 F g^{-1} at 2 A g^{-1} [97]. Predominantly ultra-microporous carbon prepared using pine cones also showed good specific capacitance of 320 F g^{-1} at 0.5 A g^{-1} [98]. A high volumetric capacitance can also be achieved using ultra-microporous carbon. With bacterial cellulose as a precursor, thiourea for heteroatom doping and KOH as an activating agent, carbon material with pores of 0.53 nm was obtained. The gravimetric and volumetric capacitance of the obtained carbon was 430 F g^{-1} and 507 F cm^{-3}, respectively, at 0.5 A g^{-1} [99]. Similarly, KOH-activated carbon from jujube biochar with pore size in the sub-microporous and microporous region showed a high volumetric capacitance of 476 F cm^{-3} in 6 M KOH electrolyte [100].

4.3 Mesoporous Carbon

As mentioned above, the limitation associated with microporous carbon is its lower capacitance retention with increasing current density due to sluggish kinetics of the

electrolyte ions while accessing the pores. In the case of mesoporous carbons, this problem is resolved. However, a trade-off needs to be balanced as high mesoporosity can decrease the overall volumetric energy density of the porous carbon material as high porosity and low density limits the volumetric capacitance between 60–130 F cm^{-3} [101]. The mesoporous carbon rods prepared from ethyl cellulose could deliver a specific capacitance of 239 F g^{-1} at 1 A g^{-1}. Even when the current density was increased to 100 A g^{-1}, 53% of the capacitance was retained. This high capacity retention behavior was observed due to fast electronic and ion transport offered by mesoporous carbon [64]. Fuertes et al. reported that the pore size of the mesopore affects the electrochemical behavior. Two different mesoporous carbons with a pore size distribution of 3 and 8 nm were prepared by template method using furfuryl alcohol as a carbon source. The specific capacitance for carbon with a smaller mesopore was higher. On the contrary, when the current density varied from 0.1 to 1 A g^{-1} in the H_2SO_4 electrolyte, the capacitance retention was higher for carbon having a larger mesopore size [102]. With lignin-derived carbon material using surfactant Pluronic F127 as pore dictating agent, mesoporous carbon with very broad pores varying from 2 to 16 nm was obtained. Further activation using CO_2 and KOH was performed to increase the specific capacitance from 77 F g^{-1} to 102 and 92 F g^{-1}, respectively [59]. Biogas slurry was converted to mesoporous carbon having a pore size distribution of 3–4.5 nm using KOH: feedstock in a 3:1 ratio, and a specific capacitance of 289 F g^{-1} was obtained. Decreasing the activation time or KOH amount had a negative effect on the charge storage capability of the carbon material [103]. Mesoporous carbon material prepared using bamboo biomass showed excellent supercapacitor performance displaying a specific capacitance of 293 F g^{-1} at 0.5 A g^{-1}. Upon increasing the current density to 20 A g^{-1}, 194 F g^{-1} specific capacitance was still retained [104].

A high operating potential window can also be used for mesoporous carbon, as reported by Bello et al. Pinecone was used as a carbon precursor, and mesopore generation was carried out using the hydrothermal treatment and its subsequent KOH activation. A specific capacitance of 137 F g^{-1} was achieved with a 2 V potential window and Na_2SO_4 electrolyte [105]. Mesoporous carbon obtained through ZnO-templated activation bark of Platanus. In the Et_4NBF_4 organic electrolyte, a high potential window of 3 V can be achieved, and a specific capacitance of 116 F g^{-1} at 1 A g^{-1} was observed [106]. Mesoporous carbon nanosheets were prepared from camellia oleifera residue through carbonization and microwave-assisted KOH activation. The obtained material exhibited a high specific capacitance of 367 F g^{-1} at 1 A g^{-1} with 66% capacitance retention when the current density was increased 20 times. The high performance was attributed to its nanosheet-like structure with abundant mesopores resulting in a shorter path for ion diffusion during the charging-discharging process [107]. Through controlled pyrolysis of sugarcane bagasse at 800 °C and quenching in ice water, mesoporous carbon with a high specific capacitance of 314 F g^{-1} at 9 A g^{-1} current density was obtained. Compared to the usual cooling method at room temperature, this capacitance value was 22% higher [108]. The expansion of pores during the quenching resulted in mesoporous carbon with a better specific surface area, resulting in better charge storage properties. In the

presence of thiourea, sodium alginate was converted to mesoporous carbon through activation using zinc acetate and calcium acetate. In-situ template formation of ZnO and $CaCO_3$ was observed, which were removed by acid washing. A specific surface area between 900 and 1900 $m^2\ g^{-1}$ was obtained, and pore size could be optimized by controlling the type of activating agent and the amount of thiourea. The electrochemical performance of ZnO-templated carbon was better than that obtained by $CaCO_3$. Moreover, thiourea also resulted in the formation of N and S surface functionalities and a specific capacitance of 350 F g^{-1} was obtained at 1 A g^{-1} [109].

In-situ activation strategies have also been investigated to develop mesoporous carbons from biomass rich in $CaCO_3$. Through direct carbonization of crab shell, mesoporous carbon was prepared as naturally present $CaCO_3$ acted as the in-situ template. The resulting biocarbon showed a specific capacitance of 220 F g^{-1} [110]. In the study reported by Yu et al., one-pot microwave-assisted phosphoric acid activation of sucrose and rice husk mixture in a 6:2:2 ratio (H_3PO_4: rice husk: sucrose) at 600 W in 20 min resulted in mesoporous carbon with 3.68 nm average pore size. The obtained material could store 150 F g^{-1} at 0.1 A g^{-1} current density [111].

4.4 Hierarchical Porous Carbon

HPCs typically have a better charge storage performance than other porous carbon materials. Due to the multimodal pore size available with micro-, meso-, and macropores, these carbon materials provide a better electrochemically available surface area, short ionic diffusion paths, and fast ion transport [112]. This ultimately results in better rate capability of HPCs. The macropores act as ion reservoirs for the HPC, while the mesopores provide diffusion pathways resulting in a high ion transfer rate [113]. HPC and microporous carbon produced from the same feedstock were investigated for their charge storage behavior. KOH-activated microporous carbons possessed a higher surface area and showed higher capacitance at low current density than HPC. When the current density was increased from 0.2 A g^{-1} to 50 A g^{-1}, the capacitance of HPC decreased from 150.1 F g^{-1} to 91.6 F g^{-1}, and that of microporous carbon fell from 160.2 F g^{-1} to 42 F g^{-1}. This shows that a hierarchical porous structure increases the available surface for electrolyte storage [71].

KOH activation reportedly prepared 1D HPC from *Metaplexis Japonica* filament. The inherent tube-like morphology was preserved in the carbon material obtained after carbonization, while after activation, pores emerged on the surface of the hollow tubular structure. The resulting carbon material exhibited 256.5 F g^{-1} specific capacitance [114]. Replacing water in the hydrothermal carbonization process with ionic liquid (1-butyl-3-methylimidazolium tetrachloroferrate) resulted in the generation of HPC from grass and KOH activation. The resulting HPC showed a capacitance value of 336 F g^{-1} at 1 A g^{-1}. Even upon increasing the current density by ten times, 222 F g^{-1} capacitance was still retained [115]. The carbon obtained after one pot activation using $KHCO_3$ showed the presence of micro-meso-macropores resulting in a

high specific capacitance of 253 F g^{-1} and 187 F g^{-1} from cellulose and bamboo-derived porous carbon, respectively [74]. Foxtail grass was used to prepare HPC using a Na_2CO_3-K_2CO_3 mixture. The material exhibited gravimetric and volumetric capacitance of 358 F g^{-1} and 243 F cm^{-3}, respectively, at 0.5 A g^{-1} [116].

Hu et al. prepared HPC with a large specific surface area (3188 m^2 g^{-1}) and pore volume (3.20 cm^3 g^{-1}) from in-situ hard template activation of lotus seeds shell with sodium phytate and subsequent chemical activation using NaOH. The material exhibited exceptional capacitance of 241 F g^{-1} at a high current density of 200 A g^{-1} in alkaline electrolyte [117]. A mixture of coconut shell and sewage sludge was hydrothermally carbonized and further activated using KOH to obtain an HPC structure with a specific capacitance of 420 F g^{-1} at 0.5 A g^{-1} [118]. In the case of onion-derived HPC using the same activation method, 179.5 F g^{-1} specific capacitance at 0.5 A g^{-1} was achieved [119].

Other activation strategies to obtain HPCs have also been reported. In a dual activation strategy, Co^{2+}-impregnated Chinese parasol fluff was KOH activated and then further activated using CO_2 to get HPC with 682 F g^{-1} at 0.2 A g^{-1} current density [120]. In this strategy, Co^{2+} acted as a template for converting the biomass to a carbon nanosheet-like structure through catalytic graphitization. At the same time, the KOH and CO_2 were responsible for providing the pores to the HPC structure. Through K_2CO_3 activation of banana leaves, micro-mesoporous HPC was obtained with a specific capacitance of 190 F g^{-1} using an ionic liquid electrolyte and a 3 V potential window [121]. Dual salt activation of Zanthoxylum leaves using ferric nitrate and zinc chloride resulted in a 3D HPC framework with a hollow nanostructure and a specific surface area of 1243 m^2 g^{-1}. The specific capacitance of the material was around 200 F g^{-1} and the fabricated symmetric device showed an energy density of 18.7 Wh kg^{-1} at a power density of 225 W kg^{-1} [122]. 3D HPC nanosheets were synthesized from Prosopis juliflora wood with a high specific surface area of 2943 m^2 g^{-1} and a high specific capacitance of 426 F g^{-1}. Owing to stable large electrochemical potential window of 2 V in Na_2SO_4 electrolyte, an energy density of 56.7 Wh kg^{-1} was obtained at a power density of 248.8 W kg^{-1} [123].

Fibrous carbon with hierarchical porosity is in huge demand due to its flexibility and high capacitance, which makes them useful in portable electronic devices. For such materials, feedstocks with inherent fibrous nature have been explored using green processing technologies like electro-spinning, spraying, coating, or ink-jet printing [124]. Nonetheless, activation techniques that do not alter the fibrous microstructure are in the nascent stage. HPC from cellulose using a zinc-ethylenediamine complex activating agent was prepared after freeze-drying and spraying, followed by carbonization at a high temperature between 700 and 1000 °C. A stable and flexible supercapacitor electrode with a specific surface area of 1095 m^2 g^{-1} and capacitance of 216 F g^{-1} (at 1 A g^{-1}) was obtained [125]. A flexible carbon supercapacitor electrode from the bamboo pulp was prepared by Ying et al. through a facile and mild activation strategy by employing N-methylmorpholine-N-oxide solution and freeze-drying it to form ice microcrystals. The HPC formed, retained the structural integrity, and provided a specific capacitance of 216 F g^{-1}

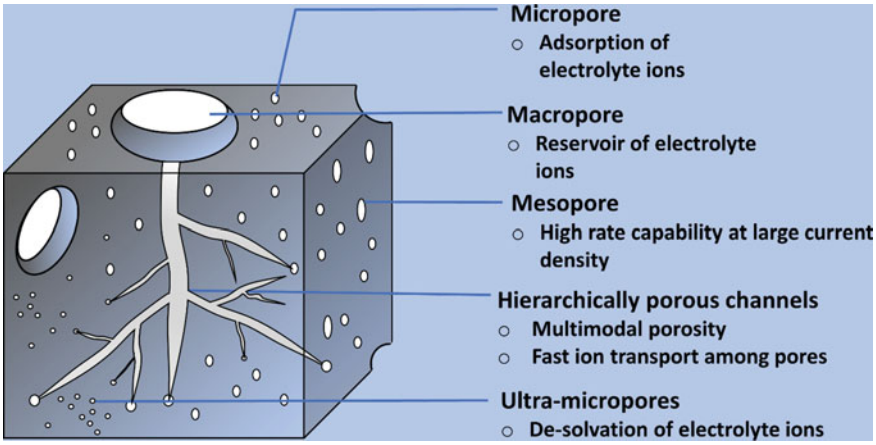

Fig. 2 Pore characteristics in porous carbon supercapacitor electrodes

at 1 A g^{-1} [126]. Similarly, a flexible carbon supercapacitor electrode with hierarchical porosity was prepared from the same feedstock (i.e., bamboo pulp) using magnesium acetate activation after hydrothermal treatment in KOH/Na_2SO_3. A high specific capacitance of 331 F g^{-1} at a current density of 1 A g^{-1} was obtained. Unlike the synthesis of the electrode using KOH or $ZnCl_2$ activation, the flexibility of $Mg(OAc)_2$ activated biocarbon showed a remarkable flexibility by retaining the fibrous structure of the carbon precursor [127].

Therefore, the porosity of carbon materials is critical in determining the intended application of carbons in the supercapacitor electrode. Each pore plays a different role in determining the overall specific capacitance of the supercapacitor. A pictorial summary of pores in biomass-derived carbons is shown in Fig. 2. The specific capacitance, energy density, and power density of various porous biocarbon are tabulated in Table 1.

5 Heteroatom-Doped Porous Nanostructures

Doping of heteroatoms like N, P, O, or S is carried out to improve the electrochemical behavior of carbon-based materials. As functional groups get removed from the biomass-derived carbon during pyrolysis/activation at high temperatures during the generation of graphitic nanostructures, the surface of carbon becomes less hydrophilic [135]. It is undoubtedly crucial that maximum contact is present between the electrode material and electrolytic solution for easy adsorption of electrolyte ions once the potential is applied. Therefore, surface functionalities need to be modified without any compromise with the porosity of carbon material. There are two strategies to impart heteroatoms in the porous carbon framework, either precursors

Table 1 Surface and energy storage properties of biomass-derived porous carbons

S. No	Feedstock	Activation	Specific surface area, $m^2\ g^{-1}$	Porosity	Specific capacitance, F g^{-1} (at current density)	Energy density, W h Kg^{-1}	Power density, kW Kg^{-1}	Refs.
1	Sodium alginate	Carbonization/KOH activation	1695	Ultra-microporous	342 (2 A g^{-1})	3.8	0.246	[97]
2	Pinecone	Carbonization/KOH activation	2000–2500	Ultra-microporous	320 (0.5 A g^{-1})	7	1	[98]
3	Bacterial cellulose	Carbonization/Thiourea + KOH activation	1554	Ultra-microporous	430 (0.5 A g^{-1})	–	–	[99]
4	Walnut shell	Carbonization/KOH activation	2373	Ultra-microporous	298 (1 A g^{-1})	82.8	7	[128]
5	Apple bagasse	Carbonization/KOH activation	2023	Ultra-microporous	300	–	v	[129]
6	Ginger	Carbonization/ No activation	320	Microporous	390 (1 A g^{-1})	9.67	0.2	[90]
7	Melon seeds	Carbonization/ Sodium alginate activation	2310–3001	Microporous	385 (0.5 A g^{-1})	–	–	[83]
8	Konjac gel	Carbonization with $NaHCO_3$	2119	Microporous	274 (1 A g^{-1})	–	–	[85]
9	Flaxseed residue	Carbonization/KOH activation	3326	Microporous	344 (1 A g^{-1})	43.5	13.3	[84]
10	Fish skin	Carbonization/KOH activation	1017	Microporous	381 (0.1 A g^{-1})	12.5 Wh L^{-1}	24 W L^{-1}	[89]
11	Squid gladius	Carbonization/KOH activation	1081	Microporous	204 (0.5 A g^{-1})	4.53	9.9	[130]
12	Almond shell	Carbonization/ HNO_3 activation	373	Microporous	171 (1 A g^{-1})	53.6	1.1	[131]
13	Coconut shell	Hydrothermal carbonization/$ZnCl_2$ activation	2440	Mesoporous	246	7.6	4.5	[61]

(continued)

Table 1 (continued)

S. No	Feedstock	Activation	Specific surface area, $m^2\ g^{-1}$	Porosity	Specific capacitance, F g^{-1} (at current density)	Energy density, W h Kg^{-1}	Power density, kW Kg^{-1}	Refs.
14	Lignin	MgO and Pluronic F127 template-assisted carbonization	712	Mesoporous	186	–	–	[132]
15	Pinecone	Hydrothermal carbonization/KOH activation	1515	Mesoporous	137	19	0.1	[105]
16	Camellia oleifera residue	Carbonization/Microwave activation	1726	Mesoporous	275 (1 A g^{-1})	9.5	0.478	[107]
17	Crab shell	Carbonization/Self-templating	634	Mesoporous	220	–	–	[110]
18	Green tea waste	Carbonization/KOH activation	1058	Mesoporous	162 (0.5 A g^{-1})	–	–	[133]
19	Rice husk + sucrose	H_3PO_4 impregnated microwave activation	1399	Mesoporous	150 (0.1 A g^{-1})	4.5	1.05	[111]
20	Cornstalk	Carbonization with $K_2C_2O_4$ and $CaCO_3$	2054	HPC	387 (1 A g^{-1})	42.5	0.374	[70]
21	Onion	KOH pretreatment/Pyrolysis	1915	HPC	132 (20 A g^{-1})	–	–	[119]
22	Coconut shell + sewage sludge	Hydrothermal carbonization/$CaCO_3$, SiO_2 activation	2049	HPC	420 (0.5 A g^{-1})	25.4	0.225	[118]
23	Lotus seed shells	Sol gel with Sodium phytate/Carbonization/NaOH activation	3188	HPC	241 (200 A g^{-1})	10.9	102.6	[117]
24	Corn husk	KOH pretreatment/pyrolysis	928	HPC	356 (1 A g^{-1})	21	0.875	[79]
25	Grape marcs	Urea doping/KOH activation	2221	HPC	446 (0.5 A g^{-1})	16.3	0.348	[134]

of heteroatoms can be added to biomass/biocarbon as a dopant and carbonized, or process parameters can be optimized so that the inherent heteroatoms are maintained in the porous biocarbon.

For N-doped porous carbon, NH_3 treatment is the most common activation strategy. Cellulose fiber carbonized in NH_3 atmosphere at 800 °C resulted in microporous carbon with 3.9 atomic % N content and a specific surface area of 1072 $m^2\ g^{-1}$. When used as a binder-free supercapacitor electrode, the resulting material possessed a specific capacitance of 172 F g^{-1} at 1 A g^{-1}. N and O surface functionalities also resulted in low charge-transfer resistance [136]. Hydrothermally treated glucose-derived carbon was activated in the NH_3 atmosphere at 950 °C. N-doped microporous carbon with spherical morphology was obtained. High specific capacitance of 244 F g^{-1} at 0.2 A g^{-1} was obtained owing to its N-rich surface with a specific surface area of 1049 $m^2\ g^{-1}$ [137]. NH_4Cl was also reportedly used as a dopant and an activating agent to obtain HPC with 4 at. % N content from Camellia pollen [138]. N-doped HPC prepared from grape marcs with urea as dopant and KOH as activating agent. The prepared material exhibited 446 F g^{-1} at 0.5 A g^{-1} specific capacitance. When the charge storage performance was compared to the porous carbon obtained by KOH activation without doping, N-doped HPC showed more than a 45% increase in capacitance at 1 A g^{-1} under the same conditions, and even the specific surface area was almost 13% higher [134]. It demonstrated that not only the electrochemical properties but also the pore enhancement could take place while doping with urea. Deng et al. systematically investigated the effect of electrolyte and heteroatom content using gelatin as feedstock and KNO3 as activating agent. The pore size distribution and N-doping can be adjusted by optimizing the KNO_3 dosage amount. Both heteroatom doping and porosity positively influence the charge storage performance of the biocarbon. However, the factor varied for enhancement in capacitance depending upon the electrolyte. For aqueous KOH electrolyte, enhancement was dominated by the redox-active sites through pseudocapacitance. While in the case of ionic liquid electrolyte $EmimBF_4$ (1-Ethyl-3-methylimidazolium tetrafluoroborate), a broader pore size dispersion was predominant for charge storage through better charge separation in the nanopores [139]. A 3D honeycomb-like porous HPC with N, P, O, and S heteroatom was prepared from KOH tree seeds. A high specific capacitance of 384 F g^{-1} at 0.5 A g^{-1} was achieved for the material in KOH electrolyte solution with more than 95% cycling stability at 20 A g^{-1}. In a neutral Na_2SO_4 aqueous electrolyte with a large potential window of 2 V, a power density and energy density of 0.5 kW kg^{-1} and 19.17 Wh kg^{-1}, respectively [140].

N, S co-doped HPC was prepared from Ginkgo leaves using NH_4NO_3 as a dopant and activating agent. Only N was doped using an external source, while S was self-doped due to high S content in the feedstock. Activation by NH_4NO_3 resulted in a specific surface area above 500 $m^2\ g^{-1}$ and a specific capacitance of 330.5 F g^{-1} at a current density of 0.5 A g^{-1} was observed. Even when the current density was increased to 10 A g^{-1}, a capacitance of 252 F g^{-1} was retained due to the hierarchical porosity-assisted diffusion of electrolyte at a high current [141]. Walnut shell waste was converted to N, P, and S co-doped HPC with a specific surface area of 2583 $m^2\ g^{-1}$ and pore volume of 1.24 $cm^3\ g^{-1}$. The prepared HPC exhibited a specific

capacitance of 332 F g^{-1} at 0.5 A g^{-1}, and 211 F g^{-1} was retained at a high current density of 40 A g^{-1} [142].

Feedstocks with inherent heteroatoms have also been exploited to produce doped porous carbons. Sword beans are rich in N content due to their nitrogen fixation capability in legumes during the growth cycle. N-doped porous carbon with a specific surface area of 2917 m^2 g^{-1} was prepared from sword bean shells through activation using KOH. The specific capacitance was 260 F g^{-1} at 1 A g^{-1} current density [143]. Similarly, Juncus herb carbonized with $ZnCl_2$ resulted in N-doped porous carbon with a specific surface area of around 1300 m^2 g^{-1} and a specific capacitance of 290 F g^{-1} at 0.5 A g^{-1} current density [144]. Commercially available calcium lignosulphonate (a form of lignin extracted from pulping of wood) was hydrothermally carbonized and thermally annealed at high temperatures, resulting in self-doped S-rich porous carbon with micro/mesopores [145]. Various heteroatom-doped biomass-derived porous structures with respective specific capacitances are summarized in Table 2.

6 Understanding the Resistance Properties of Porous Carbons

Electrochemical impedance spectroscopy is carried out for resistance studies on electrode material. The resistance of supercapacitor electrodes negatively affects the performance and stability. A high resistance decreases the supercapacitor's energy output and power density [159]. Resistance can arise due to multiple factors, such as contact between the electrode material and current collector, limited diffusivity of electrolyte ions inside the porous electrode, solution resistance (R_s), and charge transfer resistance (R_{ct}) [160]. The diffusion-controlled resistance offered by limited mass transfer of electrolytes is also associated with carbon-based supercapacitors and is referred to as Warburg impedance [161]. R_s occurs due to the bulk resistance by the electrolyte solution and depends on its conductivity, while R_{ct} is due to the carbon particle's intrinsic electronic and ionic resistance in the electrode [162]. R_{ct} can be reduced through graphitization of carbon framework to increase the electrical conductivity, as obtained in graphene sheet-like nanostructures and doping with heteroatoms that increase the wettability of the active material [163]. Intrinsic conductivity of biomass-derived carbons can also be enhanced by increasing the carbonization temperature since it results in the formation of ordered sp^2 hybridized graphitic domains in its structure [164]. Another technique that can impart graphitic structure in biomass-derived carbon is catalytic graphitization using transition metal salts. Zhang et al. reported impregnation of Willow catkins in $Fe(NO_3)_3$-KCl solution followed by carbonization and removal of metal ions to obtain porous graphitic carbon. Here, KCl acted as a pore-forming agent, while Fe salt resulted in catalytic graphitization giving the biomass-derived carbon a porous graphitic structure [165]. Similarly, Chang et al. used Co^{2+}-assisted graphitization along with activation using

Table 2 Heteroatom-doped porous biocarbon and their specific capacitance

S. No	Feedstock	Heteroatom	Specific surface area, $m^2\ g^{-1}$	Porous structure	Specific capacitance, $F\ g^{-1}$ (at current density)	Refs.
1	Pine needles	N, O	2433	HPC	223 (0.5 A g^{-1})	[146]
2	Kraft lignin	O, N, S	1307	HPC	244.5 (0.2 A g^{-1})	[147]
3	Lignin	S	660	HPC	225 (0.5 A g^{-1})	[145]
4	Peanut meal	N, S, P	2090	HPC	525 (1 A g^{-1})	[148]
5	Peanut shells	N, O	1138	HPC	447 (0.2 A g^{-1})	[69]
6	Fir sawdust	P	1282	Microporous	292 (0.1 A g^{-1})	[149]
7	Gelatin	B, N	416	Microporous	268 (0.1 A g^{-1})	[150]
8	Dandelion fluff	B, N	1420	Microporous	355 (1 A g^{-1})	[151]
9	Coffee grounds	P	554	HPC	168 (0.05 A g^{-1})	[152]
10	Beans shells	N, S	655	HPC	202 (0.5 A g^{-1})	[153]
11	Silkworm excrement	N, P, S	2044	HPC	412 (0.5 A g^{-1})	[154]
12	Hemp fiber	B, N, P	1555	Microporous	520 (1 A g^{-1})	[155]
13	Camellia pollen	N	852	HPC	300 (1 A g^{-1})	[156]
14	Mango seed	N, O	1815	Microporous	402 (1 A g^{-1})	[157]
15	Potato peel	S, P	1911	HPC	323 (1 A g^{-1})	[158]

KOH. It was observed that both the activation resulted in porous carbon with graphitic domains [166]. Warburg impedance was reported to be less when graphene-like structures are used in fabricating the supercapacitor electrodes. It was due to the short electrolyte diffusion paths provided by the graphene-like nanosheet structure [167, 168]. It is observed that ultra-microporous carbon shows a typically higher equivalent series resistance due to limited ion transport into a constricted pore structure [169, 170]. However, it can be reduced through various activation strategies. The diffusion-controlled resistance can be decreased by introducing broader pores or hierarchical porous channels [171].

7 Challenges and Prospects

Applying porous carbon materials from biomass is undoubtedly reaching new horizons in the charge storage aspects. The pore size, pore interconnectivity, and surface area significantly impact carbon materials' charge storage properties and electrochemical behavior. From the preparation perspective, control over the pore formation and nanostructure has come a long way. Different synthetic strategies have been explored for preparing carbons with various pore structures. However, alternate activation strategies need to be investigated further. Such as, most of the activations involve using harsh alkali reagents such as KOH, NaOH, etc., with a high activating agent to feedstock loading to develop porosity. Using such reagents is harmful to the environment due to their corrosive nature. Even for flexible supercapacitors using fibrous porous carbon film as electrodes, it is essential to retain the microstructure. In those cases, activation with KOH, $ZnCl_2$, etc., can lead to a high structural deformation even though a high porosity can be obtained. In these cases, benign activation strategies need to be explored for successful porosity generation. Furthermore, several template removal strategies employ corrosive acids such as HF. Therefore, more environmentally benign and facile preparation strategies are required.

Another essential factor that must be realized is the bioavailability/abundance of biomass feedstock while using it for various value-added applications like supercapacitor electrode material discussed here. The properties of biomass-derived carbons are also found to be dependent on the feedstock used. Therefore, the geographical limitations of biomass need to be well understood so that a de-centralized approach can be adopted for large-scale production. Also, for the practical application of biomass-derived porous carbons in fabricated symmetric/asymmetric supercapacitor devices, optimization of the current collector, conducting polymer, binder, additives, or electrolyte is also required. Apart from active electrode material, these chemicals also contribute to the overall cost of the fabricated device.

8 Conclusions

Biomass-derived porous carbon nanostructures are a valuable class of materials that have shown excellent charge storage behavior. The abundant feedstocks provide green and renewable precursors for the development of porous carbon materials. The ease of tuning the pore size, pore interconnectivity, and surface area through various activation techniques offers a way to create and incorporate these materials into supercapacitor electrodes. Moreover, the difference in the charge storage property of carbon materials with varying pore size distribution provides an insight into their electrochemical behavior, which can help develop intricate supercapacitor-based devices. Advancements in preparation strategies that are environmentally friendly and non-hazardous still require further exploration by the scientific community.

Acknowledgements The authors are thankful to the Director, CSIR-Indian Institute of Petroleum, Dehradun for his support. SR and MJ thank AcSIR for granting permission to conduct research work at CSIR-IIP and University Grants Commission (UGC), New Delhi for fellowship.

References

1. Mlilo N, Brown J, Ahfock T (2021) Impact of intermittent renewable energy generation penetration on the power system networks—a review. Technol Econ Smart Grids Sustain Energy. 6(1):25. https://doi.org/10.1007/s40866-021-00123-w
2. Parwal A, Fregelius M, Temiz I, Göteman M, Oliveira JGd, Boström C, et al. Energy management for a grid-connected wave energy park through a hybrid energy storage system. Appl Energy. 2018;231:399–411. doi: https://doi.org/10.1016/j.apenergy.2018.09.146.
3. Naseri F, Karimi S, Farjah E, Schaltz E (2022) Supercapacitor management system: A comprehensive review of modeling, estimation, balancing, and protection techniques. Renew Sust Energ Rev. 155:111913. https://doi.org/10.1016/j.rser.2021.111913
4. Wang R, Yao M, Niu Z (2020) Smart supercapacitors from materials to devices. InfoMat. 2(1):113–125. https://doi.org/10.1002/inf2.12037
5. Simon P, Gogotsi Y (2008) Materials for electrochemical capacitors. Nat Mater 7(11):845–854. https://doi.org/10.1038/nmat2297
6. Libich J, Máca J, Vondrák J, Čech O, Sedlaříková M (2018) Supercapacitors: Properties and applications. J Energy Storage. 17:224–227. https://doi.org/10.1016/j.est.2018.03.012
7. An C, Zhang Y, Guo H, Wang Y (2019) Metal oxide-based supercapacitors: progress and prospectives. Nanoscale Adv. 1(12):4644–4658. https://doi.org/10.1039/C9NA00543A
8. Bokhari SW, Siddique AH, Sherrell PC, Yue X, Karumbaiah KM, Wei S et al (2020) Advances in graphene-based supercapacitor electrodes. Energy Rep 6:2768–2784. https://doi.org/10.1016/j.egyr.2020.10.001
9. Kumar S, Saeed G, Zhu L, Hui KN, Kim NH, Lee JH (2021) 0D to 3D carbon-based networks combined with pseudocapacitive electrode material for high energy density supercapacitor: A review. Chem Eng J 403:126352. https://doi.org/10.1016/j.cej.2020.126352
10. Sajjadi B, Chen WY, Egiebor N. A comprehensive review on physical activation of biochar for energy and environmental applications. Rev Chem Eng. 2018;35. doi: https://doi.org/10.1515/revce-2017-0113.
11. Sevilla M, Díez N, Fuertes AB (2021) More sustainable chemical activation strategies for the production of porous carbons. Chemsuschem 14(1):94–117. https://doi.org/10.1002/cssc.202001838

12. Rawat S, Mishra RK, Bhaskar T (2022) Biomass derived functional carbon materials for supercapacitor applications. Chemosphere 286:131961. https://doi.org/10.1016/j.chemosphere.2021.131961
13. Haldar D, Purkait MK (2020) Lignocellulosic conversion into value-added products: A review. Process Biochem 89:110–133. https://doi.org/10.1016/j.procbio.2019.10.001
14. Dahmen N, Lewandowski I, Zibek S, Weidtmann A (2019) Integrated lignocellulosic value chains in a growing bioeconomy: Status quo and perspectives. GCB Bioenergy. 11(1):107–117. https://doi.org/10.1111/gcbb.12586
15. Nimmanterdwong P, Chalermsinsuwan B, Piumsomboon P (2021) Prediction of lignocellulosic biomass structural components from ultimate/proximate analysis. Energy 222:119945. https://doi.org/10.1016/j.energy.2021.119945
16. Demirbas A (2010) Use of algae as biofuel sources. Energy Convers Manage 51(12):2738–2749. https://doi.org/10.1016/j.enconman.2010.06.010
17. Hiraoka M, Kinoshita Y, Higa M, Tsubaki S, Monotilla AP, Onda A et al (2020) Fourfold daily growth rate in multicellular marine alga Ulva meridionalis. Sci Rep 10(1):12606. https://doi.org/10.1038/s41598-020-69536-4
18. Yu KL, Show PL, Ong HC, Ling TC, Chen W-H, Salleh MAM (2018) Biochar production from microalgae cultivation through pyrolysis as a sustainable carbon sequestration and biorefinery approach. Clean Technol Environ Policy 20(9):2047–2055. https://doi.org/10.1007/s10098-018-1521-7
19. Hou ZQ, Luo MY, Yang YT, Zhou JC, Liu LC, Cai JJ (2021) Algae-based carbons: Design, preparation and recent advances in their use in energy storage, catalysis and adsorption. New Carbon Mater 36(2):278–303. https://doi.org/10.1016/S1872-5805(21)60020-3
20. Hu Y, Xie K, Wang H, Yuan C, Cao B, Qian L et al (2021) Preparation and property of N-doped porous carbon material by one-step pyrolysis of protein-rich algal biomass. J Anal Appl Pyrolysis 157:105221. https://doi.org/10.1016/j.jaap.2021.105221
21. Chatterjee S, Saito T (2015) Lignin-Derived Advanced Carbon Materials. Chemsuschem 8(23):3941–3958. https://doi.org/10.1002/cssc.201500692
22. Kosheleva RI, Mitropoulos AC, Kyzas GZ (2019) Synthesis of activated carbon from food waste. Environ Chem Lett 17(1):429–438. https://doi.org/10.1007/s10311-018-0817-5
23. Guardia L, Suárez L, Querejeta N, Pevida C, Centeno TA (2018) Winery wastes as precursors of sustainable porous carbons for environmental applications. J Clean Prod 193:614–624. https://doi.org/10.1016/j.jclepro.2018.05.085
24. Li J, Luo F, Lin T, Yang J, Yang S, He D et al (2020) Pomelo peel-based N, O-codoped hierarchical porous carbon material for supercapacitor application. Chem Phys Lett 753:137597. https://doi.org/10.1016/j.cplett.2020.137597
25. Shen F, Su J, Zhu L, Qi X, Zhang X (2017) Comprehensive utilization of dairy manure to produce glucose and hierarchical porous carbon for supercapacitors. Cellulose 24(6):2571–2579. https://doi.org/10.1007/s10570-017-1267-0
26. Zhang JJ, Fan HX, Dai XH, Yuan SJ (2018) Digested sludge-derived three-dimensional hierarchical porous carbon for high-performance supercapacitor electrode. Royal Society Open Science. 5(4):172456. https://doi.org/10.1098/rsos.172456
27. Tatrari G, Karakoti M, Tewari C, Pandey S, Bohra BS, Dandapat A et al (2021) Solid waste-derived carbon nanomaterials for supercapacitor applications: a recent overview. Mater Adv. 2(5):1454–1484. https://doi.org/10.1039/D0MA00871K
28. Zhou SY, Li XH, Wang ZX, Guo HJ, Peng WJ (2007) Effect of activated carbon and electrolyte on properties of supercapacitor. Trans Nonferrous Met Soc China 17(6):1328–1333. https://doi.org/10.1016/S1003-6326(07)60271-4
29. Feng H, Zheng M, Dong H, Xiao Y, Hu H, Sun Z et al (2015) Three-dimensional honeycomb-like hierarchically structured carbon for high-performance supercapacitors derived from high-ash-content sewage sludge. J Mater Chem A. 3(29):15225–15234. https://doi.org/10.1039/C5TA03217B
30. Lu J, Zhang Q, An Q, Bu T, Hong L, Feng Y et al (2022) Hierarchical porous carbon for high-performance capacitor derived from sewage sludge by KHCO3 activation. J Energy Storage. 50:104644. https://doi.org/10.1016/j.est.2022.104644

31. Gao S, Chen Y, Fan H, Wei X, Hu C, Luo H et al (2014) Large scale production of biomass-derived N-doped porous carbon spheres for oxygen reduction and supercapacitors. J Mater Chem A. 2(10):3317–3324. https://doi.org/10.1039/C3TA14281G
32. Chen P, Wang LK, Wang G, Gao MR, Ge J, Yuan WJ et al (2014) Nitrogen-doped nanoporous carbon nanosheets derived from plant biomass: an efficient catalyst for oxygen reduction reaction. Energy Environ Sci 7(12):4095–4103. https://doi.org/10.1039/C4EE02531H
33. Yun YS, Cho SY, Shim J, Kim BH, Chang S-J, Baek SJ et al (2013) Microporous Carbon Nanoplates from Regenerated Silk Proteins for Supercapacitors. Adv Mater 25(14):1993–1998. https://doi.org/10.1002/adma.201204692
34. Zhang S, Zheng M, Lin Z, Li N, Liu Y, Zhao B et al (2014) Activated carbon with ultrahigh specific surface area synthesized from natural plant material for lithium–sulfur batteries. J Mater Chem A. 2(38):15889–15896. https://doi.org/10.1039/C4TA03503H
35. Zhang YJ, Xing ZJ, Duan ZK, Meng L, Wang Y (2014) Effects of steam activation on the pore structure and surface chemistry of activated carbon derived from bamboo waste. Appl Surf Sci 315:279–286. https://doi.org/10.1016/j.apsusc.2014.07.126
36. Yeung PT, Chung PY, Tsang HC, Cheuk On Tang J, Yin Ming Cheng G, Gambari R, et al. Preparation and characterization of bio-safe activated charcoal derived from coffee waste residue and its application for removal of lead and copper ions. RSC Adv. 2014;4(73):38839–47. doi: https://doi.org/10.1039/C4RA05082G.
37. Ding L, Zou B, Gao W, Liu Q, Wang Z, Guo Y et al (2014) Adsorption of Rhodamine-B from aqueous solution using treated rice husk-based activated carbon. Colloids Surf, A 446:1–7. https://doi.org/10.1016/j.colsurfa.2014.01.030
38. Yadav N, Singh MK, Yadav N, Hashmi SA (2018) High performance quasi-solid-state supercapacitors with peanut-shell-derived porous carbon. J Power Sources 402:133–146. https://doi.org/10.1016/j.jpowsour.2018.09.032
39. Shen Y, Zhang N, Zhang S (2020) Catalytic pyrolysis of biomass with potassium compounds for Co-production of high-quality biofuels and porous carbons. Energy 190:116431. https://doi.org/10.1016/j.energy.2019.116431
40. Fu Y, Zhang N, Shen Y, Ge X, Chen M (2018) Micro-mesoporous carbons from original and pelletized rice husk via one-step catalytic pyrolysis. Bioresour Technol 269:67–73. https://doi.org/10.1016/j.biortech.2018.08.083
41. Titirici MM, Thomas A, Yu SH, Müller JO, Antonietti M (2007) A Direct Synthesis of Mesoporous Carbons with Bicontinuous Pore Morphology from Crude Plant Material by Hydrothermal Carbonization. Chem Mater 19(17):4205–4212. https://doi.org/10.1021/cm0707408
42. Pari G, Darmawan S, Prihandoko B (2014) Porous Carbon Spheres from Hydrothermal Carbonization and KOH Activation on Cassava and Tapioca Flour Raw Material. Procedia Environ Sci 20:342–351. https://doi.org/10.1016/j.proenv.2014.03.043
43. Chen D, Zhou H, Li H, Chen J, Li S, Zheng F (2017) Self-template synthesis of biomass-derived 3D hierarchical N-doped porous carbon for simultaneous determination of dihydroxybenzene isomers. Sci Rep 7(1):14985. https://doi.org/10.1038/s41598-017-15129-7
44. Dong X, Liu X, Chen H, Xu X, Jiang H, Gu C et al (2021) Hard template-assisted N, P-doped multifunctional mesoporous carbon for supercapacitors and hydrogen evolution reaction. J Mater Sci 56(3):2385–2398. https://doi.org/10.1007/s10853-020-05303-0
45. Bouchelta C, Medjram MS, Bertrand O, Bellat JP (2008) Preparation and characterization of activated carbon from date stones by physical activation with steam. J Anal Appl Pyrolysis 82(1):70–77. https://doi.org/10.1016/j.jaap.2007.12.009
46. Jiang C, Yakaboylu GA, Yumak T, Zondlo JW, Sabolsky EM, Wang J (2020) Activated carbons prepared by indirect and direct CO_2 activation of lignocellulosic biomass for supercapacitor electrodes. Renew Energy 155:38–52. https://doi.org/10.1016/j.renene.2020.03.111
47. Yang I, Jung M, Kim MS, Choi D, Jung JC (2021) Physical and chemical activation mechanisms of carbon materials based on the microdomain model. J Mater Chem A. 9(15):9815–9825. https://doi.org/10.1039/D1TA00765C

48. Sajjadi B, Zubatiuk T, Leszczynska D, Leszczynski J, Chen WY (2019) Chemical activation of biochar for energy and environmental applications: a comprehensive review. Rev Chem Eng 35(7):777–815. https://doi.org/10.1515/revce-2018-0003
49. Oginni O, Singh K, Oporto G, Dawson-Andoh B, McDonald L, Sabolsky E (2019) Influence of one-step and two-step KOH activation on activated carbon characteristics. Bioresour Technol Rep. 7:100266. https://doi.org/10.1016/j.biteb.2019.100266
50. Mistar EM, Alfatah T, Supardan MD (2020) Synthesis and characterization of activated carbon from Bambusa vulgaris striata using two-step KOH activation. J Mater Res Technol. 9(3):6278–6286. https://doi.org/10.1016/j.jmrt.2020.03.041
51. Chen R, Li L, Liu Z, Lu M, Wang C, Li H et al (2017) Preparation and characterization of activated carbons from tobacco stem by chemical activation. J Air Waste Manag Assoc 67(6):713–724. https://doi.org/10.1080/10962247.2017.1280560
52. Zeng K, Yang X, Xie Y, Yang H, Li J, Zhong D et al (2021) Molten salt pyrolysis of biomass: The evaluation of molten salt. Fuel 302:121103. https://doi.org/10.1016/j.fuel.2021.121103
53. Cao T, Cheng J, Ma J, Yang C, Yao M, Liu F et al (2021) Facile Synthesis of Microporous Carbons from Biomass Waste as High Performance Supports for Dehydrogenation of Formic Acid. Nanomaterials 11(11):3028. https://doi.org/10.3390/nano11113028
54. Geng Z, Xiao Q, Lv H, Li B, Wu H, Lu Y et al (2016) One-Step Synthesis of Microporous Carbon Monoliths Derived from Biomass with High Nitrogen Doping Content for Highly Selective CO_2 Capture. Sci Rep 6(1):30049. https://doi.org/10.1038/srep30049
55. Bushra B, Remya N (2020) Biochar from pyrolysis of rice husk biomass—characteristics, modification and environmental application. Biomass Convers Biorefin. https://doi.org/10.1007/s13399-020-01092-3
56. Lim E, Jo C, Lee J (2016) A mini review of designed mesoporous materials for energy-storage applications: from electric double-layer capacitors to hybrid supercapacitors. Nanoscale 8(15):7827–7833. https://doi.org/10.1039/C6NR00796A
57. Liang C, Li Z, Dai S (2008) Mesoporous Carbon Materials: Synthesis and Modification. Angew Chem Int Ed 47(20):3696–3717. https://doi.org/10.1002/anie.200702046
58. Joseph S, Lee JM, Benzigar MR, Yi J, Karakoti A, Vinu A (2021) Milk derived highly ordered mesoporous carbon with CaF_2 nanoclusters as an efficient electrode for supercapacitors. Carbon 180:101–109. https://doi.org/10.1016/j.carbon.2021.05.006
59. Saha D, Li Y, Bi Z, Chen J, Keum JK, Hensley DK et al (2014) Studies on Supercapacitor Electrode Material from Activated Lignin-Derived Mesoporous Carbon. Langmuir 30(3):900–910. https://doi.org/10.1021/la404112m
60. Kubo S, White RJ, Yoshizawa N, Antonietti M, Titirici MM (2011) Ordered Carbohydrate-Derived Porous Carbons. Chem Mater 23(22):4882–4885. https://doi.org/10.1021/cm2020077
61. Jain A, Xu C, Jayaraman S, Balasubramanian R, Lee JY, Srinivasan MP (2015) Mesoporous activated carbons with enhanced porosity by optimal hydrothermal pre-treatment of biomass for supercapacitor applications. Microporous Mesoporous Mater 218:55–61. https://doi.org/10.1016/j.micromeso.2015.06.041
62. Li J, Qin F, Zhang L, Zhang K, Li Q, Lai Y et al (2014) Mesoporous carbon from biomass: one-pot synthesis and application for Li–S batteries. J Mater Chem A. 2(34):13916–13922. https://doi.org/10.1039/C4TA02154A
63. Díez N, Sevilla M, Fuertes AB (2021) Synthesis strategies of templated porous carbons beyond the silica nanocasting technique. Carbon 178:451–476. https://doi.org/10.1016/j.carbon.2021.03.029
64. Fu Y, Liu H, Liang H, Sun L, Bu Y (2022) Mesoporous carbon rods capable of fast transport of axial electrons and radial ions for ultra-thick supercapacitor electrodes. Electrochim Acta 404:139768. https://doi.org/10.1016/j.electacta.2021.139768
65. Chen W, Qian J, Zhang M, Lu W, Zhang S, Xu H (2019) Recycle of cotton waste by hard templating with magnesium acetate as MgO precursor. Environ Sci Pollut Res 26(29):29908–29916. https://doi.org/10.1007/s11356-019-06106-w

66. Fu F, Yang D, Zhang W, Wang H, Qiu X (2020) Green self-assembly synthesis of porous lignin-derived carbon quasi-nanosheets for high-performance supercapacitors. Chem Eng J 392:123721. https://doi.org/10.1016/j.cej.2019.123721
67. Zhou XL, Zhang H, Shao LM, Lü F, He PJ (2021) Preparation and Application of Hierarchical Porous Carbon Materials from Waste and Biomass: A Review. Waste Biomass Valorization. 12(4):1699–1724. https://doi.org/10.1007/s12649-020-01109-y
68. Chen Y, Ji S, Wang H, Linkov V, Wang R (2018) Synthesis of porous nitrogen and sulfur co-doped carbon beehive in a high-melting-point molten salt medium for improved catalytic activity toward oxygen reduction reaction. Int J Hydrogen Energy 43(10):5124–5132. https://doi.org/10.1016/j.ijhydene.2018.01.095
69. Lei W, Yang B, Sun Y, Xiao L, Tang D, Chen K et al (2021) Self-sacrificial template synthesis of heteroatom doped porous biochar for enhanced electrochemical energy storage. J Power Sources 488:229455. https://doi.org/10.1016/j.jpowsour.2021.229455
70. Li J, Jiang Q, Wei L, Zhong L, Wang X (2020) Simple and scalable synthesis of hierarchical porous carbon derived from cornstalk without pith for high capacitance and energy density. J Mater Chem A. 8(3):1469–1479. https://doi.org/10.1039/C9TA07864A
71. Wang C, Wang H, Dang B, Wang Z, Shen X, Li C et al (2020) Ultrahigh yield of nitrogen doped porous carbon from biomass waste for supercapacitor. Renew Energy 156:370–376. https://doi.org/10.1016/j.renene.2020.04.092
72. Long C, Chen X, Jiang L, Zhi L, Fan Z (2015) Porous layer-stacking carbon derived from in-built template in biomass for high volumetric performance supercapacitors. Nano Energy 12:141–151. https://doi.org/10.1016/j.nanoen.2014.12.014
73. Qiu D, Guo N, Gao A, Zheng L, Xu W, Li M et al (2019) Preparation of oxygen-enriched hierarchically porous carbon by $KMnO_4$ one-pot oxidation and activation: Mechanism and capacitive energy storage. Electrochim Acta 294:398–405. https://doi.org/10.1016/j.electacta.2018.10.049
74. Deng J, Xiong T, Xu F, Li M, Han C, Gong Y et al (2015) Inspired by bread leavening: one-pot synthesis of hierarchically porous carbon for supercapacitors. Green Chem 17(7):4053–4060. https://doi.org/10.1039/C5GC00523J
75. Gopalakrishnan A, Raju TD, Badhulika S (2020) Green synthesis of nitrogen, sulfur-co-doped worm-like hierarchical porous carbon derived from ginger for outstanding supercapacitor performance. Carbon 168:209–219. https://doi.org/10.1016/j.carbon.2020.07.017
76. Luo X, Li S, Xu H, Zou X, Wang Y, Cheng J et al (2021) Hierarchically porous carbon derived from potassium-citrate-loaded poplar catkin for high performance supercapacitors. J Colloid Interface Sci 582:940–949. https://doi.org/10.1016/j.jcis.2020.08.088
77. Liu D, Xu G, Yuan X, Ding Y, Fan B (2023) Pore size distribution modulation of waste cotton-derived carbon materials via citrate activator to boost supercapacitive performance. Fuel 332:126044. https://doi.org/10.1016/j.fuel.2022.126044
78. Wang D, Nai J, Li H, Xu L, Wang Y (2019) A robust strategy for the general synthesis of hierarchical carbons constructed by nanosheets and their application in high performance supercapacitor in ionic liquid electrolyte. Carbon 141:40–49. https://doi.org/10.1016/j.carbon.2018.09.055
79. Song S, Ma F, Wu G, Ma D, Geng W, Wan J (2015) Facile self-templating large scale preparation of biomass-derived 3D hierarchical porous carbon for advanced supercapacitors. J Mater Chem A. 3(35):18154–18162. https://doi.org/10.1039/C5TA04721H
80. Salanne M, Rotenberg B, Naoi K, Kaneko K, Taberna PL, Grey CP et al (2016) Efficient storage mechanisms for building better supercapacitors. Nat Energy 1(6):16070. https://doi.org/10.1038/nenergy.2016.70
81. Ghosh S, Barg S, Jeong SM, Ostrikov K (2020) Heteroatom-doped and oxygen-functionalized nanocarbons for high-performance supercapacitors. Adv Energy Mater 10(32):2001239. https://doi.org/10.1002/aenm.202001239
82. Frackowiak E (2007) Carbon materials for supercapacitor application. Phys Chem Chem Phys 9(15):1774–1785. https://doi.org/10.1039/B618139M

83. Hu W, Zhang W, Zheng M, Xiao Y, Dong H, Liang Y et al (2021) Sodium alginate assisted preparation of oxygen-doped microporous carbons with enhanced electrochemical energy storage and hydrogen uptake. Int J Hydrogen Energy 46(1):896–905. https://doi.org/10.1016/j.ijhydene.2020.09.232
84. Li Y, Zhang D, Zhang Y, He J, Wang Y, Wang K et al (2020) Biomass-derived microporous carbon with large micropore size for high-performance supercapacitors. J Power Sources 448:227396. https://doi.org/10.1016/j.jpowsour.2019.227396
85. Li Q, Bai X, Meng Q, Chen T, Zhu W, Yao W et al (2018) Porous biochar generated from natural Amorphophallus konjac for high performance supercapacitors. Appl Surf Sci 448:16–22. https://doi.org/10.1016/j.apsusc.2018.04.086
86. Aldama I, Lillo-Rodenas MA, Kunowsky M, Ibañez J, Rojo JM (2020) Understanding the rate performance of microporous carbons in aqueous electrolytes. Electrochim Acta 350:136408. https://doi.org/10.1016/j.electacta.2020.136408
87. Shang T, Xu Y, Li P, Han J, Wu Z, Tao Y et al (2020) A bio-derived sheet-like porous carbon with thin-layer pore walls for ultrahigh-power supercapacitors. Nano Energy 70:104531. https://doi.org/10.1016/j.nanoen.2020.104531
88. Waribam P, Ngo SD, Tran TTV, Kongparakul S, Reubroycharoen P, Chanlek N et al (2020) Waste biomass valorization through production of xylose-based porous carbon microspheres for supercapacitor applications. Waste Manage (Oxford) 105:492–500. https://doi.org/10.1016/j.wasman.2020.02.042
89. Niu J, Liu M, Xu F, Zhang Z, Dou M, Wang F (2018) Synchronously boosting gravimetric and volumetric performance: Biomass-derived ternary-doped microporous carbon nanosheet electrodes for supercapacitors. Carbon 140:664–672. https://doi.org/10.1016/j.carbon.2018.08.036
90. Gopalakrishnan A, Kong CY, Badhulika S (2019) Scalable, large-area synthesis of heteroatom-doped few-layer graphene-like microporous carbon nanosheets from biomass for high-capacitance supercapacitors. New J Chem 43(3):1186–1194. https://doi.org/10.1039/C8NJ05128C
91. Kim D, Jin X, Cho Y, Lim J, Yan B, Ko D et al (2021) Facile preparation of N-doped porous carbon nanosheets derived from potassium citrate/melamine for high-performance supercapacitors. J Electroanal Chem 892:115302. https://doi.org/10.1016/j.jelechem.2021.115302
92. Li T, Ma R, Xu X, Sun S, Lin J (2021) Microwave-induced preparation of porous graphene nanosheets derived from biomass for supercapacitors. Microporous Mesoporous Mater 324:111277. https://doi.org/10.1016/j.micromeso.2021.111277
93. Xu B, Hou S, Duan H, Cao G, Chu M, Yang Y (2013) Ultramicroporous carbon as electrode material for supercapacitors. J Power Sources 228:193–197. https://doi.org/10.1016/j.jpowsour.2012.11.122
94. Prehal C, Koczwara C, Jäckel N, Schreiber A, Burian M, Amenitsch H et al (2017) Quantification of ion confinement and desolvation in nanoporous carbon supercapacitors with modelling and in situ X-ray scattering. Nat Energy 2(3):16215. https://doi.org/10.1038/nenergy.2016.215
95. Zhang K, Sun J, E L, Ma C, Luo S, Wu Z, et al. Effects of the Pore Structure of Commercial Activated Carbon on the Electrochemical Performance of Supercapacitors. J Energy Storage. 2022;45:103457. doi: https://doi.org/10.1016/j.est.2021.103457.
96. Mehra P, Singh C, Cherian I, Giri A, Paul A (2021) Deciphering the Incredible Supercapacitor Performance of Conducting Biordered Ultramicroporous Graphitic Carbon. ACS Appl Energy Mater. 4(5):4416–4427. https://doi.org/10.1021/acsaem.1c00020
97. Ye Z, Wang F, Jia C, Shao Z, Biomass-based O (2018) N-codoped activated carbon aerogels with ultramicropores for supercapacitors. J Mater Sci 53(17):12374–12387. https://doi.org/10.1007/s10853-018-2487-x
98. Gadipelli S, Howard CA, Guo J, Skipper NT, Zhang H, Shearing PR et al (2020) Superior multifunctional activity of nanoporous carbons with widely tunable porosity: enhanced storage capacities for carbon-dioxide, hydrogen, water, and electric charge. Adv Energy Mater 10(9):1903649. https://doi.org/10.1002/aenm.202070039

99. Ding C, Liu T, Yan X, Huang L, Ryu S, Lan J et al (2020) An Ultra-microporous Carbon Material Boosting Integrated Capacitance for Cellulose-Based Supercapacitors. Nano-Micro Lett. 12(1):63. https://doi.org/10.1007/s40820-020-0393-7
100. Liu X, Ma C, Li J, Zielinska B, Kalenczuk RJ, Chen X et al (2019) Biomass-derived robust three-dimensional porous carbon for high volumetric performance supercapacitors. J Power Sources 412:1–9. https://doi.org/10.1016/j.jpowsour.2018.11.032
101. Bu Y, Sun T, Cai Y, Du L, Zhuo O, Yang L et al (2017) Compressing Carbon Nanocages by Capillarity for Optimizing Porous Structures toward Ultrahigh-Volumetric-Performance Supercapacitors. Adv Mater 29(24):1700470. https://doi.org/10.1002/adma.201700470
102. Fuertes A, Lota G, Centeno T, Frackowiak E (2005) Templated mesoporous carbons for supercapacitor application. Electrochim Acta 50(14):2799–2805. https://doi.org/10.1016/j.electacta.2004.11.027
103. Enock TK, King'ondu CK, Pogrebnoi A, Jande YAC. Biogas-slurry derived mesoporous carbon for supercapacitor applications. Mater Today Energy. 2017;5:126–37. doi: https://doi.org/10.1016/j.mtener.2017.06.006.
104. Zhang G, Chen Y, Chen Y, Guo H (2018) Activated biomass carbon made from bamboo as electrode material for supercapacitors. Mater Res Bull 102:391–398. https://doi.org/10.1016/j.materresbull.2018.03.006
105. Bello A, Manyala N, Barzegar F, Khaleed AA, Momodu DY, Dangbegnon JK (2016) Renewable pine cone biomass derived carbon materials for supercapacitor application. RSC Adv 6(3):1800–1809. https://doi.org/10.1039/C5RA21708C
106. Yu F, Ye Z, Chen W, Wang Q, Wang H, Zhang H et al (2020) Plane tree bark-derived mesopore-dominant hierarchical carbon for high-voltage supercapacitors. Appl Surf Sci 507:145190. https://doi.org/10.1016/j.apsusc.2019.145190
107. Bo X, Xiang K, Zhang Y, Shen Y, Chen S, Wang Y et al (2019) Microwave-assisted conversion of biomass wastes to pseudocapacitive mesoporous carbon for high-performance supercapacitor. J Energy Chem 39:1–7. https://doi.org/10.1016/j.jechem.2019.01.006
108. Okonkwo CA, Menkiti MC, Obiora-Okafo IA, Ezenwa ON (2021) Controlled pyrolysis of sugarcane bagasse enhanced mesoporous carbon for improving capacitance of supercapacitor electrode. Biomass Bioenergy 146:105996. https://doi.org/10.1016/j.biombioe.2021.105996
109. Zhou Y, Ren X, Song M, Du Y, Wan J, Wu G et al (2020) In-situ template cooperated with thiourea to prepare oxygen/nitrogen co-doped porous carbons with adjustable pore structure for supercapacitors. Renew Energy 153:1005–1015. https://doi.org/10.1016/j.renene.2020.02.075
110. Gao Y, Zhang Y, Li A, Zhang L (2018) Facile synthesis of high-surface area mesoporous biochar for energy storage via in-situ template strategy. Mater Lett 230:183–186. https://doi.org/10.1016/j.matlet.2018.07.106
111. Yu M, Song Z, Zhang C, He X (2017) One-step synthesis of mesoporous carbons from mixed resources by microwave-assisted phosphoric acid activation for supercapacitors. Mater Technol 32(11):701–705. https://doi.org/10.1080/10667857.2017.1344370
112. Lu H, Li Q, Guo J, Song A, Gong C, Zhang J et al (2018) Hierarchically porous carbon with high-speed ion transport channels for high performance supercapacitors. Appl Surf Sci 427:992–999. https://doi.org/10.1016/j.apsusc.2017.09.065
113. Fu RW, Li ZH, Liang YR, Li F, Xu F, Wu DC (2011) Hierarchical porous carbons: design, preparation, and performance in energy storage. New Carbon Mater 26(3):171–179. https://doi.org/10.1016/S1872-5805(11)60074-7
114. Liang C, Bao J, Li C, Huang H, Chen C, Lou Y et al (2017) One-dimensional hierarchically porous carbon from biomass with high capacitance as supercapacitor materials. Microporous Mesoporous Mater 251:77–82. https://doi.org/10.1016/j.micromeso.2017.05.044
115. Liu Y, Huang B, Lin X, Xie Z (2017) Biomass-derived hierarchical porous carbons: boosting the energy density of supercapacitors via an ionothermal approach. J Mater Chem A. 5(25):13009–13018. https://doi.org/10.1039/C7TA03639F
116. Liang X, Liu R, Wu X (2021) Biomass waste derived functionalized hierarchical porous carbon with high gravimetric and volumetric capacitances for supercapacitors. Microporous Mesoporous Mater 310:110659. https://doi.org/10.1016/j.micromeso.2020.110659

117. Hu L, Zhu Q, Wu Q, Li D, An Z, Xu B (2018) Natural Biomass-Derived Hierarchical Porous Carbon Synthesized by an in Situ Hard Template Coupled with NaOH Activation for Ultrahigh Rate Supercapacitors. ACS Sustainable Chem Eng. 6(11):13949–13959. https://doi.org/10.1021/acssuschemeng.8b02299
118. Peng L, Liang Y, Dong H, Hu H, Zhao X, Cai Y et al (2018) Super-hierarchical porous carbons derived from mixed biomass wastes by a stepwise removal strategy for high-performance supercapacitors. J Power Sources 377:151–160. https://doi.org/10.1016/j.jpowsour.2017.12.012
119. Zhang W, Xu J, Hou D, Yin J, Liu D, He Y et al (2018) Hierarchical porous carbon prepared from biomass through a facile method for supercapacitor applications. J Colloid Interface Sci 530:338–344. https://doi.org/10.1016/j.jcis.2018.06.076
120. Chang CS, Wang H, Zhang YQ, Wang SL, Liu X, Li L (2019) Fabrication of Hierarchical Porous Carbon Frameworks from Metal-Ion-Assisted Step-Activation of Biomass for Supercapacitors with Ultrahigh Capacitance. ACS Sustainable Chem Eng. 7(12):10763–10772. https://doi.org/10.1021/acssuschemeng.9b01455
121. Roy CK, Shah SS, Reaz AH, Sultana S, Chowdhury AN, Firoz SH et al (2021) Preparation of Hierarchical Porous Activated Carbon from Banana Leaves for High-performance Supercapacitor: Effect of Type of Electrolytes on Performance. Chem - Asian J. 16(4):296–308. https://doi.org/10.1002/asia.202001342
122. Xu Y, Lei H, Qi S, Ren F, Peng H, Wang F et al (2020) Three-dimensional zanthoxylum Leaves-Derived nitrogen-Doped porous carbon frameworks for aqueous supercapacitor with high specific energy. J Energy Storage. 32:101970. https://doi.org/10.1016/j.est.2020.101970
123. Selvaraj AR, Muthusamy A, Inho C, Kim HJ, Senthil K, Prabakar K (2021) Ultrahigh surface area biomass derived 3D hierarchical porous carbon nanosheet electrodes for high energy density supercapacitors. Carbon 174:463–474. https://doi.org/10.1016/j.carbon.2020.12.052
124. Herou S, Schlee P, Jorge AB, Titirici M (2018) Biomass-derived electrodes for flexible supercapacitors. Curr Opin Green Sustainable Chem. 9:18–24. https://doi.org/10.1016/j.cogsc.2017.10.005
125. Wang C, Wang X, Lu H, Li H, Zhao XS (2018) Cellulose-derived hierarchical porous carbon for high-performance flexible supercapacitors. Carbon 140:139–147. https://doi.org/10.1016/j.carbon.2018.08.032
126. Ying Z, Zhang Y, Lin X, Hui S, Wang Y, Yang Y et al (2020) A biomass-derived super-flexible hierarchically porous carbon film electrode prepared via environment-friendly ice-microcrystal pore-forming for supercapacitors. Chem Commun 56(73):10730–10733. https://doi.org/10.1039/D0CC04436A
127. Zhang Y, Hui S, Lin X, Ying Z, Li Y, Xie J (2021) Novel effective strategy for high-performance biomass-based super-flexible hierarchically porous carbon fibrous film electrode for supercapacitors. J Alloys Compd 883:160713. https://doi.org/10.1016/j.jallcom.2021.160713
128. Jiang Y, Chen J, Zeng Q, Zou Z, Li J, Zeng L et al (2022) Facile method to produce sub-1 nm pore-rich carbon from biomass wastes for high performance supercapacitors. J Colloid Interface Sci 612:213–222. https://doi.org/10.1016/j.jcis.2021.12.144
129. Suárez L, Centeno TA (2020) Unravelling the volumetric performance of activated carbons from biomass wastes in supercapacitors. J Power Sources 448:227413. https://doi.org/10.1016/j.jpowsour.2019.227413
130. Raj CJ, Rajesh M, Manikandan R, Yu KH, Anusha J, Ahn JH et al (2018) High electrochemical capacitor performance of oxygen and nitrogen enriched activated carbon derived from the pyrolysis and activation of squid gladius chitin. J Power Sources 386:66–76. https://doi.org/10.1016/j.jpowsour.2018.03.038
131. Wu C, Yang S, Cai J, Zhang Q, Zhu Y, Zhang K (2016) Activated Microporous Carbon Derived from Almond Shell for High Energy Density Asymmetric Supercapacitors. ACS Appl Mater Interfaces 8:15288–15296. https://doi.org/10.1021/acsami.6b02942
132. Song Y, Liu J, Sun K, Xu W (2017) Synthesis of sustainable lignin-derived mesoporous carbon for supercapacitors using a nano-sized MgO template coupled with Pluronic F127. RSC Adv 7(76):48324–48332. https://doi.org/10.1039/C7RA09464G

133. Sankar S, Ahmed ATA, Inamdar AI, Im H, Im YB, Lee Y et al (2019) Biomass-derived ultrathin mesoporous graphitic carbon nanoflakes as stable electrode material for high-performance supercapacitors. Mater Des 169:107688. https://doi.org/10.1016/j.matdes.2019.107688
134. Zhang J, Chen H, Bai J, Xu M, Luo C, Yang L et al (2021) N-doped hierarchically porous carbon derived from grape marcs for high-performance supercapacitors. J Alloys Compd 854:157207. https://doi.org/10.1016/j.jallcom.2020.157207
135. Hong N, Cheng Q, Goonetilleke A, Bandala ER, Liu A (2020) Assessing the effect of surface hydrophobicity/hydrophilicity on pollutant leaching potential of biochar in water treatment. J Ind Eng Chem 89:222–232. https://doi.org/10.1016/j.jiec.2020.05.017
136. Li S, Fan Z (2019) Nitrogen-doped carbon mesh from pyrolysis of cotton in ammonia as binder-free electrodes of supercapacitors. Microporous Mesoporous Mater 274:313–317. https://doi.org/10.1016/j.micromeso.2018.09.002
137. Wu Q, Zhang G, Gao M, Huang L, Li L, Liu S et al (2019) N-doped porous carbon from different nitrogen sources for high-performance supercapacitors and CO_2 adsorption. J Alloys Compd 786:826–838. https://doi.org/10.1016/j.jallcom.2019.02.052
138. Cao L, Li H, Xu Z, Gao R, Wang S, Zhang G et al (2021) Camellia pollen-derived carbon with controllable N content for high-performance supercapacitors by ammonium chloride activation and dual N-Doping. ChemNanoMat. 7(1):34–43. https://doi.org/10.1002/cnma.202000531
139. Deng J, Li J, Song S, Zhou Y, Li L (2020) Electrolyte-dependent supercapacitor performance on nitrogen-doped porous bio-carbon from gelatin. Nanomaterials 10(2):353
140. You Z, Zhao L, Zhao K, Liao H, Wen S, Xiao Y et al (2023) Highly tunable three-dimensional porous carbon produced from tea seed meal crop by-products for high performance supercapacitors. Appl Surf Sci 607:155080. https://doi.org/10.1016/j.apsusc.2022.155080
141. Zheng L, Wang S, Yang Y, Fu X, Jiang T, Yang J (2019) Ammonium nitrate-assisted synthesis of nitrogen/sulfur-codoped hierarchically porous carbons derived from ginkgo leaf for supercapacitors. ACS Omega 4(3):5904–5914. https://doi.org/10.1021/acsomega.8b03586
142. Guo D, Li Z, Liu P, Sun M (2021) N, P, S co-doped biomass-derived hierarchical porous carbon through simple phosphoric acid-assisted activation for high-performance electrochemical energy storage. Int J Hydrogen Energy 46(11):8197–8209. https://doi.org/10.1016/j.ijhydene.2020.12.013
143. Chen T, Luo L, Luo L, Deng J, Wu X, Fan M et al (2021) High energy density supercapacitors with hierarchical nitrogen-doped porous carbon as active material obtained from bio-waste. Renew Energy 175:760–769. https://doi.org/10.1016/j.renene.2021.05.006
144. He G, Yan G, Song Y, Wang L (2020) Biomass juncus derived nitrogen-doped porous carbon materials for supercapacitor and oxygen reduction reaction. Front Chem 8:226. https://doi.org/10.3389/fchem.2020.00226
145. Demir M, Farghaly AA, Decuir MJ, Collinson MM, Gupta RB (2018) Supercapacitance and oxygen reduction characteristics of sulfur self-doped micro/mesoporous bio-carbon derived from lignin. Mater Chem Phys 216:508–516. https://doi.org/10.1016/j.matchemphys.2018.06.008
146. Leng C, Sun K, Li J, Jiang J (2017) From dead pine needles to O, N codoped activated carbons by a one-step carbonization for high rate performance supercapacitors. ACS Sustainable Chem Eng. 5(11):10474–10482. https://doi.org/10.1021/acssuschemeng.7b02481
147. Liu F, Wang Z, Zhang H, Jin L, Chu X, Gu B et al (2019) Nitrogen, oxygen and sulfur co-doped hierarchical porous carbons toward high-performance supercapacitors by direct pyrolysis of kraft lignin. Carbon 149:105–116. https://doi.org/10.1016/j.carbon.2019.04.023
148. Zhao G, Li Y, Zhu G, Shi J, Lu T, Pan L, Biomass-Based N (2019) P, and S self-doped porous carbon for high-performance supercapacitors. ACS Sustainable Chem Eng. 7(14):12052–12060. https://doi.org/10.1021/acssuschemeng.9b00725
149. Lin G, Wang Q, Yang X, Cai Z, Xiong Y, Huang B (2020) Preparation of phosphorus-doped porous carbon for high performance supercapacitors by one-step carbonization. RSC Adv 10(30):17768–17776. https://doi.org/10.1039/D0RA02398A

150. Ling Z, Wang Z, Zhang M, Yu C, Wang G, Dong Y et al (2016) Sustainable synthesis and assembly of biomass-derived B/N co-doped carbon nanosheets with ultrahigh aspect ratio for high-performance supercapacitors. Adv Funct Mater 26(1):111–119. https://doi.org/10.1002/adfm.201504004
151. Zhao J, Li Y, Wang G, Wei T, Liu Z, Cheng K et al (2017) Enabling high-volumetric-energy-density supercapacitors: designing open, low-tortuosity heteroatom-doped porous carbon-tube bundle electrodes. J Mater Chem A 5(44):23085–23093. https://doi.org/10.1039/C7TA07010A
152. Huang C, Sun T, Hulicova-Jurcakova D (2013) Wide electrochemical window of supercapacitors from coffee bean-derived phosphorus-rich carbons. Chemsuschem 6(12):2330–2339. https://doi.org/10.1002/cssc.201300457
153. Xu G, Han J, Ding B, Nie P, Pan J, Dou H et al (2015) Biomass-derived porous carbon materials with sulfur and nitrogen dual-doping for energy storage. Green Chem 17(3):1668–1674. https://doi.org/10.1039/C4GC02185A
154. Deng P, Lei S, Wang W, Zhou W, Ou X, Chen L et al (2018) Conversion of biomass waste to multi-heteroatom-doped carbon networks with high surface area and hierarchical porosity for advanced supercapacitors. J Mater Sci 53(20):14536–14547. https://doi.org/10.1007/s10853-018-2630-8
155. Gunasekaran SS, Badhulika S (2021) Divulging the electrochemical hydrogen storage of ternary BNP-doped carbon derived from biomass scaled to a pouch cell supercapacitor. Int J Hydrogen Energy 46(71):35149–35160. https://doi.org/10.1016/j.ijhydene.2021.08.104
156. Cao L, Li H, Xu Z, Zhang H, Ding L, Wang S et al (2021) Comparison of the heteroatoms-doped biomass-derived carbon prepared by one-step nitrogen-containing activator for high performance supercapacitor. Diamond Relat Mater 114:108316. https://doi.org/10.1016/j.diamond.2021.108316
157. Lu S, Yang W, Zhou M, Qiu L, Tao B, Zhao Q et al (2022) Nitrogen- and oxygen-doped carbon with abundant micropores derived from biomass waste for all-solid-state flexible supercapacitors. J Colloid Interface Sci 610:1088–1099. https://doi.org/10.1016/j.jcis.2021.11.164
158. Khalafallah D, Quan X, Ouyang C, Zhi M, Hong Z (2021) Heteroatoms doped porous carbon derived from waste potato peel for supercapacitors. Renew Energy 170:60–71. https://doi.org/10.1016/j.renene.2021.01.077
159. Li KB, Shi DW, Cai ZY, Zhang GL, Huang QA, Liu D et al (2015) Studies on the equivalent serial resistance of carbon supercapacitor. Electrochim Acta 174:596–600. https://doi.org/10.1016/j.electacta.2015.06.008
160. Lei C, Markoulidis F, Ashitaka Z, Lekakou C (2013) Reduction of porous carbon/Al contact resistance for an electric double-layer capacitor (EDLC). Electrochim Acta 92:183–187. https://doi.org/10.1016/j.electacta.2012.12.092
161. Muglali MI, Bashir A, Terfort A, Rohwerder M (2011) Electrochemical investigations on stability and protonation behavior of pyridine-terminated aromatic self-assembled monolayers. Phys Chem Chem Phys 13(34):15530–15538. https://doi.org/10.1039/C1CP21469A
162. Taberna PL, Portet C, Simon P (2006) Electrode surface treatment and electrochemical impedance spectroscopy study on carbon/carbon supercapacitors. Appl Phys A 82(4):639–646. https://doi.org/10.1007/s00339-005-3404-0
163. Gehring M, Tempel H, Merlen A, Schierholz R, Eichel R-A, Kungl H (2019) Carbonisation temperature dependence of electrochemical activity of nitrogen-doped carbon fibres from electrospinning as air-cathodes for aqueous-alkaline metal–air batteries. RSC Adv 9(47):27231–27241. https://doi.org/10.1039/C9RA03805A
164. Gabhi R, Basile L, Kirk DW, Giorcelli M, Tagliaferro A, Jia CQ (2020) Electrical conductivity of wood biochar monoliths and its dependence on pyrolysis temperature. Biochar 2(3):369–378. https://doi.org/10.1007/s42773-020-00056-0
165. Zhang X, Zhang K, Li H, Wang Q, Jin Le, Cao Q. Synthesis of porous graphitic carbon from biomass by one-step method and its role in the electrode for supercapacitor. J Appl Electrochem. 2018;48(4):415–26. https://doi.org/10.1007/s10800-018-1170-x

166. Chang CS, Li M, Wang H, Wang SL, Liu X, Liu HK et al (2019) A novel fabrication strategy for doped hierarchical porous biomass-derived carbon with high microporosity for ultrahigh-capacitance supercapacitors. J Mater Chem A 7(34):19939–19949. https://doi.org/10.1039/C9TA06210F
167. Veeramani V, Raghavi G, Chen S-M, Madhu R, Sivakumar M, Tashima D et al (2020) Nitrogen and high oxygen-containing metal-free porous carbon nanosheets for supercapacitor and oxygen reduction reaction applications. Nano Express 1(1):010036. https://doi.org/10.1088/2632-959x/ab9240
168. Purkait T, Singh G, Singh M, Kumar D, Dey RS (2017) Large area few-layer graphene with scalable preparation from waste biomass for high-performance supercapacitor. Sci Rep 7(1):1–14. https://doi.org/10.1038/s41598-017-15463-w
169. Liu M, Qian J, Zhao Y, Zhu D, Gan L, Chen L (2015) Core–shell ultramicroporous@microporous carbon nanospheres as advanced supercapacitor electrodes. J Mater Chem A. 3(21):11517–11526. https://doi.org/10.1039/C5TA02224J
170. Liu M, Zhao F, Zhu D, Duan H, Lv Y, Li L et al (2018) Ultramicroporous carbon nanoparticles derived from metal–organic framework nanoparticles for high-performance supercapacitors. Mater Chem Phys 211:234–241. https://doi.org/10.1016/j.matchemphys.2018.02.030
171. Borchardt L, Leistenschneider D, Haase J, Dvoyashkin M (2018) Revising the concept of pore hierarchy for ionic transport in carbon materials for supercapacitors. Adv Energy Mater 8(24):1800892. https://doi.org/10.1002/aenm.201800892

Carbon Nanomaterials from Biomass for Solar Energy Conversion and Storage

Rabia Nazar, Umer Mehmood, and Ahsan Saeed

Abstract Biomass is a carbon source that is cheap, easy to get, widely available, good for the environment, and renewable. It is a byproduct of agriculture, industry, and forestry, so it is important to figure out how to get rid of it responsibly. Carbon nanomaterials (CNMs), particularly carbon nanotubes and graphene, are in demand due to their outstanding properties and wide applications. This chapter reviews the recent progress in preparing CNMs from biomass. Supercapacitors, batteries, and thin-film solar cells are the most effective energy conversion and storage devices for practical use. However, the poor electrode performance of these devices prevents further development. Most of the carbon used in these devices comes from nonrenewable resources that are made in harsh conditions. Biomass is a green natural carbon source with many desirable properties. This chapter also covers renewable carbon materials derived from biomasses, focusing on their applications in electrochemical energy storage and conversion devices.

Keywords Biomass · Carbon material · Synthesis · Solar energy conversion · Energy storage

1 Introduction

Today's world is facing a great challenge due to the scarcity of water, food, and energy resources. Recent studies have evidenced that a sharp decline in fossil fuel resources is likely in the near future due to an increase in waste generation and expected high population growth [1, 2]. The ecosystem is on the verge of destruction due to the associated air pollution from the escalated consumption of fossil fuels. This situation is aggravated by the extremely high use of coal and fossil oils [3]. These fuels contribute a lot to the significant discharge of CO_2 and SO_x gases, which leads to catastrophic outcomes leading to the greenhouse effect and acid rain [4,

R. Nazar · U. Mehmood (✉) · A. Saeed
Department of Polymer and Process Engineering (PPE), University of Engineering and Technology (UET), Lahore, Pakistan
e-mail: umermehmood@uet.edu.pk

S. K. Tiwari et al. (eds.), *Biomass-Based Functional Carbon Nanostructures for Supercapacitors*, Green Energy and Technology,
https://doi.org/10.1007/978-981-99-0996-4_11

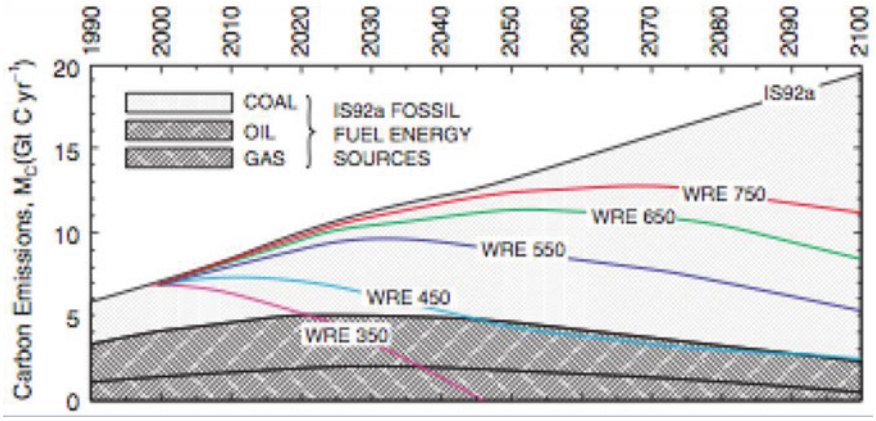

Fig. 1 The emission of CO_2 from fuel energy sources as compared to that present in the atmosphere [8]

5]. During the last century, a drastic rise in the concentration of carbon dioxide reached a high level of 383 ppm from 228 ppm [6]. With the exponential increase in the usage of fossil fuels and their different derivative products, their reserves are progressively declining. Hence, finding a replacement for conventional energy sources is crucial. Based on this evidence, it is not hard to believe that by the end of 2050, the world will be a very different place. To preserve the ecological balance and reduce the degradation of natural resources, it is necessary to investigate the use of renewable energy resources. The future could only be shaped to be able to live in harmony with nature by reducing greenhouse gas emissions and limiting the most dangerous climate changes [7]. This task can be achieved through the joint efforts of scientists from multidisciplinary scientific fields. Figure 1 represents the CO_2 emission as compared to the amount of CO_2 present in the atmosphere; this concentration should be minimized to 350 ppm (purple line in Fig. 1). However, ideally, global CO_2 emissions should be reduced to zero by the end of 2050 [8].

With the advent of new technological demands and health and environmental concerns, the world is focusing more on seeking new sources of energy. Alternative renewable sources such as nuclear, wind, solar, geothermal, and biomass are a focus of research in the twenty-first century.

This emphasis on research is aimed at maximizing the utilization of these resources and meeting global demand. For instance, a study found that to meet the 1/3 requirements of the prospective energy needed by 2050, around 10,000 nuclear plants would need to be built [8]. They are extremely expensive to build and maintain, and they are also fraught with risks and hazards.

Alternative, renewable resources to produce energy are said to be the future of this world in the absence of fossil fuels. This paradigm shift opens new opportunities for chemical processing industries and the units of biobased feedstock to produce sustainable materials capable enough to replace traditional sources of

energy. Quite recently, biomass proved to be the most promising renewable feedstock. Several processes are available through which biomass can be transformed into fuels, including green chemical and low environmental impact methods [9, 10]. The growth of dried biomass feedstock is estimated to be 118 billion tons per year across the world [10]. The agricultural share of biomass is approximately 14 billion tons per year, with approximately 85% (approximately 12 billion tons per year) discharged as AA waste.

This is a great source available to be used in many different forms at almost zero cost. One of the most researched areas is the possibility of using biomass to transform existing surplus biomass into useful products such as biofuels. The transportation is possible with zero carbon dioxide emissions. Techniques like fermentation, catalytic liquefaction, and gasification can be utilized to achieve this conversion [11, 12]. Another new application of biomass is its use in providing substitute materials to produce chemicals, vitamins, polymers, surfactants, and different solvents [13]. Polymeric foams and biodegradable polymers can be synthesized from soybean oil and keratin fibers [14]. Biomass-based polyesters [15], polyurethanes [16], and polylactic acids [17] were also developed with the help of biomass feedstock. The most recent use of biomass feedstock is in its conversion into carbon-based derivatives. This is in the critical research and development phase and is a solution to many challenges confronting the modern world. The constitution of biomass is presented in Fig. 3 [18]. There are different routes available now through which these components can be converted into biofuels, chemicals, polymers, etc. [19]. Several useful products, such as activated carbon, biochar, and fertilizers, can be obtained because of this extraordinary feature of this material [20].

The most abundant material present on the surface of the earth is carbon. The different elemental forms of it found in nature are graphite, diamond, and coal. This is one of the most highly produced elements; its products are estimated at 9 gt/year [21]. The last two decades can be associated with the nanosized allotropes of carbon, mainly due to their unique characteristics as compared to their macroform, which may allow the fine manipulation of materials' properties. Figure 2 depicts the various hybridization forms of carbon nanoallotropes. The most interesting feature of these different states is the direct correlation of their properties, i.e., electrical, chemical, thermal, and mechanical, with their size, shape, and structure. This special feature allows their use in different technological applications [22].

In the last fifteen years, three Nobel prizes have been awarded to carbon nanomaterials: fullerenes, the 1996 Nobel Prize in chemistry; CNTs, the 2008 Kavli Prize in nanoscience; and graphene, the 2010 Nobel Prize in physics [23]. As already stated, carbon is one of the most abundant materials on earth. Despite this fact, various sophisticated techniques are in use to synthesize them with the help of fossil fuel-based precursors. In the history of mankind, carbon has been obtained from biomass through the process of carbon formation. Nature is kind enough to supply this excellent material, but we can utilize a lot of synthetic methods to obtain various forms of this material.

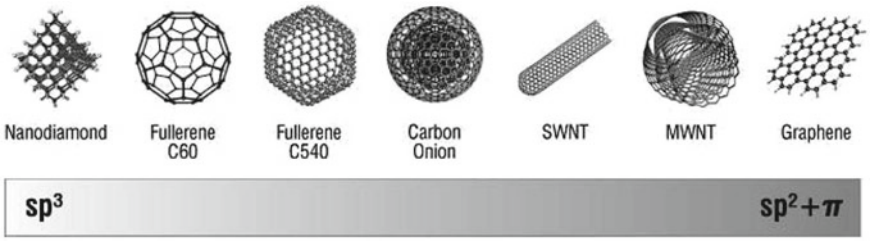

Fig. 2 Sp hybridized forms of carbon nanomaterials [22]

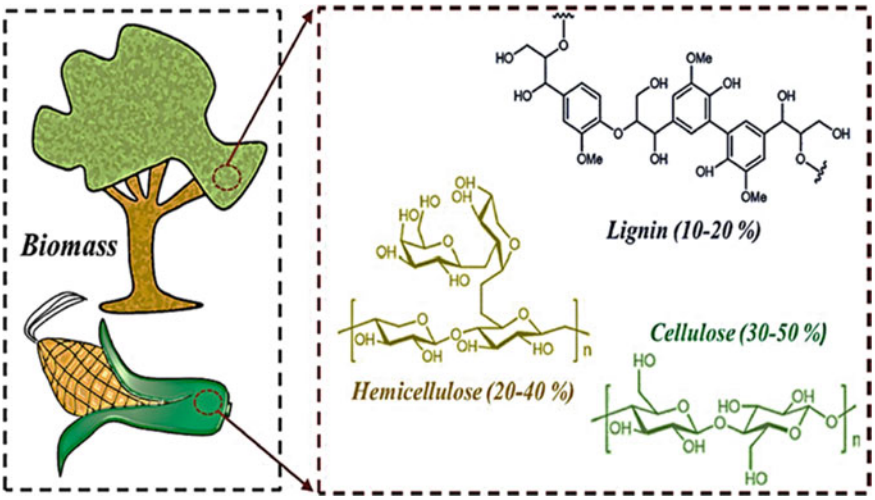

Fig. 3 Basic components and structure of biomass [18]

2 Biomass as a Sustainable and Renewable Carbon-Rich Material

Biomass is a carbon-rich material that is renewable. It is mostly composed of hemicellulose, cellulose, and lignin (shown in Fig. 3), which has been widely employed as feedstock for the preparation of various high-value-added carbon-containing products like carbon materials, chemicals, and biofuels [24]. Extensive research is being carried out to produce less expensive and greener carbon nanomaterials (CNMs) such as graphene, carbon nanofibers, carbon nanotubes, and fullerene with the help of biomass feedstock [25]. From the structure of biomass, it can be seen that it contains hydrogen, oxygen, nitrogen, sulfur, and carbon in its structure. However, the most prevalent element present in carbon nanomaterials is a pure form of carbon. The important feature in the preparation of CNMs from biomass is to keep the carbon element and remove all other elements present in its structure (N, H, O, and S); this

can be achieved by the cleavage of chemical bonds. The typical methods employed for the elimination of other elements from biomass are pyrolysis, incineration, and gasification.

The temperature has a crucial effect on the type of products obtained, the change in aromaticity of biomass derivatives indicates that H and O can be removed from the C-based structure [26]. It was also observed that with the increase in charring temperature from 100 to 700 oC, there is a physical–chemical change in the structure of biomass [26].

Based on these changes, four categories of character are obtained:

1. The first category contains the dominant crystalline character of the feed materials.
2. The second category is related to the abundant amorphous form of charcoal.
3. The next is composite charcoal, in which less ordered graphene is mixed with the amorphous phases. Turbostratic char is another form in which poorly ordered graphite crystallites are present [27]. The presence of rare earth metals such as magnesium and iron is found to be useful in the conversion of biomass to high-aromatic carbon material [28].

The fuel obtained from biomass conversion has a high concentration of carbon monoxide, hydrocarbons, phenol, and alcohol [29]. These high-purity chemicals are widely used as carbon sources to produce CNMs with the help of the CVD process [30]. Another important characteristic of biomass is the presence of mineral elements such as potassium, sodium, calcium, magnesium, and silicon, as well as small quantities of iron, copper, zinc, and other heavy metals apart from the above-stated elements [31].

These minerals are present in biomass, depending on the source from which we obtain that specific biomass feedstock. The environmental conditions, like the salinity of the soil and the presence of different mineral elements, affect the composition of the biomass obtained. The quality of biomass obtained from various parts of a single unit is also not the name; for example, a plant has various organs, such as a stem, root, shell, and leaf. But within one unit, the distribution of each mineral is generally constant. This is the reason that biomass obtained from different sources can be employed in different applications [32]. Therefore, biomass qualifies as an excellent material to be able to convert into high-quality carbon-based materials.

Nowadays, the emphasis is on thermal conversion processes, such as pyrolysis, gasification, and incineration, in order to benefit from the unique catalytic properties of mineral elements. At high temperatures of around 1200–1400 °C, silicon dioxide and silicon carbide nanowires can be synthesized with the help of elements present in a coconut shell and bamboo, i.e., Ca, Mg, and Fe [33]. Because of the presence of various active mineral elements, biomass is an effective catalyst that can be used to prepare functional materials.

The distribution of all active elements is homogeneously present in an individual organ of one product. The use of various biomass-based components in the low-cost, green synthesis of CNMs is becoming increasingly popular these days. It has a stable 3D structure, which enables it to resist certain mechanical, biological, and

chemical attacks. After surface treatment, either chemically or thermochemically, the structure becomes more stable due to the removal of easily degradable components present in its structure. Consequently, due to the removal of degradable components, holes and channels are formed in the matrix. This feature of having channels throughout the structure of biomass makes it an ideal candidate to use extensively in different areas like catalytic reactions, such as hydrolysis degradation, and synthesis techniques [34]. The abundantly available functional groups play an important role in immobilizing and dispersing the catalyst, making it a useful material to be used in catalytic reactions. In a CVD process, it is crucial to diffuse the catalyst on a spongy matrix to initiate the reaction; otherwise, there is an agglomeration of the catalyst, resulting in a low utilization efficiency and catalytic activity of the synthesized CNMs.

3 Structure of Biomass-Derived Carbon Nanomaterials

With the help of literature, a brief table (Table 1) is designed, which shows that carbon nanomaterials (CNMs) have been successfully synthesized by employing several biomass feedstocks such as seaweed, jute, ginger, glucose, rice husks, corn flour, pine nutshells, sugarcane, wheat straws, peanut shells, and seed coats.

3.1 Graphene

The single layer of graphite on an atomic scale is Graphene. The same atomic level of graphite is the structural unit of CNTs and fullerenes [35].

Graphene exists in sp^2 and sp^3 hybridized states, the structure resembles the honeycomb lattice concerning sigma and pi bonds (as shown in Fig. 2) [36]. The existence of delocalized electrons is owing to the presence of pi-orbitals of carbon atoms. The structure of graphene is 2D making it an extraordinary material, capable of having remarkable electrical, mechanical, and thermal properties. Due to these properties, graphene qualifies to be the favorite material to be used in energy-related devices, solar cells, and many other applications of the new technological era [37]. Conventionally, the production of graphene was based on single chemical precursors [38]. Recently, biomass-based feedstock has been used to synthesize graphene. In one research article, a single layer of graphene doped with nitrogen was produced at 800 °C by utilizing Chitosan [39].

Shams et al. described a novel method of using camphor leaf to synthesize graphene by pyrolysis at 1200°C [40]. They further purified the obtained product from the amorphous state of carbon.

Another scientist produced graphene using wheat straw, by utilizing a combined hydrothermal and graphitization approach [41].

Remarkable results were obtained when graphene oxide along with milled sheep horn was heated together through the pyrolysis step, and a 3D porous, sulfur, and

nitrogen-based graphene was found. This work shows that biomass can be used as the feed precursor to produce the graphene and to functionalize the obtained graphene too [42].

The recent attention designated to the synthesis of graphene from biomass materials is due to the fact that their synthesis does not require the use of any catalysts or strong acids, making the procedure a green synthesis from renewable materials.

3.2 Carbon Nanotubes (CNTs)

These are hollow cylindrical materials that are covalently bonded with sp2 carbon atoms. Just like in graphene, the properties of CNTs (mechanical, chemical, and thermal) are based on the type of hybridization demonstrating the structure of CNTs. Due to the arrangement of carbon atoms in its structure, CNTs show high tensile strength, toughness, and rigidity, qualifying them as a strong candidate to be used in different reinforcement applications [43].

CNTs are a success because of some additional properties, i.e., good electrical and thermal conductivity, and remarkable optical properties.

The electrical properties of CNTs are based on their geometry. Basically, a cylindrical shape of CNTs is created by rolling up the graphene sheet; the pattern of the resulting structure of CNTs is crucial, as it demonstrates whether the matter behaves as semiconductive or metallic. The metallic characteristics are due to their superior conductivity as compared to traditional materials available, e.g., copper. The good thermal conductivity and heat capacity of these nanotubes are manipulated to be useful in different composite systems for heat dissipation [44]. Another unique characteristic of CNTs is their optical properties, and due to this property, CNTs are applied in different applications such as electromagnetic interference shielding (EMI), coatings, films to be used in sensors, and solar cells [44].

The production of CNTs from biomass is a newer field; these can be produced from both cellulose and lignocellulosic biomass by using the pyrolysis technique. For instance, the absorbent cotton treated at a temperature range of 400–600 °C synthesized CNTs with an inner diameter of 10 nm and an outer diameter of 80 nm [45]. Similarly, another process stated in the literature stated that cellulose acetate was pyrolyzed at around 750 °C, yielding CNTs having a 24–38 nm diameter [46].

Lignocellulosic biomass such as wood sawdust and fiber can also be used to synthesize CNTs [47]. By using wood fiber, the carbonization reaction was carried out at a temperature ranging from 240 to 400 °C in an open atmosphere, and the resulting CNTs were 10–20 nm in diameter after purifying them with HCl [47].

Another study is published in which gumwood was pyrolyzed at around 500 °C to yield CNTs in an inert atmosphere; the diameter of the obtained CNTs was reported to be 50 nm [48]. Bamboo charcoal was pyrolyzed in the presence of ethanol at a very high temperature (1000–1500 °C) to produce CNTs [49]. Even grass was utilized in one study to obtain CNTs at 600 °C with a diameter between 30 and 50 nm [50].

All these examples show the successful method available now to produce CNTs from biomass derivatives. The research is still in the process of evaluating different parameters to control the diameters and lengths of CNTs produced from these green synthesis methods.

3.3 Carbon Nanofibers (CNFs)

Carbon nanofibers are a type of CNM that has straight chains arranged in a sp2-hybridized state. By observing them with the help of a scanning electron microscope, they look like CNTs. However, when viewed under high magnification with a transmission electron microscope (TEM), they appear to be solid materials with no hollow cylindrical structure, as demonstrated by CNTs.

They also exhibit high mechanical and electrical properties. Due to their good mechanical properties, they can be used in composites as a reinforcing agent. The remarkable good electrical conductivity of these nanofibers paves the way for their use in energy and sensor devices.

The synthesis of CNFs with the help of biomass materials is also in progress. A study was published in which 3D carbon nanofibers were synthesized by employing pre-treated bacterial cellulose [51].

It was reported that the resulting products need to be purified by extraction with the help of acids, due to the strategies followed to produce them. The acid treatment has an adverse effect on the morphological properties of the obtained CNFs.

3.4 Carbon Onions

Carbon onions are a relatively newer type of CNM; they are sp2-hybridized multi-faceted polyhedral quasi-spherical shaped structures with concentric layers [52]. The excellent features of this discovery are their unique physical and chemical properties. They possess exceptionally high optical properties and reasonably good capacitance, proving them to be usable in supercapacitors. They can be utilized both as active materials and as conductive materials [53]. The recent report demonstrates the production of carbon onions from wool wood pyrolysis at 600 °C in the presence of oxygen and nitrogen [54] (Table 1).

3.5 Carbon Spheres

This special class of CNMs is obtained because of broken concentric layers derived from the core. The Vander Waals forces are responsible for their unique structure.

Table 1 Characteristics of CNMs derived from biomass

Biomass	Biomass modification	Carbonization and graphitization	Method	Product	References
Corn flour	KOH	800–1500 °C, N_2	Hummer's redox method	Nano-graphene	Wu and Yu [55]
Agaric	NH_4Cl addition, KOH activation	800 °C, N_2	N/A	Carbon aerogels with graphene-like nanosheets	Zhang et al. [56]
Chitosan	Spin coating, Annealing 200 °C	600–800 °C, N_2	N/A	N-doped graphene	Primo et al. [39]
Wheat straw	KOH activation	800 °C, N_2 2600 °C, Ar		Multi-layer graphene	Chen et al. [41]
Seaweed	ChoCl-$FeCl_3$ activation	700–900 °C, N_2/H_2		Functionalized graphene	[Mondal et al. 57]
Peanut shell	KOH activation	800 °C, Ar	Probe sonication in H2SO4	Few-layer graphene	Purkait et al. [58]
Gumwood	No modification	N/A	Microwave induced pyrolysis	CNTs (50–100 nm dia)	Shi et al. [48]
Bamboo	Treated with Ferric Nitrate for 24 h	450°C, N_2	Pyrolysis Gasification-carbonization	Carbon nanoribbons CNFs Hollow carbon nanospheres	Ye et al. [59]
Palm kernel shell	Cellulose isolation method	Activated C is used as a microwave receptor	Microwave treatment process	Super long CNTs	Esohe Omoriyekomwan et al. [60]
Pine nutshell	No modification	Activated C added	Microwave pyrolysis	Hollow CNFs (400 nm Dia)	Zhang et al. [61]
Rice Husk	No modification	At 300 mTorr H_2 and Ar to generate plasma	Microwave plasma irradiation process	Graphenated CNTs	Wang et al. [62]

The carbon spheres are exclusively used as an electrode material in energy storage and conversion devices. The biomass derivatives such as cassava flour or carrageenan can be used as the feedstock to produce CSs by employing the hydrothermal carbonization method.

4 Synthesis/Production of Carbon Materials from Biomass

Efforts to continue preparing carbon materials from biomass in the future are therefore of great importance. In this chapter, various techniques for preparing carbon materials using biomass as a carbon source will be discussed in depth. These include pyrolysis, hydrothermal carbonization, cyclic oxidation, chemical vapor deposition (CVD), and combustion.

4.1 Pyrolysis

Pyrolysis of biomass refers to the process of thermal decomposition of biomass that occurs in the absence of oxygen. A natural chemical reaction takes place in the first two seconds, which is the foundational step in the combustion and gasification processes. This reaction is the precursor to both processes. The pyrolysis of biomass results in the production of several byproducts, the most notable of which are biochar and bio-oil, in addition to gases such as CH_4, H_2, CO, and CO_2 [63]. Low temperatures (less than 450 degrees Celsius) and high heating rates are required to produce biochar, while high temperatures (greater than 800 degrees Celsius) are required to produce gases [64]. When the process is carried out at a temperature in the middle of its range and at a heating rate that is in the middle of its range, the primary byproduct is bio-oil. The pyrolysis process is affected by the particle size of the feedstock. Because of the need for rapid heat transfer, most pyrolysis technologies can only process particles with a diameter of 2 mm [40]. Graphitization is a high-temperature pyrolysis that converts amorphous and turbostratic carbon into CNTs, CNFs, and nanocapsules. For graphitization to happen, the temperature must be above 2000 °C. This has led to high costs and safety risks, which have made it hard for businesses to use. Pyrolysis with a chemical activation agent like KOH or $ZnCl_2$ is a well-known way to make activated carbon from biomass with a high specific surface area (SSA) and well-developed pores. This process is called thermochemical activation. Also, the chemical activation agent is necessary for the carbon matrix to change and for porous structures to form. Recent studies have shown that biomass can be used to get carbon materials by activating them with heat [65, 66].

Catalytic graphitization favors highly graphited carbon materials, while thermochemical activation yields layered porous carbon. Combining these two methods for preparing carbon materials is receiving much attention. Su and his colleagues did a study on making carbon materials from poplar catkins. They did this by using

$Ni(NO3)_2$ and KOH as catalysts in a process called graphitization and a chemical activation process. The TEM investigation revealed that the hollow carbon nanomesh was effectively created, and additional research showed that the CNMs as created had a large SSA of 1893 $m^2\ g^{-1}$ and pore volume of 1.495 $cm^3\ g^{-1}$[67].

4.2 Hydrothermal Carbonization

Hydrothermal conditions, defined as an aqueous medium with a temperature and pressure greater than or equal to 100 °C and 0.1 MPa, occur frequently in nature. Under these conditions, a wide variety of minerals and coal can form [68]. In 1913, Bergius performed the first hydrothermal transformation of cellulose into coal-like materials [70]. After this, a number of researchers looked into how different factors such as temperature and pH affect a reaction's outcome, as well as its mechanism of formation [69].

HTC is now commonly used at room temperature (130–250 °C). Many working groups have contributed to uncovering HTC-derived carbon (HTC) structure and formation mechanism [70]. This has made it a useful methodology for producing various carbonaceous materials. Using hydrothermal treatment of biomass, reagents and solvents can interact more easily, resulting in carbon materials being formed.

Consideration should also be given to time and energy-saving concerns in the home. Since it heats quickly, consumes less energy, and takes less time than other conventional heating systems, microwave heating represents a unique intangible layout. Carbon microspheres derived from glucose were synthesized by Lee et al. using a microwave-assisted hydrothermal scheme [71]. Instead of taking an hour or more like traditional HTC (1-24 h), microwave-assisted HTC only took 15 min, saving both time and energy.

The micropore size distributions of activated carbon materials (0.7–2 nm) are inadequate for electrolyte diffusion. The template method can create tiny holes with sizes between 1 and 200 nm and also produces an ordered structure, which is not possible with conventional activation [72]. Knox et al. [73] reported the first porous carbon template synthesis. The procedure employs both hard-template and soft-template techniques. After the original parent is eliminated, porous carbon is generated. Utilizing a series of innate porous structures, this methodology has been developed [74].

Due to their low carbon content (less than 80%), HTCs are not "real" CNMs. Restrictions on energy storage and conversion can be found in HTCs made from carbohydrates that have low Specific Surface Area (SSA) (SBET less than $10m^2/g$) and poor electrical conductivity [70]. A post-thermal treatment, in which the sp^3C-X bonds transform into aromatic $sp^2C = C$ bonds, is necessary for HTCs to make a complex structure [75].

4.3 Cyclic Oxidation

The cyclic oxidation method for preparing carbon from biomass focuses on reduplicative oxidation processes. This method converts 3D biomass into tubular structure (CNTs). Kang et al. [50] used cyclic oxidation to make carbon. Grass was dried and crumbled before being heated in air to 250 °C to make CNMs. The residue was heated at 600 °C for 20 min with controlled oxygen. The system was then brought back to room temperature and given the same amount of oxygen again. Before the product was gathered, the heat treatment at around 600 °C was done almost fifty times. Images obtained using transmission electron microscopy (TEM) demonstrated that the as-prepared material, which displayed a hollow-center structure, consisted of MWCNTs with inner and outer diameters ranging from 10 to 30 and 30 to 50 nm, respectively.

Goodell's team also examined the effects of heat treatment on the synthesis of CNMs [76]. Using cyclic heat treatment, the researchers found that heat pretreatment preserved the cell wall nano-architecture, leading to the formation of tubular carbon materials. Dehydration of cellulose and stabilization of lignin were both enhanced by the low temperature pretreatment; the latter also limited lignin flow during the subsequent higher temperature process. CNTs, graphene, and carbon nanospheres were also extracted from biomass applying this method, according to Qu et al. [77].

4.4 Chemical-Vapor-Deposition (CVD)

In the CVD method, the starting materials are put into a chamber where a substrate is exposed to them. In a perfect world, the starting material would be light enough to be carried by a carrier gas. It would then react with the heat in the reactor to make carbon materials on the scaffold. The synthesis temperature is ranging from 200 to 1100 °C [78]. CVD has made a lot of progress in making carbon materials. Depending on where the catalyst is placed during the CNM preparation process, one can roughly classify these as either in situ CVD or two-stage CVD. Figure 4 compares conventional, in situ, and two-stage CVD.

During the in-situ CVD process that is used to prepare CNMs from biomass, the biomass is first converted into carbon sources, then it is broken down into carbon atoms, and finally, carbon materials are fabricated from the carbon atoms. It is essential to prepare a biomass-catalyst system that is homogeneous. A uniform mixture has the potential to supply a suitable amount of carbon sources and active catalytic sites, which are both necessary for an efficient conversion of biomass to CNM. The preparation of CVD CM is affected by a number of factors, including carbon source, catalyst, and operating parameters [80]. In order to produce CNMs from biomass using a two-step CVD method, normally two processes are required. First, the biomass must be heated to turn it into vapors, and then a catalyst must be used to transform the vapors into CMs. In most cases, these two steps will be carried

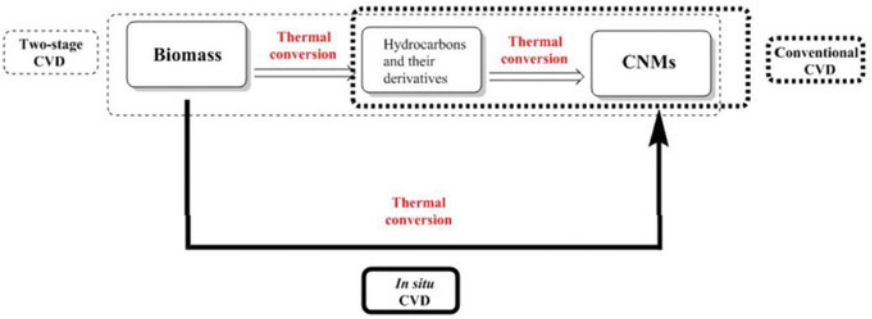

Fig. 4 Conventional, in situ, and two-step CVD relationships [79]

out in two separate reactors. The two-step CVD method for making CNMs from biomass depends on various parameters, such as the type of carbon source, the type of catalyst, and the temperature at which the process is carried out, just like the in-situ CVD method does. During the first stage of the process, the type of biomass feedstock as well as the conditions of the pyrolysis have a significant impact on the composition of the pyrolysis vapors. These vapors serve as the carbon source for the CNM synthesis that occurs during the second stage. Second-stage CNMs formation uses different catalysts. Stainless steel screens [81], NiO with/without support [82], and multi-metal catalysts were reported [83].

The CVD synthesis of carbon spheres and fullerenes is advantageous, because it produces uniformly sized structures. The CVD method is helpful in customizing the diameter, crystallinity, and fiber axis orientation of carbon nanofibers [84]. CVD is a good way to make CNTs because it gives you a lot of control over the carbon/catalyst ratio, particle size, and their orientation [84]. Because most biomass is solid, floating catalyst CVD is rarely used directly. Rice husks, wood, and corncobs are good examples of biomass that can be converted to CNMs.

5 Biomass-Derived CNMs for Energy Conversion and Storage

The demand for electric power in the modern world keeps going up. Especially in developing countries, where population and industrial growth are driving factors, there are often power outages because fossil fuels aren't always available, and electricity is sent from centralized power plants to an underdeveloped network that isn't often upgraded or maintained [85]. If there isn't enough electricity, it hurts economic growth and national security in a big way. So, the most important thing for a growing economy is to use decentralized renewable energy sources (wind, solar, hydro, and tidal power) to make electricity [86]. Solar energy is abundant in many developing

countries, so a lot of research has been done on how to capture, change, and store it [87].

5.1 Energy Harvesting/Conversion Devices

5.1.1 Thin-Film Solar Cell

Nanomaterials made of carbon have been the focus of research for a potential application in energy conversion systems. Here, we describe a comprehensive review of the wide range of applications for carbon nanomaterials and nanotechnology within the context of cutting-edge research and development (R&D) in the area of thin-film solar cells.

Polymer Heterojunction Solar Cells

Over the course of the past three decades, organic solar cells (OSC) have been developed as an alternative to silicon solar cells. They have several benefits, the most notable of which are their structural adaptability, remarkable coefficients of absorption, and the capacity to manufacture thin-film solar cells with very low thicknesses. OSCs are composed of a semiconducting material that has the capability to absorb light in the ultraviolet to the visible range of spectrum as well as the capability to carry an electric current. This material is what gives OSCs their dual absorption capabilities. An interpenetrating network is created between a fullerene derivative and a polymer in a bulk heterojunction organic solar cell, also known as a BHJ-OSC. Electron–hole pairs can be created when light-absorbing polymers are used. [88]. Excitons move towards the donor–acceptor interface. Quantification of free charge carriers can be accomplished through the generation or recombination of electron–donor–acceptor complexes. Electrodes are used to collect the charge carriers that are pushed around by the internal electric field. (Fig. 5) [89].

Interpenetrating networks, which are composed of two different semiconducting polymers, have been developed as the ideal photovoltaic material for a high efficiency. This structure offers the spatially distributed interfaces that are required for an effective photogeneration as well as an easy collection of electrons and holes [91]. As a direct result of this, recent studies have shown that photovoltaic cells that are based on interpenetrating network composites that are made up of conjugated polymer and C_{60} derivatives can achieve conversion efficiencies that are significantly higher, reaching up to 8% [92]. Thermal annealing can further enhance the performance of polymer solar cells. $PC_{61}BM$ ([6]-phenyl C61 butyric acid methyl ester) is a common acceptor in polymer solar cells, but other fullerene derivatives like $PC_{71}BM$ or $PC_{84}BM$ can be used for higher efficiency [93].

The performance of dispersed heterojunction organic photovoltaic devices has been the subject of recent research, which has investigated nanostructure of the

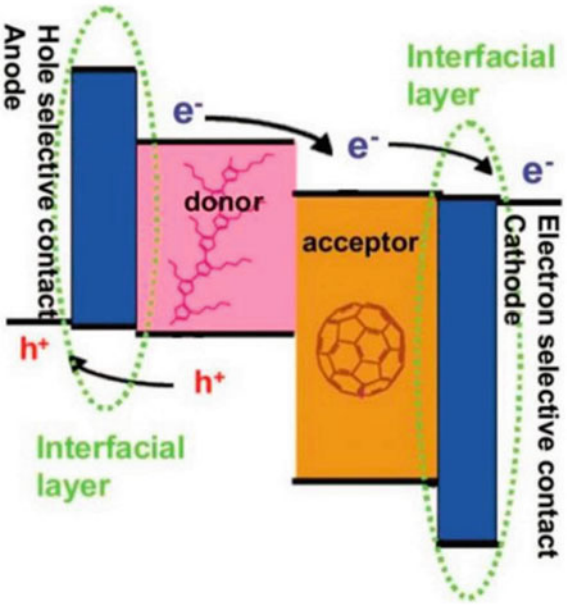

Fig. 5 Energy level diagram of polymer solar cell [90]

blends to further enhance the efficiency of cells. These studies were carried out in an effort to improve the efficiency of the devices. In order to accomplish this goal, a focus has been placed on the development of disperse heterojunctions that are constructed using polymer/CNT composite systems. It is anticipated that the CNT, which is an extended form of C60, will provide greater electron mobility while simultaneously lowering the percolation threshold. Because their field-effect electron mobility can reach up to 77,000 $cm^2\ V^{-1}\ s^{-1}$, carbon nanotubes are recognized as an extremely electron-conductive semiconductor. This is due to the fact that it has been reported that their field-effect electron mobility [94]. Time-of-flight experiments and field-effect transistor analyses determined PCBM's electron mobilities to be 10^{-6} to $10^{-1}\ cm^2\ V^{-1}\ s^{-1}$ [95]. For the first time, MWNTs and poly(p-phenylene vinylene) (PPV) were combined to form a rectifying heterojunction, as reported by Romero et al. [58]. Curran et al. [96] mixed poly(m-phenylenevinylene-co-2,5-dioctoxy-p-phenylenevinylene) and MWNTs in toluene and then solution cast. Wetting MWNTs with polymer improved photoconductivity, photoluminescence, and electroluminescence [97]. It has been hypothesized that the improved performance of the device is due to the favorable electronic properties of CNTs as well as their enormous surface areas. CNTs have the potential to provide high thermal conductivity as well as good mechanical stability. The incorporation of dye molecules into polymer–CNT solar cells may lead to an increase in the short-circuit current due to the potential for further improvement in light absorption in the ultraviolet and red regions (I_{sc}). Esterifying CH_2OH-terminated P3HT onto acid-oxidized CNTs was the method that Kuila et al. used in their investigation of charge transfer at the polymer–CNT interface. This was done using a bilayer photovoltaic device. P3HT-attached carbon nanotubes, also

known as P3CNTs, are soluble in a wide variety of organic solvents, which makes it easier for them to mix closely with free P3HT chains and produce powerful electronic interactions. It was found that nanocomposite optical and electrochemical properties differed from conventional composite. In the traditional composite, pure CNT and P3HT were mixed together [98]. When compared to CNTs, graphene's 2D carbon network possesses a significantly higher specific surface area. Even in a bulk heterojunction device, there is less chance that a short circuit will happen via the active layer [99]. The use of 2D graphene nanosheets in polymer solar cells (PSCs) in addition to 0D fullerenes and 1D CNTs has also been studied [100]. Yu et al. [101] used esterification to graft CH_2OH-terminated P3HT onto graphene oxide carboxylic groups (GO). This is interesting. The power-conversion efficiency of their fabricated device was improved by a factor of two hundred under one-sun illumination. This efficiency was measured as 0.61%. Separate research conducted by Yu and colleagues resulted in the development of a straightforward lithiation reaction that allowed for the covalent attachment of monosubstituted C60 onto graphene. C60-grafted graphene nanosheets improve electron transport and hence device performance [102, 103].

Dye-Sensitized Solar Cells

In 1991, Gratzel proposed the first dye-sensitized solar cell (DSSC) that worked well enough. Even though the DSSC turns light into electricity less well than a Si-based solar cell, it has many benefits, the most important of which is that it is cheap. Figure 6 shows the schematic illustration of DSSCs. Covalent bonds are what hold the dye molecules to the metal oxide semiconductor.

Even though pristine TiO_2 has many extraordinary properties that make it a perfect candidate for photoanode (PE), the performance of DSSCs based on pristine TiO_2 is not sufficient for use in high-performance applications [105]. Therefore, nanocomposites of carbonaceous materials with TiO_2 have been sought to make high-performance DSSCs. Allotropes of carbon have high electrical conductivity

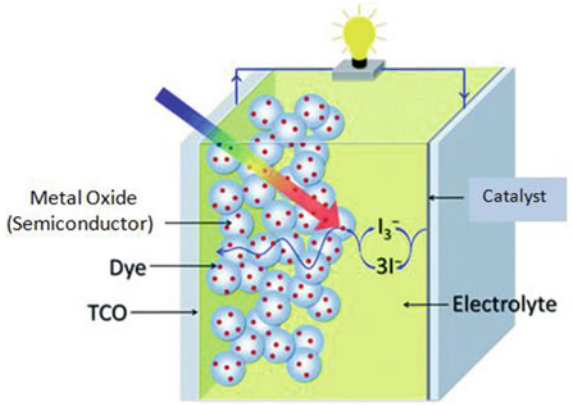

Fig. 6 Schematic illustration of DSSCs [104]

and electrolyte stability. CNTs and graphene are effective PE fillers for DSSCs. High electron mobility and light harvesting are to blame. This section reviews carbon nanocomposites with TiO_2 for efficient DSSCs.

In the production of DSSCs, carbon black (CB) is only occasionally used. The CB has a higher conduction band when compared to TiO_2, which has a lower band. It has the potential to raise the conduction band energy level of the CB/TiO_2 film. As a result, it can achieve a higher output voltage [106]. By putting TiO2/CB nanocomposite and dye in a triangle, Ting and Chao [106] were able to improve the PCE of DSSCs. The open circuit voltage (Voc) went up from 0.5 V to 0.6 V. The PCE and short-circuit current density were also made better. Kang et al. [107] made CB/TiO_2 nanocomposites with thermally treated CB. Nanocomposite thin-film photoanodes improved DSSC efficiency by 31%.

Instead of providing an effective transport path [108], CNTs' high conductivity boosts DSSC performance. High-performance CNTs require alignment and dispersion. CNT alignment made composites anisotropic in two directions. Parallel conductivity is higher than perpendicular [109]. Similarly, CNT dispersion in the base fluid affects the PCE of DSSC [110]. Conduction band of CNTs is lower than TiO2. This difference would shift the Fermi level (FL) towards more positive or downward [111].]. Figure 7a shows how MWCNTs lower Fermi level. CNTs' contents determine their positive potential. Increased CNT content shifts FL to a more positive potential, increasing charge injection efficiency [112]. Charge collection efficiency is another important factor in DSSC PE electron transport. CNTs increase PE conductivity by providing an electron transport path [113]. As can be seen in Fig. 7b, the rapid transport of electrons also helps to reduce the recombination of injected electrons with electrolyte. This decrease in recombination contributes to an increase in the overall fill factor (FF) of DSSCs, which in turn contributes to an improvement in PCE.

Semiconducting SWCNTs perform better than metallic SWCNTs, according to Guai et al. [114]. This was the case when comparing the two types of SWCNTs. It is possible that this is due to the non-continuous band structure of s-SWCNTs, whereas the bandgap of metallic-based SWCNTs is zero [115].

The bandgap, surface area, and electron mobility of graphene are all modifiable. Due to its properties, graphene is widely regarded as an excellent candidate for use as an additive material in DSSCs. Also, the 2D-graphene sheet makes it easy for electrons that have been injected to move around. PEs made from graphene have better PCE than those made from CNTs and carbon particles, according to numerous experiments [116]. Due to higher charge recombination with electrolyte, CNTs' weak interaction with spherical TiO2 nanoparticles limits DSSC efficiency. A single graphene sheet improves nanoscale TiO2 contact. Graphene's work function (–4.42 eV) [117] is between TiO_2's (–4.4 eV) and FTO's (–4.7 eV)[118]. This energy level allows stepwise transfer of photogenerated electrons from TiO_2 to conductive substrate (Fig. 8a). As can be seen in Fig. 8b, graphene serves as a connecting medium between TiO2 and FTO [119]. Because of these advances, graphene is an ideal material for the PE of a DSSC that operates at a high level of efficiency.

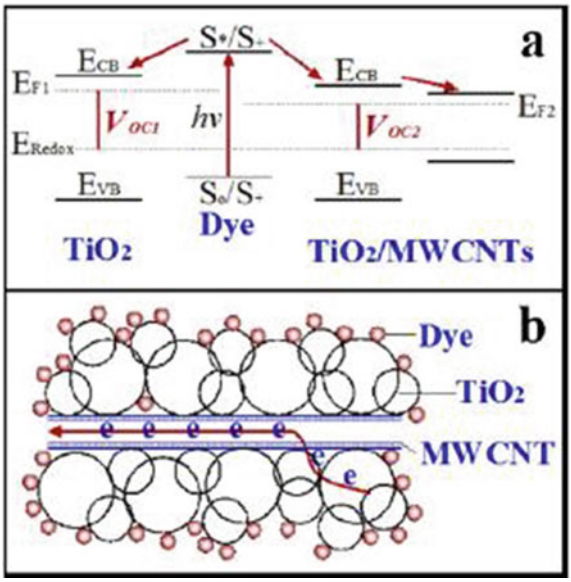

Fig. 7 The inclusion of carbon nanotubes has two effects: a) a shift in energy level, and b) an enhancement in electrical conductivity [112]

The development of a catalyst material that can be produced at a lower cost is of the utmost importance for the eventual commercialization of DSSCs. In addition to having a low cost, the catalyst should have excellent catalytic characteristics and resistance to corrosion. The most obvious candidate to take the place of Pt is carbon. It can be found in large quantities throughout the crust of the Earth. In addition to this, it possesses all the characteristics that are necessary for the material that constitutes the catalyst. Some of the carbon allotropes that have been utilized as catalysts in DSSCs include activated carbon, CB, graphene, and CNTs [120].

5.2 Energy Storage Devices

It has been demonstrated that supercapacitors and batteries belong to electrochemical energy storage devices [121]. Traditional electrode materials, however, such as graphite is neither renewable nor sustainable; however, they are essential components of the devices in question. Traditional non-sustainable electrode materials can be replaced with renewable biomass-derived materials. It could be owing to their distinct structures, mechanical strength, and conductivity. Moreover, they are versatile and tend to form hybrid composites with other materials. Biomass and its derivatives have been tried as high-performance electrode materials to enhance the power density and energy density of electrochemical storage devices. [122]. In the following, we will discuss the most recent developments in the field of supercapacitors and lithium batteries that use carbon electrode materials derived from biomass.

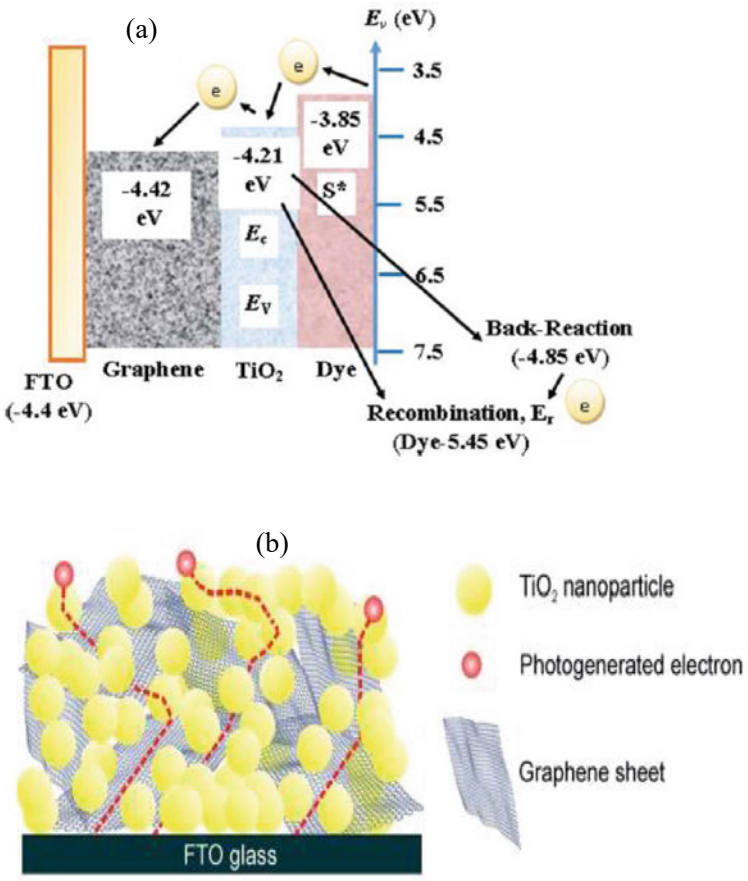

Fig. 8 **a** Graphene/TiO2-based DSSC energy level diagram [105] and **b** Charge transfer mechanism in composite anode [119]

5.2.1 Supercapacitors with Activated Carbon Nanomaterial Electrodes

Most activated carbon's surface area is micropore-sized. In general, pores of this size are inaccessible to electrolyte ions and cannot support an electrical double layer. Mesopores boost a double-layer capacitor's capacitance [123]. Recent studies demonstrate that charge storage in pores 0.5–2 nm in size rises as pore size decreases owing to the increased proximity of the ion center to the electrode surface [124]. A double layer can't form in pores that are less than 0.5 nm wide [125]. Activated carbon materials that are currently on the market have a lot of surface area but not many mesopores. This means that electrolytes can't get to them easily, which limits their capacitance. This means that the resulting supercapacitors have a low energy density. Activated carbons also don't conduct electricity well, and because they aren't easy to get to by electrolytes, they have a high internal resistance. This makes the

capacitors have a low power density. So, the activated carbon electrodes used in the supercapacitors that are currently on the market have a low energy density and a low power density.

Because of this, new materials are needed to make up for the problems with activated carbon electrodes so that supercapacitors can work better. High conductivity, mesoporosity, and electrolyte accessibility make CNTs a good electrode material for supercapacitors [126]. Researchers used the combination of CNT electrode materials and electrolytes to enhance supercapacitors' performance, safety, and lifespan. Randomly entangled CNTs were first researched for supercapacitor applications. CNTs have a moderate surface area compared to activated carbons. However, a larger capacitance has been observed for CNTs [126, 127] as compared to activated carbons. The double-layer capacitors generally possess the charge densities in the range of 20–50 μF. An et al. [128] determined that the theoretical capacitance of their CNTs was between 71 and 178 F g^{-1}. This is in close agreement with the measured values (180 F g^{-1}) in the top bound, which indicates that the CNTs have perfect electrolyte accessibility. The enhanced electrolyte accessibility and thus high capacitances found for CNT electrodes are due to the peculiar mesoporosity caused by tube entanglement [126, 128].

Since the 1990s, CNTs have been used for supercapacitance [129]. CNT-based capacitors lack the required capacitance. It is mainly due to the high interface resistance between current collector and CNT electrode, poor interaction between electrolyte and electrode, and instability of double layer. Graphene has been examined as a carbon-based electrode in supercapacitors because of its higher SSA, high electrical conductivity, and superior mechanical stability. Theoretically, a graphene electrode's double-layer capacitance can approach 550 F g^{-1}, the greatest of any carbon-based electrode [130]. Stoller et al. used electrodes made of graphene oxide that had been chemically changed to get specific capacitances of 135 F g^{-1} and 99 F g^{-1} in aqueous and organic electrolytes, respectively [131]. This group also made reduced graphene oxides with capacitance values of 191Fg^{-1} using simple microwave heating method [132].

5.2.2 Lithium-Ion Batteries (LiBs)

LiBs have been made commercially with graphite and lithium cobalt oxide as the anode and cathode, respectively [133]. The electrolytes are mostly comprised of a combination of the solvent and Li salts. The mixture of these materials results in a nominal voltage of around 3.6 V, which is approximately double the value of a conventional alkaline battery. During charging and discharging of LiBs, Li ions move from anode to cathode through electrolyte. Therefore, lithium-ion batteries have a longer cycle life than alkaline or other types of rechargeable batteries. The structure and working mechanism of LiB is shown in Fig. 9 [134]. It has been found that the electrode properties affect battery energy, power, safety, and cycle life.

Because of its comparatively large capacity and superior cyclability, graphite has traditionally been utilized as the anode material of choice for lithium-ion batteries.

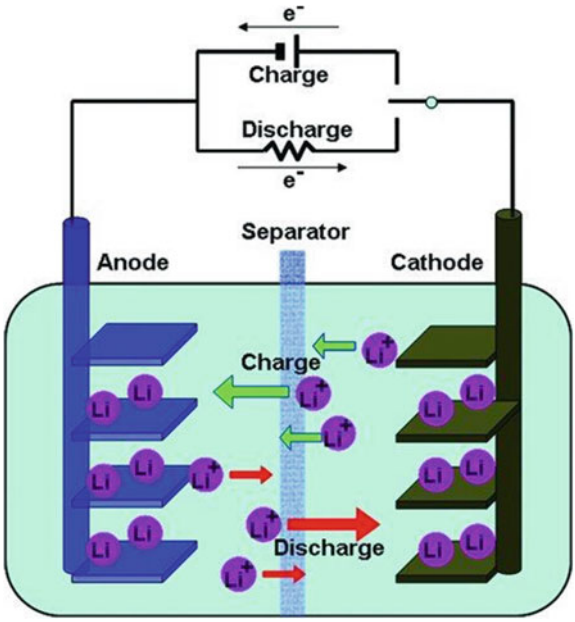

Fig. 9 Working principle of a Li-ion battery [134]

The intercalation and deintercalation of lithium ions into and out of graphite, respectively, during charge and discharge, is the fundamental mechanism behind graphite's role as the battery's anode (Fig. 9). The saturated concentration of graphite at thermodynamic equilibrium is LiC6, which is equal to a theoretical capacity of 372 mAh g^{-1}. Advanced LiBs need higher-capacity anode materials to increase energy density [134]. Also, the best anode material for LiBs should be more reversible and have a faster rate of charging and discharging than graphite [135]. To improve energy storage of LiBs, higher-capacity cathode materials are needed. Numerous studies have been conducted on nanostructured electrode materials for LiBs because they have a large SSA and make it easy for ions to move through them [136]. CNTs are promising for LiBs due to their high conductivity, high SSA, porosity, and easy electrolyte diffusivity [136]. CNTs have been investigated as host materials and conductive additions for anode applications. CNTs are an appealing host anode material for Li + intercalation. Several papers have been written about how Li + can be successfully put into both SWNTs and MWNTs [135]. On the other hand, CNT anodes have two major flaws. One of them is the capacity that can't be changed. This is caused by the formation of a layer on the surface of the carbon called the solid electrolyte interphase (SEI). This is like what happens when graphite is used as an anode [137]. The other problem is the voltage hysteresis that happens between charging and discharging. This is mostly caused by how fast the Li^+ intercalation and deintercalation reactions at the CNTs anode occur. To address these issues, for example, by shortening the nanotubes to increase the electrode's charge transfer capabilities, attempts have been made.

Graphene's excellent conductivity, high SSA, and electrochemical stability make it a suitable electrode material for LiBs [138]. However, graphene's specific capacity is quite limited, as only one lithium ion can be retained per six carbon atoms [139]. Various methods, such as generating hybrid materials with metal oxide, adding dopants, and regulating the formation of layered structures, have been built to overcome these primary constraints. Metal oxide and graphene-based hybrid materials improve the metal oxide electrode's reversible cycling performance.

6 Conclusion and Future Outlook

Carbon from biomass is used in advanced energy storage and conversion devices, especially in supercapacitors, LiBs, and thin-film solar cells. Even though there has been some progress in the field of energy conversion and storage with carbon materials made from biomass, there are still some challenges that make it hard to use them more:

1. The use of biomass in the production of high-performance carbon nanomaterials is still challenging due to the fact that biomass has a complicated 3D structure, strong chemical bonding, and a high oxygen concentration.
2. Different energy storage techniques require different architectures of biomass-derived carbon.
3. Biomass-derived carbon structure and surface chemistry should be regulated. Chemical activation promotes SSA by generating micropores. These micropores limit electrolyte ion transit and transfer, causing inadequate power. In supercapacitors, ion and electron transport is difficult when carbon materials are excessively porous.
4. Using heteroatoms in LiBs can increase interlayer spacing and active sites. Intercalation and deintercalation of lithium/sodium ions are important for battery operation. Oxygen and sulfur-containing functional groups reduce the conductivity of carbon-based materials.
5. Owing to their superior electrical conductivity and wide SSA, biomass-derived carbon materials support high pseudo-capacitance materials. However, interface combination is crucial.
6. It's important to scale up manufacturing of biomass-derived carbon compounds from the lab to industry. The production of CNMs from biomass should be low-cost and free from toxic gasses.

In a nutshell, the material structure's contradictory problems need to be balanced to offer suggestions for the design of efficient electrode materials for energy conversion and storage. Future research should be focused on the development of all biomass-based electrochemical systems that make full use of the structural variation of biomass to fulfill sustainable development approaches. These systems should take full benefit of the structural potential offered by biomass.

Acknowledgements The authors would like to thank the Higher Education Commission of Pakistan (HEC) for their support in sponsoring this work through the CPEC-Collaborative Research Grant (Project No. CPEC-8). In addition, the authors would like to thank the PPE Department at UET Lahore for providing the laboratory facilities.

References

1. Moodley, P. (2021) Sustainable biofuels: opportunities and challenges. *Sustain. Biofuels*, 1–20.
2. Chong, C.T., and Ng, J.-H. (2021) Global Aviation and Biojet Fuel Policies, Legislations, Initiatives, and Roadmaps. *Biojet Fuel Aviat. Appl.*, 1–79.
3. Goeppert A, Czaun M, Jones JP, Surya Prakash GK, Olah GA (2014) Recycling of carbon dioxide to methanol and derived products – closing the loop. Chem Soc Rev 43(23):7995–8048
4. Chandra Srivastava V (2012) An evaluation of desulfurization technologies for sulfur removal from liquid fuels. RSC Adv 2(3):759–783
5. Zhong J, Yang X, Wu Z, Liang B, Huang Y, Zhang T (2020) State of the art and perspectives in heterogeneous catalysis of CO2 hydrogenation to methanol. Chem Soc Rev 49(5):1385–1413
6. West, G.B. (2010) Integrated sustainability and the underlying threat of urbanization. *Glob. Sustain.*, 9.
7. Kamat PV (2007) Meeting the clean energy demand: Nanostructure architectures for solar energy conversion. J Phys Chem C 111(7):2834–2860
8. Lewis, N.S., and Francisco, S. (2011) Powering the Planet. *MRS Bull. 2007 3210*, **32** (10), 808–820.
9. Corma Canos A, Iborra S, Velty A (2007) Chemical routes for the transformation of biomass into chemicals. Chem Rev 107(6):2411–2502
10. Ragauskas AJ, Williams CK, Davison BH, Britovsek G, Cairney J, Eckert CA, Frederick WJ, Hallett JP, Leak DJ, Liotta CL, Mielenz JR, Murphy R, Templer R, Tschaplinski T (2006) The path forward for biofuels and biomaterials. Science 311(5760):484–489
11. Serrano-Ruiz JC, Luque R, Sepúlveda-Escribano A (2011) Transformations of biomass-derived platform molecules: from high added-value chemicals to fuelsvia aqueous-phase processing. Chem Soc Rev 40(11):5266–5281
12. Bridgwater AV (1994) Catalysis in thermal biomass conversion. Appl Catal A Gen 116(1–2):5–47
13. Pignataro, B. (2010) Ideas in chemistry and molecular sciences. Where chemistry meets life. 335.
14. Hong CK, Wool RF (2005) Development of a bio-based composite material from soybean oil and keratin fibers. J Appl Polym Sci 95(6):1524–1538
15. Gharbi, S., Andreolety, J.P., and Gandini, A. (2000) Polyesters bearing furan moieties: IV. Solution and interfacial polycondensation of 2,2′-bis(5-chloroformyl-2-furyl)propane with various diols and bisphenols. *Eur. Polym. J.*, **36** (3), 463–472.
16. Mitiakoudis A, Gandini A (1991) Synthesis and Characterization of Furanic Polyamides. Macromolecules 24(4):830–835
17. Madhavan Nampoothiri K, Nair NR, John RP (2010) An overview of the recent developments in polylactide (PLA) research. Bioresour Technol 101(22):8493–8501
18. Wang F, Ouyang D, Zhou Z, Page SJ, Liu D, Zhao X (2021) Lignocellulosic biomass as sustainable feedstock and materials for power generation and energy storage. J Energy Chem 57:247–280
19. Navakoteswara Rao V, Malu TJ, Cheralathan KK, Sakar M, Pitchaimuthu S, Rodríguez-González V, Mamatha Kumari M, Shankar MV (2021) Light-driven transformation of biomass into chemicals using photocatalysts – Vistas and challenges. J Environ Manage 284:111983

20. Adeleye AT, Akande AA, Odoh CK, Philip M, Fidelis TT, Amos PI, Banjoko OO (2021) Efficient synthesis of bio-based activated carbon (AC) for catalytic systems: A green and sustainable approach. J Ind Eng Chem 96:59–75
21. Pribula, A. (1991) The elements, their origin, abundance, and distribution (Cox, P.A.). *J. Chem. Educ.*, **68** (4), A112.
22. Babu, J.S., Prasanna, H.B.N., Babu, J.S., Rao, Y.N., and Beyan, S.M. (2022) Environmental Applications of Sorbents, High-Flux Membranes of Carbon-Based Nanomaterials. *Adsorpt. Sci. Technol.*, **2022**.
23. Luque, R., and Balu, A.M. (2013) Producing fuels and fine chemicals from biomass using nanomaterials. *Prod. Fuels Fine Chem. from Biomass Using Nanomater.*, 1–315.
24. Titirici MM, White RJ, Brun N, Budarin VL, Su DS, Del Monte F, Clark JH, MacLachlan MJ (2014) Sustainable carbon materials. Chem Soc Rev 44(1):250–290
25. Kumar R, Singh RK, Singh DP (2016) Natural and waste hydrocarbon precursors for the synthesis of carbon based nanomaterials: Graphene and CNTs. Renew Sustain Energy Rev 58:976–1006
26. Wang Z, Guo H, Shen F, Yang G, Zhang Y, Zeng Y, Wang L, Xiao H, Deng S (2015) Biochar produced from oak sawdust by Lanthanum (La)-involved pyrolysis for adsorption of ammonium (NH4+), nitrate (NO3−), and phosphate (PO43−). Chemosphere 119:646–653
27. Keiluweit M, Nico PS, Johnson M, Kleber M (2010) Dynamic molecular structure of plant biomass-derived black carbon (biochar). Environ Sci Technol 44(4):1247–1253
28. Zhang M, Gao B, Yao Y, Xue Y, Inyang M (2012) Synthesis of porous MgO-biochar nanocomposites for removal of phosphate and nitrate from aqueous solutions. Chem Eng J 210:26–32
29. Shen D, Jin W, Hu J, Xiao R, Luo K (2015) An overview on fast pyrolysis of the main constituents in lignocellulosic biomass to valued-added chemicals: Structures, pathways and interactions. Renew Sustain Energy Rev 51:761–774
30. Zhao NQ, He CN, Ding J, Zou TC, Qiao ZJ, Shi CS, Du XW, Li JJ, Li YD (2007) Bamboo-shaped carbon nanotubes produced by catalytic decomposition of methane over nickel nanoparticles supported on aluminum. J Alloys Compd 428(1–2):79–83
31. Keller C, Ludwig C, Davoli F, Wochele J (2005) Thermal Treatment of Metal-Enriched Biomass Produced from Heavy Metal Phytoextraction. Environ Sci Technol 39(9):3359–3367
32. Liu WJ, Zeng FX, Jiang H, Yu HQ (2011) Total recovery of nitrogen and phosphorus from three wetland plants by fast pyrolysis technology. Bioresour Technol 102(3):3471–3479
33. Cheung TLY, Ng DHL (2007) Conversion of Bamboo to Biomorphic Composites Containing Silica and Silicon Carbide Nanowires. J Am Ceram Soc 90(2):559–564
34. Liu WJ, Jiang H, Yu HQ (2015) Thermochemical conversion of lignin to functional materials: a review and future directions. Green Chem 17(11):4888–4907
35. Skoda, M., Dudek, I., Jarosz, A., and Szukiewicz, D. (2014) Graphene: One material, many possibilities - Application difficulties in biological systems. *J. Nanomater.*, **2014**.
36. Geim AK (2009) Graphene: status and prospects. Science 324(5934):1530–1534
37. Abergel DSL, Apalkov V, Berashevich J, Ziegler K, Chakraborty T (2010) Properties of graphene: A theoretical perspective. Adv Phys 59(4):261–482
38. Mombeshora ET, Ndungu PG, Nyamori VO (2017) Effect of graphite/sodium nitrate ratio and reaction time on the physicochemical properties of graphene oxide. New Carbon Mater 32(2):174–187
39. Primo A, Atienzar P, Sanchez E, Delgado JM, García H (2012) From biomass wastes to large-area, high-quality, N-doped graphene: catalyst-free carbonization of chitosan coatings on arbitrary substrates. Chem Commun 48(74):9254–9256
40. Shams SS, Zhang LS, Hu R, Zhang R, Zhu J (2015) Synthesis of graphene from biomass: A green chemistry approach. Mater Lett 161:476–479
41. Chen F, Yang J, Bai T, Long B, Zhou X (2016) Facile synthesis of few-layer graphene from biomass waste and its application in lithium ion batteries. J Electroanal Chem 768:18–26
42. Amiinu IS, Zhang J, Kou Z, Liu X, Asare OK, Zhou H, Cheng K, Zhang H, Mai L, Pan M, Mu S (2016) Self-Organized 3D Porous Graphene Dual-Doped with Biomass-Sponsored Nitrogen

and Sulfur for Oxygen Reduction and Evolution. ACS Appl Mater Interfaces 8(43):29408–29418
43. Abdalla S, Al-Marzouki F, Al-Ghamdi AA, Abdel-Daiem A (2015) Different Technical Applications of Carbon Nanotubes. Nanoscale Res Lett 10(1):1–10
44. De Volder, M.F.L., Tawfick, S.H., Baughman, R.H., and Hart, A.J. (2013) Carbon nanotubes: Present and future commercial applications. *Science (80-.).*, **339** (6119), 535–539.
45. Qu, J., Luo, C., and Cong, Q. (2011) Synthesis of Multi-walled Carbon Nanotubes/ZnO Nanocomposites using Absorbent Cotton. *Nano-Micro Lett. 2011 32*, **3** (2), 115–120.
46. Osman, A.I., Farrell, C., Al-Muhtaseb, A.H., Harrison, J., and Rooney, D.W. (2020) The production and application of carbon nanomaterials from high alkali silicate herbaceous biomass. *Sci. Reports 2020 101*, **10** (1), 1–13.
47. Bernd MGS, Bragança SR, Heck N, Filho LCPDS (2017) Synthesis of carbon nanostructures by the pyrolysis of wood sawdust in a tubular reactor. J. Mater. Res. Technol. 6(2):171–177
48. Shi K, Yan J, Lester E, Wu T (2014) Catalyst-Free Synthesis of Multiwalled Carbon Nanotubes via Microwave-Induced Processing of Biomass. Ind Eng Chem Res 53(39):15012–15019
49. Zhu J, Jia J, Kwong FL, Ng DHL, Tjong SC (2012) Synthesis of multiwalled carbon nanotubes from bamboo charcoal and the roles of minerals on their growth. Biomass Bioenerg 36:12–19
50. Kang Z, Wang E, Mao B, Su Z, Chen L, Xu L (2005) Obtaining carbon nanotubes from grass. Nanotechnology 16(8):1192
51. Chen LF, Huang ZH, Liang HW, Gao HL, Yu SH (2014) Three-Dimensional Heteroatom-Doped Carbon Nanofiber Networks Derived from Bacterial Cellulose for Supercapacitors. Adv Funct Mater 24(32):5104–5111
52. Bartelmess J, Giordani S (2014) Carbon nano-onions (multi-layer fullerenes): chemistry and applications. Beilstein J Nanotechnol 5(1):1980
53. Plonska-Brzezinska ME, Echegoyen L (2013) Carbon nano-onions for supercapacitor electrodes: recent developments and applications. J. Mater. Chem. A 1(44):13703–13714
54. Ghosh M, Sonkar SK, Saxena M, Sarkar S (2011) Carbon Nano-onions for Imaging the Life Cycle of Drosophila Melanogaster. Small 7(22):3170–3177
55. Wu W, Yu B (2020) Corn flour nano-graphene prepared by the hummers redox method. ACS Omega 5(46):30252–30256
56. Zhang H, Zhang Z, Luo JD, Qi XT, Yu J, Cai JX, Wei J, chao, and Yang, Z.Y. (2019) A Chemical Blowing Strategy to Fabricate Biomass-Derived Carbon-Aerogels with Graphene-Like Nanosheet Structures for High-Performance Supercapacitors. Chemsuschem 12(11):2462–2470
57. Mondal D, Sharma M, Wang CH, Lin YC, Huang HC, Saha A, Nataraj SK, Prasad K (2016) Deep eutectic solvent promoted one step sustainable conversion of fresh seaweed biomass to functionalized graphene as a potential electrocatalyst. Green Chem 18(9):2819–2826
58. Purkait, T., Singh, G., Singh, M., Kumar, D., and Dey, R.S. (2017) Large area few-layer graphene with scalable preparation from waste biomass for high-performance supercapacitor. *Sci. Reports 2017 71*, **7** (1), 1–14.
59. Ye X, Yang Q, Zheng Y, Mo W, Hu J, Huang W (2014) Biotemplate synthesis of carbon nanostructures using bamboo as both the template and the carbon source. Mater Res Bull 51:366–371
60. Esohe Omoriyekomwan, J., Tahmasebi, A., Zhang, J., and Yu, J. (2022) Synthesis of Super-Long Carbon Nanotubes from Cellulosic Biomass under Microwave Radiation. *Nanomater. (Basel, Switzerland)*, **12** (5), 737.
61. Zhang J, Tahmasebi A, Omoriyekomwan JE, Yu J (2018) Direct synthesis of hollow carbon nanofibers on bio-char during microwave pyrolysis of pine nut shell. J Anal Appl Pyrolysis 130:142–148
62. Wang Z, Ogata H, Morimoto S, Ortiz-Medina J, Fujishige M, Takeuchi K, Muramatsu H, Hayashi T, Terrones M, Hashimoto Y, Endo M (2015) Nanocarbons from rice husk by microwave plasma irradiation: From graphene and carbon nanotubes to graphenated carbon nanotube hybrids. Carbon N. Y. 94:479–484

63. Noked, M., Soffer, A., Aurbach, D., Noked, M., Soffer, : A, and Aurbach, : D (2011) The electrochemistry of activated carbonaceous materials: past, present, and future. *J. Solid State Electrochem. 2011 157*, **15** (7), 1563–1578.
64. Liu B, Liu Y, Chen H, Yang M, Li H (2017) Oxygen and nitrogen co-doped porous carbon nanosheets derived from Perilla frutescens for high volumetric performance supercapacitors. J Power Sources 341:309–317
65. Li Y, Wang G, Wei T, Fan Z, Yan P (2016) Nitrogen and sulfur co-doped porous carbon nanosheets derived from willow catkin for supercapacitors. Nano Energy 19:165–175
66. Niu Q, Gao K, Tang Q, Wang L, Han L, Fang H, Zhang Y, Wang S, Wang L (2017) Large-size graphene-like porous carbon nanosheets with controllable N-doped surface derived from sugarcane bagasse pith/chitosan for high performance supercapacitors. Carbon N. Y. 123:290–298
67. Su XL, Cheng MY, Fu L, Yang JH, Zheng XC, Guan XX (2017) Superior supercapacitive performance of hollow activated carbon nanomesh with hierarchical structure derived from poplar catkins. J Power Sources 362:27–38
68. Rabenau A (1985) The Role of Hydrothermal Synthesis in Preparative Chemistry. Angew. Chemie Int. Ed. English 24(12):1026–1040
69. Haenel MW (1992) Recent progress in coal structure research. Fuel 71(11):1211–1223
70. Falco C, Baccile N, Titirici MM (2011) Morphological and structural differences between glucose, cellulose and lignocellulosic biomass derived hydrothermal carbons. Green Chem 13(11):3273–3281
71. Jung A, Han S, Kim T, Cho WJ, Lee KH (2013) Synthesis of high carbon content microspheres using 2-step microwave carbonization, and the influence of nitrogen doping on catalytic activity. Carbon N. Y. 60:307–316
72. Kubo S, Demir-Cakan R, Zhao L, White RJ, Titirici MM (2010) Porous Carbohydrate-Based Materials via Hard Templating. Chemsuschem 3(2):188–194
73. Knox, J.H., Kaur, B., and Millward, G.R. (1986) Structure and performance of porous graphitic carbon in liquid chromatography. *J. Chromatogr. A*, **352** (C), 3–25.
74. Lee J, Kim J, Hyeon T (2006) Recent Progress in the Synthesis of Porous Carbon Materials. Adv Mater 18(16):2073–2094
75. Liu X, Giordano C, Antonietti M (2014) A Facile Molten-Salt Route to Graphene Synthesis. Small 10(1):193–200
76. Zhang XXBGYQGDD, JellisonS DCNMLPJ (2009) A method for producing carbon nanotubes directly from plant materials. For Prod J 59(1–2):26–28
77. Qu J, Luo C, Zhang Q, Cong Q, Yuan X (2013) Easy synthesis of graphene sheets from alfalfa plants by treatment of nitric acid. Mater Sci Eng B 178(6):380–382
78. Mugadza, K., Stark, A., Ndungu, P.G., and Nyamori, V.O. (2020) Synthesis of Carbon Nanomaterials from Biomass Utilizing Ionic Liquids for Potential Application in Solar Energy Conversion and Storage. *Mater. 2020, Vol. 13, Page 3945*, **13** (18), 3945.
79. Wang Z, Shen D, Wu C, Gu S (2018) State-of-the-art on the production and application of carbon nanomaterials from biomass. Green Chem 20(22):5031–5057
80. Tessonnier JP, Su DS (2011) Recent Progress on the Growth Mechanism of Carbon Nanotubes: A Review. Chemsuschem 4(7):824–847
81. Alves JO, Soares Tenório JA, Zhuo C, Levendis YA (2012) Characterization of Nanomaterials Produced from Sugarcane Bagasse. J. Mater. Res. Technol. 1(1):31–34
82. Efika CE, Wu C, Williams PT (2012) Syngas production from pyrolysis–catalytic steam reforming of waste biomass in a continuous screw kiln reactor. J Anal Appl Pyrolysis 95:87–94
83. Dong L, Wu C, Ling H, Shi J, Williams PT, Huang J (2016) Development of Fe-Promoted Ni–Al Catalysts for Hydrogen Production from Gasification of Wood Sawdust. Energy Fuels 31(3):2118–2127
84. Manawi, Y.M., Ihsanullah, Samara, A., Al-Ansari, T., and Atieh, M.A. (2018) A Review of Carbon Nanomaterials' Synthesis via the Chemical Vapor Deposition (CVD) Method. *Mater. (Basel, Switzerland)*, **11** (5).

85. Arto I, Capellán-Pérez I, Lago R, Bueno G, Bermejo R (2016) The energy requirements of a developed world. Energy Sustain Dev 33:1–13
86. Abbasi T, Abbasi SA (2011) Decarbonization of fossil fuels as a strategy to control global warming. Renew Sustain Energy Rev 15(4):1828–1834
87. Granqvist CG (2007) Transparent conductors as solar energy materials: A panoramic review. Sol Energy Mater Sol Cells 91(17):1529–1598
88. Deibel C, Dyakonov V (2010) Polymer–fullerene bulk heterojunction solar cells. Reports Prog. Phys. 73(9):096401
89. Guo J, Ohkita H, Benten H, Ito S (2010) Charge generation and recombination dynamics in poly(3-hexylthiophene)/ fullerene blend films with different regioregularities and morphologies. J Am Chem Soc 132(17):6154–6164
90. Zeng, H., Zhu, X., Liang, Y., and Guo, X. (2015) Interfacial Layer Engineering for Performance Enhancement in Polymer Solar Cells. *Polym. 2015, Vol. 7, Pages 333–372*, **7** (2), 333–372.
91. Yu G, Heeger AJ (1998) Charge separation and photovoltaic conversion in polymer composites with internal donor/acceptor heterojunctions. J Appl Phys 78(7):4510
92. Liang Y, Yu L (2010). Development of Semiconducting Polymers for Solar Energy Harvesting. https://doi.org/10.1080/15583724.2010.515765,50(4),454-473
93. He Y, Li Y (2011) Fullerene derivative acceptors for high performance polymer solar cells. Phys Chem Chem Phys 13(6):1970–1983
94. Dürkop T, Getty SA, Cobas E, Fuhrer MS (2004) Extraordinary Mobility in Semiconducting Carbon Nanotubes. Nano Lett 4(1):35–39
95. Brabec, C.J., Dyakonov, V., Parisi, J., and Sariciftci, N.S. (eds.) (2003) Organic Photovoltaics. **60**.
96. Tsuchiya T, Terabe K, Aono M (2014) In Situ and Non-Volatile Bandgap Tuning of Multilayer Graphene Oxide in an All-Solid-State Electric Double-Layer Transistor. Adv Mater 26(7):1087–1091
97. Coleman J, Curran S, Dalton A, Davey A, McCarthy B, Blau W, Barklie R (1998) Percolation-dominated conductivity in a conjugated-polymer-carbon-nanotube composite. Phys Rev B 58(12):R7492
98. Kuila BK, Park K, Dai L (2010) Soluble P3HT-grafted carbon nanotubes: Synthesis and photovoltaic application. Macromolecules 43(16):6699–6705
99. Liu Q, Liu Z, Zhang X, Yang L, Zhang N, Pan G, Yin S, Chen Y, Wei J (2009) Polymer Photovoltaic Cells Based on Solution-Processable Graphene and P3HT. Adv Funct Mater 19(6):894–904
100. Liu Z, Liu Q, Huang Y, Ma Y, Yin S, Zhang X, Sun W, Chen Y (2008) Organic photovoltaic devices based on a novel acceptor material: Graphene. Adv Mater 20(20):3924–3930
101. Yu D, Yang Y, Durstock M, Baek JB, Dai L (2010) Soluble P3HT-grafted graphene for efficient bilayer-heterojunction photovoltaic devices. ACS Nano 4(10):5633–5640
102. Yu D, Park K, Durstock M, Dai L (2011) Fullerene-grafted graphene for efficient bulk heterojunction polymer photovoltaic devices. J Phys Chem Lett 2(10):1113–1118
103. Bakr OM, Amendola V, Aikens CM, Wenseleers W, Li R, Dal Negro L, Schatz GC, Stellacci F (2009) Silver Nanoparticles with Broad Multiband Linear Optical Absorption. Angew. Chemie 121(32):6035–6040
104. Yang X, Yanagida M, Han L (2013) Reliable evaluation of dye-sensitized solar cells. Energy Environ Sci 6(1):54–66
105. Low FW, Lai CW (2018) Recent developments of graphene-TiO2 composite nanomaterials as efficient photoelectrodes in dye-sensitized solar cells: A review. Renew Sustain Energy Rev 82:103–125
106. Ting CC, Chao WS (2010) Efficiency improvement of the DSSCs by building the carbon black as bridge in photoelectrode. Appl Energy 87(8):2500–2505
107. Kang SH, Kim JY, Kim YK, Sung YE (2007) Effects of the incorporation of carbon powder into nanostructured TiO2 film for dye-sensitized solar cell. J Photochem Photobiol A Chem 186(2–3):234–241

108. Liu Y, Zhang J, Cheng Y, Jiang SP (2018) Effect of Carbon Nanotubes on Direct Electron Transfer and Electrocatalytic Activity of Immobilized Glucose Oxidase. ACS Omega 3(1):667–676
109. Guan G, Yang Z, Qiu L, Sun X, Zhang Z, Ren J, Peng H (2013) Oriented PEDOT:PSS on aligned carbon nanotubes for efficient dye-sensitized solar cells. J. Mater. Chem. A 1(42):13268
110. Sun S, Gao L, Liu Y (2011) Optimization of the cutting process of multi-wall carbon nanotubes for enhanced dye-sensitized solar cells. Thin Solid Films 519(7):2273–2279
111. Anusorn Kongkanand, Rebeca Martínez Domínguez, and, and Kamat*, P. V. (2007) Single Wall Carbon Nanotube Scaffolds for Photoelectrochemical Solar Cells. Capture and Transport of Photogenerated Electrons.
112. Du P, Song L, Xiong J, Li N, Wang L, Xi Z, Wang N, Gao L, Zhu H (2013) Dye-sensitized solar cells based on anatase TiO2/multi-walled carbon nanotubes composite nanofibers photoanode. Electrochim Acta 87:651–656
113. Patrick Brown, Kensuke Takechi, and, and Kamat*, P. V. (2008) Single-Walled Carbon Nanotube Scaffolds for Dye-Sensitized Solar Cells.
114. Guai GH, Li Y, Ng CM, Li CM, Chan-Park MB (2012) TiO2 Composing with Pristine, Metallic or Semiconducting Single-Walled Carbon Nanotubes: Which Gives the Best Performance for a Dye-Sensitized Solar Cell. ChemPhysChem 13(10):2566–2572
115. Dang X, Yi H, Ham MH, Qi J, Yun DS, Ladewski R, Strano MS, Hammond PT, Belcher AM (2011) Virus-templated self-assembled single-walled carbon nanotubes for highly efficient electron collection in photovoltaic devices. Nat Nanotechnol 6(6):377–384
116. Yang N, Zhai J, Wang D, Chen Y, Jiang L (2010) Two-Dimensional Graphene Bridges Enhanced Photoinduced Charge Transport in Dye-Sensitized Solar Cells. ACS Nano 4(2):887–894
117. Tang Y-B, Lee C-S, Xu J, Liu Z-T, Chen Z-H, He Z, Cao Y-L, Yuan G, Song H, Chen L, Luo L, Cheng H-M, Zhang W-J, Bello I, Lee S-T (2010) Incorporation of Graphenes in Nanostructured TiO_2 Films *via* Molecular Grafting for Dye-Sensitized Solar Cell Application. ACS Nano 4(6):3482–3488
118. Thomas S, Deepak TG, Anjusree GS, Arun TA, Nair SV, Nair AS (2014) A review on counter electrode materials in dye-sensitized solar cells. J. Mater. Chem. A 2(13):4474–4490
119. Dembele KT, Selopal GS, Milan R, Trudeau C, Benetti D, Soudi A, Natile MM, Sberveglieri G, Cloutier S, Concina I, Rosei F, Vomiero A (2015) Graphene below the percolation threshold in TiO_2 for dye-sensitized solar cells. J. Mater. Chem. A 3(6):2580–2588
120. Murakami TN, Grätzel M (2008) Counter electrodes for DSC: Application of functional materials as catalysts. Inorganica Chim. Acta 361(3):572–580
121. Larcher, D., and Tarascon, J.M. (2014) Towards greener and more sustainable batteries for electrical energy storage. *Nat. Chem. 2014 71*, **7** (1), 19–29.
122. Abioye AM, Ani FN (2015) Recent development in the production of activated carbon electrodes from agricultural waste biomass for supercapacitors: A review. Renew Sustain Energy Rev 52:1282–1293
123. Kastening, B., and Spinzig, S. (1986) Electrochemical polarization of activated carbon and graphite powder suspensions: Part II. Exchange of ions between electrolyte and pores. *J. Electroanal. Chem. Interfacial Electrochem.*, **214** (1–2), 295–302.
124. Chmiola, J., Yushin, G., Gogotsi, Y., Portet, C., Simon, P., and Taberna, P.L. (2006) Anomalous increase in carbon at pore sizes less than 1 nanometer. *Science (80-.).*, **313** (5794), 1760–1763.
125. Rufford TE, Hulicova-Jurcakova D, Zhu Z, Lu GQ (2009) Empirical analysis of the contributions of mesopores and micropores to the double-layer capacitance of carbons. J Phys Chem C 113(44):19335–19343
126. Niu C, Sichel EK, Hoch R, Moy D, Tennent H (1998) High power electrochemical capacitors based on carbon nanotube electrodes. Appl Phys Lett 70(11):1480
127. Zilli D, Bonelli PR, Cukierman AL (2006) Effect of alignment on adsorption characteristics of self-oriented multi-walled carbonnanotube arrays. Nanotechnology 17(20):5136

128. An KH, Kim WS, Park YS, Moon J-M, Bae DJ, Lim SC, Lee YS, Y.H.L. (2001) Electrochemical Properties of High-Power Supercapacitors Using Single-Walled Carbon Nanotube Electrodes. Adv Funct Mater 11(5):387–392
129. Liu CG, Liu M, Li F, Cheng HM (2008) Frequency response characteristic of single-walled carbon nanotubes as supercapacitor electrode material. Appl Phys Lett 92(14):143108
130. Xia, J., Chen, F., Li, J., and Tao, N. (2009) Measurement of the quantum capacitance of graphene. *Nat. Nanotechnol. 2009 48*, **4** (8), 505–509.
131. Stoller MD, Park S, Yanwu Z, An J, Ruoff RS (2008) Graphene-Based ultracapacitors. Nano Lett 8(10):3498–3502
132. Zhu Y, Murali S, Stoller MD, Velamakanni A, Piner RD, Ruoff RS (2010) Microwave assisted exfoliation and reduction of graphite oxide for ultracapacitors. Carbon N. Y. 48(7):2118–2122
133. Dunn B, Kamath H, Tarascon JM (2011) Electrical energy storage for the grid: a battery of choices. Science 334(6058):928–935
134. Dai L, Chang DW, Baek JB, Lu W (2012) Carbon nanomaterials for advanced energy conversion and storage. Small 8(8):1130–1166
135. Frackowiak E, Béguin F (2002) Electrochemical storage of energy in carbon nanotubes and nanostructured carbons. Carbon N. Y. 40(10):1775–1787
136. Poizot, P., Laruelle, S., Grugeon, S., Dupont, L., and Tarascon, J.M. (2000) Nano-sized transition-metal oxides as negative-electrode materials for lithium-ion batteries. *Nat. 2000 4076803*, **407** (6803), 496–499.
137. Aurbach, D. (2002) The Role of Surface Films on Electrodes in Li-Ion Batteries. *Adv. Lithium-Ion Batter.*, 7–77.
138. Li, X., Wang, X., Zhang, L., Lee, S., and Dai, H. (2008) Chemically derived, ultrasmooth graphene nanoribbon semiconductors. *Science (80-.).*, **319** (5867), 1229–1232.
139. Liang M, Zhi L (2009) Graphene-based electrode materials for rechargeable lithium batteries. J Mater Chem 19(33):5871–5878

Recent Development in the Production and Utilization of Plant Biomass-Based Nanomaterials

Mohammed Aslam, Anjali Rani, Bhaskara Nand Pant, Prashant Singh, and Garima Pandey

Abstract The conventional procedures for the production of nanomaterials result in the generation of a significant amount of chemical waste. In recent years, there has been a lot of focus placed on the idea of using plant biomass as a viable alternative substrate in the production of bulk chemicals, liquid biofuels, and synthetic materials. This concept has garnered a lot of interest in recent times because, contrary to traditional physical and chemical techniques, bio-resource-based nanomaterial synthesis is cost-effective, environmentally safe, and appropriate for mass manufacturing. The synthesis of nanomaterials with an abundance of beneficial qualities from renewable biomass, including plants, marine organisms, biomass waste, etc., can be one of the major sources for the production, due to the presence of biomolecules, especially polyphenols, which act as a reducing agent and stabilizer. Also, the size of different nanomaterials has been discussed, which plays an important role in their properties. These nanomaterials are lethal to resistant bacteria and present a significant opportunity for the maximization of energy production and storage. It can be used for a broad variety of purposes, including the treatment of wastewater and various other means of cleaning the environment. This chapter provides an update on the plant biomass-based synthesis of various nano-ranged nanomaterials that can be characterized using appropriate techniques. Also, all the growing uses and applications of nanomaterials in different sectors, such as imaging, drug delivery, ion detection, energy storage, photodegradation, etc., are briefly discussed.

Keywords Nanomaterial · Plant biomass · Classification · Synthesis · Applications

M. Aslam · A. Rani · G. Pandey (✉)
Department of Chemistry, Delhi-NCR Campus, SRM-Institute of Science and Technology, Modinagar, Ghaziabad, UP, India 201204
e-mail: garimap@srmist.edu.in

B. N. Pant · P. Singh
Department of Chemistry, Atma Ram Sanatan Dharma College, University of Delhi, New Delhi 110021, India

S. K. Tiwari et al. (eds.), *Biomass-Based Functional Carbon Nanostructures for Supercapacitors*, Green Energy and Technology,
https://doi.org/10.1007/978-981-99-0996-4_12

Abbreviations

Ultraviolet-visible	UV-Vis
Transmission electron microscopy	TEM
Scanning electron microscopy	SEM
Fourier transform infrared	FTIR
Dynamic light scattering	DLS
Energy dispersive X-ray	EDX
Carbon quantum dots	CDQ
Carbon dots	CD
Nanometers	Nm
Nanomaterials	NMs
Nanoparticles	NPs
Laser ablation	LA
Chemical vapor deposition	CVD
X-ray diffraction	XRD
Temperature	Temp.

1 Introduction

Biomass contains a wealth of interesting biomaterials that might be used in a variety of ways. These include as a source for polymers and innovative composites, which could find endless applications, and as a precursor to the production of platform chemicals and biofuels. Biomass' adaptability stems from its various morphological, biocompatible, biodegradable, and chemical characteristics [1, 2]. It has become increasingly common to contemplate using biological approaches for the synthesis of NPs due to the fact that these techniques mitigate many of the negative side effects associated with mass-producing nanoparticles. The biological and green approach uses bacteria, yeasts, fungi, algae, and plants for the industrial synthesis of green NMs, with biomass acting as the reducing agent as well as the stabilizing agent [3–5].

Nanomaterials, materials ranging from 1 to 100 nm, can be categorized as natural, accidental, or engineered (ENMs). Because of their small sizes, they possess unique qualities. [6–8]. Computer chips, environment and energy, biomedicine, health, cosmetics, aerospace, and defense are among the many sectors that utilize them. Nanomaterials are also added to fundamental materials to improve their performance. Nanomaterials are typically composed of inorganic, organic, carbon, and composite components. Metallic oxides and other nanosized metals are examples of inorganic nanomaterials. Titanium dioxide (TiO_2), zinc oxide (ZnO), and iron oxide (Fe_3O_4) are common metal oxide-based nanomaterials, along with silica (SiO_2), copper oxide (CuO), and oxides of iron (such as Fe_2O_3). Organic nanomaterials are composed of carbon-containing organic compounds, excluding carbon-based substances like

cyclodextrin, micelles, dendrimers, and liposomes. Graphene, multi-walled carbon nanotubes, carbon fiber, fullerene, carbon black, single-walled carbon nanotubes, and activated carbon are carbon-based nanomaterials. Metal–metal oxide, organic or carbon, and metal–organic framework-based compounds are the three main types of composite nanomaterials [9–12]. Nanomaterials have been synthesized using various plant parts, such as petals, roots, stems, leaves, fruits, etc. [13–16]. Lemongrass, aloe vera, neem, tamarind, and geranium extracts, among others, have been extensively researched for their potential use in the synthesis of gold and silver NMs [17–19]. The introduction of NPs has revolutionized the healthcare industry, drug and gene transfer, and optical engineering. Enhanced optical detection capabilities, where incident light is connected with plasmon excitation of the metal, result in a millionfold more light scattering compared to any other molecule, making metal NPs the promising biological detection instruments [20]. Recent years have seen extensive research on the potential benefits of incorporating nanotechnology and nanomaterials into biofuel production. By modifying the properties of feed materials and biocatalysts, nanomaterials can be used in the development of a novel hybrid nanobiocatalytic system that brings together biotechnology and nanotechnology [21]. Nanomaterials' unique characteristics, including their small size, large surface area, abundance of surface-active functional groups, and unusual shape, present exciting prospects in a wide range of environmental contexts. These inherent properties of nanoparticles make them excellent candidates for removing harmful pollutants from wastewater [22] (Figs. 1 and 2).

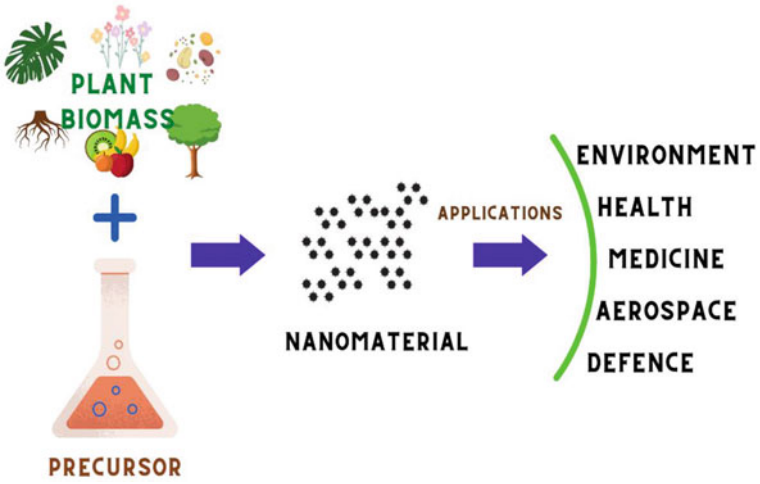

Fig. 1 Plant biomass-based nanomaterials synthesis and applications

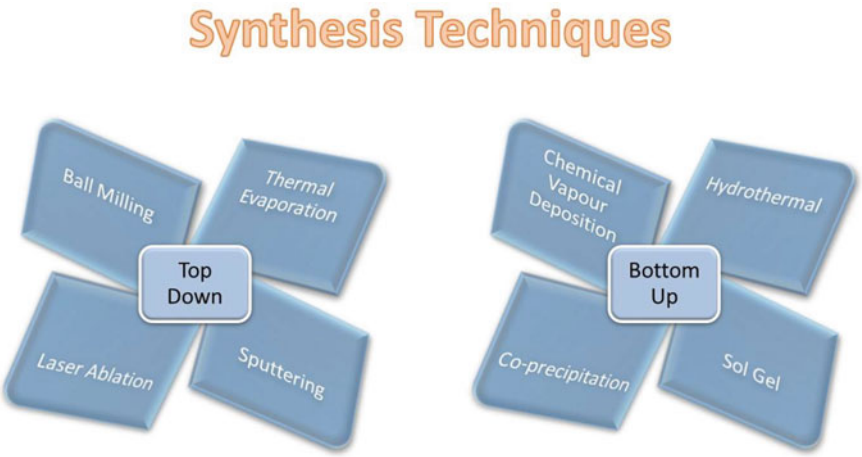

Fig. 2 Methods for synthesis of nanomaterials using different techniques

1.1 Classification of the Nanomaterials Based on Their Dimensions is As

(1) Zero-dimensional nanomaterials (0-D): This means that the NMs have all 3 of their dimensions inside the range of the nanoscale. This category will eventually include nanoparticles.
(2) One-dimensional nanomaterial (1-D): For this, if you choose any 1 dimension, it will be within the nanoscale range, while the other 2 dimensions will be outside the range of the nanoscale. This category is associated with nanotubes, nanowires, and nanorods, among other similar structures.
(3) Two-dimensional nanomaterials (2-D): Only two dimensions fall inside the range of nanoscales, whereas the third dimension remains outside of it. Nanolayers, nanocoatings, and nanofilms are all types that fall under this category.
(4) Three-dimensional or bulk nanomaterials (3-D): These nanoparticles don't fall within the range of the nanoscale in any of the dimensions. This indicates that in three dimensions, they are larger than 100 nm in scale. Nanocomposites, multi-nanolayer structures, bundles of nanowires, core shells, and bundles of nanotubes are some examples of these [23, 24].

1.2 Types of Nanomaterials

One of the many characteristics that can be used to categorize nanomaterials is the type of constituent materials that they are made up of. On the basis of the many different types of materials, we can broadly divide them into the following categories:

1. Metallic nanomaterials
2. Polymeric nanomaterials
3. Ceramic-based nanomaterials
4. Carbon-based nanomaterials.

Metal based nanomaterials

Nanomaterials based on metals have seen widespread use in a variety of different applications. They are able to be separated into a variety of categories, including metal NPs, metal oxide NPs, bimetallic NPs, trimetallic NPs, among others. Because of their smaller particle size, increased surface area, and increased reactivity, certain metal nanoparticles, such as gold and silver, exhibit exceptional optical, electric, and molecular capabilities when compared with the bulk materials. In general, the synthesis method will dictate the size of the metal NPs that are produced. Metal nanoparticles have interesting size- and shape-dependent characteristics, which results in a wide variety of interesting applications [25].

Polymeric nanomaterials

Polymeric nanostructures with particle sizes ranging from 1 to 1000 nm at minimum in one dimension have garnered a significant amount of interest in a variety of scientific applications. This is primarily due to the considerable rise in the ratio of surface area to volume that these materials exhibit. In comparison to bulk polymers, they have a number of advantageous characteristics. They exhibit outstanding characteristics in the optical and electrical domains [26].

Ceramic-based nanomaterials

Phosphates, carbides, oxides, etc., of metals or metalloids are the primary building blocks of ceramic nanomaterials. Ceramic nanoparticles based on silica and alumina are the ones that are used most frequently. They are protected from degranulation and degradation, thanks to their porous structure at the nanoscale. There are three subtypes of nanoceramics: nanostructured scaffolds, nanoclay, and nanomaterials [27].

Carbon-based nanomaterials

Because of the superior properties they possess, nanoparticles based on carbon have found widespread use in a vast array of applications. Carbon quantum dots (CQDs), graphene, and a few other materials, such as carbon nanotubes (CNTs), are among the best-known examples of this kind of material. CQDs are zero-dimensional carbon nanoparticles with a size smaller than 10 nm and internal dimensions in the region of nanometers, although their lengths are in the region of micrometers. CNTs have lengths in the range of micrometers [28–30]. Nanomaterials, due to their small size and unique properties, play an important role in moving towards a greener future, and their diverse applications in medicine, environment, cell imaging, drug inhibition, photocatalytic degradation, defense, health, and other fields pique the interest of researchers. This not only paves the way for the conversion of biomass waste into

useful reducing and capping agents for nanomaterials and other analogues, but it also offers a concept for multistep processing of waste materials that could result in many new and useful materials for various purposes. Furthermore, by effectively turning biomass waste into valuable products, this will serve as an example for promoting a sustainable economy and providing actual solutions to problems.

2 Routes for Synthesis of Nanomaterials

Being in demand, new and different routes for the synthesis of nanomaterials have been developed that can be chemical-free and suitable for different applications. In this respect, aspects such as reducing agent, solvent, and capping agent should be examined from a green chemistry viewpoint, including the usage of nontoxic capping agents, less hazardous reducing agents, and environmentally safe solvents. Another element gaining great attention is the creation of green synthetic procedures that solve the heating efficiency difficulties faced by conventional methods [30]. Generally, nanomaterials can be synthesized using both top-down and bottom-up approaches to obtain different spatial arrangements, sizes, and shapes.

2.1 Top-Down Approach

Large pieces of material can be divided into smaller, nano-sized fragments with this technique. Top-down techniques are easier to use, but they are ineffective when trying to create particles with complex forms or sizes. The main disadvantage of this approach is the challenges involved in obtaining the correct particle size and morphology (Fig. 3).

2.1.1 Ball Milling Process

Ball milling, which generates NPs through the attrition process, is the mechanical method of a top-down approach that is both the simplest and most effective. The process of "grinding," which consists of the transfer of kinetic energy from the grinding media to the substance being reduced, is applied to the material being reduced. The use of this method results in the production of a variety of NPs and alloys of metals. A regular amount of powder is added to the milling vial, where it is processed by friction and the movement of the balls inside the vial. At high temperatures, the temperature and pressure produced by the contact between the balls and the vessel wall, as well as the contact between the balls and the wall, can cause a violent change of phase. To reduce the size of the particles, it is used in a variety of materials. The reduction of particles, surface modification, crystallite size, potential generation of metastable phases, and mechanical dislocation are all

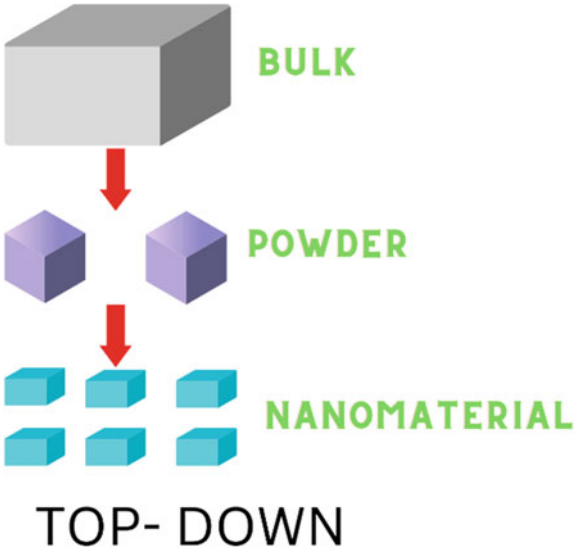

Fig. 3 Schematic diagram for top-down approach for the synthesis on nanomaterial

significantly impacted by this process for powdered samples. A large variety of reactions that don't happen naturally at the temperature of the environment can be manufactured [31–33].

2.1.2 Thermal Evaporation

During this endothermic reaction, the heat generated causes degradation. The heat produced destroys the chemical bond of a substance [34]. Among the numerous approaches for the synthesis of inorganic nanoparticles, this method is regarded as one of the most frequent for the development of stable, highly dispersed suspensions with the capacity for self-assembly. Various substances are coated with thin films, utilizing thermal evaporation [35]. There are a number of elements that can have an effect on the thermal evaporation process. Experimental conditions for the creation of nanocrystals include the heating in the furnace, the length of time that evaporation lasts, and the distance from the source to the substrate [36]. Thermal evaporation does not require a solvent, is suitable for low melting-point materials, and is simple to monitor. It is possible to deposit materials on surfaces in an even and homogeneous manner, which is of critical importance when working with ultrathin layers [37, 38].

2.1.3 Laser Ablation

Laser ablation (LA), which essentially uses a laser to eliminate molecules from the surface of a substrate in order to form micro- or nanostructures, has a broad range of applications in ceramics, polymers, metals, and glasses. By focusing a laser

source from above, it is a method for extracting chemicals from a substrate. Ablation occurs when the substance consumes sufficient energy to melt or vaporize. LA is a continuous process in laser machining such as drilling, high-precision, and laser beam milling [39]. Nd:YAG lasers, which produce light at a wavelength of 1064 nm, are the most common source of near-infrared laser radiation. The wavelength range of diode lasers, which emit light, is 800–970 nm [40]. A popular method includes directing the beam of a laser at a metal target that is partially submerged in liquid. This results in the formation of vapor, drops of molten material, or plasma, which combines with the liquid media to produce certain entities and ultimately nanomaterials [41].

2.1.4 Sputtering

Vacuum sputtering is an established top-down technique for fabricating thin films by blasting a substrate with powerful gas ions derived from Ar, O_2, N_2, or H_2, among others. The bombardment ejects atoms or clusters from the substance, which can subsequently be deposited on a substrate introduced into the vacuum sputtering chamber. To obtain NPs as opposed to large aggregates or thin films, extremely brief sputtering times, on the scale of a few to several tens of seconds, have been obtained through post-heat treatment or low pressure clusters from the substance, which can subsequently be deposited on a substrate introduced into the vacuum sputtering chamber. To obtain NPs as opposed to large aggregates or thin films, extremely brief sputtering times, on the scale of a few to several tens of seconds, have been obtained through post-heat treatment or low pressure. By alternately sputtering two or more targets, NPs can be placed between two solid layers to restrict their growth and distribute a greater quantity of nanoparticles in solid media [42]. Sputtering is a technique for depositing NMs on the surface of a substrate by emitting particles with high-energy charged particle strikes. This is done during the process of sputtering. The sputtering method can be utilized for a variety of applications, including thin-layer deposition, surface etching, and surface coating [42].

Sputtering with an ion beam is an alternative way to the ones that have been discussed previously. Ions are directly sputtered onto a target by an ion beam emanating from the source of the ions, and the plasma from which the ions are extracted is contained within the discharge vessel of the ion source. This indicates that the working gas and substrate do not come into contact with one another [43].

2.2 Bottom-Up Approach

The technique that begins from the bottom-up is also referred to as the "constructive approach." The bottom-up strategy is diametrically opposed to the top-down strategy. The formation and self-assembly of molecules and atoms as their basis produces nanomaterials with characteristic size, shape, and chemical composition (Fig. 4) [44]. This method is used to synthesize the majority of plant biomass-based nanomaterials.

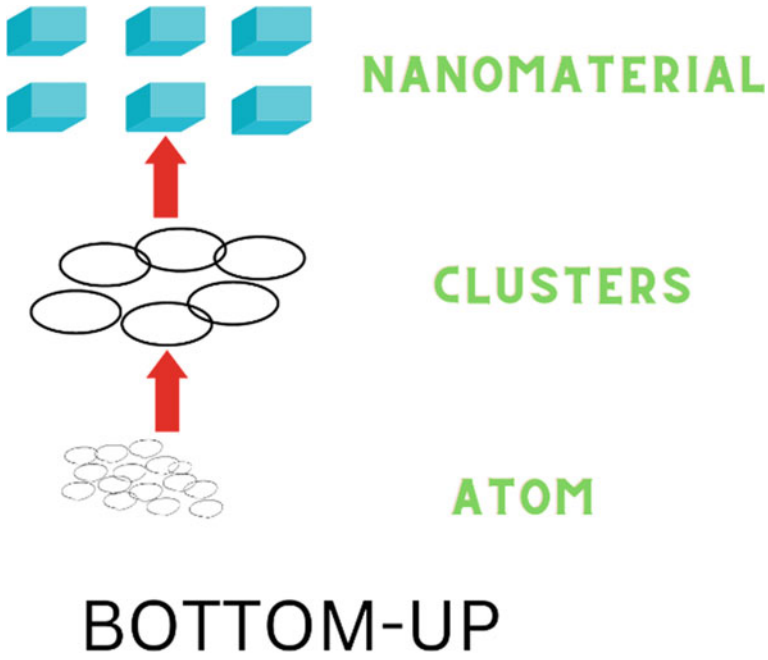

Fig. 4 Schematic diagram for the bottom-up approach for the synthesis of nanomaterial

2.2.1 Chemical Vapor Deposition (CVD)

CVD is a versatile and effective technique for producing nanoparticles. CVD was a significant technology in the microelectronics industry for years, and it continues to be one of the most compelling techniques capable of resolving the issues posed by contemporary technologies [45]. This method produces NMs using relatively simple components. Using this method, a substrate is covered with a thin layer of gaseous molecules. A chemical reaction happens when gas is brought into contact with a heated substrate in a reactor vessel. The result is the formation of a thin layer on the substrate's surface [46]. Changing the CVD process parameters can result in different amounts of NMs being produced. Processes are carried out at moderate pressure; similarly, operations can be carried out at low pressure (1 Torr) or at an extremely high vacuum (100 Torr). A uniform coating influences the quality of the materials as well as the deposition, all of which are controlled by the pressure. The type of precursors, catalysts, and temperature, as well as the state of the gas flow, the substrate, and the physical properties of the vapor, are all important. The vast majority of conventional CVD techniques are performed at extremely high temperatures, frequently around 1000 °C; however, when the material cannot withstand high temperatures, moderate temperatures (around 300 °C) are used (Fig. 5) [47].

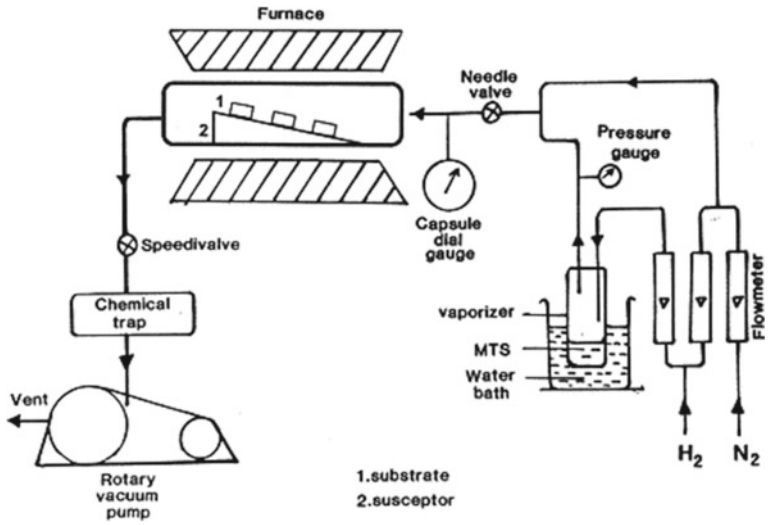

Fig. 5 A schematic diagram of a laboratory CVD equipment [48]. Reprinted under terms of the Creative Commons license from ref (Choy et al. 2021). Copyright 2021 Springer Nature

2.2.2 Hydrothermal

Heterogeneous reactions in aqueous media at 100 °C and 1 bar of pressure are the hallmark of hydrothermal synthesis. It's still a go-to technique for making ultrafine oxide powders [48]. In this process, cations precipitate as polymeric hydroxides, which then undergo dehydration and speed up the development of the metal oxide crystal structure. When a base is introduced to a metal salt solution, a second metal cation forms that is useful for regulating the particle formation process by inhibiting the production of complex hydroxide [49]. The hydrothermal method has contributed significantly to the contemporary domains of science and technology due to its pure end product, homogeneous precipitation, relative affordability, and environmentally friendly conditions. In addition, this technique can be subdivided into hydrothermal synthesis, crystal development, and treatment, as well as the preparation of functional ceramic powder and the treatment of organic waste [49, 50].

2.2.3 Co-precipitation

Co-precipitation is the combination of more than two salts of water-soluble metal ions, typically divalent and trivalent. In such compounds, the bulk of the dissolved salts are composed of trivalent metal ions. These hydrophilic salts act as reducing agents to produce at least one water-insoluble salt that precipitates. Continuous agitation of the solution is required, which may or may not coincide with the proper temperature based on the reaction circumstances and reducing agent [23]. Co-precipitation

Fig. 6 Schematic process of Co-precipitation method

is the technique of establishing a consistent distribution of two or more ionic species via a precipitation reaction in a homogenous solution (Fig. 6). Through a series of chemical processes in solution, this method produces homogeneous nanomaterials with small diameters and narrow size distributions. For pH maintenance, the solution is blended directly or drop-by-drop with the other solution that contains soluble precipitation reagents. In this method, chlorides, hydroxides, carbonates, hydroxides, and oxalates are the most commonly used precipitants. The aged precipitates are next filtered or centrifuged to remove the larger particles. To eliminate impurities and obtain NPs of purity, additional washing with deionized water, ethanol, or other solvents is necessary. Post-treatment like sintering, calcination, and annealing is employed to generate NMs with the required crystalline structure and morphology [51].

2.2.4 Sol–Gel

It is the process wherein suitable chemical solutions serve as precursors. In the sol–gel technique, metal oxide and chloride are frequent precursors. The precursor is distributed in the host liquid by several processes, such as sonication. Various processes, such as filtering, sedimentation, and centrifugation, are used to separate the solid phase from the liquid in order to extract the nanoparticles from the resulting solution. Condensation and hydrolysis reactions are involved in the process of transforming sol into gel [34]. This approach is able to produce two or more distinct types of nanoparticles at the same time, which means that alloy products can be produced in a single step by combining two or even more metal (or metal oxide) precursors in a specific ratio. The transition from the liquid to the solid state, known as the sol–gel process, can be accomplished through a number of different methods, the vast majority of which entail a slow drying process to get rid of the solvent. In this process, providing the appropriate circumstances to prevent the creation of splits is one of the most significant concerns to address. This is because the drying of the gel is associated with its shrinkage (Fig. 7) [52].

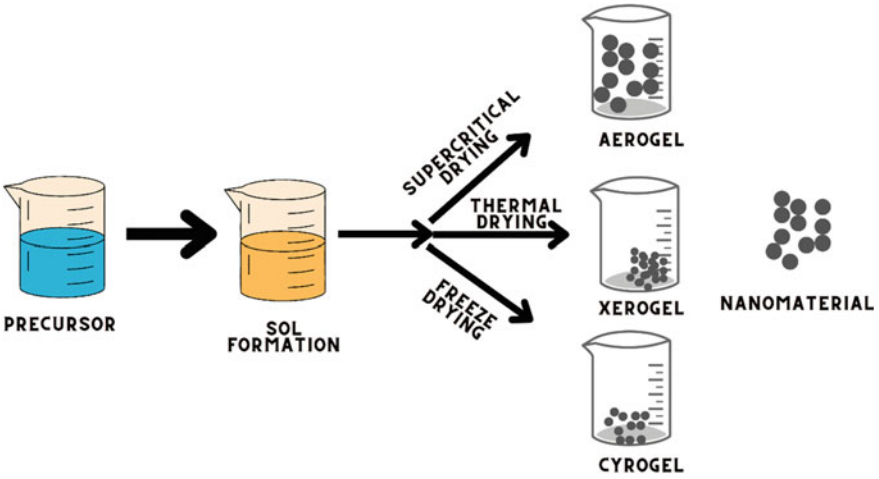

Fig. 7 Schematic of sol gel including different stages

For instance, the techniques utilized in the synthesis include ultrasonic treatment, solid-state microwave radiation, and thermal breakdown, which require a great deal of energy, space, and costly equipment [53]. To minimize all the effects, a natural source of synthesis can be highly effective. Fungi, bacteria, sawdust, animal-based gelatin, and many more Out of all this, we have chosen to discuss plant biomass-based synthesis, which can be done from various parts of the plant.

3 How Plant Driven Synthesis of Nanomaterials is Beneficial

Variable-sized and shaped NMs are generated from many plant parts, including the root, stem, leaves, flowers, latex, and seeds. The study shows that plant elements are favored due to their exceptional ability to decrease metal ions. In addition, plants are readily available and safe to handle. Alkaloids, diterpenoids, salicylic acids, steroids, tannins, polysaccharides, glycosides, flavonoids, phenolic acids, vitamins, enzymes, minerals, lectones, saponins, amino acids, and sterols are bioactive substances derived from plants that serve as reducing and stabilizing agents [54]. The use of green synthesis over chemical processes is due to its significant benefits, including cost-effectiveness, lower toxicity, environmental friendliness, and improved application.

4 Synthesis of Nanomaterials Using Plant Biomass

Nanomaterials can be synthesized from various techniques which involve both chemical and biologicals processes but one of the primary reason for choosing plant biomass is that they are environment friendly and cost effective. Some of the synthesizing methods are included in Table 1.

4.1 Titanium Dioxide (TiO_2)

Srinivasan et al. [13] added 25 mL of Sesbania grandiflora plant extract, which they mixed with 225 mL of a 5 mM TiO_2 solution and incubated for 1 day at room temperature under stable conditions. The development of a greenish color suggested the formation of TiO2 NPs. Rajendhiran et al. used Carissa carandas fruit extract for producing TiO_2. 100 mL of ethanol was added to 6 mL of titanium isopropoxide with continuous stirring for 2 h. To this solution, plant extract was added in different ratios, stirred for 80 min, filtered, and dried. The nanomaterial formed is characterized by SEM, as shown in Fig. 5 [55]. TiO_2 was produced by extracting the leaves of the Acoruscalamus (A. calamus) plant and using them as a capping and reducing agent. This created a new biogenic source. It was discovered that the nanoparticles had a globular shape and ranged in size from 15 to 40 nm on average. Strong photocatalytic activity was demonstrated by the biosynthesized TiO_2 nanoparticles, which resulted in the degradation of 96.59% of the RhB dye [82]. Titanium dioxide nanoparticles (TiO_2 NPs) were produced by a green manufacturing process that was kind on the environment and made use of the root extract of the Withania somnifera plant. To evaluate the antimicrobial properties of the TiO_2 NPs against Pseudomonas aeruginosa, Serratia marcescens, Staphylococcus aureus, Escherichia coli, Candida albicans, and Listeria monocytogenes, the minimum inhibitory concentration (MIC) was calculated.

4.2 Metal Nanoparticles (MNPs)

The synthesis of silver nanoparticles (AgNPs) using an aqueous root extract of the Salvadora persica plant as a reducing agent is environmentally friendly. Salvadora persica nanoparticles with an average size of 37.5 nm demonstrated remarkable antibacterial activity [14]. Moringa and neem plant extracts were used in the production of silver nanoparticles by Solaiman and colleagues. The researchers determined the size of the particles to be 3.82–16 and 8.34–13.7 nm, respectively, and discovered that the particles had a spherical shape [83]. Another study created silver nanoparticles from an extract of Wedelia chinensis leaves and tested them for their potential as cytotoxic, antioxidant, and antibacterial agents. Yu et al. discussed eco-friendly silver nanoparticles (AgNPs) made from Eriobotrya japonica (Thunb.) plant leaves

Table 1 Synthesis and characterization of plant biomass-based nanomaterials

S. No.	Nanomaterial	Plant family name (common name)	Part of plant	Characterization	Size (nm)	References
1	TiO_2	Sesbania grandiflora (Vegetable hummingbird, West Indian pea, Agati)	Leaves	UV, XRD, FT-IR, SEM, TEM	43–56	[13]
2	TiO_2	Carissa Carandas (Karaunda)	Fruit	UV, XRD, FT-IR, SEM, EDX	10–21	[55]
3	TiO_2	Cuminumcyminum (Jeera)	Seed	UV, XRD, FT-IR, SEM, TEM, EDX	15.17	[56]
4	TiO_2	Kniphofiafoliosa	Root	TGA-DTA, XRD, HRTEM, FTIR	8.2–10.2	[57]
5	$ZnFe_2O_4$	MoringaOleifera	Leaves	HRTEM, XRD, EDS	5–10	[58]
6	Ag	Salvadorapersica	Root	UV–Vis, FTIR, DLS, TEM, P-XRD	37.5	[14]
7	Ag	Alpinianigra	Fruit	UV–Vis, XRD, XPS, EDX, TEM, FTIR, SEM	6	[59]
8	Ag	Cannabis sativa	Stem Fiber	TEM, SAED, DLS, UV–Vis, FTIR	20–40	[15]
9	Ag	Phaseolus vulgaris	Seed	UV, Vis, HR-TEM, FTIR, SAED	10–20	[60]
10	Multi walled carbon nanotubes (MWCNTs)	C. dactylon, Rosa, A. indica, Thevetiaperuviana, andJ. regia	Leaves	FESEM, EDS, HRTEM, FTIR	8–15	[61]
11	Pt	Antigononleptopus	Leaves, stem, root	UV–Vis, SEM, TEM, XRD, FTIR, EDX	5–190	[62]
12	Au	Gnidiaglauca	Flower	UV–Vis, TEM, HRTEM, DLS, XRD	10	[63]

(continued)

Table 1 (continued)

S. No.	Nanomaterial	Plant family name (common name)	Part of plant	Characterization	Size (nm)	References
13	Au	Moringaoleifera	Petals	UV–Vis, TEM, DLS, SEM, FTIR	3–5	[16]
14	Au	Garcinia mangostana	Fruits peel	FESEM, XRD, TEM, FESEM, FTIR and UV–Vis	32.96 ± 5.25	[64]
15	Au	Elettaria cardamomum	Seed	FTIR, TEM, XRD,	15.2	[65]
16	Au	Capsicum annuum var. grossum	Pulp	UV–Vis, XRD, TEM, EDS, FTIR	20	[66]
17	Carbon quantum dots	Bamboo	Leaves	UV–Vis, TEM, FTIR, Zeta potential	2–6	[67]
18	Fe_2O_3	(Punicagranatum) pomegranate	Seed	UV–Vis, SEM, EDX, XRD	25–55	[68]
19	Fe	Green tea	Leaves	TEM, SEM, EDS, XRD, FTIR	20–50	[69]
20	Fe	Citrus maxima	Peel	TEM, EDS, XPS, FTIR, DLS	10–100	[70]
21	ZnO	Allium sativum (garlic), Allium cepa (onion) and Petroselinum crispum (parsley)	Garlic bulb, Parsley leaves	XRD, FTIR, UV–Vis, TEM, EPR	14–70	[71]
22	ZnO	Heritierafomes	Bark and leaves	UV–Vis, FTIR, DLS, XRD	40–50	[72]
23	Carbon dots (C-dots)	Lotus	Root	TEM, FTIR, XPS, UV–Vis	9.41	[73]
24	C-dots	Saffron		UV–Vis, FTIR, DLS, TEM, zeta potential	6	[74]
25	C-dots	Lemon	Peel	UV–Vis, FTIR, XPS, FESEM	1–3	[75]
26	$ZnFe_2O_4$	Limoniaacidissima	Juice	XRD, FTIR, SEM with EDAX, TEM, UV-DRS, luminescence	20	[76]

(continued)

Table 1 (continued)

S. No.	Nanomaterial	Plant family name (common name)	Part of plant	Characterization	Size (nm)	References
27	MnO_2	Gardenia resinifera	Leaves	SEM-EDAX, PSA, UV–Vis, XRD, SEM-EDAX, HR-TEM	17–35	[77]
28	SnO_2	Lycopersiconesculentum	Peel	XRD, FTIR, HRTEM, SAED	4–5	[78]
29	CeO_2	DaturametelL	Leaves	UV–Vis, FTIR, SEM, EDX, TEM, XRD	5–15	[79]
30	Sm_2O_3	Andrographispaniculata	Leaves	PXRD, DLS, SEM, HRTEM	30–50	[80]
31	$AgCoPO_4$	Canna indicia	Leaves	XRD, TEM, SAED, EDS	31.94 ± 8.99	[81]

and their application in the catalytic degradation of dyes [84]. Bhagat et al. developed an effective, quicker, and more environmentally friendly process for the biosynthesis of Au-NPs using the leaf extract of Citrus limonum. The protocol was helped by an ultrasonicator. These Au-NPs have the potential for use in the qualitative and quantitative examination of the organophosphate pesticide dichlorvos with great success. It was discovered that this procedure was helpful in determining whether or not an organophosphate pesticide was present in two extracted samples, such as soil and fabric [85]. The Anbara fruit, also known as Phoenix dactylifera L., is used in the synthesis of platinum nanoparticles (PtNPs), which are then characterized by the application of a variety of spectroscopic analytical techniques. These PtNPs were put through their paces in an experiment to investigate the hepatotoxic and hepatoprotective effects of CCl4's acute liver injury in Wister rats [86]. Under the influence of daylight, a method for the synthesis of Cu nanoparticles (CuNPs) utilizing the extract from Jatropha curcas (JC) leaves has been recorded for possible photocatalytic activity towards methylene blue (MB), in comparison with other dyes [87].

4.3 Other Nanomaterials

Another group of researchers manufactured multiwalled carbon nanotubes using a catalyst generated from plants. They employed the CVD process for the synthesis to obtain nanomaterials of 8–15 nm [61]. The carbon sources for the hydrothermal synthesis of carbon quantum dots were fresh bamboo leaves. These leaves were washed with distilled water and then air-dried. For cold crushing, a predetermined amount (2.0 g) of dry bamboo leaves are cooled and grinded with liquid nitrogen. The fine powder resulting from the grinding process is dispersed in 25 mL of distilled water. The combined mixture is then transferred to a Teflon-lined 50 mL autoclave and boiled at 200 °C for 6 h. It was centrifuged and filtered to yield 2–6 nm-sized material [67].

Stan et al. [71] synthesized ZnO nanomaterials from aqueous Allium cepa (onion), Petroselinum crispum (parsley), and Allium sativum (garlic). They used 20 mL of plant extract and added 2 g of zinc nitrate, which was stirred for 20 min, and the mixture obtained after 12 h at 95 °C was then heated in an air furnace at 400 °C for 2 h. The dried mass was characterized, and the size was found to be between 14 and 70 nm. Matinise et al. [58] used 50 ml of Moringa oleifera leaf extract and one hour of magnetic stirring to dissolve 5 g of $Fe(NO_3)3.9\ H_2O$ and $Zn(NO_3)2.6\ H_2O$. The combination was kept covered for 18 h. It was then rinsed multiple times with deionized water and heated at 500 and 700 °C for two hours. HRTEM and SAED characterization, as shown in Fig. 8, confirm the formation of nanomaterials. An environmentally friendly method was used to synthesize the nanomaterial $ZnFe_2O_4$ using an extract of the plant Limoniacidissima. After characterization, the size was found to be around 20 nm [76].

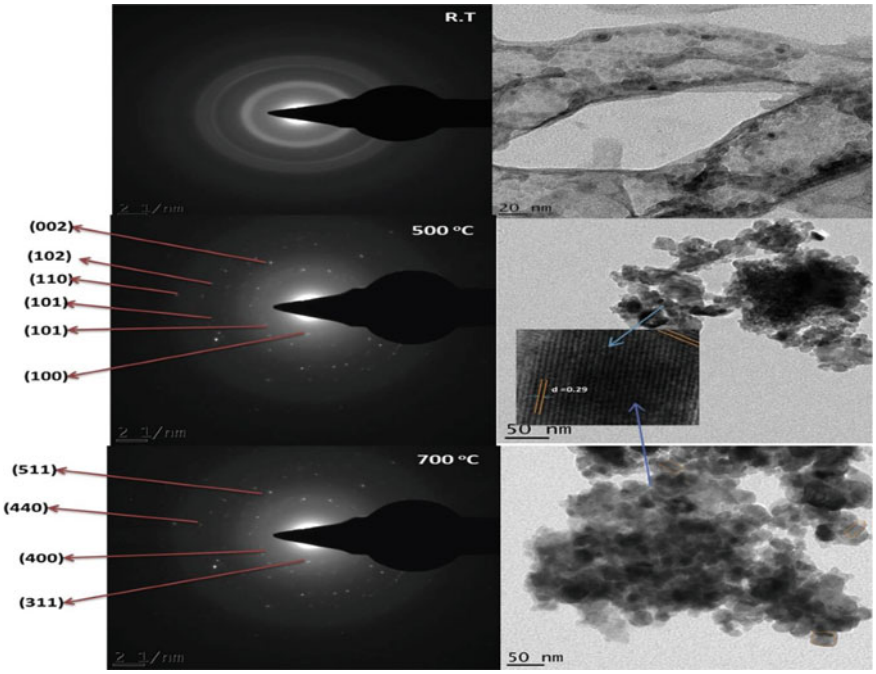

Fig. 8 HRTEM and SAED images of $ZnFe_2O_4$ nanocomposites (R.T, 500 and 700 °C) [70]. Reprinted under terms of the Creative Commons license from ref (Matinise et al.). Copyright 2021 Springer Nature

These nanomaterials have characteristic properties, and their sizes vary according to the conditions and plant biomass used. Nanomaterials synthesized from different plant biomass have been discussed in Table 1.

All these nanomaterials are of great potential in various walks of life from daily activities to industries. Having a good size to volume ratio helps these nanomaterials to have unique characteristics.

5 Applications

Nanomaterials, due to their easy synthesis from plant-based biomass, are extensively used in different fields and walks of life for everything from the enhancement of materials to defense to manufacturing new materials to drug delivery. NMs have the potential to be utilized in industries and are now used in a variety of applications [88–90]. Following are some of the daily use applications explained in the area of research and development (Fig. 9).

Fig. 9 Applications of plant biomass-based nanomaterials

5.1 Biomedical Applications

The advent of novel microbiological species, including the SARS-CoV2 virus that caused the current COVID-19 epidemic and multidrug-resistant pathogenic microorganisms, has resulted in an increase in healthcare concerns for humanity [91, 92]. Numerous pharmacotherapeutic uses of NMs have been investigated, as well as their antibacterial, antioxidant, and anti-inflammatory capabilities, and as a result, potent new therapeutic choices are now readily available. The metals gold, palladium, selenium, and silver have all shown anti-disease activity in nanostructures [93]. It was discovered that platinum nanomaterial produced with Saccharomyces boulardii possessed anticancer effects against A-431 and MCF-7 cell lines [94]. Ortega et al. found that silver nanoparticles generated by Cryptococcus laurentii had the same impact as chemotherapy on breast cancer cell lines [95]. The investigation of NPs in leukocytes to find out what role they play in gut inflammation has revealed that they stop a molecule called Cyclin D1 from working. Cyclin D1 controls the cell cycle. Kumar et al. [96] investigated that, through the metabolic pathway, the nanomaterials might come into contact with the cell walls and membranes of bacteria. The nanoparticles then stick to the basic parts of bacterial cells, like enzymes, DNA, and ribosomes. They are much more likely to prevent enzymes and proteins from doing their important tasks [97].

5.1.1 Antimicrobial Applications

Nanomaterials (NMs) have been extensively studied for their potential to be antimicrobial, and it is possible that this potential is due to the production of reactive oxygen species (ROS), which can damage cell proteins and disrupt nuclear membranes [96]. One of the following inhibitory processes may be a component of the antiviral mechanism of NMs: viral adsorption on NMs [98], fragmentation of the viral envelope [99], free radical generation, and a reduction in the ability of viruses to adhere to cell membranes [100]. Because NMs are tiny and have a large surface area, they have a significant antibacterial potential because they can quickly cross cell membranes and halt microbial development. According to several studies, bacteria's cellular membranes are harmed by zinc-based metallic NMs, which cause the contents of the cells to leak out and cause cell death [101]. In a study, many NMs based on gum karya were created and evaluated against various Chlamydomonas and microalgae species [102]. In order to prevent superinfections, zinc NMs work well in wound dressings [103], and they have a significant antioxidant potential [104]. Numerous investigations have demonstrated the capability of numerous additional metallic NMs, such as Fe_3O_4, NiO, MgO, and CO_3O_4 [105, 106]. HIV, CoxB4, HSV1, and dengue viruses can all be treated using biogenic silver nanoparticles (NMs) [107, 108]. Furthermore, biogenic ZnO nanorods have been shown to be antibacterial against the dengue vector Aedes aegypti [109]. In addition, oxidized copper NMs dramatically reduce the "oncolytic virus" activity. Thatoi et al. [72] developed a method for the synthesis of silver and zinc oxide nanomaterials for microbial pathogens using mangrove plants with a wavelength of 9–16 nm. Cittrarasuet al. tested seNP's antimicrobial activity with gram-positive and gram-negative bacteria (B. subtilis and E. coli) at various concentrations, and the inhibition results were compared with the normal antibiotic methicillin (standard). It was found that seNPs show an increase in inhibition activity with increasing concentrations of 25–100 uL/mL at the inhibition range between 14 and 20 mm diameter [110]. The high inhibition range (7–10 mm) of selenium is shown in Fig. 10.

5.1.2 Anticancer Applications

Green metallic nanoparticles derived from plants have been reported to be effective anticancer agents. The safety of cytotoxic, biogenic NMs is a top priority because they should only act on cancerous cells instead of healthy ones. An excellent antitumor medication should be impactful, safe, and selective to the cancer site, and it shouldn't need to be monitored [93]. As a result, scientists and doctors have been working to create antineoplastic medicines that have a wide margin of safety, are affordable, biodegradable, and biocompatible, and have no off-site consequences. The plant, Cassia auriculata, was used to make gold NMs, which have demonstrated an anticancer effect at a concentration of 30 μg/ml, while silver NMs derived from Cassia auriculata leaves have been employed to destroy A459 lung cancer cells at a low dose of 10 μg/ml [111]. Biogenic gold NMs made from the plant Cajanus cajan have

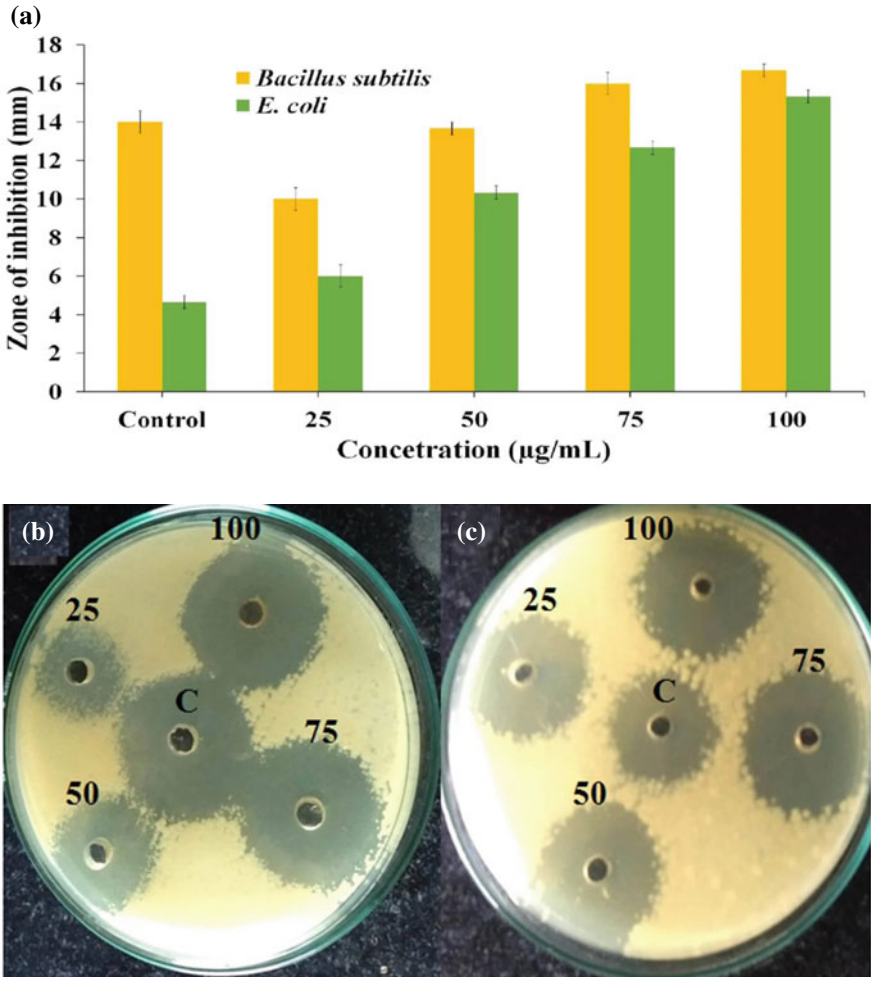

Fig. 10 (**a**–**c**) The antibacterial activity of selenium NMs on different pathogenic strains. Reprinted under terms of the Creative Commons license from ref [110]. Copyright 2021 Springer Nature. TEM, transmission electron microscopy

been shown to kill HepG2 liver cancer cells for 24 h with an LD50 of 6 µg/ml [112]. A recent study discovered that HepG2, A459, and HeLa cells were more harmful to biogenic silver nanoparticles (NMs) [113]. Green zinc sulfide NMs based on Bertoni are also efficient at eliminating cancer, with an IC50 of 400 µg/ml against MCF-7 cells [113]. At a minimum concentration of 50 µg/ml, cynodondactylon leaf-based TiO2 NMs demonstrated superior anticancer capability to NMs produced chemically in opposition to a lung cancer cell line (A549) [114]. A similar anticancer potential has been shown by biogenic Mg oxide and Sn oxide NMs against MCF-7 cells [115, 116], and green silver nanoparticles made from Rhus coriaria have been evaluated

and found to be effective at inhibiting the cellular line for breast cancer, MCF-7 [117]. With regard to Bacillus subtilis, E. coli, colon, breast, and liver cancer cells, Saudi date extract-based Platinum NMs show significant antibacterial and anticancer activity [118]. Other top-notch evaluations provide in-depth insights into the anticancer applications of green metallic NMs [119–121]. Zubair et al. [122] produced NPs of silver, cerium, and copper from the leaf extracts of T. portulacastrum and C. quinoa. The NPs were tested on the HepG2 cell line, and the normal human embryonic kidney cell line (HEK-293) was used to measure the cell cytotoxicity. The cell was treated with 10, 50, and 100 μg/ml concentrations for 24 h, and the result shows a high cytotoxicity effect of 90% at 50 μg/ml. These results show that applying lower concentrations of nanoparticles shows a high cytotoxicity effect (Fig. 11) [122].

5.1.3 Regenerative and Tissue Engineering Medical Applications

Green NMs have the potential to be used in regenerative medicine as well as the engineering of dysfunctional or damaged tissue structures due to their distinct size, shape, and ability to be hemostatically tailored. The development of tissue scaffolds based on nanoscale materials is an example of the advancement of a substance that successfully mimics extracellular matrix and can be used to not only provide mechanical strength but also to transport payloads of growth precursors. For this purpose, a variety of polymeric and metallic NMs can be utilized, and they will aid in tracking cellular activity in tissues that are being designed or are undergoing tissue regeneration [123, 124]. Vial et al. [125] have claimed that green and biogenic gold NMs can be used to improve the mechanical and adhesive qualities of tissue scaffolds. This improvement would then encourage the normal differentiation and proliferation of cells. In one study, the introduction of bioactive MgO NMs into the system of polymers dramatically improved the differentiation, adhesion, and development of osteoblast-like MG 63 cells [126]. The increased compatibility of green magnesium oxide NMs produced by C. gigantea with developing zebrafish compared to chemically produced magnesium oxide NMs suggests that green NMs have stronger morphological and size-based stability than NMs made conventionally [127]. Biogenic Au NMs have been investigated for usage in immunostaining and cellular internalization, and they've been applied to tumor identification [128]. It has been observed that iron oxide is suitable as a component of magnetic resonance imaging of many biological systems, including the spleen, lymph-nodes, bone marrow, and liver. This is because iron oxide's supramagnetic properties make it a good contrast agent [129]. Srinivasan et al. [13] used photosynthesized TiO_2 in research on the toxicity of zebrafish embryos, which was carried out to monitor changes in toxicological effects. In addition, the model utilized in this study was ideal for investigating the toxicity of zebrafish. TiO_2 nanoparticles improved bioavailability and cellular uptake [13].

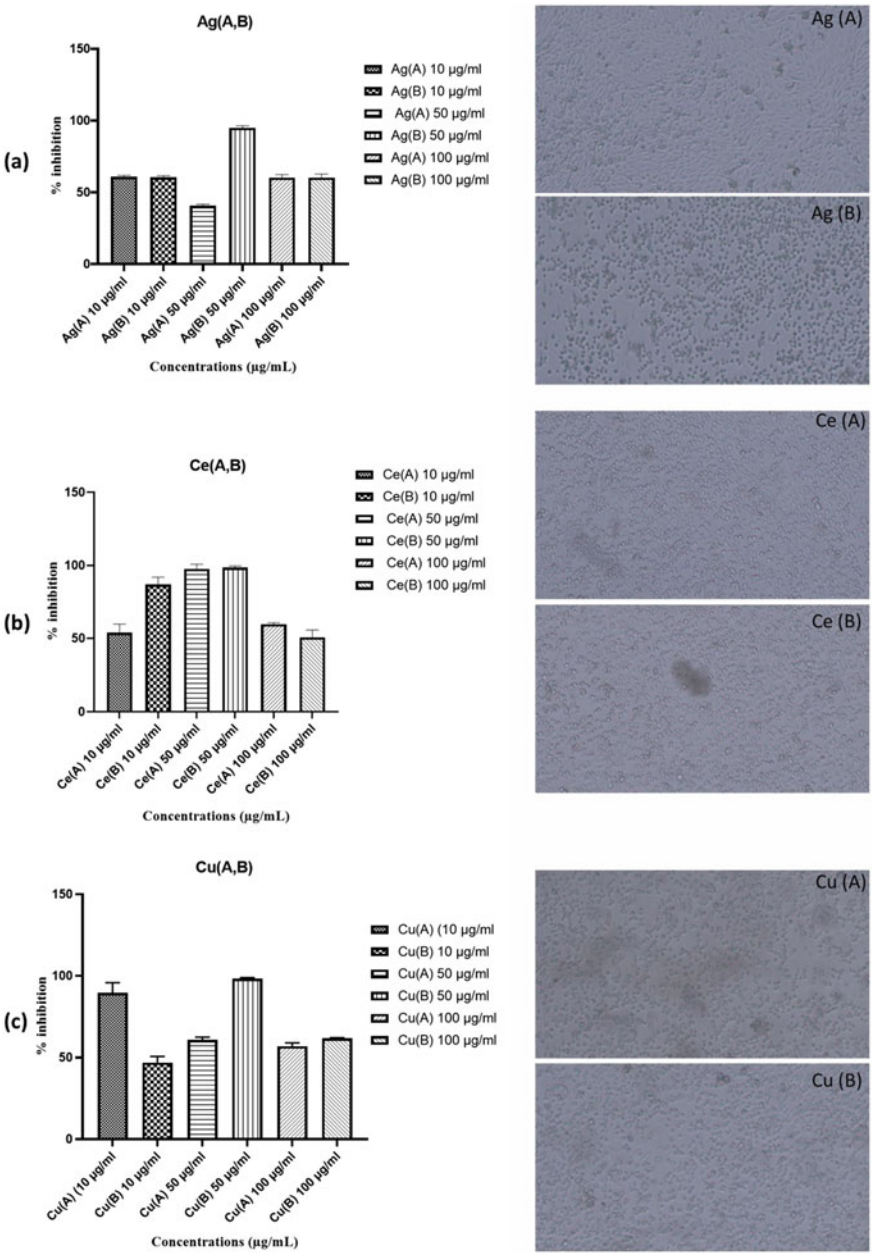

Fig. 11 Cytotoxicity effect of three types nanoparticles Ag, Ce, Cu which are synthesized by using the leaf extract of *T. portulacastrum and C. quinoa against* HepG2 cell line. Ag (A, B), Ce (A, B), and Cu (A, B) represents the Silver, cerium, and copper nanoparticles prepared by *T. porulacastrum* and *C. quinoa* respectively. Reprinted under terms of the Creative Commons license from ref (Zubair et al. 2021). Copyright 2021 Springer Nature

5.1.4 Drug Delivery

One of the developing approaches in current medical research on the deadliest pathological disorders, including cancer, is the administration of therapeutic molecules [130]. Conventional dosage forms do not exhibit sustained and regulated release, which leads to a number of drawbacks, including quick elimination, non-specificity, and limited bioavailability. Green-metallic NMs can be employed to address the shortcomings mentioned above by slowly releasing the medication molecules where they are needed without causing any side effects off-site [131]. When used to distribute gemcitabine, green, biocompatible gold nanoparticles based on gum karaya showed pronounced dose-dependent suppression with the use of the lung tumor cell line A549 in the production of ROS [132]. Doxorubicin-loaded, green produced zinc oxide NMs have demonstrated greater anti-tumor activity than doxorubicin alone [133]. Drug delivery uses are also possible for green NMs produced transdermally. It is significant in this context that a semi-solid gel containing both zinc oxide nanoparticles and ketoconazole demonstrated improved antifungal activity on canine skin [134]. Huang et al. [135] synthesized high-yield carbon dots (CDs) for identification of colitoxin DNA in human serum using banana peels of sizes 5–15 without any surface passivation agents. Manivasagan et al. [136] synthesized gold NMs loaded with doxorubicin for drug delivery from Fucus vesiculosus. They tested AuNMs on human breast cancer cells (MDA-MB-321) with different concentrations (5-50 μg/ml) for 24 h incubation, and the result showed that in 24 h, 50% of the cells died, showing IC50 values of fucoidan, Fu AuNPs, DOX, and DOX-Fu AuNPs against MDA-MB-231 cells, and the experiments proved the excellent anticancer activity (Fig. 12).

5.2 Sensors

Nanomaterials made from biomass are effective for various sensing applications due to their high sensitivity to the chemical environment. Surface phenomena have a significant impact on electrical processes, hence, preferred materials are quickly selected as nanostructures due to their high surface area [24]. Shen et al. [137] synthesized fluorescence carbon dots for cell-imaging and Fe^{3+} sensing using sweet potatoes of sizes 1–5 nm, which were accomplished via hydrothermal treatment. The resulting CDs have soluble functional groups on their surfaces, which have a quantum yield of 8.64%, are easily dispersed. Ajitha et al. [138] synthesized silver nanoparticles from Monordica charantia leaf extract. The prepared AgNPs show excellent catalytic activity on the reduction of methylene blue. Au-NPs have also been used to tell when meat is going bad. The biogenic amines that are made when bacteria break down amino acids are tyramine, histamine, cadaverine, and phenylalanine. Their storage at 5 °C has kept the mystery around the fake odor intact. One study measured histidine and histamine levels in chicken using Au-NPs with detection limits of 0.6 μM and 6.59×10^{-4}, respectively [139]. Ag-NPs-based detection is a

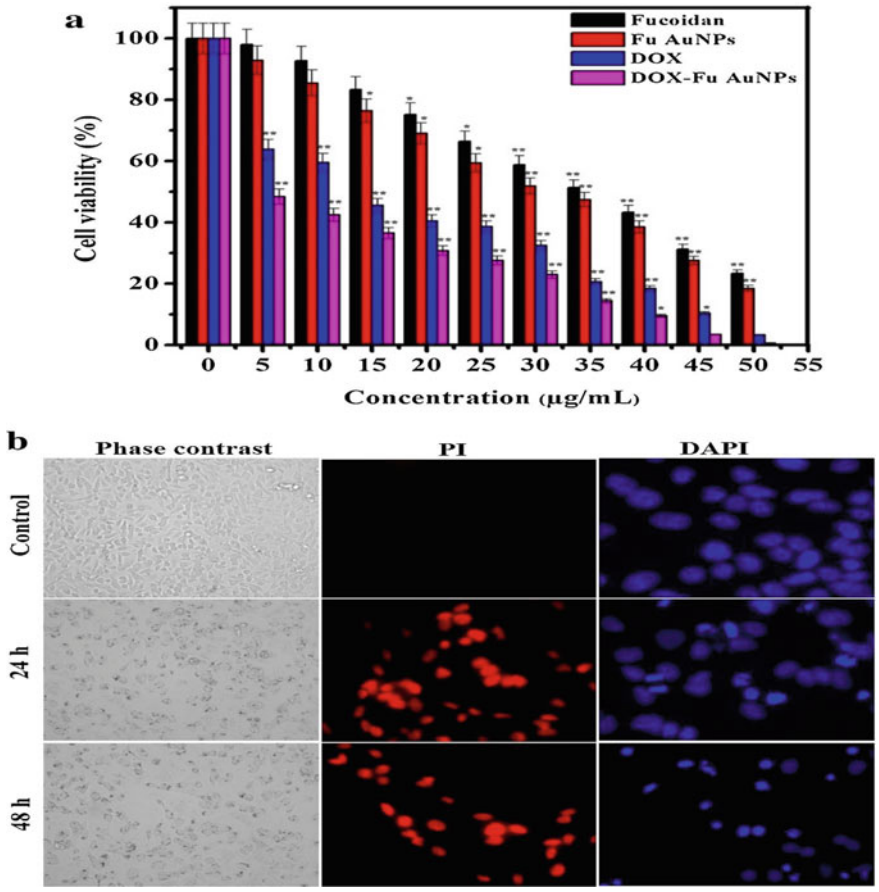

Fig. 12 **a** Results confirming the in vitro cytotoxicity effect of fucoidan, fucoidan capped gold nanoparticles, native DOX, and DOX-loaded fucoidan capped gold nanoparticles against MDA-MB-231 cells for 24 h. **b** Morphological alterations in MDA-MB-231 cells incubated with 5 μg/mL of DOX-loaded fucoidan capped gold nanoparticles for 24 and 48 h, as assessed by contrast phase microscopy. Reprinted under terms of the Creative Commons license from ref [136]. Copyright 2021 Springer Nature

very good way to figure out how many agricultural and horticultural crops have gone bad after harvest. For example, Bacillus subtilis causes spoilage in Musa acuminata and makes 1,2-benzenedicarboxylic acid and bis (2-methylpropyl) ester, which is a volatile compound, during its spoilage. When the ruined bananas were treated with the colloidal solution Ag-NPs, they took on a reddish brown appearance. The same strategy can be used with various types of fruit trees [140].

5.3 Cellular Imaging

NMs are useful for characterizing and imaging tissues, lesions, and cells, which have been applied as biomarkers for the early diagnosis of disease. In order to verify a particular illness-related malfunctioning, they are placed inside cells at a specified spot [93]. Nanotechnology can deliver the next-generation instruments needed for illness detection as well as precise regulators that make it easier to recognize clinical circumstances than ever before [141]. Quantum nanobeads made using the green method are used in an accurate assay for the detection of the hepatitis B virus [142]. Carbon quantum dots (CQDs) are effective for detecting poisons in food and for medical imaging. Carbon quantum dots with a size of 2.7 nm were produced with a yield of 38.8% by Qianchun Zhang et al. In addition, the CQDs as-prepared not only exhibit high blue fluorescence but also low toxicity and benign biocompatibility. Because of this, MCF7 cells can be imaged using CQDs. Our findings suggest that the suggested CQDs based on ginkgo kernel biomass have significant promise for NO_2 detection and cell imaging [143]. Alam et al. [144] synthesized luminescent carbon quantum dots for cellular imaging using cabbage of sizes 2–6 nm by a simple, one-step green process for low-temperature carbonization. Excellent aqueous solubility and stability, as well as enhanced resistance to photobleaching, were all displayed by the CQD with a quantum yield of 16.5%.

5.4 Thermal Properties of Nanomaterials

The films' thermal characteristics are a crucial factor to consider when assessing their potential for use in food packaging. Typically, differential scanning calorimetry (DSC) and thermogravimetric analysis (TGA) are used to examine the thermal characteristics of films [145]. The impact of various nanomaterials on the thermal properties of films made of plant proteins has been assessed using the DSC and TGA techniques. Cellulose in several nanoforms, including CNC and CNF, is the most often employed nanoreinforcement to enhance the thermal characteristics of plant-protein-based films. Researchers used TGA to evaluate how licorice residue-derived nanocellulose affected the thermal characteristics of SPI-based films. In two periods of 240–260 and 360 °C, they asserted that incorporating nanocellulose into the SPI-based films reduced weight loss. The improvement in SPI film's thermal stability caused by the addition of nanocellulose has been linked to this phenomenon. Furthermore, it has been noted that the addition of CNC raised the degradation temperatures of peptide backbones in SPI films [146, 147].

5.5 *Food Applications of Plant-Based Nanomaterials*

Researchers, the food industry, and consumers have all shown a great deal of interest in the use of packaging-based active plant proteins, including NPs, on food. Utilizing nanocomposite films made of plant proteins and coatings on diverse food products will be the main topic of the sections that follow [145]. Unquestionably, fruits and vegetables are important to a balanced diet. Fruits and vegetables have a naturally limited shelf life and are a major challenge to preserve due to their high moisture content, rapid biochemical modifications, physiological ageing, and microbial infections that hasten disintegration and make them appear unappealing during storage and transportation [148]. Böhmer-Maas et al. studied the storage of cherry tomatoes over a 22-day period using a mixture of Zn and TiO_2 nanofibers. Thus, the results show that the addition of TiO_2 increases thermal stability up to 600 °C while decreasing nanofiber diameter. Additionally, the reduction of weight for the samples is noticeably improved when TiO_2 is used in the creation of the nanocomposite; for example, the weight loss of the solely zinc-based nanocomposite was approximately 69.83% [149].

5.6 *Environmental Remediation Applications*

Concerning worldwide issues of environmental contamination, certain metallic NMs and dendrimers have the potential to be employed in the treatment of soil, water, and air pollution due to their distinctive physicochemical characteristics. Particularly, the use of zerovalent iron has the ability to clean up soil and groundwater contamination brought on by heavy metals and halogenated hydrocarbons [150, 151]. The literature has also discussed the potential of biologically generated tin oxide NMs to degrade dyes and other contaminants, with a clearance effectiveness of about 76.48% for chromium. Researchers have looked into the capacity of certain NMs to convert toxic contaminants into less dangerous moieties [152]. Water is essential to life on earth, hence, it is currently a serious concern that water sources are contaminated. It's notable in this respect that a number of metallic NMs have been investigated for the effective removal of hazardous metal, organic and inorganic contaminants, and pathogenic bacteria from water reservoirs [153]. Various applications of different plant biomass-derived nanomaterials are summarized in Table 2.

6 Conclusions

With expanding research and technological advancements in science and engineering, interest in nanomaterials has increased. Nanomaterials are successfully synthesized by various plant biomasses such as Capsicum annuum var. grossum

Table 2 Application of different plant biomass-derived nanomaterials

S. No.	Plant biomass	Nanomaterial	Size(nm)	Application	References
1.	Sweet potato	Fluorescence carbon dots	1–5	Used for cell imaging and Fe^{3+} sensing	[137]
2.	Banana peels	Pd-Au@ CDs/GCE	5–15	Identification of colitoxin DNA in human serum	[135]
3.	Cabbage	Luminescent Carbon quantum dots	2–6	Cellular imaging	[144]
4.	Sugarcane bagasse	Carbon quantum dots with a blue emission	8–11	Fluoride ion detection in water	[154]
5.	Apple juice	Fluorescence carbon dots	3.6–5.5	Bio-imaging of mycobacterium and fungi cells	[155]
6.	Waste biomass Mainly dead neem leaves	Graphene quantum dots	5–6	Fluorescence quenching, photoluminescence "on–off-on" performance to indicate the presence of Ag+ ions in aqueous solution	[156]
7.	Sugarcane stalk	Fluorescent carbon dots	1.8–2.0	Bioimaging and multicolorbiolabeling in cancer cells	[157]
8.	Catharanthusroseus	Green carbon quantum dots	5	Multi-ion detection	[158]
9.	Bamboo shells	Ultra-pure carbon	–	Energy storage	[159]
10.	Watermelon waste	Magnetic carbon nanocomposite	90–250	Removal of heavy metals from drinking water	[160]
11.	Dead pine needles	N&O Co-doped Nano structures	–	Supercapacitors	[161]
12.	Pomegranate seeds	Iron oxide	25–55	Evaluation of photocatalytic activity for degradation of textile dye	[68]

(continued)

Table 2 (continued)

S. No.	Plant biomass	Nanomaterial	Size(nm)	Application	References
13.	Green tea extract	Iron	20–50	Promoter for Fenton like dye degradation reactions	[69]
18.	Plant extract like garlic, onion	Zinc oxide	9–55	Photodegradation of methylene blue dye	[71]
19.	Mangrove plant	Silver and zinc oxide	9–16	Microbial pathogens	[72]
20.	Wood apple (Limoniaacidissima) juice	Zinc ferrite	20	Photodegradation for Evans blue and Methylene blue, Antibacterial activity	[76]
21.	Gardenia resinifera	Manganese oxide	17–35	Antibacterial activity against all tested bacterial pathogens	[77]
22.	Daturametel L	CeO_2	5–15	Degradation activity (DPPH)	[79]
23.	Lycopersiconesculentum	SnO_2	–	Photocatalytic degradation	[78]
24.	Andrographispaniculata	Samarium oxide	30–50	Inhibition action	[80]
25.	Combretumerythrophyllum	Gold	13.20	Antibacterial and anticancer	[162]
26.	Jasminumauriculatum	Gold	8–37	Wide-ranging antibacterial effects, notably against fungi	[163]
27.	Mimosa tenuiflora	Gold	2–40	Delivery of drugs using a fluorescent probe	[164]
28.	Cestrum nocturnum	Silver	20	Antioxidant and Antibacterial	[165]
29.	Adeniumabesum	Silver	–	DNA fragmentation, antioxidants, and anticancer	[124]
30.	M. glabrata	Silver	2–30	Decomposition of an antibiotic, methyl orange, and rhodamine B	[166]
31.	Eucalyptus	Iron	80–90	Phosphate and chromium removal	[167]
32.	Daphne mezereum	Iron	6.5–14.9	Discolorations of dye	[168]
33.	Dolichos lablab L	Iron	12.5	Dye absorption from oil sludge	[169]

(continued)

Table 2 (continued)

S. No.	Plant biomass	Nanomaterial	Size(nm)	Application	References
34.	Orobancheoccidentale	Copper	50	Nematicidal	[170]
35.	Tridaxprocumbens	Copper	71	Degradation of Bismarck brown	[171]
36.	Calotropisgigantea	Zinc	10–50	Nitrite sensing, photocatalysis, and antimicrobial	[172]
37.	Berberisaristata	Zinc	90–110	Prevention of infections in the urinary system	[173]
38.	Peganumharmala	Platinum	1.9–33.5	Antioxidant, anticancer, and inhibitor of cystine proteinase	[174]
39.	Cotton boll peels	Palladium	9.44	Capacity for catalysis against hazardous	[175]

pulp, Bamboo leaves, Punica bamboum (pomegranate) seed, Citrus maxima peel, and green tea leaves, which are environmentally friendly, have high efficiency, and are easily available. The plant biomass consists of various functional groups, mainly polyphenols that behave as both reducing and capping agents for the synthesis of nanomaterials. Some of the characterization techniques that can be used to obtain the morphology and size of the nanomaterials are TEM, XRD, and others. This method can be used to create nanomaterials of various types, such as TiO_2, $ZnFeO_4$, Carbon quantum dots, $AgCoPO_4$, MnO_2, and others, which have potential applications in a variety of fields, such as drug delivery, agriculture, cellular imaging, ion detection in water, selective photoluminescence, and so on. Various productive nanomaterials have also been engineered in recent years to make the process chemical-free and simple to synthesize. In this chapter, we have briefly discussed some of the applications and synthesis of the nanomaterials from different plant biomasses, which can have a larger future scope.

References

1. Teo HL, Wahab RA (2020) Towards an eco-friendly deconstruction of agro-industrial biomass and preparation of renewable cellulose nanomaterials: a review. Int J Biol Macromol 161:1414–1430
2. Tiwari SK, Bystrzejewski M, De Adhikari A, Huczko A, Wang N (2022) Methods for the conversion of biomass waste into value-added carbon nanomaterials: Recent progress and applications. Prog Energy Combust Sci 92
3. Zeghoud S, Hemmami H, Ben B, Amor I. Ben B, Kouadri I (2022) Journal Mater Today Commun 104747. https://doi.org/10.1016/j.mtcomm.2022.104747

4. Jain A (2022) Algae-mediated synthesis of biogenic nanoparticles. Adv Nat Sci Nanosci Nanotechnol 13
5. Chouke PB et al (2022) Bioinspired metal/metal oxide nanoparticles: A road map to potential applications. Mater Today Adv 16:100314
6. Cho HJ, Lee WS, Jeong J, Lee JS (2022) A review on the impacts of nanomaterials on neuromodulation and neurological dysfunction using a zebrafish animal model. Comp. Biochem. Physiol. Part C Toxicol. Pharmacol. 261:109428
7. Mu Q et al (2014) Chemical basis of interactions between engineered nanoparticles and biological systems. Chem Rev 114:7740–7781
8. Gigault J et al (2021) Nanoplastics are neither microplastics nor engineered nanoparticles. Nat Nanotechnol 16:501–507
9. İnada AA, Arman S, Safaei B (2022) A novel review on the efficiency of nanomaterials for solar energy storage systems. J. Energy Storage 55
10. Aithal PS (2016) A monthly double-blind peer reviewed refereed open access international e-Journal-Included in the International Serial Directories Nanotechnology Innovations and Business Opportunities : A Review. 6:182–204
11. Norizan MN et al (2022) Nanocellulose-based nanocomposites for sustainable applications: a review. Nanomaterials 12:1–51
12. Cao Y, Zhang J, Wei S Application and Safety Performance of Nanomaterials in Clothing Design Engineering. Adv Mater Sci Eng 2022 (2022)
13. Srinivasan M et al (2019) Green synthesis and characterization of titanium dioxide nanoparticles (TiO_2 NPs) using Sesbania grandiflora and evaluation of toxicity in zebrafish embryos. Process Biochem 80:197–202
14. Arshad H, Sami MA, Sadaf S, Hassan U (2021) Salvadora persica mediated synthesis of silver nanoparticles and their antimicrobial efficacy. Sci Rep 11:1–11
15. Singh P et al (2018) Green synthesis of gold and silver nanoparticles from Cannabis sativa (Industrial hemp) and their capacity for biofilm inhibition. Int J Nanomedicine 13:3571–3591
16. Anand K, Gengan RM, Phulukdaree A, Chuturgoon A (2015) Agroforestry waste moringa oleifera petals mediated green synthesis of gold nanoparticles and their anti-cancer and catalytic activity. J Ind Eng Chem 21:1105–1111
17. Shankar SS, Ahmad A, Pasricha R, Sastry M (2003) Bioreduction of chloroaurate ions by geranium leaves and its endophytic fungus yields gold nanoparticles of different shapes. J Mater Chem 13:1822–1826
18. Asghar MA et al (2018) Iron, copper and silver nanoparticles: Green synthesis using green and black tea leaves extracts and evaluation of antibacterial, antifungal and aflatoxin B1 adsorption activity. Lwt 90:98–107
19. Ankamwar B, Chaudhary M, Sastry M (2005) Gold nanotriangles biologically synthesized using tamarind leaf extract and potential application in vapor sensing. Synth React Inorganic Met Nano-Metal Chem 35:19–26
20. IET Nanobiotechnology (2018) Nazli—Plant-based metallic nanoparticles as potential theranostics agents bioinspired.pdf.
21. Ahmed SF et al (2023) Utilization of nanomaterials in accelerating the production process of sustainable biofuels. Sustain Energy Technol Assess 55:102894
22. Jelonek Z, Drobniak A, Mastalerz M, Jelonek I (2020) J Sci Total Environ 141267. https://doi.org/10.1016/j.energy.2022.125507
23. Kolahalam LA et al (2019) Review on nanomaterials: synthesis and applications. Mater Today Proc 18:2182–2190
24. Ayoub I et al (2022) Advances in ZnO: manipulation of defects for enhancing their technological potentials. Nanotechnol Rev 11:575–619
25. Mody V, Siwale R, Singh A, Mody H (2010) Introduction to metallic nanoparticles. J Pharm Bioallied Sci 2:282
26. Han J et al (2018) Polymer-based nanomaterials and applications for vaccines and drugs. Polymers (Basel) 10:1–14

27. Singh D, Singh S, Sahu J, Srivastava S, Singh MR (2016) Ceramic nanoparticles: recompense, cellular uptake and toxicity concerns. Artif Cells Nanomedicine Biotechnol 44:401–409
28. Roldo M, Fatouros DG (2013) Biomedical applications of carbon nanotubes. Annu Reports Prog Chem Sect C 109:10–35
29. Lee XJ et al (2019) Review on graphene and its derivatives: Synthesis methods and potential industrial implementation. J Taiwan Inst Chem Eng 98:163–180
30. Duan H, Wang D, Li Y (2015) Green chemistry for nanoparticle synthesis. Chem Soc Rev 44:5778–5792
31. Ravnsbaek DB, Sørensen LH, Filinchuk Y, Besenbacher F, Jensen TR (2012) Screening of metal borohydrides by mechanochemistry and diffraction. Angew Chemie 124:3642–3646
32. Černý R et al (2013) Trimetallic borohydride $Li_3MZn_5(BH_4)$ 15 (M = Mg, Mn) containing two weakly interconnected frameworks. Inorg Chem 52:9941–9947
33. Verdian MM, Raeissi K, Salehi M (2010) Electrochemical impedance spectroscopy of HVOF-sprayed NiTi intermetallic coatings deposited on AISI 1045 steel. J Alloys Compd 507:42–46
34. Ijaz I, Gilani E, Nazir A, Bukhari A (2020) Detail review on chemical, physical and green synthesis, classification, characterizations and applications of nanoparticles. Green Chem Lett Rev 13:59–81
35. Salavati-Niasari M, Davar F, Mir N (2008) Synthesis and characterization of metallic copper nanoparticles via thermal decomposition. Polyhedron 27:3514–3518
36. Zahra R et al (2019) Effect of secondary phases on the thermoelectric properties of Zn_2GeO_4 nano-crystals grown by thermal evaporation on Au coated Si substrate. Phys B Condens Matter 564:143–146
37. Mattox DM (2000) Physical vapor deposition (PVD) processes. Met Finish 98:410–423
38. Wang S, Li X, Wu J, Wen W, Qi Y (2018) Fabrication of efficient metal halide perovskite solar cells by vacuum thermal evaporation: a progress review. Curr Opin Electrochem 11:130–140
39. Ravi-Kumar S, Lies B, Zhang X, Lyu H, Qin H (2019) Laser ablation of polymers: a review. Polym Int 68:1391–1401
40. Saccomandi P, Lapergola A, Longo F, Schena E, Quero G (2018) Thermal ablation of pancreatic cancer: a systematic literature review of clinical practice and pre-clinical studies. Int J Hyperth 35:398–418
41. Mintcheva N, Yamaguchi S, Kulinich SA (2020) Hybrid TiO_2-zno nanomaterials prepared using laser ablation in liquid. Materials (Basel) 13:11–15
42. Nguyen MT, Yonezawa T (2018) Sputtering onto a liquid: interesting physical preparation method for multi-metallic nanoparticles. Sci Technol Adv Mater 19:883–898
43. Becker M, Gies M, Polity A, Chatterjee S, Klar PJ (2019) Materials processing using radio-frequency ion-sources: Ion-beam sputter-deposition and surface treatment. Rev Sci Instrum 90
44. Mokhena TC et al (2020) Nanomaterials: types, synthesis and characterization. 115–141. https://doi.org/10.1007/978-981-13-9333-4_5
45. Sayago I, Hontañón E, Aleixandre M (2020) Preparation of tin oxide nanostructures by chemical vapor deposition. Tin Oxide Mater (Elsevier Inc.). https://doi.org/10.1016/b978-0-12-815924-8.00009-8
46. Bhaviripudi S et al (2007) CVD synthesis of single-walled carbon nanotubes from gold nanoparticle catalysts. J Am Chem Soc 129:1516–1517
47. Choy KL (2003) Chemical vapour deposition of coatings. Prog Mater Sci 48:57–170
48. Ahmadi S, et al (2014) The role of physical techniques on the preparation of photoanodes for dye sensitized solar cells. Int J Photoenergy 2014
49. Jamkhande PG, Ghule NW, Bamer AH, Kalaskar MG (2019) Metal nanoparticles synthesis: an overview on methods of preparation, advantages and disadvantages, and applications. J Drug Deliv Sci Technol 53:101174
50. Machmudah S et al (2014) Synthesis of ZrO_2 nanoparticles by hydrothermal treatment. AIP Conf Proc 1586:166–172
51. Abid N et al (2022) Synthesis of nanomaterials using various top-down and bottom-up approaches, influencing factors, advantages, and disadvantages: a review. Adv Colloid Interface Sci 300:102597

52. Sravani GM et al (2022) Structural and electrical properties of Ca doped $BiFeO_3$ multiferroic nanomaterials prepared by sol-gel auto-combustion method. J Indian Chem Soc 99:100465
53. Dihom HR et al (2022) Photocatalytic degradation of disperse azo dyes in textile wastewater using green zinc oxide nanoparticles synthesized in plant extract: a critical review. J Water Process Eng 47:102705
54. Sunny NE et al (2022) Green synthesis of titanium dioxide nanoparticles using plant biomass and their applications—a review. Chemosphere 300:134612
55. Rajendhiran R, Deivasigamani V, Palanisamy J, Masan S, Pitchaiya S (2021) Terminalia catappa and carissa carandas assisted synthesis of Tio_2 nanoparticles—a green synthesis approach. Mater Today Proc 45:2232–2238
56. Mathew SS, Sunny NE, Shanmugam V (2021) Green synthesis of anatase titanium dioxide nanoparticles using Cuminum cyminum seed extract; effect on Mung bean (Vigna radiata) seed germination. Inorg Chem Commun 126:108485
57. Bekele ET, Gonfa BA, Zelekew OA, Belay HH, Sabir FK (2020) Synthesis of titanium oxide nanoparticles using root extract of Kniphofia foliosa as a template, characterization, and its application on drug resistance bacteria. J Nanomater 2020:1–10
58. Matinise N et al (2018) Green synthesis of novel zinc iron oxide ($ZnFe_2O_4$) nanocomposite via Moringa Oleifera natural extract for electrochemical applications. Appl Surf Sci 446:66–73
59. Baruah D, Yadav RNS, Yadav A, Das AM (2019) Alpinia nigra fruits mediated synthesis of silver nanoparticles and their antimicrobial and photocatalytic activities. J Photochem Photobiol B Biol 201:111649
60. Rani P et al (2020) Highly stable AgNPs prepared via a novel green approach for catalytic and photocatalytic removal of biological and non-biological pollutants. Environ Int 143:105924
61. Tripathi N, Pavelyev V, Islam SS (2017) Synthesis of carbon nanotubes using green plant extract as catalyst: unconventional concept and its realization. Appl Nanosci 7:557–566
62. Ganaie SU, Abbasi T, Abbasi SA (2018) Biomimetic synthesis of platinum nanoparticles utilizing a terrestrial weed Antigonon leptopus. Part Sci Technol 36:681–688
63. Ghosh S et al (2012) Gnidia glauca flower extract mediated synthesis of gold nanoparticles and evaluation of its chemocatalytic potential. J. Nanobiotechnol 10:1–9
64. Xin Lee K, et al (2016) Green synthesis of gold nanoparticles using aqueous extract of Garcinia mangostana fruit peels. J Nanomater 2016
65. Rajan A, Rajan AR, Philip D (2017) Elettaria cardamomum seed mediated rapid synthesis of gold nanoparticles and its biological activities. OpenNano 2:1–8
66. Yuan CG, Huo C, Yu S, Gui B (2017) Biosynthesis of gold nanoparticles using Capsicum annuum var. grossum pulp extract and its catalytic activity. Phys E Low-Dimens Syst Nanostructures 85:19–26
67. Liu Y, Zhao Y, Zhang Y (2014) One-step green synthesized fluorescent carbon nanodots from bamboo leaves for copper(II) ion detection. Sens Actuators B Chem 196:647–652
68. Bibi I et al (2019) Green synthesis of iron oxide nanoparticles using pomegranate seeds extract and photocatalytic activity evaluation for the degradation of textile dye. J Mater Res Technol 8:6115–6124
69. Truskewycz A, Shukla R, Ball AS (2016) Iron nanoparticles synthesized using green tea extracts for the fenton-like degradation of concentrated dye mixtures at elevated temperatures. J Environ Chem Eng 4:4409–4417
70. Wei Y, Fang Z, Zheng L, Tan L, Tsang EP (2016) Green synthesis of Fe nanoparticles using citrus maxima peels aqueous extracts. Mater Lett 185:384–386
71. Stan M et al (2015) Enhanced photocatalytic degradation properties of zinc oxide nanoparticles synthesized by using plant extracts. Mater Sci Semicond Process 39:23–29
72. Thatoi P et al (2016) Photo-mediated green synthesis of silver and zinc oxide nanoparticles using aqueous extracts of two mangrove plant species, Heritiera fomes and Sonneratia apetala and investigation of their biomedical applications. J Photochem Photobiol B Biol 163:311–318
73. Gu D, Shang S, Yu Q, Shen J (2016) Green synthesis of nitrogen-doped carbon dots from lotus root for Hg(II) ions detection and cell imaging. Appl Surf Sci 390:38–42

74. Ensafi AA, Hghighat Sefat S, Kazemifard N, Rezaei B, Moradi F (2017) A novel one-step and green synthesis of highly fluorescent carbon dots from saffron for cell imaging and sensing of prilocaine. Sensors Actuators B Chem 253:451–460
75. Tyagi A, Tripathi KM, Singh N, Choudhary S, Gupta RK (2016) Green synthesis of carbon quantum dots from lemon peel waste: applications in sensing and photocatalysis. RSC Adv 6:72423–72432
76. Madhukara Naik M, et al (2019) Green synthesis of zinc ferrite nanoparticles in Limonia acidissima juice: characterization and their application as photocatalytic and antibacterial activities. Microchem J 146:1227–1235
77. Manjula R, Thenmozhi M, Thilagavathi S, Srinivasan R, Kathirvel A (2019) Green synthesis and characterization of manganese oxide nanoparticles from Gardenia resinifera leaves. Mater Today Proc 26:3559–3563
78. Garrafa-Galvez HE et al (2019) Green synthesis of SnO_2 nanoparticle using Lycopersicon esculentum peel extract. J Mol Struct 1197:354–360
79. Yulizar Y, Kusrini E, Apriandanu DOB, Nurdini N (2020) Datura metel L. Leaves extract mediated CeO_2 nanoparticles: synthesis, characterizations, and degradation activity of DPPH radical. Surf Interfaces 19:100437
80. Muthulakshmi V, Balaji M, Sundrarajan M (2020) Biomedical applications of ionic liquid mediated samarium oxide nanoparticles by Andrographis paniculata leaves extract. Mater Chem Phys 242:122483
81. Akinsiku AA, Ajani OO, Adekoya JA, Emetere ME, Dare EO (2020) Green synthesis of triclinic (anorthic) phase $AgCoPO_4$ nanoparticles: optical studies and theoretical modelling. Heliyon 6:e05029
82. Ansari A, et al (2022) Green synthesis of TiO_2 nanoparticles using acorus calamus leaf extract and evaluating its photocatalytic and in vitro antimicrobial activity. Catalysts 12
83. Solaiman MA, Ali MA, Abdel-Moein NM, Mahmoud EA (2020) Synthesis of Ag-NPs developed by green-chemically method and evaluation of antioxidant activities and anti-inflammatory of synthesized nanoparticles against LPS-induced NO in RAW 264.7 macrophages. Biocatal Agric Biotechnol 29:101832
84. Yu C et al (2019) Green biosynthesis of silver nanoparticles using eriobotrya japonica (thunb.) leaf extract for reductive catalysis. Materials (Basel) 12
85. Bhagat DS, Gurnule WB, Pande SG, Kolhapure MM, Belsare AD (2019) Biosynthesis of gold nanoparticles for detection of dichlorvos residue from different samples. Mater Today Proc 29:763–767
86. Al-Radadi NS, Adam SIY (2020) Green biosynthesis of Pt-nanoparticles from Anbara fruits: toxic and protective effects on CCl4 induced hepatotoxicity in Wister rats. Arab J Chem 13:4386–4403
87. Ghosh MK, Sahu S, Gupta I, Ghorai TK (2020) Green synthesis of copper nanoparticles from an extract ofJatropha curcasleaves: characterization, optical properties, CT-DNA binding and photocatalytic activity. RSC Adv 10:22027–22035
88. Stark WJ, Stoessel PR, Wohlleben W, Hafner A (2015) Industrial applications of nanoparticles. Chem Soc Rev 44:5793–5805
89. Rameshkumar P, Ramaraj R (2013) Gold nanoparticles deposited on amine functionalized silica sphere and its modified electrode for hydrogen peroxide sensing. J Appl Electrochem 43:1005–1010
90. Balantrapu K, Goia DV (2009) Silver nanoparticles for printable electronics and biological applications. J Mater Res 24:2828–2836
91. Elemike EE, Onwudiwe DC, Ekennia AC, Sonde CU, Ehiri RC (2017) Green synthesis of Ag/Ag_2O nanoparticles using aqueous leaf extract of Eupatorium odoratum and its antimicrobial and mosquito larvicidal activities. Molecules 22:1–15
92. Zhu Y, Li J, Pang Z (2021) Recent insights for the emerging COVID-19: drug discovery, therapeutic options and vaccine development. Asian J Pharm Sci 16:4–23
93. Ullah A, Lim SI (2022) Plant extract-based synthesis of metallic nanomaterials, their applications, and safety concerns. Biotechnol Bioeng 119:2273–2304

94. Borse V, Kaler A, Banerjee UC (2015) Microbial synthesis of platinum nanoparticles and evaluation of their anticancer activity. Int J Emerg Trends Electr Electron 11:2320–9569
95. Ortega FG et al (2015) Study of antitumor activity in breast cell lines using silver nanoparticles produced by yeast. Int J Nanomedicine 10:2021–2031
96. Sirelkhatim A et al (2015) Review on zinc oxide nanoparticles: Antibacterial activity and toxicity mechanism. Nano-Micro Lett. 7:219–242
97. Kumar H, et al (2020) Flower-based green synthesis of metallic nanoparticles: applications beyond fragrance. Nanomaterials 10
98. Nangmenyi G, Li X, Mehrabi S, Mintz E, Economy J (2011) Silver-modified iron oxide nanoparticle impregnated fiberglass for disinfection of bacteria and viruses in water. Mater Lett 65:1191–1193
99. Mazurkova NA et al (2010) Interaction of titanium dioxide nanoparticles with influenza virus. Nanotechnologies Russ 5:417–420
100. Rai M et al (2016) Metal nanoparticles: the protective nanoshield against virus infection. Crit Rev Microbiol 42:46–56
101. Ruparelia JP, Chatterjee AK, Duttagupta SP, Mukherji S (2008) Strain specificity in antimicrobial activity of silver and copper nanoparticles. Acta Biomater 4:707–716
102. Nguyen NHA, Padil VVT, Slaveykova VI, Černík M, Ševců A (2018) Green Synthesis of Metal and Metal Oxide Nanoparticles and Their Effect on the Unicellular Alga Chlamydomonas reinhardtii. Nanoscale Res Lett 13
103. Khatami M et al (2018) Applications of green synthesized Ag, ZnO and Ag/ZnO nanoparticles for making clinical antimicrobial wound-healing bandages. Sustain Chem Pharm 10:9–15
104. Suresh D et al (2015) Green synthesis of multifunctional zinc oxide (ZnO) nanoparticles using Cassia fistula plant extract and their photodegradative, antioxidant and antibacterial activities. Mater Sci Semicond Process 31:446–454
105. Kganyago P et al (2018) Synthesis of NiO nanoparticles via a green route using Monsonia burkeana: the physical and biological properties. J Photochem Photobiol B Biol 182:18–26
106. Khalil AT, et al (2020) Physical properties, biological applications and biocompatibility studies on biosynthesized single phase cobalt oxide (Co_3O_4) nanoparticles via Sageretia thea (Osbeck.). Arab J Chem 13:606–619
107. Sujitha V et al (2015) Green-synthesized silver nanoparticles as a novel control tool against dengue virus (DEN-2) and its primary vector Aedes aegypti. Parasitol Res 114:3315–3325
108. Yugandhar P et al (2018) Cost effective, green synthesis of copper oxide nanoparticles using fruit extract of Syzygium alternifolium (Wt.) Walp. Characterization and evaluation of antiviral activity. J Clust Sci 29:743–755
109. Ashokan AP et al (2017) Toxicity on dengue mosquito vectors through Myristica fragrans-synthesized zinc oxide nanorods, and their cytotoxic effects on liver cancer cells (HepG2). J Clust Sci 28:205–226
110. Cittrarasu V et al (2021) Green synthesis of selenium nanoparticles mediated from Ceropegia bulbosa Roxb extract and its cytotoxicity, antimicrobial, mosquitocidal and photocatalytic activities. Sci Rep 11:1–15
111. Parveen A, Rao S (2015) Cytotoxicity and genotoxicity of biosynthesized gold and silver nanoparticles on human cancer cell lines. J Clust Sci 26:775–788
112. Ashokkumar T et al (2014) Apoptosis in liver cancer (HepG2) cells induced by functionalized gold nanoparticles. Colloids Surf B Biointerfaces 123:549–556
113. Alahmad A et al (2021) Hypericum perforatum L.-mediated green synthesis of silver nanoparticles exhibiting antioxidant and anticancer activities. Nanomaterials 11:1–26
114. Hariharan D, Srinivasan K, Lc N (2017) Synthesis and characterization of Tio_2 nanoparticles using cynodon dactylon leaf extract for antibacterial and anticancer (A549 Cell Lines) activity. J Nanomedicine Res 5:1–4
115. Kgosiemang IK et al (2020) Green synthesis of magnesium and cobalt oxide nanoparticles using Euphorbia tirucalli: characterization and potential application for breast cancer inhibition. Inorg Nano-Metal Chem 50:1070–1080

116. Khan SA, Kanwal S, Rizwan K, Shahid S (2018) Enhanced antimicrobial, antioxidant, in vivo antitumor and in vitro anticancer effects against breast cancer cell line by green synthesized un-doped SnO_2 and Co-doped SnO_2 nanoparticles from Clerodendrum inerme. Microb Pathog 125:366–384
117. Kubatka P, et al (2021) Rhus coriaria l. (sumac) demonstrates oncostatic activity in the therapeutic and preventive model of breast carcinoma. Int J Mol Sci 22:1–30
118. Al-Radadi NS (2019) Green synthesis of platinum nanoparticles using Saudi's dates extract and their usage on the cancer cell treatment. Arab J Chem 12:330–349
119. Jabeen S, et al (2021) Application of green synthesized silver nanoparticles in cancer treatment—a critical review. Mater Res Express 8
120. Khan ZUH et al (2017) Biomedical applications of green synthesized Nobel metal nanoparticles. J Photochem Photobiol B Biol 173:150–164
121. Bharadwaj KK, et al (2021) Green synthesis of gold nanoparticles using plant extracts as beneficial prospect for cancer theranostics. Molecules 26
122. Younas M, Rizwan M, Zubair M, Inam A, Ali S (2021) Biological synthesis, characterization of three metal-based nanoparticles and their anticancer activities against hepatocellular carcinoma HepG2 cells. Ecotoxicol Environ Saf 223:112575
123. Laurenti M, Cauda V (2017) ZnO nanostructures for tissue engineering applications. Nanomaterials 7
124. Fathi-Achachelouei M et al (2019) Use of nanoparticles in tissue engineering and regenerative medicine. Front Bioeng Biotechnol 7:1–22
125. Vial S, Reis RL, Oliveira JM (2017) Recent advances using gold nanoparticles as a promising multimodal tool for tissue engineering and regenerative medicine. Curr Opin Solid State Mater Sci 21:92–112
126. Suryavanshi A, Khanna K, Sindhu KR, Bellare J, Srivastava R (2017) Magnesium oxide nanoparticle-loaded polycaprolactone composite electrospun fiber scaffolds for bone-soft tissue engineering applications: in-vitro and in-vivo evaluation. Biomed Mater 12
127. Verma SK et al (2020) Green synthesized MgO nanoparticles infer biocompatibility by reducing in vivo molecular nanotoxicity in embryonic zebrafish through arginine interaction elicited apoptosis. Sci Total Environ 713:136521
128. Jana S, Jana S (2017) Particulate technology for delivery of therapeutics. Part Technol Deliv Ther. https://doi.org/10.1007/978-981-10-3647-7
129. Singh J, Kumar V, Kim KH, Rawat M (2019) Biogenic synthesis of copper oxide nanoparticles using plant extract and its prodigious potential for photocatalytic degradation of dyes. Environ Res 177:108569
130. De Jong WH, Paul JB (2008) Drug delivery and nanoparticles: applications and hazards. Int J Nanomed 3:133–149
131. Cho K, Wang X, Nie S, Chen Z, Shin DM (2008) Therapeutic nanoparticles for drug delivery in cancer. Clin Cancer Res 14:1310–1316
132. Pooja D et al (2015) Natural polysaccharide functionalized gold nanoparticles as biocompatible drug delivery carrier. Int J Biol Macromol 80:48–56
133. Sharma H, Kumar K, Choudhary C, Mishra PK, Vaidya B (2016) Development and characterization of metal oxide nanoparticles for the delivery of anticancer drug. Artif Cells Nanomedicine Biotechnol 44:672–679
134. Viswanathan K et al (2018) Ketoconazole-conjugated ZnO nanoparticles based semi-solid formulation and study their impacts on skin disease. IET Nanobiotechnol 12:1097–1101
135. Huang Q, Lin X, Zhu JJ, Tong QX (2017) Pd-Au@carbon dots nanocomposite: Facile synthesis and application as an ultrasensitive electrochemical biosensor for determination of colitoxin DNA in human serum. Biosens Bioelectron 94:507–512
136. Manivasagan P et al (2016) Doxorubicin-loaded fucoidan capped gold nanoparticles for drug delivery and photoacoustic imaging. Int J Biol Macromol 91:578–588
137. Shen J, Shang S, Chen X, Wang D, Cai Y (2017) Facile synthesis of fluorescence carbon dots from sweet potato for Fe^{3+} sensing and cell imaging. Mater Sci Eng C 76:856–864

138. Ajitha B, Reddy YAK, Reddy PS (2015) Biosynthesis of silver nanoparticles using Momordica charantia leaf broth: evaluation of their innate antimicrobial and catalytic activities. J Photochem Photobiol B Biol 146:1–9
139. Kumar N, Seth R, Kumar H (2014) Colorimetric detection of melamine in milk by citrate-stabilized gold nanoparticles. Anal Biochem 456:43–49
140. Kumar A, Choudhary A, Kaur H, Mehta S, Husen A (2021) Metal-based nanoparticles, sensors, and their multifaceted application in food packaging. J Nanobiotechnol 19
141. Nath D, Banerjee P (2013) Green nanotechnology—a new hope for medical biology. Environ Toxicol Pharmacol 36:997–1014
142. Yuen C, Liu Q (2013) Optimization of Fe_3O_4@Ag nanoshells in magnetic field-enriched surface-enhanced resonance Raman scattering for malaria diagnosis. Analyst 138:6494–6500
143. Zhang Q et al (2022) Targeted ginkgo kernel biomass precursor using eco-friendly synthesis of efficient carbon quantum dots for detection of trace nitrite ions and cell imaging. Inorg Chem Commun 140:109442
144. Alam AM, Park BY, Ghouri ZK, Park M, Kim HY (2015) Synthesis of carbon quantum dots from cabbage with down-and up-conversion photoluminescence properties: excellent imaging agent for biomedical applications. Green Chem 17:3791–3797
145. Jafarzadeh S et al (2022) Plant protein-based nanocomposite films: A review on the used nanomaterials, characteristics, and food packaging applications. Crit Rev Food Sci Nutr 0:1–27
146. Han Y, Yu M, Wang L (2018) Soy protein isolate nanocomposites reinforced with nanocellulose isolated from licorice residue: water sensitivity and mechanical strength. Ind Crops Prod 117:252–259
147. Xiao Y, Liu Y, Kang S, Xu H (2021) Insight into the formation mechanism of soy protein isolate films improved by cellulose nanocrystals. Food Chem 359:129971
148. Jafarzadeh S, Mohammadi Nafchi A, Salehabadi A, Oladzad-abbasabadi N, Jafari SM (2021) Application of bio-nanocomposite films and edible coatings for extending the shelf life of fresh fruits and vegetables. Adv Colloid Interface Sci 291:102405
149. Böhmer-Maas BW, Fonseca LM, Otero DM, da Rosa Zavareze E, Zambiazi RC (2020) Photocatalytic zein-TiO_2 nanofibers as ethylene absorbers for storage of cherry tomatoes. Food Packag Shelf Life 24:100508
150. Machado S, Grosso JP, Nouws HPA, Albergaria JT, Delerue-Matos C (2014) Utilization of food industry wastes for the production of zero-valent iron nanoparticles. Sci Total Environ 496:233–240
151. Das S, Sen B, Debnath N (2015) Recent trends in nanomaterials applications in environmental monitoring and remediation. Environ Sci Pollut Res 22:18333–18344
152. Gómez-Pastora J, et al. (2017) Review and perspectives on the use of magnetic nanophotocatalysts (MNPCs) in water treatment. Chem Eng J 310:407–427
153. El-Kassas HY, Aly-Eldeen MA, Gharib SM (2016) Green synthesis of iron oxide (Fe_3O_4) nanoparticles using two selected brown seaweeds: characterization and application for lead bioremediation. Acta Oceanol Sin 35:89–98
154. Boruah A, Saikia M, Das T, Goswamee RL, Saikia BK (2020) Blue-emitting fluorescent carbon quantum dots from waste biomass sources and their application in fluoride ion detection in water. J Photochem Photobiol B Biol 209:111940
155. Mehta VN, Jha S, Basu H, Singhal RK, Kailasa SK (2015) One-step hydrothermal approach to fabricate carbon dots from apple juice for imaging of mycobacterium and fungal cells. Sensors Actuators B Chem 213:434–443
156. Suryawanshi A et al (2014) Large scale synthesis of graphene quantum dots (GQDs) from waste biomass and their use as an efficient and selective photoluminescence on-off-on probe for Ag+ ions. Nanoscale 6:11664–11670
157. Du F, et al (2014) Economical and green synthesis of bagasse-derived fluorescent carbon dots for biomedical applications. Nanotechnology 25

158. Arumugham T, Alagumuthu M, Amimodu RG, Munusamy S, Iyer SK (2020) A sustainable synthesis of green carbon quantum dot (CQD) from Catharanthus roseus (white flowering plant) leaves and investigation of its dual fluorescence responsive behavior in multi-ion detection and biological applications. Sustain Mater Technol 23:e00138
159. Lu B et al (2016) Preparation and application of capacitive carbon from bamboo shells by one step molten carbonates carbonization. Int J Hydrogen Energy 41:18713–18720
160. Muneeb Ur Rahman Khattak M, et al (2017) Removal of heavy metals from drinking water by magnetic carbon nanostructures prepared from biomass. J Nanomater 2017
161. Leng C, Sun K, Li J, Jiang J (2017) From dead pine needles to O, N codoped activated carbons by a one-step carbonization for high rate performance supercapacitors. ACS Sustain Chem Eng 5:10474–10482
162. Fanoro OT, et al (2021) Facile green, room-temperature synthesis of gold nanoparticles using Combretum erythrophyllum leaf extract: antibacterial and cell viability studies against normal and cancerous cells. Antibiotics 10
163. Balasubramanian S, Kala SMJ, Pushparaj TL (2020) Biogenic synthesis of gold nanoparticles using Jasminum auriculatum leaf extract and their catalytic, antimicrobial and anticancer activities. J Drug Deliv Sci Technol 57:101620
164. Saravanakumar K et al (2019) Unveiling the potentials of biocompatible silver nanoparticles on human lung carcinoma A549 cells and Helicobacter pylori. Sci Rep 9:1–8
165. Keshari AK, Srivastava R, Singh P, Yadav VB, Nath G (2020) Antioxidant and antibacterial activity of silver nanoparticles synthesized by Cestrum nocturnum. J Ayurveda Integr Med 11:37–44
166. Francis S, Joseph S, Koshy EP, Mathew B (2017) Green synthesis and characterization of gold and silver nanoparticles using Mussaenda glabrata leaf extract and their environmental applications to dye degradation. Environ Sci Pollut Res 24:17347–17357
167. Gan L, Lu Z, Cao D, Chen Z (2018) Effects of cetyltrimethylammonium bromide on the morphology of green synthesized Fe3O4 nanoparticles used to remove phosphate. Mater Sci Eng C 82:41–45
168. Beheshtkhoo N, Kouhbanani MAJ, Savardashtaki A, Amani AM, Taghizadeh S (2018) Green synthesis of iron oxide nanoparticles by aqueous leaf extract of Daphne mezereum as a novel dye removing material. Appl Phys A Mater Sci Process 124:1–7
169. Basavaiah K, Kahsay MH, RamaDevi D (2018) Green synthesis of magnetite nanoparticles using aqueous pod extract of Dolichos lablab L for an efficient adsorption of crystal violet. Emergent Mater. 1:121–132
170. Akhter G et al (2020) Antibacterial and nematicidal properties of biosynthesized Cu nanoparticles using extract of holoparasitic plant. SN Appl Sci 2:1–6
171. Kalpana VN, Chakraborthy P, Palanichamy V, Devi Rajeswari V (2016) Synthesis and characterization of copper nanoparticles using Tridax procumbens and its application in degradation of bismarck brown. Int J ChemTech Res. 9:498–507
172. Kumar CRR et al (2020) One-pot synthesis of ZnO nanoparticles for nitrite sensing, photocatalytic and antibacterial studies. J Inorg Organomet Polym Mater 30:3476–3486
173. Chandra H, Patel D, Kumari P, Jangwan JS, Yadav S (2019) Phyto-mediated synthesis of zinc oxide nanoparticles of Berberis aristata: characterization, antioxidant activity and antibacterial activity with special reference to urinary tract pathogens. Mater Sci Eng C 102:212–220
174. Fahmy SA, et al (2021) Green synthesis of platinum and palladium nanoparticles using Peganum harmala L. Seed alkaloids: biological and computational studies. Nanomaterials 11:1–15
175. Narasaiah BP, Mandal BK (2020) Remediation of azo-dyes based toxicity by agro-waste cotton boll peels mediated palladium nanoparticles. J Saudi Chem Soc 24:267–281